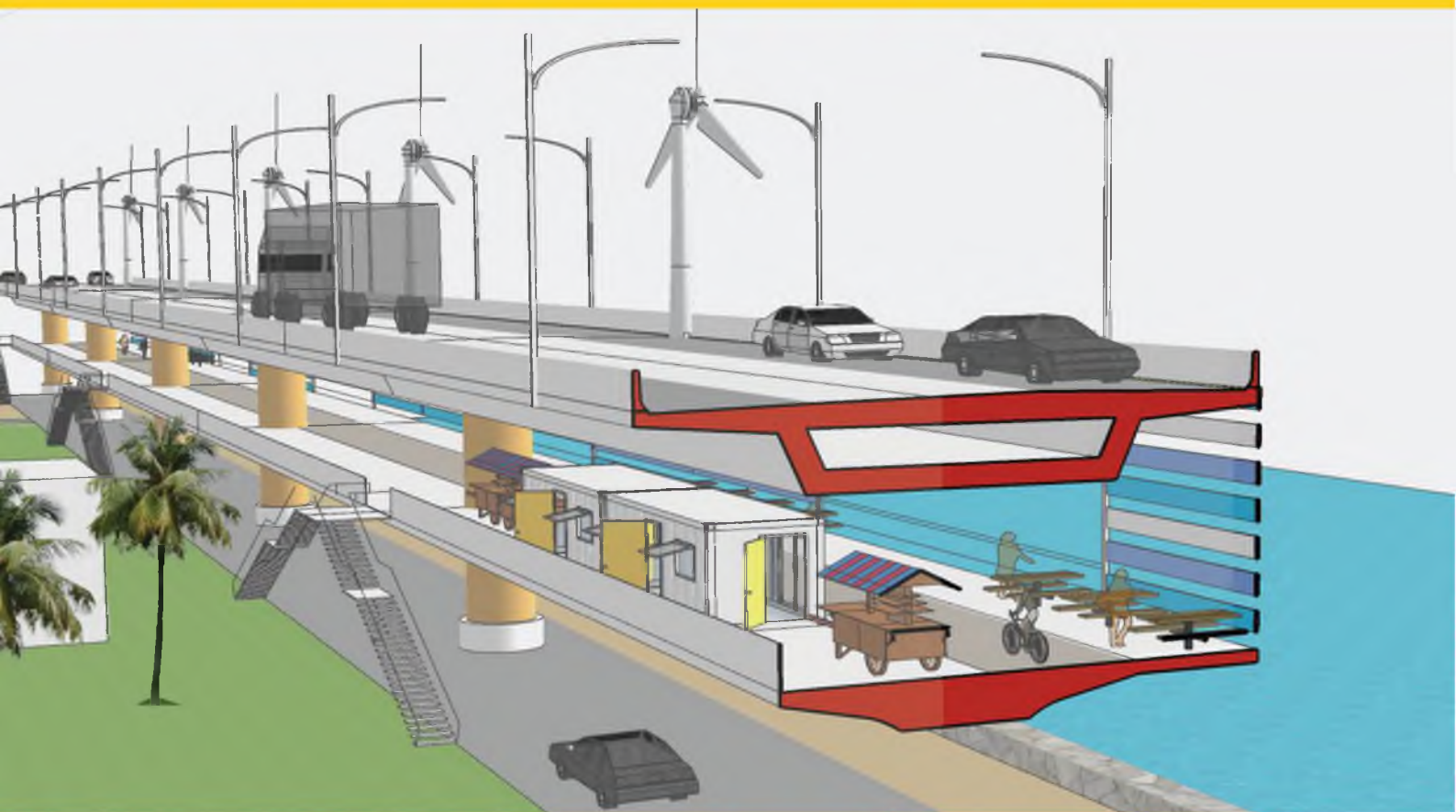




INTERNATIONAL CONFERENCE ON INFRASTRUCTURE DEVELOPMENT : ISSUES, INNOVATIONS AND THE WAY FORWARD

21-23 JUNE, 2018

PROCEEDINGS



MAR BASELIOS
COLLEGE OF ENGINEERING AND TECHNOLOGY

Department of Civil Engineering



Defining the Future

**KERALA INFRASTRUCTURE
INVESTMENT FUND BOARD**



Department of Civil &
Environmental Engineering

AMMANN

SUPPORTED BY:



WIRTTGEN
GROUP

Zydex
Innovating for Sustainability

MESSAGE FROM CEO & Member Secretary, KIIFB



21st June 2018

Message

We are extremely pleased to associate with Mar Baselios College of Engineering and Technology, Nalanchira to organize an International Conference on Infrastructure Development: Issues, Innovations and the Way Forward (ICID 2018). The Kerala Infrastructure Investment Fund was established with the main objective of providing investment for projects in the State of Kerala in sectors like Transport, Water Sanitation, Energy, Social & Commercial Infrastructure, IT and Telecommunication etc. KIIFB aims to facilitate planned and sustained development of both physical and social infrastructure ensuring all round well-being and prosperity in the State.

The conference is intended to provide a platform for the academicians and industry experts to interact and arrive at novel solutions to existing problems. This goes hand-in-hand with the vision of KIIFB - to provide quality infrastructure for the well-being of society. I hope that the association with this conference will pave the way for significantly improving the quality and efficiency of infrastructure development in our state.

With the warmest of wishes for a fruitful and rewarding conference!!

Dr. K.M.Abraham, CFA, IAS
Ex-officio Secretary, Finance (Infrastructure)
CEO & Member Secretary, KIIFB

MESSAGE FROM BURSAR



It is a matter of great pleasure that the Department of Civil Engineering, MBCET is organizing the INTERNATIONAL CONFERENCE ON INFRASTRUCTURE DEVELOPMENT: ISSUES, INNOVATIONS AND THE WAY FORWARD (ICID 2018) from 21-23 June 2018 in association with Kerala Infrastructure Investment Fund Board (KIIFB). The focus of the conference is to provide an opportunity for the engineers, planners, researchers, faculty and students to come together, discuss and seek sustainable solutions related to infrastructure development.

A good conference is always more than just an exchange of papers and ideas, it's a place to stop and reflect, a place to inspire and be inspired. I hope that you will have a productive time at this very special conference.

I convey my best wishes to every participant and congratulate all members of the Department of Civil Engineering for successfully organizing the conference.

I wish the conference a grand success.

Rev. Fr. John Vilayil
Bursar, MBCET

MESSAGE FROM PRINCIPAL



It is with great pleasure; I welcome you to participate in the **International Conference on Infrastructure Development: Issues, Innovations and the Way Forward (ICID 2018)**, which will be held in Trivandrum from **21-23, June 2018**. The conference is organized by Mar Baselios College of Engineering and Technology, Trivandrum, jointly with Kerala Infrastructure Investment Fund Board (KIIFB).

Infrastructure is a vital component for any country aspiring for growth and development. India being a fast developing country will have to spend trillions of rupees for modernization and expansion of water, electricity and transportation systems in order to achieve a developed nation's crown. Alarming increase in the rate of urbanization and consequent industrialization has posed challenges on natural resources and construction materials, forcing new ways and means for infrastructure development.

This conference is aimed at engaging and interacting with the researchers, industry leaders and government agencies to address the various issues of infrastructure development. We sincerely hope that the scope of the conference will serve the interest of the community in shaping the future directions as well as key priorities. In addition, the conference will serve as a platform for the participants to get in touch with their peers who share similar interest.

I extend a hearty welcome to all the participants and the sponsors to ICID 2018.

Dr. T M George
Principal, MBCET

MESSAGE FROM HEAD OF THE DEPARTMENT



International conferences are awesome open base for specialists, researchers, strategy creators, graduates and understudies. Attending conferences, particularly the global one allows tuning into various perspectives and learning new thoughts and patterns in the field. Infrastructure is a fundamental piece of social prosperity of any country and this can be assembled under the umbrella of manmade structures to encourage temperate advancement for the welfare of mankind. This conference gives a stage to investigate the conceivable outcomes of the utilization of nontraditional material and their financial reasonability as other option to regular developmental option, for monetary and ergonomic infrastructures.

I wish ICID2018 a grand success.

Dr. M. Satyakumar
Professor & HOD, Dept. of Civil Engineering
MBCET

MESSAGE FROM CONVENER

Infrastructure development refers to the system of Networks of roads, highways, and railways for transportation into and out of a community, Water and sewage systems that ensure an adequate supply of clean water as well as the disposal of waste, Power grids that can handle the needs of the entire community. The impact of construction technology and transport infrastructure development is known to be significant on the economy of any country. It gives us immense pleasure to organize this International Conference on INFRASTRUCTURE DEVELOPMENT: ISSUES, INNOVATIONS AND THE WAY FORWARD (ICID2018) from 21-23 Jun, 2018 in association with Kerala Infrastructure Investment Fund Board (KIIFB).

The purpose of this conference is to bring together academics and other professionals from all over the world, for the presentation and exchange of their thoughts and experiences on concepts, trends and practices in infrastructure development. All the papers in this conference proceeding have undergone an intensive review process, and only accepted papers are included which covers all streams in civil engineering namely, Structural Engineering, Geotechnical Engineering, Transportation Engineering, Hydraulics Engineering and Environmental Engineering.

It is our pleasant duty to acknowledge the financial support from KIIFB. We would like to acknowledge and give special appreciation to our keynote speakers for their valuable contribution, our delegates for being with us and sharing their experiences, and our invitees for participating in this conference. We also wish to express the sense of gratitude to the college management for their abundant support and encouragement.

Convener

ABOUT THE INSTITUTE

Mar Baselios College of Engineering & Technology was started in 2002 and is administered by the Malankara Catholic Educational Society of the Major Archdiocese of Thiruvananthapuram, Kerala. It is the first self-financing engineering college in Kerala accredited by NAAC with A grade (CGPA 3.13) and all B.Tech programmes provisionally accredited by NBA since July 2016. The college is KTU approved research center.

Mar Baselios College of Engineering and Technology (MBCET) inspires the aspirations of generations of knowledge-seekers. Dedicated to mould morally upright, socially committed and intellectually trained Engineers, the College strives to realize its dreams. Situated amidst 17 Educational Institutions in the Mar Ivanios Vidyanagar, just 5 kms from the heart of the city of Thiruvananthapuram, MBCET stands tall as a symbol of the quest for Professional and Technological Studies set against the backdrop of the serene and panoramic Mar Ivanios Vidyanagar away from the hustle and bustle of the city life. The campus provides the ideal milieu for academic pursuits.

The aesthetically designed buildings in nine blocks spread over the campus have a total built-up area of over 32000 sq. m. An eco-friendly infrastructure concept, causing least disturbance to the landscape has been executed. Rain water harvesting has been implemented right from the beginning of the College.

VISION AND MISSION

Vision

To be an institution moulding globally competent professionals as epitomes of noble values.

Mission

To transform the youth as technically competent, ethically sound and socially committed professionals, by providing a vibrant learning ambience, for the welfare of humanity.

ABOUT KIIFB

Kerala Infrastructure Investment Fund Board (KIIFB) came into existence on 11.11.1999 under the Kerala Infrastructure Investment Fund Act 1999 (Act 4 of 2000) to manage the Kerala Infrastructure Investment Fund. The objective was to provide investment for critical and large infrastructure projects in Kerala. Comprehensive modification of the Act and Scheme has been made through an amendment Ordinance in August 2016. KIIFB will assist the Government and its agencies in the various aspects pertaining to Infrastructure Development namely, Management Consultancy, Financial Consultancy, Issue Advisory and Legal Consultancy. With the restructured and rejuvenated KIIFB the future looks bright for the development of key infrastructure in Kerala. With new strategy and structure, KIIFB aims to dynamically mobilize funds for the infrastructure development of Kerala which includes the major land acquisition needs of the State. KIIFB have recourse to the advanced financial instruments approved by SEBI & RBI and is expecting an upspring of sustainable infrastructure development of the State. KIIFB through its well organised and professional approach will act as the key arm of Government to facilitate planned, hassle-free and sustained development of both physical and social infrastructure ensuring all round well being and prosperity in the State.

ABOUT THE CIVIL DEPARTMENT

The Department of Civil Engineering, established in the year 2005, is a vibrant place for learning, where the students pursue their educational interests in order to lead the next generation to better prospects. The students develop high quality technical expertise with a sound knowledge in basic engineering principles, technical skills and innovative research capabilities. The students have access to state-of-the art facilities and well-equipped laboratories. They are also provided with opportunities to earn valuable experience in the field through value added courses frequently conducted in the Department. The Civil Engineering Department moulds, organizes and structures the students to be good citizens, competent Civil Engineering Professionals and to be the architects of a better world. To excel in Civil Engineering means to have proper reasoning skill, good knowledge of geometry, good creativity and above all good imagination.

The Department is rich with a group of Faculty Members with knowledge and passion to deliver their experience to the future leaders. The Department offers B.Tech and M.Tech programmes. In addition to the Teaching Staff, a team of experienced technicians are also in position to gain most from our well equipped laboratories and other facilities available: The Strength of Materials Lab, Concrete Lab and Survey Lab are functioning at the ground floor and Environmental Engineering Lab and Transportation Lab are situated on the first floor. Our teaching block is large and refurbished with Lecture Rooms, Staff Rooms, Seminar Halls and Department Library, where students pursue their educational interests in order to lead the next generation in transforming the disciplines of Civil Engineering.

Vision

To be a Centre of Excellence in Civil Engineering education with a global perspective, creating ethically strong engineers for the service of society.

Mission

To provide engineering education which can create exemplary professional Civil Engineers of high ethics with strong conceptual foundation coupled with practical insight, to serve the industry and community.

ICID 2018

The Department of Civil Engineering is organizing the **International Conference on Infrastructure Development: Issues, Innovation and the Way Forward** from **21 - 23 June 2018**. ICID 2018 aims to present the state-of-art in infrastructure development as it exists today, around the world and its applicability in the Indian scenario. It will provide a platform for all stakeholders, academicians, and practitioners to amalgamate and seek sustainable solutions for challenges in technology implementation. Presentations, keynote addresses, and pre-conference workshops will cover aspects of infrastructure development including design, construction, maintenance & quality control of various infrastructure facilities. Discussions on real-time research finding adaptations will be beneficial for practicing Engineers. Devising ways of optimizing the benefits of infrastructure development is yet another focus area.

Infrastructure is an essential part of the social well-being of any nation and this can be grouped under the umbrella of man-made structures to facilitate economic development for the welfare of the humankind. Such infrastructure includes buildings, roads, pipelines, dams and power plants, to list a few. Providing quality infrastructure without aggravating the existing issues related to environment, economy and sustainability is a major challenge to the engineering community. The recent decades have witnessed extraordinary strides made in the efficient engineering of such infrastructure projects.

The conference will have keynote addresses & paper presentations in the following areas:

- Pavement, Traffic & Transportation Engineering
- Structural & Construction Engineering
- Environmental Engineering
- Geotechnical Engineering
- Hydraulics & Water Resources Engineering

PRE-CONFERENCE WORKSHOPS

Sustainable Pavements & Asset Management

This workshop combines aspects of sustainable pavements and recycling, road asset management, advances in quality control, management and innovative technologies in condition evaluation of roads.

Structural Simulations using FEAST^{SMT} Software

FEAST (Finite Element Analysis of Structures) is ISRO's structural analysis software based on Finite Element Method realized by the Structural Engineering Entity of VSSC. The current version of FEAST 2014 R2 includes linear analysis capabilities. This has basic modules such as linear static analysis, free vibration analysis, buckling analysis etc. and supplementary modules such as transient response, frequency response, fluid-structure interaction etc. Workshop includes technical session handled by experts from VSSC and hands-on training in FEAST^{SMT}.

A Technical Tour of Greenfield International Stadium, Kerala

This workshop provides the delegates a rich experience of understanding the technical aspects & having a close look at the various features of the Sports Hub, Trivandrum, commonly known as Trivandrum International Stadium or Greenfield Stadium. It includes a technical session on various aspects of the stadium such as design, safety, maintenance etc. and a guided tour of the stadium.

INTERNATIONAL TECHNICAL COMMITTEE



Dr. K R Rajagopal
Distinguished Professor
Texas A&M



Prof. Rajib B Mallick
Professor
Civil and Environmental Engineering
Worcester Polytechnic Institute
(WPI) Worcester, Massachusetts



Dr. Gopu R Potty
Professor
University of Rhode Island University



Dr. Anuj Sharma
Associate Professor
IOWA State University

NATIONAL TECHNICAL COMMITTEE



Dr J Murali Krishnan
Professor
IIT Madras



Dr Lelitha Devi Vanajakshi
Professor
IIT Madras



Dr Veeraragavan
Professor
IIT Madras



Dr Shiva Nagendra S M
Associate Professor
IIT Madras



Dr U Saravanan
Associate Professor
IIT Madras



Dr Radhakrishna G Pillai
Associate Professor
IIT Madras



Dr R G Robinson
Professor
IIT Madras



Dr Thyagaraj T
Associate Professor
IIT Madras



Dr V Sunitha
Assistant Professor
NIT Trichy



Dr Santosh G Thampi
Professor
NIT Calicut



Dr Venkaiah Chowdary
Assistant Professor
NIT Warangal



Dr Padmarekha A
Associate Professor
SRM University



Dr A N Brijesh Nair
Professor
VIT University



Dr Manju V S
Associate Professor
CET



Ms. Thushara V T
Assistant Professor
GEC Bartonhill

ADVISORY COMMITTEE



Dr. T M George
Principal
MBCET



Prof. S Viswanatha Rao
Vice Principal
MBCET



Prof. M K Giridharan
Dean (Academic)
MBCET



Prof. K M Raju
Dean (Administration)
MBCET



Prof. P S Abraham
Professor
Dept. of Civil Engg
MBCET



Prof. P N Mohan
Professor
Dept. of Civil Engg
MBCET

ORGANISING COMMITTEE



Organising Chair
Dr. M Satyakumar
Professor & HOD,
Dept. of Civil
Engineering, MBCET



**Technical
Programme Chair**
Dr. Neethu Roy
Professor, Dept. of
CE, MBCET



Convener
Bindu Biju
Asst. Professor,
Dept. of CE, MBCET



Convener
Dr. Senthilkumar R
Asst. Professor,
Dept. of CE, MBCET



Dr. Jayasree S
Assoc. Professor



Ann George
Asst. Professor



Tisny D B
Asst. Professor



Muthulakshmi P
Asst. Professor



Jean Molly Simon
Asst. Professor



Jaya S Pillai
Asst. Professor



Tom George
Asst. Professor



Aneena Babu
Asst. Professor



Anjana Krishnan
Asst. Professor

KEYNOTE SPEAKERS



Dr. Rajib B Mallick

Rajib Basu Mallick is currently the Ralph White Family Distinguished Professor of Civil and Environmental Engineering at WPI. He graduated from Jadavpur University, India, in 1989 and received his master's degree and Ph D from Auburn University, USA. He also worked as a senior research associate at the National Center for Asphalt Technology, USA.

His main research interests are in the optimum utilization of natural resources and sustainable construction, specifically related to the pavement industry. His work focuses on recycling of asphalt pavements, understanding and modeling the behavior of recycled materials, reducing the urban heat island effect, harvesting energy from pavements, understanding temperature profiles, and reducing temperatures in pavement layers.

He has close to 100 publications, including a textbook, and also a U.S. patent. He has conducted numerous research projects and has consulted in the area of both highway and airport pavements. He is a registered Professional Engineer in the state of Massachusetts.

KEYNOTE SPEAKERS



Dr. J Murali Krishnan

Dr. J. Murali Krishnan is currently a Professor in the Department of civil Engineering at IIT Madras. His main interest includes bituminous material characterization, pavement engineering and viscoelasticity.

He did his diploma in civil engineering, followed by AMIE and ME from NIT-Trichy (REC Trichy in his time). He did his Ph D at IIT Madras and spent 5 years at Texas A&M/ Texas Transportation Institute as a post-doctoral fellow/visiting faculty/engineering scientist.

He is currently an associate editor of International Journal of Pavement Engineering and serves in the editorial board of pavement engineering journals.

KEYNOTE SPEAKERS



Dr. P. K. Sikdar

Professor P. K. Sikdar is Advisor, International Road Federation (India Chapter), while he is a President at ICT Pvt Ltd. He is former Professor of Civil Engineering and Dean at Indian Institute of Technology (IIT), Bombay. Dr. Sikdar is also Former Director, Central Road Research Institute (CRRI), New Delhi, a constituent laboratory of Council of Scientific & Industrial Research (CSIR). He obtained Canadian Commonwealth Scholarship for his Doctor of Philosophy (Ph.D.) study from University of Waterloo, Canada; and he is also a recipient of Leverhulme Foundation Fellowship of UK (1981-82) for post-doctoral research.

Prof. Sikdar has been involved in the teaching, research and R&D management for Road and Road Transport Sector including highway planning and management for more than three decades. Prof. Sikdar is member of a large number of national and international bodies for policy making and standardization in the road sector. He is also a Fellow of Institution of Engineers (India), The Chartered Institute of Logistics & Transport (CILT, UK) and Indian National Academy of Engineering (INAE).

KEYNOTE SPEAKERS



Mr. K Vasudevan

Mr. K Vasudevan, General Manager – International Marketing, SEA, is a business management professional with an experience of 25 years in the field of specialty chemicals. He's been associated with Zydex since 2014 and has been driving their Roads Division in Southern India and South East Asia.

He regularly participates in public forums for technology presentations, in close correspondence with major concessionaires, government officials, university departments and consultants in all these markets.

KEYNOTE SPEAKERS



Dr. T Thyagaraj

Dr. T Thyagaraj is currently the Associate Professor, Department of Civil Engineering, Indian Institute of Technology Madras, India, July 2015 - till date. He worked as Assistant Professor, Department of Civil Engineering, Indian Institute of Technology Madras, India, from August 2008 - July 2015. He was also the Assistant Professor at King Saud University, Riyadh, Saudi Arabia, April 2008 - August 2008. He also worked as Research Fellow in, King Saud University, Riyadh, Saudi Arabia, January 2008 - March 2008 and Lecturer, Department of Civil Engineering, National Institute of Technology Warangal, from November 2006 - December 2007.

He graduated from Osmania University, Hyderabad and received his master's degree and PhD from Indian Institute of Science, Bangalore. His main research interests are in ground improvement techniques, unsaturated soil behaviour and geo-environmental engineering.

KEYNOTE SPEAKERS



Mr. K.Saravanakumar

Mr. Saravanakumar is a Graduate Mechanical Engineer with a Masters' degree in Business Management and over 24 years of experience in the asphalt road construction equipment industry. He commenced his career as a Project Engineer with Gujarat Apollo Industries Limited and has worked in various capacities in the asphalt pavement construction industry – project management, adoption of new technologies, sales & marketing. During his tenure he has worked with almost all the prestigious construction companies in India and with Government organisations like Border Roads Organization. He is currently working as Deputy General Manager (South) Ammann India Private Ltd. He has good knowledge on production of asphalt mix both by Batch & Continuous process.

After the Joint Venture of Apollo with Ammann, he attended the paving campus of Ammann at Czech Republic and has been making technical presentations on the latest technologies in production of asphalt mix and construction of asphalt pavements. He is an active participant in Indian Roads Congress and delivers lectures on the latest flexible pavement technologies.

KEYNOTE SPEAKERS



Mr. Rithesh J Parmar

Mr. Rithesh J Parmar is currently the Assistant Product Manager of Cold Milling Technology, Wirtgen India Pvt. Ltd. He has an experience of 8 years as Assistant Manager in After Market Customer Support for Equipments mainly used in roads and mineral technology specialized in Milling Machines, Asphalt & Concrete Pavers & Compactors.

He deals with customer service and involved in training and development field for a period of 7 years at Wirtgen Group and currently deals with the Sales and Service for Product Development of Cold Milling Technology in Western Regions of India.

KEYNOTE SPEAKERS



Mr. Arashdeep Singh

Mr. Arashdeep Singh is Deputy Manager with Wirtgen group from August 2012 till date. He has also worked with Soma Enterprises Ltd. He is experienced in Project support for Cold In situ Recycling and Soil stabilization in Roads & Mineral Technologies. He is specialized in the Application of Projects of Recyclers and Stabilizers.

He is responsible for assisting the VP–Business Development & VP–Sales & Service for Product, development of Cold Recycling and Soil stabilization Technology in India, addition of new cities and customers for recycling and stabilization technology, market development etc.

KEYNOTE SPEAKERS



Dr U Saravanan

Dr. Saravanan U is Associate Professor at the Department of Civil engineering, IIT Madras. Having obtained his B Tech in Civil Engineering from IIT madras, he took his Masters in Mechanical Engineering from Texas A&M University. Subsequently, he obtained his Doctoral Degree in Mechanical engineering from Texas A&M University.

His area of expertise includes Continuum Mechanics, Constitutive Modelling and non-linear analysis. He has co-authored numerous cited journal publications and conference articles in the aforementioned topics, and has received several awards and scholarships.

KEYNOTE SPEAKERS



Dr. Santhosh G Thampy

Dr. Santhosh G Thampy is presently the professor of NIT Calicut. He graduated from Calicut University and received his masters in Agriculture Engineering from Kerala agricultural university and Hydraulics and water resources engineering from IIT madras. He is being honoured doctorate in Environmental hydraulics from IISC, Bangalore.

His area of expertise includes Pipe and channel flows, Hydrologic Processes and modelling, water quality modelling, water and waste water treatment, Water resource systems analysis and management and application of remote sensing and GIS in natural resource management. He has worked as Assistant engineer in Kerala State Rural Development Board and senior project officer in IIT, Madras.

KEYNOTE SPEAKERS



Mr. Shreeganesh V Nair

Mr. Shreeganesh V Nair is a complete building physics expert with 24 years of experience in design of buildings, services, Infrastructures, factories and industries. He is currently the managing director and Chief Consultant at GTCS and Master Trainer in ECBC. He is also a BEE certified energy manager and GRIHA certified Trainer and evaluator. He has an experience of 22 years in core construction industry and specialized in cost analysis for buildings and MEP services, task analysis with planning schedule breakdown and hindrance analysis. He designed rainwater harvesting reservoirs in association with DuPont liners. He mainly focused his efforts on reducing energy cost in operations and incorporating green building practices.

KEYNOTE SPEAKERS



Dr. Gopu R Potty

Dr. Gopu R Potty is currently working as Associate Research Professor of Department of Ocean Engineering at the University of Rhode Island. He graduated from Kerala University, in 1985 and received his master's degree from IIT Madaras. He completed his PhD in Ocean Engineering from University of Rhode Island, USA.

He is actively involved in field data collection and analysis in the areas of underwater acoustics, acoustical oceanography and marine bio acoustics. He has conducted numerous research projects in his subject area Physical Oceanography.

LIST OF PAPERS ACCEPTED FOR PRESENTATION

STRUCTURAL ENGINEERING			
Sl. No.	Paper ID	Title	Authors
1	SE 101	Fire Resistance of Steel-Concrete Composite Bridge Girders	Anusree Venugopal Tom George
2	SE 102	Analysis of Concrete Silo by Using ETabs 2016	Neeraja R
3	SE 103	Finite Elemental Analysis of Idukky Dam	Asna Yasmin Yassid Devika B Gayathri D S Gayathri G R Lekshmi Rajan B S Ramya Raveendran
4	SE 104	Seismic Analysis of RCC Buildings Considering the Flexibility of Soil	Fathima S Jisha S V
5	SE 105	Effect of Containment Reinforcement on the Seismic Performance of Un-Reinforced Masonry Buildings	Vaidehi S R Aiswaria G R Jisha S V
6	SE 106	Along and Across Wind Responses of Tall Buildings Considering Soil Structure Interaction	Aiswaria G R Jisha S V
7	SE 107	Eco- Friendly Cement Blocks	Arathy K Chandran Aiswarya.A Irfana.S U Jayanarayanan Anjana Krishnan
8	SE 108	Effect of Steel and Polypropylene Fibre on the Tension Stiffening of Ultra High Performance Concrete	Lijina Thomas Jithin J S
9	SE109	Development of Stress Block Parameters of Concrete with Metakaolin Admixed Recycled Concrete Aggregate	Shin Elizabeth Shaji Jithin J S

10	SE 110	Study on Properties of Polythene Fibre Reinforced Concrete with Partial Replacement of Coarse Aggregate as Coconut Shell (PFRCS)	Swathi M S Anu A
11	SE 111	Comparative Study on Hysteretic Performance of Semithrough Connections in CFT Beam - Column Joint	Ajith M S Dr. Beena K P Dr. S Sheela
12	SE 112	Effect of Swimmer Bars on the Behaviour of Exterior Beam Column Joints Under Reverse Cyclic Loading	Shahana S Tom George
13	SE 115	Experimental and Analytical Study on Geopolymer Concrete Beam with Hollow Space Below Neutral Axis	Sherin Kurikesu Abhirami S
14	SE 116	Thermal Response of Concrete Filled Fibre Reinforced Polymer Tube Columns	Sneha S B Anjana Krishnan
15	SE 118	Partial Replacement of Fine Aggregate With Crumb Rubber	Madhavi G Saneeth S Anju P Babu
16	SE 119	Strengthening of Self Compacting Concrete using Polypropylene and Strips of Steel Scrubber	Amritha V R Adarsh S Anil Anju P Babu
17	SE 120	Experimental Investigation on Torsional Behaviour of RCC Beams Retrofitted with High Strength Ferrocement Jacketing and GFRP	Shine R. Sylus Tom George
18	SE 121	Seismic Evaluation of Different Structural Systems in Stepped Building Frame	Yamuna S R Aneena Babu
19	SE 122	Study on the Mechanical and Flexural Properties of Concrete by the Addition of Black Liquor Sludge as Admixture	Nikhil NadhV S Jayasree S
20	SE 123	Study on Flexural Behaviour of RCC Beams Retrofitted with Biplanar Geonet	Sherine Stanly Tisny D B
21	SE 124	Study on Behaviour of Normal Concrete Column and Modified Reactive Powder Column	Neethu S Deth Sreejith R

22	SE 125	Response of Conventional and Virtual Outrigger System Subjected to Seismic Load	Visakh V S Akhil Raj S R
23	SE 126	Shear Behaviour of RCC Beams Retrofitted With Ultra High Performance Fibre Reinforced Concrete	Swarup S S Bindu Biju
24	SE 127	Effect of Near Surface and Externally Bonded Retrofitting on Exterior Beam-Column Joint	Akash S Dr. Jayasree S
25	SE128	Effect of Nonlinear Viscous Dampers on Irregular Shaped Buildings	Rakhimol.S Smrithi Cheriya
26	SE 129	Flexural Behaviour of RCC Beams Retrofitted with Engineered Cementitious Composite (ECC)	Jackson Vincent Jean Molly Simon
27	SE 130	Numerical Study on the Flexural Behaviour of Concrete Filled Steel Tube Beam Strengthened With CFRP	Neethu Prakash Jisha S V
28	SE 132	Flexural Behaviour of Hybrid Fibre Reinforced High Strength Concrete	Kalyani Laxman Akhil Raj S R
29	SE 133	Strength and Behaviour of RCC Beams Retrofitted by Textile Reinforced Concrete	Sunoj J S Dr. Jayasree S
TRANSPORTATION ENGINEERING			
30	TE 201	Use of Recycled Premix Chipping Carpet (RPCC) for Rural Road Construction	Jesh Jayakumar Anil R
31	TE 203	Accurate Identification of Pavement Materials that are Susceptible to Moisture Damage with the use of Advanced Conditioning and Test Methods and the use of Machine Learning Techniques	Ram Kumar Veeraragavan Nivedya, M K Rajib B Mallick
32	TE 204	Comparing the Properties of HMA with Warm Asphalt Mixes by Varying Temperatures using Sasobit and Stearic Acid as Additives	K Govind Goud Dr. P Sravana A Nitish
33	TE 205	Environmental Impact Assessment of Thrissur-Vadanapally Road Project	Rosmy Sebastian Vincy Verghese M G Cyriac
34	TE 206	Development of a Relation between Structural and Functional Characteristics of the Pavement	Janani L Raunak Dixit Sunitha V Samson Mathew

35	TE 207	Effect of Accessibility on Potential Tourist Destinations –A Case Study of Kozhikode District in Kerala	V S Sanjay Kumar Saleel K Teena John
36	TE 208	Activity Based Transportation Modeling for Chelakottukara ward of Thrissur District	Midhun. T Dr. Anitha Jacob
37	TE 209	Urban Resident’s Awareness and Readiness for Sustainable Transportation: A Case Study	Leejiya Jose Vincy Verghese
38	TE 210	Use of Data Mining Technique for Systematic Road Safety Audit of Non-urban Highways	Bincy B J Dr. Anitha Jacob
39	TE 211	A Study on Profit Optimisation of Kerala State Road Transport Corporation	Anusree P P Jomy Thomas
40	TE 212	Estimation of PCU and Saturation Flow for Mixed Traffic Condition at Urban Signalized Intersections	Minu Mol Raju Subhash Chand Jomy Thomas
41	TE 213	Analysis and Development of Traffic Speed-Flow-Density Relationships for Urban Roadway	Thasneem Nadirsha Archana S
42	TE 214	Managing Traffic Congestion using GIS – A Case Study in Attingal Town	Anjana U Ashtami Hari Ayana Asok G Greeshma M J Riya Sreekumar Anoja B V
43	TE 215	Overtaking Behaviour of Vehicles on Undivided Roads Under Heterogeneous Traffic	Ameera V U Vincy Verghese
44	TE 218	Quantification and Analysis of Blindspots for Light Motor Vehicles	Aleena Mathew E. S. Krishna Ram Elizabeth Maria Alex Gokul G Kumar Jeslin Elizabeth M Satyakumar
45	TE 219	Comparative Study on Cell Filled and Whitetopped Concrete Overlay with Human Hair as Pavement Rehabilitation Methods	Gokul.K.L M Satyakumar
46	TE 220	Influence of Gauge Length on the Measurement of Resilient Modulus of Bituminous Mixtures	Arbin Raj J Murali Krishnan

47	TE 221	Influence of Rest Period and Confinement Pressure on the Measurement of Dynamic Modulus of Bituminous Mixtures	Devika R Sriram. V J Murali Krishnan
48	TE 222	How to consistently collect Rheological data for Bitumen in a Dynamic Shear Rheometer?	P S Divya J Murali Krishnan
49	TE 223	Moisture Conditioning Process for Large-Sized Prismatic Straight Beam Specimens of Bituminous Concrete	Utsav Vishal Venkaiah Chowdary J Murali Krishnan
530	TE 224	Surrogate Safety Assessment Models for Interurban Corridors	Bhamini B A. Mohan Rao S Velmurugan Jomy Thomas
51	TE 225	Use of Statistical Methods for the Analysis of Axle Load Data for Pavement Design	Donia Savio J Murali Krishnan
52	TE 226	Feasibility Study of Provision for Exclusive Bus Lanes on Urban Roads	Arathi A R Vincy Verghese
ENVIRONMENTAL ENGINEERING			
53	EE 301	Environmental Issues of Buildings – Green Solutions	Aaliya Azeem
54	EE 302	Development of Noise Map using GIS for Lucknow Metropolis	Sudhanshu Bhushan A.K. Shukla
55	EE 303	Comparitive Study of Noise Descriptors and Noise Exposure Level due to Diwali Noise in Metropolitan City: Lucknow	Ajay Kumar Vasanwal A K Shukla J B Srivastava
56	EE 304	Treatment of Industrial Effluent with Coir pith and Charcoal Infused Soil Media	Aravind M A Rahna L
57	EE 305	Optimisation of Phosphate Removal from Fertiliser Waste Water using Polysulphone Chitosan Nanosilica Membrane	Krishnaveni S Meera V Megha M
58	EE 306	Trend and Change point Analysis of Extreme Temperature over India using Non-Parametric Methods and Empirical Mode Decomposition	Drisya S Dharan Anuja PK Govindan Unnithan Anand Vishnu B Adarsh S

59	EE 307	Evaluation of Groundwater Quality at Eloor, Ernakulam District, Kerala Using GIS	Fehmida Fatima S Bindu A G
60	EE 308	Biodiesel Production from Waste Oil using Mussel Shell as Catalyst	Sona Gloriya Antony Nithya Kurup
61	EE 309	Landfill Site Selection using GIS and Landfill Design in Trivandrum District	Arathy Nair G R Lakshmi R Vasanth Namratha Lekshmi Silpa B Santhosh Mini M. Anoja B. V.
GEOTECHNICAL ENGINEERING			
62	GT 402	Influence of Nano-Silica on Unconfined Compressive Strength of Marine Clay with Curing Time	Joju M R S Chandrakaran
63	GT 403	Effect of Enzymatic Lime on Engineering Behaviour of Clay	Dani Jose S Chandrakaran
64	GT 404	Skirted Stone Column with Bamboo and Coir in Kuttanadu Clay	S J Ganesh K Balan
HYDRAULICS ENGINEERING			
65	HE 501	Trend and Change Point Analysis of Annual Maximum Streamflows of Krishna Basin using Non- Parametric Tests and Empirical Mode Decomposition	Athul MM Nandhu AR Adarsh S
66	HE 502	Modeling of Bharathapuzha River Basin using SWAT Model and SUFI-2	Dila John Chithra N.R.
67	HE 503	Assessment of Meteorological Drought in Anantapur District Using Standardized Precipitation - Evapotranspiration Index (SPEI)	Athira K Chithra N R Sathish Kumar D

Fire resistance of steel-concrete composite bridge girders

Anusree Vemugopal (PG student)

Department of Civil Engineering
Mar Baselios College of Engineering and Technology
Thiruvananthapuram, India
anusreevenu@gmail.com

Mr. Tom George (Assistant Professor)

Department of Civil Engineering
Mar Baselios College of Engineering and Technology
Thiruvananthapuram, India
tomgeorge1507@gmail.com

Abstract—Bridge fires have become relevant issue in recent years due to rapid development of navigational systems as well as increasing transport of hazardous materials. Fire is one of the most dreadful hazards that bridges may be subjected to during their whole lifespan. Due to high intensity of fires, significant structural damage, even collapse of bridges occur which lead to large economic loss and traffic delay. In this paper, the fire response of a composite bridge girder is evaluated using the FEM computer program ANSYS. Numerical simulation results demonstrate that the composite action from steel-girder-concrete-slab interaction significantly elevates the fire resistance of a composite bridge girder under fire conditions.

Index Terms—Fire resistance, Shear connectors, Bridge fires, Thermo-structural analysis

INTRODUCTION

Bridge fires caused by crashing of vehicles with different components of bridges and burning of highly flammable gases are much more hazardous than building fires and are differentiated by a rapid heating rate and a higher peak temperature which could lead to bridge collapse. Bridge failures during a fire can result in the disruption of commerce and services, and most importantly the loss of human life. The fire thus produced is highly dangerous as compared to building fires and they spread in different directions with rapid heating pace. These high intensity fires can pose a severe peril to structural members and can lead to disintegration of structural members of a bridge.

The most significant example is the demolition of the I-20/I-59/I-65 interchange in Birmingham, AL, USA on January 5, 2002. A gasoline tanker overturned and started a fire under the bridge. The main span sagged about 3 meters and the bridge had to be replaced. The bridge damage level was estimated to be 4 [3].

Construction of composite steel-concrete composite bridges is a major trend in recent years. Advantageous properties of both concrete and structural steel are effectively utilized in a composite bridge. Due to the composite action developed, all loads including traffic, surfacing, wind, water, pressure, seismic loads) are shared by the steel/concrete composite. They are endowed with higher strength, ductility, and less dead weight. Nevertheless, steel structural members exhibit lower fire resistance when compared to concrete members due to rapid rise in steel temperatures resulting from different thermal properties such as high thermal conductivity, low specific heat, and lower sectional mass of steel. This ultimately leads to reduced load carrying capacity under fire conditions.



Fig.1 Bridge constructed over Zolotoi Rog Bay caught fire, Vladivostok

The steel structure of a bridge is connected to the concrete structure of the deck so that the steel and concrete act together, and thereby reducing deflections and enhancing stiffness. This is accomplished by 'shear connectors' connected to the steel beams and then embedded in the concrete. Steel-concrete composite beams are mainly used in bridges and industrial buildings due to their potential in developing high flexural strength and stiffness. Structural steel sections with no fire insulation, when subjected to fire, are having limited fire resistance due to the rapid rise of temperature in the member. This rapid rise in temperature is pursued by a rapid loss in strength and stiffness. Fire resistance can be significantly increased when steel elements interact with structural materials characterized by low thermal conductivity such as concrete. Even though bridge fires pose a real threat, this field is not considered in current design codes.

In current practice, there are no special measures adopted for enhancing structural fire safety of bridge girders. Moreover, there is very limited information and research data in the literature on the fire resistance of structural members in bridges. This paper presents results from an analytical study on the fire rating of composite bridge girders.

OBJECTIVES

The main objective of this project work is:

- To study the fire resistance of symmetric steel-concrete composite bridge girder of symmetric when subjected to fire
- To investigate the influence of composite action and stiffeners on the response of girder under fire

MODELLING

A numerical study is carried out using the FEM computer software ANSYS to illustrate the response of a steel girder exposed to fire. For thermal and structural analyses, two sets of discretization models has been developed. The thermal-analysis results are imported to structural model and applied as thermal-body load on it uniformly along the girder span. Thermal and mechanical properties of steel and concrete have been incorporated in the analysis. ASTM E119 fire curve is given as fire load. Deflection limit state is adopted for defining failure, and the failure is said to occur when the deflection becomes span/20. Both heat-convection and radiation loads have been applied at the exposed surface areas of the solid element. Convection coefficient of $\alpha = 35 \text{ W/m}^2 \text{ }^\circ\text{C}$ is used in the thermal analysis under and this is based on Eurocode 1 [European Committee for Standardization (CEN) 2002] recommendations. A Stefan-Boltzmann radiation constant of $5.67 \times 10^{-8} \text{ W/m}^2 \text{ }^\circ\text{C}$ is applied in the thermal analysis.

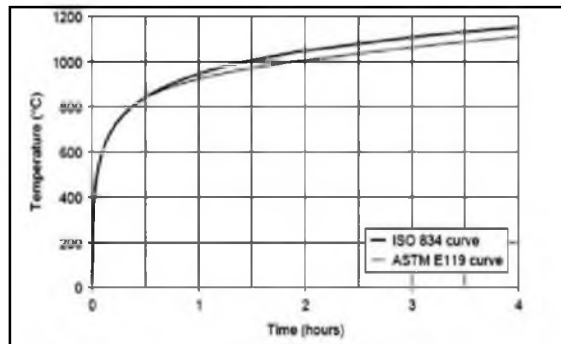


Fig.2 Fire loading curve

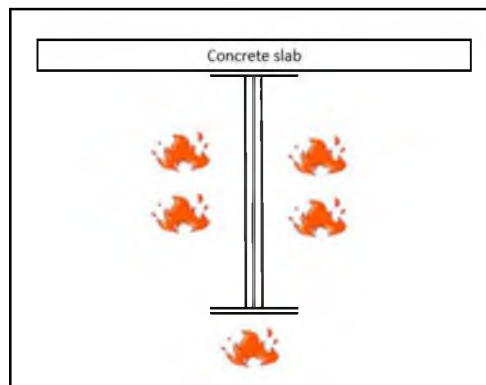


Fig.3 Fire exposure

Discretization for Thermo-structural analysis

The thermal analysis of the steel-concrete girder is carried out using, SOLID70 elements and SURF 152 elements. SOLID70 has a three-dimensional thermal conduction capability. The element has eight nodes with a single degree of freedom, temperature, at each node. The element is applicable to a three-dimensional, steady-state or transient thermal analysis. The element also can compensate for mass transport heat flow from a constant velocity field. LINK 33 is used to model the reinforcement. To account for the action between the concrete slab and the top flange of the steel girder, bonded contact is considered. SURF152 is used for thermal load and surface effect applications. The whole model has been meshed with 50mm size after conducting mesh convergence study. For welding simulation bonded contact modelling has been used. Linear analysis is considered in contact modelling (bonded contact).

For structural analysis, the bridge girder was modelled with two elements, namely, element SHELL181 and SOLID185. For the bottom flange, web, top flange, and stiffeners, SHELL 181 is used and for concrete slab SOLID 185 is used. SHELL181 can capture buckling of flange and web as well as lateral torsional buckling of the member and therefore is well suited for large-rotation, large-strain, and nonlinear problems. SOLID185 has eight nodes with three degrees of freedom, namely, three translations in the x, y, and z-directions. This element is used for 3D modelling of solids with or without reinforcement and is capable of accounting for cracking of concrete in tension, crushing of concrete in compression, creep, and large strains. To the structural model, the output from thermal analysis has been imported as thermal load. Node merging concept has been adopted for composite action simulation between concrete deck slab and steel beam. The model is shown in fig 3.

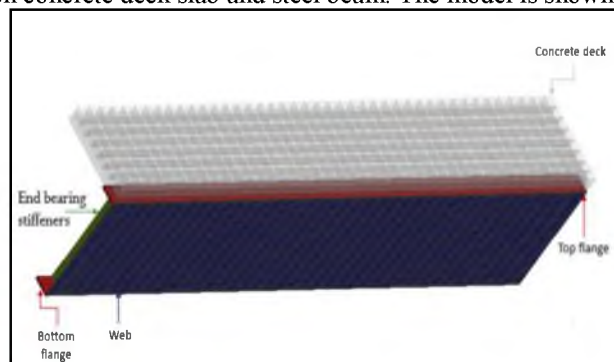


Fig.4 Composite bridge girder modelled in ANSYS

Methodology

The thermal properties of component materials, namely, thermal conductivity, specific heat, and thermal expansion, which vary as a function of temperature are given as input to determine the thermal progression among steel beam and concrete slab. Reduction factor for modulus of elasticity of steel and concrete at each temperature is also considered. The mechanical properties of steel and concrete were also given as input. The thermal and mechanical properties of steel and concrete are adopted from Eurocode 2 (CEN 2004) and Eurocode 3 (CEN 2005) codes.

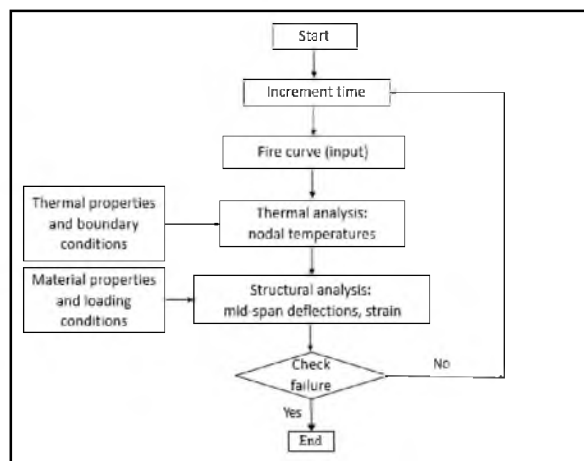


Fig.5 Thermo-structural analysis

The methodology for this work is explained as a flowchart in fig. 5.

Model Validaton

The validation process comprises of comparison of thermal results from the analysis with that obtained from the fire test conducted by Aziz [1]. The fire analysis experiment is conducted inside a specially designed furnace. The analysis is carried out with the mesh discretization of 50mm size and material properties. The assembly is exposed to ASTM E119 fireexposure as in the fire test. The geometric and materiel properties of the tested girder are taken from the literature.

Fig.6 shows a comparison of predicted temperatures by the FEM model with those measured in the fire test. It can be seen that percentage error is about 3-4% when comparing the FEA and experimental results. This slight difference can be imputed to the change in the heat-transfer parameters, such as emissivity and convection coefficients used in the analysis compared with the actual values in the test (furnace).

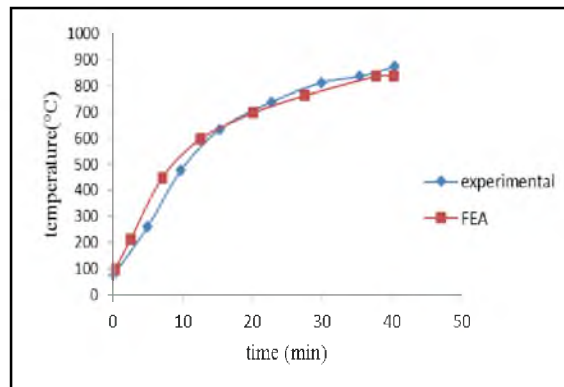


Fig.6 Comparison of temperatures in bottom flange as per FEA analysis with test data

Case study

To evaluate the response of a typical bridge girder under fire conditions, a simply supported steel bridge girder is selected for analysis. The bridge consists of five girders supporting a RC slab 200mm thick. The steel girder is assumed to be in full composite action with the slab. The bridge girder is 25.8 m span length. The girders are fabricated from 415 Mpa steel and the concrete used in the slab has a compressive strength of 25 MPa.

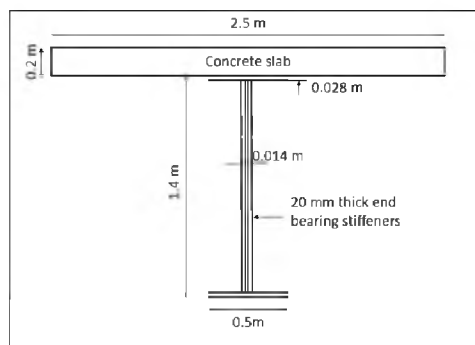


Fig.7 Cross section of the girder

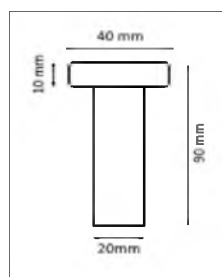


Fig.8 Cross section of shear stud

RESULTS AND DISCUSSIONS

The thermo-structural analysis on the girders carried out under the loading which consists of dead load plus live load and thermal load. The dead loads include self-weight of the girder, self-weight of effective width of concrete slab, and weight of wearing coat which is 14.5kN/m. For the live load, a uniformly distributed load of 9.5kN/m representing Class AA wheeled vehicle is considered. Symmetric criteria is considered for analysis.

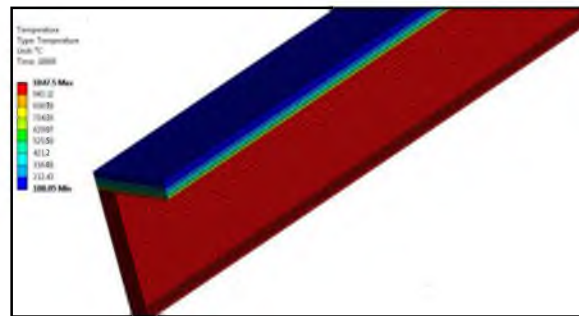


Fig.9 Thermal distribution along cross section

Fig.9 shows the temperature distribution of the steel-concrete composite bridge girder with time. The maximum temperature applied is 1047.6°C. It can be seen that maximum temperature occurs within steel due to high thermal conductivity of steel.

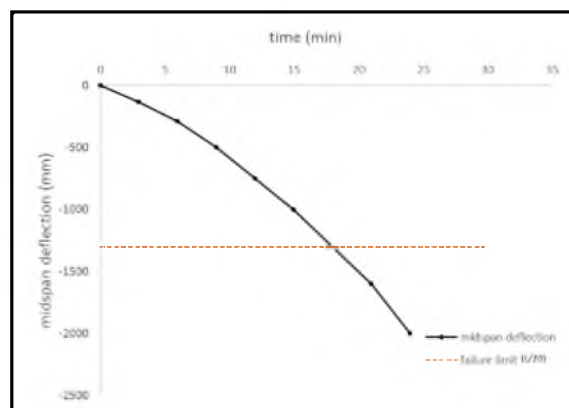


Fig.10 Effect of midspan deflection on thermo-structural loading

From fig.10 it is observed that the fire resistance of the bridge girder is about 18 minutes. It is also observed that mid-span vertical deflection increases linearly with fire exposure time initially. With the increase of temperature, higher rate of midspan deflection is observed, which is due to the strength reduction resulting from increased temperatures in the steel girder. The third stage includes rapid increase in deflection which ultimately results in spalling of concrete and finally collapsing of the structure. This is because of the formation of plastic hinges in the steel beam and also buckling of the web.

A. Influence of composite action

In order to study the effect of composite action on response of girders under fire conditions, girder with partial shear connection as well as girder with no composite action is considered.

TABLE I. INFLUENCE OF COMPOSITE ACTION

Parameter	Fire resistance(min)
No composite action	17.1
Partial composite action	18
Full composite action	19.8

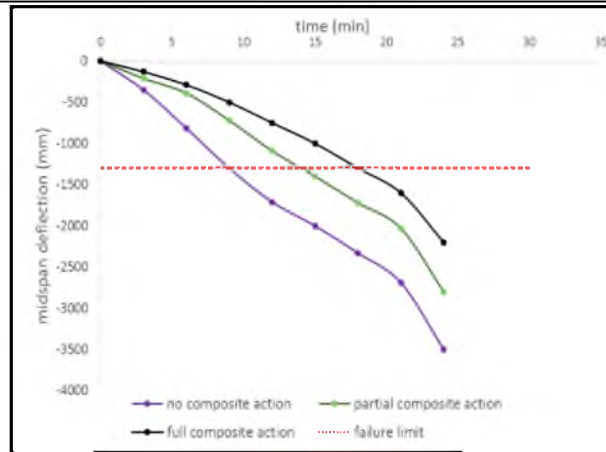


Fig. 11 Effect of composite action on thermo-structural loading

From Fig.11 it can be seen that maximum fire resistance is for girders with full composite action since it transfers load from fire induced steel beam to deck slab and thereby reducing deflection.

B. Influence of stiffeners

To investigate the effect of stiffeners on fire resistance, the girder is analyzed considering two cases. First case includes girder with midspan and end bearing stiffeners. Second case includes girder with end bearing stiffeners only. The results shown in Fig.12 indicate that no fire resistance enhancement is indicated with including the stiffeners.

TABLE II. EFFECT OF STIFFENERS

Parameter	Fire resistance(min)
Unstiffened girder	17.6
Stiffened girder	18

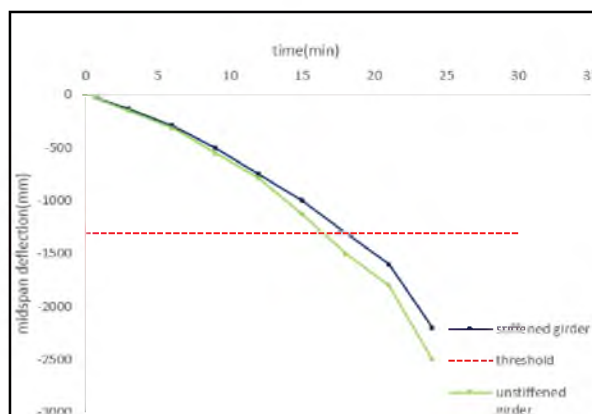


Fig. 12Influence of stiffeners on thermo-structural loading

C. Influence of web thickness

Varying the thickness of web changes the slenderness ratio and this variation is plotted in Fig.13

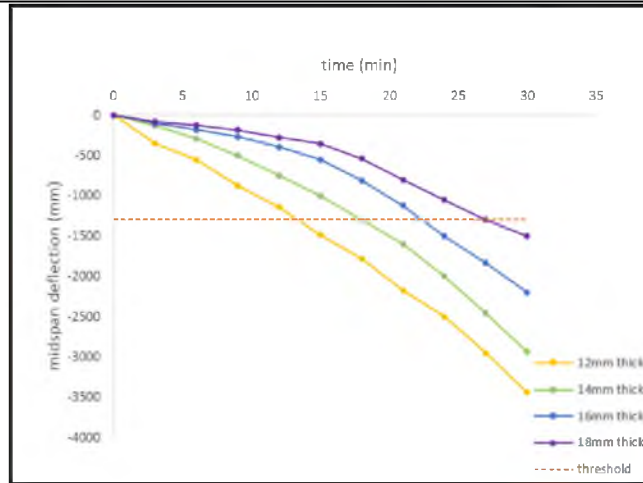


Fig.13 Effect of web thickness on the response of steel bridge girders

TABLE III. EFFECT OF WEB THICKNESS

Web thickness (mm)	Slenderness ratio	Fire resistance(min)
12	112	13.5
14	96	18
16	84	22.5
18	75	27.3

CONCLUSIONS

The following are the conclusions obtained from this study:

- The fire resistance of the girder with composite action is twice the girder with no composite action. Hence composite action plays an important role in enhancing fire resistance.
- Presence of stiffeners does not have significant effect in increasing fire resistance
- An increase of 21-33% in fire resistance is observed by increasing the web thickness of the steel beam

ACKNOWLEDGMENT

The authors would like to express their sincere gratitude to the Principal and Department of Civil Engineering, MBCET, Thiruvananthapuram, Kerala for the support and facilities provided for completion of this work.

REFERENCES

[1] Naser, Z. and Kodur, V. (2017) "Comparative fire behaviour of composite girders under flexural and shear loading", *Thin-Walled Structures*, 116, 82-90

[2] Reis, A., Nuno, L. and Paulo, V. (2016) "Numerical study of steel plate girders under shear loading at elevated temperatures", *Journal of Constructional Steel Research*, 117, 1-12

[3] Albrifkani, S. (2016) "Explicit modelling of large deflection behaviour of restrained reinforced concrete beams in fire", *Engineering Structures*, 14, 115-123

[4] Aziz, M., Kodur, V. and Maria, E. (2015) "Behaviour of steel girders under fire conditions", *Journal of Constructional Steel Research*, 106, 11-22

[5] Naser, Z. (2014) "Effect of shear on fire response of steel beams", *Journal of Constructional Steel Research*, 97, 48-58

[6] Moya, J. and Zaforteza, P. (2014) "Analysis of a bridge failure due to fire using computational fluid dynamics and finite element models", *Engineering Structures*, 68, 93-110

[7] Kodur, V., Aziz, E. and Dwaikat, M. (2013) "Evaluating fire resistance of steel girders in bridges", *Journal of Bridge Engineering*, 18, 633-643

- [8] Zaforteza, P. and Garlock, M., E. (2012) "A numerical investigation on the fire response of a steel girder bridge", *Journal of Constructional Steel Research*, 43, 93-103
- [9] Kodur, V. and Dwaikat, M. (2010) "Effect of high temperature creep on fire response of restrained steel beams", *Journal of Materials and Structures*, 43, 1327-41
- [10] White, D. and Barker, M. (2008) "Shear resistance of transversely stiffened steel girders", *Journal of Structural Engineering*, 134, 1425-1436
- [11] Vimonsatit, V., Tan, K. and Qian, Z. (2007) "Testing of plate girder web panel loaded in shear at elevated temperature", *Journal of Structural Engineering*, 133(6), 815-824
- [12] Wald, F., Silva, L., Moore, B. and Santiago, A. (2006) "Experimental behaviour of a steel structure under natural fire", *Fire Safety Journal*, 41(7), 509-22
- [13] Li1, G., Jiang, S., Yin, Y., Chen K., and Li, M. (2003), "Experimental Studies on the Properties of Constructional Steel at Elevated Temperatures", *Journal of Structural engineering*, 21, 231-245
- [14] Baskar, K., Shanmugam, E. and Thevendran, V. (2002) "Finite element analysis of steel - concrete composite plate girder", *Journal of Structural Engineering, ASCE*, 128, 1158-1168
- [15] <https://www.rt.com/news/vladivostok-bridge-construction-fire-681>
- [16] Eurocode 2 (EN 1992-1-2), Design of concrete structures Part 1-2: General rules Structural Fire Design, Commission of European Committee for Standardization, Brussels, 2004
- [17] ANSYS. ANSYS metaphysics. Version 17 ANSYS Inc. Canonsburg, PA, USA

Analysis of concrete silo by using ETABS 2016

Neeraja R.

Research Scholar Professor
Department of civil engineering
Younus college of engineering, Kollam
e-mail: neerajarsingh@gmail.com

Liji A.

Assistant Professor
Department of Civil Engineering
Younus College of Engineering, Kollam
e-mail: a_liji@yahoo.co.in

Abstract— The demand for storage structures has increased due to increase of population. Hence RCC silos are widely used for storage of granular materials as they are an ideal structural material for the building of permanent bulk storage facilities for dry granular like fillings. Initially concrete storage units are economical in design and reasonable in cost. Silos are very demanding in cement industries. Concrete can offer the protection to the stored materials, requires little maintenance, is aesthetically pleasing, and is relatively free of certain structural hazards such as buckling or denting. Adequate seismic design of silos is especially important in the field of plant engineering since structural damage often leads to consequential damage such as fires, explosions, and the release of toxic substances into the air and soil.

The silo walls are subjected to pressure in terms of vertical friction that is engendered by the material that is stored within the silo and walls of silo, the properties of material stored are the cause for the quantity and distribution of both vertical and horizontal pressure over the wall height and additionally it depends on the whether the silo is being filled or evacuating case. In the present paper it deals with analysis of concrete silo with varying wall thickness with empty, partially and fully filled conditions and to study the stress concentration at the joints where the wall thickness is changed. To find the best suited cross section of silo wall thickness for different loads and stresses and to compare the cross section of silo walls. Also examines the effect of wind and earth quake loads on the concrete silo.

Keywords: Silo, Concrete, Pressure, Wall thickness

INTRODUCTION

In recent years, silos are used by a wide range of industries to store bulk solids in quantities ranging from a few tones to hundreds or thousands of tones. The term silo includes all forms of particulate solids storage structure that might otherwise be referred to as a bin, hopper, grain tank or bunker. They can be constructed of Steel or Reinforced concrete and may discharge by gravity flow or by mechanical means. Steel bins range from heavily stiffened flat plate structures to efficient unstiffened shell structures. They can be supported on columns, load bearing skirts, or they may be hung from floors. Flat bottom bins are usually supported directly on foundations. Concrete silo is much stronger in compression than tension, so

the silo is reinforced with steel hoops encircling the tower and compressing the staves into a tight ring. The vertical stacks are held together by intermeshing of the ends of the staves by a short distance around the perimeter of each layer, and hoops which are tightened directly across the edges.

Now a day, many engineers have aim to renovate, reinforced concrete silos, they are not only renovated but also strengthened. Most of them lost their designed durability life with many reasons. The basic reason of this state is carbonation of concrete, corrosion of reinforcement, chemical activity on objects, loss of concrete cover, number of wider crack width, too large deformations and deflections, etc. The walls of the silos are typically subjected to both normal pressure and vertical frictional shear or traction produced by the material stored inside the silo. Other potential loads, including seismic and wind loads, stresses created by temperature difference between the silo wall and the stored bulk solids, potential expansion of the stored material, and differential settlement of the foundation or support columns, should also be considered during the design process.

The silo walls are subjected to pressure in terms of vertical friction that is engendered by the material that is stored within the Silo and walls of Silo, the properties of material stored are the cause for the quantity and distribution, of both vertical and horizontal pressure over the wall height and additionally it depends on the whether the silo is being filled or evacuating case. The variant of loads that can act are self weight of the Silo, wind loads, temperature stress, and seismic loads, properties of material to be stored, and differential settlement of substratum, and various loads should be considered during design.

The design of silos is done generally by two methods:

1. Janssen's Theory

The assumption of this theory is that the friction between the material stored and walls of silo supports the large portion of weight of material store and hopper bottom supports only small portion of weight. Hence Rankine's or coulomb's theory of lateral pressure cannot be directly applied, the walls of silo are subjected to direct compression as well as lateral pressure.

2. Airy's Theory

This theory uses coulomb's theory of earth pressure. Due to which it is possible to determine the horizontal loads on walls per unit length of the periphery and position of plane of rupture.

OBJECTIVES

- To find where the maximum load acting along the height of concrete silo
- To analyze the concrete silo with varying wall thickness at empty, partially and fully filled conditions
- To study the effect of stress concentration at the joints where the wall thickness is changed
- To find the best suited cross section of silo wall for different loads and stresses
- To compare the cross section of silo wall at empty, partially and fully filled conditions
- To study the effects of loads acting on the concrete silo and find out the dominant load

III.MODEL DESCRIPTION

A concrete circular silo with 20m height and 6m diameter is selected as a model (Fig.1) for the study. Properties of the structure selected for the study is given in TABLE 1. Modeling and analysis are carried out by using ETABS 2016.

TABLE 1 PROPERTIES OF THE STRUCTURE SELECTED FOR THE STUDY

Type of the structure	Concrete silo
Height of the structure	20m
Diameter of the structure	6m
Thickness of the structure	200mm
Type of material stored	Cement
Density of material stored	16 kN/m ³
Coefficient of friction	0.70
Angle of repose	25
Thickness of the Plate	100mm
Zone	V
Response reduction factor	3
Importance factor	1
Damping of structure	5%
Grade of concrete	M30
Poisson ratio for concrete	0.20
pressure intensity	0.40



Fig. 1 Model of concrete silo

Structural loads

Different structural loads that the structure typically must carry are

- Dead load
- Live load
- load due to storage material
- wind load
- Seismic load

Forces that act vertically are gravity loads like dead load, live load. Forces that act horizontally, such as wind and seismic events require lateral load resisting systems to be built into structures.

- Earthquake Forces Data: Earthquake load for the structure has been calculated as per IS-1893-2002:
 - ✓ Zone (Z) =V
 - ✓ Response Reduction Factor (RF) = 3
 - ✓ Importance Factor (I) = 1
 - ✓ Soil condition = Hard
 - ✓ Zone factor = 0.36
- Wind Forces Data: Wind load for the structure has been calculated as per IS 875(part-3):
 - ✓ Wind speed =39 m/s
 - ✓ Terrain category = 2
 - ✓ Structure class = B
 - ✓ Risk coefficient (K1 factor)=1
 - ✓ Topography (k3 factor) = 1

Load combinations

Load combinations for the analysis shall be the one that produces maximum forces in the members and consequently maximum stresses. The effect of wind and earthquake load is taken into account. The load combinations are considered for

the analysis as per IS 1893(part 1)-2002 as shown in TABLE 2, Where

DL= Dead Load

LL= Live Load

PR = Load due to stored material

WIND-X, WIND-Y = Wind load in X & Y direction respectively

EQX, EQY = Earthquake load in X & Y direction respectively

RSX, RSY = Response Spectrum Load in X & Y direction respectively

TABLE 2 LOAD COMBINATIONS

Load Combination	Load Factors
Gravity Analysis	DL+LL
	DL+LL+PR
Wind Analysis	0.75(DD+LL+PR+WINDX)
	0.75(DD+LL+PR+WINDY)
	0.675DL+0.75WIND-X
	0.675DL+0.75WIND-Y
Response Spectrum Analysis	0.75(DD+LL+PR+RSX)
	0.75(DD+LL+PR+RSY)
	0.675DL+0.75RSX
	0.675DL+0.75RSY

IV RESULTS AND DISCUSSION

The results are presented for each of the model considered, for the static and dynamic analyses carried out by ETAB 2016 package. Both wind and earthquakes cause dynamic action on Concrete silo. However, in the analysis of silo is subjected to maximum pressure at its base, which induces inertia forces in the model that in turn cause stresses; this is displacement-type loading. Comparison of different performance characteristics are made to check the performance of concrete silo with different filled conditions. The results are in terms of stresses, lateral displacements and forces for different models are presented and compared.

Maximum Load

From the TABLE 3 it was observed that the maximum load was acting at the bottom section of the concrete silo and minimum at the top of the section.

TABLE 3 MAXIMUM LOADS ON EACH LEVEL

LEVEL	Maximum Loads(kN)
1	470.502
2	376.40
3	282.30
4	188.20
5	94.14

Effect of stress

The stress values of each story of different models are compared. In fully filled condition models with 50mm offset (Fig.2), 100mm offset (Fig.3) and 150mm offset (Fig.4) are compared. Three stepped section with 150mm offset shows the least value of stresses with when compared with the plane section. In partially filled condition models with 50mm offset (Fig.5), 100mm offset (Fig.6) and 150mm offset (Fig.7) are compared. Three stepped section with 150mm offset shows the least value of stresses with when compared with the plane section. In empty filled condition models with 50mm offset (Fig.8), 100mm offset (Fig.9) and 150mm offset (Fig.10) are also compared. Three stepped section with 150mm offset shows the least value of stresses with when compared with the plane section.

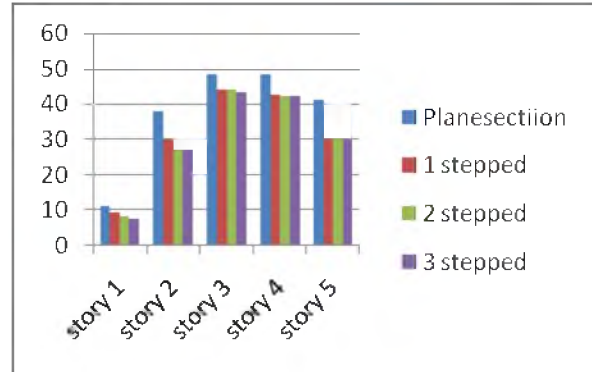


Fig.2 50mm offset in fully filled condition

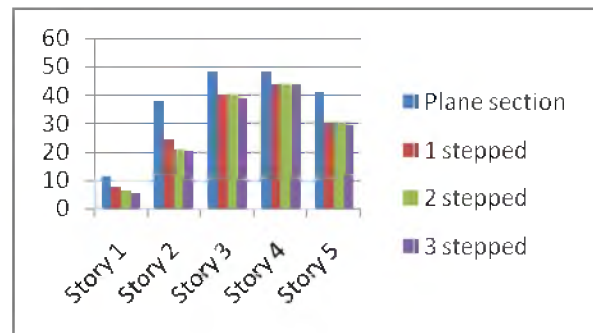


Fig.3 100mm offset in fully filled condition

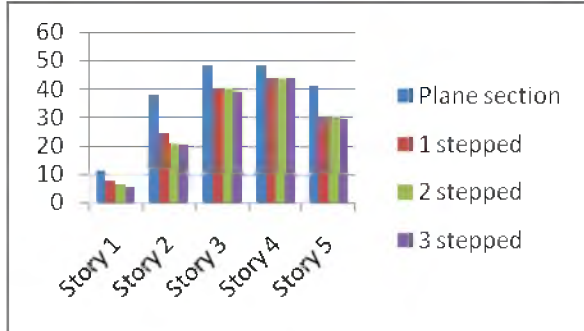


Fig.4 150mm offset in fully filled condition

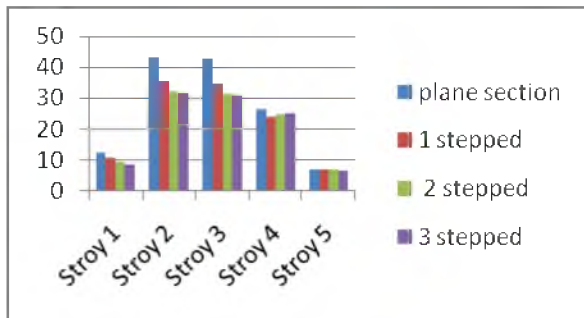


Fig.5 50mm offset in partially filled condition

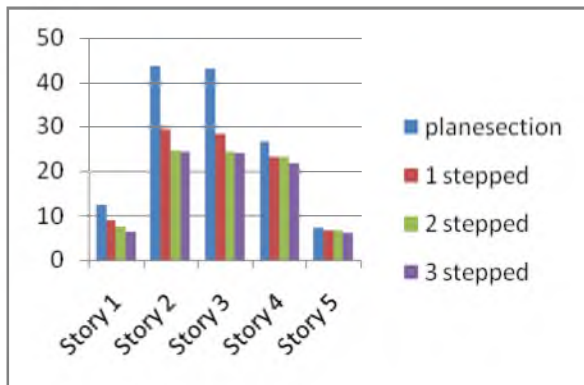


Fig.6 100mm offset in partially filled condition

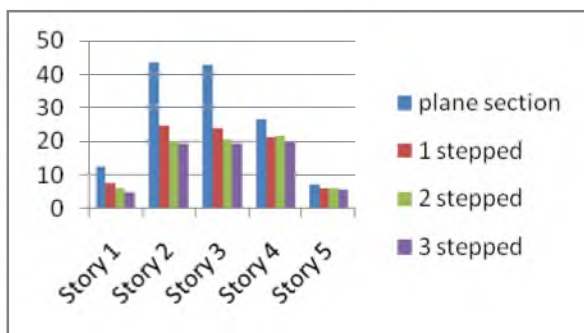


Fig.7 150mm offset in partially filled condition

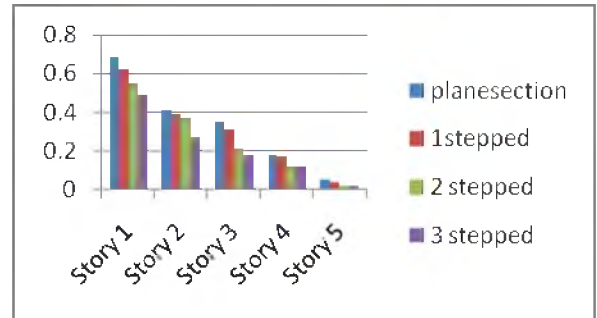


Fig.8 50mm offset in empty filled condition

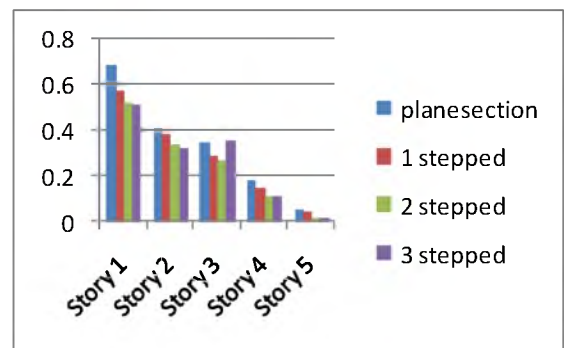


Fig.9 100mm offset in empty filled condition

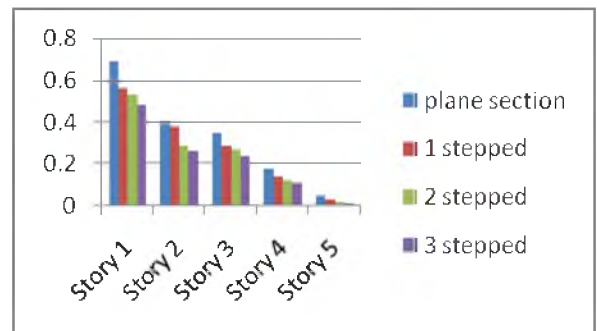


Fig.10 150mm offset in empty filled condition

Lateral displacement

Lateral displacement profiles for different models obtained by both wind and seismic effect. In seismic analysis response spectrum method are used. From the analysis it is observed that that the maximum displacement occurs at the middle portion of the structure. Thus the offset of the sections are provided from the middle portion of the sections.

Maximum storey displacement curve obtained for plane section and 150mm offset at fully filled condition as shown in Fig. 11 and Fig. 12

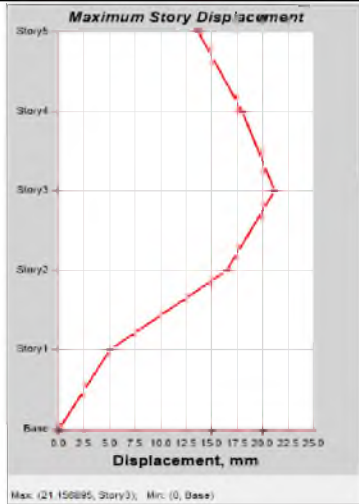


Fig. 11 Story displacement of plane section at fully filled condition

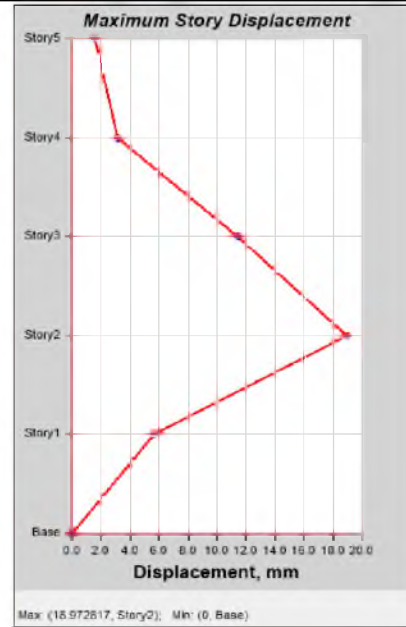


Fig. 13 Story displacement of plane section at partially filled condition

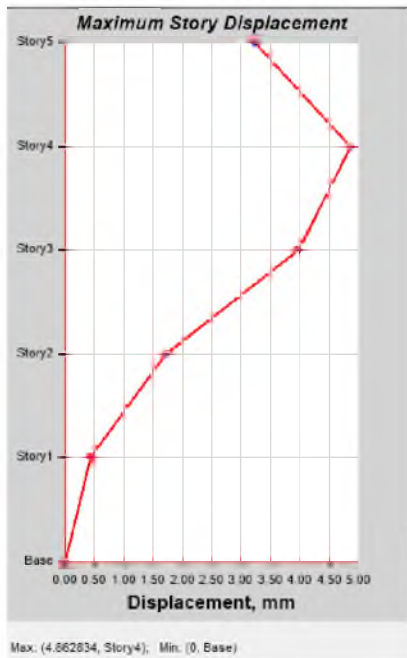


Fig. 12 Story displacement of 150mm offset at fully filled condition



Fig.14 Story displacement of 150mm offset at partially filled condition

In the case of fully filled condition the maximum displacement occurred at third story about 21.15mm. But considering the three stepped 150mm offset section the displacement is reduced to 4.13mm at the third story. Percentage reduction in the displacement is about 78.34%

Maximum storey displacement curve obtained for plane section and 150mm offset at partially filled condition as shown in Fig. 13 and Fig.14.

In the case of partially filled condition the maximum displacement occurred at second story about 18.97mm. But considering the three stepped 150mm offset section the displacement is reduced to 2.168mm at the second story. Percentage reduction in the displacement is about 88.15%.

Maximum storey displacement curve obtained for plane section and 150mm offset at empty condition as shown in Fig. 15 and Fig.16.

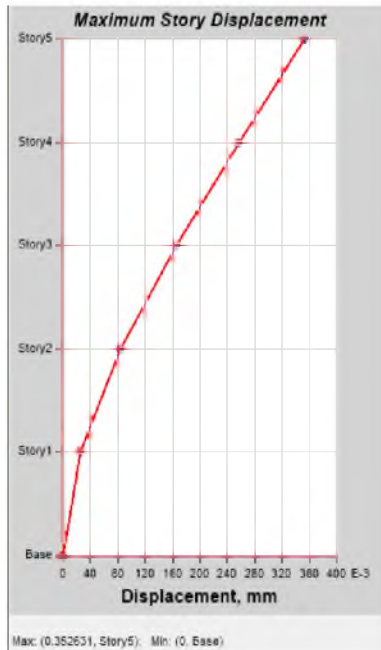


Fig 7.15 Story displacement of plane section at empty filled condition

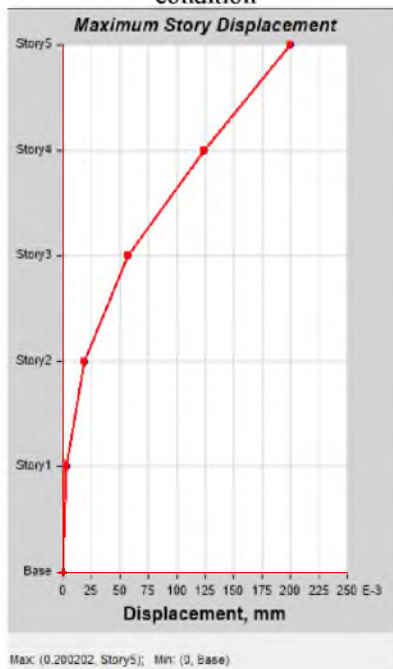


Fig 7.16 Story displacement of 150mm offset section at empty filled condition

In the case of empty condition the maximum displacement occurred at top story about 0.325mm. But considering the three stepped 150mm offset section the displacement is reduced to 0.2mm at the top story. Percentage reduction in the displacement is about 43.18%

The aim of project work is mainly based on the study of stress concentration at different cross sections with different filled conditions. The parameters like maximum loads, stress concentration, story displacement etc are analyzed and some of the important points are summarized below,

- The effectiveness of stresses due to the different loads at different levels was tabulated for Concrete silo.
- The maximum load was acting at the bottom section of the silo but the deformations are found to be critical at the middle portion of the structure.
- The behaviour of stress and displacement of Concrete silo with various thickness and different filled conditions were tabulated.
- It is found that in each filled condition the three stepped cross section with 150 mm offset was the best suited section for different loads and stresses.
- The effect of stress concentration at the joints is minimum, when maximum offset is provided.
- The effect of lateral displacement was reduced at each story level when maximum offset is provided

REFERENCES

- [1] Anand Adi and Hemant L. Sonawadekar (2013) Parametric Study On Dynamic Response Of Silo, *International Journal of Engineering Research & Technology (IJERT)* Vol. 2 Issue 7, ISSN: 2278-0181
- [2] Afzal Ansari, Kashif Armaghan and Sachin S.kulkarni (2016).Design and Optimization of RCC Silo, in *International Journal for Research in Applied Science and Engineering Technology*, Vol.4, Issue 6,ISSN: 2321-9653
- [3] Indrajit Chowdury and Raj Tilak (2010). Dynamic Pressure on Circular Silos under Seismic Force, in *14th Symposium on Earthquake Engineering, IIT Roorkee, Paper A009*.
- [4] IS 4995 (Part 1&2) V 1974. Criteria for design of reinforced concrete bins for the storage of granular & powdery material.
- [5] Md. Alauddin and Sohrabuddin Ahmad (1995). Design forces and moments in circular silos based on finite element analysis, *Journal of civil engineering division, the institution of Engineers, Bangladesh*, Vol. CE23 No. 1.

Finite Element Analysis of Idukki Arch Dam

Ramya Raveendran¹, Asna Yasmin Yassid², Devika.B³, Gayathri D.S⁴, Gayathri G.R⁵, Lekshmi Rajan B.S⁶

¹Assistant professor, Department of Civil Engineering, LBS Institute of Technology for Women

^{2,3,4,5,6} UG Scholar, Department of Civil Engineering, LBS Institute of Technology for Women, Trivandrum

Abstract

Arch dams have the most suitable geometry for efficient load transfer and optimum volume to achieve economy. It can also be fitted to nearly every asymmetric valley shape. Idukki dam is the second arch dam built in the world and first in Asia. It is constructed across the Periyar river in a narrow gorge. Idukki dam was constructed along with two other dams at Cheruthoni & Kulamavu. In this thesis, dynamic analysis of the 50 year old Idukki arch dam was done using Finite Element Method (FEM). FEM is a method used for studying complex structures by dividing them into finite elements and analyzing for suitable boundary conditions. ABAQUS software was chosen for modelling due to its precision and wide material modelling capability. The geometry of the dam was generated using spatial global coordinates. Static analysis was done for the dam model. The results obtained from the static analysis were compared with the available results from the literature and the model was validated. Further, seismic response of the validated model was obtained by nonlinear time history analysis. Two parametric studies were conducted; one by varying the peak ground acceleration for maximum water level and other by varying peak ground acceleration for different water levels.

Keywords: arch dam, finite element method, ABAQUS software, mesh convergence study, seismic analysis.

1. Introduction

Idukki dam is a double curvature arch dam, which is curved vertically as well as horizontally. The dam is constructed across the Periyar River in a narrow gorge between two granite hills locally known as Kuravan and Kuravathi in Kerala, India. The arch dam has a height of 169.16 m and situated 732.62 m above MSL. This dam was constructed along with two other dams at Cheruthoni and Kulamavu. The stored water is used to produce electricity at the Moolamattom Power house, which is located inside nearby rocky caves. Moolamattom hydroelectric power station has a capacity of 780 W and it constitutes nearly 30% of Kerala's power generation. The Government of Canada aided in the building of the dam with long term loans and grants. It is one of the highest arch dams in Asia. Heavy loss in human life and economy can be affected by the failure of such a massive structure. The concerns about seismic safety of concrete dams have been growing during recent years, partly because the population at risk in locations downstream of dams continues to expand. This is evident from the up gradation in the seismic zone of Kerala from Zone II to Zone III. It is proposed to acquire a well knowledge about structural actions of concrete dams and decisive tool to study the dynamic response of a structure.

2. Scope of Research and Objectives

Studies on dynamic analysis of massive structures especially dams etc. are relevant. Static analysis of Idukki arch dam has been reported in literature. Dynamic behavior of the dam is yet to be studied comprehensively. This thesis investigates static and dynamic response of Idukki dam by finite element method using the software ABAQUS.

The specific objectives of the research are the following

1. To develop a model of the Idukki dam using ABAQUS software.
2. To validate the model with the results available in literature.
3. To analyze the stresses and deflections that would occur in the dam for dynamic load.

3. Finite Element Method

Finite Element Method (FEM) is a numerical method for solving problems of engineering and mathematical physics. It is also called Finite Element Analysis (FEA). It has developed simultaneously with the increasing use of high-speed electronic digital computers and with the growing emphasis on numerical methods for engineering analysis. The method can be systematically programmed to accommodate complex and difficult problems such as non-homogeneous materials, nonlinear stress-strain behavior, and complicated boundary conditions.

The basis of finite element method is the representation of a body or a structure by an assemblage of subdivision called finite elements. These elements are considered inter connected at joints which are called nodes or nodal points. Simple functions are chosen to approximate the distribution or variation of the actual displacements over each finite element. Such assumed functions are called displacement functions or displacement models. Displacement model can be expressed in various simple forms, such as polynomials and trigonometric functions. Since polynomials offer ease in mathematical manipulations, they have been employed commonly in finite element applications. The equilibrium equations for the entire body are then obtained by combining the equations for the individual elements. In many types of problems, the desired solution is in terms of the strains or stresses rather than the displacements, so additional manipulations or calculations may be necessary.

4. Static analysis of Idukki dam

The actual structure consists of horizontal inspection galleries and vertical shafts connecting them. These structures were not considered while modelling and analysis. The dam section actually consists of steel reinforcements to support the inspection galleries and shafts which was neglected in this study. Since the two ends and the bottom of the dam comprises completely of rigid rocks, fixed boundary conditions were assumed.

Thus the dam was modelled by inputting the global coordinates of 80 points obtained from Abraham (2007). Individual coordinates were connected using wire edge. The edges of this wire frame were individually selected and covered to form shell model. Then the whole structure was selected and converted into a solid. The solid model consist of 28 cells, 123 solid faces, 175 edges and 81 vertices.

The material properties obtained from Menon et al. (2014) [1], were assigned to the solid dam model. The details about the material properties are given in table 1.

Table 1- Material Properties

(Source: Menon et al., 2014)

PROPERTY	VALUE	UNIT
MODULUS OF ELASTICITY	2.1×10^{10}	N/m ²
DENSITY	2400	kg/m ³
COEFFICIENT OF THERMAL EXPANSION	1.2×10^{-5}	/K
POISSON'S RATIO	0.17	-
COMPRESSIVE STRENGTH	26.5	MPa

The solid model was discretized into finite elements. The element used for meshing was C3D8R (Continuum, 3-D, 8-node, Reduced integration). C3D8R element is a general purpose linear brick element with reduced integration. The dam model was analyzed for a combination of dead load and maximum water load. Optimum mesh size is to be found for computational efficiency. The obtained maximum displacement for various discretization at node 75. And optimum mesh size obtained is 4m is shown in figure 3.

4.1 Static Behavior of Idukki Dam

The loads considered for the static analysis were concrete dead weight, maximum flood level, full silt level and minimum concrete temperature. The details of the loads applied are given in Table 2. The boundary surfaces were defined as fixed.

Table 2- Load Combination

(Source: Menon et al., 2014)

PARAMETER	VALUE	UNIT
DEAD LOAD OF CONCRETE	24	kN/m ³
DEAD LOAD OF WATER	10	kN/m ³
SILT LOAD	11.86	kN/m ³
MAXIMUM WATER LEVEL	156.5	m
MAXIMUM SILT LEVEL	72.9	m
MINIMUM TEMPERATURE	21	°C

The result obtained for the static analysis of the dam model is shown in Figure 1.

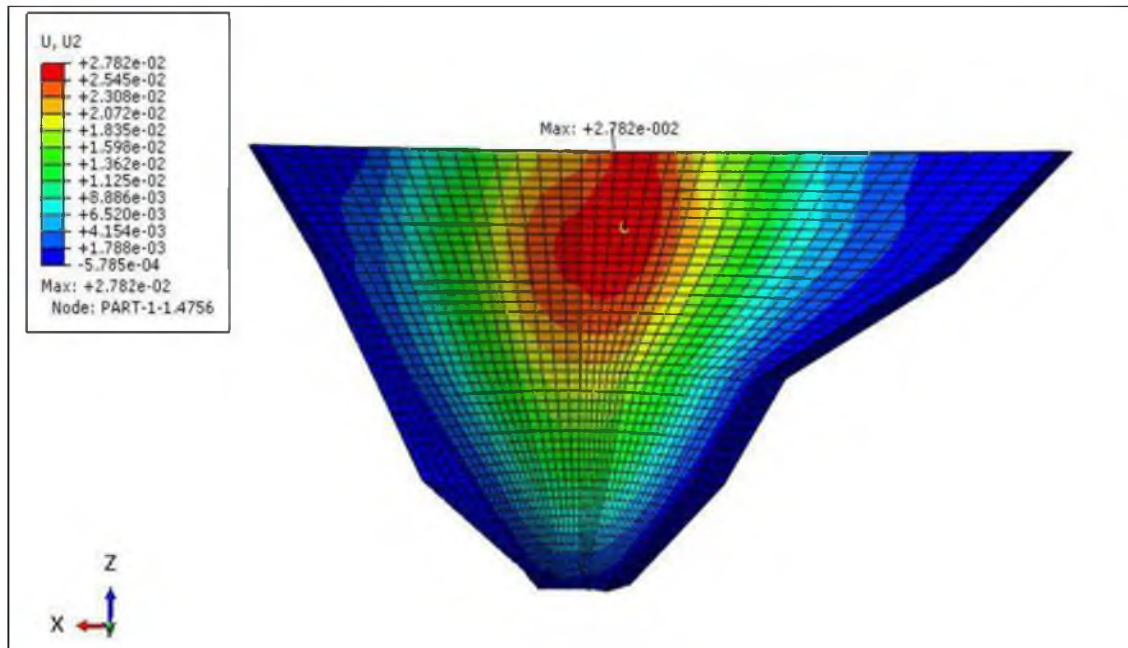


Figure 1 - Maximum Displacement in Static Analysis

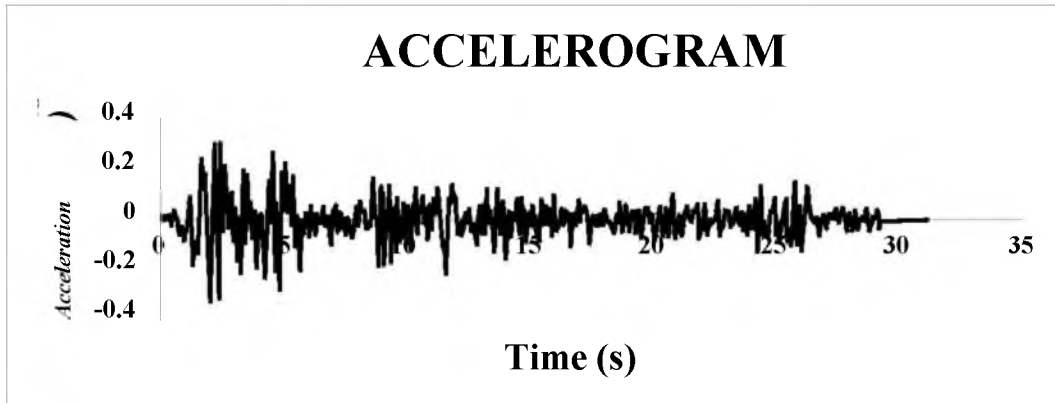
The maximum displacement obtained was 2.782 cm. In Menon et al. (2014) [1], the maximum displacement obtained for the same load combination is 2.689 cm. Suresh (1996) [4] gives the maximum displacement values obtained by Trial Load Analysis, Finite Element Analysis and Model Test as 2.87 cm, 4.06 cm and 4.83 cm respectively. The obtained maximum displacement was comparable with the available results. Hence the dam model was validated.

The maximum displacement was occurred in a node situated at the middle-crest portion of the dam model. The portions of the dam adjacent to the boundaries were having almost negligible values for displacement. This may be due to the fixed boundary conditions on the two sides and bottom of the dam.

5. Seismic Analysis of Dam

The concerns about seismic safety of concrete dams have been growing during recent years, partly because the population at risk in locations downstream of dams continues to expand. This is evident from the up gradation in the seismic zone of Kerala from Zone II to Zone III. Dynamic analysis can be broadly divided into two – Linear Analysis and Non-linear Analysis. Response spectrum analysis is a linear dynamic statistical analysis method which measures the contribution from each natural mode of vibration to indicate the likely maximum seismic response of an essentially elastic structure. Time history analysis is a non-linear method of seismic analysis for the simulation of an earthquake motion. In a non-linear time history analysis time-acceleration data is given as an input function and then performance of the arch dam is evaluated with displacement and stress results. To perform the analysis, a representative earthquake

time history is required and time history data of El Centro earthquake occurred in California in 1940 was chosen. It had a moment magnitude of 6.9. In this seismic study, the time acceleration data in North – South direction was considered, which is shown in Graph 1.



Graph 1-Accelerogram of El Centro Earthquake

(Source: www.vibrationdata.com)

5.1 Seismic Behavior of Idukki Dam

For dynamic analysis, two steps were created in the software – Static step and Dynamic step. In the static step, fixed boundary condition and the loads were created. In dynamic step, two boundary conditions were created. First one was for controlling the displacement, in which the displacement in X and Z directions were restrained. The second one was for controlling the acceleration. The time – acceleration data was defined in this boundary condition with the time data squeezed up by a factor of 10 to increase the response of the structure. The fixed boundary condition was deactivated in the dynamic step and the loads were propagated from the static step. The results obtained are shown in Figure 2 and Figure 3.

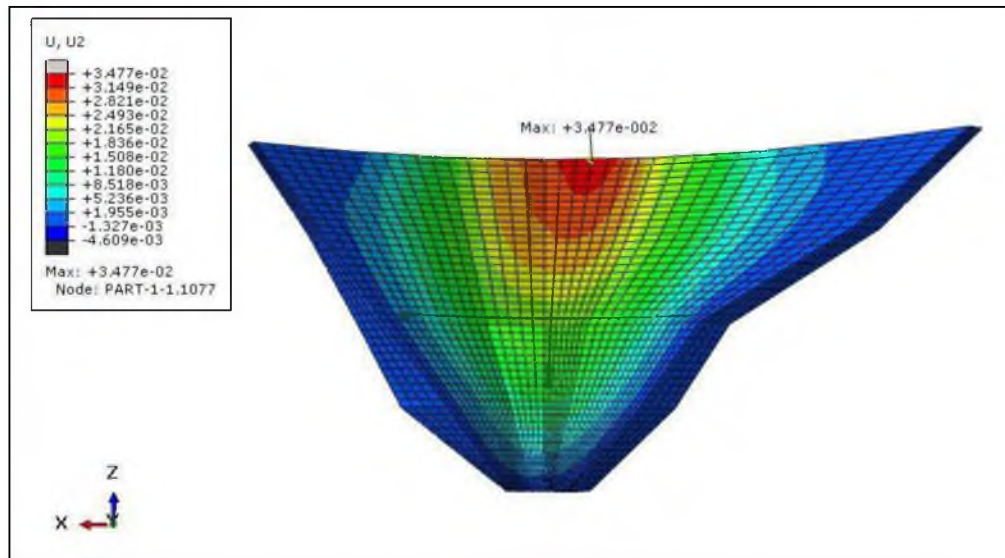


Figure 2- Maximum Displacement

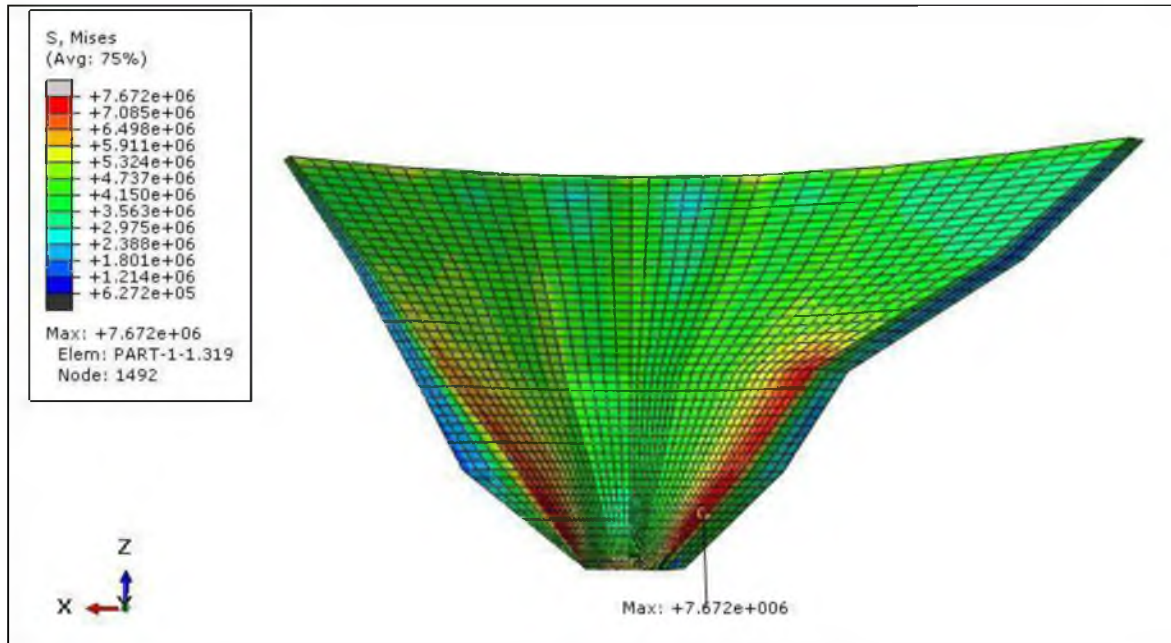
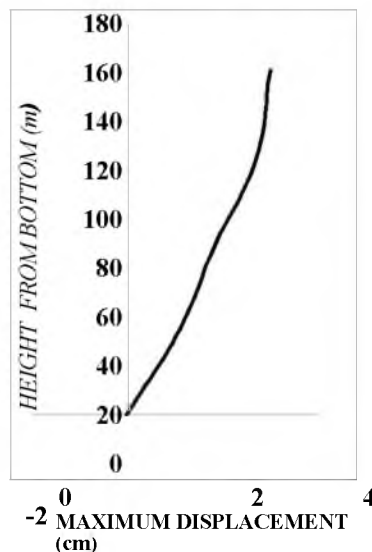


Figure 3 – Maximum stress

A maximum displacement of 3.477 cm was obtained at the crest level in node 1077. A maximum stress value of 7.672 MPa was obtained at the bottom portion of right abutment in node 1496.

A set of 24 nodes along the height of the dam, were selected for studying the variation of displacement from bottom to crest level under the seismic load. And the variation obtained is shown in Graph 2.



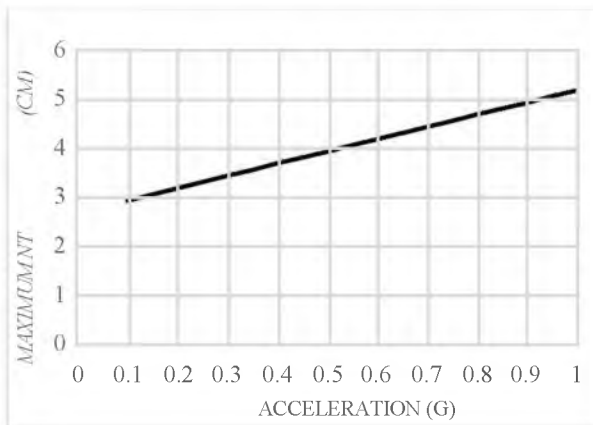
Graph 2 – vertical profile of displacement

It is clear from the graph that the displacement reaches its maximum at the crest level. Displacement increases with increasing distance from the boundary.

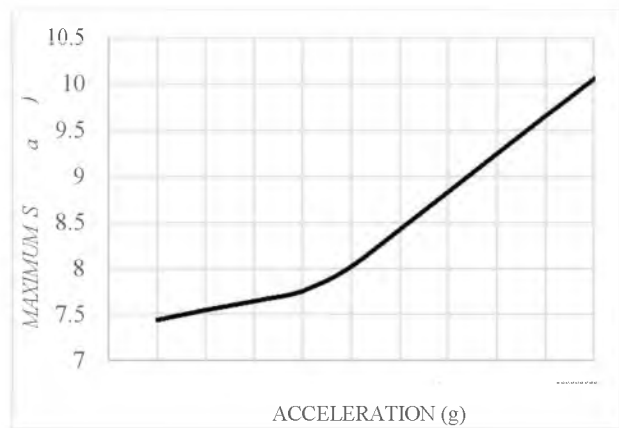
6. Parametric Study

6.1 Effect of Peak Ground Acceleration

The Peak Ground Acceleration (PGA) of the El Centro earthquake used for the non-linear time history analysis was 0.31882g. The variation of maximum displacement and maximum stress was studied by increasing value of PGA from 0.1g to 1g. The graphs shown below shows the results obtained. Maximum displacement is increasing linearly with increasing PGA. The accelerogram of 0.1g PGA is derived from real accelerogram of El Centro earthquake using a scale factor of 0.1/0.31882.



Graph 3 – PGA v/s Maximum Displacement

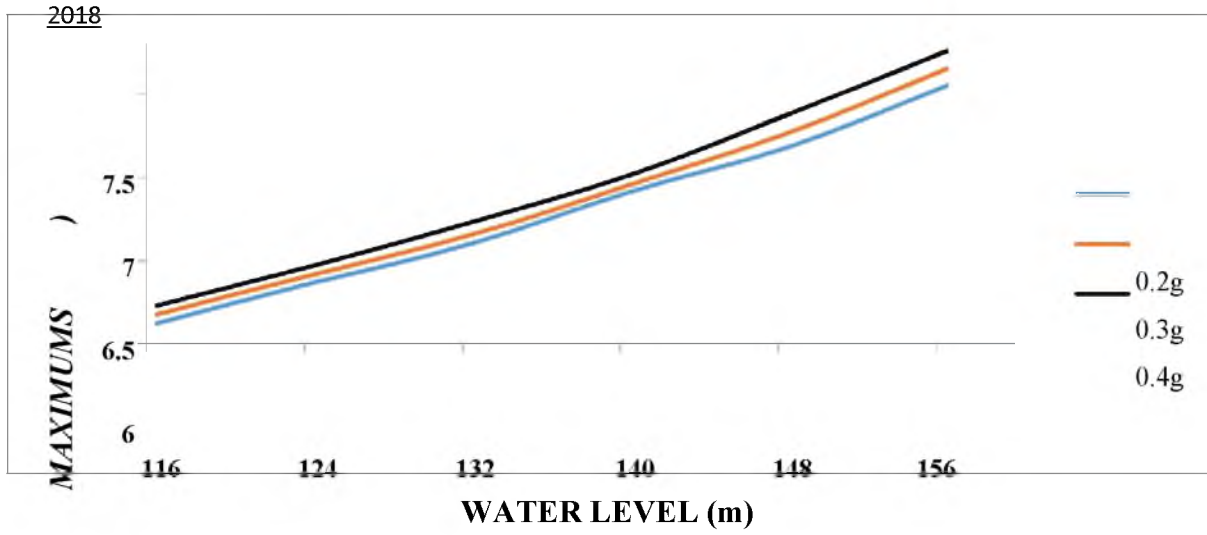


Graph 4 – PGA v/s Maximum stress

From the Graph 4, it is clear that the maximum stress value exceeds the permissible direct stress when PGA reaches 0.5g. The original design of the dam accounts for earthquakes with PGA up to 0.2g. According to the revised seismic zone of Kerala, the Zone Factor is 0.16g. The results obtained conform to the design criteria of the dam and also show that the dam can withstand earthquakes with PGA up to nearly 0.5g.

6.2 Effect of Water Level

The variation in maximum stress value under different water levels for peak ground accelerations of 0.2g, 0.3g and 0.4g were studied. The water level at 8m intervals was used. The figure below shows the result obtained.



Graph 5- Water Level v/s Maximum Stress

It can be seen that the maximum stress in the dam increases almost linearly with increase in water level. Also, it increases with PGA for a particular water level. Hence, it can be concluded that the dam condition is critical under specific ground acceleration when the water in the reservoir is at the maximum water level.

7. Conclusion

A solid model of Idukki arch dam was developed in ABAQUS software by inputting the global special coordinates of the dam. A static analysis of the dam with a load combination of dead load, maximum water load and maximum silt load, resulted in a value of deflection comparable with the results in Suresh (1996) and Menon et al. (2014). Thus the dam model was validated. Subsequently, a non-linear time history analysis of the dam was conducted using a representative accelerogram of El Centro earthquake. The maximum deflection of 3.477 cm was found to occur at the crown portion on the downstream side. A maximum stress of 7.672 MPa was obtained at the bottom of right abutment. From the vertical profile of displacement obtained, it was seen that the deflection is more at the central crest level which may be due to its increased distance from the boundary. From the parametric studies it can be concluded that the critical condition of failure of dam is reached when reservoir water level is maximum and earthquakes with PGA is 0.5g or more occurs.

8. Scope for Future Work

Keeping in view the limitations of time and its scope of present investigation, only a part of the area is investigated. It is necessary to investigate the possible further research work in this area which is detailed below.

- (i) The effect of galleries, vertical shafts and the steel reinforcements to support them.
- (ii) Influence of weather conditions.
- (iii) The effect of waves in the reservoir.
- (iv) Incorporation of actual support conditions.

9. References

- [1] Rohith Menon V P, Girija K, Deepa Raj S, "Safety Evaluation of Idukki Arch Dam", *International Journal of Scientific and Engineering Research*, vol. 5, issue. 7, July 2014.
- [2] Binol Varghese, Arya Saju, Simi John, "Finite Element Analysis of Arch Dam", *International Journal of Research in Engineering and Technology*, vol. 3, issue. 7, July 2014.
- [3] M. A. Lotfollahi Yaghin, M. A. Hisari, "Dynamic analysis of the arch concrete dam under earthquake force with ABAQUS", *Journal of Applied Sciences*, vol. 8, issue. 15, 2008.
- [4] G Suresh, "A Study of the Structural Behaviour of Idukki Arch Dam", University of Roorkee, December 1996.
- [5] Susan Abraham, "Finite Element Method in the Context of Arch Dams – A Critical Study", Government Engineering College, Thrissur, Kerala, December 2007.
- [6] Peizhen Zhang, Zhi-xian Yang, Harsh K.Gupta, Satish C. Bhatia and Kaye M. Shedlock, "Global Seismic Hazard Assessment Program (GSHAP) in Continental Asia", *Annali Di Geofisica*, vol. 42, December 1999.

- [7] Lars V. Andersen, "Non Linear Analysis of Earthquake Induced Vibrations", Aalborg University, Denmark, January 2016.
- [8] "Engineering Guidelines for the Evaluation of Hydropower Projects", Federal Energy Regulatory Commission Division of Dam Safety and Inspections Washington, DC, 1999.
- [9] ABAQUS 6.13 Documentation and User Manual.
- [10] IS 456:2000
- [11] IS 1893 Part 1 : 2002
- [12] <http://www.mathrubhumi.com/tv/ReadMore1/34461/idukki-dam/E>

Seismic Analysis of RCC Buildings Considering the Flexibility of Soil

Fathima S ¹[0000-1111-2222-3333] and Jisha S. V ²[1111-2222-3333-4444]

¹P G Student, Department of Civil Engineering, Mar Baselios College of Engineering and Technology, Thiruvananthapuram, India
fatimzainu@gmail.com

²Assistant Professor, Department of Civil Engineering, Mar Baselios College of Engineering and Technology, Thiruvananthapuram, India
jpn.nitk@gmail.com

Abstract. Detailed investigations on the behaviour of buildings considering Soil Structure Interaction (SSI) can be obtained by conducting nonlinear finite element analysis. Three dimensional reinforced concrete buildings with aspect ratios varying from 1 to 3 considering SSI are studied in this paper. The plan area of the building is kept same for all the buildings and the heights of the buildings varied based on the aspect ratios. To study the effect of underlying soil medium, different geotechnical properties are selected. Time history analyses are conducted for the integrated structure-soil system assuming the nonlinear behaviour of soil medium. Drucker Prager model is selected for the three dimensional soil medium. The analysis was carried out using finite element method on the basis of direct method of SSI. The responses such as maximum lateral deflection, base shear and base moments are investigated. It is found that, the variation of deflection on building with aspect ratio 1.0 supported on soft soil strata compared to fixed base is approximately 80%. The variation is reducing to 50% and less than 20% for buildings with aspect ratio 2.0 and 3.0.

Keywords: Soil Structure Interaction, nonlinear, Drucker Prager, time history analysis, finite element analysis.

1. Introduction

More high-rise concrete buildings are built over the years especially in the high seismic areas. The buildings in a seismically active zone are generally expected to go through many small, some moderate, few large, and possibly one very severe earthquake. It is uneconomical or impractical to design buildings to resist the forces resulting from large or severe earthquakes. In severe earthquakes, most buildings are designed to experience yielding in at least some of their members. Properly designed and detailed buildings can limit the damage upto energy-absorption capacity of yielding. These can survive earthquake forces substantially greater than the design forces associated with an allowable stress in the elastic range. Soil Structure Interaction (SSI) is one of the significant topics in the field of earthquake engineering, in recent decades. In the conventional design, superstructure and substructure are analysed separately considering fixed base for the super structure. Conventionally, the ground motions are given directly to an analysis of the structure based on codal provisions without any consideration of interaction with supporting soil strata and the foundation is designed separately. In most of the cases, ignoring SSI is conservative. However, it is important to consider SSI effects to reduce risk when buildings with a deep basement or pile foundation system are dependent on the foundation reaction with the soil. It is difficult to determine the effective ground excitation and the structural inertia forces in the case of pile foundations. SSI analysis is also performed to work out the construction cost savings by reducing the conservatism in the conventional approach. This is useful on sites with relatively soft soils where the flexibility of the soil-foundation system significantly elongates the effective natural periods of the structure and increases the damping, leading to reduced earthquake design forces [1]. Observations in different parts of the world provided direct evidence of the significance of nonlinear site effects. Nonlinearity under strong ground shaking depends on the physical properties of soil strata. It may be considerable for soft clays and sands, but negligible for stiffer materials. Considering all these facts, in spite of the huge uncertainties in the earthquake motions, its effect on buildings considering the nonlinearities of soil strata will give the most reliable results while evaluating the dynamic response of a realistic structure.

SSI

The phenomenon of SSI is mainly affected by energy exchange mechanism between soil and structure. SSI analysis has become a prominent feature of structural engineering with the advent of massive constructions on soft soil strata. If the

structure is very massive or stiff and the foundation is relatively soft, the motion at the base of the structure may be significantly different than the free-field surface motion. Suyehiro (1932) introduced the theory of SSI and described the responses of various buildings on soft clay and hard rock. In 1970s, many researchers put effort into estimating the SSI effect on elastic response of structures. After 1994 Niigata earthquake (M 7.5), it was evident that damage to the structure not only depend on the behaviour of super-structure, but also on the sub-soil below it. Since then, many researchers have studied the behaviour of the soil subjected to the dynamic loading. Also, investigations had been performed experimentally, analytically, numerically and by field observations. Numerous studies starting from origin of SSI have been carried out to investigate the dynamic effects of buildings due to earthquake forces considering soil-flexibility. A seismic design procedure for the structures with embedded foundations is studied by Kashima et al. (1988). It can take into account the soil flexibility and the effect of spatial variability of ground motions with the help of a numerical example. A shaking table model test results of dynamic interaction between two identical foundations conducted by Shohara et al. (1992) proved that the SSI effect was found to be relatively small in terms of foundation displacement and acceleration but more significant in terms of soil pressure. Halabian and Naggar (2002) established that the non-linearity of soil strata might vary the base forces of high rise slender structures depending on the type of structure, frequency content of the input motion and the dynamic properties of the near-field soil strata. RCC structures in the places with weak soil have to be founded on piles to avoid excessive ground settlements. These piles may be subjected to dynamic forces in addition to static loads transferred from the dead load of the structures. Past earthquake events demonstrate that damages in piles are commonly induced during moderate to strong earthquakes [6]. The degree of influence of SSI on response of structures depends on the stiffness of soil and dynamic characteristics of structure such as natural period, damping factor, stiffness and mass of structure. There are two different approaches for interaction effects namely direct and indirect approach. In the direct approach, structure is modelled explicitly with the soil strata and a complete solution is obtained in a single analysis. In the substructure method, the soil-structure system is analysed separately as two substructures; a structure which may include a portion of non-linear soil strata and the unbounded soil. If the structural foundations were perfectly rigid, the solution arrived by substructure approach and direct-method will be identical. Both approach gives correct result, however second approach is easy to implement and therefore often specified in the most of design codes.

It is well established in geotechnical engineering that response of soil strata is nonlinear beyond a certain level of deformation. The soil system nonlinearity under strong ground shaking depends on the physical properties of soils. Many constitutive models are available to simulate the nonlinear soil behaviour in the finite element modelling. Drucker-Prager model is a simplified Mohr-Coulomb model. Drucker-Prager model had been widely used in geotechnical engineering to predict failure strength. It is a pressure-dependent model for determining whether a material has failed or undergone plastic yielding [7]. This study quantifies the effects of SSI using an integrated three dimensional (3D) soil-structure systems considering nonlinear soil behaviour.

2. Methodology

RCC buildings with aspect ratios 1.0, 2.0 and 3.0 considering nonlinear behaviour of soil strata are selected for the study. Finite element models of RCC buildings supported by piled raft foundations resting on 3 different soil strata are developed. Time history analyses were conducted on all these buildings with and without considering SSI and the responses obtained from the analyses are compared.

Idealisation of Buildings

RCC buildings with number of storeys 10, 20, and 30 with a typical storey height of 3.0 metres are selected. Preliminary analysis is done to fix the sizes of structural elements for superstructure and piled raft foundations. The building names are designated as BL1, BL2, and BL3 for the different storey heights, respectively. The plan dimensions of the buildings are kept same, as shown in Fig. 1. Geometric parameters of buildings are tabulated in Table 1.

Table 1 Geometric parameters of buildings

Building designation	Aspect ratio	Nos. of Storeys	Height of building (m)
BL1	1.0	10	30
BL2	2.0	20	60
BL3	3.0	30	90

M25 grade concrete of density 25 kN/m³ and poisson’s ratio of 0.15 and Fe 415 grade reinforcement with density of 78.50 kN/m³ and poisson’s ratio of 0.3 were selected as the materials for building.

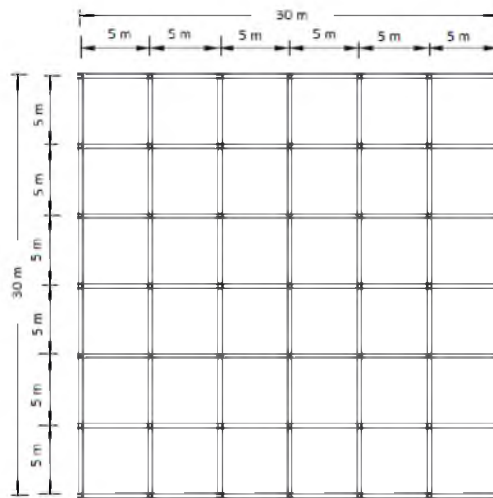


Fig.1. Typical plan of building

The static loads are considered based on IS 875 (Part 1 & 2)[8,9]. The dead load includes self weight of the building components & average live loads on each story are taken as 2.0 kN/m², and additional dead loads of 2.0 kN/m² is considered for the finishes and light weight partitions. The foundation system is assumed as piled raft foundations for all the buildings. Based on the preliminary study, the typical dimensions of beam in the building are taken as 0.3 x 0.5 m. The column dimensions taken are as shown in Table 2.

Table 2 Sizes of columns

Building designation	Column size (mm x mm)	Nos. of storeys
BL1	400 x 400	1-10
BL2	600 x 600	1-10
	400 x 400	11-20
BL3	800 x 800	1-10
	600 x 600	11-20
	400 x 400	21-30

Characteristics of piled raft foundations

The plan area of Raft foundation is taken as 35x35 m for all the buildings. Bored cast in situ Piles of length 30.0 m with diameter varying from 800 mm to 1000 mm is taken and the number of pile foundations required for each building is found out based on the preliminary design. Capacity of piles are designed based on the soil criteria in conformance with IS 2911 (Part 1/Sec 2) 2010 [10]. Thickness of raft, number and diameter of piles are taken as shown in the Table 3.

Table 3 Geometric parameters of piled raft foundations

Building designation	Raft thickness (mm)	Details of pile foundations	
		Nos.	Dia. of pile (mm)
BL1	800	49	800
BL2	1200	49	1000
BL3	1200	85	1000

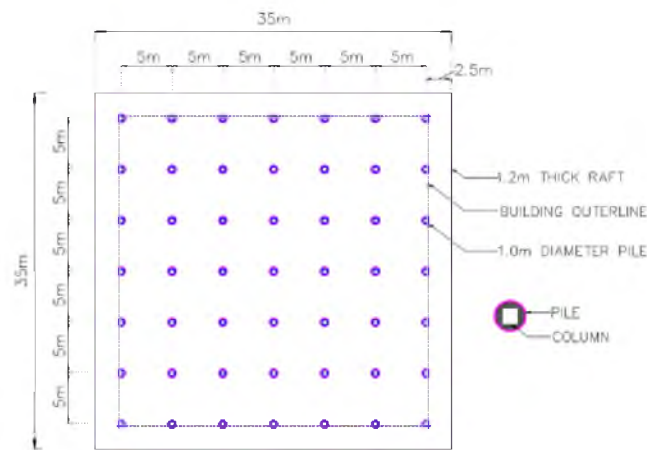


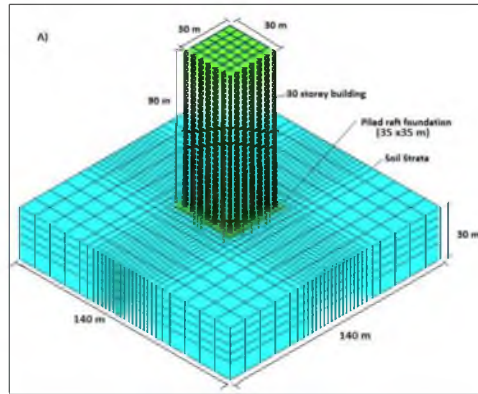
Fig.2. Plan of piled raft foundation of building-BL1

Geotechnical Characteristics

It is important to properly consider the geometric and material properties of both the buildings and the soil strata. A depth of 30m homogenous soil stratum with Soft (S), Medium (M) and Hard (H) clayey sand (c-φ) was considered in the analysis. Bedrock was assumed at a depth of 30m below the soil stratum. The dimension of the soil stratum was taken as four times the external dimension of the raft [11]. The properties of the soil strata are defined by its mass density, shear wave velocity, modulus of elasticity, poisson’s ratio and angle of internal friction [12,13] as shown in Table 4. Drucker-Prager model is used to define the non-linear soil model. The base of soil strata is assumed as fixed.

Table 4 Properties of soil types

Soil type	Shear Wave Velocity (m/s)	Poisson’s Ratio, μ	Density, γ (kN/m ³)	Elastic modulus, E (kN/m ²)	Angle of friction, Ø (°)	Cohesion, C (kN/m ²)
S	125	0.20	16	50000	30	50
M	150	0.25	18	100000	34	100
H	200	0.30	20	250000	38	200



3D integrated soil – structure system

Finite element meshing and analyses of 3D integrated soil-structure system were carried out by using the finite element software. In the 3D system, two noded beam element with six degrees of freedom is used to model the beam, column and pile elements. Degrees of freedom include translations in the x, y, and z directions and rotations about the x, y, and z directions. Shell element is used to model the slab and raft elements. It is a four-node element with six degrees of freedom at each node: translations in the x, y, and z directions, and rotations about the x, y, and z-axes [14]. The nonlinear soil stratum is modelled using solid elements having eight nodes and three translational degrees of freedom at each node. Three dimensional finite element model of the building is generated in the finite element programme. Fig. 3 shows the finite element meshing of Building BL3.

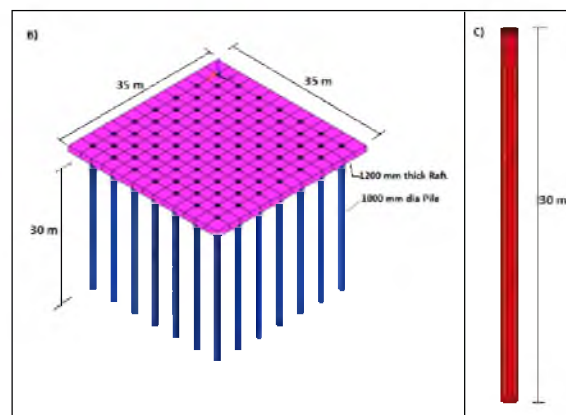


Fig.3. Finite element meshing of (A) Integrated building-piled raft-soil system (B) Piled raft foundation (C) Single pile

In the finite element analysis, the boundary of infinite soil medium needs to be restricted to a finite distance. The non-reflecting boundaries were kept at the soil boundaries to prevent the reflection of waves propagated from the soil at the soil finite boundary. In this analysis, the lateral boundaries are assumed to provide a non reflecting boundary (special artificial or transmitting boundaries also known as viscous boundaries – Fig. 4) to accommodate a seismic excitation that is assumed to be vertically propagating [12] from the base of the model. The ground motions are applied at special boundaries at the base and sides of the model, and the kinematic interaction is modeled directly. The medium beneath the lower boundary of the model is modelled as grounded linear viscous dampers, to which the desired ‘bedrock’ ground motions are induced via applied force history. This is done to prevent spurious stress wave reflection at the lower boundary.

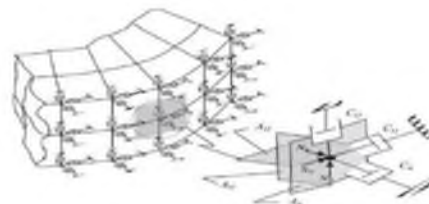


Fig.4. Viscous boundaries in three dimensional finite element SSI model [12]

3. Time History Analysis

Time history analysis of three dimensional integrated SSI system was done considering Elcentro ground motion based on longitudinal component of Imperial Valley earthquake (1940) [15]. The peak ground acceleration of Elcentro was 0.319g and its magnitude was 7.0. Acceleration time history and associated fourier spectrum of this ground motion are shown in Fig. 5. The time history acceleration was applied in the global X direction of the integrated building–foundation–soil model. Fourier spectrum is used to study the influence of frequency content of the ground motion. Rayleigh damping was taken into consideration in the seismic analyses. 5% of critical damping was assumed as structural damping. The horizontal loading due to wind and other causes were neglected.

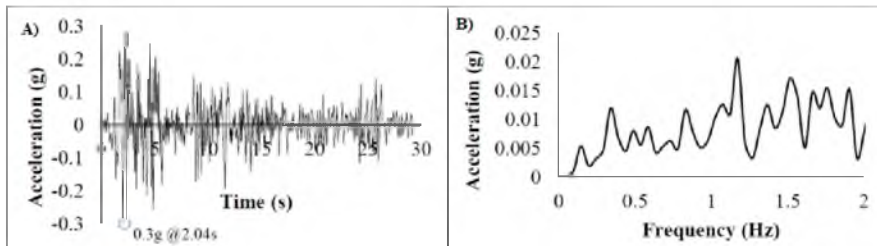


Fig.5 (A) Time history and (B) Fourier spectrum of Elcentro ground motion [15]

4. Results and Discussion

The change in frequencies of buildings with reference to buildings with flexible foundation and the effect of frequency content in the ground motion were studied. Three different soil conditions were taken for analysis of buildings with flexible base. The absolute maximum responses namely lateral tip deflection, base shear and base moments corresponding to fixed base buildings were evaluated. The variation of these responses of buildings with flexible base from that of buildings with fixed base was computed.

4.1 Effects of free vibration analysis

Fundamental natural frequency obtained from buildings with fixed base is higher than that obtained from SSI analysis. Variation of fundamental frequency of building with flexible base from that of building with fixed base is more for building- BL1 resting on soil type S and the maximum variation is about 40%. Variation is less than 25% and 15% respectively for buildings- BL2, and BL3 rests on soil type S. Fig.6 shows the normalized natural frequencies (ratio of frequency of building with flexible base to that with fixed base) of the buildings. The frequency variation is only 10% for buildings- BL2 and BL3 supported on hard soil strata.

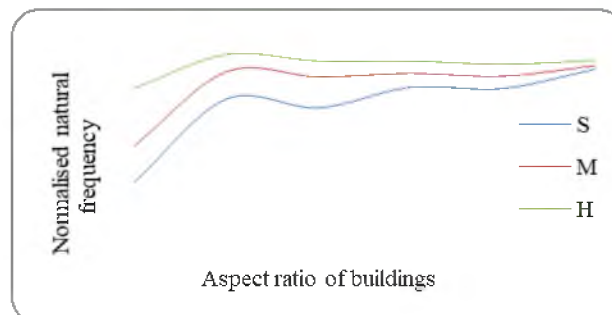


Fig.6. Normalised natural frequency of buildings with different aspect ratios

4.2 Effects of time history analysis

Responses of buildings namely lateral tip deflection, inter-storey drift, base shear & base moments were studied.

4.2.1 Variation of tip deflection

Variation in tip deflection of building with flexible base from that with fixed base is high for buildings with aspect ratio 1.0. Fig.7 shows the time history plot of lateral tip deflection of building-BL1.

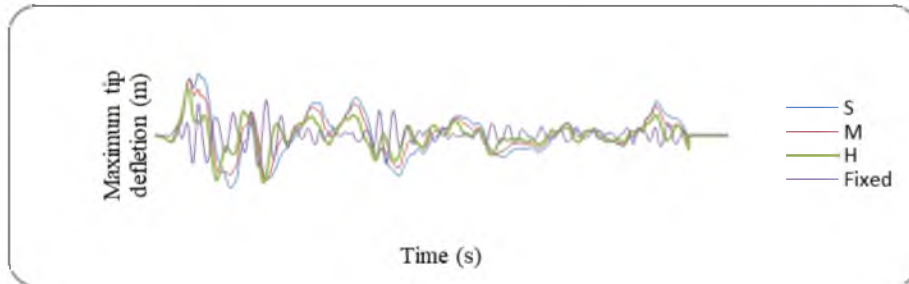


Fig.7. Time history plot of lateral tip deflection of building- BL1

It is seen that the variation is approximately two times for building with aspect ratio 1.0. There is a sudden increase in the deflection of building with aspect ratio 3.0 supported on hard soil strata due to resonance effect. The percentage variation of deflection is 80% for BL1 supported on soft soil strata. The variation reduced to 40% and less than 20% for the same building supported on medium and hard strata respectively.

4.2.2 Variation of Base shear and Base moment

Variation in base shear and base moment of buildings considering flexible base with respect to fixed base is high for all buildings. Base shear and base moment got reduced by 85% approximately for all buildings. Variation corresponding to increase in stiffness of supporting soil stratum is approximately 2 times. Table 3 and 4 show the percentage variation in base shear and base moment of buildings with fixed base compared to flexible base.

Table 3 Percentage variation of base shear of buildings due to ground motions

Building designation	Base shear (fixed base) (kN)	Percentage variation of base shear of buildings		
		S	M	H
BL1	39903.54	-93.8	-89.3	-80.9
BL2	57796.32	-79.2	-66.0	-39.5
BL3	68470.35	-79.4	-73.2	-55.5

Table 4 Percentage variation of base moment of buildings due to ground motions

Building designation	Base moment (fixed base) (kNm)	Percentage variation of base moment of buildings		
		S	M	H
BL1	55911.52	-93.6	-89.0	-80.4
BL2	67634.52	-75.9	-60.6	-30.0
BL3	75439.90	-77.2	-72.7	-56.1

5. Conclusions

The analysis buildings with 30m, 60m and 90m with piled raft were from SSI analysis based on finite element analysis and compared that with conventional analysis. The properties of the soil types were varied to study the effect of SSI. The effect of frequency content of ground motion was also investigated. The responses in terms of tip deflection, base shear

and base moment were considered for study. The absolute maximum responses obtained from conventional analysis are compared with that obtained from SSI analysis. The following conclusions are derived from the present study:

1. Frequency variation is 40% for building with aspect ratio 1.0 resting on soft soil.
2. The effect of SSI is to be considered for the response of tip deflection of short buildings with aspect ratio one. Such buildings, the maximum deflections are increased by 2 times when the flexibility of soil stratum is accounted for.
3. The inter-storey drift is more in the lower half of the height of buildings with fixed base.
4. The effect of SSI is less significant in the study of base moment and base shear as it is found to be conservative.

References

- Deierlein, G. G., Reinhorn, A. M., Willford, M. R.:** Nonlinear structural analysis for seismic design, *NEHRP Seismic Design Technical Brief No. 4*, Gaithersburg, MD, NIST GCR 10-917-5(2010).
- Suyehiro, K.:** Engineering seismology notes on American lectures, *Proc. ASCE*, 58,4,1-110 (1932).
- Reissner, E.:** Stationäre, axialsymmetrische, durch eine schüttelnde Masseerregte Schwingung eines homogenen elastischen Halbraum, *Ingenieur-Archiv*, 7, 6, 381-396 (1936).
- Kashima, N., Kawashima, K., Harada, T., Ioyama, R., Masuda, S.:** Soil structure interaction and its implication for seismic design of structures. In: *Proc. 13th World Conf on Earthq. Eng.*, Tokyo, Kyoto, Japan(1988).
- Shohara, R., Kurosawa, I., Shinozaki, Y., Sakamoto, D.:** Tests on dynamic interaction between foundations, *Proc. of the 10th world conference on earthquake engineering*. Balkema, Rotterdam(1992).
- Hokmabadi, A. S., Fatahi, B., Samali, B.:** Physical modelling of seismic soil-pile-structure interaction for buildings on soft soils, *Int. J. Geomech.*, 04014046-1-18(2014).
- Drucker, D. C., Prager, W.:** Soil mechanics and plastic analysis or limit design, *Quart. Applied Math.*, 10, 2, 157-165 (1952).
- IS 875 (Part 1):1987** Indian code of practice for design loads (other than earthquake) for buildings and structures, *Bureau of Indian Standards*, New Delhi
- IS 875 (Part 2):1987** Indian code of practice for design loads (other than earthquake) for buildings and structures, *Bureau of Indian Standards*, New Delhi
- IS 2911 (Part 1/Sec2):2010** Indian code of practice for design and construction of pile foundations, *Bureau of Indian Standards*, New Delhi
- Jisha, S. V., Jayalekshmi, B. R., Shivashankar, R.:** Evaluation of the effect of soil-structure interaction on the raft of tall reinforced concrete chimneys under across wind load, *The Eighth Asia-Pacific Conf on Wind Eng.*, 58-67 (2013)
- Bowles, J. E.:** "Foundation analysis and design." *McGraw-Hill International Editions*, Singapore(1997).
- Jayalekshmi, B. R., Jisha, S. V., Shivashankar, R., SooryaNarayana, S.:** Effect of dynamic soil-structure interaction on raft of piled raft foundation of chimneys, *ISRN Civil Engineering*, 16, 1-11(2016).
- Ansys Inc.** Theory Reference – Ansys Manual, <http://www.ansys.com>.
- PEER Strong Motion Database** The Pacific Earthquake Engineering Center and the University of California(2000).

Effect of Containment Reinforcement on the Seismic Performance of Un-Reinforced Masonry Buildings

Vaidehi S. R.¹, Aiswaria G. R.² and Jisha S. V.³

^{1,2}PG Research Scholar, Structural Engineering, Mar Baselios College of Engineering and Technology, Thiruvananthapuram, Kerala, India

vaidehivr781@gmail.com

³Assistant. Professor, Department of Civil Engineering, Mar Baselios College of Engineering and Technology, Thiruvananthapuram, Kerala, India

jpn.nitk@gmail.com

Abstract. Un-Reinforced Masonry (URM) construction is the most common type of construction in rural as well as urban areas due to its lower cost and ease of construction. However, these are weak in resisting lateral loads. The main objective of this study was to investigate the effectiveness of vertical containment reinforcement in mitigating seismic vulnerability of URM buildings using finite element method. URM building of dimensions 6×3×3m with openings in the buildings have been considered. All the walls were assumed to be fixed at their bases along their length. 12mm diameter steel bars were used as vertical containment reinforcement and it was laid on the surface of the walls on both the faces at a spacing of 1m. In this study, time history analysis of the building was carried out for Bhuj ground motion. The responses such as base shear and storey deflection of URM buildings were evaluated. The study was concluded that on providing the vertical containment reinforcement along with roof slab and lintel band, the deflection gets reduced by 96 % from that of the building without roof slab, lintel band and reinforcement.

Keywords: Laterite masonry, Containment reinforcement, Time history analysis

1. Introduction

Masonry is generally a highly durable form of construction throughout the world. The common materials of masonry construction are brick, limestone, laterite stone, concrete block etc. Among them laterite is the most favoured masonry material in south-west coastal areas of India due to its availability in abundance. Un-Reinforced Masonry (URM) construction is the most common type of construction in rural as well as urban areas due to its lower cost, ease of construction and good aesthetics.

When such a masonry structure is subjected to lateral inertial loads during an earthquake, the walls develop shear and flexural stresses. A masonry wall can also undergo in-plane shear stresses if the lateral forces are in the plane of the wall. Shear failure in the form of diagonal cracks is observed due to this. However, catastrophic collapses take place when the wall experiences out-of-plane flexure. This can bring down a roof and cause more damage. Fig 1 shows typical failure of an URM building during 2010 Haiti earthquake [1]. Masonry buildings with light roof such as tiled roof is more susceptible to out-of-plane vibrations, since the top edge can undergo large deformations due to lack of lateral restraint. Damage to masonry buildings in earthquakes may be influenced by four general categories namely quality of materials and construction, connections between structural elements, structural layout and soil structure interaction.



Fig.1. Failure of an URM building during 2010 Haiti earthquake [1]

2. Background of study

Numerous experimental investigations were carried out on URM walls which shows the seismic behaviour of brick masonry walls [2,3]. While considering the influence of flanges on the in-plane behaviour of URM walls it is observed that for a diagonal tension-controlled wall, once a stair stepped crack is opened up, sliding can be expected to occur along the bed joints and deformation can be expected [4]. The seismic performance of URM with different types of failures such as lack of anchorage between floor and walls, anchor failure when joists are anchored to walls, in-plane failure [5], out-of-plane failure, a combined in-plane and out of plane effects showed that in-plane failure may not lead to collapse since the load carrying capacity of a wall is not completely lost by diagonal cracking, whereas, out-of-plane failure leads to unstable and explosive collapse [6].

In containment reinforcement, vertical reinforcement is wrapped around the masonry unit at the foundation and tied at the top in lintel band. Such vertical reinforcement is to be provided at an appropriate spacing along the length of the wall. The reinforcements on the two faces are tied together through links or ties provided at a definite vertical spacing. Fig 2 displays masonry with containment reinforcement and links connecting them through bed joints. As the masonry wall bends, one face of masonry would be subjected to tension and the reinforcement on that side would bend to its profile while the reinforcement on the compression side would tend to become slack and the reverse happens as the wall bends the other way. Here the reinforcement is intended to prevent the growth of flexural tensile cracks that lead to failure. The containment reinforcement will prevent brittle failure due to tension cracks and permit larger deflections and hence a much higher absorption of energy without a substantial increase in strength.

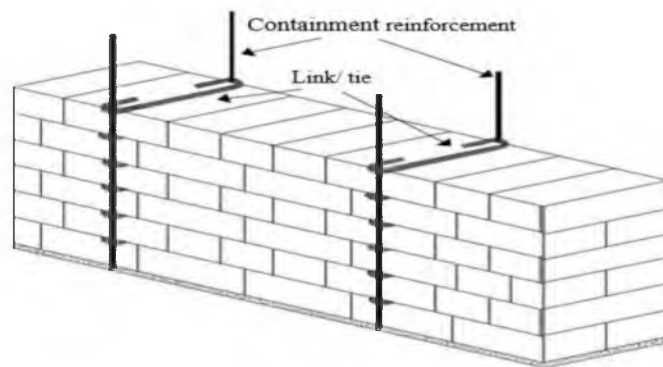


Fig. 2. Masonry with containment reinforcement and links [7]

The behaviour of brick masonry structures during the Bhuj earthquake of January 2001 reported that higher bond strength improves the earthquake resistance of masonry, use of lintel band, seems to introduce a rigid box-like behaviour in the upper portion of the buildings while the portions below the lintel bands cracked badly suggesting the need for more horizontal bands at different levels and provision of corner reinforcement in corners and junctions, as suggested by IS 4326-1993, has to be properly bonded with the surrounding masonry possibly with dowels or keys to prevent separation [8]. Containment reinforcement is intended to control post-cracking deflections, stresses and impart flexural ductility to masonry buildings [9]. From shock table test results on 1/6th of the buildings, it is observed that reserve energy capacity of the masonry building is vastly enhanced due to the presence of ductile containment reinforcement [10]. In some studies, the seismic strengthening of URM elements such as walls with glass fibre reinforced polymers [11] and piers with steel elements [12] were carried out. The strengthening system showed significant improvement in stiffness and ductility.

Consideration of ductility for earthquake resistant design is important for buildings, structures and building materials. When a structure undergoes lateral forces, the structure could not remain elastic anymore and the next stage is damage. It can go through plastic stage or fracture or damage, where stiffness will decrease significantly and deformations will be drastically increasing even for a small load. So, there is a need for providing reinforcement for making the structure ductile. These reinforcements are called containment reinforcement. The effect of containment reinforcement on the seismic response of a single storeyed URM buildings was investigated and is being outlined here.

3. Idealisation of the building

A URM building with plan dimensions of 6m x 3m x 3m have been considered for the analysis. Provisions of openings in the buildings have been considered with one door opening (of size 1m x 2m) and one window opening (of size 1m x 1m) on both the longer walls. Each of the short walls was assumed to be provided with one central window opening. All the walls of the building were assumed to be fixed at their bases, all along their lengths. The top nodes were free in structures without roof, and merged to roof nodes, in structures with roof. The different types of single storeyed laterite masonry structures used for the analysis are given in Table 1. Vertical containment reinforcement made of 12mm diameter steel bars was provided on the surface of the walls on both the faces at a spacing of 1m. M25 grade concrete and Fe250 grade steel reinforcement was used. Table 2 provides the properties of masonry, RCC and vertical containment reinforcement bars used in the finite element analysis.

Table 1. Types of single storeyed laterite masonry structures analysed

Designation	Building description
U	URM building without roof slab and lintel band
UL	URM building without roof slab and with lintel band
ULR	URM building with roof slab and lintel band
ULRC	URM building with roof slab, lintel band and containment Reinforcement

Table 2. Material properties [10]

Property	Laterite masonry in 1:6 cement mortar	Reinforced concrete	Vertical reinforcement (steel)
Modulus of Elasticity (GPa)	1.20	25	200
Poisson's Ratio (assumed)	0.15	0.15	0.30
Mass Density (kg/m ³)	2500	2500	7850

4. Seismic Forces

Non-linear time history analysis was conducted for URM buildings for Bhuj ground motion. The responses of a structure to any earthquake can be computed by time history analysis. A part of the Bhuj ground motion acceleration recorded at Ahmedabad during earthquake of January 26, 2001 which lasted over 2 minutes is shown in Fig 3. This was considered for the analysis. The peak ground acceleration is 0.11g at time 46.94 s for Bhuj ground motion. The earthquake reached a magnitude of 7.7 on the moment magnitude scale. The Fourier amplitude spectrum of Bhuj earthquake is revealed in Fig 4.

Damping in a structure increases with displacement amplitude since with increasing displacement more elements may crack or become slightly non-linear. For linear seismic analysis, viscous damping is usually taken as 5% of critical as the structural response to earthquakes are usually close to or greater than the yield displacement [9]. Hence, damping ratio of the building was chosen as 5%. The time history analysis was performed by applying each acceleration value to the building step by step in time domain.

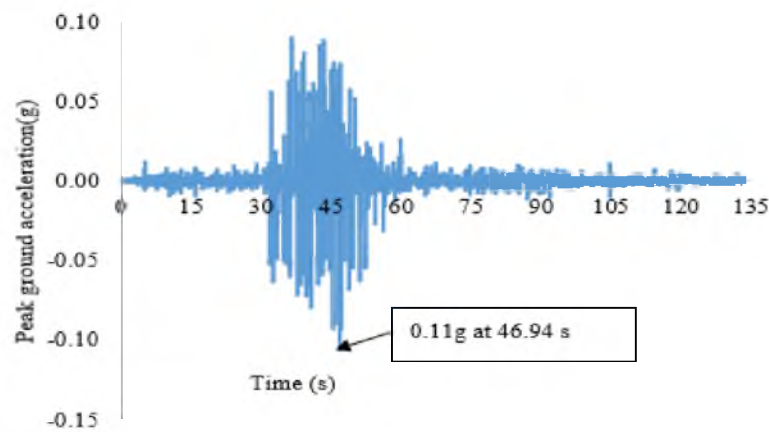


Fig.3. Acceleration time history of Bhuj earthquake [13]

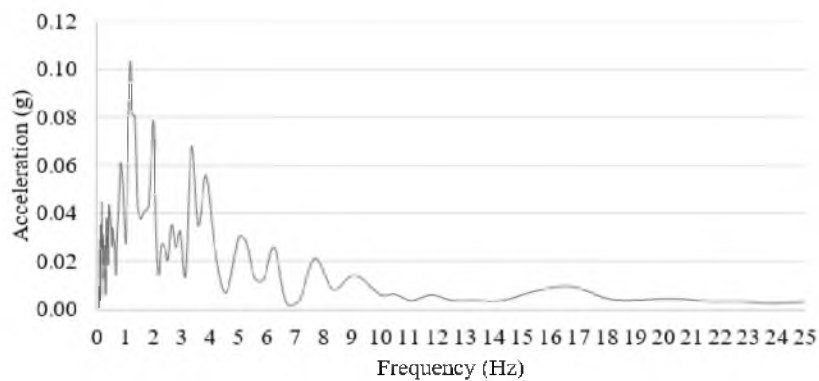


Fig.4. Fourier amplitude spectrum of Bhuj earthquake [13]

5. Finite Element Analysis

The URM building with lintel band, roof slab and containment reinforcement was analysed by finite element method. Eight noded brick (SOILD185) elements were used for the masonry of URM building. It is having three translational degrees of freedom at each node. For roof slab, four noded elastic SHELL181 element was used. The element has six degrees of freedom at each node and has both bending and membrane capabilities. Truss elements (LINK180) were used for the vertical reinforcements which is a uniaxial tension-compression element, also with three translational degrees of freedom at each node. The discrete modelling was used for the bars of steel reinforcement. In the discrete model, for the reinforcement, bar element was used to connect concrete mesh nodes. Therefore, the concrete and the reinforcement mesh share the same nodes and concrete occupies the same regions occupied by the reinforcement.

Vertical reinforcements called containment reinforcement were provided at a horizontal spacing of 1 m on both the faces of the walls, as shown in Fig 5. The whole building was discretised with element of 0.2 m size. Four types of building are chosen for analysis. Configurations of the four types of buildings analysed are illustrated in Fig 6.

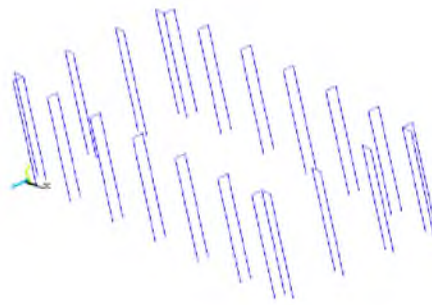


Fig.5.Configurations of containment reinforcement in URM buildings[9]

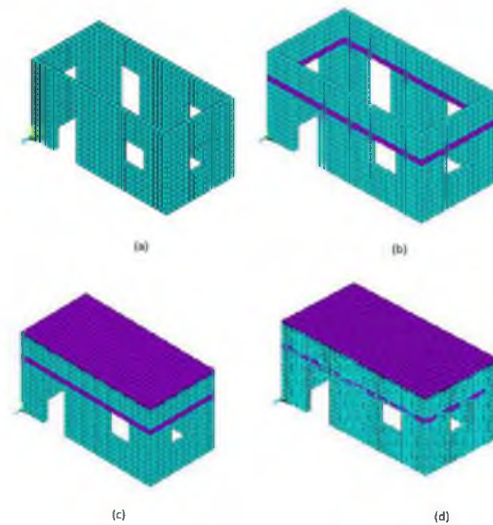


Fig.6.Configurations of URM buildings (a) U (b) UL (c)ULR (d)ULRC type[9]

6. Results and Discussion

Different configurations of URM building with lintel band, roof slab and containment reinforcement were selected for the study. Analysis was carried out by considering the base of the building as fixed. From the free vibration analysis, the frequency and mode shape of the buildings were obtained. Structural response in terms of storey deflection of building and base shear were evaluated.

6.1 Natural Frequencies

Free vibration studies were conducted to find the natural frequencies and mode shapes of all the four types of buildings, the results of which are tabulated in Table 3.

Table 3. Natural Frequencies

Mode No.	Natural Frequencies (Hz)			
	Designation			
	U	UL	ULR	ULRC
1	4.950	6.904	11.058	12.397
2	5.303	7.550	11.356	17.649
3	10.232	15.800	15.588	18.528
4	11.585	15.965	16.794	21.021
5	14.124	20.519	18.063	22.192

In the above table, there is an increase of 37% and 45% in frequency from U type building to UL type building and ULR type building respectively. But while considering ULRC type building there is an increase of 81.45% in frequency than U type building. Therefore, it is clear that for URM buildings with lintel band, roof slab and containment reinforcement, there is an increase in the natural frequencies of the structure. This is due to the increase in the stiffness of the building.

6.2 Time History Responses

Storey Deflection

All the four types of URM buildings discussed earlier were analysed to find their responses to Bhuj acceleration. In URM building without roof (U), the maximum deformation was observed above the openings. Table 4 gives the maximum storey deflections of different type of URM buildings.

Table 4. Maximum deflection

Designation	Deflection (mm)
U	3.717
UL	2.109
ULR	0.160
ULRC	0.150

For the buildings of Type UL, Type ULR and Type ULRC respectively, a reduction of 43.26%, 95.69% and 95.96% from Type U. Thus, in single-storeyed URM building, vertical containment reinforcement seems to help in controlling the total deformation significantly. Again, the displacements in the various URM buildings with roof are quite small as compared to structures without roof.

Base shear

Base shear is an estimate of the maximum expected lateral force that will occur due to seismic ground motion at the base of a structure. Table 5 conveys the base shear values of URM buildings. In the above table, there is an increase of 35% of base shear in ULRC type building than U type building. Therefore, base shear of a building with lintel band, roof slab and containment reinforcement are much higher than that of building without these.

Table 5. Base Shear

Designation	Base Shear (kN)
U	179.98
UL	194.10
ULR	236.31
ULRC	243.06

7. Conclusions

The effect of strengthening factors like lintel band, roof slab and containment reinforcement on the natural frequencies were analysed. Response of URM buildings, to Bhuj acceleration was obtained using time-history analysis. From the above results, it is concluded that URM buildings with lintel band, roof slab and containment reinforcement are more effective in mitigating seismic vulnerability as they reduced storey deflection and base shear.

References

1. Huffpost homepage, https://www.huffingtonpost.in/entry/haiti-earthquake-anniversary-photos_n_6456888, last accessed on 16/05/2018.
2. Anthonie, A., Magonette, G., and Magenes, G.: Shear compression testing and analysis of brick masonry walls. Proceedings of 10th European Conference on Earthquake Engineering, Taylor and Francis, 1657-1662, (1995).
3. Dolatshahi, K.M., and Aref, A.J.: Multi-directional response of unreinforced masonry walls: experimental and computational investigations, Earthquake Engineering and Structural Dynamics, Wiley Online Library 45, 1427-1449, (2016).

4. Khanmohammadi, M., Behnamb, H., and Marefata, M.S: Seismic behaviour prediction of flanged unreinforced masonry (FURM) walls, *Journal of Earthquake Engineering*, 18(5), 759-78, (2015).
5. Singh, Y., Lang, D.H., Prasad, J.S.R., and Deoliya, R.: An analytical study on the seismic vulnerability of masonry buildings in India, *Journal of Earthquake Engineering*, 17, 399–422, (2013).
6. Bruneau, M.: State-of-the-art report on seismic performance of unreinforced masonry buildings, *Journal of Structural Engineering*, ASCE,120(1),231-251, (1994).
7. Online civil engineering homepage, [http://civil-online2010.blogspot.in/2010/02/earthquake resistant features in html](http://civil-online2010.blogspot.in/2010/02/earthquake-resistant-features-in-html), last accessed on 24/03/2018.
8. Jagadish, K.S., Raghunath, S., and Rao, N.K.S.: Behaviour of masonry structures during the Bhuj earthquake of January 2001, *Proceedings of Indian Academy of Science (Earth Planetary Sciences)*, 112(3), 431-440, (2003).
9. Unnikrishnan, S., Mattur, N.C., and Venkataramana, K.: Effect of containment reinforcement on the seismic response of box type laterite masonry structures – an analytical evaluation, *Earthquakes and Structures*, 5(1), 067-081, (2013).
10. Jagadish K.S., Raghunath S. and Rao N.K.S.: Shock table studies on masonry building model with containment reinforcement, *Journal of Structural Engineering*, 29(1), 9-17, (2002).
11. Kalali, A, and Kabir M.Z.: Cyclic behaviour of perforated masonry walls strengthened with glass fibre reinforced polymers. *Scientia Iranica*, Elsevier, 19(2), 151–65 (2012).
12. Rai, D.C. and Goel, S.C.: Seismic strengthening of unreinforced masonry piers with steel elements, *Earthquake Spectra*, 12(4),845-862, (1996).
13. COSMOS homepage, <http://www.strongmotioncenter.org/vdc/scripts/vent.plx?evt=785>, last accessed on 23/03/2018.

Along and Across Wind Responses of Tall Buildings Considering Soil Structure Interaction

Aiswaria G. R.¹ and Jisha S. V.²

¹PG Student, Structural Engineering, Mar Baselios College of Engineering and Technology, Thiruvananthapuram, Kerala, India
aiswariagr@gmail.com

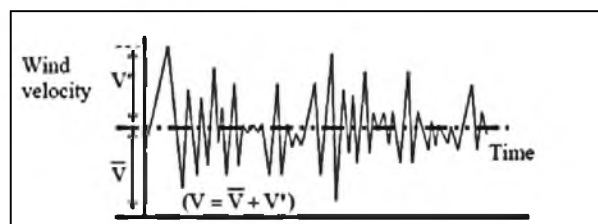
²Asst. Professor, Department of Civil Engineering, Mar Baselios College of Engineering and Technology, Thiruvananthapuram, Kerala, India
jpn.nitk@gmail.com

Abstract. For a good wind resistant design, the exact behaviour of a building needs to be assessed. Thus it is important to consider the effect of the foundation and the underlying soil stratum flexibility along with the building during analysis which is investigated in this paper. A 180m high tall RCC building with piled raft foundation founded on different soil conditions is being considered here. The building is assumed to be located in terrain category IV and interference zone IV as per the IS: 875 (Part 3): 2015 subjected to an average wind speed of 50 m/s. Linear analysis performed on the building with rigid base is compared with the integrated building-foundation-soil system considering material non-linearity of the soil. Drucker Prager model is used to represent the material non linearity of the soil stratum to consider soil structure interaction (SSI). Using numerical finite element analysis, the 3D structure is analysed for wind induced responses such as maximum lateral deflection and base moment with and without considering soil flexibility. On considering SSI, free vibration analysis, showed that the frequency decreases with increase in flexibility. It was also observed that, on considering SSI, displacement got increased by 18% and base moment got reduced by 85% of the structure without SSI effect for the building considered.

Keywords: Along wind force, across wind force, soil structure interaction, finite element analysis

1. Introduction

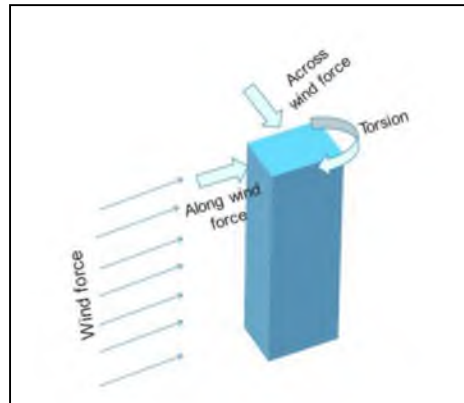
To improve and optimise the designing of buildings, the responses and behaviour must be studied and analysed in detail. In tall buildings, wind is the critical load especially in cyclone prone areas. These structures are susceptible to vibration problems caused by wind due to their low damping characteristics. The wind is generated by the differential heating of the atmosphere by the sun. The two major driving factors of large-scale wind patterns are the differential heating between the equator and the poles due to difference in absorption of solar energy. The two types of effects exerted by wind on to a structure are static and dynamic effects. Static effect causes elastic bending and twisting of the structure while dynamic effect causes vibrations or oscillations. The dynamic character of wind is a constant mean wind velocity and a varying gust velocity. Thus, there is a mean and a fluctuating response to wind force. This is shown in Fig. 1. where ' \bar{v} ' is the mean velocity and ' v' ' is the fluctuating velocity.



Variation of wind velocity with time [1]

Flexible structures, such as tall buildings, subjected to dynamic wind loading experience fluctuating deflections in primarily three directions namely along-wind deflections in the direction of the wind, across-wind deflections in the direction normal to the wind and torsional deflections which are due to the non-uniform wind pressures over the surface of the building. This is illustrated in Fig. 2. One of the main tasks while designing tall buildings is its ability to absorb the horizontal forces and to transmit the resulting moment into the foundation. Any unexpected deflection can lead to additional lateral forces and must

be considered. Hence, for a wind resistant design, there is an extreme need to assess the true behaviour of the building under wind.



Components of building response to wind excitation

In conventional engineering practice, structures are often designed considering the base of the structure fixed to the ground neglecting the flexibility of soil strata. Although this can be considered reasonable for low rise structures on relatively stiff soils, the effect of soil–foundation–structure interaction becomes prominent for heavy structures.

In this paper, effect of along and across wind responses of tall buildings considering soil structure interaction is studied using numerical finite element analysis.

2. Soil Structure Interaction (SSI)

It is the process in which response of the soil influences the motion of the structure and the motion of the structure influences the response of the soil [2]. SSI effects can amplify the lateral deflections and corresponding inter-storey drifts of unbraced building structures founded on soft grounds, forcing the structure to behave in the inelastic range, resulting in severe damage of the building structures.

Methods that can be used to evaluate the SSI effects can be categorized as direct and substructure approaches [2]. In a direct analysis, the entire structure foundation- soil system is modelled and analysed in a single step as a complete system using a finite element platform. The soil is often represented as a continuum along with foundation and structural elements, transmitting boundaries at the limits of the soil mesh, and interface elements at the edges of the foundation as depicted in Fig. 3. In a substructure approach, the SSI problem is partitioned into distinct parts that are combined to formulate the complete solution using principle of superposition.

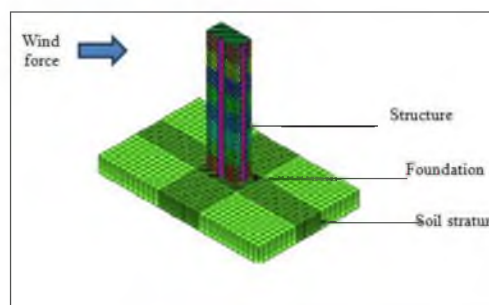


Fig. 3. Direct approach of SSI

There are various types of soil models used in SSI such as Winkler model, Filanenکو Borodich model, Hetenyi's model, Pasternak model, Kerr model, elasto-plastic model, elastic continuum models, Mohr-Coulomb model, Drucker-Prager (DP) model etc. The DP yield criterion is a pressure-dependent model for determining whether a material has failed or undergone

plastic yielding. The criterion was introduced to deal with the plastic deformation of soils and have been applied to rock, concrete, polymers, foams, and other pressure-dependent materials. In DP, parameters related to friction angle and cohesion govern the yielding and hardening criteria, while the parameter related to plastic dilation determines the flow rule.

Extensive studies have been conducted on the role of SSI in seismic response of structures considering 3D structural system [3-6] and it was deduced that SSI affects the responses of structures such as increased the displacements, reduced base shear and base moments etc. It was also observed that failure sequences are influenced by SSI [4]. Effect of SSI on wind responses were also investigated [7-12] by idealising the structure to equivalent lumped mass system. It was deduced that SSI effect on wind responses are detrimental. Based on literature studies it was observed that very few researches have been undergone on the wind responses of an integrated structure-foundation-soil system. In this study, direct approach of SSI is used to determine the along and across wind responses by considering the material non-linearity of the soil stratum using DP model.

3. Idealisation of the Structure

A tall 180m high RCC building with core having a base dimension of 30 m x 60 m was analysed for along and across wind loads. The storey height was taken as 3m. For a high rise structure, incorporation of shear wall system is necessary to resist the lateral forces and hence, shear walls were placed on the periphery and at the centre to act as the lateral load resisting system. Piled raft foundation with piles located at a minimum spacing of 3 times the pile diameter [13] was chosen for the building. The plan view of building showing shear walls and the piled raft foundation are illustrated in Fig. 4 and Fig. 5 respectively. The parameters of the building and foundation are listed in Table 1. The sizes of RCC columns considered are enlisted in Table 2.

Table 1. Structural Parameters of Building

Building	-	RC building with core and shear walls
Foundation type	-	Piled raft foundation
Plan dimension	-	30m x 60m
Plan area	-	1800 m ²
Storey height	-	3m
Number of storeys	-	60
Grid size	-	5m x 5m
Beam size	-	0.3m x 0.5m
Slab thickness	-	0.125m
Shear wall thickness	-	0.25m
Pile diameter	-	1.2m
Raft dimension	-	45 x 75 x 2.5 m
No. of piles	-	247

Table 2. Dimension of column

Storey		Size of column (m)
0-10	-	1.20 x 1.20
10-20	-	0.85 x 0.85
20-30	-	0.75 x 0.75
30-40	-	0.60 x 0.60
40-50	-	0.50 x 0.50
50-60	-	0.40 x 0.40

The grade of concrete was chosen as M40 for the building and M25 for the piled raft foundation whose modulus of elasticity [14] are 3.16×10^4 N/mm² and 2.50×10^4 N/mm² respectively and the grade of steel was chosen as Fe 415. The Poisson's ratio of concrete and steel were taken as 0.15 and 0.3 respectively. The density of concrete and steel was taken as 2500 kg/m³ and 7850 kg/m³ respectively.

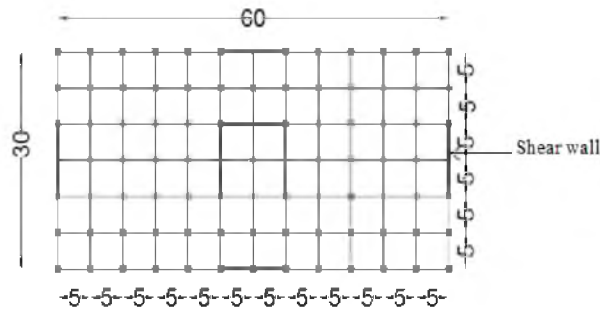


Fig 4. Plan view of the building

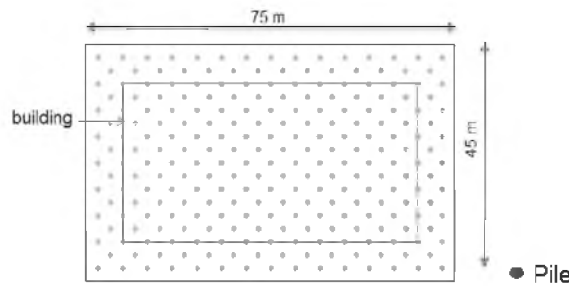


Fig 5. Plan view of piled raft foundation

4. Calculation of Wind Loads

Gravity load of the structure [15], an imposed load of 2kN/m² [16] and wind load [17] were calculated and applied to the building. As per IS 875 (Part 3):2015, there are two methods for determining wind loads acting on a structure namely force coefficient method and dynamic analysis method. For structures with aspect ratio of more than five or natural frequency less than 1Hz, dynamic method of load determination is recommended as per the above IS specification. Both along and across wind loads were calculated considering wind direction at 0° and 90°. The wind action at 0° shall be designated as long body orientation and that at 90° shall be designated as short body orientation. This is shown in Fig. 6. The structure is assumed to be located in wind terrain category IV and interference zone IV as per IS 875 Part 3: 2015 subjected to a basic wind speed of 50 m/s. Modal analysis was performed to obtain the modal frequencies for the building with lateral load resisting system. The wind loads were computed based on this without considering soil stratum flexibility. The procedure for wind load estimation is outlined in the following subsections.



Fig 6. Different plan orientations of the building subjected to wind force (a) Long body, (b) Short body

a. Along Wind Load

The along wind load on a structure on a strip area at any height z is [17]

$$F_z = C_{f,z} \cdot A_z \cdot \overline{p_d} \cdot G \tag{1}$$

where $C_{f,z}$ is the drag force coefficient for the building corresponding to A_z ; A_z is the effective frontal area considered for the structure at height z in m^2 ; \bar{p}_d is the design hourly mean wind pressure at height z due to hourly mean wind and G is the gust factor.

Then the design peak along wind base bending moment can be obtained by summing the moments resulting from design peak along wind loads acting at different heights along the height of the building as

$$M_{\alpha} = \sum F_z Z \quad (2)$$

b. Across Wind Load

The across wind design peak base bending moment M_c for enclosed buildings is given by the following formula [17]

$$M_c = 0.5g_h\bar{p}_h b h^2 (1.06 - 0.06k) \sqrt{\frac{\pi C_{fs}}{\beta}} \quad (3)$$

where g_h is a peak factor in cross wind direction for resonant response; \bar{p}_h is hourly mean wind pressure at height h (Pa); k is a mode shape power exponent for representation of the fundamental mode shape and C_{fs} is across wind force spectrum coefficient generalized for a linear mode.

Then, the across wind load distribution on the building obtained from M_c using linear distribution of loads as:

$$F_{z,c} = \left(\frac{3M_c}{h^2} \right) \frac{z}{h} \quad (4)$$

5. Soil Stratum Idealisation

Three types of clayey sand c - ϕ soil were considered for the analyses and these include soft, medium and hard clayey sand which shall be designated as S, M and H respectively. The compressibility of underlying soil stratum was idealized using Drucker Prager model. The bedrock was assumed to be at a depth of 30m below the soil stratum. The lateral boundaries of the supporting soil medium are taken as four times the respective lateral dimensions of the raft for which the response as static load is expected to be died out [18]. This leads to a finite domain for the soil which was modelled similar to the structure. The structural system was analysed based on direct method of SSI. The properties of the soil stratum chosen are listed in Table 3. The analysis in which soil structure effect is ignored will be designated as fixed base.

Table 3. Properties of soil stratum [2, 19]

Designation of soil	Cohesion, C (kN/m ²)	Elastic modulus, E_s (kN/m ²)	Poisson's ratio, μ	Unit weight, γ (kN/m ³)	Angle of friction, ϕ (°)
S	50	50×10^3	0.3	1.6	32
M	100	100×10^3	0.25	1.8	34
H	200	150×10^3	0.2	2	48

6. Finite Element Analysis (FEA)

The integrated building-foundation-soil system was analysed using FE method. The types of elements used are shown in Fig. 7.

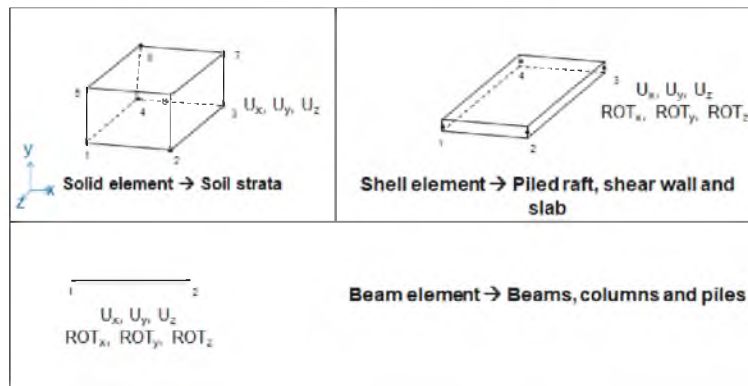


Fig 7. Elements used for FEM

Using FEM, modal analysis was performed to find the frequency of the building for calculating the wind forces. The columns were meshed to an element aspect ratio of three while beams, raft and slabs were meshed to an element aspect ratio of 2.5. The piles and the soil stratum were meshed to an element aspect ratio of ten. The FEM model of the building and the integrated building-foundation-soil structure is shown in Fig. 8 and Fig. 9 respectively. Isometric view of the piled raft foundation and the enlarged view of pile are shown in Fig. 10. The base and lateral boundaries of the soil stratum were constrained in all degrees of freedom. Free vibration analysis was performed to obtain the fundamental frequencies of the building for wind load computation. Then, the wind forces computed as per IS 875 (Part 3): 2015 were applied as point loads at every floor level. The responses in terms of maximum deflection and base moment of the non-linear structure considering SSI were compared with that of the linear structure with fixed base in order to assess the effect of SSI.

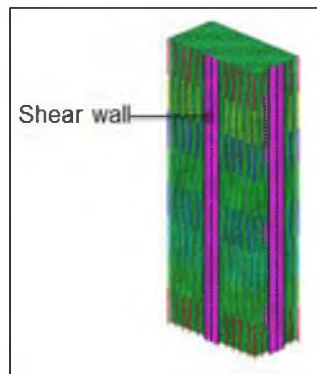


Fig. 8. Isometric view the building

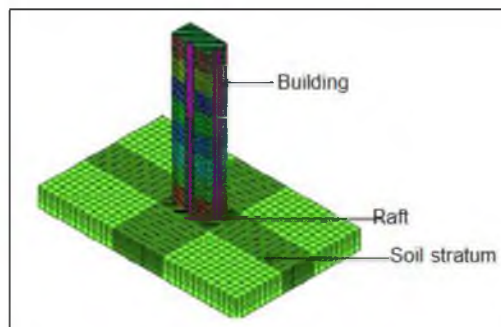


Fig. 9. Isometric view the integrated building-foundation-soil structure

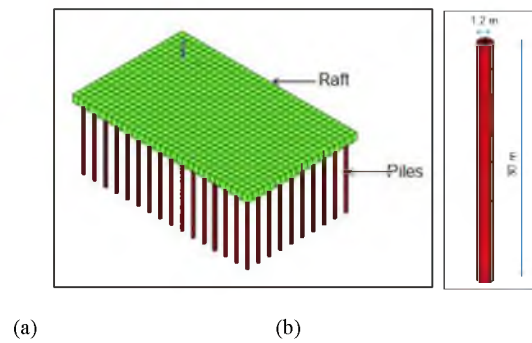


Fig 10. Isometric view of foundation (a) Piled raft, (b) Enlarged view of one pile

7. Results and Discussion

In order to investigate the effect of SSI on wind responses of a tall building, FEA was conducted on the 180m high building-foundation-soil system. The along and across wind loads acting on the building for long body and short body orientation was computed as per IS 875 (Part 3): 2015. The base moment obtained are shown in Table 4. It was observed that the along and across wind forces acting on short body orientation were greater than that for short body orientation and hence response to wind in short body orientation was considered for analysis.

Table 4. Base moment as per IS 875 (Part 3): 2015

Base moment (kNm)	Long body orientation	Short body orientation
Along wind induced	3.10×10^6	6.42×10^6
Across wind induced	6.84×10^5	7.92×10^5

Across wind induced base moment were found to be lesser than the along wind induced base moment by 78 and 88% for long and short body orientation respectively. Hence along wind loads corresponding to the short body orientation (at a wind angle of 90°) shall be considered as the governing wind load for the building considered.

The along and across wind loads were applied as point loads to the integrated building-foundation-soil system for FEM analysis. Free vibration analysis was conducted to assess the effect of SSI on modal frequencies. The responses in terms of maximum lateral deflection and base moment variations were assessed and compared with respect to the conventional analysis in which SSI effect is ignored. Normalised responses which is the ratio of response by the structure considering SSI to that of the structure without SSI is being used to express the effect of SSI.

7.1. Variation of frequency

Free vibration analysis was conducted to analyse the effect of SSI on modal frequency of the building. The modal frequencies corresponding to first three modes under varying conditions of flexibility are tabulated in Table 5. The natural frequency is corresponding to the first mode is found to be reduced more compared to the other two modes on considering SSI. For all the type of soil strata considered, natural frequency becomes 0.94 times that of the fixed system. It is observed that frequency decreases with increase in flexibility of the structural system. The maximum variation of frequency from that of the fixed base was seen when founded on soft soil strata 'S'. This might be because as the flexibility of the system increases, number of vibrations increases thereby increasing its time period and hence frequency of vibration decreases.

Dynamic behaviour of a building is dependent on its frequency. Overestimations of frequencies without considering SSI while designing for lateral loads may affect the structural stability and serviceability especially when dampers which require tuning are used. Hence, the effect of SSI should be considered in free vibration analysis.

Table 5. Frequency

Structure-soil system	Mode 1	Mode 2	Mode 3
S	0.248	0.272	0.312
M	0.249	0.274	0.313
H	0.250	0.275	0.314
Fixed	0.265	0.287	0.325

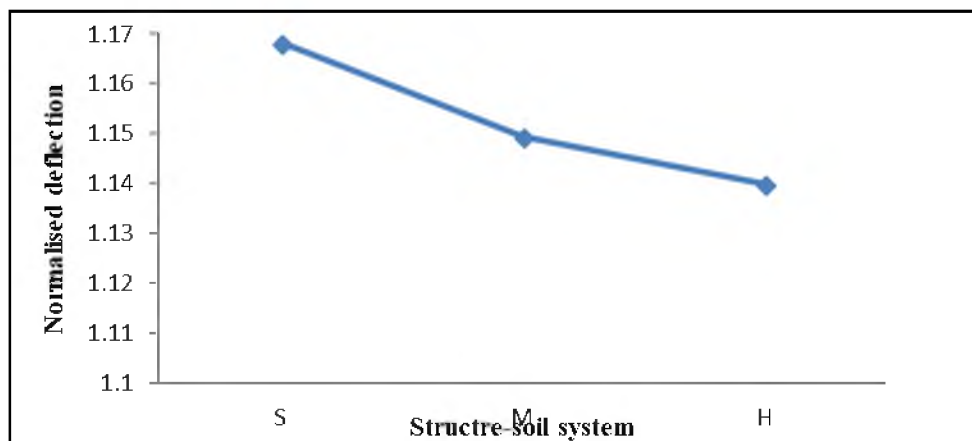
7.2. Variation of maximum lateral deflection

The maximum deflection for along wind and across wind loads were obtained from FEM analysis. These deflections were found to be increased with increase in flexibility. The variation of deflection with varying conditions of soil flexibility is shown in Table 6. The along wind induced deflection is found to be greater by 74% compared to the across wind induced response for all the structure-soil system. This may be because the across wind forces acting on the building is much less than the along wind forces. Hence responses corresponding to along wind loads shall be assessed to investigate the effect of SSI.

Upon considering SSI effect, the maximum variation in deflection compared to the fixed base system was found to be for the soft soil strata. The deflection got increased by 17, 15 and 14% of that of the fixed base system for the soil strata types S, M and H respectively. The variation of normalised along wind induced maximum deflection is shown in Fig. 10. It can be observed from the figure that on considering SSI effect, the wind induced deflection becomes almost 1.2 times that of the building system without SSI for all the types of soil strata considered. This increase in deflection owes to the flexibility incorporated on considering the SSI effect.

Table 6. Maximum lateral deflection

Structure-soil system	Maximum lateral deflection (m)	
	Along wind induced	Across wind induced
S	0.251	0.066
M	0.246	0.065
H	0.244	0.064
Fixed	0.214	0.056

**Fig.10.** Normalised maximum deflection

7.2 Variation of base moment

The base moment induced by along wind force was considered for assessing the effect of SSI. The base moment was found to be decreased with increase in flexibility. On considering SSI, base moment got reduced by 86, 85 and 78% of that of the system without SSI effect for the soil strata types S, M and H respectively. The variation of the normalised base moment is shown in Fig. 11. On considering SSI, base moment was found to be 0.14 times that of the fixed base system when founded on lower strength soil strata types and 0.22 times of the fixed base system when founded on hard strata. Thus SSI effect was found to be conservative in case of base moment. It may be due to the stiffness offered by the piled raft foundation.

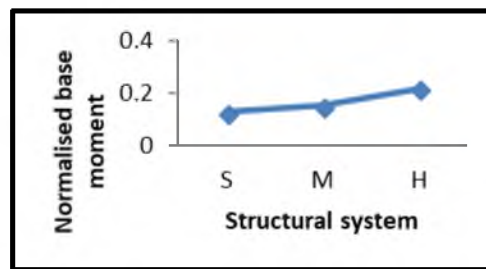


Fig. 11. Normalised base moment

8. Conclusions

To assess the effect of SSI on wind responses of tall buildings, FEM analysis was conducted on 180m high building with piled raft foundation founded on three types of soil conditions. The wind loads calculated as per IS 875 (Part 3):2015 were applied as point loads at every floor level to compare the responses with and without considering SSI. On comparing the variation of various responses of integrated structure-soil system with respect to the structure system without SSI, the following conclusions can be made.

- (i) Modal frequency decreases with increase in flexibility of the soil strata.
- (ii) The maximum lateral deflection was found to be 1.2 times that of the building without effect. Hence SSI effect is significant in the case of deflection response.
- (iii) On considering the SSI effect, the base moment of the building got reduced by 86-78% of that of building which ignores SSI effect.

Hence for the better optimised performance of the structure, effect of SSI should be considered in the design phase.

References

1. Bhandari, N. M., Krishna, P., Kumar, K and Gupta, A.: A Handbook of on Proposed IS 875 (Part 3) Wind Load on Buildings and Structures, IITK, (2003).
2. Bowles, J. E.: Foundation analysis and design, McGraw Hill Companies International Edition, fifth edition, Singapore, (1997).
3. Farr, H and Clifton, T.: Significance of considering soil-structure interaction effects on seismic design of unbraced building frames resting on soft soils, Australian Geomechanics, 51 (1), 55-65, (2016).
4. Mengke, L., Xiao L., Xinzheng, L and Lieping, Y.: Influence of soil-structure interaction on seismic collapse resistance of super-tall buildings, Journal of Rock Mechanics and Geotechnical Engineering, 6, 477-485, (2014).
5. Tabatabaiefar, H. R and Massumi, A.: A simplified method to determine seismic responses of reinforced concrete moment resisting building frames under influence of soil-structure interaction, Soil Dynamics and Earthquake Engineering, 30, 1259-1267, (2010).
6. Jayalekshmi, B. R., Jisha, S. V., Narayana, S and Shivashankar, R.: Effect of dynamic soil-structure interaction on raft of piled raft foundation of chimneys, ISRN Civil Engineering, 2014, 1-11, (2014).
7. Venanzi, I., Salciarini, D and Tamagnini, C.: The effect of soil-foundation-structure interaction on the wind-induced response of tall buildings, Engineering Structures, 79, 117-130, (2014)
8. Liu, M. Y., Chiang, W. L., Huang, J. H and Chu C.: Wind-induced vibration of high-rise building with tuned mass damper including soil-structure interaction, Journal of Wind Engineering and Industrial Aerodynamics, 96, 1092-1102, (2008).
9. Halabian A. M., El Naggat M. H and Vickery, B. J Reliability analysis of wind response of flexibly supported tall structures, Structural Design of Tall and Special Buildings, 12, 1-20, (2003).
10. Galsworthy, J. K and El Naggat, M. H.: Effect of foundation flexibility on the across- wind response of reinforced concrete chimneys with free-standing liners, Canadian Geotechnical Journal, 37, 676-688, (2000).
11. Xu, Y. L. and Kwok, K. C. S.: Wind-induced response of soil-structure-damper systems, Journal of Wind Engineering and Industrial Aerodynamics, 41-44, 2057-2068, (1992)
12. Novak, M. and Hifnawy, L. E.: Structural response to wind with soil structure interaction, Journal of Wind Engineering and Industrial Aerodynamics, 28, 329-338, (1988).
13. IS 2911 (Part 1/Sec 1): 2010, Code of practice for design and construction of pile foundations- Part 1: Concrete piles, Section 1: Driven cast in-situ concrete piles (Second revision), Bureau of Indian Standards, New Delhi, India
14. I.S:456 2000, Plain and Reinforced Concrete - Code of Practice, Bureau of Indian Standards, New Delhi, India
15. I.S: 875 (Part-1) 1987-Re:2008, Code of practice for the design loads (other than earthquake) for buildings and structures- Part 1: Dead loads-unit weights of building materials and stored materials (second revision), Bureau of Indian Standards, New Delhi, India

16. I.S: 875 (Part-2) 1987, Code of practice for the design loads (other than earthquake) for buildings and structures- Part-2, Imposed loads (Second revision), Bureau of Indian Standards, New Delhi, India
17. I.S: 875 (Part-3) 2015, Code of practice for the design loads (other than earthquake) for buildings and structures (Part-3, Wind loads), Bureau of Indian Standards, New Delhi, India
18. Wolf, J. P.: Dynamic Soil Structure Interaction, Prentice- Hall, INC., Engelwood Cliffs, 1985
19. Carter, M. and Bentley S. P.: Correlations of soil properties, Pentech Press Ltd., London, 1991

Eco- Friendly Cement Blocks

Arathy K Chandran.*, Aiswarya.A*, Irfana.S*, U.Jayanarayanan* and

Ms.Anjana Krishnan**

*B. Tech Student, Department of Civil Engineering,
Mar Baselios College of Engineering and Technology, Nalanchira, Thiruvananthapuram, Kerala - 695 015 Corresponding
author,email -arathykchandran03@gmail.com.

**Assistant Professor, Department of Civil Engineering,
Mar Baselios College of Engineering and Technology, Nalanchira, Thiruvananthapuram, Kerala - 695 015, gmail -
anjana.mbcet@gmail.com

Abstract

Eco friendly Cement Blocks (ECB) consists of plastic bottle bricks (plastic bottles filled with waste materials) which are cast in 1:3 cement mortar. ECBs offer solution to the problem of plastic waste disposal and scarcity of construction material. It can be used as a substitute for normal bricks and hollow bricks. ECBs are very cheap since it uses mostly waste materials and has a simple manufacturing process. A single ECB is capable of replacing nine normal bricks with respect to its size. This reduces the time and cost of construction. The objective of this paper is to check the feasibility of using ECB as a substitute to conventional bricks. Compressive strength tests are conducted on ECBs with different orientation of bottles, size of bottles used and reinforcement within bottles. It is seen that compressive strength is max for ECBs filled with alternate layers of one litre bottles placed parallel to the mould. Finally a wall specimen was constructed and tested. The compressive strength of wall specimen falls well within the limits specified for its use in a masonry structure.

Key words: Eco-bricks, waste PET bottles, construction material, masonry structures.

Introduction

Ecofriendly Cement Blocks (ECB) are cement blocks made of discarded plastic bottles which are filled with compacted waste materials. It can be used as a substitute for normal bricks, hollow bricks etc. ECB solves mainly two major issues of plastic waste disposal and scarcity of construction materials (bricks). ECB is very cheap since it is made with waste materials and has a simple manufacturing process. A single block is capable of replacing a minimum 6 normal bricks with respect its size

which reduces the cost of construction to a great extent. ECB can be used for constructing retaining walls, check dams, canal walls etc.

Plastic is a non-bio-degradable substance which takes thousands of years to decompose hence creating land

pollution as well as water pollution. Taking into account the increase in pollution, new concept of

eco bricks has been introduced. These bricks are manufactured by using the non-biodegradable wastes such as plastic bottles, plastic bags and other non-biodegradable substances. Use of such bricks helps in reducing the overall cost of the buildings. Chlorinated plastic can release harmful chemicals into the surrounding soil, which can then seep into groundwater or other surrounding water sources and also the ecosystem. This can cause serious harm to the species that drink the water. Components of plastics currently being studied for their health effects include polyhalogenated flame retardants, poly-fluorinated compounds (known as PFOS or PFOA) and microbial compounds such as triclosan and trichlorocarban.

ECBs are low cost, non-brittle, Bio climatic, re-useable, easy to build, absorbs abrupt shock loads, green construction and uses less construction material. But it is non-decomposable and non-destructible. On melting it releases a compound gas which is very harmful to the health and environment and it weakens the ozone layer. Most of the plastic is produced from oil which is a scarce resource. But these disadvantages can be reduced by recycling of the plastic waste and promoting renewable plastic. ECBs can be used for the construction of culverts, Drainage lining, columns for supporting roofs and waiting shed, Interlocking Block Paver and bench.

The main objective of this paper is to study the strength of eco-friendly cement blocks in comparison with conventional bricks and to evaluate the compressive strength of ECB made using three layers of one litre plastic bottles. This paper also aims to find out the optimum orientation of one litre bottle bricks in the ECB with respect to its compressive strength and to estimate the load carrying capacity of an ECB wall.

This study is limited to the usage of C&D waste, fabric waste and locally available soil as filler materials for plastic bottles. Only one litre plastic bottles are studied. ECBs with only three layers each of 3 bottle bricks each are studied.

A number of experimental investigations have been conducted in recent years on usage of plastic bottles in construction field. Manisha et al. (2016) investigated the properties of waste plastic bottles like density, solubility, resistance to chemicals etc. in order to find the compatibility of materials used along with plastic bottles. The strength of individual materials used as fillers were also studied.

Kansal et al. (2014) studied the strength of bottle bricks by conducting various experiments like compression test on single bottle etc. and concluded that no curing time is required if waste PET bottles are used as building material as compared to bricks which require 28 days curing time. Also while baking of bricks there is a major issue of carbon emission which is negligible in using PET bottles. PET bottles generally have a durability of over 300 years which is more as compared to standard bricks. Cost of construction in case of brick bottle is more economical than standard bricks. Weight of a unit bottle brick was found to be less than that of a standard brick. Compressive strength of the bottle brick is also nearly equal than that of a standard brick. The concept of brick bottles is cost effective, energy efficient and commercially feasible. Using PET bottles is also bio-climatic and it is a Green construction.

Wankhade et al. (2017) concluded that the strength of bottle brick equalizes with normal bricks. The insulation properties of bottle bricks are much better than conventional bricks. He also concluded that thermal comfort can be provided to the

residents those who cannot afford heating and cooling appliances by constructing houses from eco bricks. This will help in providing shelter to the poor people in India. They also said that bottle bricks are nearly 20 times stronger than the baked bricks.

Singh et al. (2017) mentioned that the construction cost of plastic bottle bricks is very cheap when compared to the construction with the baked bricks. They have shown a profit of Rs.5 in each brick. They also concluded that the weight of the bottle brick is very less than the baked brick. Pratima et al. (2016) investigated that the plastic bottles are cheaper in comparison to bricks.

clear cover was provided all around. Once the first layer had been placed, three same sized (1000ml) mix filled plastic bottles were placed on this first layer of mortar. Then another layer of mortar is placed in the mould covering them evenly. The second and third layers of bottles were placed similarly with cement mortar in between the bottles. The step by step process in which a total of nine bottles are inserted into the mould is shown in Figure 1.



Layer 1

Layer 2

Layer 3

Figure 1: Casting of ECB



Figure 2: Casted ECB

Methodology

Materials and Experimental Methods

The materials used for the experimental program are locally available soil, fabric waste, and construction and demolition waste. The optimum mix proportion was found by conducting tests on specific gravity, void ratio test and value obtained is 1:1:7 (weight proportion).

Preparation of plastic bottle bricks

Waste plastic bottles of same capacity were collected and washed. The filler mix was filled into these bottles in five layers; each layer compacted with 25 blows using tamping rod.

Preparation of Eco-friendly cement Blocks (ECB)

Wooden mould (28cm × 28cm × 25cm) were made to prepare the ECB. The cement mortar for the ECB were made of 1:3 (65%Puzzalona Portland cement & 35% fly ash: sand) by weight with a water cement ratio of 0.5. A 2 cm thick

Compressive strength test of plastic bottle bricks

A Compression testing machine of 2000 kN capacity was used for compression test. The brick was placed between loading plates of the machine. The load was applied gradually. The first crack that appears on the plastic bottle brick was considered as the failure point. The ultimate load was recorded and compressive strength of plastic bottle brick was obtained by

$$\text{Compressive strength} = \frac{\text{Maximum Load (N)}}{\text{Cross Sectional Area (mm}^2\text{)}}$$

Compressive strength test of ECB

Compressive strength is tested on the specimen of size 28 x 28 x 25mm at the age of 7, 14 and 28 days as per IS 516:1959. Three cube samples were cast. After curing, the cube specimens were placed in 1000kN Compression Testing Machine and loaded to failure.

Orientation Test

This test was conducted in order to find the optimum possible orientation of laying plastic bottles to achieve maximum compressive strength. In this test mainly two types of orientation are studied. The first orientation is obtained by laying bottles parallel to mould in the first layer. In second layer the bottles are placed in perpendicular to mould. Again the third layer is placed parallel to the mould. The second orientation is obtained by laying all the three layers parallel to the mould. After the casting of these specimens, the specimens were kept for curing for 7 days. Then compression test was conducted.

Capacity of Bottle Test

This test was conducted to study whether the capacity of bottles affect the compressive strength of ECB. For this mainly two types of bottles are used i.e., 1000ml plastic bottles and 600ml plastic bottles. In both the cases the size of specimen, number of bottles, number of layers and number of bottles per layer were kept constant. These specimens were cured for 7 days. Compression test was conducted after curing period.

ECB – Masonry Structure

The dimensions of wall specimen constructed was 0.86m x 1.15m x 0.3 m. Plastering provided was 2 cm all around the specimen. The wall specimen constructed was placed on loading frame in such a way that the position of hydraulic jack is at the center of gravity of specimen. An I-section was placed on top of specimen for uniform distribution of load throughout the specimen. Load is applied through load cell from hydraulic jack and load is recorded automatically. Load is applied manually by using hydraulic jack.



Figure 3: Construction of Wall

Results

Compressive strength test of plastic bottle bricks

The bottle was placed between the between loading plates of the machine. The bottles didn't break but did deform. The load was increased until the reading showed a sudden drop of force. The load at which it started to drop was recorded as the maximum load.

The ultimate load = 180 kN

Area of bottle = 62407.5mm²

Compressive Strength = 9.2 N/mm²

Compressive strength of a masonry brick is only found to be 3.5 N/mm². Hence the strength of a waste filled bottle itself proves to be higher than the normal conventional brick.



Figure 4 : Testing of Bottle brick



Fig 5 : Bottle before testing Fig 6: Bottle after testing

Compressive strength test of ECB

The test was performed according to IS 516: 1959. Compressive strength test were performed on ECBs after curing of 7 days, 14 days and 28 days. The results obtained are:

Table 1: Result of ECB compression test

Specimen	7 th day		14 th day		28 th day	
	Load (kN)	Strength (N/mm ²)	Load (kN)	Strength (N/mm ²)	Load (kN)	Strength (N/mm ²)
1	185	2.3	245	3.1	418	5.3
2	180	2.3	240	3.1	410	5.2
3	187	2.4	249	3.2	423	5.4
Average compressive strength		2.3		3.1		5.3

Orientation test

Plastic bottles which are placed in different orientation were tested for compressive strength and were compared with normal ECB. In this case, all bottles are placed parallel to the mould.

Table 2 : Results for Orientation test

Specimen	Orientation	
	All layers parallel to mould	Alternate layers parallel to mould
No of bottles	9	9
No of layers	3	3
Load maximum (kN)	150	185
Average compressive strength, N/mm² (7 days)	1.913	2.360

From the strength results of both orientation it is found that alternate layers of bottles placed parallel to the mould, will have more strength than all layers placed parallel to the mould. This shows that when all layers laid parallel to the mould the specimen will fail suddenly.

Capacity of bottle test

ECBs made of 600 ml and 1000 ml bottles were tested for compressive strength and following results were obtained.

Hence from the results it is found that ECBs made of higher capacity bottles will have more strength. This shows that the compressive strength of ECB is independent of thickness of bottle and purely based on the compaction mix. As the size of the bottle increases, the strength also increases. Thus it is better to use 1000 ml bottle made ECB for construction purpose.

Table 3: Results for Capacity of bottle test

Specimen	Capacity of plastic bottles used	
	600ml	1000ml
No of bottles	9	9
No of layers	3	3
Load maximum (kN)	114	185
Average compressive strength, N/mm ² (7 days)	1.454	2.360

ECB – Masonry Structure

The load was applied axially on specimen using hydraulic jack, through load cell. The load at which initial crack occurred was noted. The ultimate load is also recorded directly using load cell apparatus. The dimensions of the specimen were known.

Self-Weight of I-section = 0.6 kN

Load at which initial crack occurs = 116.2 kN

Ultimate load capacity = 288.8 kN

Face area on which load is acting = $0.3 \times 0.54 = 0.162 \text{ m}^2$

Compressive strength of specimen = 1.78MPa



Figure 7: Failure mode of wall

The compressive strength obtained is greater than the minimum allowable compressive strength of masonry structures. Thus ECB wall can be used as load bearing structure.

Conclusions

The compressive strength of a single ECB of size $28 \times 28 \times 25 \text{ cm}$ was found to be $5.318/\text{mm}^2$. The optimum orientation of plastic bottle bricks in ECB is an arrangement with alternate layers placed parallel to the mould. ECBs with 1000ml bottle bricks have a higher strength than those with 600ml bottle bricks which clearly shows that the bottle bricks are efficient in load transmission. Testing of wall specimen yielded a compressive strength of 1.78 N/mm^2 which shows the suitability of ECB as a load carrying member [4]. The cost of a single block of ECB was calculated and it is found to be less when compared to conventional bricks. Therefore ECB can be used for constructing low cost housing, retaining walls, paver blocks etc.

References

- [1] Patel.A.P,Shah.A,Patel.H(2016),“Waste Plastic Bottles Offering Innovative Building Materials With Sustainable Application”, *International Journal of Innovative and Emerging Research in Engineering*, Volume 3(3), pp 38-45
- [2] Goyal.N, Manisha(2016),“Constructing Structures using eco-bricks”, *International Journal of Recent Trends in Engineering & Research*, Volume 2(4), pp 159-164
- [3] Rawat.A.S, R. Kansal (2014), “PET Bottles as Sustainable Building Material: A Step towards Green Building Construction”, *Journal of Civil Engineering and Environmental Technology*, Volume1 (6), pp 1-3
- [4] Investigating the compressive strength of plastic bottles as masonry, KalumireKusimwiragi, A report submitted in part requirement for the degree of Bachelor of Environmental Design with Honours, Faculty of the Built Environment, Uganda Martyrs University, June, 2011.
- [5] Pandey.S.P, Gotmare.S,Wankhade.S.A (2017), “Waste Plastic Bottle as Construction

- Material”, *International Advanced Research Journal in Science, Engineering and Technology*, Vol. 4, Special Issue 3,pp 1-6
- [6] Rawat.A.S, ,Kansal.R (2014),“PET Bottles as Sustainable Building Material: A Step TowardsGreen Building Construction”,*Journal of Civil Engineering and Environmental Technology*,Volume 1(6), pp. 1-3
- [7] Dakwale.V.A,Ralegonkar.R,(2014),“Development of sustainable construction material using construction and demolished waste”, *Indian Journal of Engineering and Material Science*, Vol.21, pp 451-457

Effect of Steel and Polypropylene Fibre on the Tension Stiffening of Ultra High Performance Concrete

Lijina Thomas¹ and Jithin J S²

¹PG Research Scholar, Structural Engineering, Mar Baselios College of Engineering and Technology,
Thiruvananthapuram, Kerala, India
lijinathomas2017@gmail.com

²Asst. Professor, Department of Civil Engineering, Mar Baselios College of Engineering and Technology,
Thiruvananthapuram, Kerala, India
jithinjs003@gmail.com

Abstract. Tension stiffening is one of the important properties of concrete that reduces the strain in steel and leads to reduction in width and spacing of cracks in reinforced flexural members. The tensile strength of concrete between cracks in a reinforced concrete member represents the tension stiffening effect. Several attempts have been made in the past to improve the tension stiffening effect of conventional concrete by adding short discrete fibre in the matrix, but a few studies have been conducted to find out the tension stiffening effect of steel fibre and polypropylene fibre on the cracking behaviour of ultra high performance concrete. So this study investigates the effect of metallic fibre (crimped steel) and non metallic fibre (polypropylene fibre) on tension stiffening characteristics and the cracking behaviour of ultra high performance concrete. The variables included in this study are volume fractions of crimped steel fibre (0.25, 0.5%, 0.75% and 1%) and polypropylene fibre (0.1, 0.15 and 0.2) The optimum content of steel fibre and polypropylene fibre and their effect on the tension stiffening and cracking behaviour is finding out by studying the load deformation behaviour, crack width, crack spacing and crack pattern of the prismatic tension specimen subjected to uniaxial tension.

Keywords: Ultra high performance concrete, Load-deformation behaviour and Tension stiffening bond factor

1. Introduction

Although concrete is the most universally used material in building there are still some limitations to its use, such as tensile strength and brittleness. Ultra high performance concrete is a type of concrete (UHPC), may able to overcome these concerns. The concept of UHPC was first developed by Richard and Cheyrezy and was produced in the early 1990s at Bouygues laboratory in France [1, 2]. UHPC consists of a combination of Portland cement, fine silica sand, silica fume, quartz flour, high-range water reducer and discontinuous internal steel or organic fibers. Depending on the application, different combination of these materials may be used [3, 4]. Addition of fibres improves the engineering properties of concrete like ductility, post crack resistance, energy absorption capacity etc. Thus addition of fibres in cement concrete matrix bridges these cracks and restrains them from further opening. UHPC offers more than 150MPa compressive strength and greater than 5Mpa post cracking tensile strength [1, 5]. Compressive strength and modulus of elasticity of UHPC was 3 to 4 times greater than normal strength concrete according to Mohamadreza S. studies [2]. Hannawi K. (2016) investigates the effect of adding different type of fibres (steel, mineral and synthetic fibers) on the microstructure and the mechanical behaviour of UHPC. Results show that the fibre has a relatively slight influence on the compressive strength and elastic modulus of concrete except for steel fibre which improves the strength because of its intrinsic rigidity. Among the steel fibre crimped and twisted fibres gives better performance. The addition of steel fibres generally contributes towards the improvement of an energy-absorbing mechanism whereas the non-metallic fibre such as polypropylene fibre plays a vital role in delaying the formation of micro cracks [6].

Because of its weakness in tension, concrete is reinforced by steel bars which can carry tensile forces across the cracks after tensile failure of concrete. With tensile reinforcement, concrete can transfer tensile stresses across cracks as the result of bond action between concrete and reinforcement. Consequently, concrete can still carry a part of tensile force even if cracks are induced into RC element and tensile stress carried by RC element as a whole becomes superior to that carried by only bare steel bars at the same deformation. This phenomenon is called tension

stiffening effect. Due to tension stiffening effect of concrete, the free elongation of steel under tension is prevented. This led to reduction in crack width and improves the serviceability of the structure [8, 11]. Tension stiffening would prevent free elongation of steel under tension and hence reduces the crack width in concrete. Finer cracks would prevent the entry of moisture and CO into the cracks and thus prevents corrosion and carbonation in concrete.

There are many studies in UHPC with micro and macro steel fibres of different type and aspect ratio. The tension stiffening effect can be used as post-cracking stress-strain response of the reinforced concrete. Several attempts have been conducted to find out the tension stiffening effect of conventional and other concrete by adding short discrete fibres in the matrix. But only few studies have been conducted to find out the tension stiffening effect of ultra high performance fibre reinforced concrete. The effect of adding steel fibres (crimped steel fibre) and polypropylene fibre on the cracking behaviour of UHPC was investigated in this study. The main aim of this study is to investigate the effect of metallic (crimped steel fibre) and non-metallic (polypropylene fibre) on the tension stiffening characteristics and the cracking behaviour of Ultra High Performance Concrete (UHPC).

2. Experimental Program

The experimental work consisted of casting and testing reinforced concrete prismatic tension members with dimensions of 60 x 60 mm x 600mm and it was axially reinforced with a 10mm diameter high yield strength deformed steel bar with a reinforcement ratio of 2.18%. The reinforcement bar was extended 200mm on either side for proper gripping in the testing equipment as shown in figure 1. The variable includes the volume fraction of crimped steel fibres (0.25%, 0.5%, 0.75% & 1%) and volume fraction of polypropylene fibres (0.1%, 0.15% & 0.2%).

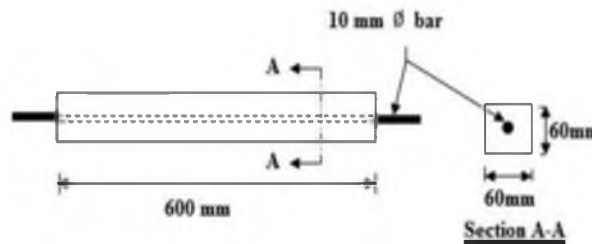


Fig 1. Specimen details

2.1 Materials Used

Ordinary portland cement (53 grade) conforming to IS: 12269-1987 (reaffirmed 2004)[13], 75% of fine aggregate passing through 600µm and retained on 300µm, 25% of fine aggregate passing through 300µm and retained on 150µm conforming to [383- 1970 (Reaffirmed 2002) [14], IS 2386 (Part III) - 1983 (Reaffirmed 2002)[15]], silica fume, glass powder and superplasticizer were used for the investigation. The mix proportion for UHPC is selected from the optimum mix obtained from the trial mixes conducted in previous study [12]. The cube compressive strength and prismatic specimen(60mm x 60mm x 600mm) for uniaxial tension test is to be casted and cured in water. The details of tested specimens and variables are given in table 3

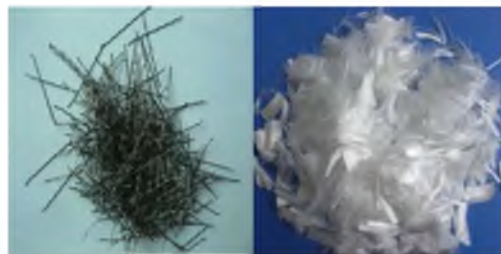


Fig 2. Steel fibres Fig 3. Polypropylene fibres

Table 1. Properties of fibres

Type of fibre	Crimped steel fibre	polypropylene fibre
---------------	---------------------	---------------------

Length, mm	30	12
Diameter, mm	0.5	0.8
Aspect ratio	60	15

Table 3. Details of specimens and variables

Specimen designation	Volume fraction of fibres %		No. of Specimens
	Steel	Polypropylene	
C	0	0	3
S ₀ P _{0.10}	0	0.10	3
S ₀ P _{0.15}	0	0.15	3
S ₀ P _{0.20}	0	0.20	3
S _{0.25} P ₀	0.25	0	3
S _{0.50} P ₀	0.50	0	3
S _{0.75} P ₀	0.75	0	3
S ₁ P ₀	1	0	3

2.2 Testing of specimens

The specimens of each steel fibre reinforced UHPC mixes and polypropylene fibre reinforced UHPC mixes were tested under uniaxial tension in a Universal Testing Machine (UTM) with a capacity of 1000 kN. The axial elongation of the specimen was monitored by a Linear Variable Differential Transducer (LVDT). The location of each crack is to be marked on the specimen immediately after its appearance during the test. The crack spacing was measured along the centreline of the front face of specimen. Crack widths were measured along the specimen at regular intervals using a crack detection microscope. The load-control condition and contained until yielding occurred. One longitudinal reinforcement bar was also tested under the same loading condition to obtain the response of the bare bar. For each mix, three specimens were cast and test. The average values of three results are to be taken as the final value. Figure 4 shows the test setup.

**Fig. 5.** Casting of prismatic specimen



Fig 4. Test setup

3. Results and Discussion

3.1 Load Deformation Behaviour

The axial load-deformation behaviour of the specimen was obtained by plotting the axial load against member strain. The load deformation behaviour of all the specimens was linear up to first crack load. All the specimens showed a higher initial stiffness compared to bare steel bar. Figure 5 & 6 shows the axial load-deformation behaviour of different steel fibre and polypropylene fibre reinforced UHPC specimens. All the fibre reinforced specimens showed a higher stiffness compared to normal UHPC and bare steel bar. Also there was a considerable increase in the stiffness with increase in fibre content. Maximum stiffness was observed in that specimen with steel fibre content of 0.75% and polypropylene fibre content of 0.15%. Specimen with steel fibre content of 0.75% exhibited the maximum first crack load and yield load. The specimen with 0.75% steel fibre content to have higher number of smaller cracks than to have smaller number of wider cracks compared to other steel fibre reinforced UHPC mixes. Similarly among the polypropylene fibre reinforced UHPC mixes 0.15% polypropylene fibre content mixes have higher number of smaller cracks. It may be due to the ability of UHPFRC to carrying tensile stresses at the cracks and the between cracks.

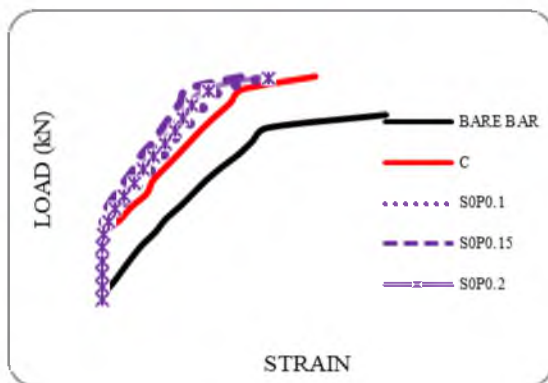


Fig 6. Load deformation behaviour of steel fibre reinforced UHPC

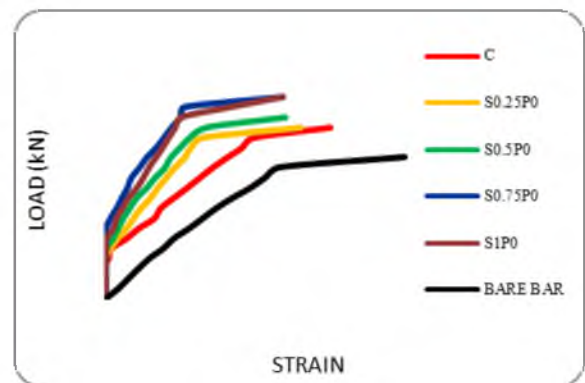


Fig 7. Load deformation behaviour of polypropylene fibre reinforced UHPC

Table 4. Test results

Designation	First crack load (kN)	Yield load (kN)	Crack spacing (cm)	No. of cracks
C	17.5	40.69	9	6
S ₀ P _{0.10}	18	42.02	7.1	8
S ₀ P _{0.15}	21.4	42.33	4.94	9
S ₀ P _{0.20}	20.2	42.1	5.92	7
S _{0.25} P ₀	19.2	41.87	5.38	8
S _{0.50} P ₀	20	44.68	5.2	10
S _{0.75} P ₀	23.2	49.8	4.59	12
S ₁ P ₀	22	49.6	5.35	11

3.2 Tension stiffening bond factor (β)

The tension stiffening contribution of each mixture is represented by the tension stiffening bond factor, which is calculated by dividing P_{cm} with P_{cr} , where P_{cm} is average load carried by cracked concrete and is obtained by subtracting the bare steel response from the specimen responses, and P_{cr} is the load carried by concrete at first cracking [[11].

The above figure 8 & 9 shows the variation of tension stiffening bond factor of UHPC mix having different volume fractions of steel fibre and polypropylene fibre. An increase in the tension stiffening bond factor indicates an increase in the stiffness of the member. From the graph, all fibre reinforced specimens showed considerable tension stiffening effect compared to UHPC specimen. Also the bond factor increases with increase in the volume fraction of fibres up to optimum percentage variation of fibre content. The maximum tension stiffening bond factor was exhibited by the specimen with 0.75% steel fibre and 0.15% polypropylene fibre content. It may be due to the balling effect of fibres S₁P₀ and S₀P_{0.2} gives lesser bond factor values than S_{0.75}P₀ and S₀P_{0.15}. The average tensile strength in concrete increases even after the first crack, which leads to enhanced values of bond factor.

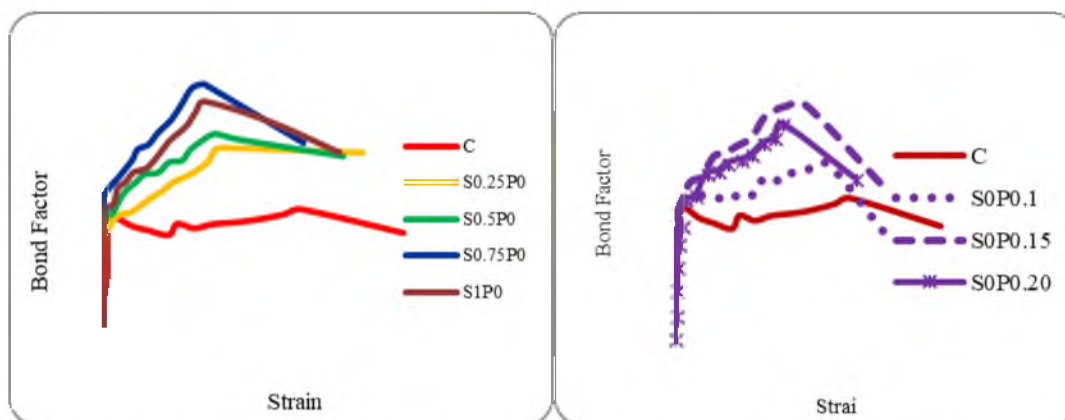


Fig 8. β of steelfibre reinforced UHPC

Fig 9. β of polypropylenefibre reinforced UHPC

3.3 Crack pattern, crack spacing and crack width



Fig 10.Crack pattern of steel fibre reinforced UHPC



Fig 11.Crack pattern of polypropylene fibre reinforced UHPC

Figure 10 & 11 shows the crack pattern of steel fibre and polypropylene fibre reinforced UHPC prismatic tension specimens subjected to uniaxial load. The first transverse crack appeared near the middle portion of the specimen. The first crack widened and additional cracks appeared as the load increased. On all sides of the specimen the development of cracks was not uniform. Also the longitudinal splitting cracks were appeared with transverse cracks. The number of transverse cracks increased and the spacing of cracks decreased with increasing fibre content. Maximum number of transverse cracks was obtained for UHPC specimen with 0.75% steel fibre and 0.15% polypropylene fibre content compared to other fibre reinforced UHPC specimens.

4. Conclusions

The tension stiffening and cracking behaviour of UHPC and fibre reinforced mixes were studied in this work. An optimum steel fibre and polypropylene fibre volume fractions were found out based on the tension stiffening and cracking behaviour of specimens subjected to uniaxial tension test. Based on the results of this study, the following conclusions are made:

- In steel fibre reinforced UHPC mix, the maximum tension stiffening and yield load is obtained for the mix with 0.75% steel fibre content, it may be due to good confinement effect of fibres and ability of UHPFRC to carrying tensile stresses at the cracks.
- 0.75% steel fibre content increases the yield load, compressive strength and first crack load by 18%, 3% and 25% respectively than normal UHPC mix
- In polypropylene fibre reinforced UHPC mix, the maximum tension stiffening and yield load is obtained for the mix with 0.15% polypropylene fibre content, it may be due to good confinement effect of fibres and ability of UHPFRC to carrying tensile stresses at the cracks.
- 0.15% polypropylene fibre content increase the yield load, compressive strength and first crack load by 4%, 1% and 18% respectively than normal UHPC mix.

References

20. Prabhat, R., P., B.H. Bharatkumar and Nagesh R., I.: Mechanical properties of ultra high performance concrete, *International Journal of Civil, Environmental, Structural, Construction and Architectural Engineering* 6, 670-675, (2012)
21. Mohamadreza, S., Mahsa, F. and Atorod, A.: Experimental and numerical study on mechanical properties of ultra high performance concrete (UHPC), *Construction and Building Materials*, 156, 402-411, (2017)
22. Chong, W., Changhui, Y., Fang, L., Chaojun, W. and Xincheng, P.: Preparation of ultra-high performance concrete with common technology and materials, *Cement and Concrete Composites*, 34, 538-544, (2012)

23. Benjamin, G. and Jussara, T.: Durability of ultra high performance concrete, *Journal of Materials in Civil Engineering*, 19, 848-854, (2007)
24. Doo, Y. Y., Sung, W. K. and Jung, J. P.: Comparative flexural behavior of ultra high performance concrete reinforced with hybrid straight steel fibers, *Construction and Building Materials*, 132, 219-229, (2017)
25. Hannawi, K., Hui, B., William, P. A. and Balaji, R.: Effect of different types of fibers on the microstructure and the mechanical behavior of ultra high performance fiber reinforced concretes, *Composites Part B*, 86, 214-220, (2016)
26. Petr, M., Radosav, S. and Tomas, V.: Experimental investigation of mechanical properties of UHPFRC, *Procedia Engineering*, 65, 14-19, (2013)
27. Bischoff, P. H.: Tension stiffening and cracking of steel fiber-reinforced concrete, *Journal of Materials in Civil Engineering*, 15, 174-182, (2003)
28. Caroline, S. R., Mayara, A., Pepe, M., Yao, Y., Mobasher, B. and Romildo, D.: Tension stiffening approach for interface characterization in recycled aggregate concrete, *Cement and Concrete Composites*, 20, 1-10, (2017)
29. Moreno, D. M., Trono, W., Jen, G., Ostertag, C., and Billington, S. L.: Tension stiffening in reinforced high performance fiber reinforced cement-based composites, *Cement and Concrete Composites*, 50, 36-46, (2014)
30. Ganesan, N., Indira, P. V. and Sabeena, M. V.: Tension stiffening and cracking of hybrid fibre reinforced concrete, *ACI, Materials Journal*, 110, 715-722, (2014)
31. Bindu, B. and Krishnan, H.: Development of ultra high performance concrete by normal curing method, *Proceedings of National Conference on Recent Trends in Computer Science & Engineering and Sustainability in Civil Engineering*, 2, 116-118, (2016)
32. IS 12269-1987 (Reaffirmed 2004), Indian Standard specification for 53 grade Ordinary Portland Cement, Bureau of Indian Standards, New Delhi, India, 1988
33. IS 383- 1970 (Reaffirmed 2002), Specification for Coarse and Fine Aggregates from Natural Sources For Concrete, Bureau of Indian Standards, New Delhi, India, 1970
34. IS 2386 (Part III) - 1983 (Reaffirmed 2002), Methods of test for aggregates for concrete, Bureau of Indian Standards, New Delhi, India, 1983.
35. IS 1608- 2005 (ISO 6892- 1998), Metallic Materials- Tensile Testing at Ambient Temperature, Bureau of Indian Standards, New Delhi, India, 2005

Development of Stress Block Parameters of Concrete with Metakaolin Admixed Recycled Concrete Aggregate

Shin Elizabeth Shaji¹ and Jithin J S²

¹PG Research Scholar, Structural Engineering, Mar Baselios College of Engineering and Technology,
Thiruvananthapuram, Kerala, India
shinelizabethshaji@gmail.com

²Asst. Professor, Department of Civil Engineering, Mar Baselios College of Engineering and Technology,
Thiruvananthapuram, Kerala, India
jithinjs003@gmail.com

Abstract. This paper deals with the evaluation of stress-block parameters for concrete with metakaolin admixed recycled concrete aggregate. An experimental investigation was carried out on the stress-strain characteristics of concrete by replacing 100% of coarse aggregate by recycled aggregate for varying design strength of 20 MPa and 30 MPa under increasing axial compression. As these recycled aggregate causes reduction in strength, mineral admixture was used to improve the properties of recycled aggregate. In this study, metakaolin was used by 2.5%, 5%, 7.5%, 10% and 12.5% of recycled aggregate and the optimum value of metakaolin was obtained as 10% in M20 and M30 mixes. A total of 18 cylinders were prepared to develop a stress strain model for concrete with metakaolin admixed recycled concrete aggregate. The results indicated that Saenz stress-strain model was applicable for concrete with metakaolin admixed recycled concrete aggregate and the proposed stress-block parameters could be used to determine the flexural strength of members made using above composites.

Keywords: Metakaolin, Admixed, Recycled concrete aggregate, Stress block parameters, Saenz model.

1. Introduction

Concrete is a major construction material and plays a crucial role in the improvement of infrastructures such as highways, bridges, buildings etc. It is estimated that the total annual concrete production over the world is more than 10 billion tons. The concrete industry alone uses 20 billion tons of aggregates, 1.5 billion tons of cement and 800 million tons of water [1]. The idea of the conservation of natural aggregate (NA) has been largely ignored despite the fact that coarse aggregates make up 40–50% of a concrete mix by volume while cement makes up about 10% [2]. Volume of cement and concrete production probably will continue to increase. The overexploitation of NA may reduce the resources to a crucial level, compromising the needs of future generation. Thus the necessity of conservation of NA leads to the use of recycled concrete aggregates (RCA) and this may provide sustainable development. RCA has lower compressive strength, less stiffness, increased creep, increased shrinkage, weak interfacial transition zones, high porosity, high levels of sulphate and chloride contents, impurities, poor grading, and lower quality as compared to NA concrete. Mineral admixtures can be successfully used as partial replacement of cement in order to mitigate the poor performance of the RCA, thus obtaining admixed recycled concrete aggregate. Mineral admixtures such as fly ash (FA), silica fume (SF), metakaolin (MK) and Ground granulated blast slag (GGBS) have been utilized for many years either as supplementary cementitious materials in Portland cement concrete or as a component in blended cement. Generally, due to their high pozzolanic activity, the mineral admixture improves the mechanical and durability properties of the concrete [3]. Two stage mixing approach (TSMA) is used to mix recycled concrete aggregate, in which the mixing process is divided into two parts and the required water is proportionally split into two, which is added at different timing. First, fine and coarse aggregates are mixed for 60 s before half of the water required is added and mixed for another 60 s; then cement is added and mixed for 30 s before the remaining half of water is added and mixed for 120 s. Improvement of strength is achieved up to 21.19% for 20% of RA used under 28-day curing conditions under TSMA [4].



Fig.1. Interfacial zones in RCA

Stress block parameters are extensively used in the analysis and design of concrete structural members and offer a convenient way to determine flexural capacity. Better the stress-strain model, more reliable is the estimate of strength and deformation behaviour of concrete structural members.

In this paper, an attempt has been made to develop a stress-strain model for concrete with metakaolin admixed recycled concrete aggregate and to evaluate the stress block parameters such as, the effective average concrete stress ratio (α_1) and the effective stress-block depth factor (β_1).

2. Experimental Programme

a. Materials and Mix Proportions

The materials used in this study includes Portland pozzolana cement conforming to IS 1489 (1) – 1991, river sand passing through 4.75mm IS sieve conforming to grading zone II of IS 383:1970 (reaffirmed 2002) having specific gravity of 2.75 and coarse aggregate with a maximum size of 20mm and specific gravity of 2. The mixes were designed using IS 10262:2009. Slump was fixed as 85-90mm. Polycarboxylate ether based super plasticizer was used to improve the workability of the mix. Mix proportion of M20 and M30 mixes were 1:1.97:3.81 and 1:1.93:3.58.

Recycled concrete aggregate (RCA) was obtained from the demolished building wastes and was sieved to get a maximum size of 20mm. The specific gravity of RCA obtained was 2.69, which was lower than coarse aggregate. Also the water absorption was obtained as 2.1%, which was higher than coarse aggregate. Coarse aggregate was then replaced by 100% RCA.

Metakaolin admixed RCA was obtained by mixing metakaolin with RCA by replacing RCA by 2.5,5,7.5,10 and 12.5% by weight of RCA in each mixes.

As the 100% replacement of coarse aggregate with RCA, the mixes were found to be less workable and thus, the amount of super plasticizer was increased, so that the mixes achieve a slump of 85-90mm. Cube specimens of size 150mm were cast and tested for 28 day compressive strengths to obtain the optimum percentage of metakaolin in each mixes.

Table 1. Mix proportion of cylindrical specimens for 1m³

Mix	Cement (kg)	FA (kg)	CA (kg)	RCA (kg)	Metakaolin (kg)	Water (L)	Super plasticizer (L)
M20			1268	-	-		-
M20R100	340	674	-	1148	-	193	0.002
M20R100-10			-	1033	114		0.0035
M30			1289	-	-		-
M30R100	360	693	-	1196	-	163	0.004
M30R100-10			-	1077	119		0.0047

b. Testing

The determination of stress-strain characteristics was carried out by testing 18 cylindrical specimens of diameter 150mm and height 300mm using an UTM of 1000 kN capacity. For each mix, three specimens were cast and tested and the average of the test results was taken for analysis. While casting the specimen, two steel flats were inserted into the core concrete through the slots made in the cylinder moulds so that the vertical distance between the inserted flats was 100mm. The core deformations corresponding to every 10 kN increment of load were recorded during loading using Linear Variable Differential Transducer (LVDT) attached to the flats. The test setup is shown in Fig.2. The specimens were subjected to monotonic axial compression until failure. The tests were terminated when the load suddenly dropped to a fraction of the maximum and resulted in complete destruction of the specimen. The failure pattern of the specimen was also observed.



Fig.2. Testing of cylindrical specimen

3. Saenz stress-strain model

For the formulation, it was assumed that no exact theory is available for stress-strain curve of concrete. However, the theoretical stress-strain curve can be verified by comparing it with experimental stress-strain curve developed from the observed data. The procedure adopted in this model is explained below [7].

Saenz proposed the following equation to represent stress-strain relationship of concrete in compression.

$$f = \frac{A\varepsilon}{1 + B\varepsilon^2} \tag{1}$$

where,

ε = Strain in concrete

f = Stress corresponding to strain in concrete

A and B are the constants for a stress-strain curve without normalizing and are calculated by the equations (3) and (4)

Expressing the stress-strain relation in non-dimensional form,

$$\frac{f}{f_u} = \frac{A' \left(\frac{\varepsilon}{\varepsilon_u}\right)}{1 + B' \left(\frac{\varepsilon}{\varepsilon_u}\right)^2} \tag{2}$$

where,

A' and B' are constants of stress-strain curve

f_u = peak stress

ε_u = peak strain

f/f_u = stress ratio

$\varepsilon/\varepsilon_u$ = strain ratio

The constants A' and B' can be find out by using the following boundary conditions:

(i) At the point where the curve departs from its straight line portion

(ii) The strain ratio and stress ratio at the peak of the non dimensional stress-strain curve is unity

. Then, the constants A & B in the stress-strain relation without normalizing are calculated as follows:

$$A = A'(f/f_u) \tag{3}$$

$$B = B' (1 / \epsilon_u)^2 \quad (4)$$

Using the values of constants A and B for each mix, the theoretical stresses are calculated by keeping the experimental strain as such in Eqn.(1). The obtained theoretical stresses were then normalized by dividing each value by their peak stress. And a graph is plotted between normalized theoretical stress v/s normalized experimental strain. Again a graph is plotted between normalized experimental strain and normalized experimental stress. If the normalized theoretical stress-strain curve matches with the normalized experimental stress-strain curve, then Saenz's stress-strain model will be applicable. If this model is satisfied, the equations pertaining to this model would be used to find out the stress block parameters which are explained below.

Expressions for compressive force and tensile force

The expression for compressive force (C) is written as:

$$C = \alpha_1' f_{cu} b X_u \quad (5)$$

where,

- X_u = Depth of neutral axis
- f_{cu} = Stress corresponding to ultimate strain in concrete
- C = compressive force
- α_1' = stress block parameter without partial safety factor

The idealization of stress-strain curve is assumed as shown in Fig.3. And the area under stress-strain curve (A_b) is given by:

$$A_b = \alpha_1' f_{cu} \epsilon_{cu} \quad (6)$$

Thus,

$$\alpha_1' = A_b / f_{cu} \epsilon_{cu} \quad (7)$$

Where, α_1' is a stress block parameter without partial safety factor and the modified parameter is found by dividing this by partial safety factor of 1.5. Thus α_1 is the stress block parameter, called effective average concrete stress ratio.

Now, by substituting Eqn. (7) in Eqn. (5),

$$C = \frac{b X_u}{\epsilon_{cu}} A_b \quad (8)$$

Then, the tensile force (T) is expressed as

$$T = f_y A_{st} \quad (9)$$

As per clause 38.1 of IS 456:2000

$$\epsilon_s = \frac{(0.87 f_y)}{E_s} + 0.002 \quad (10)$$

Hence,

$$f_y = E_s \left(\frac{\epsilon_s - 0.002}{0.87} \right) \quad (11)$$

Substituting Eqn. (7.11) in Eqn. (7.9), we get

$$T = E_s \left(\frac{\epsilon_s - 0.002}{0.87} \right) A_{st} \quad (12)$$

To derive the expression for compressive force, idealization of stress-strain curve was assumed. The assumption of idealization was proved with respect to each mix. For idealization, the stress-strain curve obtained from experimental data was extrapolated beyond the experimental ultimate stress point. The extrapolation of the curve was done by obtaining further theoretical ultimate values of stress and strain by considering the condition of equilibrium of forces (Compressive force = Tensile force)

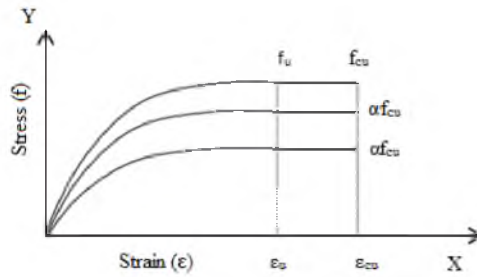


Fig.3. Assumed idealized stress-strain curve^[7]

The area under the stress-strain curve (A_b) is given by

$$A_b = \frac{A}{2B} \log \frac{1 + B\epsilon_{cu}^2}{1 + B\epsilon_1^2} \tag{13}$$

By substituting Eqn. (7.13) in Eqn. (7.8), we get

$$C = \frac{bX_u A}{\epsilon_{cu} B} \log \frac{1 + B\epsilon_{cu}^2}{1 + B\epsilon_1^2} \tag{14}$$

where,

b = breadth of the section

ϵ_1 = Initial strain in concrete

ϵ_{cu} = Ultimate strain in concrete

A & B = constants obtained from Eqns. (2) & (3)

For idealizing stress-strain curve, different values of compressive force were generated. For this, values were assigned for the parameters X_u , ϵ_1 , ϵ_{cu} , and b in Eqn. (14). Similarly, to generate different values for tensile forces, values were assigned for the parameters A_{st} , E_s , and ϵ_s in Eqn. (12). While the parameters ϵ_1 , b , A_{st} , and E_s were considered as constants & the remaining parameters were considered as variables.

The values for various parameters were assumed as follows:

$\epsilon_1 = 0$, $b = 100\text{mm}$, $d = 125\text{mm}$, $E_s = 2.1 \times 10^5 \text{ MPa}$

$X_u = 0.1d$ to $0.5d$ with an incremental value of $0.1d$

$\epsilon_{cu} = 1 \times 10^{-4}$ to 1×10^{-3} at an interval of 1×10^{-4}

2×10^{-3} to 1×10^{-2} at an interval of 1×10^{-3}

2×10^{-2} to 1×10^{-1} at an interval of 1×10^{-2}

$\epsilon_s = 2.2 \times 10^{-3}$ to 1×10^{-2} at an interval of 1×10^{-3}

The value of X_u at which the compressive force (C) is equal to the tensile force (T) was identified and the exact value of strain at which $C=T$, was found by plotting the force against the strain. The theoretical ultimate value of strain, in concrete was thus obtained. Then, area under the stress-strain curve (A_b) was calculated using Eqn. (7.13) and by taking $f_u = f_{cu}$, the stress block parameter was obtained from Eqn. (7.7). The theoretical ultimate value of stress, f_{cu} was then obtained from Eqn. (7.5) as all other parameters being known. Now, using the value of f_{cu} , the stress-strain curve is extrapolated until this value and the idealization of stress-strain curve is compared. If the experimental and theoretical stresses are almost same then the assumption is valid. The same procedure was repeated for all the mixes. The stress block diagram is shown in Fig.4.

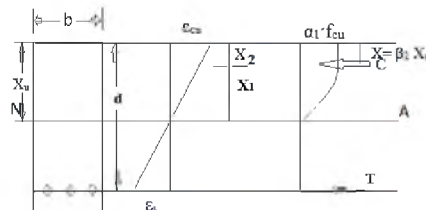


Fig.4. Stress block diagram ^[7]

From the above figure, using similar triangles, the values of x_1 and x_2 was found using Eqns. (15) and (16)

$$X_1 = \frac{\varepsilon_u}{\varepsilon_{cu}} x_u \quad (15)$$

$$X_2 = \frac{\varepsilon_{cu} - \varepsilon_u}{\varepsilon_{cu}} x_u \quad (16)$$

Where ε_{cu} is substituted as 0.0035 here as it is the ultimate strain in any concrete as per IS 456:2000. X_1 is the depth of the parabolic portion of the stress-block & X_2 is the depth of the rectangular portion of the stress block.

The compressive force component for parabolic portion of stress block without partial safety factor is given as:

$$C_1 = \frac{2}{3} X_1 (\alpha_1' f_{cu}) b \quad (17)$$

The compressive force component for rectangular portion of stress block without partial safety factor is given by

$$C_2 = X_2 (\alpha_1' f_{cu}) b \quad (18)$$

Thus, the total compressive force (C) is given by:

$$C = C_1 + C_2 \quad (19)$$

Let X be the distance of the line of the action of compressive force from the extreme top fibre, then

$$X = \frac{C_1 \left(\frac{3}{8} X_1 + X_2 \right) + C_2 \left(\frac{X_2}{2} \right)}{C} \quad (20)$$

Let,

$$X = \beta_1 X_u \quad (21)$$

where,

β_1 = effective stress block depth factor & is a function of X_1 , X_2 , C_1 , C_2 and C

Thus, we get X in terms of X_u and the constant connecting that gives the value for β . By using the principle of equilibrium, the compressive force equal to the tensile force, the value of X_u/d was calculated.

Thus a new set of stress block parameters were obtained by using this model which could be used for rapid design checks. This procedure was adopted for all the mixes.

4. Results and Discussion

Three specimens were tested to determine the stress-strain characteristics in M20 and M30 mixes and the average value of the three results were taken for the analysis. The stress-strain curves were then plotted for M20 and M30 mixes and shown in Fig.5 & Fig.6.

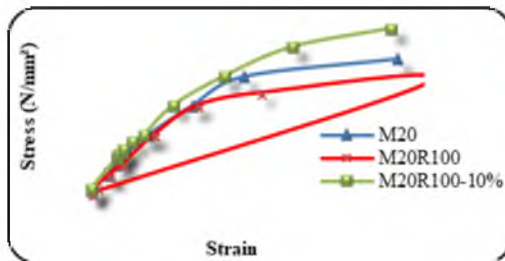


Fig.5. Stress-strain curve of M20 mixes

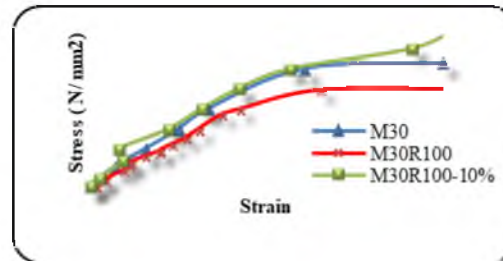


Fig.6. Stress-strain curve of M30 mixes

The peak stress and strain values of each mixes can be seen from the Fig.5 and Fig.6. It was observed that when the recycled aggregate is used, the stress value decreased and the strain value increased comparing to control mix. This is because of the low strength of recycled aggregate. Also, when metakaolin is used, the stress value increased and strain value decreased comparing to control mix. And this is because of the high strength of the mix. Due to the filler effect of metakaolin, it reduces the pores in the recycled aggregate and reduces the water absorption and thus increased the strength of the mix.

All the stress-strain curves show a linear behaviour till the first crack load and at higher levels of stress, the behaviour was highly non-linear. As a result of formation of micro cracks, the softening behaviour of concrete started at early stages and this was continued up to the peak load. These micro cracks developed both in mortar and

mortar-aggregate interface. When stress was increased beyond peak stress, micro cracks propagate suddenly and this increases the compressive strain. At this stage cracks got widened and failure occurred.

A typical failure pattern of M20 and M30 cylinder specimens observed after the test is shown in Fig.7 and Fig.8.



Fig.7. Failure pattern of M20 mixes

a. Illustration of Evaluation of Stress Block Parameters

A typical illustration of the Saenz stress-strain model has been done for M30R100-10. The normalized experimental and theoretical stress and normalized experimental strain data derived from Eqn. (1) and Eqn. (3). By applying boundary conditions, the values of A' and B' are 3.216 and 2.216. Hence by solving Eqn. (3) and Eqn. (4), the values of A and B are obtained as 60430.41 and 246619.79. Using the values of A' and B', the theoretical stress-strain curve is drawn and it is seen to be in good agreement with the experimental curve (Fig.9). Hence the assumption of Saenz's stress-strain model is valid for M30R100-10



Fig.8. Failure pattern of M30 mixes

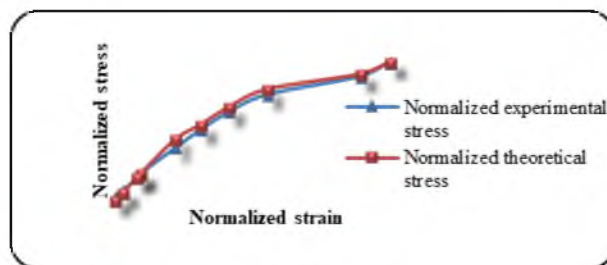


Fig.9. Non-dimensionalised stress-strain curve for M30R100-10

The experimental peak stress and strain corresponding to peak stress obtained are 23.12 MPa and 0.00193 respectively. Different values for compressive force (C) and tensile force (T) by substituting the values of the parameters in Eqn. (14) and Eqn. (12). The values of the force was plotted against the strain values as shown in Fig.10 and the value of ϵ_{cu} at which the compressive and tensile stresses were found to coincide was obtained as 0.0035. Knowing the value of ϵ_{cu} , the values of A_b and f_{cu} were calculated from Eqn. (13) and Eqn. (5) as 0.0415mm^2 and 24.05 MPa respectively. The idealized stress-strain curve was found to be coinciding with the extrapolated stress-strain curve as shown in Fig. Hence the assumption of idealization of stress-strain curve is also proved.

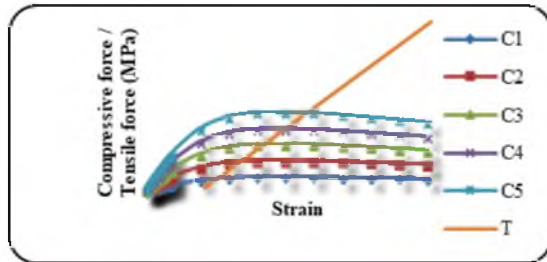


Fig.10. Force-strain curve for M30R100-10

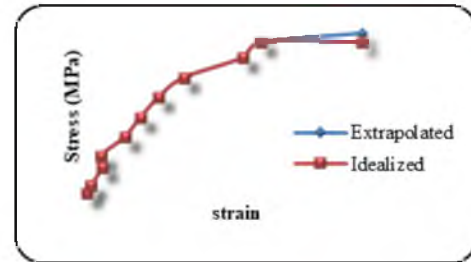


Fig.11. Idealized stress-strain curve for M30R100-10

The depth of parabolic portion and rectangular portion of stress block and the corresponding compressive force component were then obtained as

$$X_1 = 0.63X_u$$

$$X_2 = 0.365X_u$$

$$C_1 = 740.352X_u$$

$$C_2 = 185.088X_u$$

Thus, the total compressive force, $C = 925.44X_u$

The stress block parameters were obtained as follows:

$$\alpha_1' = 0.54$$

$$\alpha_1 = 0.36$$

$$\beta_1 = 0.381$$

Considering the equilibrium condition,

$$T = 52056 \text{ N}$$

Equating C and T, $X_u/d = 0.452$

This procedure was adopted for all considered mixes of M20 and M30 and the stress-strain relation and stress block parameters were evaluated. The values of the constants in the stress-strain relation for various mixes along with the proposed values are shown in Table. The correlation coefficient for actual values and proposed values of the constants were calculated and all the values were found to be nearly equivalent to unity. The average values of stress block parameters for M20 and M30 mixes were found and shown in Table 2.

Table 2. Average values of stress block parameters for M20 and M30 mixes

Mix Designation	Stress block parameters		
	α_1	β_1	X_u/d
MxR100-y	0.33	0.39	0.44

MxR100	0.32	0.41	0.42
Mx (IS 456:2000)	0.36	0.42	0.48

x denotes the grade of concrete and y denotes the optimum percentage of metakaolin

5. Conclusions

The following are the conclusions obtained from this study:

- Saenz model was found to be applicable for all M20 and M30 mixes.
- The effective average concrete stress ratio (α_1), the effective stress block depth factor (β_1), neutral axis depth to effective depth ratio (X_u/d) were found to be comparable with the values for concrete as per IS 456: 2000.
- As the regression coefficients are closer to unity, the proposed values of stress block parameters could be used to determine the flexural strength of members made using the above composites.

References

1. Takahashi, h., Satomi, t. and Bui, k.: Improvement of Mechanical Properties of Recycled Aggregate Concrete Based on a New Combination Method Between Recycled Aggregate and Natural Aggregate, *construction and building materials*, 148, 376-385 (2017)
2. Kurama, C., Weldon, d., Rosa, A., Davis, A. and McGinnis, J.: Strength and Stiffness of Concrete With Recycled Concrete Aggregates, *construction and building materials*, 154, 258-269, (2017)
3. Szpetulski, J., Koper, A., Jaskulski, R. And Kubissa, A.: Properties of Concretes With Natural Aggregate Improved by RCA Addition, *procedia engineering*, 108, 30-35, (2015)
4. Aggoun, S., Debieb, F., Bouvet, A., Kadri, E., Ngo, T. and Tahar, Z.: Effect of Cement and Admixture on the Utilization of Recycled Aggregates in Concrete”, *construction and building materials*, 149, 91-102, (2017)
5. Buabin, K., Sossou, G., Meisuh, K. and Kankam, C.: Stress-Strain Characteristics of Concrete Containing Quarry Rock Dust As Partial Replacement of Sand”, *case studies in construction materials*, 7, 66-72, (2017)
6. Ganesan, N., Ruby, A. and Deepa, R.: Stress–Strain Behaviour of Confined Geopolymer Concrete, *construction and building materials*, 73, 326–331, (2014)
7. Ganesan, N., Bharati, R., J. and Shashikala, A., P.: Evaluation of Stress Block Parameters for Self Compacting Rubberized Concrete Composites, *the Indian concrete journal*, 89 (2), 24-38, (2015)
8. Shah, P., Corr, J., Wengui, L. and Xiao, j.: Simulation Study on the Stress Distribution in Modeled Recycled Aggregate Concrete Under Uniaxial Compression, *Journal of materials in civil engineering*, 25(4), 504-518 (2013)
9. Bhikshma, V. and Kishore, R.: Development Of Stress Block And Design Parameters for Recycled Aggregate Concrete, *Asian Journal of Civil Engineering (Building and Housing)*, 12 (2), 179-195, (2011)
10. IS 516 – 195 (Reaffirmed 2004), “*Methods of Test for Strength of Concrete*”, Bureau of Indian Standards, Newdelhi, india, 1959

STUDY ON PROPERTIES OF POLYTHENE FIBRE REINFORCED CONCRETE WITH PARTIAL REPLACEMENT OF COARSE AGGREGATE AS COCONUT SHELL (PFRCS)

Swathi M S¹, Anu A²,

¹ M.Tech student,

² Assistant Professor,

Dept. of Civil Engineering, Younus College of Engineering & Technology (YCET),

Pallimukku P O, Kollam 10, Kerala, India

Contact E-mail: swathimohan55@gmail.com

Aggregates generally occupy 60% to 75% of the concrete volume and strongly influence the fresh and hardened properties and economy of concrete. The continued extraction of aggregates from nature has caused its depletion at an alarming rate. The worldwide depletion of natural resources and the simultaneous accumulation of waste materials call for the need for sustainable development in the construction industry. Hence, recent researches have been focussed on the use of locally available waste materials such as coconut shell, plastic, etc., in concrete to replace the mineral aggregates. This study deals with the strength characteristics of PET fibre reinforced coconut shell concrete (PFRCS). Earlier studies have shown that when coconut shell was used in concrete to replace the coarse aggregates, compressive strength was decreased considerably. But, this reduction in strength was significantly low for 10% coarse aggregate replacement. Also, the inclusion of polythene fibres made from waste plastic bottles was noted to improve the strength characteristics of concrete. Hence, an attempt has been made to combine the positive characteristics of both coconut shell concrete (CSC) and PET Concrete. M30 normal concrete and CSC concrete with 10% coarse aggregate of normal concrete replaced by coconut shell has been taken as the control mixes. PET fibres made from waste plastic bottles were added at volume fractions of 0, 0.5, 1, 1.5, 2 and 2.5%. The mechanical properties such as density, compressive strength, tensile strength and flexural strength were determined and compared with the control mixes. The experimental investigations were carried out on a total of 180 specimens which includes cubes, cylinders and prisms. The results indicate that PFRCS is a sustainable, eco-friendly and economical concrete with better engineering properties and strength characteristics in comparison with normal concrete and coconut shell concrete.

Key Words: coconut, fibres, plastic, polythene, and sustainable

-----***-----

1. INTRODUCTION

Sustainability in building developments is a vast and complex subject that must be considered from the very earliest stages as the potential environmental impacts are very significant. In the present day construction industry, the rising cost of building construction materials is becoming a factor of great concern. The prices of building materials are rising day by day. Concrete has always been considered as the premier building material and aggregates form the main ingredient of concrete. The continued extraction of aggregates from nature has caused its depletion at an alarming rate. The worldwide depletion of natural resources and the simultaneous accumulation of waste materials have called for the need for sustainable development in the construction industry. This mainly involves the use of locally available materials as replacement of the natural aggregates, both coarse and fine aggregates. Hence, recent researches have been focussed on the use of locally available waste materials such as coconut shell, plastic, etc., in concrete to replace the mineral aggregates.

Coconut shells are one of the agricultural waste products abundantly available from local coconut fields in Kerala and accounts for around 45% of the production in India. In many countries, coconut shell is subjected to open burning which contributes significantly to CO₂ and methane emissions. The disposal of coconut shell poses various environmental issues as it is not easily degradable and it is an agricultural waste. In India, coconut shell when used as an agricultural waste requires huge dumping yards. The dumping of coconut shell also causes breeding place for mosquitoes. If this material can be utilised to replace the coarse aggregates in concrete, then it should be a boon to the civil engineering society. Various researchers [1-5] have investigated the use of coconut shells and their derivatives in civil engineering construction. This will not only reduce the weight of the resulting concrete, but also provides an efficient solution to the disposal of coconut shells.

Plastic waste is yet another crucial issue posing various environmental hazards. The amounts of plastics, especially the plastic bottles consumed annually have been increasing steadily. There are several factors that contribute to the rapidly growth of plastics consumption such as low density, fabrication capabilities, long life, lightweight, and low cost of production. The problem gets further complicated since plastic waste is not degradable and may cause environmental disturbance. Treatment method through incineration will provide toxic gas like dioxin that could be dangerous to human health. The main disadvantage of PET (Polyethylene Terephthalate) bottles is the sheer amount of time they take to decompose, an average plastic bottle takes 500 years. The decomposition can be affected by various factors, such as climate and acids in the landfill. Of the mass numbers of plastic bottles consumed throughout the world, most of them are not recycled because only certain types of plastic bottles can be recycled by certain municipalities. They either end up lying stagnant in landfills, leaching dangerous chemicals into the ground, or they infiltrate our streets as litter. They are found on sidewalks, in parks, front yards and rivers, and even if you chop them into tiny pieces they still take more than a human lifetime to decompose.

A possible application of disposing these hazardous PET bottles is to chop them into fibres and use Polyethylene Terephthalate (PET) fibres obtained from waste plastic bottles as short fibre reinforcement in structural concrete. It can improve its tensile strength as concrete is good in compressive strength but lack tensile strength. The reduced strength is mainly due to presence of micro and macro cracks due to shrinkage of concrete. PET comes in the category of low modulus synthetic fibres along with fibres of polyethylene, nylon, polyester which are effective in controlling shrinkage cracking but is not so effective in increasing tensile strength. Also, PET bottles are being experimented to act as non-load bearing and partition walls in many parts of world. Previous researches [6,8,9,11,14] revealed that PET waste fibre in concrete has significant role in terms of bonding and strength. Increasing the PET waste increases the size of porosity and interfacial transition zone in concrete matrix and resulted in reduction in strength of concrete.

2. SIGNIFICANCE OF THE WORK

Though there are various waste materials that form a part of garbage, non-biodegradable wastes like plastic are more visible than other trash. This is especially true in case of PET (Polyethylene Terephthalate) bottles. These bottles not only result in waste of expensive material but also increase plastic waste which can cause environment pollution in the form of their disposal. Today, PET bottle wastes are seen everywhere: on the road, in garbage bins, railways tracks, play grounds, etc. This calls for a need for using these waste materials in a useful manner.

Studies have revealed that the addition of fibres improves the engineering properties of concrete such as ductility, post crack resistance, energy absorption capacity, etc. The inclusion of fibres also imparts better flexural strength, cracking resistance and toughness characteristics to the concrete. Research has been carried out on the properties of concrete including polythene fibres obtained from plastic bottles and it has been noted that the compressive strength was improved when the polythene fibre volume fraction was increased from 0 to 2.5%. Hence, the inclusion of such fibres would prove to be beneficial to the concrete properties.

This creates a possibility of including PET fibres to the Coconut Shell Concrete (CSC) to improve the strength characteristics of concrete. Research available on coconut shell concrete and polythene fibre concrete has been restricted to the studies on mechanical properties such as compressive strength, tensile strength, density, water absorption and flexural strength. The possibility of inclusion of polythene fibres to coconut shell concrete has not been explored so far.

This paper aims at analysing the mechanical properties of Polythene Fibre Reinforced Coconut Shell Concrete (PFRSC).

The major objectives are

- To study the characteristics of coconut shell concrete with 10% coconut shell as partial replacement of coarse aggregates.

- To analyse the possibility of inclusion of polythene fibres to coconut shell concrete at volume fractions of 0, 0.5, 1, 1.5, 2 and 2.5%.
- To evaluate the engineering properties such as density, compressive strength, tensile strength and flexural strength of Polythene Fibre Reinforced Coconut Shell Concrete

3. EXPERIMENTAL PROGRAMME

3.1 Materials and Mix Proportions

Ordinary Portland cement of 53 Grade having specific gravity 3.15 and normal consistency of 38% and conforming to IS:12269-1987(Reaffirmed 2004) [15] was used. M sand passing through 4.75 mm IS sieve conforming to grading Zone II of IS 383-1970 (Reaffirmed 2002) [16] was used as fine aggregate. Crushed stone having effective size of 10.2mm conforming to IS: 2386-1997 [17,18] and IS: 383-1970 (Reaffirmed 2002) [16] was used as coarse aggregate.

The mix designs were carried out for obtaining 28day concrete compressive strengths of 30MPa. Locally available coconut shells were crushed and sieved to get coarse particles with effective size of 15 to 20mm and bulk density 1.69 g/cc as shown in Fig.1. The natural coarse aggregates were replaced at a volume fraction of 10% with coconut shell and polythene fibres obtained from polythene bottles were added at volume fractions of 0, 0.5, 1, 1.5, 2 and 2.5%.



Fig 1 Coconut shell

The coconut shell content was restricted to 10% by volume of coarse aggregates as the optimum value of coconut shell content for desirable compressive strength for the mix was found to be 10% from past literature [7,12,13]. Polyethylene terephthalate (PET) fibres having an aspect ratio of 88 were cut from waste PET bottles (Fig.2). The length of the fibres was 40mm. Potable water available in the laboratory, which satisfies drinking standards, was used for the concrete mixing and its subsequent curing. The mix proportion used is as given in Table 1.



Fig 2 PET Fibres

Table 1 Mix proportions

Cement (kg/m ³)	Coarse Aggregate (kg/m ³)	Fine Aggregate (kg/m ³)	Water (L)	Water Cement Ratio
360	1285	710	192	0.4

3.2 Testing and specimen details

The specimens were designated as shown in Table 2. A total of 180 specimens were cast and tested to obtain the mechanical properties of NC, CSC and PFRCS. The details of specimens cast for each mix are as follows.

- (i) 18 cube specimens of 150mm size to evaluate the unit weight, 28 day, 45 day and 60 day compressive strength
- (ii) 6 cylindrical specimens of 150mm Φ and 300mm height for the split tensile strength
- (iii) 6 prisms of 100 x 100 x 500mm for the modulus of rupture

Table 2 Designation of specimens

Designation	Details	Coconut shell %	Volume fraction of PET fibres (%)
NC	Normal Concrete	0	0
CSC	Coconut Shell Concrete	10	0
PFRCS1	PET Fibre Reinforced CSC	10	0.5
PFRCS2			1.0
PFRCS3			1.5
PFRCS4			2.0
PFRCS5			2.5

4. RESULTS & DISCUSSIONS

4.1 Workability

The concrete mixes with coconut shell aggregates were found to have better workability because of the smooth surface on one side of the coconut shells. The workability in terms of slump value was seen to follow an increasing trend with addition of coconut shells as well as PET fibres. The slump values increased by 13.7% between NC and CSC. The slump values gradually increased from 33 to 45mm as the PET fibre volume fraction was increased from 0.5 to 2% as shown in Fig 3. For PFRCS with 2% fibres, the increase in workability was 55.17% and 36.36% with respect to NC and CSC respectively.

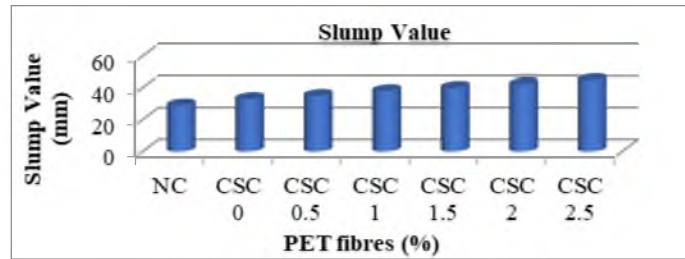


Fig 3 Slump values of mixes

The workability based on compaction factor was observed to increase from 0.91 to 0.924 as the percentage of PET fibres in CSC increased from 0 to 2% as shown in Fig 4. Increase in compaction factor between NC and CSC was noted to be 19%. For PFR CSC with 2% fibres, the increase was 12% and 6.4% with respect to NC and CSC respectively.

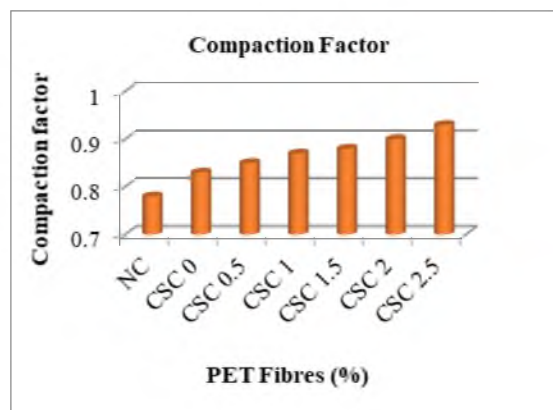


Fig 4 Compaction factor values of mixes

4.2 Density

The density of PFR CSC was seen to decrease with increase in fibre volume fraction. The maximum value of density for CSC was observed to be 2540.2 kg/m³ as shown in Fig 5. The density dropped down to 2056.3 kg/m³ (20%) as volume fraction PET fibres in CSC was increased to 2%. The decrease in density between NC and CSC was 2.8%. It was also observed that the density values obtained for CSC and PFR CSC were lesser than the density of normal concrete, which usually ranges between 2300 to 2600 kg/m³. Hence the concrete obtained by adding coconut shell and PET fibres could be categorised as light weight concrete.

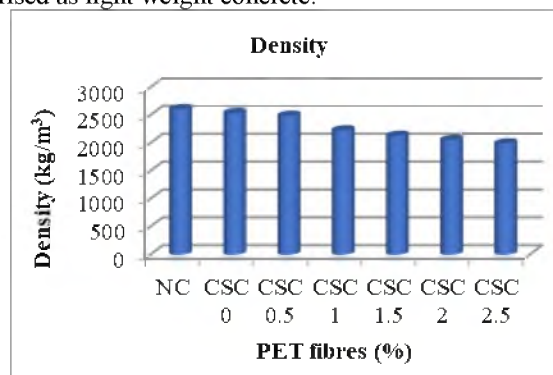


Fig 5 Density

4.3 Compressive Strength

Compressive strength of all concrete mixes was determined at 7 and 28 days of curing. The compressive strength test results are given in Table 4.4. The variation of compressive strength at 7 and 28 days with different mixes is shown in Fig 4.5. It has been observed that the polythene fibre reinforced concrete show an increasing trend in the compressive strength with increase in PET content. From these results, it was observed that compressive strength of all mixes was found to increase till 2% and that compressive strength of all mixes was greater than the control mix. Compressive strength decreases for addition of fibres above 2%. Maximum strength at all ages occurs with 2% addition of fibre. From test results it was concluded that there is an increase in the early age compressive strength due to the addition of fibre in concrete. Comparing to CSC 0, CSC 2 has showed an increase in strength of 15% at 28 days. When compared to NC, CSC 2 has showed an increase in strength of 23.43% at 28 days. From the compressive strength test, CSC 2 was obtained as the optimum percentage.

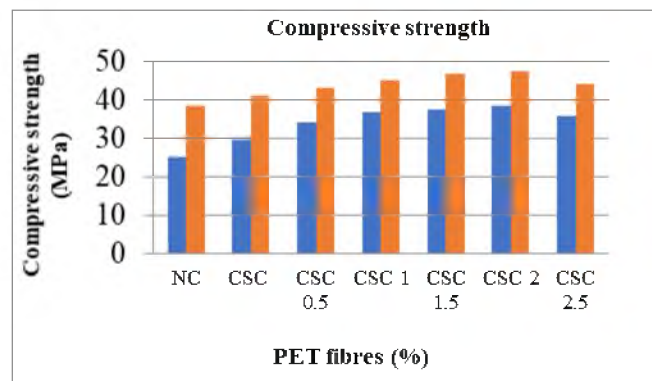


Fig 6 Compressive strength

4.4 Splitting Tensile Strength

Splitting tensile strength test was carried out on cylindrical specimens horizontally placed between the loading surfaces of the compression testing machine. The load was applied until failure of the cylinder along the vertical diameter was observed. Split tensile strength was found to increase with increase in percentage of PET fibres as shown in Fig 7. The split tensile strength values increased to 4.56 MPa as the fibre percentage was increased from 0 to 2%. The tensile strength for PFR CSC with 2% fibres, that splitting tensile strength of cylinder of CSC 2 was higher than CSC 0. Percentage increase in strength of CSC 2 was 27.97% than CSC 0 and 31.73% when compared to Normal concrete. So 2% PET Fibre addition can be considered as optimum content.

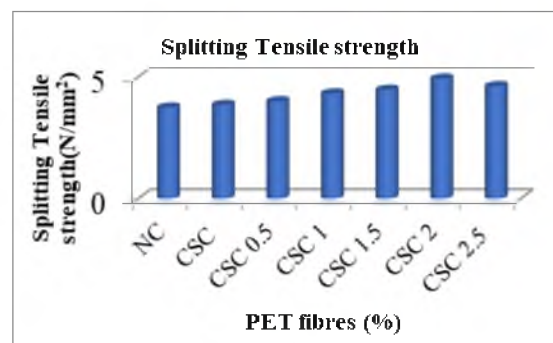


Fig 7 Split tensile strength

4.5 Flexural Strength

Flexural strength or the modulus of rupture (extreme fibre stress in bending) was found out by testing prisms under two-point loading. Flexural strength was observed to follow an increasing trend with increase in percentage of PET fibres as shown in Fig 8. But, when compared to NC, Flexural strength decreased by 42.8 % between normal

concrete and CSC. For coconut shell concrete with 2% fibres the increase was 32.203 % with respect to normal concrete and 28.57% with respect to CSC 0.

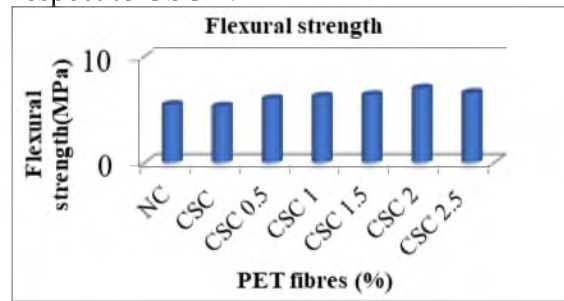


Fig 8 Flexural strength

5. Cost analysis

According to the mix design, weight of coarse aggregate for one cubic meter is 1153.75 kg which costs Rs.1396. By the replacement of 10% of coarse aggregate with coconut shell, the weight of coarse aggregate obtained is 1038.375 kg, which costs Rs.1256. This gives a reduction of Rs.140 for CSC when compared to normal concrete. The PET fibres and coconut shell are completely a waste material which does not cause any additional cost to the work. Hence, it was observed that around 25% cost reduction was obtained by using coconut shell and PET fibres in concrete and our project work was economical.

CONCLUSIONS

An attempt has been made to effectively utilise waste materials like coconut shell and PET bottles in concrete as a solution to the huge disposal problems and environmental pollution hazards posed by these waste materials. Based on the above studies, the following conclusions are arrived at;

- CSC and PFRCS are concretes which promote green construction.
- Coconut shell and PET fibres are compatible with the cement in concrete and improves the workability of the concrete mix.
- PFRCS exhibits improvement in compressive strength, flexural strength and split tensile strength in comparison to conventional concrete and coconut shell concrete.
- 2% PET Fibre addition considered as optimum percentage.
- PFRCS can be categorised as light weight concrete.
- PFRCS also contributes to the reduction of coarse aggregate usage in concretes, thereby reducing the production cost and depletion of natural resources.

Hence it can be concluded that PFRCS is a low cost, light weight and an eco-friendly concrete with improved strength characteristics.

REFERENCES

1. Akshay, S S, Kalyani, R N, Pooja, P K, Shraddha, P G.,(2014) *Coconut shell as partial replacement for coarse aggregate: Review*, International Journal of civil engineering research, 5(3), 211-214.
2. Amarnath, Y, and Ramachandrudu, C.,(2012) *Properties of concrete with coconut shells as aggregate replacement*, International Journal of engineering Inventions, 1(6), 21-31.
3. Anjali, S K, Priyanka, A B, Shashiraj, S C.,(2015)*Investigation of coconut shell as a replacement of coarse aggregate in concrete*, Journal of information, knowledge and research in civil engineering, 3(2), 195-198.
4. Daniel,Y.,(2013) *Experimental assessment on coconut shells as aggregate in concrete*, International Journal of engineering science inventions, 2(5), 7-11.
5. Dewanshu, A. and Kalurkar, L G.,(2014), *Coconut shell as partial replacement of coarse aggregate in concrete*, IOSR Journal of Mechanical and Civil engineering, International Conference on Advances in Engineering and Technology,61-64.
6. Ganesh P, Arunkumar C, Pandiyaraj R, Rajesh P, Sasikumar L (2014) *Study on utilisation of waste PET bottle fiber in concrete*, International Journal of Research in Engineering and Technology 2(5),233-240.
7. Gopal, C. and Ranjan, K.,(2013), *Effect of coconut shell aggregate on normal strength concrete*, International Journal of engineering research and technology, 2(6), 2405-2415.

8. Irwan J M, Asyraf R M, Othman N, Koh H B, Annas M M K, Faisal S K.,(2013) *The mechanical properties of PET fiber reinforced concrete from recycled bottle wastes*, *Advanced Materials Research*,795, 347-351.
9. Kandasamy R., and Murugesan R., (2011), *Fibre reinforced concrete using domestic waste plastics as fibres*,*ARNP Journal of Engineering and Applied Sciences*,6(3),75-82.
10. Maninder, K, Manpreet, K.,(2012), *A Review on utilisation of coconut shell as coarse aggregates in mass concrete*, *International journal of applied engineering research*, 7(11).
11. Nibudey R N, Nagarnaik P B, Parbat D K, Pande A K.,(2013)*Strength and fracture properties of post consumed waste plastic Fiber reinforced concrete*, *International Journal of Civil, Structural, Environmental and Infrastructure Engineering*, 3(2),9-16.
12. Rajeevan, B.,(2015) *A study on the utilisation of coconut shell as coarse aggregate in concrete*, *International Journal of engineering research and technology*, 4(7), 77-80.
13. Sreenivasulu, D, Praveen, K, Satish, K, Sri Harsha, K, Mahesh, V.,(2014) *Laboratory investigation on coconut shell in concrete: An alternative low cost building*, *Journal of chemical and pharmaceutical sciences*, 4, 41-43.
14. Suganya, Aastha T M, Swaptik C.,(2013)*Polyethylene terephthalate waste as building solution* *International Journal of Chemical and Biological Sciences*,1(2).
15. IS 12269: 1987 (reaffirmed 2004): Specifications for 53 Grade ordinary Portland cement, Bureau of Indian Standards, New Delhi, P.5
16. IS 383: 1970 (reaffirmed 2002): Specification for coarse and fine aggregates from natural sources for concrete, Bureau of Indian Standards, New Delhi, P.19
17. IS 2386 (Part I): 1963 (reaffirmed 2002): Methods of Test for Aggregates for Concrete, Bureau of Indian Standards, New Delhi, P.17.
18. IS 2386 (Part III): 1963 (reaffirmed 2002): Methods of test for aggregates for concrete Part 3 - Specific gravity, density, voids, absorption and bulking, Bureau of Indian Standards, New Delhi, P.17.

Comparative Study on Hysteretic Performance of Semi Through Connections in CFT Beam - Column Joint

Ajith M. S.¹, Dr. Beena K. P.¹ and Dr. S. Sheela.²

¹ College of Engineering, Trivandrum, India

² Mohandas College of Engineering, Trivandrum, India
ajithms83@gmail.com

Abstract. The concrete filled tubes (CFT) have the complete utilization of strength of its components both steel and concrete due to its peculiar positioning. The presence of outer steel improves the confinement of concrete which leads to high stiffness and strength, where as core concrete will support the steel tube from local buckling and enhance the overall performance. The application of CFT is limited due to the lack of design guidelines for the joint between CFT and structural steel beams especially in seismic regions. This paper attempts to evaluate and compare the hysteretic performance of two extended end plate exterior beam column connection suitable for square and circular CFT by investigating the strength, stiffness, ductility and energy dissipation. The results indicate the adaptability of both connections for Special moment resisting structure with consistently stable, ductile and good energy dissipation nature .

Keywords: CFT column, Through bolt, Cyclic loading.

1 Introduction

Recent research focus on the ways to improve the strength of joint region to avoid connection failure before reaching ductility of components under seismic action by maintaining strength hierarchy . During a seismic event the overall performance of the CFT building will be characterized by the connection pattern. The connection between steel beams and CFT columns can be broadly classified into two categories namely exterior and interior connections. Exterior joints are made by attaching the steel beam to the outer steel tube alone, which may lead to high distortion on tube wall. From the literature review joint failures reported in Northridge Earthquake were weld failures which were categorized under exterior joint. The second method is interior connection which allows stress transfer to concrete core also, by penetrating extended beam elements or beam itself through the column. Even though this method will improve the seismic performance, practical construction difficulties prevails. Alternate solution to these problems are use of semi through type connections in which the entire beam is not passing through, instead extended anchor rods or bolts are transmitting the stresses to concrete core and making the confined concrete to actively participate in lateral stability. The selection of semi through connection has to be properly analyzed for easiness in construction, location of plastic hinge and cost benefit ratio[1-5]. On comparison circular CFT has better performance than square CFT due to higher confinement. But the application limited due to the difficulties in joint configuration and performance [6-8]. Current study aims to the performance evaluation of semi rigid semi through exterior connection of extended end plate steel beam to CFT square and circular columns under cyclic loading. This kind of bolted connection helps to avoid field weld completely which in turn increases the speed as well as quality of construction [9]. This paper describes the guidelines for design, methodology for testing and analyzing the performance of exterior joint under cyclic loading and results were compared in detail. It also evaluates the adaptability of split bolt assembly for circular CFT compared to square CFT with normal through bolt assembly [10].

2 Experimental Programme

2.1 Specimen Design

The design criteria selected was Four Bolt Stiffened Extended (4ES) End-Plate connection configuration, as per the capacity design approach [11]. The presence of stiffener helps to push the location of plastic hinge away from the face of column which will in turn improve the joint performance [12]. End plate thickness was arrived on the assumption to avoid prying force, which leads to the fixation of required diameter of bolts and pretension force. Representative sub assemblage of exterior joints were selected by assuming inflection points on the midspan of beam and column. Square CFT joint was considered as control specimen and its modified version was adopted for circular CFT specimen.

2.2 Test Specimen Fabrication

Control specimen 1ESFF220 illustrated in Fig.1(a) composed of square tube $220 \times 220 \times 8$ mm with 300 grade and beam ISMB175 with 250 grade. The steel beam is welded to extended end plate of 16mm thick using 6mm fillet weld at factory. 10mm thick triangular Stiffeners were provided above and below the top and bottom flanges. 16mm rod with 8.8 grade were specially fabricated to form through bolts.

Specimen 2ECSC220 shown in Fig. 1(b) was fabricated with circular tube of 220 mm diameter and 8mm thick with 300 grade and beam remains same. For the connection curved endplate was chosen with a special split bolt assembly which allows diametrical intersection of through bolt at same level as shown in fig. 3.

M30 grade concrete from 12mm aggregate, with plasticizer for 100mm slump was used to fill the steel tube. Mix design was carried out as per IS10262-2009 by considering good workability without compromising the strength requirement. Overall height of 1500mm and cantilever projection of 800mm were selected for all specimens considering the convenience of testing. After the fabrication of assembly the through bolts were placed as snug tight. Bolts were post tensioned after 28 days of concrete placing inside the tube. 100Nm torque was applied on either side of the rod using a calibrated torque wrench.

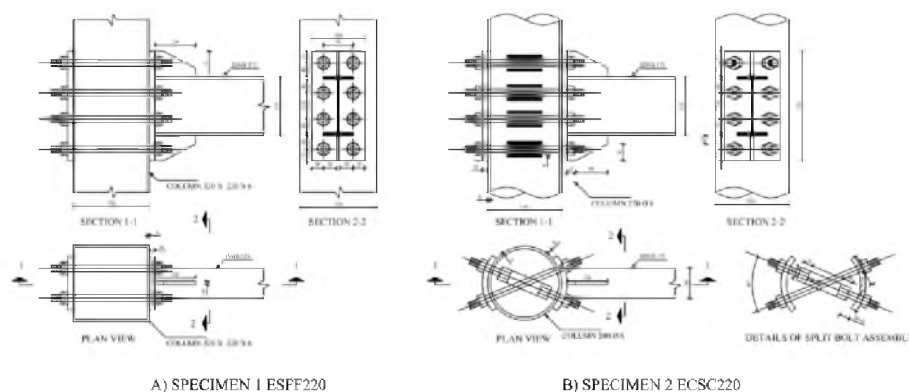


Fig.1. Exterior Joint Details

Mechanical properties of steel used for column, beam and HSFG bolt were identified using tension test and the values are presented in table 1, which shows that all the test results satisfies the design requirement. Concrete

strength properties were characterized by cube and cylinder compression test and tensile properties using split tensile test.

Table 1.Material Properties

Specimen	Yield Strength (MPa)	Ultimate Strength (MPa)
HSFG bolt (8.8 grade)	640	835
Steel Tube square	322	465
Steel Tube Circular	346	492
ISMB175 (flange)	284	393
(web)	268	381



Fig.2. Split Bolt Assembly

2.3 Test setup and Instrumentation

The test setup shown in Fig 3 was designed to simulate seismic loading effect on exterior joint by giving displacement controlled cyclic loading vertically on the free end of the beam by the use of manually controlled 750kN hydraulic actuator. 15% of the axial capacity of the column was given as static axial load over the top of the column and this minimum maintained throughout the test. Bolt prestress level also kept same for both specimen and its variation was monitored during the testing. High precision LVDT of LC 0.001 were used to capture the displacements accurately. Universal load cells were placed above the double acting hydraulic jack to measure both push as well as pull over the cycles. 5mm electric foil strain gauges were attached over the bolts and other critical locations of the specimen where high stress variations are expected. All data were collected by a 40 channel data acquisition system and recorded in an automated computer using lab view software with 80Hz frequency. The real time response was monitored continuously and the feedback used to control displacement excitation of quasi static cyclic loading.

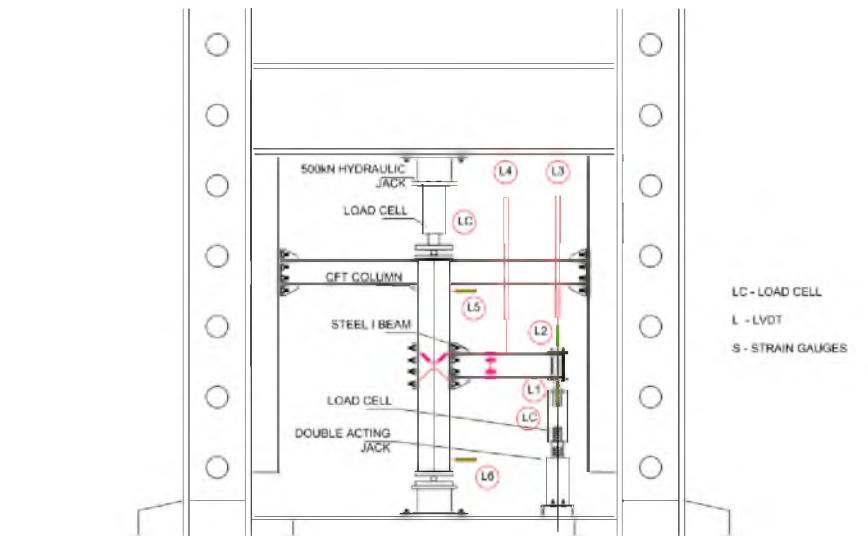


Fig.3. Schematic diagram of test setup

The loading protocol was chosen as ANSI/AISC 2002 cyclic loading programme as shown in Fig. 4 [13]. The rotation mentioned in the protocol was converted as tip displacement of the beam and was monitored in real time, according to these measurement corresponding vertical load were captured and stored continuously. Experimental setup photograph is shown in Fig. 5.

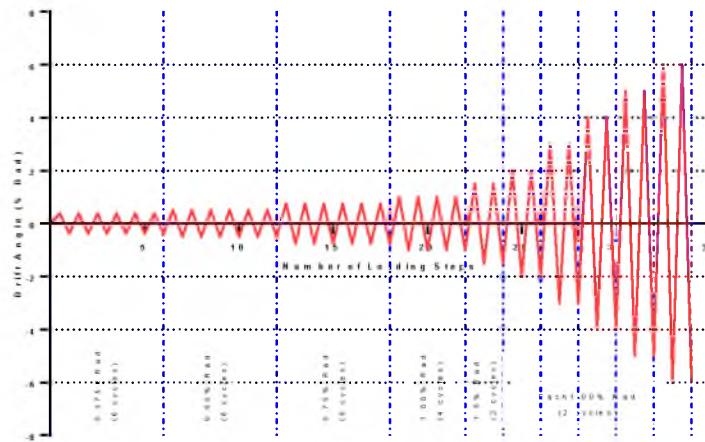


Fig.4. Loading protocol



Fig.5. Test Arrangement

3 Experimental Results and Discussions

The observed physical phenomenon and key structural response parameters captured during the experiment are presented and discussed in detail in the following sections.

3.1 General observations

The test specimen ESFF220 exhibited good ductile properties with characteristics of plastic hinge formation on beam near the vertical stiffener. Actual material test data was used to find out the plastic flexural strength of beam (M_p). In order to calculate moment, force at the tip of beam multiplied by the distance between face of the column to the loading line were used. The initial cycles were perfectly elastic. During 0.02rad cycle of loading peeling of surface paint on the beam near the stiffener region was observed. Slight buckling of top flange was observed during the second cycle of 0.05 rad and which almost get flattened over the negative cycle. Weld failure occurred during the first cycle of 0.06rad and the load dropped to 90% of the peak load. The experiment stopped at an angular rotation of 5.663%rad on the negative side.

Second Specimen ECSC220 also showed similar ductile behaviour. When the angular displacement reaches 0.03rad cracks perpendicular to the beam length originating from top and bottom flange location were visible in the painted area of beam near the vertical stiffener. During the second cycle of 5%rad specimen showed drop in moment capacity with slight torsional buckling which may be due to non uniform distribution of stresses between end plate and steel beam.

For both the specimens peak minimum rotation observed was greater than 0.04 rad in both positive and negative cycles, which satisfy the guidelines provided by AISC 341-10 for composite special moment resisting frame. Hence this type of semi through type connection can be utilized for seismic region.

3.2 Moment Rotation relation

The hysteretic loops of moment at the column face and angular rotation in % rad is presented in Fig.6. The total rotation of the structure is contributed by beam, column and panel zone. From the experimental data evaluation of local and total rotation it was clear that major contribution was from beam because of the design philosophy, strong column strong joint and weak beam. The result shows a stable hysteretic pattern with increase in loop area for both the specimen.

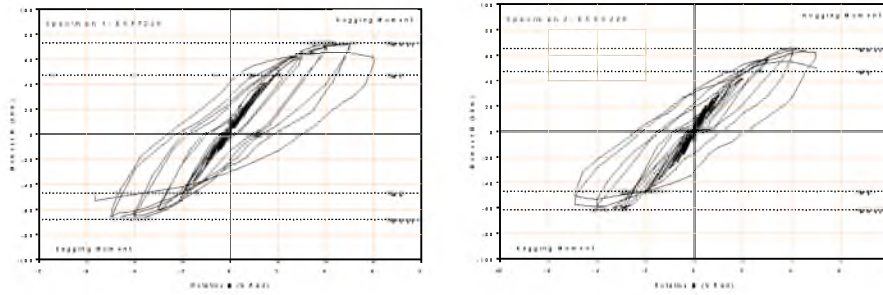


Fig.6. Moment Rotation hysteresis curve

Envelope curve of the moment rotation relationship were extracted from hysteretic curve and plotted in Fig. 7 for detailed investigation on stiffness comparison. The experimental results of flexural strength and comparison with beam plastic moment capacity are listed in Table 2. Beam plastic moment capacity was calculated based on the true strength observed from coupon test.

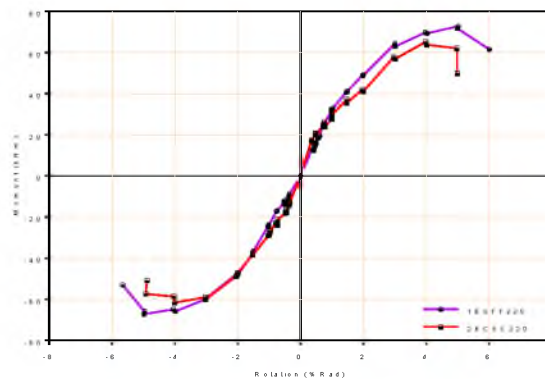


Fig.7. Moment – Rotation Envelop curve

General yield point method was adopted to find the yield point from the skeleton curve. The ductility of the joint can be evaluated by using displacement ductility coefficient, given by the ratio of ultimate displacement to the yield displacement. The yield point was corresponding to 45.57MPa moment for 1ESFF220 and 43.09MPa for 2ECSC220.

$$\mu = \frac{\Delta_u}{\Delta_y} \tag{1}$$

For the first specimen displacement ductility coefficient calculated was 4.36 while specimen 2 was having higher value of 5.27 even though total drift angle observed was lesser by 1%rad. Maximum displacement was chosen corresponding to last successful cycle before failure whose moment resisting capacity of specimen does not fall below beam plastic moment capacity M_p .

Table 2. Test Results

Specimen	Peak Moment (MPa)		M _{test} /M _p		Initial stiffness (kNm/Rad)	
	+M _{max}	-M _{max}	Hogging	Sagging	Hogging	Sagging

1ESFF220	72.813	67.221	1.544	1.425	33.0	24.66
2ECSC220	65.126	61.664	1.38	1.308	44.8	34.09

The initial stiffness of the circular specimen 2ECSC220 was higher than that of square CFT specimen by 35.7% and 38.24% respectively on hogging and sagging.

3.3 Energy Dissipation capacity

Energy dissipation can be found by calculating area bounded by each loop of hysteretic curve. Cumulative energy dissipation is plotted in Fig. 8. Plot shows remarkable increase in energy dissipation capacity after reaching 0.01rad. This parameter gives a clear picture of rate of stiffness degradation and deformation occurred during the increment of rotation cycles. Both the specimen follow almost same path which indicate that split bolt assembly is comparable to conventional straight bolt configuration.

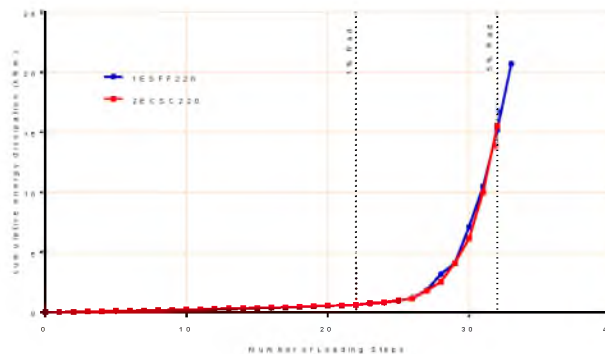


Fig.8. Moment – Rotation Envelop curve

3.4 Failure Mode

During the first cycle of 6% rad. there was a breaking sound followed by initiation of weld crack occurred between top flange and endplate. After that there was no increment in loading but rotation was increasing. Once the load was reduced to 85% of the ultimate load, experiment terminated. On removal of load the beam shows permanent overall deflection and slight local flange buckling at plastic hinge location. The photograph of the joint region after testing is shown in Fig.9. The confinement effect of prestress induced by bolt tightening increases the strength and stiffness of panel zone, which reduces the chance of panel zone failure at seismic regions. No inelastic deformations were observed at the endplate and predrilled hole locations on the column as in case of surface bolted connection [14]. Photograph showing the plastic hinge formation and weld failure is marked in Fig. 9.

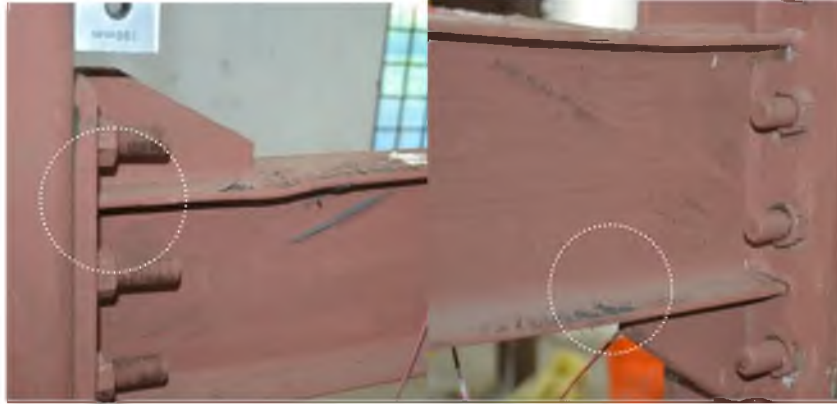


Fig.9. Photograph of specimen after test

For circular specimen experiment was terminated at second cycle of 5% rad were moment resistance tends to fall below M_p and observed minor torsional buckling of beam which leads to non uniform distribution of stress at joint. There was difference between through bolt and split bolt on maintaining the prestress force during the cyclic loading. Split bolt assembly strength depends on the bolt lap length and bond between bolt and concrete which usually reduce during cyclic loading. After debonding the resistance to bending and axial pull/push depends on the tread capacity of the bolt and split assembly.

4 Conclusions

The proposed connection allows to completely avoid field weld. So the erection speed can be increased, thus reducing construction uncertainties.

The presence of triangular stiffener is effective in reducing the local distress like prying on end plate and successfully moves the plastic hinge away from the face of the column which reduces early stage failures of joint.

The test structure response indicate that connection using through bolt can achieve excellent seismic performance by incorporating the participation of the panel zone in resisting the story drift without physical damage for both circular and square specimens.

The specimens shows good hysteretic behaviour with enough energy absorption capacity and stable rotation more than 0.04 rad. The joint can be classified as composite special moment resisting frame as per AISC 341-10. Split bolt assembly configuration proves to be practically good choice for circular column joint without compromising the seismic performance when compared to conventional straight through bolt in square sections.

The failure mode observed was weld cracking at the beam flange - endplate connection region and shows ductile failure pattern with better deformation ability when compared to surface bolting.

The total rotation of the connection is largely contributed by the bending of beam by yielding. Also stiffness degradation was predominant when compared to strength degradation, which ensure the elimination of brittle failures.

Acknowledgment

The authors acknowledge the financial support from Kerala State Council for Science, Technology & Environment (KSCSTE) (project No ETP/05/2016/KSCSTE)

References

1. Ahmed Elremaily, Atorod Azizinamini, "Experimental behavior of steel beam to CFT column connections" , Journal of Constructional Steel Research 57, pp1099–1119 (2001).
2. Lai-Yun Wu, Lap-Loi Chung, Sheng-Fu Tsai, Tung-Ju Shen, Guo-Luen uangSeismic behavior of bolted beam-to-column connections for concrete filled steel tube, Journal of Constructional Steel Research 61, 1387–1410 (2005).
3. Su-Hee Park , Sung-Mo Choi , Yo-Suk Kim, Young-Wook Park , Jin-Ho Kim (2010) Hysteresis behavior of concrete filled square steel tube column-to-beam partially restrained composite connections, Journal of Constructional Steel Research 66 943_953
4. W.H. He , Y. Xiao, Y.R. Guo, Y.L. Fan, Pseudo-dynamic testing of hybrid frame with steel beams bolted to CFT columns, Journal of Constructional Steel Research 88, 123–133. (2013).
5. Ying Qin, Zhihua Chen , Xiaodun Wang Experimental investigation of new internal-diaphragm connections to CFT columns under cyclic loading, Journal of Constructional Steel Research 98, 35–44 (2014).
6. J. Beutel , D. Thambiratnam, N. Perera, Cyclic behaviour of concrete filled steel tubular column to steel beam connections, Engineering Structures 24, 29-38 (2002).
7. X. Li, Y. Xiao, Y.T. Wu , Seismic behavior of exterior connections with steel beams bolted to CFT columns, Journal of Constructional Steel Research 65 1438_1446 (2009).
8. Daxu Zhang, Shengbin Gao , Jinghai Gong,Seismic behaviour of steel beam to circular CFST column assemblies with external diaphragms, Journal of Constructional Steel Research 76 155–166 (2012).
9. Zhong Tao, Wei Li, Bo-Lin Shi, Lin-Hai Han, Behaviour of bolted end-plate connections to concrete-filled steel columns, Journal of Constructional Steel Research 137 194-2018 (2017)
10. Ikhlas S. Sheet, Umarani Gunasekaran, Gregory A. MacRae, Experimental investigation of CFT column to steel beam connections under cyclic loading, Journal of Constructional Steel Research 86 167–182 (2013).
11. ANSI/AISC 358-10 Prequalified Connections for Special and Intermediate Steel Moment Frames for Seismic Applications, Chicago: American Institute of Steel Construction; 2010.
12. Roozbeh Kiamanesh, Ali Abolmaali, Mehdi Ghassemieh, The effect of stiffeners on the strain patterns o the welded connection zone", Journal of Constructional Steel Research 66 2010, 19_27. (2010).
13. ANSI/AISC 341-10 Seismic Provisions for Structural Steel Buildings, Chicago: American Institute of Steel Construction; 2010.
14. Walid Tizani, Zhi Yu Wang, Iman Hajirasouliha Hysteretic performance of a new blind bolted connection to concrete filled columns under cyclic loading: An experimetal investigation" Engineering Structures 535_546 (2013).

Effect of Swimmer Bars on the Behaviour of Exterior Beam column joints under Reverse Cyclic Loading

Shahana S¹ and Tom George²

¹PG Research Scholar, Structural Engineering, Mar Baselios College of Engineering and Technology,
Thiruvananthapuram, Kerala, India
Shahanashajahan2014@gmail.com

²Asst. Professor, Department of Civil Engineering, Mar Baselios College of Engineering and Technology,
Thiruvananthapuram, Kerala, India
Tomgeorge1507@gmail.com

Abstract. Beam-Column Joint is the portion of column where a beam is used to join. These joints are the most critical portions of a Reinforced Concrete Moment Resisting Framed structures (MRF) because, the loads from adjacent beams and columns are transferred through the joint. Joints have no problem when it is subjected to dead load and live load only, but when it is subjected to seismic load the condition will be different and large. These would be developed even with dead load and live load, concentrated at the critical zone ie, joints. Failure due to shear is often sudden and catastrophic. The shear cracks progress rapidly without warning, and the diagonal cracks are considerably wider than the flexural cracks. Usually vertical stirrups are provided as shear reinforcement. Here in this study two types of shear reinforcements will be provided :- traditional stirrups and swimmer bars. Swimmer bar system is defined as inclined bars, with its both ends bent horizontally for a short distance and welded to both top and bottom flexural steel reinforcement. Eight exterior beam column joints were cast and tested under reverse cyclic loading in this study. The specimens with swimmer bars exhibited better performance in terms of ultimate strength, energy absorption, dissipation, displacement ductility and stiffness.

Keywords: Swimmer bars, exterior beam column joints, moment resisting structures, reverse cyclic loading

1. Introduction

Moment Resisting Frames (MRF) are the rectilinear assemblages of structural elements such as beams and columns, with beams rigidly connected to the column [1]. In the times when the importance of earthquake was unknown, the buildings were designed only for gravity loads. So such buildings will be in a safe zone until it is affected by an earthquake. Earthquake is a destructive phenomenon which causes severe damage to structures. In most of the structures, failure occurs in the joint portion. So that is why beam-column joint is considered as the major failure zone of a structure.

The portion of the column at which beam is used to join is called beam-column joints. Beam-column joints are the most vulnerable part of a MRF system because of that the forces from adjacent beams and columns are transferred through the joint. As a result of that brittle shear failure will occur at the joint. A beam-column joint has no problem if it is subjected to normal dead load and live loads. When it is subjected to lateral loads such as seismic load, the behavioural action of beam-column joints are entirely different. To enhance the safety of a Reinforced Concrete (RC) structures against seismic loadings, designers should mainly concentrate on the shear strength and ductility performance of joints and ensure that brittle shear failure at joint should be avoided. Shear strength of a beam-column joint is the resistance of the joint against the shear forces developing in it. Shear strength is an important criterion of design considerations in beam-column joints of both exterior and interior types. During the construction of RC structures congestion of reinforcement normally occurs at beam-column joints. In exterior joints, longitudinal bars of beam should be properly anchored into the column for ensuring good bond of bars in joint. The transverse reinforcement help to provide adequate ductility of beam-column joints and also resist shear force which helps to reduce the cracking and crushing of concrete. Stirrups are most commonly used as transverse reinforcement.

The beam-column joint is defined as the portion of the column within the depth of the deepest beam that frames into the column [2]. In a MRF structure three different varieties of joints can be found out

(i) Exterior Beam-Column Joints

(ii) Interior Beam-Column Joints

(iii) Corner Beam-Column Joints

In concrete building construction, stirrups are most commonly used as shear reinforcement, for their simplicity in fabrication and installation. Stirrups are spaced closely at the high shear region. Congestion near the support of the reinforced concrete structures due to the presence of the closely spaced stirrups, increases the cost and time required for installation. Bent up bars are also used as shear reinforcement along with the normal stirrups in order to resist the applied shear force. Bent up bars also used as shear reinforcement. The use of bent-up bars is not preferred nowadays. Inclined bars also used as shear reinforcement, they are known as swimmer bars. There are three types of inclined bars. They are single, rectangular and rectangular with cross bracings.



Fig.1 Swimmer bars

Inclined bars are very effective in beams as transverse reinforcement. Heba(2017) investigated the effect of swimmer bars on the behavior of normal and high strength reinforced concrete beams. The test result showed that swimmer bars increases the shear capacity and reduces the number and propagation of shear cracks. Also showed that the shear strain by using swimmer bars were higher than those by using traditional stirrups [5]. Saravanakumar and Govindaraj (2016) conducted an experimental study on RCC beams to investigate the strength and shear resisting capacity of various shear reinforcements such as traditional shear reinforcements, inclined shear reinforcements, combination of vertical and inclined shear reinforcement and vertical shear reinforcement with inclined cross bracings. The various parameters like load deflection characteristics, strength characteristics, shear cracks and failure mode of concrete were investigated. It was found that the shear reinforcement configuration influence the strength characteristics of the beam [6]. Omar and Sinan (2014) investigated the effect of position and type of shear reinforcement of high strength reinforced concrete deep beams. Test was conducted on eight reinforced concrete deep beams with stirrups in different type and position using high strength concrete. The test variables were type and position of web reinforcement, shear stress on horizontal stirrups and shear stress of inclined stirrups with in shear span, within middle span and along the beam. The test results indicated that beam with vertical an inclined bars with in the shear span has better shear carrying capacity than others [8]

Only few studies were conducted to study the effect of inclined bars as shear reinforcement. This paper aimed to investigate the effect of inclined bars on the behavior of beam column joints.

2. Research significance

The present study demonstrates the effect of using swimmer bars instead of traditional stirrups on improvement of shear performance in exterior beam column joints and to identify the most efficient shape of swimmer bars in the critical zone of beam column joint

3. Experimental investigations

Four types seismically detailed exterior beam column joint specimens were cast and tested. The cross sectional dimensions adopted were 200mm x 200mm for column and 150mm x 200mm for beam. M40 grade concrete and Fe 415 grade steel are adopted for design. The exterior beam column joint is considered and designed as per the norms specified in IS 456:2000[20]. The mix design was conducted as per IS 10262:2009. The reinforcement detailing as shown in fig 2.

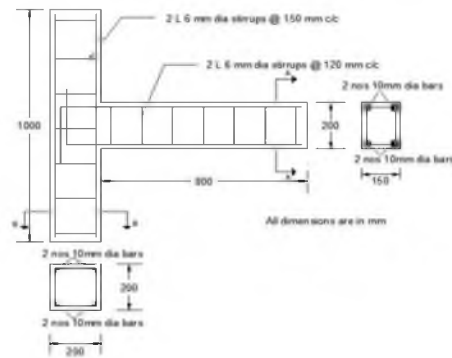


Fig. 2 Reinforcement detailing of beam column joint

3.1 Characteristics of specimen

Four types of joint detailing are considered for the present study. All joints are identical in cross-sectional dimensions and the variations are limited in transverse reinforcement detailing. The conventional ductile beam column joint specimen satisfying joint detailing stipulated in IS 456:2000 is referred to as specimen C. The newly proposed detailing essentially involves the use of diagonal welded bars in the joint region. The ties in the joint region is replaced by diagonal welded bars. The specimen with welded diagonal bars at the joint region is referred to as CX. Other two types of specimens are CXS and CXX. CXS with diagonal bars at the joint and single swimmer bars at the critical zone of beam. In CXX specimen instead of single bars rectangular with cross bracings are provided. These specimens are shown in the fig. 3.



a) C

b) CX

c) CXS

d) CXX

Fig. 3. Specimens

The specimen are cast using Portland Pozzolona Cement. Manufactured sand (M sand) conforming to zone II is used as fine aggregate. Crushed granite stone of maximum size not exceed 20 mm is used as coarse aggregate. The mix proportion arrived at is 1:1.81:3.36 by weight and water cement ratio kept as 0.4. The 28th day average compressive strength from 150 mm size size cube test is obtained as 48.65 N/mm².

3.2 Test setup and loading

The schematic diagram of test set up is shown in Fig.4. The specimens are tested in an upright position in a 1000 kN capacity loading frame after 28 days of curing. The bottom end portion of column is kept fixed and top end is kept as hinge support. The hinged condition was incorporated by using a steel ball which is placed in-between the groove portions of the two identical plates made of steel. To make joint in stable condition during reverse cyclic load, the column of each beam column joint was subjected to an axial load of 20% of the axial load carrying capacity of the column was applied over it by using a hydraulic jack. Reverse cyclic load was applied at the tip of beam through a hydraulic jack. A load cell, attached to the plunger measures the load. The deflection of beam tip is measured at every 2 kN load interval for forward and backward cycles using LVDTs. The test setup in the laboratory is shown in fig 5.

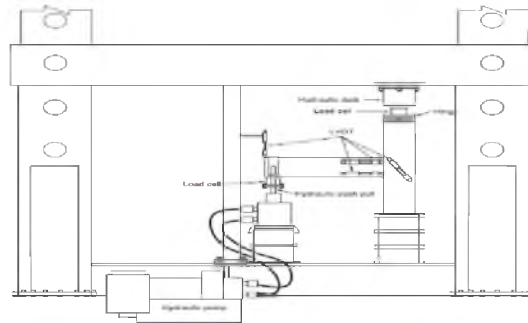


Fig.4 Schematic diagram of test setup



Fig.5 Test setup in the laborato

4. Results and discussion

The behaviour of beam-column joints under reverse cyclic loading is determined and parameters such as failure crack pattern, load-deflection characteristics, envelop curve, first crack load, ultimate load, energy absorption capacity, energy dissipation capacity, displacement ductility factor and stiffness degradation are discussed. The observations during the test and the results are briefly described below

4.1 Crack pattern

Cracking pattern is very important parameter in assessing the performance of a beam column joint. Failure of beam column joint by formation of brittle joint shear cracks are undesirable. The crack pattern of the specimens are shown in fig 6.

In the control beam column joint, the first crack was observed near the joint portion. The further increasing load causes additional formation of cracks on beam portion of joints, extending and widening of initial cracks were also occurred. The failure of control specimen was seen at the interface between beam and column. In the case of CX, CXS and CXX specimens, no cracks were seen during the initial load cycles. As load increases horizontal and inclined cracks were seen in the effective depth portion. At ultimate load CX specimen failed at the effective depth portion of beam. It is away from the beam column interface. CXS specimen also failed as in the same pattern. But so many thin hairline cracks are observed at failure. In the specimen CXX, first crack observed in the fifth loading cycle when the load reached 10 kN in the upward cycle. The specimen were failed at the interface between beam and column.

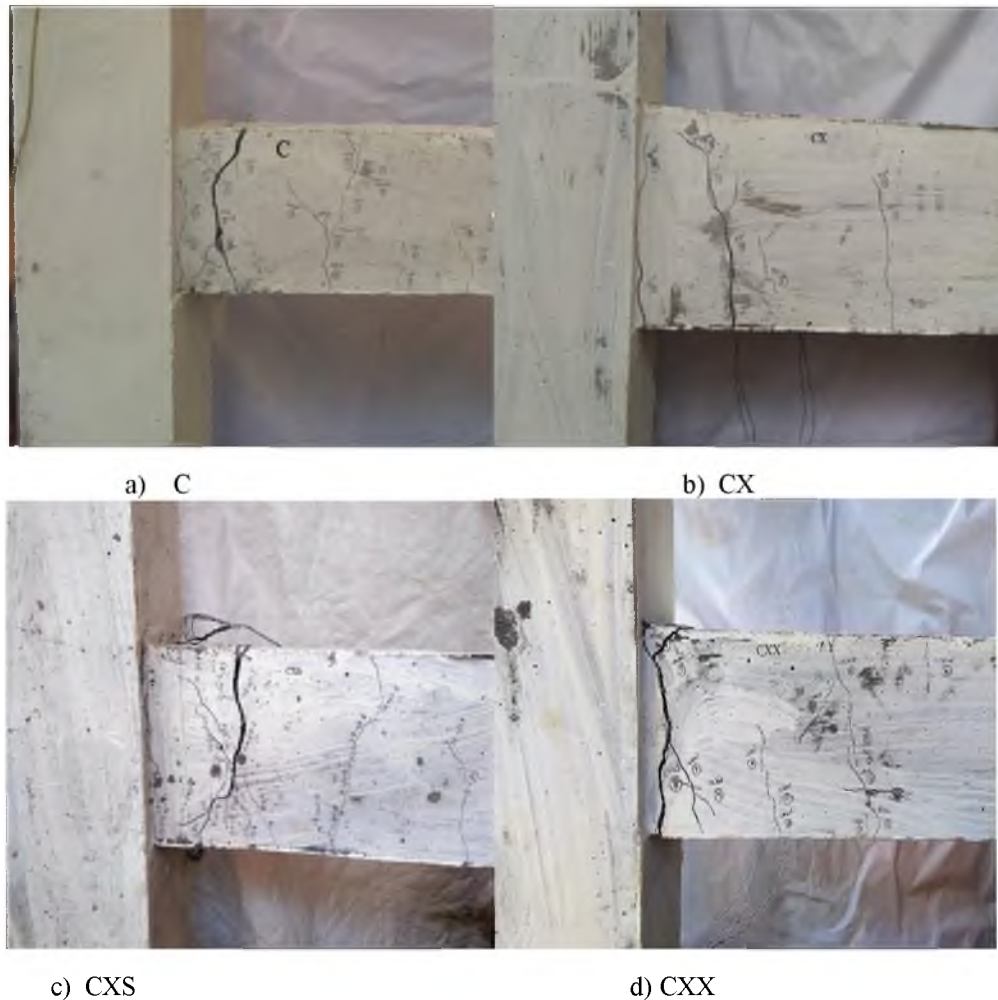


Fig.6 Crack pattern of specimens

4.2 First crack load and ultimate load

Table 1 summarizes the details of first and ultimate load carrying capacity of tested specimens. Swimmer bars improved the load carrying capacity of the exterior beam column joints. The specimen with diagonal bars at the joint and rectangular bracing with cross bracings at the effective depth in the beam portion have more load carrying capacity. The ultimate strength of the specimens CXX, CXS and CX showed a percentage improvement of 35%, 17% and 16% respectively over control specimen C.

Table 1. First crack load and ultimate load of specimens

Specimen designation	First crack load(kN)	Ultimate load(kN)			Percentage increment
		Forward cycle	Backward cycle	Average	
C	6	16	-15.2	15.6	-
CX	8	18.1	-18	18.05	16
CXS	8	18.4	-18.1	18.25	17
CXX	10	21.4	-20.6	21	35

4.3 Hysteresis loops

The force-displacement hysteresis loops for the specimens are shown in the fig 7. Hysteresis loops show the performance of beam column joint under reverse cyclic loading. The area under the curve denotes the potential

energy stored in the structure at the maximum displacement position. The wider the loop, the larger will be the energy dissipation capacity and better will be the seismic performance. The shear strength possessed by the joint CXX was observed to be higher compared to the specimens C, CX and CXS as evident in the load cycles sustained

by specimen. The shear strength of the joints is in the order of CXX, CXS, CX and C. CXS and CX specimen's shows similar results. From the hysteresis curves it can be clearly seen that the area enclosed by the hysteresis curve of specimen CXX is large compared to the area enclosed by the remaining three specimens. The performance of the specimen CXX in the context of energy dissipation and strength was far superior to that of specimen CX, CXS and C. This shows that addition of inclined welded bars improves the seismic resistant behaviour of joints.

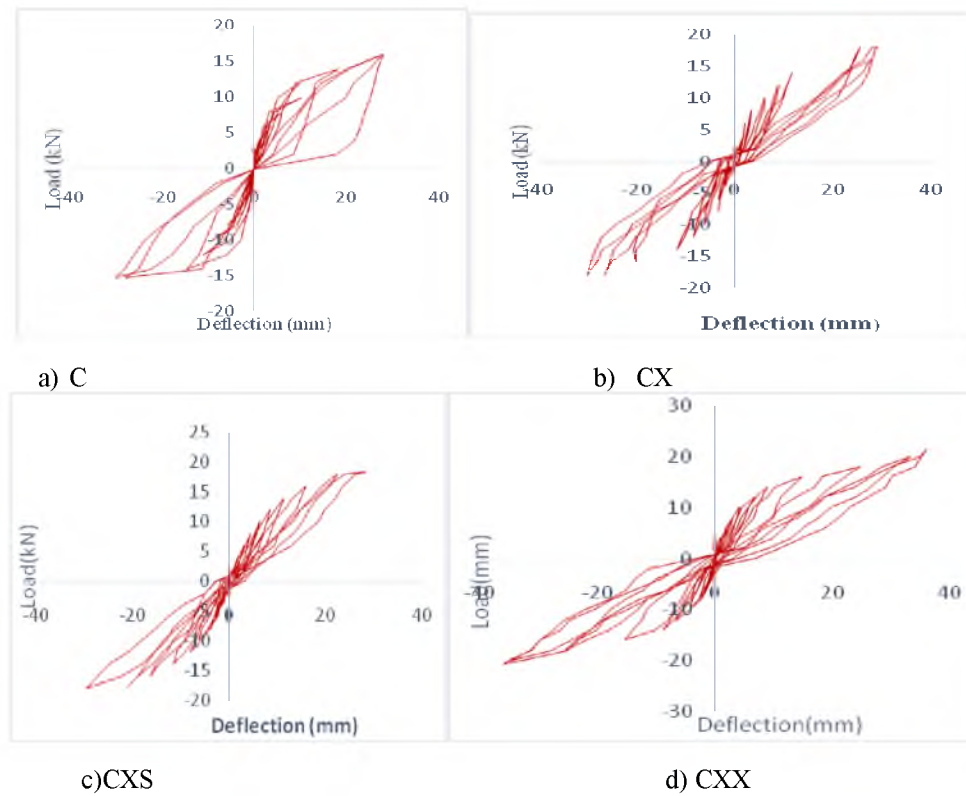


Fig. 7 Hysteresis loops of specimens

4.4 Energy dissipation capacity

Energy dissipation capacity is another important parameter that helps to assess the behaviour of beam column joint under reverse cyclic loading. Fig.8 summarises the details of energy absorption capacity of tested specimens. The specimen CXX shows more energy dissipation capacity than others. Which shows better performance under seismic excitation.

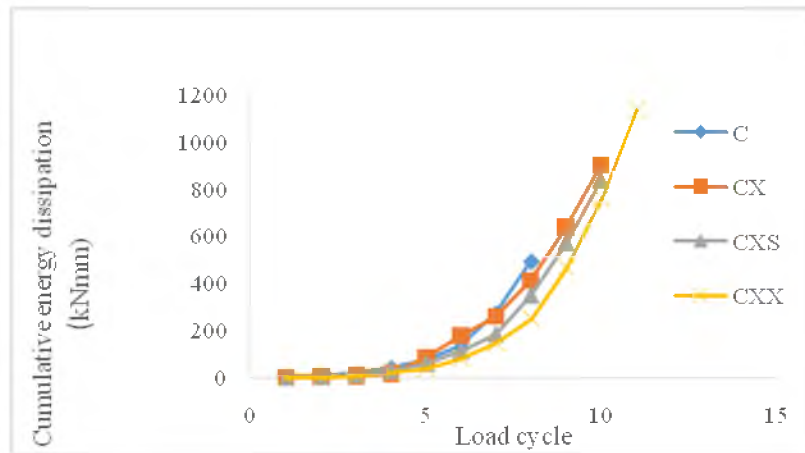


Fig.8 Energy dissipation capacity of specimens

4.5 Envelope curve

The envelop curves for the control and retrofitted joints are plotted in fig. 9. The envelop curve is a curve obtained by joining the peak points of all the cycles of hysteresis loop. It was used to calculate the first crack load, ductility factor and energy absorption capacity of each specimens.

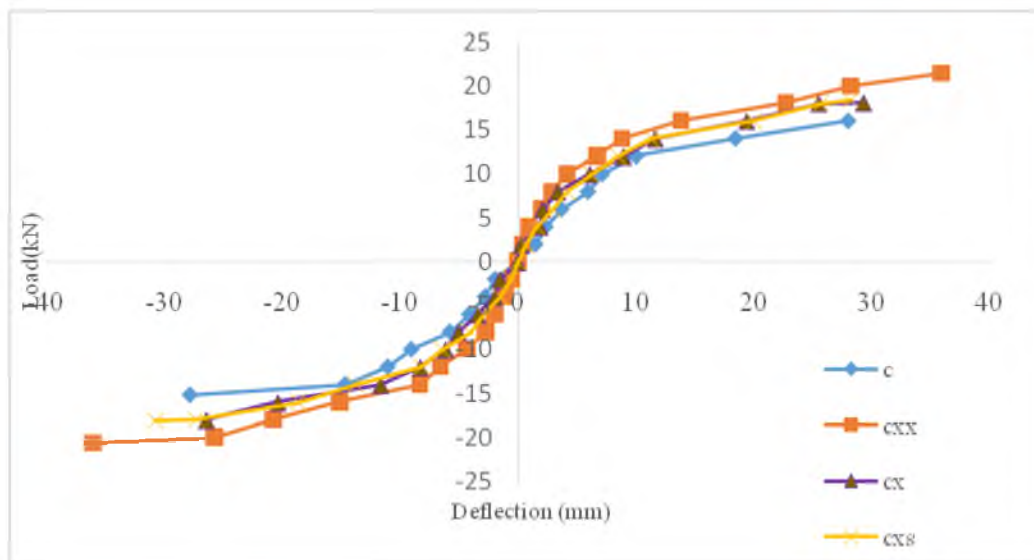


Fig.9 Envelope curve

4.6 Energy absorption capacity

Energy absorption capacity is another important parameter that helps to assess the behaviour of beam column joint under seismic loading. Table 2 summarizes the details of energy absorption capacity of tested beams. The specimen CXX exhibited an increase of 71% in energy absorption capacity.

Table 2. Energy absorption capacity of specimens

Specimen designation	Energy absorption capacity(kNmm)			Percentage Increment
	Forward	Reverse	Average	

	cycle	cycle		
C	295.14	287.80	291.47	-
CX	348.80	365.67	357.24	23
CXS	344.58	362.06	353.32	21
CXX	496.83	499.61	498.22	71

4.7 Displacement ductility factor

Ductility of a structure is its ability to undergo deformation beyond the initial yield deformation while still sustaining load. The displacement ductility factor is the measure of ductility of a structure. It is calculated by taking ratio of maximum displacement (δ_m) to the yield displacement (δ_y). The yield displacement, (δ_y) is calculated from the line which is extended from first crack load point of the load deflection plot, this line is extended and allowed to intersect with the 80% load capacity horizontal line. The corresponding displacement is considered as yield displacement. The other point of intersection of the curve on the 80% of the ultimate load capacity line is the ultimate displacement, (δ_m). The displacement ductility factor of control and retrofitted specimens are given in table 3.

Table 3. Displacement ductility factor

Specimen designation	Displacement ductility factor	Percentage increment (%)
C	1.79	-
CX	2.33	30
CXS	2.35	31
CXX	3.23	81

The ductile nature of the structure allows it to dissipate the energy induced during earthquake. The ductility of a structure is commonly measured in terms of displacement ductility factor. Ductility factor of CXX specimen has the maximum value as compared to other specimens. The percentage increase in ductility factor is in the order of CXX followed by CXS and CX, and corresponding values are 31, 31 and 81% respectively as compared to control specimen. The usage of diagonal bars in the joint portion and effective depth of beam portion has clearly influence the ductile behaviour of CXX specimen.

4.8 Stiffness degradation

Stiffness is defined as the load required to produce a unit deflection. Stiffness of the reinforced concrete beam-column joint gets reduced when the joint is subjected to cyclic or reverse cyclic load. This stiffness reduction of the specimens can be calculated by computing the secant stiffness and which is the measure of stiffness degradation of the beam-column joints. The secant stiffness of each cycles was calculated by drawing a line between the maximum positive and negative displacement points in each halves of a cycle and takes the slope. Stiffness degradation curve of each specimen is given in fig. 10.

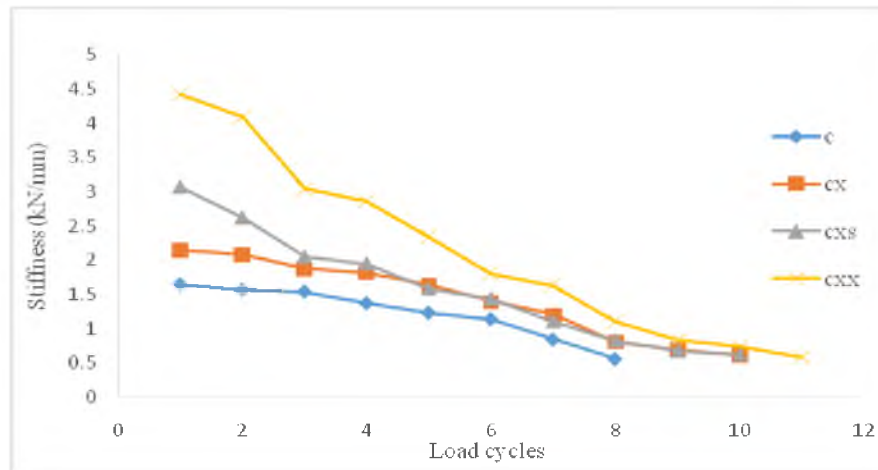


Fig. 10 Stiffness degradation

From the graph it is understood that joint confinement could increase the initial stiffness as compared to the control specimens. Maximum value of initial stiffness is obtained for CXX specimens. The increase in initial stiffness values is in the order of CXX followed by CXS and CX respectively as compared to control specimen.

5. Conclusion

Here the effect of swimmer bars as transverse reinforcement on the behaviour of exterior beam-column joints was studied. Behaviour of control and non-conventional beam-column joints were studied under reverse cyclic load and their performance was compared based on the parameters such as crack pattern, first crack load, ultimate load, energy absorption capacity, energy dissipation capacity, displacement ductility factor and stiffness degradation values. The energy absorption capacity was found to increase by 21, 23 and 71 percentage for CXS, CX and CXX respectively when compared to the control specimen. Likewise the ultimate load value was found to increase by 16, 17 and 35 percentage for CX, CXS and CXX respectively as compared to the control specimen. Similarly the ductility factor also increased by 32, 31 and 81 percentage for CX, CXS and CXX respectively. The crack pattern of the non-conventional joints were also flexural but was found to shift more towards the joint region. Ductility behaviour and energy dissipation capacity of non-conventional beam column joints were found to be better than the conventional joints. The increase in initial stiffness values is in the order of CX followed by CXS and CXX respectively as compared to control specimen and after each cycle of reverse cyclic load the stiffness of joint reduces upto failure.

From the results it is understood that all of the parameters were improved significantly for the non-conventional specimens. Among the non-conventional specimens CXX exhibited better performance and can be a possible alternative to avoid reinforcement congestion in the joint region.

References

- [1] Titiksh, A. and Gupta, M. K.: A Study of the Various Structural Framing Systems Subjected to Seismic Loads”, *SSRG International Journal of Civil Engineering (SSRG-IJCE)*, 2, 23-30 (2015)
- [2] Kaliluthin, A.K., Kothandaraman, S. and Ahamed, T.S.: A Review on Behavior of Reinforced Concrete Beam-Column Joint, *International Journal of Innovative Research in Science, Engineering and Technology*, 3, 11299-11312(2014)
- [3] “Types of beam column joints”, <http://www.masterbuilder.co.in> accessed on 13/11/2017
- [4] Najmi, N., Al-Nasra, M. and Asha, M.: Investigating the Use of swimmer Bars in the Reinforced Concrete Beams, *International Journal of Civil and structural Engineering*, 3, 313-320(2013)
- [5] Heba, A.: Effect of using swimmer bars on the behavior of normal and high strength concrete beams, *Ain Shams Engineering Journal*, 8, 29-37(2017)

- [6] Saravanakumar, P. and Govindaraj, A.: Influence of Vertical and Inclined Shear Reinforcement on the Behavior in Reinforced Concrete Beams, *International Journal of Civil Engineering and Technology*, 7, 602-610(2016)
- [7] Al-Nasra, M. and Asha, M.: Investigating the Use of spliced swimmer Bars as shear Reinforcement in Reinforced Concrete Beams, *Journal of Engineering*, 5, 47-54(2015)
- [8] Omar, Q. A. and Sinan, A. Y.: Effect of type and Position of Shear Reinforcement of High Strength Reinforced Concrete Deep Beams, *Al-Rafidain Engineering Journal*, 21, 69-79(2013)
- [9] Al-Nasra, M., Najmi, S. and Ibrahim, A.: Effective Use of Space Swimmer bars in Reinforced Concrete Flat Slabs, *International Journal of Engineering Science & Research Technology*, 2, 195-201(2013)
- [10] Al-Nasra, M. and Asha, A.: shear Reinforcements in the Reinforced Concrete Beams”, *American journal of Engineering Research*, 2, 191-199(2013)
- [11] Najmi, s., Al-Nasra, M. and Asha, M.: Improved Shear Performance of Bent- Up Bars in Reinforced Concrete Beams, *International Journal of Engineering Science & Research Technology*, 2, 1264-1268(2013)
- [12] Noor, H.: The Use of Horizontal and Inclined Bars as Shear Reinforcement”, Master Thesis, University of Technology Malaysia(2005)
- [13] Piyamahant: Shear Behaviour of reinforced concrete beams with small amount of web reinforcement”, M. Eng. Dissertation Kochi University of Technology Japan(2002)
- [14] Tran, T. M.: Influence Factors for the Shear Strength of Exterior and Interior Reinforced Concrete Beam Column Joints, *Sustainable Development of Civil, Urban and Transportation Engineering Conference Procedia Engineering*, 63-70(2016)
- [15] Beydokhty, E. Z. and Shariatmadar, H.: Behavior of Damaged Exterior RC Beam-Column Joints Strengthened by CFRP Composites”, *Latin American Journal of Solida and Structures*, 13, 880-896(2016)
- [16] Bindhu, K. R., Sukumar, P. M. and Jaya, K.P.: Performance of Exterior Beam-Column Joints under seismic type loading, *Journal of earthquake Engineering*, 46, 47-64(2009)
- [17] Somma, G.: Shear strength of fiber reinforced concrete beam-column joints under seismic loading, *The 14th World Conference on Earthquake engineering* (2008)
- [18] Ahmed, G. and Said, A.: Shear strengthening of beam-column joints, *Engineering Structures*, 24, 881-888(2002)
- [19] Ganesan, N., Indira P.V. and Ruby, A.: Steel Fibre Reinforced High Performance Concrete Beam-Column Joints Subjected to Cyclic Loading”, *ISETJ Earthq Technol.* 44, 445-456(2007)
- [20] IS 456: 2000 (Reaffirmed 2005): Plain and Reinforced Concrete- Code of Practises, Bureau of Indian Standards, New Delhi, India, 2000.
- [21] Anjana, V. G.: Experimental Study on Fibre Reinforced High Performance Concrete Beam Column Joints with Recycled Concrete Aggregates, Thesis report(2015)
- [22] Bindhu, K., Mohana, N., and Sivakumar, S.: New Reinforcement Detailing for Concrete Jacketing of Non ductile Exterior Beam Column Joints, *Journal of performance of constructed facilities*, 9, 1-9(2014)
- [23] Ganesan, N., Indira P. V and Sabeena, M. V.: Behaviour of Hybrid Fibre Reinforced Concrete Beam-Column Joints Under reversed Cyclic Loads, *Materials and Design*, 54, 686-693(2014)

Experimental and Analytical Study on Geopolymer Concrete Beam with Hollow Space below Neutral Axis

Sherin kurikesu¹, Abhirami S²

¹MTech student

SreeNarayana Institute of Technology

Theppupara, Adoor, Kerala

sherinkurikesu06@gmail.com

²Assistant Professor, Department of Civil Engineering

SreeNarayana Institute of Technology

Theppupara, Adoor, Kerala

sabhirami91@gmail.com

Abstract. In this paper, a detailed study was carried out on strength behaviour of flyash based geopolymer concrete with hollow space below neutral axis. Use of hollow space at and near the neutral axis will reduce the selfweight and saves concrete materials. This paper focuses on material minimization by introducing hollow space using pvc pipe in tension zone of beams. By this method, we can reduce the dead loads which contribute to seismic effect in high rise structures. Geopolymer concrete shall be produced without using any amount of ordinary Portland cement. Alkaline solution produced aluminosilicate gel that acts as the binding material for the concrete. Thus many efforts are being made to reduce the usage of opc which responsible for carbondioxide emission. M30 grade concrete is used for ordinary and geopolymer concrete. Experimental validation was done by ANSYS software.

Keywords: Fly ash, alkaline solution, opc ,pvc.

1. Introduction

The global warming is an environmental problem caused due to the emission of greenhouse gases, such as carbon dioxide (CO₂), to the atmosphere. As the demand for concrete increases in construction field, the demand for Portland cement also increases. Cement industry is held responsible for some of the CO₂ emissions. Thus many efforts are being made to reduce the usage of cement. The concrete just above neutral axis is less stressed whereas the concrete below the neutral axis acts as a shear transmitting media. Sustainability can be achieved by replacing the partially useful concrete, by saving concrete, which reduces the demand for material and cost. So new technology materials like geopolymers offer waste utilization and emissions reduction, in which fly ash is used as a base material instead of OPC in geopolymer concrete. Geopolymer concrete is an innovative construction material which is produced by the chemical action of inorganic molecules. Fly Ash, a by-product of coal obtained from the thermal power plant is available in plenty worldwide. Flyash is rich in silica and alumina reacted and an excellent alternative construction material to the existing plain cement concrete. In this work flyash based geopolymer is used. Flyash is a waste product generated from thermal power plant. Hence we can protect water bodies from contamination due to flyash disposal and by creating hollow space at tension zone by inserting the pvc pipe we can reduce the quantity of concrete and cost can be reduced. The electrical conduits, air conditioning small ducts etc. also been taken through these hollow beams.

2. Objective

The main objectives of the present study is

- The main aim of this study is to find the structural behaviour of hollow GPC beam.
- To study the flexure behaviour of hollow pcc concrete beam at different diameter pvc pipe.
- To determine the flexural strength.
- To determine the load carrying capacity of hollow concrete beams.

3. Methodology

The work methodology consist of,

- 1) Selection of grade of concrete; M30 for opc and geopolymer concrete.
- 2) Mix design of M30 grade concrete.
- 3) Creating the hollow section inside the beam with two dia 25mm pipes and 32mm pipe.
- 6) Casting, Curing and Testing
- 7) Result and discussion

4. Material Used

4.1. Flyash

Fly ash is a by-product of coal-burning power plants. Therefore, huge quantities of fly ash will be available for many years in the future. Fly ash can be used in Portland cement concrete to enhance the performance of the concrete. Flyash has been successfully used to manufacture geopolymer concrete when the silicon and aluminum oxides constituted about 80% by mass.

4.2. Alkaline solution

A combination of sodium silicate solution and sodium hydroxide (NaOH) solution can be used as the alkaline liquid. It is recommended that the alkaline liquid is prepared at least 24 hours before use. The addition of sodium silicate solution to the sodium hydroxide solution as the alkaline activator enhanced the reaction between the source material and the solution. The concentration of sodium hydroxide solution was 16 Molar.

4.3. Coarse aggregate

Coarse aggregate used was locally available crushed angular granite metal of 20mm size. These aggregates are bound together by the cement and fine aggregate in the presence of water to form concrete.

4.4. Fine aggregate

Fine aggregate consist of natural sand or crushed stone sand. It should be hard, durable and clean and be free from organic matter .sand conforming to zone II is used.

5. Material Test

Test results on cement, fly ash, and fine aggregate and coarse aggregate are given in table 1.

Table 1:Material property

TEST	MATERIAL USED	VALUES OBTAINED
Specific gravity	Cement (53grade)	3.16
Specific gravity	Fine aggregate (m sand)	2.56
Specific gravity	Coarse aggregate	2.96
Specificgravity	Fly ash	2.3
Water absorbtion	Fine aggregate	2.01%
Water absorbtion	CoarseAggregate	0.326%
workability	Geopolymer M30 grade	100mm
Workability	Opc concrete (M30 grade)	120mm

6. Mix design

The compressive strength and the workability of geopolymer concrete are influenced by the proportions and properties of the constituent materials .Table 3 and 4 shows the mix proportion of geopolymer concrete and OPC concrete

TABLE 2: Mix Design of GPC

Flyash(kg/m ³)	550
Sodium silicate(kg/m ³)	239.64
Sodium hydroxide(kg/m ³)	95.86
Fine aggragte(kg/m ³)	576.51
Coarse aggregate(kg/m ³)	854.68
Extra water(l/m ³)	16.5

TABLE 3:Mix Design Of OPC

cement(kg/m ³)	394.32
Fine aggregate(kg/m ³)	643.15
Coarse aggregate(kg/m ³)	1246.6
water(kg/m ³)	197.16
Water cement ratio(kg/m ³)	0.5

7. Experimental setup

7.1 Mixing of geopolymer

In the laboratory, the fly ash and the aggregates were first mixed together for about three minutes. The alkaline solutions, sodium hydroxide solution and sodium silicate solution were prepared separately before one day of casting to get the required strength and mixed together at the time of casting. Since lot of heat is generated when sodium hydroxide pellets react with water, the sodium hydroxide solution was prepared a day earlier to casting. The alkaline solutions were added to mixed materials. The mixing of total mass was continued until the mixture become homogeneous and uniform in colour.

7.2 Curing of geopolymer

After casting the specimens, they are kept in rest period in room temperature for one day. Heat-curing substantially assists the chemical reaction that occurs in the geopolymer paste the geopolymer concrete is de-moulded and then placed in an autoclave for steam curing for 24 hours at a temperature of 60degree Celsius. The compressive strength of geopolymer concrete cubes increase with the increase in age.

8. Test Procedure

Geopolymer concrete cubes, cylinder and beam according to standard dimension were cast. cube compressive strength, cylinder split tensile strength and beam flexural strength are determined by UTM .7,14,28 days results were taken. Typical PCC beams of size 100x100x500mm were used with hollow neutral axis are made by PVC pipes of 25 mm ϕ and 32 mm ϕ . For plain geopolymer beam the neutral axis will be at the centre. The length of the pipe inside the beam neutral axis is 450mm and an anchorage length of 25mm on each side is provided for the transfer of load. The depth of neutral axis is taken as half of total length. All the beams were subjected to 2-point flexural test. Figure 1 shows the beam with pipe.



Fig 1: Beam with pipe

9. Result and Discussion

9.1. Comparison of geopolymer and conventional concrete

PARAMETRES	GPC	OPC
Compressive strength	31.01N/mm ²	30.82 N/mm ²
Tensile strength	4.46N/mm ²	4.3 N/mm ²
Flexural strength	4.85N/mm ²	4.5 N/mm ²
Poisson's ratio	0.224	0.2
Modulus of elasticity	22360Mpa	27386Mpa

From this it is observed that geopolymer concrete has same properties as that of ordinary Portland cement concrete

9.2 Comparison of solid geopolymer and geopolymer with two diameter pipe beam.

PARAMETRES	Solid GPC	25mm dia	32mm dia
Ultimate load	9.7KN	10.2KN	11.8KN
Flexural strength	4.85N/m ²	5.1N/mm ²	5.9N/mm ²
Bending moment	1.21KNm	1.29KNm	1.47KNm
Deflection	0.135mm	0.142mm	0.164mm

9.2.1 Ultimate load carrying capacity

Fig.1 show the Ultimate load comparison of solid and hollow beams

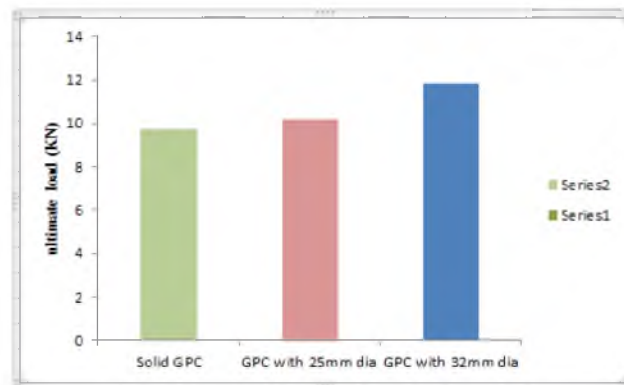


Figure 2: Comparison of load

It is observed that ultimate load carrying capacity of GPC beam with hollow space is higher than the geopolymer solid beam

9.2.2 Flexural strength

In this test, plain geopolymer concrete beam was subjected to flexure using symmetrical two point loading until failure occurs. The comparative study of flexural strength of control beams with beams having hollow near neutral axis zone is as shown in Fig. 3

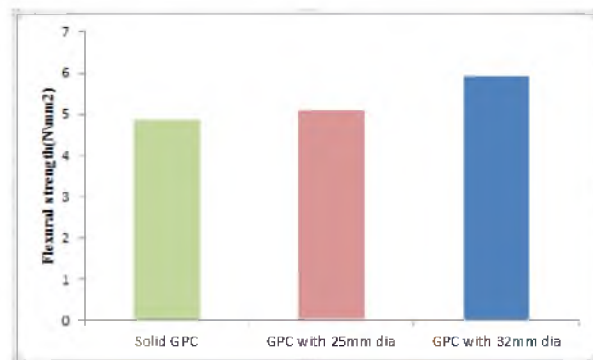


Figure 3: Comparison of flexural strength

9.2.3 Deflection

The corresponding deflection of solid control beam and beam with hollow neutral axis is given in fig:4 from manual calculation.it shows that it lies within the limit as per code IS456-2000.

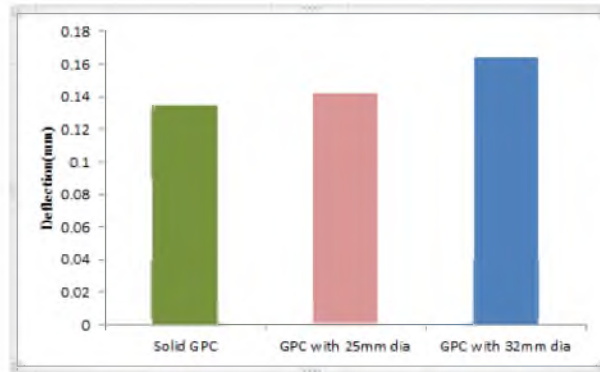


Figure 4: Comparison of deflection

9.3 Crack pattern

In initial stages of loading, all beams were un-cracked beam. When the applied load reached the rupture strength of the concrete on specimens, the concrete started to crack. The failure pattern in all the tested beams was observed as a flexure failure. All the beams showed the same pattern of failure.

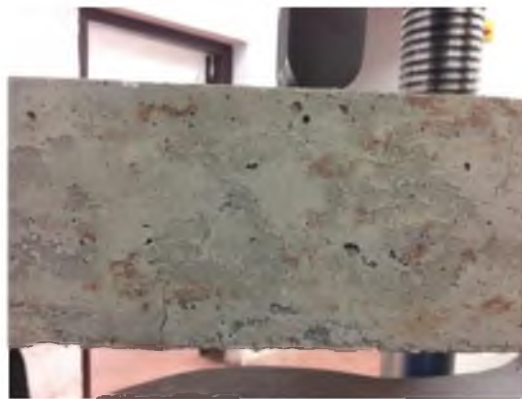


Figure 6: Crack pattern

10. Analytical Investigation

ANSYS was employed to simulate the flexural and shear behaviour of the beam by finite element method. ANSYS is a general purpose finite element analysis (FEA) software package. FEA is a numerical method of deconstructing a complex system into very small pieces called element. The software implements equations that govern the behaviour of these elements and solves them all. These results can be presented in tabulated or graphical forms. This type of analysis is typically used for the design and optimization of a system far too complex to analyze by hand.

Element Types and Real constants

Table 5 :Element Types For Model

Material type	Element type
Concrete	Solid 65
Pvc pipe	4 noded quad shell element

10.1.Material Properties

Table 6: Material Properties Of Elements

	Young's modulus	Poissons ratio	density
PVC	4.7Gpa	0.4	1.38g/cm ³
GPC	22360Mpa	0.224	2400Kg/m ³

10.2. Modelling Of Beam:

The analysis has been carried out for the comparison and the study of effect of GPC with and without pvc pipe experimental and ANSYS results. The beams modelled in ANSYS for the same Load from experiment.

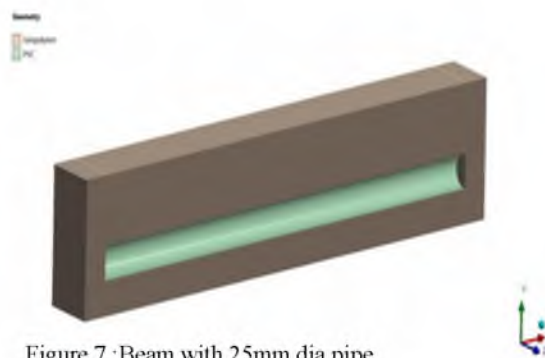


Figure 7 :Beam with 25mm dia pipe

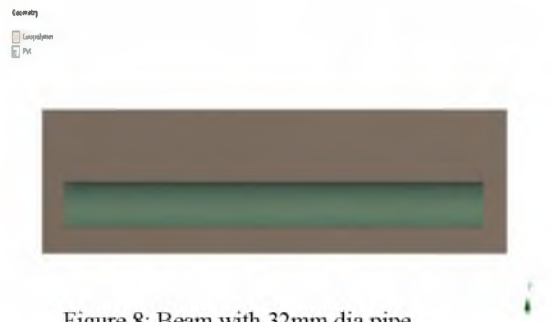


Figure 8: Beam with 32mm dia pipe

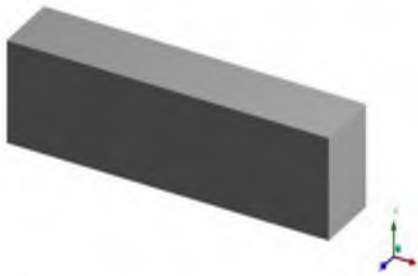


Figure 9: Beam without pipe

11. Results From Analysis

11.1.Total deflection

Deflection or deformation is the degree to which a structural element is displaced under a load. It may refer to an angle or a distance. The deflection distance of a member under a load is directly related to the slope of the deflected shape of the member under that load. The maximum deformation for static loading from experiment is given below.

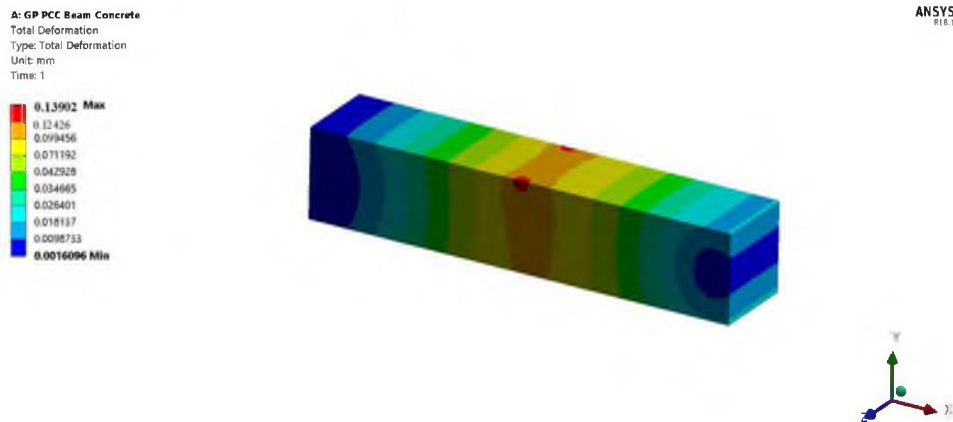


Figure 10 :Beam without pipe

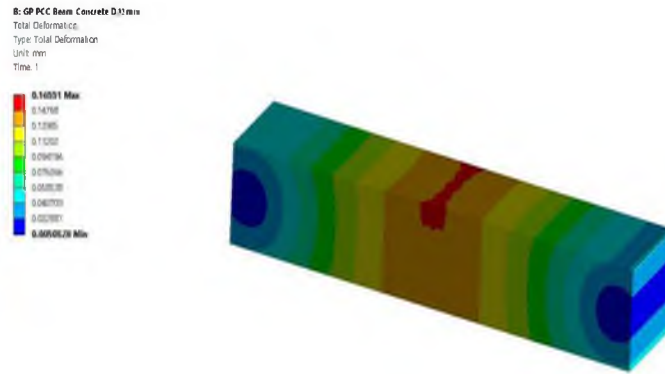


Figure11 :Beam with 25mm dia pipe

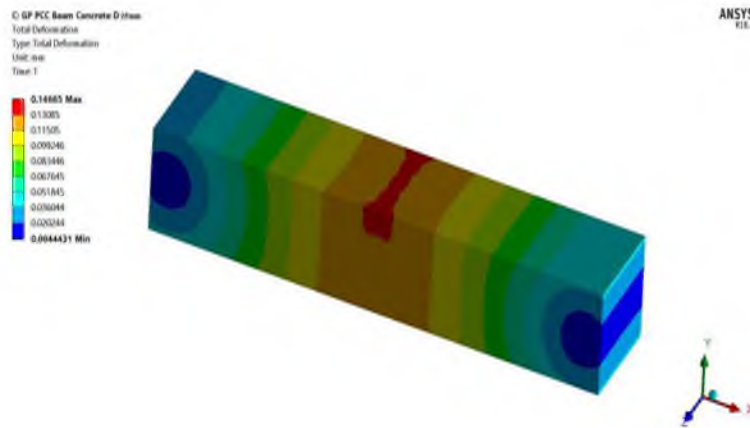


Figure12:Beam with 32mm dia pipe

11.2 Equivalent Bending Stress

Equivalent stress (also called *von Mises stress*) is often used in design work because it allows any arbitrary three-dimensional stress state to be represented as a single positive stress value. Equivalent stress is part of the maximum equivalent stress failure theory used to predict yielding in a ductile material.

A: GP PCC Beam Concrete
 Equivalent Stress
 Type: Equivalent (von-Mises) Stress
 Unit: MPa
 Time: 1

ANSYS
 R18.1

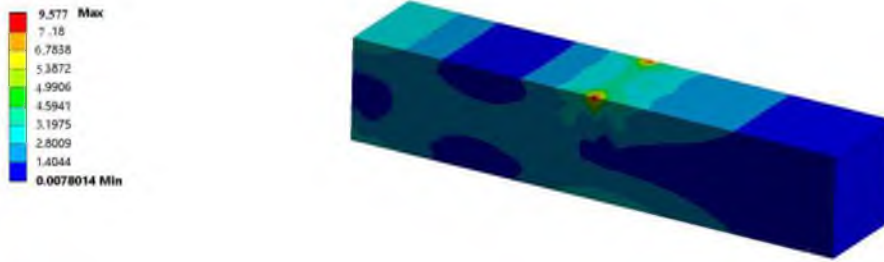


Figure 13 :Beam without pipe

C: GP PCC Beam Concrete D25mm
 Equivalent Stress
 Type: Equivalent (von-Mises) Stress - Top/Bottom
 Unit: MPa
 Time: 1

ANSYS
 R18.1

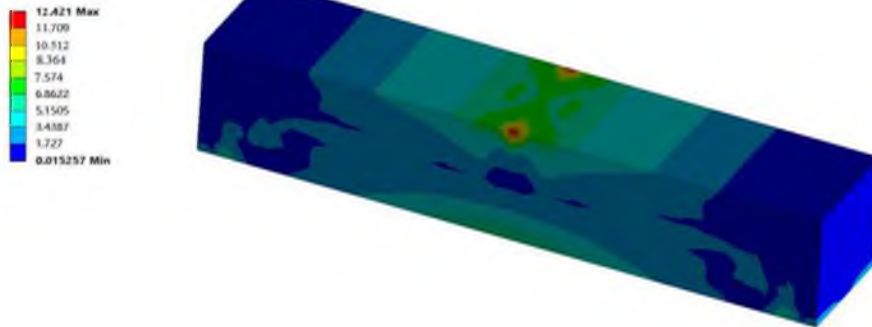


Figure14 :Beam with 25mm dia pipe

B: GP PCC Beam Concrete D32mm
 Equivalent Stress
 Type: Equivalent (von-Mises) Stress - Top/Bottom
 Unit: MPa
 Time: 1

13.861 Max
 12.878
 11.835
 10.911
 9.928
 7.9447
 5.9614
 3.978
 1.9947
 0.011367 Min

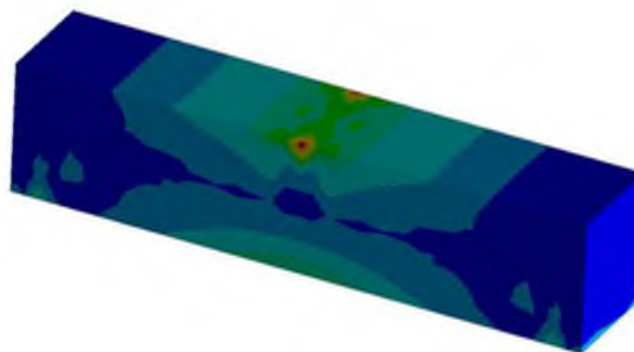


Figure 15:Beam with 32mm dia pipe

11.5.3 Equivalent Elastic Strain

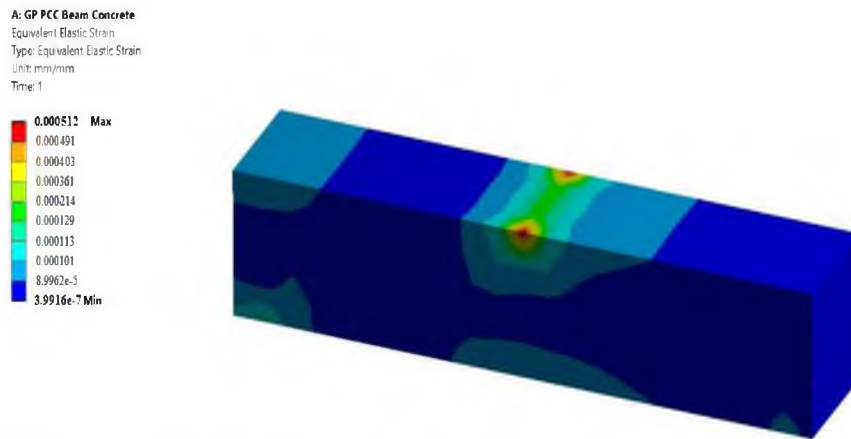


Figure 16 :Beam without pipe

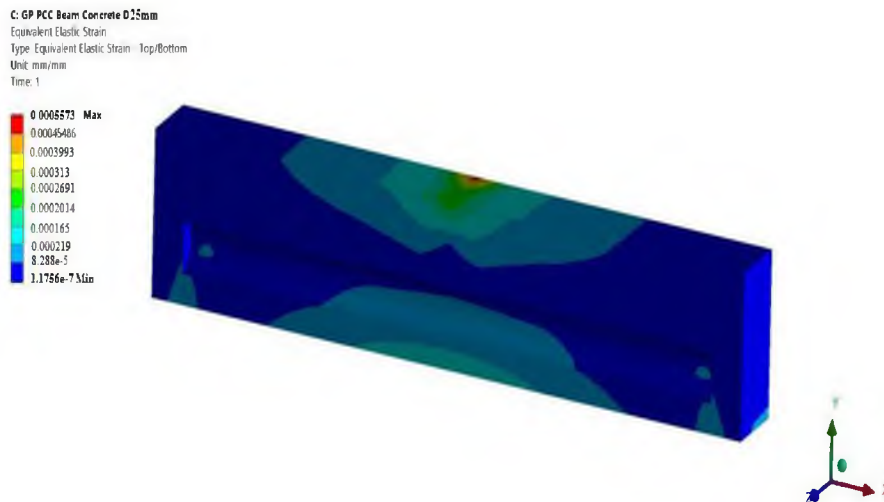


Figure 17:Beam with 25mm dia pipe

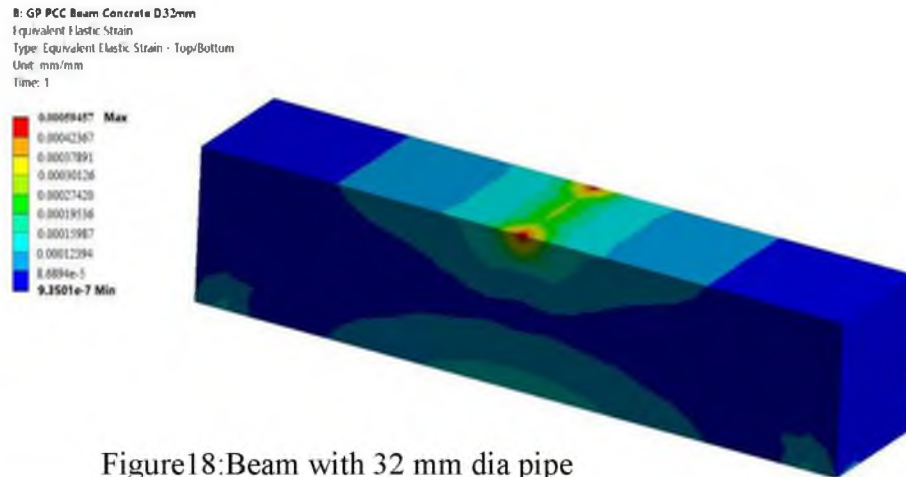


Figure18:Beam with 32 mm dia pipe

12. Comparison of Results

Analytical and experimental results were compared and it is found that geopolymer with hollow space shows same properties as that of without hollow space.

	PROPERTIES	ANALYTICAL	EXPERIMENTAL
Without Pipe	Deflection	0.13902mm	0.135mm
	Bending stress	9.571N/mm ²	7.26N/mm ²
	Strain	0.000512	0.000327
	Shear force	4910N	4850N
25mm Dia Pipe	Deflection	0.14665mm	0.142mm
	Bending stress	12.42N/mm ²	7.54N/mm ²
	Strain	0.0005573	0.000339
	Shear force	5186.5N	5100N
32mm Dia Pipe	Deflection	0.16551mm	0.164mm
	Bending stress	13.861N/mm ²	8.641N/mm ²

	Strain	0.000594	0.000398
	Shear force	5981.3N	5900N

12.1. Concrete

Total Volume beam $V_1 = 0.1 \times 0.1 \times 0.5 = 0.005 \text{ m}^3$

Volume of pipe $V_2 = \pi \times 0.0125 \times 0.45 \times 2 = 0.00221 \text{ m}^3$

% of reduction in concrete = $(V_1 / V_2) \times 100 = 14.20\%$

Since we have assumed a small

beam, the percentage reduction is also small. When we assume this for a larger section, the percentage reduction will be larger.

12.2. Labour Reduction:

Labours are one of the major factors in construction industries. Construction labour is most disorganised in India. Direct labour cost is also a part of the prime cost. It is clearly evident from the study that the total volume saving in concrete is directly proportional to the percentage reduction in labour. Concreting works in construction industry is labour intensive. When the volume of concreting works reduce, the need for labour also get decreased simultaneously, which in turn minimise the production cost.

12.3. Cost reduction:

In current days of competition, it is necessary that a business concern should have utmost efficiency and minimum possible wastages and losses to reduce the cost of production. If the cost of input increases, then naturally, the cost of the production will go up. The inputs in construction fields include material, machines, labour and other overhead expenses. From the above conducted study we have come to a conclusion that by using geopolymer beam with hollow neutral axis, we can save significant amount of concrete without compromising the strength up to a limit. This saving in material cost is more effectively utilised when considering large depth and length of beam or in similar other works, where abnormal reduction of concrete occurs. This can be compared to a chain reaction because as the volume of concrete decreases, the material cost reduces which decreases the labour cost, which in turn minimises the construction cost.

12.4 Decrease in self weight

Dead load shall include weight of all structural and

Architectural components which are permanent in nature. It includes self-weight of the structure. The unit weight of concrete is 23 kN/m^3 . If we can reduce the volume of concrete then the self-weight of the beam also get reduced.

Weight of 1 m^3 concrete = 2300 kg

Weight of beam, $W_1 = 12 \text{ kg}$

Weight of concrete replaced by pipe, $W_2 = 0.83 \text{ kg}$

Weight of hollow beam = $W_1 - W_2 = 11.4 \text{ kg}$

Since we have assumed a small beam, the self-weight reduction is also small. When we assume this for a larger section, the weight reduction will be larger.

13. Conclusion

1. GPC has almost same properties as that of OPC.
2. From the above results, it is concluded that Hollow beam of 25mm and 32mm diameter provides higher strength and better performance and hence it is used for structure in effective way as electrical conduits, when compared to the solid conventional beam
3. Mode of failure is flexural in hollow beam of 25mm and flexure in solid and hollow (32mm)
4. It is seen that there is not much difference in the flexural strength of control beams and that of beams with low grade concrete near neutral axis zone and hollow neutral axis.
5. It can also be seen that with the increase in size of pipe replaced at neutral axis, there is no large difference in flexural strength
6. Thus in the overall study, it can be concluded that behaviour of PGC beams with hollow neutral axis behaves almost in the same manner as that of conventional concrete.

Reference

- [1] Jain Joy and Rajesh Rajeev (2014)—Effect of Reinforced Concrete Beam with Hollow Neutral Axis, *International Journal for Scientific Research and Development* (2014), volume 3, November.
- [2] Dr. G. Hemalatha And W. Godwin Jesudhason (2013), —Experimental Investigation On Beams Partial Replacement Below The Neutral Axis, *International Journal Of Civil And Structural Engineering Research*, Vol. 2, January.
- [3] Manikandan, Dharmar, Robertravi “Experimental study on flexural behaviour of reinforced concrete hollow core sandwich beams” *International Journal of Advance Research In Science And Engineering*, IJARSE, Vol. No.4, Special Issue (01), March 2015
- [4] Shankar H. Sanni, Khadiranaikar, R. B., “Performance of geopolymer concrete under severe environment conditions, *International Journal Of Civil and Structural Engineering* Volume 3, No 2, 2012.
- [5] Anuar K.A, Ridzuan A.R.M., Ismail S. (2011) 10. —Strength Characteristic of Geopolymer Concrete, *International Journal of Civil & Environmental Engineering*, Selangor, Malaysia
- [6] Raijiwala D.B. Patil H. S – Geopolymer Concrete- a Concrete of next decade, *Journal of Engineering Research and Studies*, March 2011.
- [7] Hardjito, D., S. Wallah, D. M. J. Sumajouw, and B. V. Rangan. 2004. “On the Development of Fly Ash-Based Geopolymer Concrete.” *ACI Materials Journal*, vol. 101, no. 6, pp. 467–472.

[8] Rangan, B. V. 2008. "Low-Calcium, Fly-Ash-Based Geopolymer Concrete." Concrete Construction Engineering Handbook. Taylor and Francis Group, Boca Raton, FL

[9] Aleem A., Arumairaj P.D. (2012), —Geopolymer Concrete- A Review—, IJEST.

[7] Hardjito, D., S. Wallah, D. M. J. Sumajouw, and B. V. Rangan. 2004. "On the Development of Fly Ash-Based Geopolymer Concrete." ACI Materials Journal, vol. 101, no. 6.

[10] Concrete in Australia, "Geopolymer Concrete for Construction", News, Vol 39, Issue No 4, December, 2013, pp 4-5.

Thermal response of concrete filled fibre reinforced polymer tube columns

Sneha S. B.¹ and Anjana Krishnan.²

¹PG Research Scholar, Structural Engineering, Mar Baselios College of Engineering and Technology,
Thiruvananthapuram, Kerala, India
snehasbs@gmail.com

²Asst. Professor, Department of Civil Engineering, Mar Baselios College of Engineering and Technology,
Thiruvananthapuram, Kerala, India

Abstract. Bridge columns are the most critical components of a bridge responsible for its overall stability. In recent years, concrete-filled fiber reinforced polymer (FRP) tube (CFFT) system has been widely investigated as a durable and cost-effective alternative design for robust bridge columns. This study summarizes the results of thermal analysis of RCC and CFFT columns of same axial capacity. The resilience of the CFFT system to each type of hazard is measured as column's capability to retain its axial characteristics after thermal analysis. The axial performance of CFFT columns subjected to each threat is quantified in terms of axial capacity, axial ductility and initial axial stiffness. The results show that CFFT column system can be used an effective fire-resistant bridge column system.

Keywords: CFFT column, bridge piers, fire resistance, Residual axial capacity, finite element analysis

1. Introduction

Columns are the most critical structural elements of a bridge for its overall stability. Traditional column materials for bridge include steel, concrete, and timber and these have limited service life and high maintenance costs when used in marine environments due to corrosion, degradation and marine borer attack. Concrete filled fiber reinforced polymer (FRP) tube (CFFT) columns were first introduced as marine piles by Mirmiran and Shahaway (1995). in corrosive environments. This column system can be used as bridge columns to enhance the durability and corrosion resistance of bridge columns. Recently, the CFFT column system has been validated as a high-performance alternative to RCC columns for multi-hazard resilience.

CFFT system consists of an external FRP tube and a regular concrete fill inside. Minimum number of longitudinal reinforcements is provided and spirals are provided to hold the longitudinal reinforcement in its place. It was discovered that an FRP tube system with fibers wound at $\pm 55^\circ$ provides comparable capacity and superior ductility to conventional RCC columns when filled with lightly reinforced regular concrete. Experiments have proved that the $\pm 55^\circ$ fiber orientation is optimal for the flexural capacity and ductility of CFFT columns. The durability of these composite tubes has been proven through several instances where they have stayed in-service in highly corrosive environments for nearly forty years [1].

CFFT column system provides several advantages over RCC columns in terms of structural performance and construction including:

- Sufficient longitudinal strength and confinement to the core concrete, which allows for elimination of the entire lateral steel reinforcement and a significant reduction of longitudinal bars
- A self-curing environment for the concrete core
- Omission of the scaffolding, frame work, and frame removal stages of column construction
- Protection of the inner core in highly corrosive environments

Unlike FRP wrapping or jacketing that serve as retrofit measures for existing columns, the FRP tube of the CFFT column system serves as both formwork and reinforcement for precast or cast-in-place construction. Static and pseudo dynamic test results showed that the structural performance of this column system was improved from the composite action of FRP tube that acts as both longitudinal and transverse reinforcement and provides confinement for the concrete core. Prior to 2012, specifications regarding the design and implementation of CFFT members were absent. In 2012, AASHTO released the 1st Edition LRFD Guide Specifications for Design of CFFTs for Flexural and Axial Members (2012b), referred as "Guide Specification" [3]. The main objective of this study is to compare and study the axial performance of RCC and CFFT columns of same axial capacity under fire loading. This study

consists of an analytical research program comparing the fire resistant capability of RCC and CFFT columns of same axial capacity. The comparative basis for the fire resistance of the columns is in terms of axial load carrying capacity, axial ductility and initial axial stiffness.

2. Methodology

2.1 Details of RCC and CFFT column

The details of RCC column was adopted from the bridge column located at Mohan Nagar junction in Ghaziabad, Uttar Pradesh. The column had a diameter of 1.3 m and a height of 8m. The longitudinal reinforcement consisted of 30#, 32 mm diameter bars. The transverse reinforcement of the RCC column was provided by 10 mm diameter spirals at a pitch of 240 mm. The axial capacity of this bridge column is 20400 kN [4]. A CFFT column was designed for an axial capacity of 20400 kN as per AASHTO LRFD guide specifications for design of concrete filled FRP tubes for flexural and axial members. The CFFT column designed as AASHTO LRFD guide specifications had a diameter of 700 mm and a height of 8m. The transverse reinforcement consisted of six number of 32 mm diameter bars and no transverse steel reinforcement was included. Only spirals were provided at top and bottom to hold the longitudinal reinforcement in its place. Fig. 1 shows the details of RCC and CFFT columns.

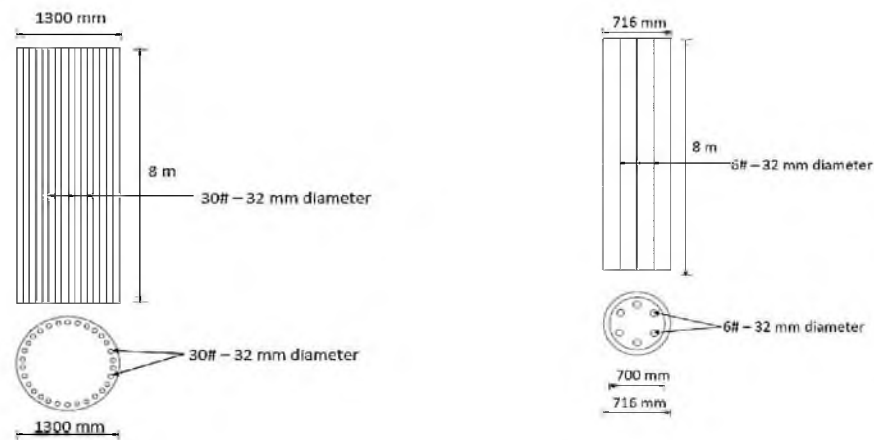


Fig.1. (a) RCC column [4]

(b) Designed CFFT column

2.2 Finite element modelling of columns

Concrete Modelling

Linear and non-linear properties were to be assigned for concrete. For linear properties modulus of elasticity and Poisson's ratio were given. Poisson's ratio was given a value of 0.2 and modulus of elasticity was determined with concrete strength ($f_{ck} = 25\text{MPa}$) using the equation 2. Solid65 element requires linear isotropic and multi-linear isotropic material properties to properly model concrete. The multi-linear isotropic material uses the Von-Mises failure criterion to define the failure of the concrete. Simplified stress strain relationship for concrete in compression is obtained and is shown in Fig. 2.

$$E = 5000 \sqrt{f_{ck}} \tag{1}$$

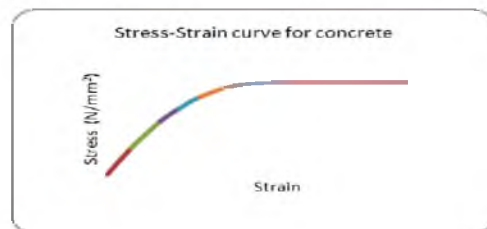


Fig.2. Stress strain relationship for concrete in compression [2]

The non-linear properties for concrete are provided as given in Table 1.

Table 1. Non-linear material properties of concrete [2]

Shear transfer coefficients for an open crack	0.3
Shear transfer coefficients for a closed crack	1
Uniaxial tensile cracking stress	3.5
Uniaxial crushing stress	1

Fibre reinforced polymer tube modelling

An assumption commonly made in FRP modelling is that FRP is a linear elastic material until it reaches its tensile strength and has orthotropic material properties, even when a very large pressure load is applied. It is commonly modelled as an orthotropic material. Input data needed for the FRP composites in the finite element models is given in the Table 2.

Table 2. Orthotropic material properties of FRP tube [5]

Elastic Modulus (GPa)			Shear Modulus (MPa)			Poisson's ratio		
E_x	E_y	E_z	G_{xy}	G_{yz}	G_{xz}	ν_{xy}	ν_{yz}	ν_{xz}
200	48	48	3270	3270	1860	0.22	0.22	0.3

Reinforcement modelling

An elastic- perfectly plastic material model was assumed for steel. Elastic properties such as Young's Modulus and Poisson's ratio were as 200000 N/mm² and 0.3. The bilinear model was considered for the stress-strain relation which is defined by the yield stress ($f_y=415$ MPa) and the tangent modulus of the steel as 1480 MPa.



Fig.3. (a) CFFT column



(b) Reinforcement of CFFT column

Contact modelling

The contact between the inner surface of steel and outer concrete surface of concrete was provided using surface to surface contact elements. The 3-D contact surface elements CONTA174 is associated with the 3-D target segment element TARGE170 via a shared real constant set. ANSYS looks for contact only between surfaces with the same real constant set. Here the FRP tube is the target surface and concrete core is the contact surface. The concept is that contact surface moves in to the target surface.

Loading and Boundary Conditions

Displacement boundary conditions of the model were constrained to get a unique solution. Fixed-pinned conditions are used in the FE model. Bottom end of the column is given fixed support. A pinned support can resist both vertical and horizontal forces but not a moment. They will allow the structural member to rotate, but not to translate in any

direction. A pinned connection could allow rotation in only one direction; providing resistance to rotation in any other direction. The compression load is applied to the top along z axis.

3. Direct coupled thermal analysis

The fire performance of RCC and CFFT columns is studied by performing direct coupled thermal structural analysis in finite element analysis software, ANSYS Workbench. When coupling is considered in both directions, it can be modelled with two way or direct coupling. In this study, two way or direct coupling was done to obtain the thermal response of RCC and CFFT columns. To represent direct coupling, APDL commands should be used. Coupled field elements were selected for the analysis. Coupled field elements can include several degrees of freedom and the associated couplings between them are represented in the equation 2 and 3.

$$[M] \{\ddot{u}\} + [C] \{\dot{u}\} + [K] \{u\} = \{F(t)\} \quad \text{(Structural solution)} \quad (2)$$

$$[C] \{T\} + [K] \{T\} = \{Q\} \quad \text{(Thermal solution)} \quad (3)$$

Where [M]= mass matrix

[C] = damping matrix

[K] = stiffness matrix

{ \ddot{u} } = nodal acceleration vector

{ \dot{u} } = nodal velocity vector

{u} = nodal displacement vector

{F(t)} = load vector

[C] = specific heat (J/kg-K)

{T} = Temperature

[K] = thermal conductivity (W/m-K)

{T} = Rate of temperature change

{Q} = Total heat energy

Firstly, a static structural analysis was done followed by time- transient thermal analysis by describing bulk temperature loads and convective heat transfer coefficients as a function of time. Then transient structural analysis was done in the thermal coupled model. Structural loads and boundary conditions were applied as usual. Thermal loads were applied on nodes and elements, via Named Selections. The surface of a structural member exposed to a fire is subjected to heat transfer by convection and radiation. The influence of convection and radiation were included in, and the heat convective coefficient of the fire side is taken as 25 W/ (m²°C), the adiabatic surface taken as 9 W/ (m²°C); the surface radiation emissivity is selected as 0.5 (ECCS 1998).

3.1 Coupled Field Elements

For coupled model for concrete, SOLID5 element is used and is shown in Fig.4 (a) was used in this study. SOLID5 has a 3-D magnetic, thermal, electric, piezoelectric, and structural field capability with limited coupling between the fields. The element has eight nodes with up to six degrees of freedom at each node. When used in structural analysis, SOLID5 has large deflection and stress stiffening capabilities [6]. A three-dimensional coupled-field element, SOLID226 was used to model outer FRP tube and is shown in Fig.4 (b). The element has twenty nodes with up to five degrees of freedom per node. Structural capabilities include elasticity, plasticity, hyper-elasticity, creep, large strain, large deflection, stress stiffening effects, and prestress effects. For modelling reinforcement bars, LINK33 element shown in Fig.4 (c) was used. It acts as a three- dimensional conduction bar. LINK33 is a uniaxial element with the ability to conduct heat between its nodes. The element has a single degree of freedom, temperature, at each node point. The conducting bar is applicable to a steady-state or transient thermal analysis.

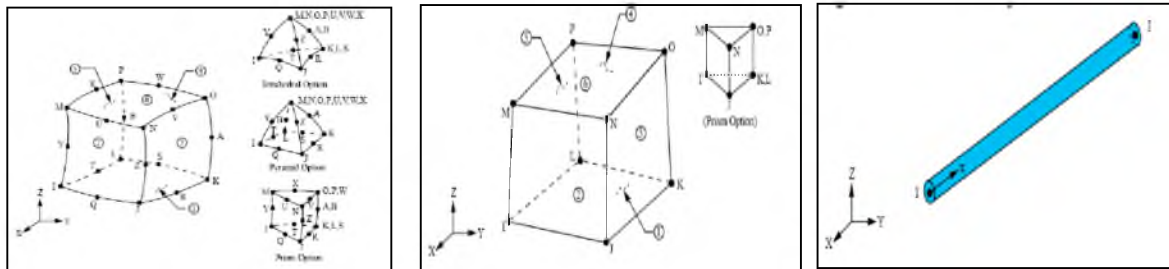


Fig.4. (a) SOLID5 Coupled thermal element

[6] (b) SOLID226 element [6] (c) LINK33 element [6]

3.2 Thermal properties of concrete and FRP

Time dependent thermal properties such as thermal conductivity, specific heat and stress-strain relationships for concrete were given as input and the variation of these properties with temperature is shown in Fig.5-7 respectively. The orthotropic thermal parameters for the FRP tube was provided as in the Table 1. For a structural-thermal analysis, UX, UY, UZ and TEMP are the DOF labels for SOLID226 coupled element and force and heat flow are the reaction solution.

Table 3. Input thermal properties for FRP tube [5]

Density (ρ) kg/m ³	Specific heat (C) J/kg K	Conductivity(k) W/m K			Diffusivity (α) 10 ⁻⁶ m ² /s		
		Parallel to fiber axis	45 ⁰ to fiber axis	90 ⁰ to fiber axis	Parallel to fiber axis	45 ⁰ to fiber axis	90 ⁰ to fiber axis
1530	950	4.5	2.95	0.67	3.096	2.029	4.609

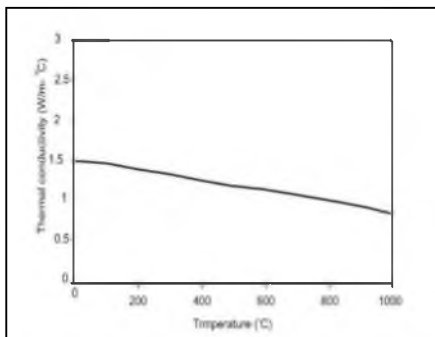


Fig.5. Variation in thermal conductivity of concrete

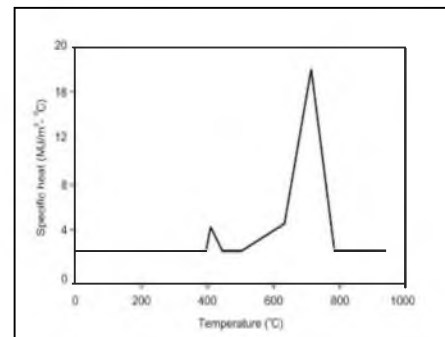


Fig.6. Variation in specific heat of concrete [7]

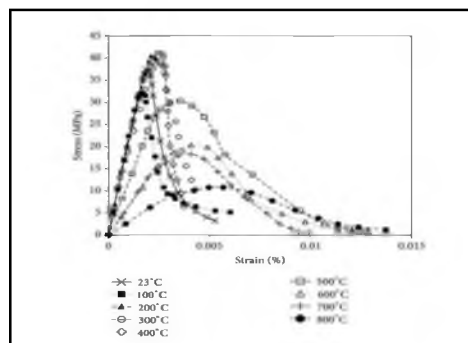


Fig.7. Stress-strain response of normal strength concrete at elevated temperature[7]

Because FRP materials are vulnerable to extreme temperatures, the insulation system was applied to the surface of the CFFT columns and was modelled using SOLID70 element. The initial temperature was defined as 20°C. The RCC and CFFT columns were subjected to fire according to ASTM E119 standard fire curve for one hour and two hours separately and the post-fire resistance of each column was studied by comparing the axial strength parameters. The columns were fixed at the bottom and hinged at the top and axial load was applied and corresponding axial deformation were obtained by performing coupled thermal analysis. The columns were exposed to fire from one side providing the actual furnace conditions as in the fire testing laboratory. Firstly, the load was

applied to the design value at the ambient temperature, after which the temperature field results calculated above were imported, during heating and load was increased until the failure of columns occurred.

3.3 Thermal boundary and loading conditions

Only one face of the columns was exposed to fire in this study as shown in Fig. 8. Convective type heat transfer was considered with a coefficient of heat transfer equal to $25 \text{ W/m}^2 \text{ }^\circ\text{C}$ and a conduction coefficient of $200 \text{ W/m}^2\text{K}$ was adopted in the contact between FRP tube and the concrete.

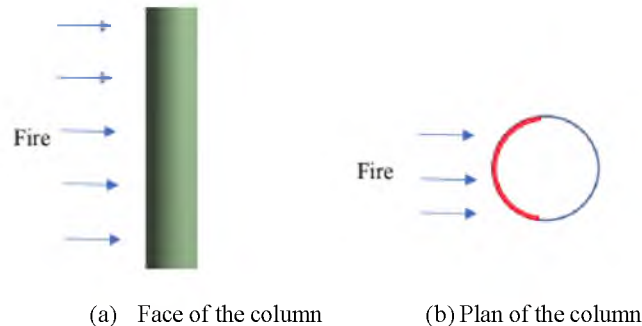


Fig.8.Schematic representation of fire exposure

For this study, two types of fire exposure were selected to simulate a moderate and severe fire hazard. In the moderate test, RCC column and CFFT column were subjected to one hour of extreme temperature following the ASTM E119 curve and for severe test, columns were subjected to two hours of the ASTM E119 temperature curve and is referred to as the 1-hr test and 2-hr test, respectively. The standard ASTM E119 fire curve used in 1-hr test and 2-hr is given in Fig. 9 (a) and (b) respectively.

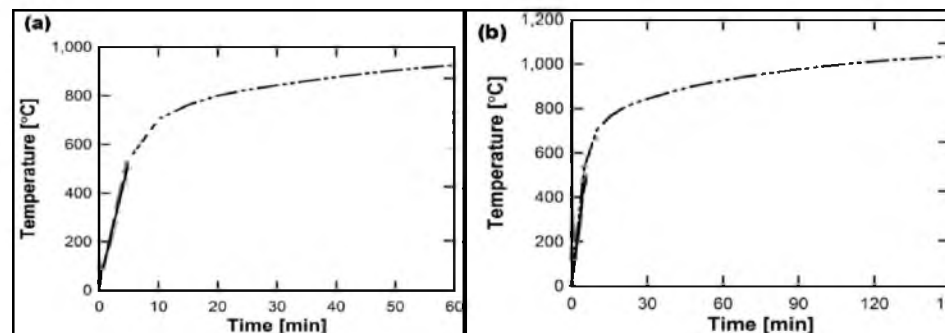


Fig.9. (a) 1-hr and (b) 2-hr ASTM E119 curve [7]

The failure mode selected was the maximum strain. The deformation response of RCC and CFFT columns after thermal analysis were plotted for each load until failure. From the load- deformation behavior, the residual axial capacity of columns, axial stiffness and axial ductility were evaluated. The ductility value less than one indicates buckling collapse mode and ductility value greater than one indicates yielding type collapse mode [8].

4. Thermal response of RCC and CFFT columns

When concrete columns are exposed to fire, the material properties of concrete and the reinforcements change as a result of the increase in temperature. Temperature propagation inside the concrete structure is non-uniform and results in the degradation of the structure and leads to the failure of the entire structure. The decreases in yield

strength and modulus of elasticity reduce the overall strength of the column. Columns fail by crushing or by flexural buckling when the column strength decreases lower than the applied load. In experimental fire performance testing, a column is placed in furnace and subjected to a controlled fire while being axially loaded. The length of time from the beginning of fire exposure to failure is the fire resistance rating of a column. The modes of concrete failure under fire exposure depend on the nature of fire, loading system, and types of structure. Failure can also be due to reduction of bending or tensile strength, loss of shear or torsional strength, loss of compressive strength.

The response of CFFT and RCC columns were evaluated after direct coupled thermal analysis for 1-hr and 2-hr fire exposure. The temperature distribution of RCC and CFFT columns subjected to 1- hr and 2- hr fire exposure was obtained as shown in Fig.10 and 11. The load- deformation behavior was presented in Fig.12. The summary of axial test results of fire damaged columns was given in Table 4.

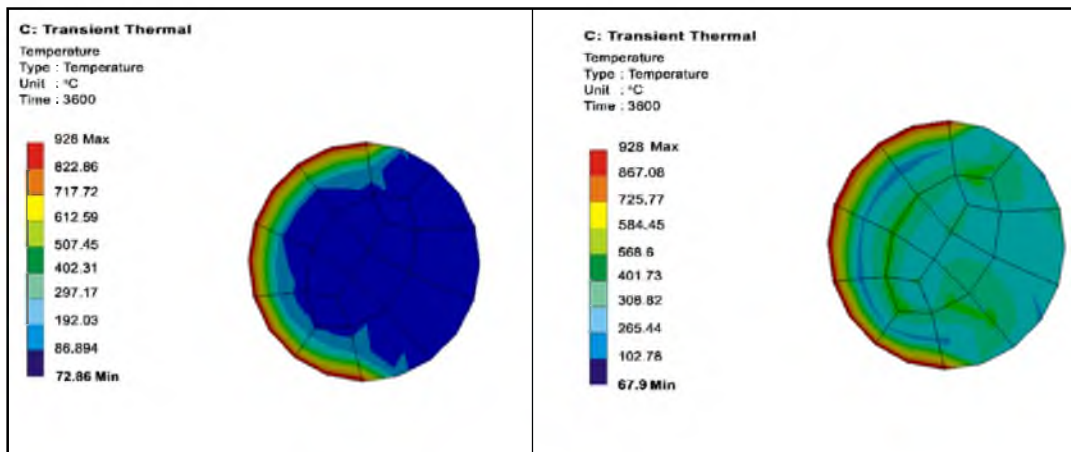


Fig.10. Temperature distribution of columns under moderate fire(a) RCC - Moderate (b) CFFT - Moderate

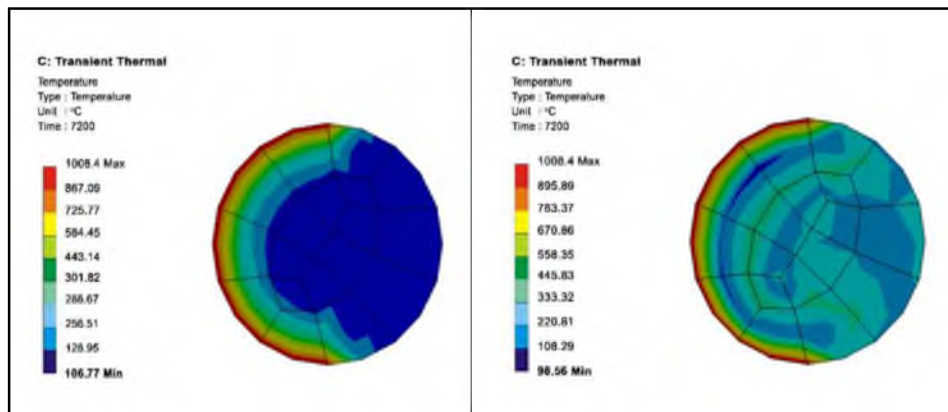


Fig.11. Temperature distribution of columns under severe fire (a) RCC - Severe (b) CFFT - Severe

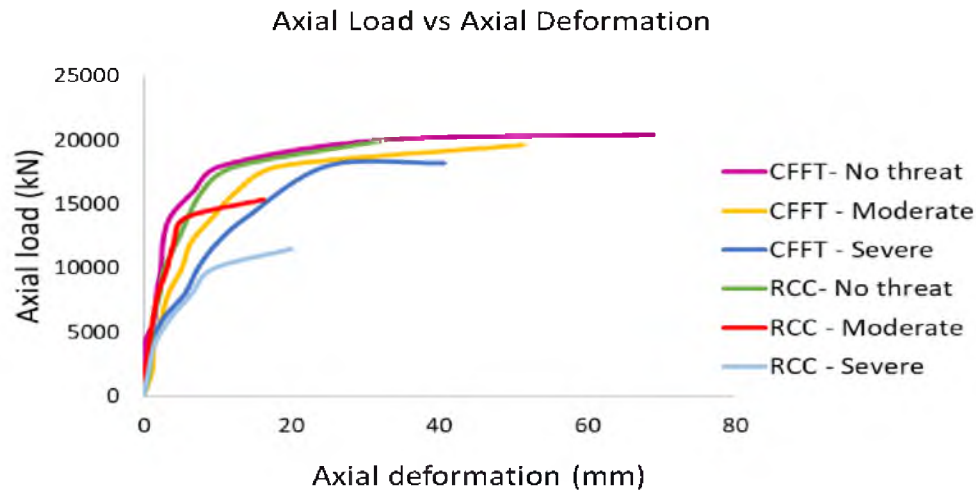


Fig.12. Load-deformation relationship of RCC and CFFT fire damaged columns

Table 4. Axial capacity parameters for fire damaged columns

Column type	Threat level	Axial capacity (kN)	Axial stiffness (kN/mm)	Axial ductility	Percentage reduction (%)		
					Axial capacity	Axial stiffness	Axial ductility
RCC	No threat	20400	1630	2.06	-	-	-
	Moderate	15398	1083	1.02	25	34	50
	Severe	11510	668	1.22	44	59	41
CFFT	No threat	20400	1810	4.38	-	-	-
	Moderate	19646	1111	3.21	4	38	27
	Severe	18160	1090	2.52	11	40	42

Although CFFT column exhibited rupture of the FRP tube after 2-hr exposure, the Tyfo® VG system provided sufficient fire protection to the CFFT columns allowing them to maintain their axial load carrying capabilities after more than two hours of extreme temperature exposure. The significant loss of axial strength and stiffness observed in the 2-hr fire damaged RCC columns resulted in larger values of axial ductility when compared to the 1-hr fire damaged column. On an average, axial ductility of CFFT columns were 3 times that of RCC columns for each damaged state which indicates the high deformability of CFFT columns before reaching failure.

6. Conclusions

The following conclusions are made from the study

- The RCC columns exhibited losses of 25% and 44% in axial capacity and 34% and 59% in initial axial stiffness after one hour and two hours of exposure to extreme temperature, respectively.
- The percentage loss in axial capacity observed in CFFT columns was low when compared to that of RCC columns under moderate and severe fire exposure.
- Axial ductility of the CFFT columns were 3 times the axial ductility of the RCC columns, for each damaged state
- The significant loss of axial strength and stiffness observed in the 2-hr fire damaged RCC columns resulted in larger values of axial ductility when compared to the 1-hr fire damaged column.

References

1. Echevarria, A., Zaghi, A., Christenson, R and Plank, R: Residual axial capacity comparison of CFFT and RC Bridge columns after fire, *Polymers*, 7(5), 876–895(2015)
2. Echevarria, A., Zaghi, A.E., Christenson, R and Accorsi, M: CFFT Bridge Columns for Multihazard Resilience, *Journal of Structural Engineering*, 142(8)(2016)
3. AASHT. LRFD guide specifications for design of concrete-filled FRP tubes for flexural and axial members, Washington, DC, (2012b)
4. Wilbur Smith, *Detailed Design, DPR for bridge at Mohan Nagar Junction in Ghaziabad*, (NCRPB), TA No. 7055-IND), Vol V A-2, (2010)
5. Pan, C., and Hocheng, H: Evaluation of anisotropic thermal conductivity for unidirectional FRP in laser machining, *Composites Part A: Applied Science and Manufacturing*, 32(11), 1657–1667, (2001).
6. ANSYS, ANSYS User's Manual Revision 15, ANSYS, Inc.
7. ASCE, Structural Fire Protection, ASCE Committee on Fire Protection, Structural Division, American Society of Civil Engineers, New York, NY, USA, 1992.
8. Khan, Q.S., Sheikh, M.N and Hadi, M.N: Axial compressive behavior of circular CFFT: Experimental database and design-oriented model, *Steel and Composite Structures*, 21(4), 921–947(2016)
9. Agarwal, A and Varma, A.H: Fire induced progressive collapse of steel building structures: The role of interior gravity columns. *Eng. Struct.*, 58, 129–140 (2014)
10. Green, M.F., Bisby, L.A., Fam, A.Z and Kodur, V.K: FRP confined concrete columns: Behaviour under extreme conditions. *Cement Concrete Composites*, 28, 928–937 (2006)
11. Chowdhury, E.U., Bisby, L.A., Green, M.F and Kodur, V.K: Investigation of insulated FRP-wrapped reinforced concrete columns in fire. *Fire Safety Journal*, 42, 452–460 (2007)
12. Garlock, M.E., Paya-Zaforteza, I., Kodur, V.K and Gu, L: Fire hazard in bridges: Review, assessment and repair strategies, *Engineering Structures*, 35, 89-98 (2012)
13. ACI 216.1, “Code requirements for determining fire resistance of concrete and masonry construction assemblies,” ACI 216.1-07/TMS-0216-07, American Concrete Institute, Farmington Hills, Mich, USA, 2007.
14. ACI-318, Building Code Requirements for Reinforced Concrete and Commentary, American Concrete Institute, Farmington Hills, Mich, USA, 2008.
15. Vincent, T and Ozbakkaloglu, T: Influence of slenderness on stress-strain behavior of concrete-filled FRP tubes: experimental study, *Journal of Structural Engineering*, 4014029, 1-13 (2015)

PARTIAL REPLACEMENT OF FINE AGGREGATE WITH CRUMB RUBBER

Madhavi G¹, Saneeth S¹, Anju P Babu^{2*}

¹UG Scholar, Department of Civil Engineering, RIET, Trivandrum, Kerala, India

²Assistant Professor, RIET, Trivandrum, Kerala, India

*Corresponding author email: 6666babuanju@gmail.com, Tel.:8848939842

Abstract: The undegradable nature of the rubber and consequent disposal problem has lead to a serious environmental issue in the recent decades. To overcome this problem, usage of this waste tire in concrete can be done, along with which natural resources can also be preserved. In this research a study was carried out on the use of recycled rubber tyre as a partial replacement for the fine aggregate in concrete construction using locally available waste tyre. The specimens were cast percentage replacement of fine aggregate 5%, 10%, 15% and 20% by the crumb rubber aggregate and 10% of silica fume with cement.. The data collection was mainly based on the tests conducted on the prepared specimens in the laboratory.

Key Words: waste tire, recycled rubber tyre, silica fume

I. INTRODUCTION

During the last three decades, there have been dramatic changes in the way of thinking about industrial processes and the approach and evaluation of new and innovative materials. Concrete, in its most basic form, is one of the world's oldest building materials. Concrete is a substance composed of only a few simple and commonly available ingredients that when properly mixed and cured, may last for centuries. New ingredients to include in concrete mixes are also constantly being researched and developed. In general, concrete has low tensile strength, low ductility, and low energy absorption. Concrete also tends to shrink and crack during the hardening and curing process. These limitations are constantly being tested with hopes of improvement by the introduction of new admixtures and aggregates used in the mix. One such method may be the introduction of rubber to the concrete mix. Shredded or crumbed rubber is waste being of non-biodegradable and poses severe fire, environmental and health risks.

II. OBJECTIVES

The objective of this study is to test the properties of concrete when crumbed rubber used as aggregate by partial replacement of fine aggregates and silica fume foe cement. The parameters of this investigation include the compressive strength, flexural strength and split tensile strength of concrete specimens. Cubes of 15 x 15 x 15cm size for compressive strength, cylinders of diameter 15cm and height 30cm size for split tensile strength and beams of size 50 x 10 x 10cm for flexural strength are casted for the testing of concrete. The concrete having compressive strength of 25 N/mm² (M₂₅) is used and percentages of rubber aggregates are 0, 5, 10, 15 and 20% of fine aggregates and 10% of cement with silica fume. The natural aggregates are replaced by rubber aggregates on volume basis. The strength performance of modified concrete specimens was compared with the conventional concrete.

III. MATERIALS USED

The basic materials for mixing Concrete are required such as

A. Cement

The cement used for the present investigation was ordinary Portland cement. OPC 53 Grade cement is required to conform to BIS specification IS: 12269-1987 with a designed strength for 28 days being a minimum of 53 MPa or 530 kg/ sqcm.

Table 1: Properties of Cement

Sl No	Property	Value	Range
1	Fineness	8%	< 10%
2	Standard consistency	30%	26%-33%
3	Initial Setting Time	35 min	Not less than 30 minutes

4	Final Setting Time	510 min	Not greater than 600 minutes
---	--------------------	---------	------------------------------

B. Fine Aggregate

The locally available river sand is used as fine aggregate in the concrete design mix. Sand is of Zone-II as per IS: 383-1970.

Table 2: Properties of Fine Aggregate

Sl No	Property	Value
1	Specific gravity	2.6
2	Bulk density	1.67 g/cc
3	Void ratio	.447
4	porosity	30.9%

C. Coarse Aggregate

Aggregates are the most mined material in the world. Aggregates are a component of composite materials such as concrete and asphalt concrete; the aggregate serves as reinforcement to add strength to the overall composite material. Coarse aggregate of size 16mm is sieved and used.

Table 3: Properties of Coarse Aggregate

Sl No	Property	Value
1	Specific gravity	2.7
2	Bulk density	1.78 g/cc
3	Void ratio	.67
4	porosity	40.05%

D. Crumb Tire

Crumb rubber is recycled rubber produced from automotive and truck scrap tires. During the recycling process, steel and tire cord (fluff) are removed, leaving tire rubber with a granular consistency. Continued processing with a granulator or cracker mill is done. Specific gravity is evaluated in accordance with ASTM 127 [ASTM, 1997a] and the range is in between 1.14 to 1.27

E. Water

Water containing less than 2000 parts per million (ppm) of total dissolved solids can generally be used satisfactorily for making concrete.

F. Silica Fume

The main field of application is as pozzolanic material for high performance concrete. This makes it approximately 100 times smaller than the average cement particle. The bulk density of silica fume depends on the degree of densification and varies from 130 (undensified) to 600 kg/m³. The specific gravity of silica fume is generally in the range of 2.2 to 2.3.

IV. EXPERIMENTAL INVESTIGATIONS

Study the feasibility of incorporating crumb tyre rubber as fine aggregate in concrete mixes and determine the change in the properties after the incorporation of the rubber into the concrete mix. Investigation on the influence of the rubber content on the properties of rubberized concrete starting with the 0% rubber content (i.e., without rubber) and up to 20% rubber content and cement with 10% of silica fume in the M₂₅ grade concrete (i.e., with a partial replacement of the fine aggregate by 0%, 5%, 10%, 15% and 20% by volume of the total fine aggregate). For convenience, the mix design for M₂₅ grade concrete has been done according to IS: 10262 (1982).

In the present study we are designing a Concrete Mix for M25 Grade concrete is (1:1:2) and the water cement ratio is 0.55 below the different percentage of rubber aggregate is replaced by fine

aggregate and cement with 10% silica fume. Then cubes, cylinders and beams were tested for compressive strength, split tensile strength and flexural strength for 7th day, 14th day and 28th day.

Table 4: Mix Proportion Of M25 Grade Concrete

Crumb tire (%)	Silica Fume (%)	Cement (%)	Fine Aggregate (%)	Coarse aggregate (%)
0	0	100	100	100
5	10	90	95	100
10	10	90	90	100
15	10	90	85	100
20	10	90	80	100
	w/c ratio	0.55		

V. TESTS AND RESULTS

A. Slump Cone Test

Ingredients of mixes are properly mixed so as to produce homogeneous and uniform fresh concrete in macro-scale in order to know its workability using slump test. Since as the rubber content in the concrete mix increases, the workability of the mix decreases. So for every 5% increase in rubber content 5% of water is also be increased.

Table 5: Observation of Slump test for percentage of rubber with increased water

Percentage of Sludge added	Water cement ratio	Water content	Slump value	Slump type
0	0.5	50	70	True slump
5	0.5	55	60	True slump
10	0.5	60	55	True slump
15	0.5	65	50	True slump
20	0.5	70	50	True slump

It is noted that with altered water content workability seemed to be increasing along with the addition of rubber. For normal mix, the slump value is 70 cm and when rubber content increases along with increases water content, the slump value tends to be 50cm.

B. Compaction Factor Test

As percentage of sludge added increases, compaction factor value decreases. Compacting factor of the prepared concrete is in the range of 0.85 to 0.89. So degree of workability is medium

Table 6: Observation of compaction factor test for percentage of sludge

Percentage of crumb rubber added	Compaction factor
0%	0.89
5%	0.877
10%	0.872
15%	0.86
20%	0.85

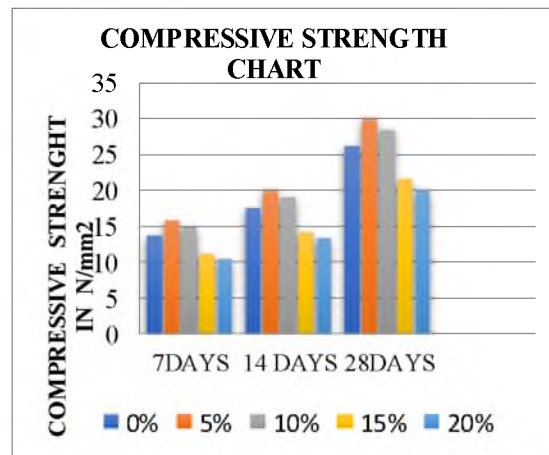
It is noted that compaction factor value decreases but remains within the limit.

C. Compressive Strength

Compressive strength test on cubes were carried out using the Compression Testing Machine. Compressive test were carried out on cubes of dimensions 150 × 150 × 150 mm after 7 days, 14 and 28 days. .

Table 7: Observation and calculation

Mix No	% Of Crumb Tire Added	% Of Silica Fume Added	7 th day Strength (N/mm ²)	14 th day Strength (N/mm ²)	28 th day Strength (N/mm ²)
M1	0	0	13.66	17.487	26.1
M2	5	10	15.648	20.03	29.9
M3	10	10	14.86	19.028	28.4
M4	15	10	11.12	14.2	21.5
M5	20	10	10.3	13.28	19.83

**Fig 1** Variation of Compressive strength

The test results show that addition of rubber aggregates resulting to significant reduction in compressive strength compared to conventional concrete. This is due to the weakness of the rubber particles compared to the fine aggregate particles. However, the partial replacement of fine aggregates with 5% of rubber can potentially be used in low strength concrete applications.

D. Flexural Strength

Increasing the content of rubber leads to an increase in the flexural strength of the concrete upto 5% of replacement of fine aggregate. Then this significant drop can be attributed to poor bonds between rubber aggregate and cement paste and the presence of more air voids due to rubber.

Table 8: Observation and calculation

Mix no	Crumb Tire %	Silica Fume %	7 th day strength (N/mm ²)	14 th day strength (N/mm ²)	28 th day strength (N/mm ²)
M1	0	0	2.11	2.71	3.8
M2	5	10	2.5	3.285	4.62
M3	10	10	2.28	2.9	4.1
M4	15	10	1.896	2.428	3.41
M5	20	10	1.58	2.02	2.84

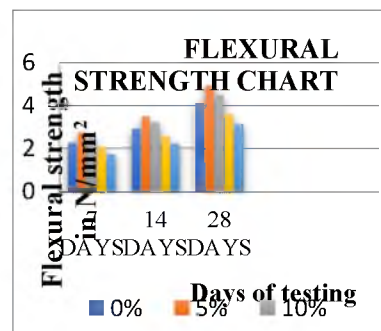


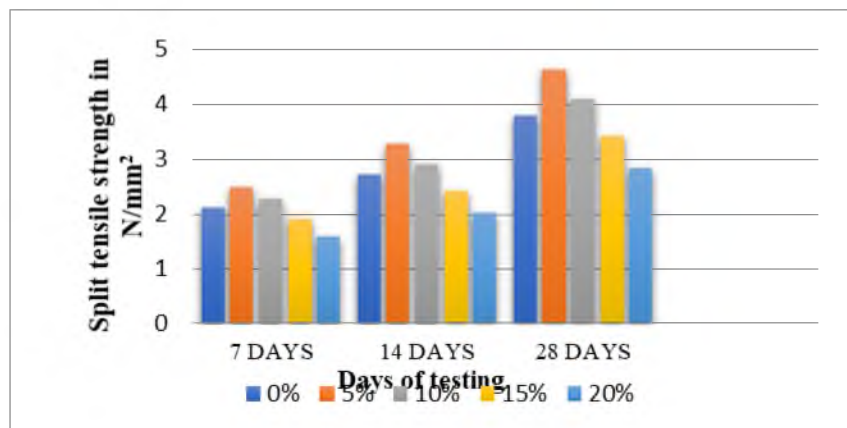
Fig 2 Variation of Flexural strength

E. Split Tensile Strength

Results indicate that as the tire content increases from 5% to 10% along with the addition of 10% silica fume, maximum strength is shown at the M2 mix where silica fume content is more than the crumb tire content. On further increase of rubber leads to the decrease in tensile strength.

Table 9: Observation and calculation

Mix No	Crumb Tire %	Silica Fume %	7 th day strength (N/mm ²)	14 th day strength (N/mm ²)	28 th day strength (N/mm ²)
M1	0	0	2.28	2.92	4.1
M2	5	10	2.73	3.5	4.9
M3	10	10	2.50	3.21	4.5
M4	15	10	2.07	2.57	3.6
M5	20	10	1.741	2.228	3.12

**Fig 3** Variation of split tensile strength

VI. CONCLUSION

- Compressive strength, split tensile strength and flexural strength were obtained by testing.
- The minimum and maximum 28th day compressive strength obtained are 19.83N/mm² and 29.9N/mm²
- The test results show that the addition of crumb rubber alone reduces the compressive strength. The main reason for strength reduction is due to the lack of adhesion at boundaries of rubber aggregate. These soft rubber particles behave as voids in the concrete mix.
- But both the compressive strength and split tensile strength increases by the addition of silica fume. It is mainly because of filling capability of silica fume which provides good adhesion between the rubber and the cement paste
- There is an increase in flexural strength which can be achieved by limiting the replacement amount to only 5% of fine aggregate. For 15% and 20% rubber content, flexural strength reduction was observed.

- It indicates that the improvement in flexural strength is limited to relatively small rubber content. By the increasing rubber content in the concrete, the workability of concrete decreases.
- So for every 5% increase in rubber content, 5% extra water was added. Thus for altered water content, the workability of concrete mix increased.
- For the combination mixes as the percentage of crumb rubber increases the strength reduces gradually.
- Based on this study, the use of crumb rubber aggregates in concrete produces light weight concrete and is economical and environmentally effective.
- Use of the waste rubber tyre in concrete is a techno- economically feasible and environmentally consistent method of waste disposal.
- Large volumes of waste rubber are generated, because of stricter environmental regulations, landfill disposal has become difficult and therefore disposal cost is escalating. Recycling is the best option over disposal; it helps in reducing disposal costs, conserves natural resources. Substitution of conventional materials by recycled waste materials helps in efficient use of waste material and sustainable use of natural resources.

REFERENCE

- [1] Paillere, A.M., Buil, M. and Serrano, J.J. (1989), "Effect of Fibre Addition on the Autogeneous Shrinkage of Silica Fume Concrete" *ACI Materials Journal*, Vol. 86, No. 2, pp. 139-144.
- [2] Cong, X., Gong, S., Darwin, David and McCabe, S.L. (1992), "Role of Silica Fume in Compressive Strength of Cement Paste, Mortar and Concrete." *ACI Materials Journal*, Vol. 89, No. 4, pp. 375-387.
- [3] Eldin, N.N., and Senouci, A.B. (1993). "Rubber Tires As Concrete Aggregate". *Journal of Materials in Civil Engineering*, 5(4), 478-496.
- [4] Barris C, LI Torres ,Turon A and Baena M(1994), "Investigation of crumb rubber concrete for blast", *Cement & Concrete Composites*, Vol. 16, pp. 287-298.
- [5] Fattuhi, N.I., and Clark, L.A. (1996)."Cement-based materials containing shredded scrap tyres rubber". *Construction Building Materials*, 10(4), 229-236.
- [6] Bakri, A. M. M. A., Fadli, S. A. S. N., Bakar, M. D. A., and Leong, K. W. (2007)."Comparison of rubber as aggregate and rubber as filler in concrete",*First International Conference on Sustainable Materials 2007*, Penang.
- [7] Panda, K. C, Parhi, P. S and Jena, T (2012),"Scrap-TyreRubberReplacement for Aggregate in cement Concrete: Experimental Study", *International Journal of Earth and Science Engineering* ISSN 0974-5904, Vol. 05, No.06.
- [8] Akinwonmi, Ademola Samuel and Emmanuel(2013), *Department of Mechanical Engineering University Of*
- [9] Mines, "Mechanical Strength of Concrete with Crumb Tyre as Aggregate", *IJERA*
- [10]DhirajAgarwal ,Pawan Hinge, U.P. Waghe, S.P. Raut (2014) "Utilization of Industrial waste in construction material – A Review" *International Journal of Innovation Research in Science, Engineering and Technology* Vol. 3, Issue 1.

STRENGTHENING OF SELF COMPACTING CONCRETE USING POLYPROPYLENE AND STRIPS OF STEEL SCRUBBER

Amritha V R¹, Adarsh S Anil¹, Anju P Babu^{2*}

¹UG Scholar, Department of Civil Engineering, RIET, Trivandrum, Kerala, India

²Assistant Professor, RIET, Trivandrum, Kerala, India

*Corresponding author email: 6666babuanju@gmail.com, Tel.:8848939842

ABSTRACT: Self compacting concrete (SCC) is defined as the concrete which compact and settle under its own weight. The aim of this project is to study the performance of self compacting concrete containing fibres such as polypropylene and strips of steel scrubber fibre. Four mixes with different mix proportions are casted for this. All four mixes containing equal proportion of polypropylene (0.25%) and steel scrubber fibre is used in different proportion such as 0.1%, 0.15%, 0.2%, 0.25%. After casting, studies are carried out on the fresh and mechanical properties of self compacting concrete for all the mix. The hardened properties such as compressive strength, flexural strength, split tensile strength are determined by conducting suitable testes on SCC.

I. INTRODUCTION

The present day civil engineering constructions have their own structural and durability requirements related with concrete to better suit the intended function of the structure. It is therefore necessary to develop self compacting concrete of special properties, so that the structures continue to perform the intended purpose. Internal micro-cracks are inherently present in the concrete and its poor tensile strength is due to propagation of such micro-cracks, leading to brittle failure of concrete. This weakness can be considerably overcome by the inclusion of polypropylene and steel scrubber fibres in the concrete mix. Polypropylene and steel scrubber fibres are added to concrete to improve the structural properties, particularly tensile, compressive and flexural strength. The extent of improvement in the mechanical properties achieved with polypropylene and steel scrubber reinforced self compacting concrete over those of plain concrete depends on several factors, such as shape, size, volume, percentage and distribution of fibres.

II. OBJECTIVES

- To find the workability of different mixes of SCC and SCC with polypropylene and steel scrubber fibre
- To find the compressive strength and flexural strength of SCC and SCC with polypropylene and steel scrubber fibre
- To find the split tensile strength of SCC and SCC with polypropylene and steel scrubber fibre
- To compare the results of SCC and SCC with polypropylene and steel scrubber fibre.

III. SCOPE OF THE STUDY

- The study deals with the determination of slump flow of SCC and SCC with polypropylene and steel scrubber fibre.

- The study deals with determination of the maximum load by the application of compressive load on the cube specimen of 150 x 150 x 150 mm in Compression testing machine.
- The study deals with the determination of the breaking load by two point loading on beam of size 500 x 100 x 100 mm in flexural testing machine.
- The study deals with determination of the breaking load by the application of tensile load on the cylinder specimen of 150 x 300 mm in Compression testing machine.

IV. MATERIALS USED

A. CEMENT

Ordinary Portland cement of grade 53 conforming to IS8112:1981 was used. The physical properties are shown in Table 1.

Table 1: Physical Properties of cement

Property	Values
Specific gravity	3.10
Initial setting time	58 min
Final setting time	280 min
Standard consistency	27.5%
Fineness	4.5%

B. Fine Aggregate

Tests were done according to IS 2386 (part 3):1963, river sand passing through 4.75mm sieve conforming to zone 2 as per IS 383:1970 was used for experiment. The properties of fine aggregate are given in Table 2.

Table 2 properties of fine aggregate

Sl. No	Property	Value
1	Specific gravity	2.63
2	Fineness modulus	2.125
3	Void ratio	0.53
4	Porosity	29%

C. Coarse Aggregate

As per IS 2386 (part 3):1963 tests were conducted on coarse aggregate to determine the different physical properties. The physical properties are shown in Table 3.

Table 3 Properties of Coarse aggregate

Sl. No	Property	Value
1	Specific gravity	2.68
2	Bulk density	1.66 g/cc
3	Void ratio	0.69
4	Porosity	41.07%

D. Polypropylene

Polypropylene also known as polypropene is a thermoplastic polymer used in wide variety of applications. Usually polypropylene of 12mm length is used for construction purposes. It has the ability to prevent crack formation in concrete. Polypropylene of diameter 75 μ m and length 12mm is used.

E. Steel scrubber fibre

Steel scrubber fibres of 12mm length and 0.5 mm diameter are used. It has the ability to prevent crack formation in concrete.

F. Cerahyperplast

Cerahyperplast XR W40 is used as superplasticizer. The Superplasticizer or high range water reducing admixtures are chemical admixtures that are added to concrete mixtures to improve workability.

G. Viscocrete

Viscocrete is a high range water reducing and superplasticizing admixture. It is ideal for production of self compacting concrete. The superplasticizing action of viscocrete provides excellent workability and may be placed with minimal vibration even at very low water cement ratio.

H. Water

Drinking water directly drawn from the water supply line was used for the entire casting work.

V. MIX PROPORTION

The mix design was done by trial and error method. There is no standard method for mix design of self compacted concrete. Mix design was done for M₃₀ grade. The quantity of ingredients fixed by trial and error method is shown in table 4.

Table 4 Quantity of materials per cubic meter of concrete

Sl. No	Ingredients	Quantity
1	Cement	240 Kg/m ³
2	Fine aggregate	915 Kg/m ³
3	Coarse aggregate	720 Kg/m ³
4	Cerahyperplast	1.5% of cement
5	Viscocrete	2.5% of cement
6	water	192 Kg/m ³

After finalizing the proportion of ingredients, following mix proportions with different designations according to Polypropylene and Steel scrubber fibre content were used.

Table 5 Mix designations used

Sl. No	Mix designation	% polypropylene fibre by weight of cement	% steel scrubber fibre by weight of cement
1	SCC	0%	0%
2	SCC ₁	0.25%	0.1%
3	SCC ₂	0.25%	0.15%
4	SCC ₃	0.25%	0.2%
5	SCC ₄	0.25%	0.25%

VI. EXPERIMENTAL INVESTIGATIONS

Mixing procedure and mixing time are more critical in SCC as compared to conventional concrete mixtures. The coarse and fine aggregate are initially dry mixed for about 30 sec, this was followed by the addition of cement and 1/3 of total mixing water. After 1.5 minutes of mixing, the rest of the mixing water together with the superplasticizer and viscocrete was added. All batches were mixed for a total mixing time of 4 minutes in the mixer. Then fibers were added and mixed for 1 minute. After the mixing procedure is completed, tests are conducted on the fresh concrete. Two types of workability tests were performed on fresh concrete mixtures, Slump flow and V-funnel test.

Standard moulds were used for casting 150mm cube specimens of three numbers, 150mm diameter and 300mm height cylinders of three numbers and 100 x 100 x 500 mm size beam specimens of three numbers. All specimens are cast in one layer without any compaction. After 24 hours, the specimens were de-moulded and cured in water. These specimens are used for the determination of compressive strength, split tensile strength and flexural strength of concrete respectively.

VII. TESTS AND RESULTS

A. SLUMP FLOW TEST

The test is done to assess the horizontal flow of concrete and the filling ability of the mix in the absence of obstructions. The higher the slump flow value, the greater its ability to fill formwork under its own weight.

B. V-FUNNEL TEST

V-funnel test is used to determine the filling ability (flowability) of the concrete with a maximum aggregate size of 20mm.

The results of various workability testes are given in table 6

Table 6 Results of fresh property testes

Mix	Fibre content (%)		Slump diameter mm	V-funnel sec
	Polypropylene	Steel scrubber		
SCC	0	0	745	8.1
SCC ₁	0.25	0.1	726	9.8
SCC ₂	0.25	0.15	710	10
SCC ₃	0.25	0.2	690	12.2
SCC ₄	0.25	0.25	666	13

From the above data it is clear that the workability of the mix reduces with increase in fiber content as compared to plain self compacting concrete. The workability results of different mixes are given in table 7

Table 7 Workability results of all mixes

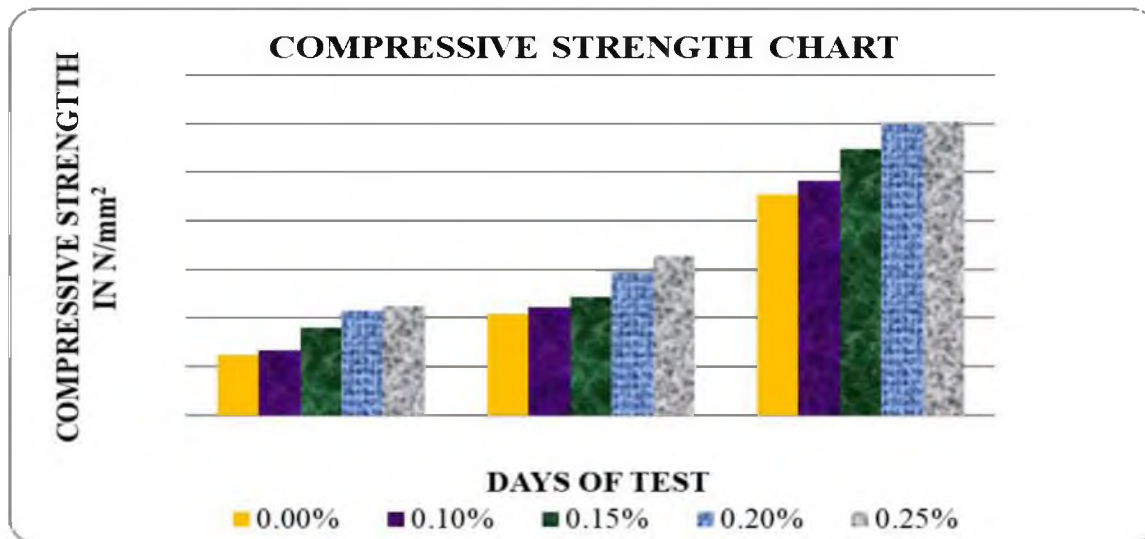
Mix designation	Workability results
SCC	SCC achieved
SCC1	SCC achieved
SCC2	SCC achieved
SCC3	SCC achieved but little bit difficulty for passing ability
SCC4	SCC achieved but little bit difficulty for passing ability

C. COMPRESSIVE STRENGTH

The compressive strength is the characteristic value for classification of concrete in various grades. The testing was done by compression testing machine and load was applied at a rate of 14 N/mm²/min, then failure load was noted and compressive strength is calculated. The test results and variation of 7th, 14th and 28th day compressive strength are shown in Table 8 and Fig1.

Table 8 Compressive strength results of cubes

Mix No	Polypropylene %	Steel scrubber %	7 th day compressive strength (N/mm ²)	14 th day compressive strength (N/mm ²)	28 th day compressive strength (N/mm ²)
SCC	0	0	12.31	20.83	45.3
SCC ₁	0.25	0.1	13.41	22.14	48.22
SCC ₂	0.25	0.15	17.91	24.23	54.72
SCC ₃	0.25	0.2	21.5	29.36	59.85
SCC ₄	0.25	0.25	22.43	32.71	60.3

**Fig 1 Variation of compressive strength of different mixes**

It was observed that there is a considerable increase in compressive strength with the increase in fibre content. About 15% to 37% increase in compressive strength was observed when volume fraction was changed from 0% to 0.25%. The maximum compressive strength is achieved when the percentage of Polypropylene is 0.25% and steel scrubber fibre is 0.25% .

D. SPLIT TENSILE STRENGTH

Three cylinder samples were tested for each mix to determine split tensile strength after 7th, 14th and 28th days using Compression Testing Machine. The test results obtained for the split tensile strength of SCC and SCC with different percentage of fibre content are shown in table 9 and fig2. It was observed that split value increases with increase in fibre content. The maximum strength is obtained when the percentage of polypropylene is 0.25% and steel scrubber fibre is 0.25%.

Table 9 Split tensile strength results

Mix No	Polypropylene %	Steel scrubber %	7 th day split tensile strength (N/mm ²)	14 th day split tensile strength (N/mm ²)	28 th day split tensile strength (N/mm ²)
SCC	0	0	1.82	2.43	3.42
SCC ₁	0.25	0.1	2.01	2.56	3.5
SCC ₂	0.25	0.15	2.11	2.76	3.71
SCC ₃	0.25	0.2	2.56	3.41	4.24
SCC ₄	0.25	0.25	2.81	3.63	4.26

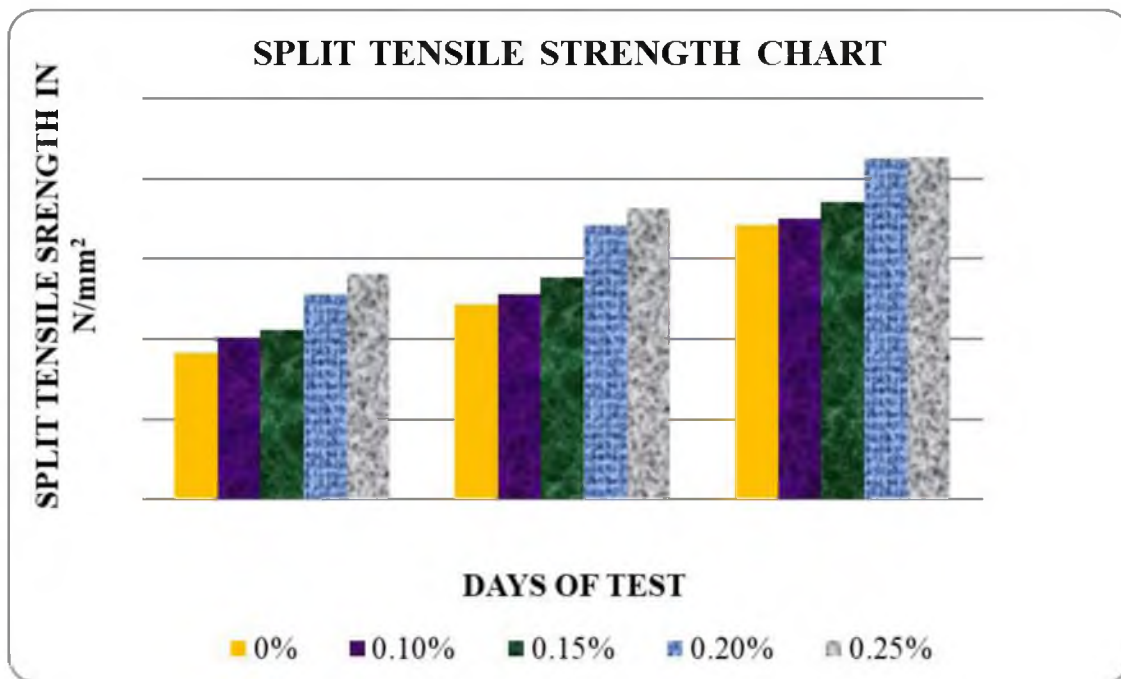


Fig 2 Variation of split tensile strength of different mixes

E. FLEXURAL STRENGTH

Three beam samples were tested for each mix to determine flexural strength after 7th, 14th and 28th days using Flexural Testing Machine as per IS specifications. The test results obtained for flexural strength of SCC and SCC with different percentage of fibre content are shown in Table 10 and fig 3. The flexural strength increases with increase in fibre content. The maximum flexural strength is obtained when the percentage of polypropylene and steel steel scrubber fibre are in equal proportion, ie 0.25%.

Table 10 Flexural test results

Mix No	Polypropylene %	Steel scrubber %	7 th day flexural strength (N/mm ²)	14 th day flexural strength (N/mm ²)	28 th day flexural strength (N/mm ²)
SCC	0	0	2.82	3.62	4.32
SCC ₁	0.25	0.1	2.91	3.82	4.5
SCC ₂	0.25	0.15	3.25	4.25	5.63
SCC ₃	0.25	0.2	3.52	4.86	6.75
SCC ₄	0.25	0.25	3.56	4.97	6.83

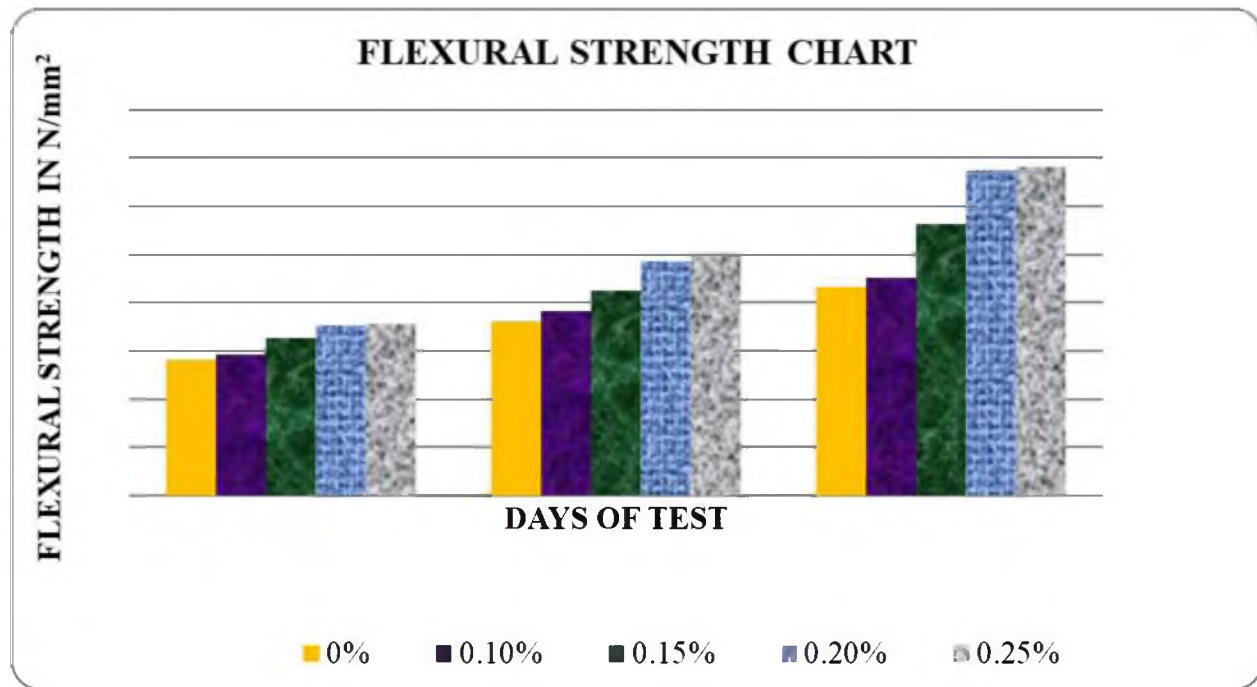


Fig 3 Variation of Flexural strength of different mixes

VIII. CONCLUSION

Studies were conducted by the addition of different percentage of fibres. The even dispersion of polypropylene and steel scrubber fibres increases the compressive strength, split tensile strength and flexural strength of self compacting concrete. The developed SCC mix with fibre content has satisfied almost all requirements of self compacting concrete.

- Compressive strength, split tensile strength and flexural strength were obtained by testing.
- The maximum 28th day compressive strength is obtained when polypropylene and steel scrubber fibre are in equal proportion, i.e., 0.25%.
- The minimum and maximum 28th day compressive strength obtained are 45.3 N/mm² and 60.3 N/mm².
- This result shows that the addition of polypropylene and steel scrubber fibre increases the compressive strength of SCC.
- The main reason for strengthening of SCC is due to addition of fibres. Addition of fibres reduces the crack propagation and increases the load carrying capacity.
- Along with compressive strength, the split tensile strength and flexural strength increase due to the addition of fibres.
- The minimum and maximum 28th day split tensile strength obtained are 3.42 N/mm² and 4.26 N/mm², which indicate the increase in split tensile strength.
- The minimum and maximum 28th day flexural strength obtained are 4.32 N/mm² and 6.83 N/mm², which also indicate increase in flexural strength.
- Polypropylene is a relatively inexpensive material which can be used to process high flexural strength in SCC.
- Polypropylene helps to reduce crack propagation in concrete which offers high strength to SCC.
- Addition of polypropylene and steel scrubber fibre to the concrete can improve the mechanical properties of specimens and reduce workability. Fresh self compacting concrete with considerable fibre inclusion can obtain desired workability by proper adjustment of superplasticizer dosage.
- Use of polypropylene and steel scrubber fibre in SCC is a techno-economically feasible method of strengthening of SCC.

REFERENCE

- [1] Okamura and Ouchi, (2003) "Self Compacting Concrete", Journal of Advanced Concrete Technology, vol- 1, No: 1, pp 5-15.
- [2] EFNARC, (European Federation For Specialist Construction Chemicals And Concrete Systems), (2003), "Specification and Guideline for Self Compacting Concrete".
- [3] Apoorva Chandak, Nitin Agrawal, Divyansh Thakur and Abhyuday Titiksh, (2016) "Analysis of Self Compacting Concrete Using Hybrid Fibres"; International Journal of Trend in Research and Development, Vol- 3(2)

- [4] Ahmed Fathi Mohamed Salih, Nasir Shafiq, Muhd Fadhil Nuruddin, Ali Elheber, (2014) "Performance of Fibre Reinforced Self – Compacting Concrete Containing Different Pozzolanic Material: State of the Art"; IJCSE vol 1, issue 1
- [5] Avinash Thankur, Hemant Sood, (2017) "A Review Study of Strength Properties of Hybrid Fibre Reinforcement Concrete Using PPC", IRJET, vol – 4.
- [6] Gandi Sathi Babu, P Rama Mohan Rao, "Properties of Self Compacting Concrete Using Polypropylene Fibres", SSRG – IJCE, vol -3.
- [7] Mallesh M, Shwtha G C, Reena K, Madhukaran, "Experimental Studies on M₃₀ Grade Self Compacting Concrete", vol -4.
- [8] Nan Su, Kung- Chung Hsu, His- Wen Chai (2001), "A Simple Mix Design Method for Self- Compacting Concrete" Journal of Cement And Concrete Research 31(2001) pp 1799-1807

Experimental investigation on torsional behaviour of RCC beams retrofitted with high strength ferrocement jacketing and GFRP

Shine R. Sylus¹ and Tom George²

¹PG Research Scholar, Structural Engineering, Mar Baselios College of Engineering and Technology, Thiruvananthapuram, Kerala, India
shinersylus127@gmail.com

²Asst. Professor, Department of Civil Engineering, Mar Baselios College of Engineering and Technology, Thiruvananthapuram, Kerala, India
tomgeorge1507@gmail.com

Abstract. Torsion occurs in many reinforced concrete structures in combination with flexure and shear. Structural components can fail due to severe torsional effects. An introduction to torsion, retrofitting using high strength ferrocement mortar and GFRP discussing in this project. There are total 12 specimens divided into four groups, each having three specimens each. First group is the control specimen group. Second group specimens retrofitted with high strength ferrocement mortar. Third group is test specimens retrofitted with GFRP wrapping. Fourth group is test specimens retrofitted with inclined GFRP wrapping. A normal M20 mix was designed for the beams. Special mixing, placing, and curing practices may be needed to produce and handle high-strength mortar. Wrapping with GFRP can significantly improve the strength and ductility. The behavior and performance of RC members strengthened with externally bonded GFRP sheets subjected to torsion and is presented in this paper. The test is done using a push pull jack on one end of the beam and giving a reaction to the floor on the other end of the beam. Load is transferred using fabricated lever arms fixed on the beam. The twisting of the beam is measured using dial gauges. Also the torsional behaviors are studied. First cracks occurred at the middle of the beam. They circulated along the periphery of the beam like a continuous spiral crack. Torsional resistance of retrofitted beams increased than that of normal beams.

Keywords: High strength ferrocement mortar, Glass fiber reinforced polymer

1. Introduction

When external loads act far away from the vertical plane of bending, the beam gets subjected to twisting about its longitudinal axis which is known as torsion. Numerous structural members are subjected to torsional moments which are critical in design. Torsion occurs in many reinforced concrete structures in combination with flexure and shear. Depending on the load transfer mechanism the torsion is classified as 'equilibrium' torsion' and 'compatibility torsion'. Equilibrium torsion is induced in beams supporting lateral overhanging projections, and is caused by the eccentricity in the loading. In compatibility torsion, torsion is induced in a structural member by rotations (twists) applied at one or more points along the length of the member. The twisting moments induced are generally statically indeterminate and their analysis necessarily involves compatibility conditions. Hence it is named 'compatibility torsion'. The structural elements subjected to torsion show cracking if they are not designed and detailed properly. Further, change in loading or deterioration of structural element cause the deficiency in torsional resistance. Also in recent past earthquakes, it has been seen that structures showed failure and some have been severely damaged. Such disasters have demonstrated the need for retrofitting of seismically deficient structures. Shear stresses due to torsion create diagonal tension stresses that produce diagonal cracking. If the member is not adequately reinforced for torsion, a sudden brittle failure can occur. Structural components can fail due to severe torsional effects, particularly in vertical resisting components where torsion in the horizontal plane greatly amplifies seismic effect. In a reinforced concrete member, such a crack would cause brittle failure unless torsional reinforcement is provided to limit the growth of this crack. The first cracks are observed at the middle of the longer side. Next, cracks are observed at the middle of the shorter side. After the cracks connect, they circulate along the periphery of the beam. Retrofitting allows strengthening of elements to resist the strength demands predicted by the analysis, without significantly affecting the overall response of the structure. The cracking of reinforced concrete structures under load is a natural process. Because of concrete's low ultimate tensile stress, cracks appear in it once this strength is exceeded. [2] It is often better to repair or upgrade the structure by retrofitting. Different methods of structural strengthening or retrofitting techniques that have been developed over the years include external bonding of steel plates, glass fibre reinforced plastic (GFRP), fibre reinforced polymer (FRP) sheets, external pre-stressing, carbon fibre wrapping, external bar reinforcement and very recently improved external (bars) reinforcement techniques.

2. Experimental study

A. Mix selection and casting of control beams

A concrete mix of grade M20 was designed based on the nature of the available materials. Materials used are Portland pozzolona cement, 20mm coarse aggregate and manufactured sand. Mix developed is 1:1.96:3.90 with 340gm cement content. The fresh properties were evaluated by measuring the slump according to IS 1199:1959 (Reaffirmed 2004) [21] and the hardened properties were evaluated according to IS 516:1959 (Reaffirmed 2004). Reinforcement was placed inside the beam mould with an effective cover of 25mm. The concrete was then poured inside and compacted well. It was de-moulded the next day and covered with moist rags for 28 days for curing. The reinforcement detail is as shown in fig 1.

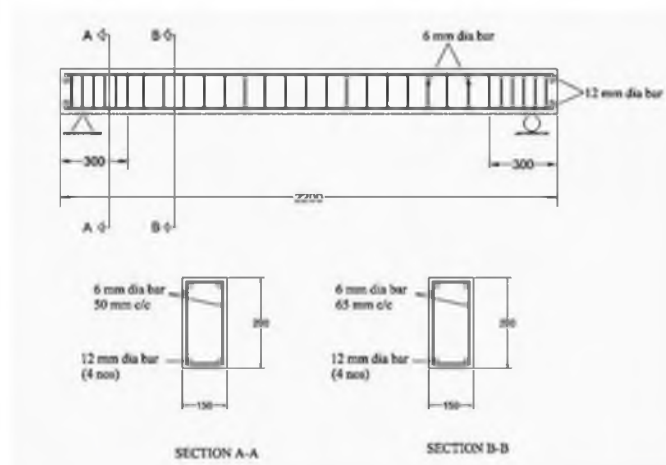


Fig.1 Layout of beam



Fig.2 Reinforcement



Fig.3 Beams kept for curing

B. Torsion test

The beams are placed on a simply supported condition. Shot put balls, of 8 pounds each, are used to create the simply supported condition. Metal plates are placed above and below the shot put balls having CNC done on the contact surface. One shot put ball is bolted to the plate below it to give the hinge effect to the plate placed above it and the other shot put ball is placed in between the CNC's to give the roller effect. Two concrete pillars were made having centre to centre distance of 2 metres and the height of the pillars were fixed according to the height required for the test setup. The shot put balls with plates were then placed on the pillars. After that the test specimen to be tested was placed on the simply supported condition. After placing the beam, fabricated lever arms of 1m length are fixed on to the ends of the beam. One lever arm is connected to a universal load cell which is connected to a push pull jack connected to a loading frame. This push pull jack pulls down the lever arm to create torsional force on the beam. The second lever arm is connected on the other end of the beam in the opposite direction and the reaction is transferred through turn buckles hooked to the anchor bolt provided on the floor. Another set of small lever arms are fixed at the ends of the test region of the beam for placing the dial

gauges to measure the angle of twist. The loading is done by using the push pull jack and as the lever at the loading end is pulled down, the other lever arm being fixed to ground using turn buckle resists the load. Since the support condition is simply supported, it allows free rotation of the lever arm which inturn ends up in twisting the beams. Loading of 0.2kN interval was applied with the hydraulic jack, having a universal load cell attached on it, until the specimen failed to take further load. Deflections were noted by dial gauges of least count 0.01mm and angle of twists were found out for the corresponding loads. Crack patterns were also noted while testing.



Fig.4 Test set up



Fig 5. Ferrocement mesh wrapped beam



Fig 6. High strength ferrocement retrofitted beam

The mortar in the ferrocement matrix was designed by adopting cement – sand ratio of 1:2 and the water cement ratio as 0.35. The silica fume replacement level was found out from the test results of compression test of mortar cubes having various percentages of silica fume. While considering the 28th day compressive strength values, 5% cement replacement showed the compressive strength equal to 56 MPa. Thus 5% silica fume by weight of cement was selected as the optimum percentage.



Fig 7. GFRP wrapped beam



Fig 8. GFRP diagonal strip wrapped beam

Table 1. Description of beams

Designation	Description	Number of beams
CB	Control beam	3
HSFB	Beam retrofitted with High strength ferrocement jacketing	3
GFRPB	Beam retrofitted with GFRP	3
GFRPB₁	Beam retrofitted with inclined GFRP	3

3. Results and discussion

A. Torque and angle of twist

Table 2. Initial and ultimate torques and corresponding angle of twists

Specimen	Initial cracking torque (kNm)	Angle of twist for initial cracking torque (rad/mm)	Ultimate cracking torque (kNm)	Angle of twist for ultimate cracking torque (rad/mm)
Control	2.6	0.0071	3.9	0.0321
HSFB	2.6	0.0068	6.0	0.055
GFRPB	3.8	0.010	4.6	0.032
GFRPB₁	4.0	0.012	5.2	0.0307

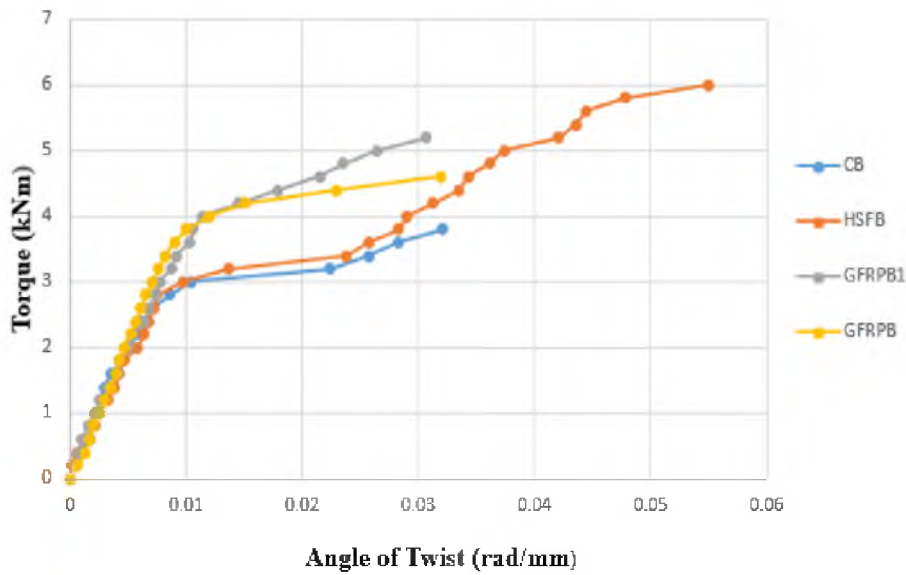


Fig.9. Torque vs angle of twist curve

The initial cracking torque of HSFB and control beams were almost similar. Ultimate cracking load of HSFB beam was 6kNm. But that of control beam was only 3.9kNm. But in the case of GFRP retrofitted beams, initial cracking torque of GFRPB and GFRPB₁ were 3.8kNm and 4.0kNm respectively. Ultimate cracking torque of GFRPB and GFRPB₁ beams were 4.6kNm and 5.2kNm respectively. The angle of twist for initial cracking torque of control and HSFB beams were 0.0071 and 0.0068 respectively. That in the case of GFRPB and GFRPB₁ beams were 0.010rad/mm and 0.012rad/mm respectively. Angle of twist for ultimate cracking torque of control and HSFB beams were 0.0321rad/mm and 0.055rad/mm respectively.

B. Crack patterns

The first cracks occurred at the middle of the beam. They circulated along the periphery of the beam like a continuous spiral crack.

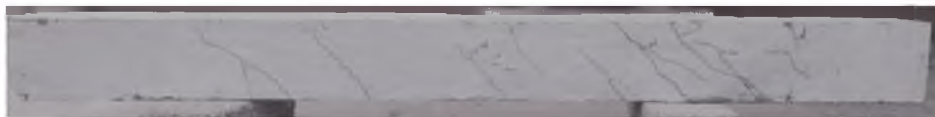


Fig.10. crack pattern in control beam



Fig.11. Crack pattern in HSFB beam



Fig.12. Crack pattern in GFRPB beam



Fig.13. Crack pattern in GFRPB₁ beam

In HSFB beam first crack occurred at the middle of the beam similar as in the control beam. De-bonding of ferrocement from the beam surface takes place during testing and the number of cracks increased considerably in this case and the space between the adjacent cracks decreased upto 15cm. The initial crack occurred at a torque of 3.6kNm. The angle of the cracks were more inclined when compared to the control beam. The number of cracks increased and it clearly had more load carrying capacity than the control beam. In GFRPB beams, crack patterns were not propagated through the retrofitted surface. Because the cracked surface was fully covered by GFRP 'U' wrap. No considerable de-bonding of GFRP sheet was occurred. The number of cracks decreased in this case and the space between the adjacent cracks remains same as in the control beam. The first cracks occurred at the middle of the beam and the initial crack occurred at a torque of 3.8kNm. Then the cracks propagated forming spiral cracks. The angle of the cracks were more inclined when compared to the control beam. While in GFRPB₁ beam, cracks can be seen through the region where strip is absent. When compare with control beam, retrofitted beams have more number of micro cracks and less number of major cracks. The diagonal strip wrapped beam (GFRPB₁) shows better crack pattern.

4. Conclusions

The torsional behaviour of M20 beams and various retrofitted beams were studied in this work. Based on the results of this study, the following conclusions are made:

- It is seen that ultimate cracking torque of high strength ferrocement retrofitted beam was about 1.5 times higher than that of M20 control beam. Ultimate cracking torque of GFRPB beam was about 1.2 times higher than that of control beam, and that of GFRPB₁ beam was about 1.35 times higher than control beam.
- Diagonal strip wrapping is more effective in resisting torsion than 'U' wrapping.
- In control beam, first cracks occurred at the middle of the beam. After the cracks connected, they circulated along the periphery of the beam like a continuous spiral crack. But in HSFB beams, De-bonding of ferrocement from the beam surface takes place.

References

5. Unnikrishna Pillai, DevdasMenon. Reinforced Concrete Design, Tata McGraw-Hill, 2003, 1998.
6. Fuad Okay, SerkanEngin.: Torsional behaviour of steel fiber reinforced concrete beams, *ELSEVIER. Construction and Building Materials*, October, 269-275(2011)
7. Rao, T. D. G, D. Rama S.: Torsional response of fibrous reinforced concrete members: Effect of single type of reinforcement, *Construction and Building Materials*, 187-192(2006)
8. Khaldoun N. Rahal.: Torsional strength of normal and high strength reinforced concrete beams, *ELSEVIER, Engineering Structures*, 56, 2206-2216(2013)
9. Khaled S. R., Ahmed, S. E.: Torsion Behaviour of Steel Fibered High Strength Self Compacting Concrete Beams Reinforced by GFRP Bars, World Academy of Science, *Engineering and Technology International Journal of Civil, Environmental, Structural, Construction and Architectural Engineering*, 7(9)(2013)
10. Pawlak, W. and Kaminski, M.: Cracking of reinforced concrete beams under torsion—theory and experimental research, *ELSEVIER. Archives of civil and mechanical engineering*, 12, 368 – 375(2012)
11. Pant A. S. and Suresh, R.: Steel fiber reinforced concrete beams under combined torsion-bending-shear, *Journal of Civil Engineering (IEB)*, 38, 31-38(2010)
12. Olivito, R. S. and Zuccarello, F. D.: An experimental study on the tensile strength of steel fiber reinforced concrete, *ELSEVIER. Composites: Part B*, 41, 246-255(2009)
13. Rao, T. D. G. and Rama, D. S.: Torsion of steel fiber reinforced concrete members, Pergamon. *Cement and Concrete Research*, 1783-1788(2003)
14. Panchacharam S., Belarbi, A.: Torsional Behaviour of Reinforced Concrete Beams Strengthened with FRP Composites, *First FIB Congress*, Osaka, Japan, October 13-19(2002)
15. Koutchoukali N.E., Belarbi, A.: Torsion of High-Strength Reinforced Concrete Beams and Minimum Reinforcement Requirement, *ACI Structural Journal*, 98(4), 462- 469(2001)
16. Rasmussen L.J., Baker, G.: Torsion in Reinforced Normal and High Strength Concrete Beams (Part 1): Experimental Test Series, *ACI Structural Journal*, 92(1), 56 – 62(1995)
17. Akhtaruzzaman A. A. and Hasnat, A.: Torsion in Concrete Deep Beams with an Opening, *ACI Structural Journal*, 86 (S3), 20- 25(1989)
18. Mansur M. A., Nagataki S., Lee S. H., and Oosumimoto, Y.: Torsional Response of Reinforced Fibrous Concrete Beams, *ACI Structural Journal*, 86 (S5), 36- 44(1989)
19. Varma, M. B. and Hajare, M. B.: Ferrocement: Composite Material and its Application, *International Journal of Pure and Applied Research in Engineering and Technology*, 3(8), 296-307(2015)
20. Structural engineering laboratory manual, Department of civil engineering, IIT Madras.

Seismic Evaluation of Different Structural Systems in Stepped Building Frame

Yamuna S R¹ and Aneena Babu²

¹ PG Scholar, Department of Civil Engineering, MBCET, Trivandrum,
yamunasebastianr@gmail.com

² Assistant Professor, Department of Civil Engineering, MBCET, Trivandrum, aneenaroshan@gmail.com

Abstract. High rise structures have fascinated mankind from the beginning of the civilization itself. In the last few decades the rate of growth in vertical structures has increased drastically. Seismic performance of a building is an important criteria to be considered in the design phase. Many building nowadays have irregular configuration both in plan and elevation. Usually, irregularities are unavoidable in the construction of buildings. This causes the structure to be more vulnerable to damages during earthquakes. Hence, it is necessary to assess the seismic performance of a structure in the design phase. In this work, a hybrid system which is a combination of conventional lateral load resisting system (bracings and shear wall) and a moment resisting frame is used, to improve the seismic performance of vertical irregular structures such as stepped building. Vertical discontinuity arises from reduction of the lateral dimension of the building along its height commonly known as stepped building. Different types of concentric bracing systems have been used. The regularity index provides a basis for assessing the degree of irregularities in a stepped building frame. Torsional effect of structures were also studied. The performance of the structure is assessed by means of modal analysis and nonlinear time history analysis in SAP 2000 (version 2014). Shear wall with concentric brace and shear wall with X brace turned out to be the best hybrid system in terms of seismic performance.

Keywords: Stepped building frame, Dual system, Hybrid system, Regularity index

1. Introduction

Many buildings in the present scenario have irregular configuration in both plan and elevation. Irregularities are not avoidable in the construction of buildings. Irregularities in buildings will cause damage during earthquakes. In multistoried buildings, damage from earthquake ground motion generally initiates at locations where the structure is weak[2]. Structural weaknesses may be caused by discontinuities in stiffness, strength and mass difference between adjacent storeys.

Real structures are mostly irregular, as perfect regularity is an idealization that occurs rarely. For practical purposes, major seismic codes distinguishes irregularity in plan and elevation.

One of the greatest causes of damage to buildings has been the use of improper architectural-structural configurations which affects building response.

A common form of vertical discontinuity arises from the reduction of the lateral dimension of the building along its height, Such buildings are commonly known as stepped buildings. Stepped buildings with vertical discontinuity have increased recently because of its functional and aesthetic architecture. Stepped form provides adequate daylight and ventilation in an urban locality with closely spaced tall buildings [5]. Stepped buildings are characterized by staggered abrupt reductions in floor area along the height of the building.

1.1 Stepped building Frame

Stepped buildings are characterized by abrupt reductions in floor area along the height of the building. Height-wise changes in stiffness and mass, imparts render the dynamic characteristics to a stepped building. Stepped buildings are a typical form of vertical geometric irregularity that required special design consideration due to transverse and torsional responses and higher mode effects. As per IS 1893:2016, stepped building forms are to be treated as vertically irregular when the lateral dimension of the maximum offset (A) at the roof level exceeds 25% of the lateral dimension of the building at the base (L) as shown in Fig.1.



Fig. 1 Stepped building frame

1.2 Structural systems

A structural system consists of elements which are used to resist the various combination of vertical and horizontal loads. The selection of one structural system depends on various factors such as location, height and architectural requirements of the building[6].

One of the major consideration in the modern office building is the requirement of large working spaces. Therefore all the load carrying members especially the lateral load resisting members are placed over the exterior periphery and at the core of the structures. Currently there are different forms of structural systems, out of which moment resisting frame, braced frame and shear wall framed system are the conventional types.

Building frame with shear wall and structural system (bracing) combination is called hybrid system. In this study various structural systems are to be used such as;

- a. Rigid Frame System
- b. Braced Frame system
- c. Shear wall frame system

2. Methodology

2.1 Problem formulation

A stepped building frame subjected to gravity loading was first modelled and designed and then design check is carried out as per IS 456: 2000. The structure was successful in the final design check carried out under gravity loads. Then seismic analysis (Modal analysis and nonlinear time history analysis) as per Indian seismic code has been carried out. After the seismic analysis, the seismic design check has been carried out. That is the structure can take gravity load but has poor performance under seismic loads. So, this structure requires an efficient lateral load system to resist the additional loads generated due to the seismic ground motion.

The reason for poor performance was investigated and it was found that mass irregularity, discontinuity in strength and stiffness.

This is how stepped building structures shows poor performance during seismic ground motions, in the absence of an efficient lateral load resisting system. The dual frame system specified by Indian seismic code and a new structural system known as the hybrid structural systems are chosen to improve the seismic performance of this structure. The data chosen for the modeling of building frame as shown in Table 1.

Table 1 Preliminary data [5]

Building type	Office
Zone factor, z	0.16
Zone	III
Importance factor, I	1
Response reduction factor, R	5
Damping (% critical)	5
Soil type	Medium
Plan dimension (m)	24x24
Bay width in x and y direction(m)	6
Upper storey height (m)	3.3
Opening area in infill (m)	1.5 x 1
Opening area in shear wall (m)	1 x 2
Ground storey height (m)	4.5

2.2 Validation

A regular bare frame has been modelled and analysed using response spectrum analysis. The base shear obtained after the analysis using SAP 2000 (version 2014) has been compared with the base shear obtained by theoretical calculation.

2.3 Modelling of building frame

The modelling of the structures had been carried out in SAP 2000(version 2014). The beams and columns are modelled as frame elements. The slab and shear wall are modelled as thin shell element. The external infill wall is modelled as diagonal strut element. The material data chosen for study is shown in Table 2. The model parameters are shown in Table3.

Table 2 Material property

Material	Type	Young's modulus, E (N/mm ²)	Density, ρ (kN/m ²)
Concrete	M25	25000	25.00
Rebar	Fe 415	200000	78.93
Brick	Class 490	5500	18.87

Table 3 Modal parameter [28]

Parameter	Dimensions
Slab thickness	150mm
Wall thickness	230mm
Shear wall thickness	250mm
Structural steel section	ISMB 300

2.4 Computational model

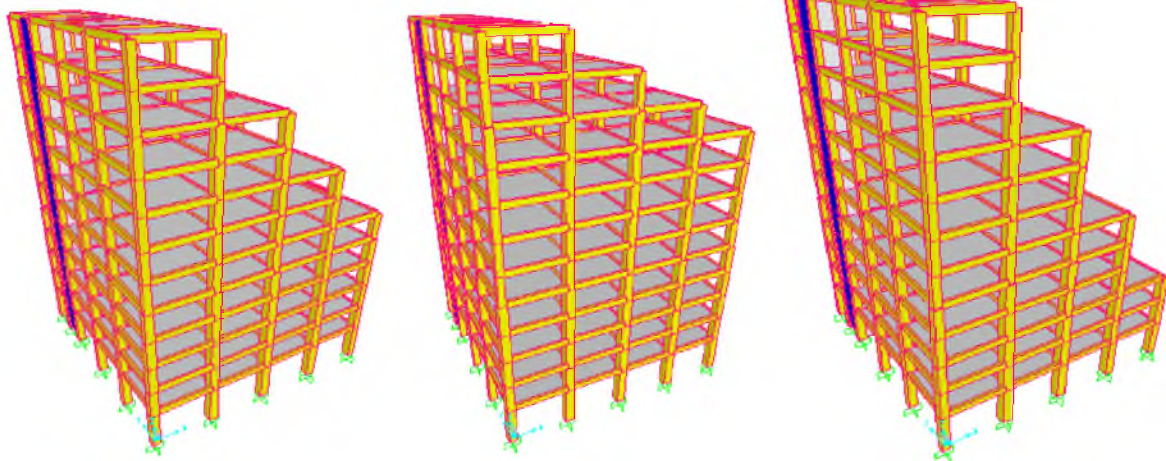
Modelling a building involves the modelling and assemblage of its various load-carrying elements. The model must ideally represent the mass distribution, strength, stiffness and deformability. Modelling of the material properties and structural elements used in the present study is described in Table 4. Building frame and notations are shown in Table 3.4. Cross section details of primary elements of 12 storeyed building frame are shown in Table 5. Different structural models chosen are shown in Fig. 2.

Table 4 Building frame and notations

Building frame	Notations
12 storey Stepped building with one floor height	S1 – 12
12 storey Stepped building with two floor height	S2 – 12
12 storey Stepped building with three floor height	S3 - 12
Bare frame	BF
X brace	XB
Diagonal brace	DB
Chevron brace	CB
Shear wall	SW
Shear wall with X brace	SW-XB
Shear wall with diagonal brace	SW-DB
Shear wall with inverted brace	SW-CB

Table 5 Cross section data of 12 storeyed building frame [10]

Storey	Beam	Outer Column	Inner column
1	300mm x 700mm	800mm x800mm	900mm x900mm
2	300mm x 700mm	800mm x800mm	900mm x900mm
3	300mm x 700mm	800mm x800mm	900mm x900mm
4	300mm x 700mm	800mm x800mm	900mm x900mm
5	300mm x 700mm	800mm x800mm	900mm x900mm
6	300mm x 700mm	700mm x 700mm	800mm x800mm
7	300mm x 700mm	700mm x 700mm	800mm x800mm
8	300mm x 700mm	700mm x 700mm	800mm x800mm
9	300mm x 700mm	700mm x 700mm	800mm x800mm
10	300mm x 600mm	700mm x 700mm	800mm x800mm
11	300mm x 600mm	600mm x 600mm	600mm x 600mm
12	300mm x 600mm	600mm x 600mm	600mm x 600mm



a) S1-12

b) S2-12

c) S3-12

Fig. 2 Structural models

3 Result and Discussions

3.1 Modal analysis

Modal analysis as per Indian seismic code were carried out on dual frame models such as XB, SW, CB, DB and on hybrid frame models such as SWXB, SWCB and SWDB. 79 models were considered for the analysis.

3.1.1 Variation in fundamental natural period

The variation in fundamental time period of setback structure with structural systems are shown in Table 6.

Table 6 Variation in fundamental natural period of 12 storeyed stepped building frame

Models	Fundamental time period (s)		
	S1	S2	S3
BF	1.47	1.22	1.18
XB	0.96	0.84	0.80
CB	1.00	0.95	0.91
DB	1.27	1.12	1.06
SW	0.66	0.63	0.59
XBDB	1.14	1.04	0.99
XBCB	1.00	0.95	0.89
DBCBC	1.20	1.14	1.06
SWDB	0.78	0.71	0.65
SWCB	0.59	0.52	0.49
SWXB	0.48	0.42	0.40

From the result obtained for the fundamental period, it is observed that the time period of the systems increase with increasing number of storeys. By using dual frame in stepped building frame fundamental natural period of structure decreased due to increase the stiffness of structure and SW dual frame system is found to be more effective in the combinations considered. And also by using hybrid frame in stepped building frame natural period of structure decreased due to increase the stiffness of structure. It can conclude that dual and hybrid systems are more effective in high rise stepped building frame.

3.1.2 Quantifying irregularity in stepped building frame

The stiffness and mass distributions in the frame have to be considered in quantifying the irregularity of a stepped building. Studying the dynamic properties of regular building it was found that the participation of the first mode is dominant. However, when the vertical irregularities (step in the

building frame) are introduced, it is observed that as the irregularity increases, participation on higher modes is prominent.

Generally, irregularity in the stepped frame can be captured by relative first mode participation factor. Accordingly, a regularity index (η) is proposed to quantifying irregularity of a stepped frame as Eqn.5.1. [5]

$$\eta = \frac{r_1}{r_{ref}} \quad (5.1)$$

Where,

r_1 is the first mode participation factor for stepped frame under consideration

r_{ref} is the first mode participation factor for regular frame without steps

Building irregularity of 12 storeyed stepped building frame is shown in Table 7 to Table 9. From Table 7 to Table 9, it can be concluded that for any stepped building the value of regularity index (η) will be less than unity as the first mode participation factor will always be less than that of regular building. This regularity index accounts for properties associated with mass and stiffness distribution in the frame. Regularity index increases with increasing in number of storeys, the rate of increasing regularity index being stiffer when the number of storeys per step increases.

Table 7 Building irregularity of 12 storeyed stepped frame with S1

Building frame	Regularity index	Percentage Variation
S1BF	0.59	-
XB	0.77	30.51
CB	0.76	28.81
DB	0.74	25.14
SW	0.95	61.02
S1 XBDB	0.76	28.81
XBCB	0.79	33.90
DBCB	0.72	22.03
SWDB	0.87	47.46
SWCB	0.90	52.54
SWXB	0.92	55.93

Table 8 Building irregularity of 12 storeyed stepped frame with S2

Building frame	Regularity index	Percentage Variation
S2BF	0.51	-
XB	0.74	45.10
CB	0.72	41.18
DB	0.70	37.25
SW	0.92	80.39
S2		
XBDB	0.72	41.18
XBCB	0.75	47.06
DBCB	0.68	33.33
SWDB	0.84	64.71
SWCB	0.88	72.55
SWXB	0.90	76.47

Table 9 Building irregularity of 12 storeyed stepped frame with S3

Building frame	Regularity index	Percentage Variation
S1BF	0.48	-
XB	0.73	54.15
CB	0.70	45.83
DB	0.67	39.58
SW	0.83	72.92
S3		
XBDB	0.70	45.83
XBCB	0.72	50.00
DBCB	0.65	35.42
SWDB	0.79	64.58
SWCB	0.84	75.00
SWXB	0.87	81.25

4 Non linear time history analysis

Time history analysis (Elcentro – earthquake data) is a step by step analysis of the dynamic response of a structure subjected to a specific ground motion. The dynamic input has been gives as a ground acceleration time – history which was applied uniformly at all the points of the base of the structure, only one horizontal component ground motion has been considered.

4.2.1 Variation of roof displacement

The variation of roof displacement of different building models are shown in Table 10 to 12. It can be concluded that the stepped building frame without structural system have higher displacement as compared to the dual and hybrid structural systems. Roof displacement of structure increase with increasing irregularity and number of storeys.

Stepped buildings with dual frame such as SW and hybrid structural system SWXB are more effective in reduction of roof displacement of structure. While with increasing number of storeys of structure, dual frame such as SW and hybrid structural systems SWXB and SWCB are more effective in reduction of roof displacement of structure. It can be concluded that hybrid structural systems are more effective in high rise structures.

Table 10 Roof displacement of 12 storeyed stepped frame with S1

Building frame	Roof displacement (mm)	Percentage Variation
S1BF	30.89	-
XB	10.11	67.27
CB	23.86	22.76
DB	26.49	14.24
SW	6.79	78.02
S1		
XBDB	17.56	43.15
XBCB	15.03	51.34
DBCB	21.95	28.94
SWDB	10.54	65.88
SWCB	9.13	70.44
SWXB	8.28	73.20

Table 11 Roof displacement of 12 storeyed stepped frame with S2

Building frame	Roof displacement (mm)	Percentage Variation	
S2BF	35.60	-	
XB	16.74	61.06	
CB	27.57	26.00	
DB	31.24	14.11	
SW	14.56	68.11	
S2	XBDB	22.07	43.80
	XBCB	18.78	54.45
	DBCB	27.12	27.45
	SWDB	14.32	68.89
	SWCB	11.02	79.57
	SWXB	8.41	88.02

Table 12 Building irregularity of 12 storeyed stepped frame with S3

Building frame	Roof displacement (mm)	Percentage Variation	
S1BF	38.00	-	
XB	19.47	59.99	
CB	30.01	25.87	
DB	34.65	10.84	
SW	16.45	69.76	
S3	XBDB	28.14	31.92
	XBCB	23.42	47.20
	DBCB	31.90	19.75
	SWDB	17.49	66.40
	SWCB	15.91	71.51
	SWXB	11.43	86.01

3.2.2 Variation of base shear

The variation of base shear of different building models are shown in Table 13 to Table 15. It can be seen that stepped building frame without structural system have lesser base shear as compared to the dual and hybrid structural systems. Base shear of structure decrease with increasing irregularity and increase with increasing number of storeys.

Stepped buildings with dual frame such as SW and hybrid structural system SWXB are more effective in improving base shear of structure. While with increasing irregularity of structure hybrid systems SWXB and SWCB are more effective. When number of storeys of structure is increased, dual frame such as SW and hybrid structural systems SWXB and SWCB are more effective in improving base shear of structure.

Table 13 Base shear of 12 storeyed stepped frame with S1

Building frame	Base Shear (kN)	Percentage Variation
S1BF	620	-
XB	654	5.48
CB	648	4.52
DB	640	3.23
SW	820	32.26
XBDB	640	3.23
XBCB	653	5.32
DBCBC	646	4.19
SWDB	720	16.13
SWCB	795	28.23
SWXB	864	39.35

Table 14 Base shear of 12 storeyed stepped frame with S2

Building frame	Base Shear (kN)	Percentage Variation
S2BF	560	-
XB	598	6.79
CB	581	3.75
DB	579	3.39
SW	710	26.79
XBDB	576	2.86
XBCB	592	5.71
DBCBC	588	5.00
SWDB	592	5.71
SWCB	694	23.93
SWXB	758	35.36

Table 15 Base shear of 12 storeyed stepped frame with S3

Building frame	Base Shear (kN)	Percentage Variation	
S3BF	495	-	
XB	535	8.08	
CB	526	6.26	
DB	519	4.85	
SW	622	25.66	
S3	XBDB	519	4.85
	XBCB	534	7.88
	DBCB	528	6.67
	SWDB	586	18.38
	SWCB	642	29.70
	SWXB	663	33.94

5 Conclusions

The seismic performance of stepped building with hybrid structural system and dual frame system was investigated. Modal analysis and non - linear time history analysis were used to study the seismic performance of the structural systems. The poor performance of stepped building can be accounted due to mass reduction at top storeys which reduces the storey stiffness. This causes an increase in lateral displacement and twisting effect in stepped building frame during seismic ground motions, which leads to catastrophic failures.

- Structural systems are found to be more effective with increasing number of storeys.
- The given configuration of shear wall dual frames system improves the seismic performance of stepped building by reducing lateral displacement and base shear.
- The implementation of hybrid structural systems has reduced the irregularity effect and increased the mass and stiffness of the system.
- The best hybrid framed systems that can be adopted in stepped buildings are SWCB and SWXB. These systems have high lateral and vertical load carrying capacity.
- While considering the practical aspects, it is better to provide SW-CB system, since it creates much convenience for the movement of peoples and vehicles in ground storey.

References

- [1] Kiran, S., Ramtekkar, G. D. and Titiksh, A. (2017) "Comparative Study for Mitigating the Soft Storey Effect in Multi Storey Buildings Using Different Structural Arrangements", *International journal of civil engineering and technology*, 8, 520 – 531.
- [2] Drazic, J. and Vatin, N. (2016) "The influence of configuration on to the seismic resistance of a building", *Procedia Engineering*, 165, 883 -890.
- [3] Draft Indian Standard for Criteria for Structural Safety of Tall Buildings, Bureau of Indian Standards, New Delhi, 2016, 1-37.
- [4] IS 1893 (Part 1): 2016, Indian Standard Criteria for Earthquake Resistant Design of Structures, Part 1 General Provisions and Buildings, Fifth Revision, Bureau of Indian Standards., New Delhi.
- [5] Sarkar, P., Prasad, M. A. and Menon, D. (2015) "Vertical geometric irregularity in stepped building frames", *Engineering Structures*, 32(2), 2175 -2186.

- [6] Ozmen, G., Girgin, K. and Drugum, Y. (2014) “Torsional Irregularity in Multi- storey Structures”, *Engineering Structures*, 6 (1),121 – 131.
- [7] Sachin, G., Maske., and Dr. Pajgade, P. S. (2013) “Torsional Behaviour of Asymmetrical Buildings”, *International Journal of Modern Engineering Research*, 3(1),1146 – 1149.
- [8] Wakchaure, M. R. and Nagare, Y. U. (2013) “Effect of Torsion Consideration in Analysis of Multi Storey Frame”, *International Journal of Engineering Research and Applications*, 3, 1828 -1832.
- [9] Dr. Dubey, S. K. and Sangamnerkar, P. D. (2011) “Seismic Behaviour of Asymmetric RC Buildings”, *Procedia Engineering*, 2,296 – 301.
- [10] Dr. Varughese, J. A., Menon, P. and Prasad, M. A. (2012) “Simplified procedure for displacement-based design of stepped buildings”, *Fifteenth World Conference on Earthquake Engineering*, 1-10.
- [11] Agarwal, P. and Shrikhande, M. (2011) “Earthquake Resistant Design of structures”, Rajkamal Electric Press.
- [12] Damodarasamy, S. R. and Kavitha, S. (2009) “Basics of Structural Dynamics and Aseismic Design”, Jay Print Pack Private Ltd.
- [13] Kim, S. and Elnashai, A. S. (2009) “Characterization of shaking intensity distribution and seismic assessment of RC buildings for the Kashmir earthquake”, *Engineering Structures*, 02(5), 105 -111.
- [14] Mondal, G. and Jain, S. K. (2008) “Lateral Stiffness of Masonry Infilled Reinforced Concrete (RC) Frames with Central Opening”, *Earthquake spectra*, 24, 701-723.
- [15] Godinez-Dominguez, E. A. and TenaColunga, A. (2008) “Behaviour of Moment Resisting Reinforced Concrete Concentric Braced Frames (RC-MRCBF) in Seismic Zones”, *The 14th World Conference on Earthquake Engineering*, Beijing, China, National Information Centre on Earthquake Engineering, Kanpur, India.
- [16] Trifunac, M. D. and Todorovska, M. I. (2008) “Origin of the Response Spectrum Method”, *The 14th World Conference on Earthquake Engineering*, Beijing, China, National Information Centre on Earthquake Engineering, Kanpur, India.
- [17] Galal, K. and Sökkary, H. (2008) “Recent Advancements in Retrofit of RC Shear Walls”, *The 14th World Conference on Earthquake Engineering*, Beijing, China, National Information Centre on Earthquake Engineering, Kanpur, India.
- [18] Karavasilis, T. L., Bazeos, N. and Beskos, D. E. (2008) “Seismic response of plane steel MRF with stepped , estimation of inelastic deformation demands”, *Journal of Constructional Steel Research*, 64, 644 – 654.
- [19] Inel, M., Ozmen, H. and Bilgin, H. (2008) “Re-evaluation of building damage during recent earthquakes in Turkey”, *Engineering Structures*, 30(8), 286 -292.
- [20] Athanassiadou, C. J. (2008) “Seismic performance of RC frames irregular in elevation”, *Engineering Structures*, 30, 1250-1261.
- [21] Gunel, M. H. and Ilgin, H. E. (2007) “A proposal for the classification of structural systems of tall buildings”, *Building and Environment*, 42, 2667 – 2675.
- [22] Freeman, S. A. (2007) “Response spectra as a Useful Design and Analysis Tool for Practicing Structural Engineers”, *Journal of Earthquake Technology*, 44 (1), 25 – 37.
- [23] IS 800: 2007, Indian Standard General Construction in Steel – Code of Practice, 3rd Revision, Bureau of Indian Standards, New Delhi.
- [24] Kaushik, H. B., Rai, D. C. and Jain, S. K. (2006) “A case study for use of dynamic analysis in designing for earthquake force”, *Engineering Structures*, 04, 674 – 679.
- [25] Sharon, B. L., and Wood, S. L. (2005) “Seismic response of RC frames with irregular profiles”, *Engineering Structures*, 08, 545 – 566.

[26] Goel , R. K. and Chopra, A. K. (2003) “Period formula for moment resisting frame buildings”, *Engineering Structures*, 123, 1454 –1461.

[27] Agarwal, P., Thakkar, S. K. and Dubey R. N. (2002) “Seismic performance of reinforced concrete building during Bhuj earthquake”, *Journal of Earthquake Technology*, 39, 195 -217.

[28] Maheri, M. R. and Sahebi, A. (2001) “Use of Steel Bracing In Reinforced Concrete Frames”, *Engineering structures*, 19, 1018-1024.

[29] IS 4326: 1993, Indian Standard Criteria for Earthquake Resistant Design and Construction of Buildings – Code of Practice, 2nd Revision,3.3rd Ed., Bureau of Indian Standards., New Delhi.

[30] IS 875 (Part 2): 1987, Indian Standard Code of Practice for Design Loads (Other than Earthquake) for Buildings and Structures, Part 2 Imposed Loads, 2nd Revision,6th Ed., Bureau of Indian Standards., New Delhi.

Study on the Mechanical and Flexural Properties of Concrete by the Addition of Black Liquor Sludge as Admixture

Nikhil Nadh V. S.¹ and Jayasree S.²

¹PG Research Scholar, Structural Engineering, Mar Baselios College of Engineering and Technology,
Thiruvananthapuram, Kerala, India
nikhilnadhvs1@gmail.com

²Associate Professor, Department of Civil Engineering, Mar Baselios College of Engineering and Technology,
Thiruvananthapuram, Kerala, India
jayasris71@gmail.com

Abstract. Water cement ratio is one of the main factors which control the strength of concrete. Though workability of concrete increases due to the increase in water cement ratio strength of concrete decreases considerably. For increasing the workability with minimum water cement ratio, admixtures are used. It is necessary to note that the addition of these admixtures should not decrease strength and durability properties of concrete. Commonly used chemical admixtures are costly. Black liquor sludge is a waste product from paper industry causes environmental pollution, which may be considered to use as a workability aid. This project work is intended to find the amount of black liquor sludge to be added in M30 and M50 concrete mixes for getting a slump of 100 mm with a water cement ratio of 0.35 for medium workability and to study its mechanical and flexural properties. All the results showed that, black liquor sludge is an effective material for the replacement of current chemical admixtures for improving workability.

Keywords: Black liquor sludge, workability, mechanical properties, flexural property

1. Introduction

Concrete admixture is defined as a material other than water, aggregates or cement, used as an ingredient of concrete and added to the batch immediately before or during its mixing to modify one or more of the properties of concrete in the plastic or hardened state. They are used to modify the properties of concrete to achieve desired workability in case of low water cement ratio and to enhance setting time of concrete for long distance transportation of concrete.

The disposal of waste material is a major problem faced by the industries. If this waste can be used in construction industry as a replacement material, then it will become a solution to the problem. Some of the industrial waste and byproducts were used as concrete admixture such as iron splinters, minced rubber, polymer fibres, mineral dust, calcium carbonate etc [1, 2, 3]. Some natural products were also used as concrete admixture like broiler hen egg and Gum Acacia Karroo (GAK) [4, 5].

Super plasticizers are added to concrete with a low water-cement ratio to make high-slump flowing concrete. The commonly used superplasticizers are ligno-sulphonates and hydrocarbolic acid salts. They are usually based on lignosulphonate, which is a natural polymer, derived from wood processing in the paper industry. The disadvantages of using most of chemical admixtures like super plasticizers are its high cost, lack of availability etc.

In the present experimental investigation, improvement of workability of concrete with a minimum water cement ratio by using black liquor sludge as admixture was studied. Black liquor sludge is a waste product of paper industry during Kraft process. This is a process for conversion of wood into wood pulp, which consists of almost pure cellulose fibers, the main component of paper. One of the main ingredients in it is lignin, the material in trees that binds wood fibers together and makes them rigid. Approximately 7 tonnes of black liquor sludge is produced in the manufacture of one tonne of pulp. It is discharged to watercourses causing toxic to aquatic life. Hence studies can be conducted to find the suitability of black liquor sludge in construction industry as admixture. This approach will help to eliminate the environmentally polluting black liquor sludge waste.

Samar et al. (2011) conducted an experiment on utilization of black liquor, produced by the pulp and paper industry, as a workability aid and retarder admixture. The properties of black liquor and its performance on concrete at two different water cement ratio were studied. Water is replaced by black liquor for 5, 10, 15, 20 percentage of water. The results showed that black liquor increases concrete workability, improve compaction and reduce honeycombing when 15% water replaced by black liquor [6].

The objectives of this study are:

- i) To develop concrete mixes of BLC30 and BLC50 (concrete of grade M30 and M50 with Black liquor sludge as admixture) for a slump of 100 mm with water cement ratio of 0.35.
- ii) To find the mechanical and flexural properties of BLC30 and BLC50.

2. Material Properties and Mix Proportion

Portland Pozzolana Cement, crushed stones of 20 mm coarse aggregate, manufactured sand passing through sieve of size 4.75 mm and conforming to zone II of IS 383-1970 (reaffirmed 2002) as fine aggregates were used [7]. Black liquor sludge procured from Hindustan newsprint limited, Vellore, Kerala, India was used as super plasticizer. The mix design was done as per IS 10262-2009, to obtain a M30 and M50 grades of concrete [8]. The mix proportion thus obtained was 1:2.1:4.1 for M30 and 1:1.1:3.2 for M50. Laboratory tests were conducted on black liquor sludge to determine the different chemical properties and the results are shown in Table 1.[9]

Table 1. Properties of Black Liquor Sludge

Properties	Values
pH	8
Bio-chemical oxygen demand (BOD) (mg/l)	16000
Chlorides (mg/l)	375
Sulphides (mg/l)	300
Total solids (mg/l)	9105
Total dissolved solids (mg/l)	2115
Total suspended solids (mg/l)	6990

3. Experimental Program

a. Fresh and Harden Properties

The workability of concrete was determined by slump test [10]. The different mechanical properties such as cube compressive strength, splitting tensile strength, flexural strength, cylinder compressive strength and modulus of elasticity were determined [11], [12].

b. Flexural Behaviour of RCC Beams

Beam specimens were used to determine the flexural strength which are subjected to two point loading using Universal Testing Machine of 1000kN capacity. Three numbers of beams were prepared for CB30 (control beam of M30 mix), CB50 (control beam of M50 mix), BLC30 and BLC50 mixes. The beam is of 100 x 150 x 1000 mm size which are provided with reinforcement as per IS 456 - 2000 [13]. The clear cover provided on all the sides was 25mm. Two numbers of 10mm diameter bars were used as tension reinforcement, 8mm diameter bars as compression reinforcement and 6mm diameter 2 legged stirrup holders at 90mm c/c. Dial gauges were used to measure the deflection and the values obtained were used to plot the load-deflection graph. Strain gauges were placed on the tension and compression reinforcement to measure the strains and to plot the moment-curvature relationship. Fig 1. represents the detailing of beam specimen.

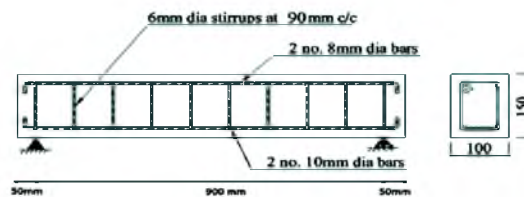


Fig 1. Details of reinforcement in beam specimen

Test set up

The beams were tested under two point loading in a Universal Testing Machine. Dial gauges and strain gauges were used to measure the mid span deflection and strain respectively. Fig 2. represents the test setup. The value of moment is given by:

$$M = \frac{Pl}{\epsilon} \tag{10}$$

Where,

- M = Moment at mid span
- P = Applied load
- l = Span of the beam between the supports

The curvature was obtained by:

$$\phi = \frac{\epsilon_s + \epsilon_c}{d} \tag{11}$$

Where,

- ϕ =Curvature
- ϵ_s =Tension steel strain
- ϵ_c =Tension steel strain [14]



Fig 2. Testing of Beam

4. Results and Discussion

c. Workability test

The amount of black liquor sludge were added for M30 and M50 control mixes by replacing water for getting a slump of 100 mm are given in Table 2.From the workability test results, the percentage of black liquor sludge to be added for M30 mix was selected as 20% by replacing water and for M50 it was 25% for getting a slump of 100mm. The increase in slump may be due to the ability of black liquor sludge to act as a dispersing agent by neutralizing the electrostatic charges of the concrete mixture, especially the cement. This neutralization minimizes assemblage of the solid particles allowing them to mix better with water.

Table 2. Percentage of black liquor sludge added in M30 and M50 mix

Black liquor sludge(% replacement of water) for M30 mix	Slump (mm)	Black liquor sludge (% replacement of water) for M50 mix	Slump (mm)
1	15	10	40
5	35	15	63
10	50	20	80
15	80	22	88
16	84	23	95
18	92	24	97
19	96	25	100
20	100	-	-

d. Mechanical properties

The mechanical properties of control BLC30 and BLC50 are shown in Table 3.All the hardened properties such as compressive strength, splitting tensile strength, flexural strength, cylinder compressive strength and modulus of elasticity are within acceptable limit for all mixes. Also all these values satisfies the IS specification.

Table 3. Mechanical properties of concrete

Properties	M30 C	BLC30	M50 C	BLC50
Compressive strength (N/mm ²)	38.44	39.12	59.11	57.85
Splitting tensile strength (N/mm ²)	3.25	3.32	5.09	4.95
Flexural strength (N/mm ²)	4.40	4.80	6.00	5.80
Cylinder compressive strength (N/mm ²)	29.60	29.37	44.80	43.58
Modulus of elasticity (N/mm ²)	2.72 x 10 ⁴	2.71x 10 ⁴	3.55 x 10 ⁴	3.54 x 10 ⁴

e. Flexural Behaviour of RCC Beams

Crack Pattern

The crack pattern obtained after testing of beams was shown in Fig 3 and Fig 4. From the figures it can be seen that, Most of the cracks initiated from the bottom of the beam and propagated to the top of the beam. Crack pattern of BLC beams were almost similar to the control beam.



Fig 3. Crack pattern of CB30 and BLC30 beams



Fig 4. Crack pattern of CB50 and BLC50 beams

Crack Width Propagations

The crack width propagation of various mixes is shown in Fig 5. The crack width propagation of BLC beams was slightly higher than control specimens but the final crack width was approximately same.

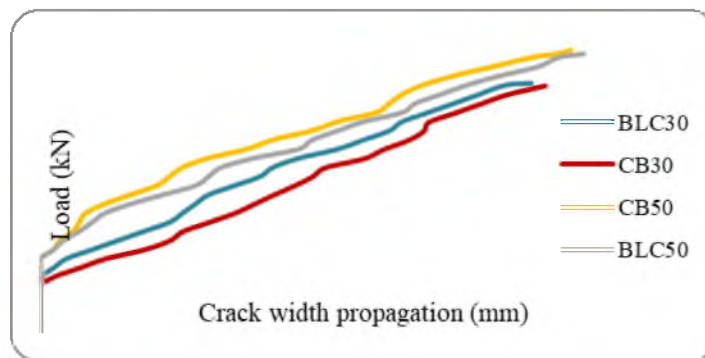


Fig 5. Crack width propagation of beams

Ultimate, Yield and Initial Crack Load

Table 4 shows the ultimate load, yield load and initial crack load of all the beams and it can be observed that ultimate load and initial crack load of BLC and control specimens were approximately same but the yield load of BLC specimens were less than control mixes.

Table 4. Initial crack, ultimate and yield load of beams

Specimen	Initial crack load (kN)	Yield load (kN)	Ultimate load (kN)
CB30	18	51	68
M30 B	17.5	47.5	67.5
CB50	21	60	77
M50 B	20	57	76

Load Deflection Plot

The load-deflection curve for each beam specimens were plotted as shown in Fig 6. It was observed that the curves for BLC specimens showed similar load-deflection behaviour with control specimens. There is a linear portion till initial cracking and thereafter, non-linearly varying curve till the yield load. Beyond the yield point, the deflection of the beams increased considerably until the ultimate load was reached.

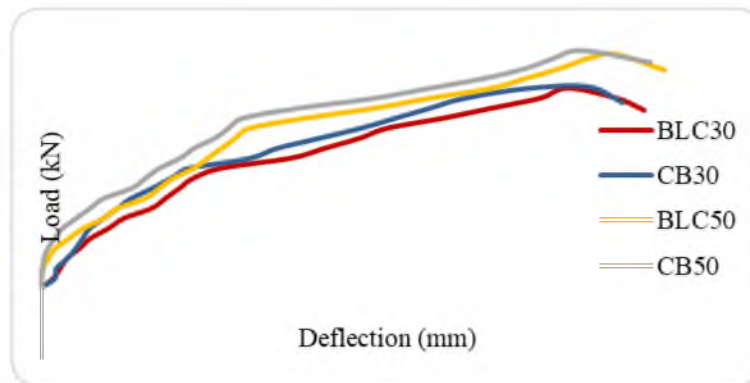


Fig 6. Load deflection plot of beams

Moment Curvature Relationship

The moment curvature obtained for control beam and BLC beams are shown in Fig7. Moment curvature graph has three stages, first stage ends at initial crack of specimen then linearly increase due to the yielding of tension steel. Final stage is contributed by the limiting value of strain taken by the concrete. Similar trend is followed by the test specimen. It has a linear portion up to initial crack and comparatively after the formation of cracks and non-linear bending behaviour till the yield point and thereafter large deformations beyond yield load. Similar trend is followed by the test specimen. It was observed that the curves for BLC specimens showed similar moment curvature behaviour with control specimens.

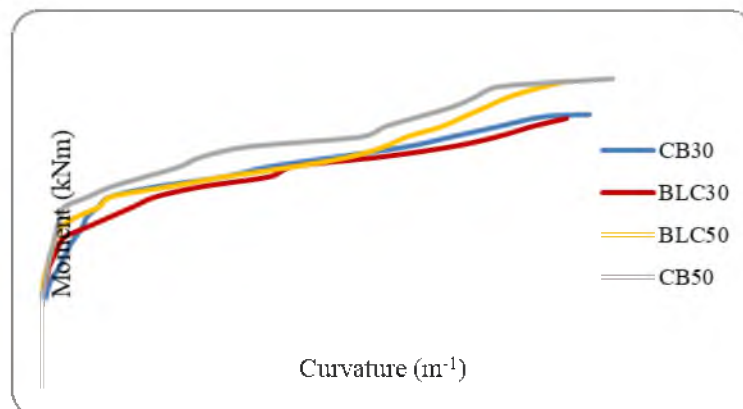


Fig 7. Moment - curvature graph

Energy absorption and ductility indices

From the load-deflection and moment-curvature plots, the energy absorption characteristics, displacement ductility and curvature ductility for each specimen was derived. Energy absorbed by each specimen during the test was calculated by the area under the load-deflection curve. Due to the limitations in the experimental set up, the load deflection graph could be plotted only up to 80% of the peak load, in the descending portion of the curve. Thus, the energy absorption was calculated as the area under the curve up to the peak load and under the descending portion up to 80% of the peak load. The displacement ductility was calculated from the load deflection plot by the ratio of deflection at ultimate load to that at the yield load and the curvature ductility was computed from the moment-curvature plot by the ratio of curvature at ultimate load to corresponding curvature at yield load. The obtained values are given in Table 5. The results show that the energy absorption, ductility index slightly reduced in the case of BLC mixes than control specimens.

Table 5. Energy absorption capacity and ductility indices of beams

Specimen	Energy Absorption Capacity(kNmm)	Displacement ductility		Curvature ductility	
		Absolute	Relative	Absolute	Relative
CB30	211.41	3.54	1.00	4.66	1.00
BLC30	192.86	3.29	0.93	4.42	0.95
CB50	251.78	4.23	1.00	6.53	1.00
BLC50	245.88	4.12	0.97	6.26	0.96

5. Conclusions

From this experimental investigation, the following conclusions were obtained:

- The addition of Black liquor sludge of 20 and 25% by replacing water provided a slump of 100 mm in M30 C and M50 C mixes respectively.
- All the mechanical properties of BLC30 and BLC50 mixes were found to be within acceptable limit and satisfies IS specification.
- The BLC30 and BLC50 beams showed similar behaviour with respect to control specimens.

Hence Black liquor sludge can be effectively used as admixture in concrete for increasing workability for both normal strength and high strength mixes. It can be also used for structural applications.

References

6. Al-Adili,A., Al-Ameer,O. A. and Raheem,E.: Investigation of incorporation of two waste admixtures effect on some properties of concrete, *Elsevier Procedia Engineering*, 74, 652-662, (2015).
7. Anna,K.: Effect of selected admixtures on the properties of ordinary concrete, *Elsevier Procedia Engineering*, 108, 504-509, (2015).
8. Okeyinka,O.M. and Oladejo,O.A.: The influence of calcium carbonate as an admixture on the properties of wood ash cement concrete, *International Journal of Emerging Technology and Advanced Engineering*, 4, 432-437, (2014).
9. Ramesh,T.S. and Neeraja,D.: An experimental study of natural admixture effect on conventional concrete and high volume class F fly ash blended concrete, *Elsevier Procedia Engineering*, 6, 43-62, (2017).
10. Rose,M., Ramadhan,S. and Julius,N.: Effect of Gum Arabic Karroo as a water-reducing admixture in cement mortar, *Elsevier Case Studies in Construction Materials*, 1, 100-111, (2016).
11. Samar,A., El-Mekkawi, Ibrahim, Ismail,M.M., El-Attar,M., Alaa,A.S., Fahmy and Mohammed: Utilization of black liquor as concrete admixture and set retarder aid, *Elsevier Journal of Advanced Research*, 121, 163-169, (2011).
12. IS 383 – 1970, Specification for coarse and fine aggregates from natural sources for concrete, Bureau of Indian Standards, New Delhi, India.
13. IS 10262-2009, Concrete mix proportioning – guidelines, Bureau of Indian Standards, New Delhi, India.
14. Colin F., Quevauviller P., Monitoring of Water Quality: The Contribution of Advanced Technologies, Elsevier, (1998).
15. IS:1199 -1959 (Reaffirmed 2004), Methods of Sampling and Analysis of Concrete, Bureau of Indian Standards, New Delhi, India.
16. IS 516 – 1959, Method of Tests for Strength of Concrete, Bureau of Indian Standards, New Delhi, India.
17. ASTM C496 / C496M – 11, Standard Test Method for Splitting Tensile Strength of Cylindrical Concrete Specimens, American Society for Testing and Materials, Philadelphia, Pennsylvania, 2006.
18. IS 456 - 2000, Plain and reinforced concrete - code of practice, Bureau of Indian Standards, New Delhi, India.
19. Park,R. and Thomas,P.T.: Reinforced Concrete Structures, Wiley India, Third Edition, (2009).

Study on Flexural Behaviour of RCC Beams Retrofitted with Biplanar Geonet

Sherine Stanly¹ and Tisny D B²

¹ PG Scholar, Department of Civil Engineering, MBCET, Trivandrum, sherinestanly4@gmail.com

² Assistant Professor, Department of Civil Engineering, MBCET, Trivandrum, tisnyarun@gmail.com

Abstract. Major problem in the construction industry is deterioration of concrete structural elements. Replacement of deficient structural elements is uneconomical and inconvenience due to interruption of function of the structure. It is often better to upgrade the structure by retrofitting. External strengthening has become an acceptable way of improving the load carrying capacity of the existing structure. The present study intended to develop a technique of retrofitting of RCC beams, using geonet. In this study biplanar geonet was used as an externally bonded material. Prior to retrofitting, the specimens were subjected to different levels of distressing, 67%, 80% and 90% of the flexural capacity of control specimen. The flexural behaviour of control specimen and retrofitted specimen were studied. From the result obtained, a significant improvement in load carrying capacity was observed, which depends upon the distressing level.

Keywords: Biplanar Geonet, Flexural Behaviour, Retrofitting.

Introduction

Reinforced concrete structures are one of the most important structure system. After a period of rapid economic growth, structural modification of existing infrastructures that have been aging rapidly. Reason for the demand for structural modification is the upgrading of load carrying capacity and resistance to withstand underestimated loads, to ameliorate the increased perceived risk from earthquakes.[1] In such circumstance replacement or retrofitting is adopted. Replacement is uneconomical and inconvenience due to interruption of function of the structure. It is often better to upgrade the structure by retrofitting. Retrofitting is the upgrading of existing structure for improving its structural performance even before or after the damage. Retrofitting is a more feasible economic alternative than demolition and reconstruction.[2] Studies were conducted on reinforced concrete members strengthened with ferrocement and steel plate bonding.[3,4] Ferrocement jacketing and steel plate bonding has become an acceptable way of improving the load carrying capacity of the existing structure. Major drawback with these retrofitting systems is the corrosion of externally bonded steel plate and wire mesh. To overcome these drawback, many alternative materials were introduced for retrofitting, which includes Textile-reinforced mortar (TRM) and Fibre reinforced polymer (FRP).[5-7] The present study intent to develop a new retrofitting system using biplanar geonet. Studies were conducted using geosynthetics as shear reinforcement. The use of geosynthetics was found to be effective in increasing the strength and ductility characteristics.[8] Biplanar geonet is a geosynthetic material consisting of two sets of intersecting ribs overlaying at different angles and spacings. Owing to the non-rusting properties of the geonet mesh, the wire mesh in the ferrocement jacketing can be replaced by the geonet.

The main aim of the paper is to introduce a new retrofitting material. In this study, the flexural behavior of pre-damaged reinforced concrete beams retrofitted with biplanar geonet was studied.

Experimental Details

Material Properties

Concrete with an average compressive strength of 28 N/mm² was used for casting the tested specimens. High tensile steel of diameter 10mm was used for bottom reinforcement and 8mm diameter was used for top reinforcement. Mild steel of diameter 6mm was used as shear reinforcement. The geonet used in the study had a thickness of 3.2mm with tensile strength of 30kN/mm².

Specimen Descriptions

Nine reinforced concrete beams were cast. All beams had a cross section of 100 mm x 150 mm, and a total length of 1m. For flexure reinforcement, two reinforcing bars of 10mm high tensile steel were used as tension reinforcement and two reinforcing bars 8mm high tensile steel were used as compression reinforcement. The shear reinforcement consist of 2 legged, 6mm diameter stirrups at 90mm spacing throughout the span. Fig. 1 shows the reinforcement details of tested specimen.

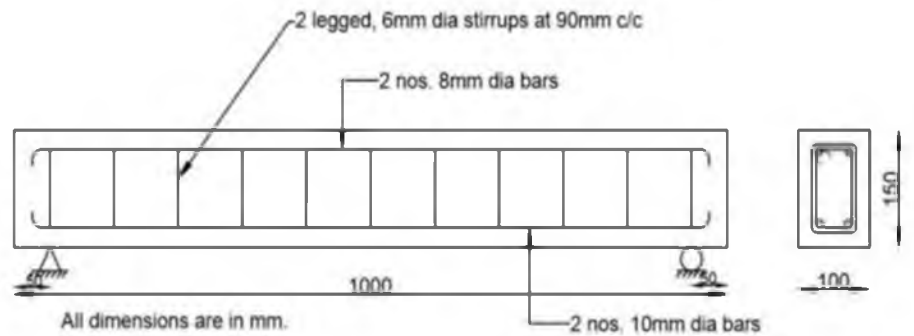


Fig. 1 Reinforcement details of tested specimens.

Table 1 presents the summary details of the beams used in the experimental study. The beams designation stands for two letters and number, CS stands for control specimen, D stands for distressing the beam and N stands for retrofitting with geonet. The number refers to the percentage of distressing with respect to the ultimate carrying capacity of control specimen.

Table 1. Designation of specimens.

Beam No.	Designation	Description
B1	CS0	Control specimen
B2	DN67	Beams distressing with 67% of ultimate load, then retrofitted using geonet
B3	DN80	Beams distressing with 80% of ultimate load, then retrofitted using geonet
B4	DN90	Beams distressing with 90% of ultimate load, then retrofitted using geonet

The retrofitting of beam was done in constant moment region of length 300mm after distressing the beam specimens. The beam surface was roughened using a grinding machine to improve the bond with concrete substrate. The concrete surface was cleaned and bonding agent was placed over the surface. Geonet was wrapped around the surface using U-wrapping technique. Finally a layer of mortar of 1:3 ratio was applied over the geonet.

Test Setup

All beams were tested under two point loading condition. The effective span of the beams was 900mm. A dial gauge was used to measure the deflection at the mid-span. These values were used to plot load-deflection relation. Strain gauges were placed on tension reinforcement and compression reinforcement to measure the strain. Loading was applied using a 1000 kN universal testing machine at 2.5 kN load increment. All readings from the dial gauge and strains were manually recorded.

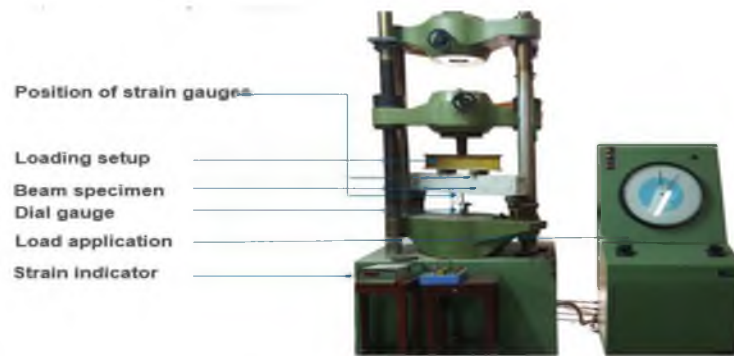


Fig. 2 Test setup.

Test Results and Discussion

Cracking behaviour and Failure Mode

The failure mode of each tested specimen was determined by referring to the initiation and propagation of the cracks. For the distressed beams, at specified distressing level, the maximum crack widths at constant moment region varies between 0.18 and 0.36. After the loading is removed, the cracks were partially closed and the maximum crack width varies between 0.04 and 0.1. The crack patterns of the beams after distressing indicates that the number and depth of the cracks increases with increase in distressing level. For all beams, crack was initiated in the span between two concentrated loads. In this region the flexural stress is highest and shear stress is zero. The cracks formed were vertical and was perpendicular to the direction of the maximum principal tensile stress induced by pure bending. The crack pattern of retrofitted beams is shown as in fig. 3.



Fig. 3 Crack patterns of the retrofitted beam specimens.

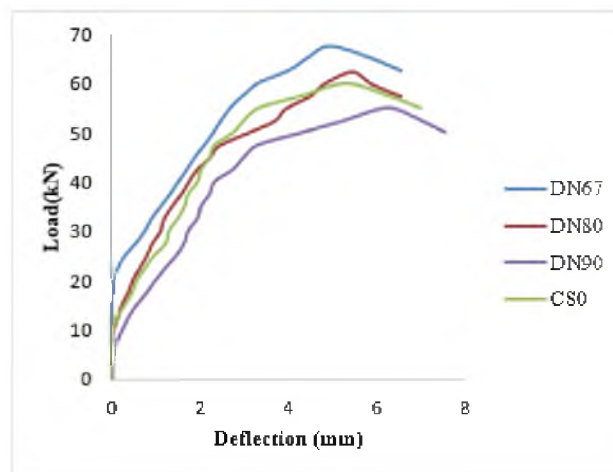
For the control specimen the first crack occurred at 18 kN and first cracks for DN67, DN80 and DN90 specimens were 22.5 kN, 20 kN and 15 kN respectively. The control specimen failed by forming large flexural cracks at the constant moment region. Intermediate flexural crack followed by tributary cracks were formed on DN67 specimen. Flexural shear cracks were formed on DN80 specimen. For DN90 specimen, the width of the flexural crack was more pronounced as compared to other specimens. The cracking loads, yield load, ultimate loads and crack pattern of specimens were given in Table 2.

Table 2. Summary of test results.

Designation	First Crack Load (kN)	Yield Load (kN)	Ultimate Load (kN)	Crack Pattern
CS0	18	48	59	Flexural crack
DN67	22.5	59	67.5	Flexural crack followed by tributary cracks
DN80	20	51	63	Flexural shear crack
DN90	15	43	55	Flexural crack followed by tributary cracks

Load – Deflection Behaviour

All the curves were characterized by three distant stages: Un-cracked beam, development of cracking up to yielding of steel reinforcement and post yielding response up to failure. Any difference between the curves of the retrofitted beams and the control specimen is attributed to the contribution of retrofitting material to the flexural performance of the beams. The effect of retrofitting was more pronounced during stage – II, where the development of flexural cracks was progress. During this stage, for specimen DN67, both the steel reinforcement and geonet were activated in tension and contributed to the increase of the beam's flexural resistance. The load – mid span deflection curves of the tested beams are as shown in fig. 4.

**Fig. 4** Load – mid span deflection of test specimens.

Energy Absorption

Energy absorption capacity of reinforced concrete specimen is one of the crucial structural properties that define the specimen's seismic resistance. The use of geonet for the retrofitting of reinforced concrete beams is predominantly motivated by the energy absorption capacity. Energy absorption is obtained by the area under the load deflection curve. Due to limitation in experimental setup, the energy absorption is calculated by successive integration method. The energy absorption of control specimen and retrofitted specimens are shown in fig. 5.

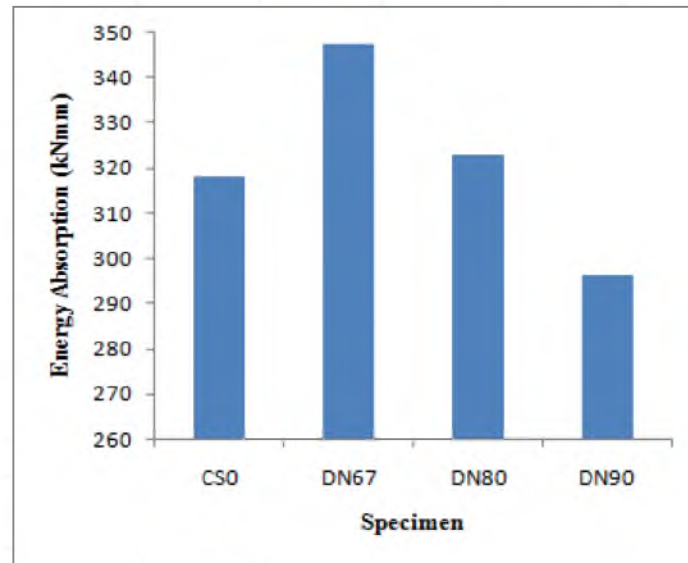


Fig. 5 Energy absorption of test specimens.

Moment – Curvature Relationship

Moment curvature relations are important to find the ductility and the amount of possible redistribution of stresses in the structure. The moment curvature relationships of the retrofitted and control beam specimens were established from the strain indicator readings taken corresponding to the load increments. The moment curvature curve had three stages. First stage is till cracking, second stage till yielding of tension steel and the third stage to limit of useful strain in concrete. The curve is linear up to first crack moment. Further when the moment increases, the curve shifts from linearity. When the moment reaches yield moment, the curves become flat. When steel yields, a large increase in curvature occurs with a small change in moment. Moment curvature relations for tested specimens are shown as in fig. 6.

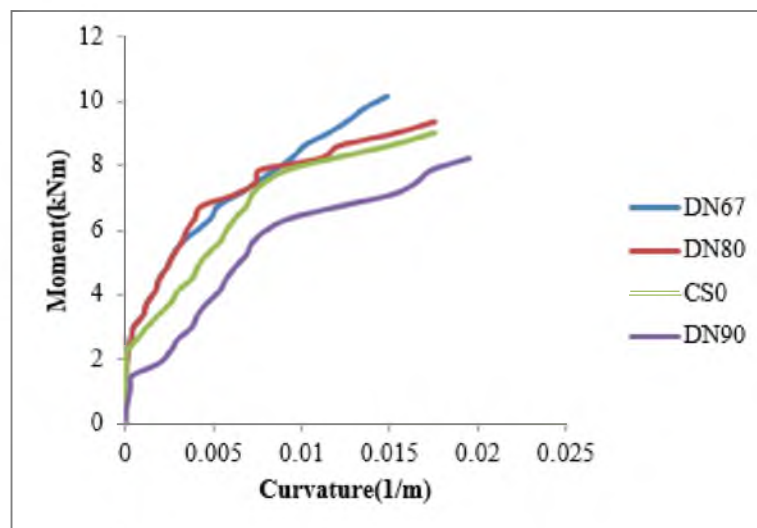


Fig. 6 Moment curvature relation for tested specimens.

Conclusions

This study investigated experimentally the flexural behaviour of reinforced concrete beams retrofitted using geonet. The obtained results revealed the following conclusions:

- Two types of crack patterns were observed in the geonet retrofitted beams. These crack patterns were found to be sensitive to the level of distressig.

- DG67 and DG80 specimens showed significant improvement in first crack load and ultimate load as compared to the control specimen.
- For the specimens DN67 and DN80, the load carrying capacity was substantially increased compared to the control specimen (up to 14% and 7%). Thus, damaged beams retrofitted with geonet appear to be structurally efficient and reliable.
- Specimens distressed with 67% of ultimate load of control beam showed significant improvement in energy absorption due to the formation of finer cracks.
- Increasing the distressing level decreases the bearing capacity of the specimen which was to be expected but unexpectedly increases the curvature of DN80 specimen. This may be due to the use of externally bonded biplanar (overlapping ribs) geonet.

References

- Guibing, L. Aihui, Z. and Yugang, G.: Effect of Preload Level on Flexural Load-carrying Capacity of RC Beams Strengthened by Externally Bonded FRP Sheets, *The Open Civil Engineering Journal*, 9, 426-434(2015).
- Obaidat, Y.T., Heyden, S., Dahlblom, O., Abu-Farsakh, G., and Abdel-Jawad, Y.: Retrofitting of reinforced concrete beams using composite laminates. *Construction and Building Materials*, 25(2), 591-597(2011).
- Hamza, S. M., Al-Saadi, Hoby, P. M. and Aravind, N.: An Experimental Study on Strengthening of Reinforced Concrete Flexural Members using Steel Wire Mesh, Curved and Layered Structure, 4, 31-37(2017).
- Ismail, M. I. Qeshta, Payam Shafiqh, Mohd, Z. J., Aziz I. A., Ubagaram, Johnson A. and Zainah, Ibrahim.: Flexural behaviour of concrete beams bonded with wire mesh-epoxy composite”, *Applied Mechanics and Materials*, 567, 411-416. (2014).
- Saad, M. Raouf, Lampros, N. Koutas and Dionysios, A. Bourmas.: Textile-reinforced mortar (TRM) versus fibre-reinforced polymers (FRP) in flexural strengthening of RC beams, *Construction and Building Materials*, 151, 279-291(2017).
- Aravind N., Amiya K Samanta., D K Singha Roy., Joseph V Thanikal.: Flexural strengthening of Reinforced Concrete (RC) Beams Retrofitted with Corrugated Glass Fiber Reinforced Polymer (GFRP) Laminates, *Curved and Layered Structures*, 2 (1), 244-253 (2015).
- Fayyadh, M. M. and Abdul Razak, H.: Assessment of effectiveness of CFRP repaired RC beams under different damage levels based on flexural stiffness, *Construction and Building Materials*, 37, 125-134(2012).
- Pankaj, Agarwal and Siva, Chidambaram, R.: Flexural and shear behavior of geo-grid confined RC beams with steel fiber reinforced concrete, *Construction and Building Materials*, 71, 628-637(2014).
- IS: 10262-2009: Concrete mix proportioning- Guidelines”, Bureau of Indian Standards, New Delhi, India, (2009).
- IS: 456 - 2000 (Reaffirmed 2005): Plain and reinforced concrete - code of practice”, Bureau of Indian Standards, New Delhi, India, (2000).

STUDY ON BEHAVIOUR OF NORMAL CONCRETE COLUMN AND MODIFIED REACTIVE POWDER CONCRETE COLUMN

Neethu S Deth¹, Sreejith R²,

¹MTech student,

²Assistant Professor

Dept. of Civil Engineering, Younus College of Engineering & Technology (YCET),
Pallimukku P O, Kollam 10, Kerala, India
Contact E-mail: neethusdeth@gmail.com

Abstract- Reactive Powder Concrete (RPC) is a developing composite material that will allow the concrete industry to optimize the material use, generate benefits by build structures that are strong, durable and sensitive to environment. This study is intended to explore the suitability of providing the reactive powder layer as cover to the normal column (M30). In this study Modified RPC is given in two different layer thickness (2.5cm thick and 5cm thick) and finding the compressive strength and durability of the newly composite structure. Modified Reactive Powder Concrete (MRPC) refers to the mix which is free from quartz sand and steel fibers, which are normally present in RPC; and MRPC column is the column having an inner core filled with normal concrete (M30) and outer portion with MRPC mix. MRPC mix is provided in two different thicknesses for checking its effectiveness and durability of each type of column. Cube specimens of 150mm were casted and determined compressive strength and compared with the control mixes. Also loading frame tests were carried out to find the buckling characteristics of column and durability test conducted for 28 day specimen. Seven day and 28 day compressive strength of the newly modified column shows more compressive strength than the normal concrete column and the 5cm thick layer shows more strength. So we can provide the MRPC as cover to the normal column.

Key Words: MRPC, strong, durability, buckling characteristics

1. INTRODUCTION

Concrete is one of the necessary elements for structural work in the modern construction. In the decade, buildings around the world have become higher and so the structural strength demand for concrete is increased as they require high strength concrete. Concrete is widely used construction material dominating the construction industry worldwide. Portland cement important ingredient in modern concrete was first used in 1824 by Joseph Aspdin in England. Today world production of concrete exceeds 1 billion tonnes per annum. High strength concrete is an important member of the concrete family. The concrete that was once known as high-strength concrete in the late 1970s is now referred to as high-performance concrete because it has been found to be much more than simply stronger; it displays enhanced performance in such areas as durability and abrasion resistance. Reactive Powder Concrete (RPC), which is an Ultra High Performance Concrete (UHPC), represents one of the most recent technological leaps witnessed by

the construction industry. Reactive powder concrete (RPC) have been

marketed as high performance concretes in various countries. This new family of materials has compressive strengths of (170MPa to 230MPa) and flexural strengths of (30MPa to 50MPa). There is a growing use of RPC owing to the outstanding mechanical properties and durability. Since the intrinsic strength of concrete is its ability to resist compressive loads, reinforced concrete members are designed to take advantage of this intrinsic strength. Therefore, the knowledge of the behaviour of concrete in compression is very important. Therefore, the behaviour of RPC under compression, flexural, tensile is of considerable interest in the design of RPC members and prediction of their structural behaviour. Compressive strengths of RPC range from 200 to 800MPa. There is a growing use of RPC owing to the outstanding mechanical properties and durability. RPC structural elements can resist chemical attack, impact loading from vehicles and vessels, and sudden kinetic loading due to

earthquakes. Ultra high performance is the most important characteristic of RPC. Reactive Powder Concrete (RPC), which is an Ultra High Performance Concrete, represents one of the most

recent technological leaps witnessed by the construction industry. Among already built outstanding structures, RPC structures lie at the forefront in terms of innovation, aesthetics and structural efficiency.

RPC is a special mixture that is cured especially to have a higher compressive strength than that of concrete. Adding steel fibres can greatly improve its tensile strength and bending strength, impact resistance and toughness. Its main features include a high percentage ingredient of Portland cement, very low water-to-binder (cement + silica fume) ratio which ranges from 0.15 to 0.25, a high dosage of super plasticizer, and the presence of very fine crushed quartz and silica fume. RPC represents one of the most recent technological leaps witnessed by the construction industry. Among already built outstanding structures, RPC structures lie at the forefront in terms of innovation, aesthetics and structural efficiency. The unique properties for RPC make it extremely attractive for structural applications.

2. SIGNIFICANCE OF THE WORK

One of the limitations of RPC is its high cost than the normal concrete. So its usage is less compared to conventional mix. This study is emerged from this limitation and leads to the provision of RPC as a protective layer to the structural element where durability issues the risk and also needs high compressive strength. Need is the mother of innovations and the need for more strength leads to the development of ultra-high strength materials like RPC.

As construction and material costs escalate, demand has increased for stronger materials like RPC. Durability of each specimen is carried out

with dipping it in potable water for seven days and then in acid solutions. Hydrochloric acid and Sulphuric acid are used for durability tests in 2% concentration. The loss of weight is the durability parameter and MRPC is highly durable and have less penetration. Different kinds of research works are carried out in normal RPC mix and this is a new attempt in this field. This positive results will definitely improve the use of MRPC as it costs less than the RPC but shows greater strength than the normal concrete.

3. EXPERIMENTAL

PROGRAMME 3.1 Materials and

Mix Proportions

Ordinary Portland cement of 53 Grade having specific gravity 3.15 and normal consistency of 32% and conforming to IS:12269-1987(Reaffirmed 2004) [15] was used. M sand passing through 4.75 mm IS sieve conforming to grading Zone II of IS 383-1970 (Reaffirmed 2002) [16] was used as fine aggregate. Crushed stone having effective size of 10.2mm conforming to IS: 2386-1997 [17,18] and IS: 383-1970 (Reaffirmed 2002) [16] was used as coarse aggregate.

The mix designs were carried out for obtaining 28day concrete compressive strengths of 30MPa. Silica fume used in MRPC mix which is collected from Chennai and also known as micro silica is an amorphous (non-crystalline) polymorph of silicon dioxide, silica. It is an ultrafine powder collected as a by-product of the silicon and ferrosilicon alloy production and consists of spherical particles with an average particle diameter of 150 nm. The main field of application is as pozzolanic material for high performance concrete. Silica fume is an ultrafine material with spherical particles less than 1µm in diameter, the average being about 0.15µm. This makes it approximately 100 times smaller than the average cement particle.



Fig 1 Silica fume

Naphthalene based super plasticizer Conplast SP430 is used as super plasticizer. The quantity of super plasticizer used was 2% of fine aggregate. Conplast SP430 disperses instantly in water and disperses the fine particles in concrete mix, enabling the water content of the concrete to perform more effectively. Conplast SP430 curing



Fig 2 Conplast SP430

Table 1 Mix proportions for normal mix

Cement (kg/m ³)	Coarse Aggregate (kg/m ³)	Fine Aggregate (kg/m ³)	Water (L)	Water Cement Ratio
480	1153.75	530.56	192	0.4

Table 2 mix proportions for MRPC mix

Particulars	Quantity (kg/m ³)
Cement	700
Fine aggregate	1230
Silica fume	105
Super plasticizer (1%)	8.05
Water	182
w/c ratio	0.26

3.2 Testing and specimen details

The specimens were designated as shown in Table 3 and 4. The details of specimens cast for each mix are as follows.

- (i) 18 cube specimens of 150mm size to evaluate the 7 day and 28 day, compressive strength
- (ii) 18 cube specimens of 100mm for the durability test of 28, 56 and 90 days

improves cohesion and particle dispersion minimizes segregation and bleeding and improves pumpability. It is chloride free and safe for use in pre-stressed and reinforced concrete. The mix proportion used is as given in Table 1.

Table 4 designation of specimens for durability test

Sl No	Specimen details	Mix designation	Number of specimens
1	Control specimen	CC	6
2	Specimen with 2.5 cm thick MRPC coat	C2.5	6
3	Specimen with 5 cm thick MRPC coat	C5	6
Total Specimens			18

4. RESULT OBTAINED

4.1 Compressive Strength

Compressive strength of all concrete mixes was determined at 7 and 28 days of curing. The compressive strength test results are given in Table 4.1. The variation of compressive strength at 7 and 28 days with different mixes is shown in Fig 4.1. It has been observed that Modified RPC exhibits less compressive strength than RPC but have a greater strength than normal concrete mix.

Table 5 - 7 day compressive strength

No:	Specimen	Compressive strength (MPa)
1	Normal concrete	20.24
2	MRPC(2.5 cm thick)	27.45
3	MRPC(5 cm thick)	36.50

Table 6 - 28 day compressive strength

No:	Specimen	Compressive strength (MPa)
1	Normal concrete	40.21
2	MRPC(2.5 cm thick)	44.94
3	MRPC(5 cm thick)	50.63

Table 3 Designation of specimens for compressive strength test

Sl no	Specimen	Size	Number
1	Cube A	(150x150x150) mm	6
2	Cube B	(150x150x150)mm with 2.5 cm thick MRPC coat	6
3	Cube C	(150x150x150)mm with 2.5 cm thick MRPC coat	6
Total Specimens			18

4.2 Durability

A. Durability Tests on Concrete

The durability of cement concrete is defined as its ability to resist weathering action, chemical attack, abrasion, or any other process of deterioration. Durable concrete will retain its original form, quality, and serviceability when exposed to its environment. For determining the resistance of concrete specimens to aggressive environment such as acid attack, the durability factors as described in ASTM C 666 has been adopted as the base.

B. Acid Attack Test

To check the durability of concrete mix against sulphuric acid, the concrete specimens were tested based on modified ASTM C 267 test method. For acid attack test concrete cubes of size 100mmx100mmx100mm were prepared for concrete with 2.5cm and 5cm MRPC coating and normal concrete mix. After 7 days of curing, the specimens were immersed in 5% sulphuric acid (H₂SO₄) solution for 28 days and the weight and compressive strength was noted. The strength loss and weight loss was calculated and compared with that of normal

concrete mix exposed to the same acid environment. From the test results it is clear that the specimen with 5cm MRPC coating was highly durable than the normal mix in acid.

C. Alkali Attack Test

Alkali attack test was conducted on the concrete with 2.5cm and 5cm MRPC coating and normal mix. The weight and compressive strength were determined for the above mixes after 7 days. Then the specimens were immersed in sodium hydroxide solution for 28 days. The weight loss and strength loss were also determined. Test results are shown in the table 4.4. From the results the specimen with 5cm MRPC coating was more durable than the control mix.

D. Sulphate Attack Test

The sulphate attack tests were conducted in specimen with 2.5cm and 5cm MRPC coating and normal mix. After 7 day curing, the specimens were immersed in the calcium sulphate (CaSO₄) solution for 28 days. The effect of sulphate attack on concrete specimens was determined by measuring the compressive strength and weight loss of the mixes. The results are shown in table 4.5. The test results show that the specimen with 5cm MRPC coating was more durable than the control mix.

E. Sea water Attack Test

The water cured specimen was then immersed in sea water till testing. The initial weight of the specimen was taken. The compressive strength of the specimens at 28 days were taken.

Table 7 Test results for acid attack (H₂SO₄)

Mix designation	Percentage strength loss			Percentage weight loss		
	28 days	56 days	90 days	28 days	56 days	90 days
Normal concrete specimen	22.46	31.59	35.5	3.05	4.53	5.06
Specimen with 2.5cm MRPC coating	9.25	14.13	24.2	1.56	2.72	3.49
Specimen with 5cm MRPC coating	4.03	7.85	15.71	1.12	2.09	3.07

Table 8 Test results for alkali attack (NaOH)

Mix designation	Percentage strength loss			Percentage weight loss		
	28 days	56 days	90 days	28 days	56 days	90 days
Normal concrete specimen	19.46	24.53	27.03	2.83	4.67	5.33
Specimen with 2.5cm MRPC coating	6.72	10.70	19.39	1.36	2.34	3.52
Specimen with 5cm MRPC coating	2.93	5.21	13.35	1.03	1.86	2.23

Table 9 Test results for sulphate attack (CaSO₄)

Mix designation	Percentage strength loss			Percentage weight loss		
	28 days	56 days	90 days	28 days	56 days	90 days
Normal concrete specimen	18.74	25.52	28.77	2.57	2.93	3.72
Specimen with 2.5cm MRPC coating	5.51	8.83	17.82	1.18	1.43	2.85
Specimen with 5cm MRPC coating	2.17	3.23	10.35	0.98	1.14	2.25

Table 10 Test results for sea water attack

Mix designation	Percentage strength loss			Percentage weight loss		
	28 days	56 days	90 days	28 days	56 days	90 days
Normal concrete specimen	11.15	12.72	15.74	2.74	4.63	5.89
Specimen with 2.5cm MRPC coating	4.68	6.66	10.75	1.04	2.43	2.69
Specimen with 5cm MRPC coating	2.02	3.13	6.42	0.86	1.24	2.01

5. RESULTS & CONCLUSIONS

The details of the results obtained from different experiments conducted are explained here.

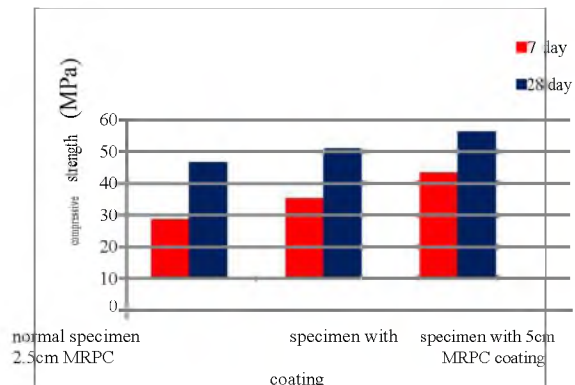


Fig 3- 28 day compressive strength

The compressive strength of MRPC is higher than that of conventional concrete. 5 cm thick layered MRPC takes more loads than 2.5 cm thick layered column and so that it can be used as a cover to the normal column.

The durability of concrete specimen is finding out by measuring the weight loss. If the weight loss is less, then it will consider as more durable than the other specimen.

The relative % of loss of compressive strength is less in 5 cm thick MRPC. Thus the result shows that that specimen is more durable in worst conditions which clear from the table 11 shown below.

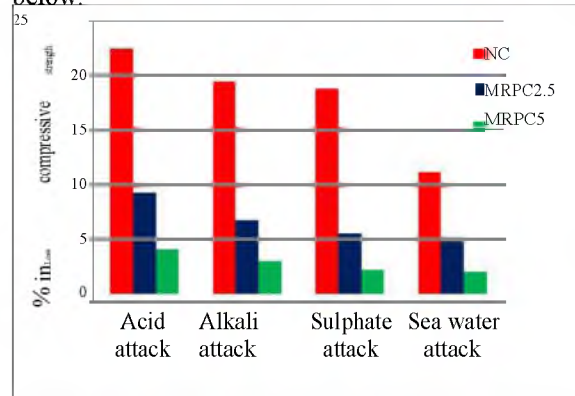


Fig 4 percentage loss in compressive strength

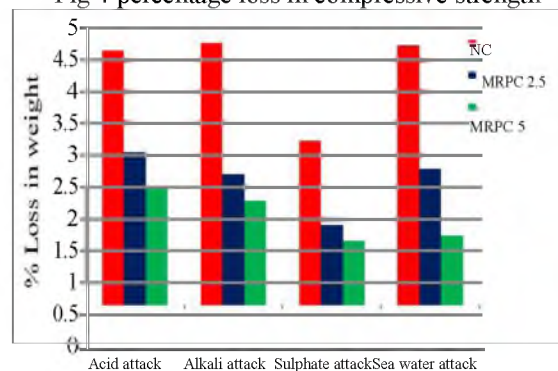


Fig 5 percentage loss in weight

All kinds of results show higher strength for 5 cm thick MRPC mix.

REFERENCES

- [1] Gökçe, H. S., Sürmeliođlu, S., Andiç-Çakir, Ö., "A new approach for production of reactive powder concrete: lightweight reactive powder concrete (LRPC)". *Materials and Structures*, 50(1) ,2017, pp.58
- [2] Prabha S. L., Dattatreya J. K., Neelamegam M., Seshagirirao M. V,“, "Study on Stress-Strain Properties of Reactive Powder Concrete Under Uniaxial Compression ", *International Journal of Engineering Science and Technology*, Vol 2, No-11,2010, pp 6408-6416.
- [3] Roux, N.; Andrade, C.; and Sanjuan, M. A. (1995), "Experimental Study of Durability of Reactive Powder Concretes," *Journal of Materials in Civil Engineering*, Vol. 2, Issue 3, March 2013.
- [4] Xiaoa, H. Schneiderb, C. Donneckeb, G. Konigb (2004), *Wedge Splitting Test on Fracture Behaviour of Ultra High Strength Concrete*, *Construction and Building Materials*, 18:359–365

Response of Conventional and Virtual Outrigger System Subjected to Seismic Load

Visakh V. S.¹ and Akhil Raj S. R.²

¹PG Student, Structural Engineering, Mar Baselios College of Engineering and Technology, Thiruvananthapuram, Kerala, India

Visakhsyama196@gmail.com

²Asst. Professor, Department of Civil Engineering, Mar Baselios College of Engineering and Technology, Thiruvananthapuram, Kerala, India

Akhil45u@gmail.com

Abstract. Tall structures are subjected to lateral loads, especially wind and earthquake loads that become judgmental in the design of these buildings. Various lateral load resisting structural systems were introduced for the analysis and design of these structures which mainly include tubular structures, outriggers with bracings, diagrid structures, etc. The core supported outrigger with bracings is one of the most commonly used structural systems to control the risk of structural and non-structural damage due to lateral load. So that, during small or medium lateral load due to either earthquake or wind load, the risk of structural and non-structural damage can be reduced. Outriggers are rigid horizontal structures used to improve stiffness and building overturning stiffness by connecting the core or spine to exterior columns. In an Outrigger system, it functions by tying together two structural systems, typically a perimeter system and have a core system to yield the whole structural behaviour that is much better than those of component system. The benefits of the outrigger system lie in the fact that the overturning moments causing building deformations getting reduced. In this work, the performance of outrigger structural system in high rise building subjected to seismic load was done. Response spectrum analysis was done to identify optimum location of outrigger system. The seismic performance was studied in terms of storey displacement and storey drift ratio by considering different bracing systems such as X brace and K brace.

Keywords: Conventional outrigger, Virtual outrigger, X bracing, K bracing, Base shear, Storey displacement, Storey drift ratio.

1. Introduction

In high rise building the height of the building plays an important role in the design of the design, construction and use that can exist common building of certain region and period. Lateral stiffness governs the structural design of tall buildings, and consequently, structural systems in tall buildings have evolved to produce higher lateral stiffness more efficiently. The outrigger system is the one of the lateral load resisting system in which the external columns are tied to the central core with very stiff outriggers and belt truss at one or more level. By this system, it can be effectively controls the excessive drift due to lateral loads during wind or earthquake loading. So that risk of structural and non- structural damage can be reduced. In high- rise buildings, particularly in seismic active zone or wind load dominant, this system can be chosen as an appropriate structure.

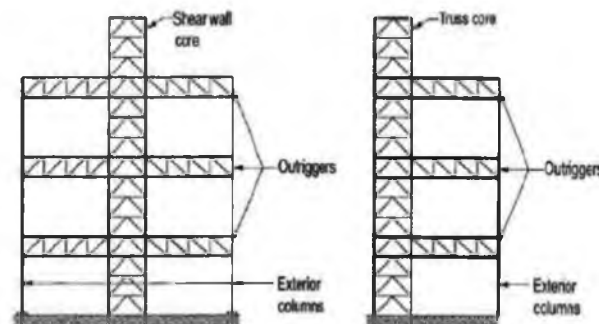


Fig. 1. Outrigger with central core [3]

2. Outrigger Structural Systems

2.1. Types of Outrigger System

In conventional outrigger system, the outrigger trusses are connected to the core and to the perimeter columns. The number of outriggers over the height of building can be varied from one to three or more levels. When lateral loads acting on the structure, the outrigger system restrain rotation of the core and convert part of the moment in the core into a vertical couple at the columns. Shortening and elongation of this columns and deformation of trusses will allow same rotation in the core at the outrigger.

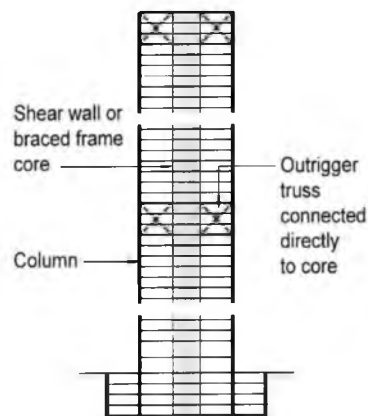


Fig. 2. Conventional outrigger system [3]

In virtual outrigger systems, this same transfer of overturning moments from the core to elements outboard of the core is achieved, but without a direct connection between the outrigger truss and the core. The basic concept of this virtual outrigger system is to use of the floor diaphragms, which are typically very stiff and strong in their plane, to transfer moment in the form of horizontal couple from the core to trusses that are not connected directly to the core.

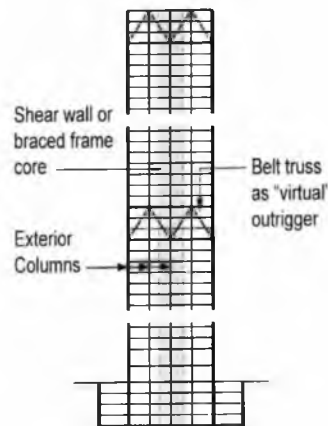


Fig. 3. Virtual outrigger system^[3]

The seismic behaviour of outrigger braced system in high-rise 2D building was investigated by Patil and Sangle (2016). It is observed that the position of outriggers influences the seismic performance by increasing the strength and stiffness, which is measured in terms of storey displacement, interstorey drift ratio, and performance point. Ho and Arup (2016) investigated the evolution of outrigger system in high rise building and it is concluded that, target of high stiffness is not always the only objective of outrigger system. The optimum position of outrigger system for high rise reinforced concrete buildings under wind and earthquake load was done by Nanduri et al. (2013). From the study, it is clear that outrigger and belt truss system increases the stiffness of building and optimum location of outrigger is 0.5 times its height. Bayati et al. (2008) studied the optimized use of multi outriggers system to stiffen tall buildings and shows that multi outrigger system can decrease element and foundation.

Most of the reviews study the performance of the outrigger structural system. The introduction of outrigger in high rise building will increase the lateral stiffness of the structure. Base shear will reduce and minimize the inter storey drift by introducing

outrigger. Outrigger structures improve the structural stability. Outriggers are the structural system, which help in reducing the lateral drift increasing the stiffness of the structure by huge amount. There were only limited studies in virtual outrigger system.

2.2. Behaviour of Outrigger System

The structural response of the outrigger system is quite simple, because of this outrigger act as a stiff arm engaging outer columns. When central core tries to tilt its rotation at outrigger level induced a tension compression couple in the outer columns and acting in opposite to that moment. By this restoring moment, the effective depth of the structure for resisting bending is increased, when the core bend as a vertical cantilever. This cantilever action is developed due the tension in the windward columns, and compression in the leeward columns.

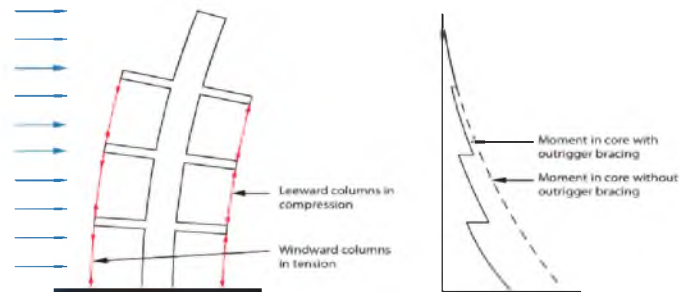


Fig. 4. Behaviour of outrigger structural system [3]

3. Methodology

3.1. Finite Element Modelling

The model considered for the present study is 96m high rise RC framed building and it represent a 30 storied building. Modelling and analysis were conducted by using the engineering software ETABS Nonlinear version 2016. The floors and roofs were modelled as rigid diaphragms. Earthquake loads were given as per IS 1893- 2016 (Part 1). The structure is analysed by response spectrum analysis.

Table 1. Structural Parameters of Building

Building	- RC building with core and shear walls
No. of storeys	- 30
Plan dimension	- 25m x 25m
Plan area	- 1800 m ²
Storey height	- 3.20m
Column size	0.60m x 0.60m
Beam size	- 0.25m x 0.40m
Slab thickness	- 0.10m
Shear wall thickness	- 0.35m
Grade of concrete	- M25
Grade of reinforcing steel	- Fe 415

Table 2. Location of structure

Location	- Delhi
Seismic zone	- IV
Seismic zone factor	- 0.24
Response reduction factor	- 5
Importance factor	- 1

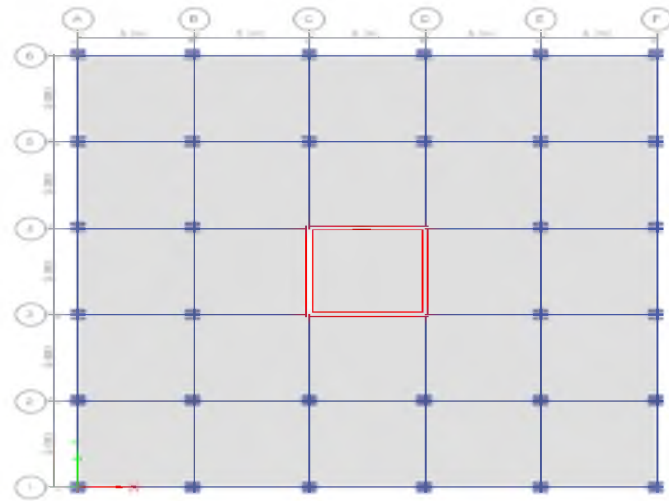


Fig. 4. Plan of structure without outrigger

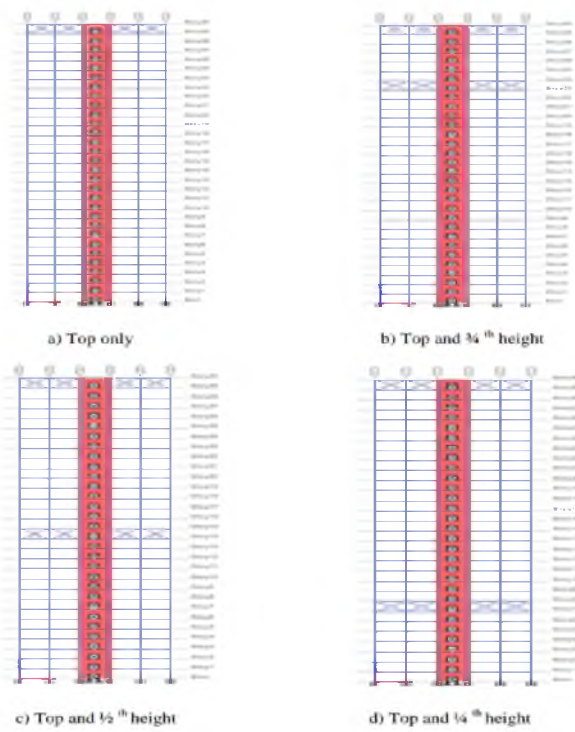


Fig. 5. X braced conventional outrigger system

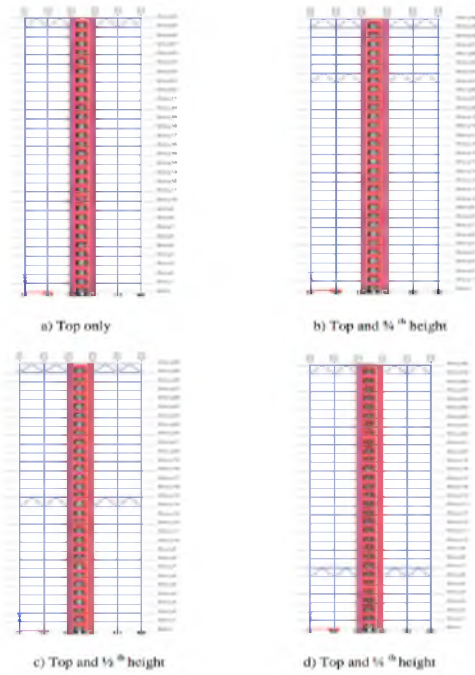


Fig. 6. K braced conventional outrigger system

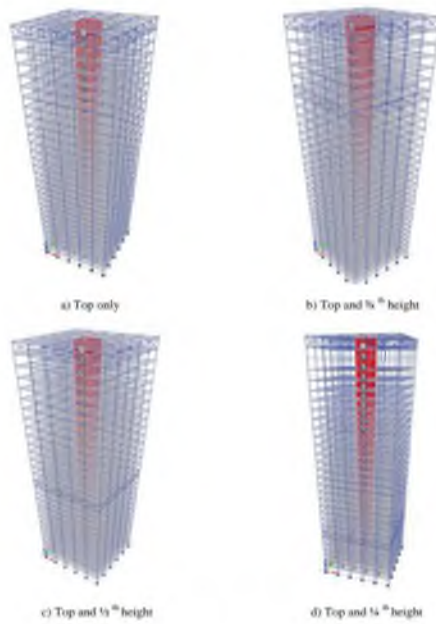


Fig. 7. X braced virtual outrigger system

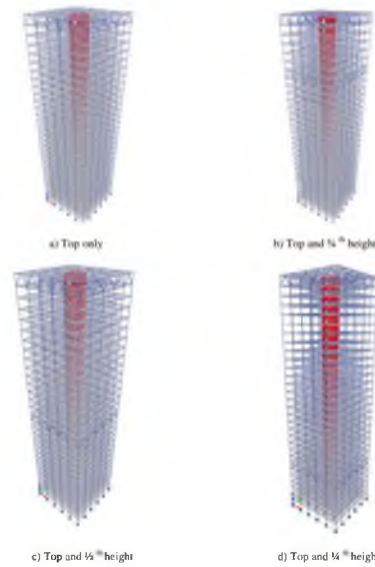


Fig. 8. K braced virtual outrigger system

3.2. Load Combinations

As per IS 1893 part 1 (2016), the assigned load combinations are:

- $1.2[DL+ LL \pm EL_x \pm 0.3EL_y]$] and $1.2 [DL+ LL \pm 0.3EL_x \pm EL_y]$]
- $1.5 [DL \pm (EL_x \pm 0.3EL_y)]$] and $1.5 [DL \pm (0.3EL_x \pm EL_y)]$]
- $0.9 DL \pm 1.5 (EL_x \pm 0.3EL_y)$ and $0.9 DL \pm 1.5 (EL_y \pm 0.3EL_x)$

4. Result and Discussions

4.1. Base Shear

Table 3. Percentage decrease in base shear

Combinations	Conventional Outrigger (% decrease)		Virtual outrigger (% decrease)	
	X brace	K brace	X brace	K brace
Top only	16.71	24.88	22.22	26.25
Top and 3/4 th height	24.71	28.39	27.86	28.15
Top and 1/2 th height	26.95	29.66	29.81	29.11
Top and 1/4 th height	24.27	28.07	27.51	27.48

a) Effect of Conventional and Virtual outrigger system: From the analysis of base shear, the minimum value of base shear obtained as 2411.64 kN for conventional outrigger system and 2406.456 kN for virtual outrigger system. From these results it is

clear that, conventional and virtual outrigger system shows nearly same reduction in the base shear value. The much better configuration is virtual outrigger system than conventional outrigger system.

b) Optimum location of outrigger system: The virtual X braced outrigger system at top and $\frac{1}{2}$ th height of the building shows better performance than other outrigger configurations.

c) Type of bracing: The higher percentage reduction in the base shear values are 29.66% for virtual X braced outrigger system and 29.66% in conventional K braced outrigger system. The X braced and K braced outrigger system shows nearly same effect in the reduction of base shear values. However, the virtual X braced system shows better performance than that of other braced configurations.

4.2. Storey Displacement

Table 4. Percentage decrease in storey displacement

Combinations	Conventional Outrigger (% decrease)		Virtual outrigger (% decrease)	
	X brace	K brace	X brace	K brace
Top only	41.25	40.61	45.26	42.7
Top and 3/4 th height	45.69	44.82	49.41	48.51
Top and 1/2 th height	47.35	45.95	51.62	50.37
Top and 1/4 th height	45.24	43.62	49.14	47.43

a) Effect of Conventional and Virtual outrigger system: From the analysis of displacement, the minimum value of displacement obtained as 72.367 mm for conventional outrigger system and 66.519 mm for virtual outrigger system. From these results it is clear that, virtual outrigger system shows nearly 6 mm reduction in displacement from conventional outrigger system. The much better configuration is virtual outrigger system than conventional outrigger system.

b) Optimum location of outrigger system: The virtual X braced outrigger system at top and $\frac{1}{2}$ th height of the building shows better performance than other outrigger configurations.

c) Type of bracing: The higher percentage reduction in the displacement values are 51.62% for virtual X braced outrigger system and 50.37% in virtual K braced outrigger system. The X braced and K braced outrigger system shows nearly same effect in the reduction of displacement values. The virtual X braced system shows better performance than that of other braced configurations.

4.3. Storey Drift Ratio

Table 5. Percentage decrease in storey drift ratio

Combinations	Conventional Outrigger (% decrease)		Virtual outrigger (% decrease)	
	X brace	K brace	X brace	K brace
Top only	65.27	62.36	74.98	72.07
Top and 3/4 th height	68.76	66.31	74.81	76.73
Top and 1/2 th height	64.68	62.18	79.05	72.36
Top and 1/4 th height	63.64	61.11	73.82	71.08

a) Effect of Conventional and Virtual outrigger system: From the analysis of inter storey drift ratio, the minimum value of inter storey drift ratio is obtained as 0.000537 for conventional outrigger system and 0.00036 for virtual outrigger system. From these results it is clear that, conventional and virtual outrigger system shows nearly same reduction in the inter storey drift ratio. The much better configuration is virtual outrigger system than conventional outrigger system.

b) Optimum location of outrigger system: The virtual X braced outrigger system at top and $\frac{1}{2}$ th height of the building shows better performance than other outrigger configurations.

c) Type of bracing: The higher percentage reduction in the displacement values are 79.05% for virtual X braced outrigger system and 76.73% in virtual K braced outrigger system. The X braced and K braced outrigger system shows nearly same effect in the reduction of inter storey drift ratio. The virtual X braced system shows better performance than that of other braced configurations.

5. Conclusions

From the analysis of parameters like base shear, displacement and inter storey drift ratio, the following conclusions are made from the present study:

- The behaviour of conventional and virtual outrigger system was found to be similar. Comparing both of this the much better performance shows in virtual outrigger system.
- Even though the virtual outrigger system perform better when compared to the convention system, due to the difficulty in installation and high construction cost conventional outrigger system is preferred.
- The optimum location of outrigger was at top and 1/2th height of the structure for both conventional and virtual outrigger system.
- X bracing shows better performance in bracing the outrigger system when compared to K bracing.
- The use of conventional and virtual outrigger system in tall buildings increases the stiffness and makes the structure efficient under seismic load .

References

1. Gorji, M. S. and Cheng, J. J. Steel plate shear wall with outriggers. Part II: Seismic design and performance, *Journal of Constructional Steel Research*, Vol.137, 311-324, (2017).
2. Patil, M. D. and Sangle, K. K. Seismic behaviour of outrigger braced system in high rise 2-D buildings, Vol.4, 282-305, (2016).
3. Gadkari, A. P. and Gore, N. J. Review on behaviour of outrigger structural system in high rise building, *International Journal of Engineering Development and Research*, Vol.4, (2016).
4. Ho, W. M. Outrigger topology and behaviour, *Advanced steel construction*, Vol.12, No.2, 83-96, (2016).
5. Mohamed, O. A. and Najm, O. Outrigger system to mitigate disproportionate collapse in building structures, *World Multidisciplinary Civil Engineering- Architecture- Urban Planning Symposium (WMCAUS)*, 839-844, (2016).
6. Ho, G. W. and Arup. The evolution of outrigger system in tall building, *International Journal for High- Rise building*, Vol.5, No.1, (2016).
7. Nanduri, R. K., Suresh, B. and Hussain, I. Optimum position of outrigger system for high rise reinforced concrete buildings under wind and earthquake load, *American Journal of Engineering Research (AJER)*, Vol.2, 76-89, (2013).
8. Bayati, Z., Mahdikhani, M. and Rahaei, A. "Optimized use of multi- outriggers system to stiffen tall building, *The 14 World Conference on Earthquake Engineering*, (2008)
9. IS 1893 (Part 1) 2016 : Criteria for Earthquake Resistant Design of Structures, Bureau Of Indian Standards, New Delhi.

Shear Behaviour of RCC Beams Retrofitted with Ultra High Performance Fibre Reinforced Concrete

Swarup S.S.¹ and Bindu Biju²

¹PG Research Scholar, Structural Engineering, Mar Baselios College of Engineering and Technology, Thiruvananthapuram, Kerala, India

nandu4828@gmail.com

²Asst. Professor, Department of Civil Engineering, Mar Baselios College of Engineering and Technology, Thiruvananthapuram, Kerala, India

bindurani92@gmail.com

Abstract. Reinforced concrete structures often needs modification and improvement in their performance during their service life and the factors mainly contributing are change in their use, new design standards, deterioration due to corrosion in the steel caused by exposure to aggressive environments and accident events such as earthquakes. In case of such circumstances there are only two possible solutions, they are either replacement or retrofitting. But full structure replacement might have determinate disadvantages such as high costs for material and labour, a stronger environmental impact and inconvenience due to interruption of the function of the structure. Whenever possible, it is often better to repair or upgrade the structure by retrofitting. In this study, shear behaviour of reinforced cement concrete beams retrofitted with Ultra High Performance Fibre Reinforced Concrete (UHPFRC) with two types of fibres (crimped and micro steel fibre) and a plain UHPC were compared with control beams. A normal M20 mix was designed for the study. Two point loading system was adopted for the test and deflection were noted for each load increment. Behaviour of retrofitted beams and control beams were studied by comparing the properties such as first crack load, ultimate load and load deflection plot. The result showed that shear performance improved by 88% for UHPFRC-C, 78% for UHPFRC-M and 36% for UHPC, showing the effect of fibres which improved the shear performance of UHPFRC retrofitted beams.

Keywords: Ultra high performance concrete, normal curing, shear performance.

1. Introduction

Existing reinforced cement concrete structures may, for a variety of reasons, be found to perform unsatisfactorily. This could manifest itself by poor performance under service loading, in the form of excessive deflections and cracking, or there could be inadequate ultimate strength. Additionally, revisions in structural design and loading codes may render many structures previously thought to be satisfactory, noncompliant with current provisions. In the present economic climate, rehabilitation of damaged concrete structures to meet the more stringent limits on serviceability and ultimate strength of the current codes, and strengthening of existing concrete structures to carry higher permissible loads, seem to be a more attractive alternative to demolishing and rebuilding. Various repair procedures are resin injection, stitching, bonding of external reinforcement, routing and sealing, drilling and plugging, chemical grouting, flexible sealing and Portland cement grouting. The techniques used for carrying out repair of damaged structures vary from one structure to the other, depending on the type of distress. Depending on the location and environmental conditions, suitable materials should be chosen for retrofitting, from the point of view of long term performance of the structures after repair. Retrofitting schemes are based on cost and availability of the materials. The different methods include patch repair, jacketing technique using concrete or steel, fibre reinforced polymer (FRP) wrapping, attaching steel plates externally to structural elements by epoxy bonding or bolting, fibre shotcreting and external prestressing[1]. But one thing that should keep in mind before adopting a technique is its overall performance in their service life, it should provide adequate strength, durable, and economic. Also inventions are being conducting to improve the process of retrofitting efficiently. Ultra High Performance Concrete is one of them which is defined by its high strength and durability. It was developed in Europe in the 1980s for specialized applications that demand higher strength and corrosion resistance for marine anchors, piers and seismic structures[2]. This concrete consists of a combination of Portland Pozallana Cement, fine aggregate, silica fume, high-range water-reducing admixture (HRWR), fibres (usually steel), and water. It have a very low water-cement ratio below 0.25. The absence of coarse aggregate was considered by the inventors to be a key aspect for the microstructure and the performance of the UHPFRC in order to reduce the heterogeneity between the cement matrix and the aggregates. However, due to the use of very fine aggregates instead of ordinary aggregate, the cement density of UHPFRC is high[3]. Petr et al. (2013)[4] investigated the mechanical properties of UHPFRC and the results showed excellent performance of UHPFRC in all categories. Fracture energy of UHPFRC was obtained five times higher than that of conventional fibre reinforced concrete. Then it was Prem et al. (2012) he studied different mixing methods and curing procedures such as normal curing, hot air curing and steam curing for the

development of UHPRC. The cube and cylinder strength observed for different mixes were recorded, which were in the range of (180 - 132) MPa and (171 - 193) MPa respectively. Flexural and split tensile strength showed a linear relationship and reinforcement index. Also from the test results obtained it was recommended that fibres with higher aspect ratio yields better tensile and flexural strength. Results also reflected that even after cracking the residual capacity is very high for both long fibres and short fibres. Durability testing were also conducted and the results shown that water absorption and sorptivity was very low thus the corrosion resistance is too high and can be used in all types of aggressive environments [3]. Later he also studied the flexural behaviour of damaged RCC beams strengthened with Ultra High Performance Fibre Reinforced Concrete overlay. For the test control RCC beams of size 100 x 200 x 1500 mm with M30 grade of concrete are tested up to failure. Damage to the beams was introduced by preloading the RC beams up to 80 and 90 % of the failure load of control RCC beam. UHPFRC overlay was added on the tension face of the beam with epoxy and tests are conducted for flexural behaviour and it was observed that there is significant increase in load carrying capacity and ductility in the case of preloaded RC beams strengthened with UHPC overlay [5]. Hannawi et al. (2016) [6] investigated the effect different type of fibres on the microstructure and the mechanical behaviour of UHPFRC. Mainly steel, mineral and synthetic fibres of different dimensions were used in the study. The microstructure of the specimens was examined by using SEM observation and by measuring the porosity, intrinsic permeability and P-wave velocity. The mechanical behaviour under loading has been studied using a uni-axial compression test and the results showed that the use of fibre has a relatively slight influence on the compressive strength and elastic modulus of concrete except for steel fibre which improves the strength because of its intrinsic rigidity. The fibres clearly restrain the cracking process in concrete under loading. Studies proved that the UHPFRC got improved mechanical as well as durability properties and thus it can be considered as a retrofitting technique. So this study focused towards the development of a retrofitting system using the addition of a thin overlay of Ultra High Performance Fibre Reinforced Concrete (UHPFRC) to reinforced cement concrete (RCC) members of M20 grade which was made deficient in shear capacity and the performance of the retrofitted beams were taken for the study.

2. Experimental Program

The experimental work consisted of casting, curing, preloading and then testing of beams of length 1000 mm and cross section 100 mm x 150 mm. The reinforcement details are shown in Fig. 1. For the beam two 10 mm diameter bars were used as tension reinforcement and, two 8 mm bars were used as compression reinforcement and 2 legged 6 mm stirrups were used at a spacing of 90 mm center to center were provided at flexural span and at two ends of the shear member to induce shear failure. Strain gauges were provided on one of the two bars of each diameter both bottom and top. The reinforcement bars were levelled smooth on the portion where strain gauge was to be attached and then is attached using suitable adhesive. The lead wires were then soldered to the strain gauge and proper insulation were provided in order to avoid damaging of the strain gauge. The strain readings were measured using strain indicator and for measuring the central deflection dial gauges were used. Testing of beams were carried out using an Universal testing machine of 1000kN capacity and deflection, strain readings and crack propagation were measured at each 2.5kN increment of loading.

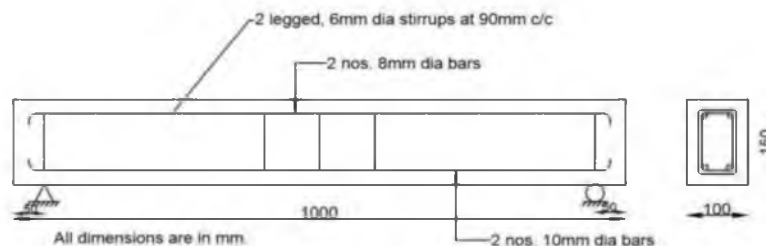


Fig.1. Reinforcement detailing for shear beam [2]

2.1 Materials Used

Ordinary Portland cement of 53 grade conforming to IS: 12269-1987 (reaffirmed 2004) [16], 75% of fine aggregate passing through 600 μ m and retained on 300 μ m, 25% of fine aggregate passing through 300 μ m and retained on 150 μ m, silica fume, glass powder and super plasticizer were used for the investigation. The basic design philosophy lies in complete elimination of the coarse aggregate to impart greater homogeneity, with mineral and chemical admixture to get stronger gel formation during hydration. Two types of fibres were used in the study both of same aspect ratio 60 (crimped steel fibre 30mm length and 0.5mm diameter and micro steel fibre 6mm length and 0.1mm diameter). The mix proportion was selected from the optimum mix obtained from the trial mixes conducted in previous study [8]. The mechanical properties were also determined for finding the optimum mixes.



Fig. 2. Micro steel fibres



Fig. 3. Crimped steel fibres

Table 1. Properties of fibres

Type of fibre	Crimped steel fibre	Micro steel fibre
Length (mm)	30	6
Diameter (mm)	0.5	0.1
Aspect ratio	60	60

Table 2. Mix proportion of M20 and UHPC mix

Mix	Cement (kg/m ³)	Fine aggregate (kg/m ³)	Coarse aggregate (kg/m ³)	Silica fume (kg/m ³)	Glass powder (kg/m ³)	Super plasticizer (L/m ³)	Water (L/m ³)	Compressive strength (MPa)
UHPC	712	733	-	178	178	24	144	153
M20	340	666.4	1326	-	-	-	153	28.50

Table 3. Mix proportion of UHPFRC Mixes

Mix	Cement	Fine Aggregate	Silica Fume	Glass powder	Super plastisizer	Water	Steel fibre	
							Micro	crimped
	Kg/m ³			L/ m ³		Percentage volume		
UHPC	712	733	178	178	24	144	0	0
UHPFRC-C0.25	712	733	178	178	24	144	0	0.25
UHPFRC-C0.5	712	733	178	178	24	144	0	0.50
UHPFRC-C0.75	712	733	178	178	24	144	0	0.75
UHPFRC-C1.00	712	733	178	178	24	144	0	1.00
UHPFRC-C1.25	712	733	178	178	24	144	0	1.25
UHPFRC-C1.5	712	733	178	178	24	144	0	1.5
UHPFRC-M0.25	712	733	178	178	24	144	0.25	0
UHPFRC-M0.5	712	733	178	178	24	144	0.5	0
UHPFRC-M0.75	712	733	178	178	24	144	0.75	0
UHPFRC-M1.00	712	733	178	178	24	144	1.00	0
UHPFRC-M1.25	712	733	178	178	24	144	1.25	0
UHPFRC-M1.5	712	733	178	178	24	144	1.5	0

Optimum fibre content was found out and retrofitting was carried out only with the optimum mixes.

2.2 Preparation of specimens

Total of 12 beam specimens were prepared with M20 grade concrete. All the specimens were prepared and cured for 28 days. And then the control specimens were tested and then preloading was done. The reinforcement provided on beams was given in Fig.4.

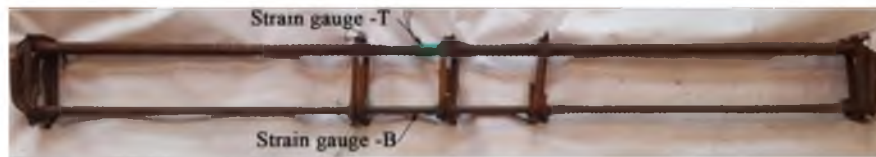


Fig. 4. Reinforcement provided on beams

Table 4. Specimen details

Specimen ID	Size	No. of specimens
CB		3
UHPC	100mm x 150mm x	3
UHPFRC-C	1000mm	3
UHPFRC-M		3

2.3 Test Procedure

The beams were tested under two point loading. The deflection values obtained from the dial gauge at the mid span were used to plot the load deflection curve. Values of strain obtained from the strain gauges connected to the strain indicator were used for plotting the moment curvature relationship. The moment was obtained from the loading configuration. The loading configuration for two points loading is shown in Fig.5.

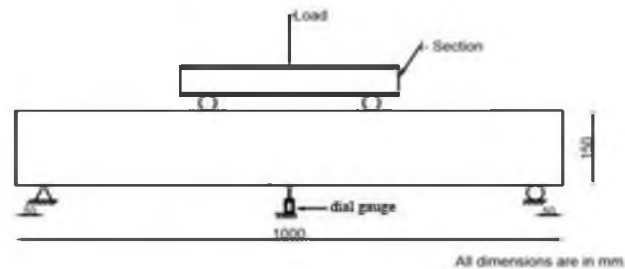


Fig.5.Loading configuration

2.4 Distressing of beam specimen

The three control beams (CB) were loaded up to failure and their ultimate loads were determined. The remaining nine beams were then distressed up to 67% of the ultimate load.

2.5 Retrofitting of Pre-Loaded Beams

The preloaded beams were then U-wrapped with UHPC and UHPFRC's, 2.5cm was adopted as overlay thickness and was done over the full span. Retrofitting was made easily with the help of moulds and they were demoluded and kept for curing. Procedure adopted for retrofitting was given in Fig. 6.

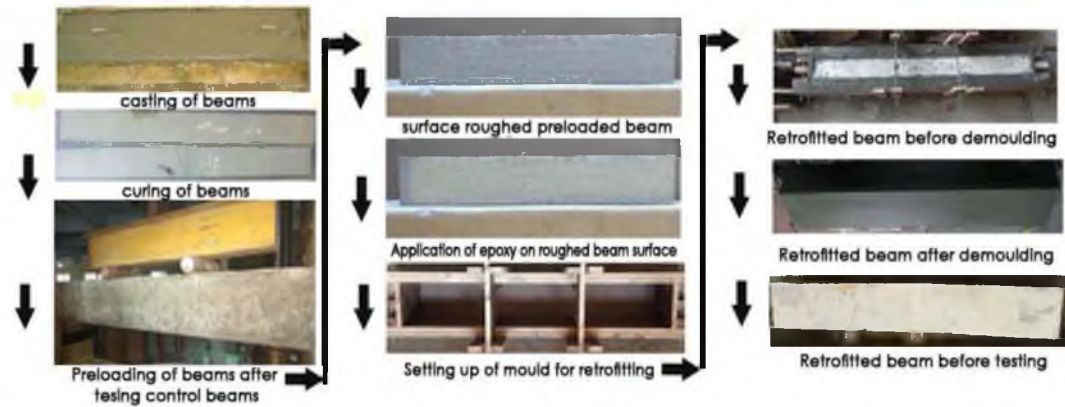


Fig. 6. Retrofitting procedure

2.6 Shear Test on Retrofitted Beams

After the curing period, the beams were tested in the Universal Testing Machine (UTM) with the same test procedure as mentioned earlier. The flexure and shear behaviour of the UHPC retrofitted and UHPFRC's retrofitted beams were compared to that of the control beams. Fig.7 shows the test setup used for the study.



Fig.7. Test setup

3. Results and Discussion

3.1 Compressive strength and slump values of UHPC and UHPFRC mixes

Compressive strength and slump values of trial mixes were given in Table 5 and from the results optimum fibre content for crimped steel were found out as 1.00 % and that for micro steel were found out as 1.25%.

Table 5. Compressive strength and slump values of UHPC and UHPFRC mixes

Mix designation	Compressive strength (N/mm ²)	Slump(mm)
UHPC	151	247
UHPFRC-C0.25	153	243
UHPFRC-C0.5	155	238
UHPFRC-C0.75	157	234
UHPFRC-C1.00	158	230
UHPFRC-C1.25	145	218
UHPFRC-C1.5	132	198
UHPFRC-M0.25	153	246
UHPFRC-M0.5	155	241
UHPFRC-M0.75	158	237
UHPFRC-M1.00	160	234
UHPFRC-M1.25	163	231
UHPFRC-M1.50	153	221

3.2 Hardened properties of UHPC and UHPFRC mixes

Some of the hardened properties were also studied and the results were given in Table 6. All the tests were done according to ASTM and BS codes.

Table 6. Hardened properties of UHPC and UHPFRC mixes

Mix Designation	Compressive strength(N/mm ²) ASTM C 109[21]	Modulus of rupture(N/mm ²) ASTM C 1609[22]	Modulus of elasticity(N/mm ²) ASTM C 469[23]	Split tensile strength(N/mm ²) BS 1881:1983[24]
UHPC	151	18.2	4.04x10 ⁴	12.8
UHPFRC-C1.00	158	33.6	4.71x10 ⁴	20.1
UHPFRC-M1.25	163	31.5	4.48x10 ⁴	18.6

From the results it was clear that the addition of steel fibre had improved the mechanical properties of the mix

3.3 Crack Pattern and Failure

The crack pattern for normal as well as beams was shown in Fig.8. Cracks was not observed at the beginning of the test. After some time, shear cracks initiated at shear zone. As the load got increased, the existing cracks started to propagate and also new cracks were also developed.



Fig. 8. Crack pattern

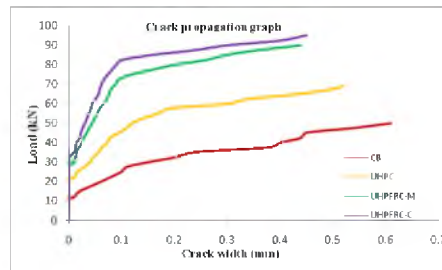


Fig.9. Crack propagation graph

At the ultimate stage most of the cracks travelled up to the top of the beam, even though the number and size of the cracks were different in normal and retrofitted beam. In retrofitted beam all the cracks were shear type. In the control specimen comparatively wider cracks was noticed at shear region. During testing, the crack width were measured using crack detection microscope of 50x magnification at load increment of 2.5 kN. Crack propagation graph of all the tested beams were given in Fig.9. The crack width pattern was different in normal and retrofitted beam, in the case of UHPFRC-M and UHPFRC-C the crack width was comparatively smaller when compared to the control beam. The maximum value of crack width was observed in control beam which was 0.64 mm.

3.4 Load-Deflection Behaviour at mid span

The load and deflection values recorded during the testing of beams were used to draw the load deflection graphs. Fig.10 shows the load-deflection plot of the control beam specimen and retrofitted specimens. From the load-deflection plot of shear beams, it was observed that initially the curve was linear up to certain load for the control as well as for the retrofitted specimens.

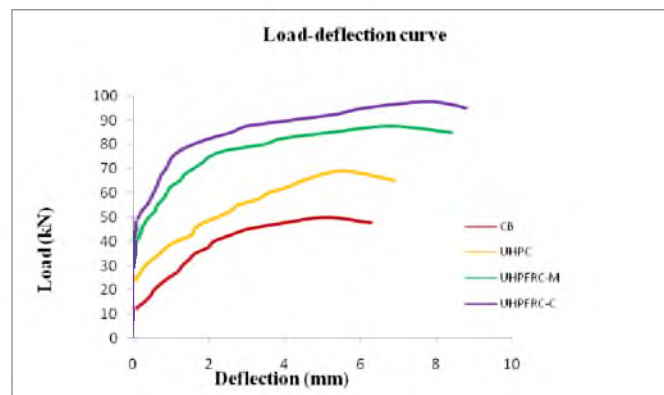


Fig. 10. Load-deflection plot for shear retrofitted beams

For the control beam, it was observed that the linearity was up to the first crack load and further increase in load causes the curve to deviate from linearity. The load carrying capacity of retrofitted beams increased. The steel fibres in UHPFRC's arrested the micro cracks developed thus improved the load carrying capacity than UHPC. For UHPFRC-C, the load carrying capacity was much improved when compared to UHPFRC-M and this may be due to the proper bonding provided by the crimped steel fibre which is much longer compared to micro steel fibre. The initial, yield and ultimate loads are given in Table 7. Energy absorption was also found by calculating the area under the load deflection plot. Due to the limitations in the

experimental set up, the load deflection graph could be plotted only up to 80 % of the peak load, in the descending portion of the curve. Thus, the energy absorption was calculated as the area under the curve up to the peak load and under the descending portion up to 80 % of the peak load. The energy absorption of beams is shown in Table 8.

Table 7 Initial, yield and ultimate load values

Beam ID	Initial Crack load (kN)	Yield load (kN)	Ultimate Load (kN)	
			Absolute	Relative
CB	13	41	50	1
UHPC	23	56	68	1.38
UHPRFC-M	30	74	89	1.78
UHPRFC-C	35	79	94	1.88

Table 8. Energy absorption

Specimen	Energy absorption (kNmm)
CB	289.25
UHPC	370.88
UHPRFC M	631.82
UHPRFC C	718.23

3.5 Moment curvature relationship

Moment curvature plot for the control and retrofitted beams were given in Fig.11. The moment curvature can be said to have three stages.

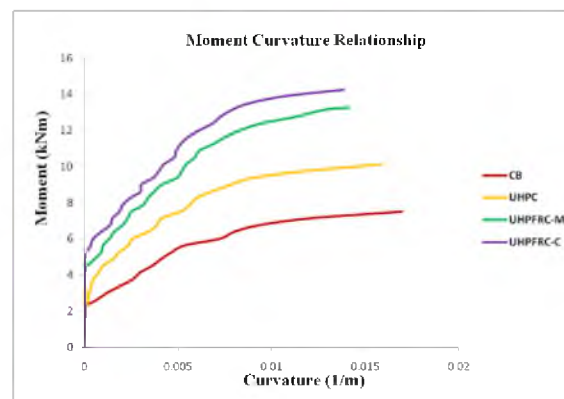


Fig. 11. Moment curvature relationship

divided into three stages, first stage is till initial cracking, second stage till yielding of tension steel and then the third stage to limit of useful strain in concrete. The curve is linear up to first crack moment. Further when the moment increases, the curve

shifts from linearity. When the moment reaches the yield moment, the curves become flat. When steel yields, a large increase in curvature occurs with a small change in moment.

3.6. Ductility indices

Displacement ductility was calculated as the ratio of the displacements at ultimate load to the displacement at yield load. The ductility could be considered at 80% of the peak load, because this takes into account, the softening part of load deflection curve. Hence for calculating the ultimate deflection, 80% of peak load was considered. Softening ductility consideration is important in seismic design and where large deformations are involved. Failure of an under reinforced beam is called tension failure.

Table 9.Ductility indices of the beams

Beam ID	Displacement Ductility		Curvature Ductility	
	Absolute	Relative	Absolute	Relative
CB	2.11	1	2.07	1
UHPC	2.26	1.07	2.19	1.05
UHPFRC-M	3.12	1.47	2.33	1.12
UHPFRC-C	3.2	1.51	2.45	1.18

This is because the primary reason for failure is the yielding of reinforcement. The large increase in the curvature, before collapse of the beam is an indication of the ductile failure of beam. Curvature ductility was calculated as the ratio of the curvature at ultimate load to that of the curvature at yield load. The ductility index of the beams is shown in Table 9.

3.7 Shear behaviour of beams

Behaviour of retrofitted beams under shear was evaluated by calculating the maximum shear force at the supports and the results were shown in Table10. The results showed that the shear carrying capacity of all the retrofitted specimens when compared to the control specimens.

Table 10.Shear behaviour of beams

Beam ID	Ultimate shear force (kN)
	Absolute
CB	25
UHPC	34
UHPFRC-M	44.5
UHPFRC-C	47

Results showed that the ultimate shear capacity got improved by the addition of fibers, for UHPFRC-M it got improved by 88% for UHPFRC-C, 78% for UHPFRC-M and 36 % for UHPC when compared to the control specimens.

4. Conclusions

From the experimental investigation conducted, the load deflection behaviour, crack width, energy absorption, ultimate load carrying capacity, moment curvature relationship and ductility indices mixes were studied and based on the results obtained, the following conclusions were made:

- Both UHPFRC-M and UHPFRC-C shown good crack arresting capacity compared to beams retrofitted with UHPC
- The ultimate capacity was improved by 88% for UHPFRC-C, 78% for UHPFRC-M and 36 % for UHPC, showing the effect of fibres which improved the shear performance of UHPFRC retrofitted beams.
- The energy absorption capacity was increased by 148% for UHPFRC-C retrofitted beam and 118 % for UHPFRC-M, but for beams retrofitted with UHPC, an increase of 28% was only observed.

References

1. Hemaanitha,R and Kothandaraman,S.: Materials and Methods for Retrofitting of RC Beams – A Review, *International Journal of Civil Engineering and Technology*, 5,01-14, (2014).
2. Richard, P. and Cheyrezy, M.: Reactive Powder Concretes with High Ductility and 200 to 800 MPa Compressive Strength, *ACI*, 44, 507–518, (1995)
3. Prem,P.R., Bharatkumar,B.H and Iyer,N.G. .:Mechanical Properties of Ultra High Performance Concrete, *International Journal of Civil, Environmental, Structural, Construction and Architectural Engineering*, 6, 670-675, (2012).
4. Petr, M., W.: Mechanical properties of Ultra High Performance Fibre Reinforced Concrete, *International Journal of Civil and Structural Engineering*, 3, 122-135, (2013)
5. Prem, R. P., Bharatkumar, B. H.,Iyer, N. Gand Murthy, R. A. and Gopal, A.: Flexural behaviour of damaged RC beams strengthened with Ultra High Performance Concrete, *Research Gate-Advances in Structural Engineering*, 1, 2056-2068, (2017).
6. Hannawi, T.: Effect of different types of fibres on the microstructure and the mechanical behaviour of UHPC, *Journal of Construction and Building Materials*, 3, 113-123, (2016).
7. Ataur, R. M. and Tyler, M. Q.: Application of Ultra High Performance Concrete in expediting the replacement and rehabilitation of highway bridges,*International Journal for Civil Engineering*, 4, 1-9, (2016).
8. Biju, B. and Krishnan, H.: Development of Ultra High Performance Concrete by normal curing method,*Proceedings of National Conference on Recent Trends in Computer Science & Engineering and Sustainability in Civil Engineering*, 3, 116-118,(2016).
9. Tahenni, T., Chemrouk, M., and Lecopte, T.: Effect of steel fibres on the shear behaviour of high strength concrete beams,*Journal of Construction And Building Materials*, (105), 14-28, (2016).
10. Hussein, L. and Amleh, L.: Structural behaviour of ultra-high performance fibre reinforced concrete-normal strength concrete or high strength concrete composite members, *Journal of Concrete Technology*, 3, 1105-1116, (2015).
11. Feng, J., and Sun, W.: Mechanical analyses of hooked fibre pullout performance in Ultra High Performance Concrete, *Journal of Concrete Technology*, 9, 403-410, (2014).
12. Ruano, G., Isla, F., Pedraza, R. I., and Sfer, D.: Shear retrofitting of reinforced concrete beams with steel fibre reinforced concrete, *Journal of Construction And Building Materials*, 54, 646- 658, (2014).
13. Behzad, M., Raizal, S. M. R. and Mohd S. J.:A Review on Ultra High Performance Concrete (UHPC) Technology,*International Journal of Civil and Structural Engineering*, 2, 994-1009, (2012).
14. Graybeal, B.: Ultra High Performance Concrete,*Federal Highway Administration*, 25, 11-38, (2011).
15. Stephen, J. F.: Construction of a 50 MetreLong Ultra High Performance Ductile Concrete Composite Road Bridge, *International Journal of Civil and Structural Engineering*, 2, 228-240,(2011).
16. Mostosi, S., Meda,A.,Riva, P., and Maringoni, S.: Shear strengthening of RC beams with High Performance Jacket,*Proceeding of fib Symposium PRAGUE*, CBS, 1-9,(2011).
17. Lei, Y.: Ultra High Performance Concrete technology towards sustainable construction, *International Journal for Sustainable Construction Engineering& Technology*,1,105-126, (2010).
18. Yang, I.H., and Kim, B.: Structural behaviour of ultra high performance concrete beams subjected to bending, *Journal of Concrete Technology*, 1, 1-10, (2010).
19. IS 2386 (Part III) - 1983 (Reaffirmed 2002),Methods of test for aggregates for concrete, *Bureau of Indian Standards*, New Delhi, India, 1983.
20. IS 10262-2009, Concrete mix proportioning- Guidelines, *Bureau of Indian Standards*, New Delhi, India, 2009.
21. ASTM C-109,Standard Test Method for Compressive Strength of Hydraulic Cement Mortars, *American Society for Testing and Materials Standard Practice*, Philadelphia, Pennsylvania, 2016.

22. ASTM C-1609, Standard Test Method for Modulus of rupture of Hydraulic Cement Mortars, *American Society for Testing and Materials Standard Practice*, Philadelphia, Pennsylvania, 2013.
23. ASTM C-469, Standard Test Method for Modulus of elasticity of Hydraulic Cement Mortars, *American Society for Testing and Materials Standard Practice*, Philadelphia, Pennsylvania, 2013.
24. BS-1881-1983, Method for determination of tensile splitting strength, British standards Institute, London, U.K.

Effect of Near Surface and Externally Bonded Retrofitting on Exterior Beam-Column Joint

Akash S.¹ and Jayasree S.²

¹ PG Research Scholar, Structural Engineering, Mar Baselios College of Engineering and Technology, Thiruvananthapuram, Kerala, India

akashsanal15@gmail.com

² Associate Professor, Department of Civil Engineering, Mar Baselios College of Engineering and Technology, Thiruvananthapuram, Kerala, India

jayasris71@gmail.com

Abstract. To prevent the loss due to structural damages that can be resulted from the seismic activity, it is important that the structural elements should be retrofitted as soon as possible. Beam-column joints are the most vulnerable part of a structure, as the forces from adjacent beams and columns are transferred through the joint. In this study, a method for retrofitting RCC exterior beam-column joints using externally bonded Glass Fiber Reinforced Polymer (GFRP) sheet and Near Surface Mounted (NSM) GFRP strips (at different orientations such as 30°, 45° and 60°) is proposed. All specimens were tested under reverse cyclic loading. The performance of beam-column joints was evaluated with respect to strength, ductility, energy absorption and stiffness degradation. The results show that the NSM retrofitted specimens with orientation of 30° have significantly enhanced all the above properties.

Keywords: Beam-column joints, Near surface mounted retrofitting, Reinforced concrete

1. Introduction

In RCC structures, beam-column joints are the critical members for transferring forces and moments between beams and columns. Due to the moment reversal across beam-column joints, when subjected to seismic action, higher stresses are formed in the joint cores. Such beam-column joints become vulnerable members in moment resisting structures and display poor performance under seismic action according to post-earthquake investigations. Therefore, it is necessary to rehabilitate existing substandard beam-column joints for enhancing their seismic performance and extending their design life span [1]. Retrofitting can be done in two ways either in global manner or in local level. In the case of structures with higher level of flexibility or when no uninterrupted transverse load path is available, global retrofitting techniques are considered. This method includes addition of shear walls, bracings, infill walls, base isolation etc. In case of local retrofitting, the main aim is to improve the capacity of deteriorated isolated members. It is economical as compared to global retrofitting techniques. Local retrofitting techniques consist of jacketing of columns, beams, beam-column joints, strengthening of foundations etc. In this technique, the sheets of different materials such as GFRP, CFRP, ferrocement etc. will be bonded to the surfaces of the structural members to increase its strength. But debonding failure is a major disadvantage in these external retrofitting techniques, where rupture occurs suddenly once the ultimate strength is reached [2]. To improve this aspect in retrofitting, new strengthening methods are developed and Near Surface Mounted retrofitting is one among them.

2. NSM Retrofitting Technique

In the NSM method, grooves are first cut into the concrete cover of an RCC element and the FRP reinforcement is bonded within it using an appropriate groove filler such as an epoxy paste or cement grout [3].

NSM steel rebars has been used in Europe for the strengthening of RCC structures which date back to the early 1950s. More recently, NSM stainless steel bars has been used for the strengthening of masonry buildings and arch bridges [2]. The advantages of FRP over steel as NSM reinforcement are better resistance to corrosion, increased ease and speed of installation due to its lightweight, and a reduced groove size due to the higher tensile strength and better corrosion resistance of FRP. Fig. 1 depicts the ways by which NSM systems can be applied to the structural component.

The objectives of this study are,

- (i) To study the effect of orientation of NSM Glass Fiber Reinforced Polymer (GFRP) strips on the performance of exterior beam-column joint
- (ii) To compare the performance of the exterior beam-column joint retrofitted with NSM technique (GFRP strips) and with externally bonded GFRP wrapping

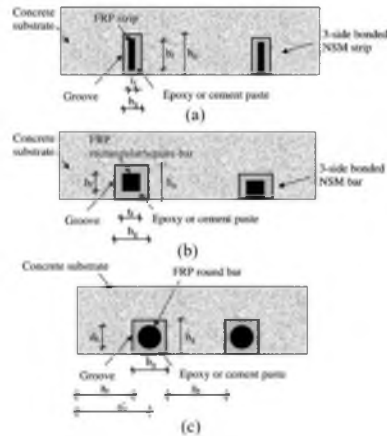


Fig. 1 NSM retrofitting with (a) Rectangular FRP strips, (b) Square FRP strips, (c) Round FRP bars [3]

3. Experimental Study

3.1 Materials used

Portland pozzolana cement, natural coarse aggregate with maximum size 20 mm, manufactured sand of fineness modulus 2.65, Glass Fibre Reinforced Polymer (GFRP) sheets and strips, epoxy adhesive. Table 1 shows the mechanical properties for both GFRP strips and sheets and Table 2 shows that of the epoxy resin supplied by manufacturer. Fig. 3 shows the GFRP sheets and strips used.

3.2 Mix Design

Mix design for M20 was done by the method given in IS 10262:2009 [4]. Water cement ratio was fixed as 0.45. The fresh properties of the mix were evaluated by measuring the slump according to IS 1199-1959 [5].



Fig. 2 (a) GFRP sheet, (b) GFRP strips

Table 1. Properties of GFRP sheet*

Table 2. Properties of EP103 epoxy resin*

Particulars	Values
Fibre thickness	0.90mm
Tensile strength	3400 N/mm ²
Tensile modulus	73000 N/mm ²

Particulars	Values
Application temperature	15- 40°C
Density	1.25-1.26 gm/cc
Pot life	2 hours at 30°C
Full cure	5days at 30°C

* (Source: Obtained from the supplier)

3.3 Casting of exterior beam-column joint specimen

A total of 10 numbers of exterior beam-column joints were prepared. The dimensions of the specimens are as shown in Fig. 2 and the specimen designation are shown in Table 3. The size of the beam-column joint was selected as a scaled down model of 1/3rd of its original dimension.

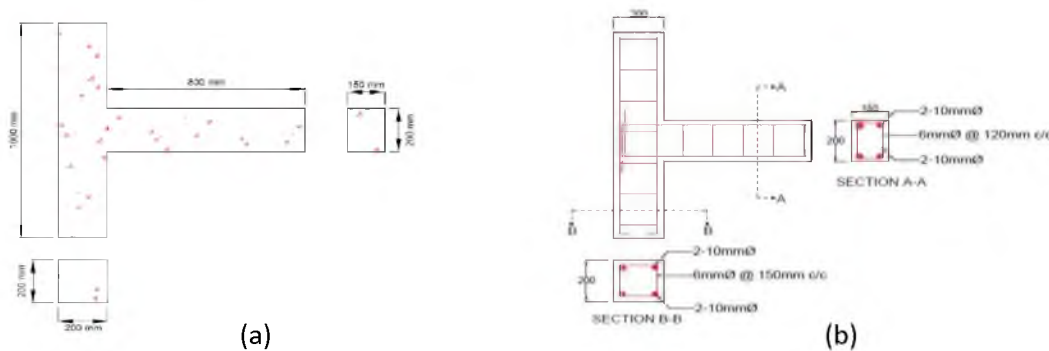


Fig. 3 (a) Dimensions of the beam-column joint specimen, (b) Reinforcement detailing of beam-column joint [6]

Table 3. Specimen designation

Sl. No.	Specimen name	Strengthening method	No. of specimen
1	BCJC	Control specimen	2
2	BCJN30	NSM retrofitting at an angle of 30°	2
3	BCJN45	NSM retrofitting at an angle of 45°	2
4	BCJN60	NSM retrofitting at an angle of 60°	2
5	BCJEB	Wrapping of GFRP sheets on the beam-column joint	2

3.4 Test setup

All the specimens were tested under reverse cyclic loading, in a 1000 kN capacity loading frame. The bottom end portion of column is kept partially fixed and top end is kept as hinge support. The hinged condition was incorporated by using a steel ball which is placed in-between the groove portions of the two identical plates made of steel. To make joint in stable condition during reverse cyclic load, 20% of the axial load carrying capacity of the column was applied over it by using a hydraulic jack. Reverse cyclic load was applied at the tip of beam through a hydraulic jack. A load cell, attached to the plunger measures the load. The deflection of beam tip is measured at every 2 kN load interval for forward and backward cycles using LVDTs. A schematic diagram of the test setup is shown in Fig. 3. The control specimens (BCJC), were tested as mentioned above and the ultimate load was obtained.

3.5 Preloading of specimens

The beam-column joint specimens designated as BCJ30, BCJ45, BCJ60 and BCJEB were subjected to a preload of 67% of ultimate load of BCJC specimen in reverse cyclic loading condition.

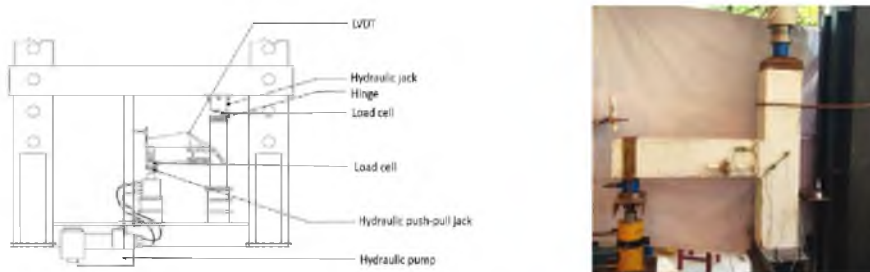


Fig. 4 (a) Schematic diagram of test setup [7], (b) Test setup of beam-column joints

3.6 Strengthening methods

The following strengthening methods were adopted for retrofitting the beam-column specimens. Fig. 5 shows the specimen after strengthening.

Externally bonded retrofitting of specimens

Specimens designated as BCJEB, after preloading were retrofitted as follows

- A length equal to the effective depth of beam was selected on all the three sides of the joint for retrofitting
- The surface of the concrete was made smooth and free of grout holes
- Epoxy base and hardener were mixed in a ratio of 10:1 and was applied over the dust free surface of concrete
- GFRP sheet was then cut in to required size and then the sheet is pressed on the epoxy paste applied area by gloved hand and a surface roller was rolled over the surface to remove air bubbles
- One more coat was applied over the glass fabric after drying and the retrofitted specimens were cured for 2 days

NSM retrofitting of specimens

Specimens designated as BCJ30, BCJ45 and BCJ60, after preloading were retrofitted as follows:

- Grooves were cut at angles of 30°, 45° and 60° for specimens designated as BCJ30, BCJ45 and BCJ60 respectively
- The spacing between the NSM-GFRP strips remain as 50 mm in all the cases
- The surface was cleaned from dust and loose particles and the groove was filled halfway with epoxy adhesive and GFRP strip was inserted and pressed to let the adhesive flow around the strips
- The specimens were cured for 2 days



Fig. 5 (a) Externally bonded beam-column joint, (b) Grooves cut on beam-column joint

4 Results and Discussion

4.1 Crack pattern

In all specimens, the cracks propagated towards the joint and initial cracks started widening. The crack pattern is shown in Fig. 5 (a) - (f).

From the figures it can be observed that the cracks were considerably reduced in the NSM retrofitted specimens and the major crack was observed closer to the joint than in the control specimen. No cracks were found in between the retrofitted grooves.

4.2 Load-deflection plots

The load-deflection plots of specimens are shown in Fig. 6. The retrofitted specimens have wider loops. Among the retrofitted specimens, the BCJN30 specimens show better load carrying capacity than that of the BCJEB specimens. The reason for lesser performance of BCJEB specimen may be due to the debonding of GFRP sheet.

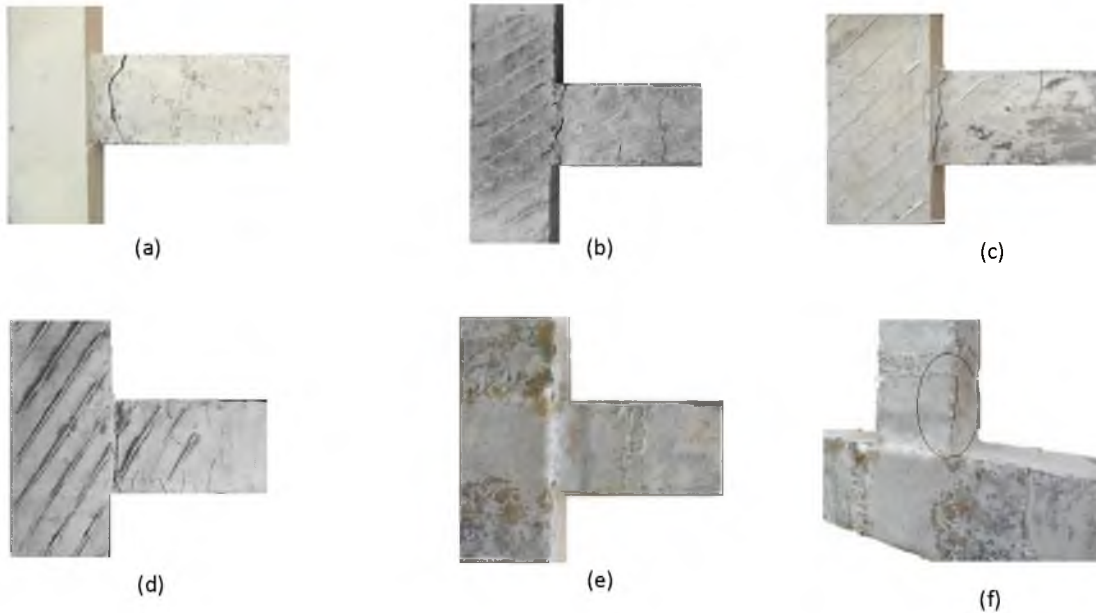


Fig. 6 Crack pattern of (a) BCJC specimen, (b) BCJN30 specimen, (c) BCJN45 specimen, (d) BCJN60 specimen, (e) BCJEB specimen, (f) Delamination of BCJEB specimen

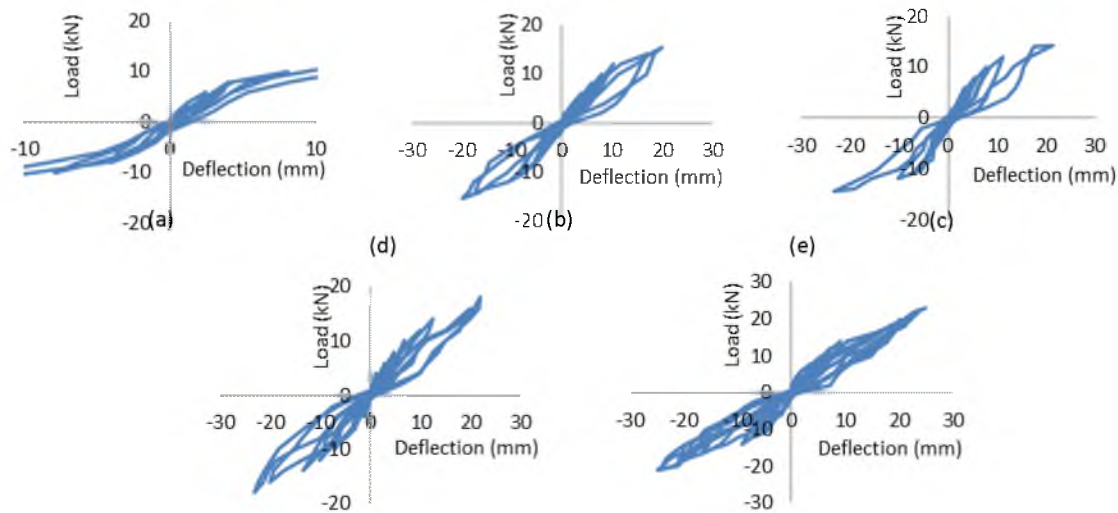


Fig. 7 Load-deflection plot of (a) BCJC specimen, (b) BCJEB specimen, (c) BCJN60 specimen, (d) BCJN45 specimen, (e) BCJN30 specimen

4.3 Load-deflection envelope plot

The envelope plot is obtained by joining the peak points of each cycle. A comparison of envelope plot for the control and retrofitted joints are shown in Fig. 7.

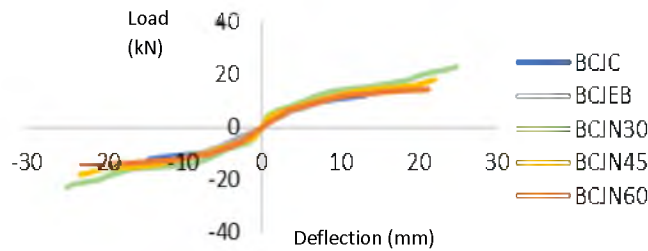


Fig. 8 Load-deflection Envelope curve of specimen

4.4 First crack load and ultimate load

The first crack load and ultimate load of the specimens are given in Table 4. First crack load was determined from the envelope curve of the load deflection plot corresponding to the point at which the curve deviated from linearity. From the table it can be observed that, first crack load increased for the NSM retrofitted specimens, which may be due to the better bond between NSM strips and specimens. Among the retrofitted specimens BCJN30 specimen had the highest first crack and ultimate load.

Table 4. First crack and ultimate load of specimens

Specimen Designation	First crack load (kN)	Ultimate load (kN)			Percentage increment
		Forward cycle	Reverse cycle	Average	
BCJC	4.20	12.10	-12.00	12.05	-
BCJEB	6.00	15.30	-15.00	15.15	26.00
BCJN60	6.00	14.30	-14.60	14.45	20.00
BCJN45	6.20	18.10	-18.00	18.05	50.00
BCJN30	10.00	23.00	-22.80	22.90	90.00

4.5 Energy absorption

The area under the load deflection plot indicates the energy absorption capacity. Energy absorption capacity was calculated and the values obtained are given in Table 5. From the table it is clear that all the retrofitted specimens have greater energy absorption capacity than the control specimen and it is maximum for BCJN30 specimen. BCJEB specimen had a much lower energy absorption capacity than that of NSM retrofitted specimens. This may be due to debonding failure of BCJEB specimens.

In NSM retrofitted specimens, the narrow GFRP strips maximize the surface area to sectional area ratio for the given volume and thus minimize the risk of debonding. But this is not the case for BCJEB specimen. As soon as the bonding between the retrofitted material and concrete surface is broken, the specimen will not be able to take up much load.

Table 5. Energy absorption capacity of specimens

Specimen Designation	Energy absorption capacity (kNmm)			Percentage increment
	Forward cycle	Reverse cycle	Average	
BCJC	113.19	125.01	119.10	-
BCJEB	199.42	198.51	198.97	67.00
BCJN60	218.06	251.87	234.97	97.00
BCJN45	257.60	273.75	265.68	123.00
BCJN30	357.50	351.33	354.42	198.00

4.6 Energy dissipation capacity

Energy-dissipation capacity is an important indicator of the seismic performance of a structure. The structural elements can withstand strong ground earthquake motions only if they have sufficient ability to dissipate seismic energy. This energy dissipation is provided mainly by inelastic deformations in critical regions of the structural system and requires adequate ductility of the elements and their connections. It can be estimated from the area within the load–displacement hysteretic loop for every cycle of load. The cumulative energy dissipated by the specimens was calculated by summing up the energy dissipated in consecutive load displacement loops throughout the test [8]. The cumulative energy dissipation of the specimens during each cycle is shown in Fig. 8. From the plot it is clear that the NSM retrofitted specimen has more cumulative energy dissipation in each cycle. BCJN30 specimen performed the best among all the other retrofitted specimen.

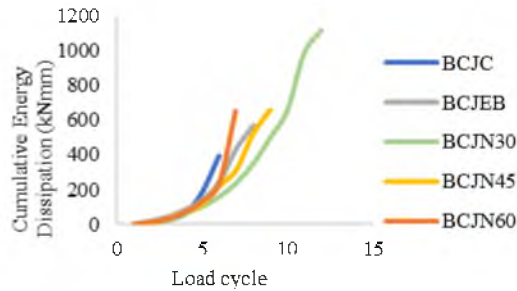


Fig. 9 Cumulative Energy dissipation capacity plot

4.7 Displacement ductility factor

Ductility of a structural element is its ability to undergo deformation beyond the initial yield deformation, while it is still sustaining load. The ductility factor, which is a measure of ductility of a structure, is defined as the ratio of maximum deflection (δ_u) to the deflection at yield (δ_y) [8]. The ductility factors were calculated and the results obtained are given in Table 6. From the Table it can be seen that NSM retrofitting influence the ductility. The ductility factor increased for all the retrofitted specimens. BCJN30 specimen had the highest ductility factor. Compared to the BCJEB specimen, the ductility factor is increased by 2.3 times for BCJN30 specimen.

Table 6. Displacement ductility factor for specimens

Specimen Designation	Displacement ductility factor	Percentage increment
BCJC	1.52	-
BCJEB	1.69	11.00
BCJN60	1.78	17.00
BCJN45	2.51	65.00
BCJN30	3.49	129.00

4.8 Stiffness degradation

Application of cyclic or repeated loading on the RCC beam–column joint causes reduction in the stiffness of the joint. This reduction in stiffness of the specimens can be assessed by computing the secant stiffness which provides a measure of the stiffness degradation in the specimens. The secant stiffness in each cycle was calculated using a line drawn between the maximum positive displacement point in one half of the cycle and the maximum negative displacement point in the other half of the cycle [8]. Stiffness degradation plot is shown in Fig. 9. It may be noted that BCJEB specimen has a low initial stiffness when compared to the NSM retrofitted specimen. The use of NSM strips significantly increased the initial secant stiffness value of the specimens. As the number of cycles increase, NSM strips intercept the macro cracks and control the widening of these cracks. This action will control further propagation of cracks and will result in higher energy demand for debonding. From the plot it can be observed that the initial stiffness for the BCJN30 specimens are greater than the other specimens.

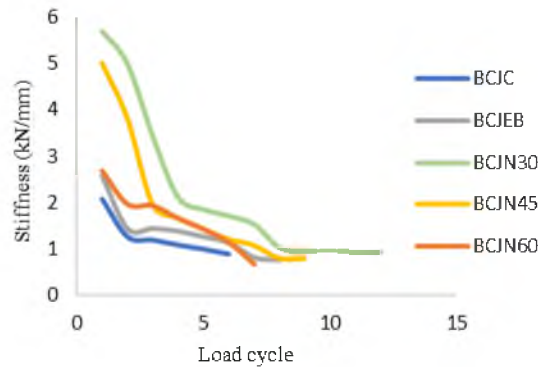


Fig. 10 Stiffness degradation plot

5 Conclusions

The following conclusions were obtained from this study.

- (i) No visible cracks were found in the case of BCJEB specimens at failure
- (ii) The cracks shifted more towards the joint region for BCJN30, BCJN45 and BCJN60 specimens when compared to BCJC specimen. This may be due to confining action in the critical region
- (iii) The ultimate load carrying capacity, energy absorption and energy dissipation capacity of all the NSM retrofitted specimens were higher when compared to BCJC and BCJEB specimens. This may be due to bridging action of NSM strips across the cracks as well as the better bond between NSM strips and specimen. Among the NSM retrofitted specimens, BCJN30 performed the best
- (iv) Debonding may be the factor that caused BCJEB specimens to fail at lesser load when compared to NSM retrofitted specimens
- (v) Initial stiffness of NSM retrofitted specimens were found to be more when compared to other specimens. The rate of degradation of stiffness was observed to be greater for BCJN30 specimen

References

1. Li,B., Lam,E.S.S., Wu,B and Wang,Y.Y.: Experimental investigation on reinforced concrete interior beam–column joints rehabilitated by ferrocement jackets, *Engineering Structures*, 56, 897–909 (2013).
2. Campione,G., Cavaleri,L and Papia,M.: Flexural Response of External RC Beam-Column Joints Externally Strengthened with Steel Cages, *Engineering Structures*, 104(1), 51-64 (2015).
3. De Lorenzis,L and Teng,J.G.: Near-surface mounted FRP reinforcement: An emerging technique for strengthening structures, *Composites*, 38(2), 119-143 (2007).
4. IS 10262:2009, Concrete Mix Proportioning- Guidelines, Bureau of Indian Standards, New Delhi, India.
5. IS 1199:1959 (Reaffirmed 2004), Methods of Sampling and Analysis of Concrete, Bureau of Indian Standards, New Delhi, India.
6. Ganesan,N., Indira,P.V and Ruby,A.: Steel Fibre Reinforced High Performance Concrete Beam-Column Joints Subjected to Cyclic Loading, *ISET Journal of Earthquake Technology*, 44(1), 445-456 (2007).
7. Anjana,V.G, Experimental Study on Fibre Reinforced High Performance Concrete Beam Column Joints with Recycled Concrete Aggregates, Mar Baselios College of Engineering and Technology, 2015.
8. Ganesan, N., Indira, P., and Sabeena, M.: Behaviour of hybrid fibre reinforced concrete beam–column joints under reverse cyclic loads, *Materials & Design (1980-2015)*, 54, 686–693 (2014).
9. Kaliluthin,A.K., Kothandaraman,S and Ahamed,T.S.: A Review on Behavior of Reinforced Concrete Beam-Column Joint, *International Journal of Innovative Research in Science, Engineering and Technology*, 3(4), 11299-11312 (2014).
10. ACI 440.2R-02 440, *Guide for the design and construction of externally bonded FRP systems for strengthening concrete structures*, American Concrete Institute Technical Committee, Farmington Hills, USA, 2002.

11. Beydokhty, E.Z and Shariatmadar, H.: Behavior of Damaged Exterior RC Beam-Column Joints Strengthened by CFRP Composites, *Latin American Journal of Solida and Structures*, 13(5), 880-896 (2016).
12. Santarsiero, G and Masi, A.: Seismic Performance of RC Beam-Column Joints Retrofitted with Steel Dissipation Jackets, *Engineering Structures*, 85(1), 95-106 (2015).
13. Esmaeeli, E., Barros, J.A.O., Sena-Cruz, J., Fasan, L., Prizzi, F.R.L., Melo, J and Varum, H.: Retrofitting of Interior RC Beam-Column Joints Using CFRP Strengthened SHCC: Cast in Place Solution, *Composite Structures*, 122, 456-467 (2015).
14. Mahmoud, M.H., Afefy, H.M., Kassem, N.M and Fawzy, T.M.: Strengthening of Defected Beam-Column Joints Using CFRP, *Journal of Advanced Research*, 5, 67-77 (2013).
15. Zhou, L., Lei, S and Jiang, Y.: Experimental Study on the Seismic Behaviour of Strengthened Concrete Column-Beam joints by Simulated Earthquake, *Procedia Engineering*, 14, 1871-1878 (2011).
16. Li, B and Kai, Q.: Seismic Behavior of Reinforced Concrete Interior Beam-Wide Column Joints Repaired Using FRP, *Journal of Composites for Construction*, 15(3), 327-338 (2011).
17. Ghobarah, A and El-Amoury, T.: Seismic Rehabilitation of Deficient Exterior Concrete Frame Joints, *Journal of Composites for Construction*, 9(5), 408-416 (2005).
18. Jiang, Y., Yan, X., Ke, Q., and Thomas, A.: Preliminary Study to Enhance Ductility of CFRP-Strengthened RC Beam, *Journal of Composites for Construction*, 21(1), 1-10 (2016).
19. Soliman, S.M., El-Salakawy, E and Benmokrane, B.: Bond Performance of Near-Surface-Mounted FRP Bars, *Journal of Composites for Construction*, 15(1), 234-251 (2011).
20. Rasheed, H.A., Harrison, R.R., Peterman, R. J and Alkhrdaji, T.: Ductile strengthening using externally bonded and near surface mounted composite systems, *Composite Structures*, 92(10), 2379-2390 (2010).
21. Oehlers, D.J., Rashid, R and Seracino, R.: IC debonding resistance of groups of FRP NSM strips in reinforced concrete beams, *Construction and Building Materials*, 22(1), 1574-1582 (2007).
22. De Lorenzis, L and Nanni, A.: Bond between near-surface mounted fiber-reinforced polymer rods and concrete in structural strengthening, *ACI Structural Journal*, 99(2), 123-132 (2002).
23. Focaci, F., Nanni, A and Bakis, C.E.: Local Bond-Slip Relationship for FRP Reinforcement in Concrete, *Journal of Composites for Construction*, 4(1), 541-555 (2000).
24. IS 1489 (Part 1): 1991 (Reaffirmed 2005), Specification for Portland Pozzolana Cement, Bureau of Indian Standards, New Delhi, India.
25. IS 4031 (Part 4): 1988 (Reaffirmed 2005), Methods of Physical Tests for Hydraulic Cement- Determination of Consistency of Standard Cement Paste, Bureau of Indian Standards, New Delhi.
26. IS 4031 (Part 5): 1988 (Reaffirmed 2005), Methods of Physical Tests for Hydraulic Cement- Determination of Initial and Final Setting Time, Bureau of Indian Standards, New Delhi.
27. IS 4031 (Part 11): 1988 (Reaffirmed 2005), Methods of Physical Tests for Hydraulic Cement- Determination of Density, Bureau of Indian Standards, New Delhi.
28. IS 383: 1970 (Reaffirmed 1997), Specifications for Coarse and Fine Aggregate from Natural Sources for Concrete, Bureau of Indian Standards, New Delhi, India.
29. IS 2386 (Part III): 1963 (Reaffirmed 2002), Methods of Test for Aggregates for Concrete, Bureau of Indian Standards, New Delhi, India.
30. IS 1608: 2005, Metallic Materials- Tensile Testing at Ambient Temperature, Bureau of Indian Standards, New Delhi, India.
31. IS 516 – 1959, Method of Tests for Strength of Concrete, Bureau of Indian Standards, New Delhi, India.
32. IS 456: 2000 (Reaffirmed 2005), Plain and Reinforced Concrete- Code of Practises, Bureau of Indian Standards, New Delhi, India.
33. Arathy, A.R., Tom, G.: Strengthening of RC Beam Using GFRP with EBR and NSM Techniques, Mar Baselios College of Engineering and Technology (2013).

Effect of Nonlinear Viscous Dampers on Irregular shaped buildings

Rakhimol.S¹and Ms. Smrithi Cheriya²

¹PG Research Scholar, Structural Engineering, Mar Baselios College of Engineering and Technology, Thiruvananthapuram, Kerala, India

rakhi7150@gmail.com

²Asst. Professor, Department of Civil Engineering, Mar Baselios College of Engineering and Technology, Thiruvananthapuram, Kerala, India

smrithicheriyath@gmail.com

Abstract. Nowadays most of the structures are constructed with irregularities to provide better architectural appearance. But it has been also noted that irregular buildings show poor seismic performance compared to regular buildings. So, it is essential to study the seismic response of these irregular shaped buildings to reduce the seismic potential damages. In order to absorb and dissipate the transmitted earthquake energy, control systems such as active, passive and hybrid systems are used. These systems aim to control the structural seismic response by improving the dynamic properties of the structure. Viscous Dampers are widely used as passive control systems which is more reliable as it requires no external power source. The current study focuses on the effect of nonlinear Viscous Damper on irregular shaped buildings. Also, the study proposes the optimum configuration and location of Viscous Damper in brace configuration system. This study includes diagonal brace configuration system. A typical G+8 story building is considered for preliminary study and then the study is further done on irregular shaped structures such as L, T and C shape. SAP2000 is used for the nonlinear dynamic analysis. Parametric study is also conducted by varying aspect ratio of the building. From the study, it is concluded that Viscous Dampers arranged in longer faces reduces the seismic response of irregular shaped buildings in terms of lateral displacement and torsion.

Keywords: Irregularities, Nonlinear Viscous Damper, Damping coefficient, Nonlinear time history analysis

1. Introduction

Earthquake is the sudden shaking of ground caused due to the passage of seismic waves. Large amount of energy is imparted into the structure during these vibrations. This will lead to collapse and damage of the structural and non-structural elements. Also, the behavior of a building during earthquake depends critically on its overall shape, size and geometry. Therefore, selection of building configuration is an important criterion in planning stage. Nowadays most of the structures are constructed in irregular shaped plan for providing better architectural appearance. These irregularities are responsible for structural collapse of buildings under dynamic loads. Conventional methods of seismic design rely on ductile behavior of structural members for energy dissipation. But retrofitting of structures is difficult in certain cases. In order to overcome this drawback, the current design practices use some special damping systems to reduce the response of the structure. Besides reducing damage, these methods have been successful in increasing safety of the structure.

There are mainly three types of control systems such as passive, active and semi active systems[1]. The basic function of the passive devices is to absorb a part of input energy, reducing energy dissipation on structural members and minimizing the damage on structures. Several different types of energy dissipation systems such as Viscous dampers, Viscoelastic dampers, Friction dampers, and Yielding metallic dampers etc. were used. This study aims to enhance the seismic response of symmetrical rectangular shaped building, C and L shaped building by using various orientations of diagonally braced Fluid Viscous Damper.

2. Fluid Viscous Damper

Fluid viscous damper is one type of passive energy dissipation systems that is used in the absorption and dissipation of the earthquake input energy. Viscous Dampers consist of a cylinder and a stainless-steel piston [2]. The cylinder is filled with incompressible silicone fluid that is divided into two compartments by a piston. The damper is activated by the stream of silicone fluid between the chambers at the opposite ends of the unit through small orifices. When the Fluid Viscous Damper strokes in compression, fluid flows from chamber 2 to 1. When the Fluid Viscous Damper strokes in tension, fluid flows from one chamber to another. The high pressure drop across the annular orifice produces a pressure differential across the piston head, which creates the damping force. The damping force of a Viscous Damper varies with the velocity of the piston. The force velocity relationship in case of a Viscous Damper is given by the following equation.

$$F = C_v v^\alpha \quad (1)$$

Where F is the damping force, C is the damping coefficient, v is the velocity of piston, α is the damping exponent. For nonlinear damper, $\alpha < 1$ and for linear damper damping exponent is equal to 1.

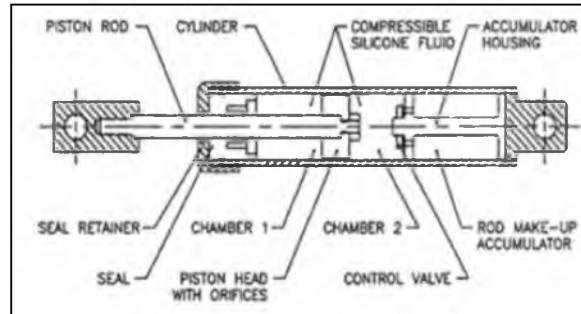


Fig 1. Components of Fluid Viscous Damper [2]

3 Methodology

3.1. Modelling

The structure considered for the study is an eight storey hospital building with towerroom at roof level. The plan area of the building is 24m x 12m. All beams along longitudinal and transverse direction are assigned with dimensions of 0.23m x 0.5m. All sub beams are assigned with dimensions of 0.23m x 0.4m and the slab thickness is taken as 0.12m. A cross section of 0.3 m x 0.6m is assigned to columns with fixed support at the base and the typical floor height is 3m. Medium soil condition is assumed as the site condition of structure and the zone is III. The building was modelled by using SAP2000 by assigning its geometric properties. Live load was calculated as per IS 875 Part I:1987 and IS 875 Part II:1987. Nlink was the element used for modelling damper in SAP2000. The value of damping exponent was taken as 0.7.

Table 1. Structural Parameters

Building	RCC building
Foundation type	Pile foundation
Plan dimension	24m x 12m
Storey height	3m
Beam size	0.23 x 0.5m
Secondary beams	0.23 x 0.4m
Column	0.6 x 0.6m
Slab thickness	0.12m

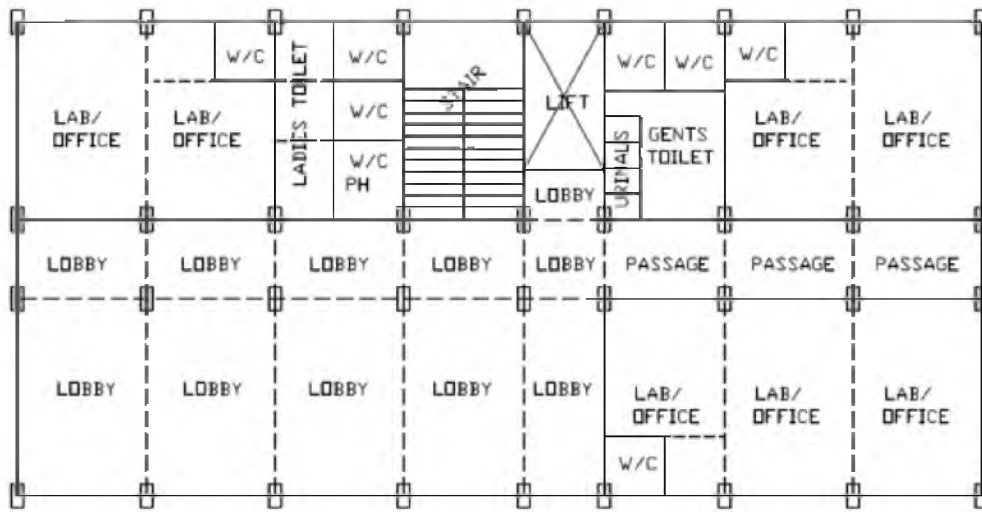


Fig 2. Plan view of building

Table 2. Descriptions and designations used

Descriptions	Designation
Longer face	X
Shorter face	Y
Alternate bays	B
Alternate floors	F
Diagonally braced damper	D

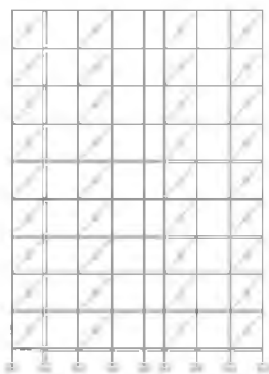


Fig 3. DXB Configuration

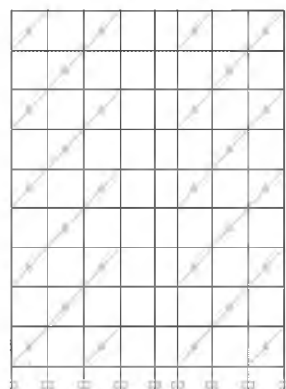


Fig 4. DXF Configuration



Fig 5. DYB Configuration

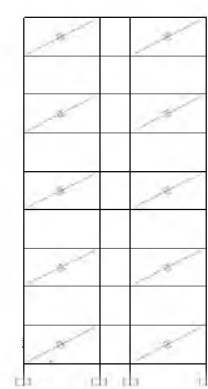


Fig 6. DYF Configuration

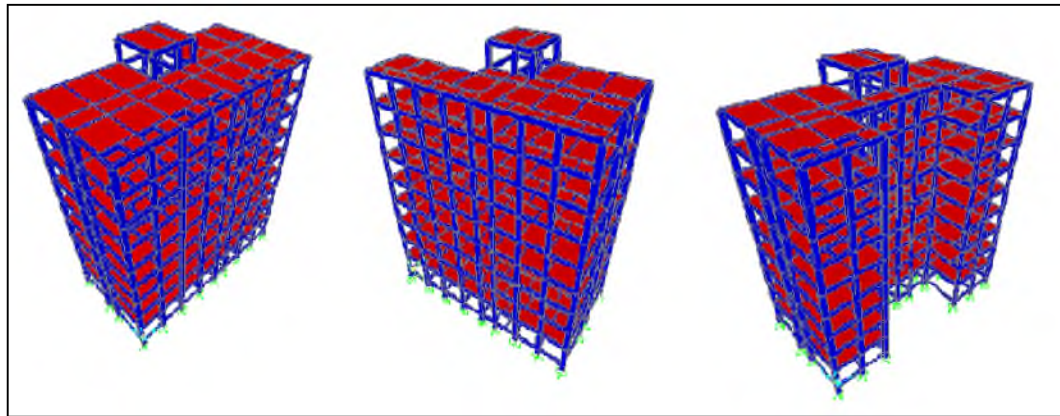


Fig 7.Symmetrical rectangular, L and C shaped building

3.2.Validation

Structure is validated by using the base shear value. Base shear value of regular building is calculated theoretically by using Equivalent lateral force method on the basis of IS 1893 (PART I):2016 code provisions and analytically by using non-linear time history analysis method.

3.3. Modal analysis

Modal analysis was carried out to determine the natural frequency and natural time period for each mode in a system. It was carried out by means of Eigen value method according to IS 1893 (Part 1): 2016.

3.4. Nonlinear time history analysis

Hilber Hughes Taylor method is used for NL-THA. Iteration procedure used for NL-THA is double integration method. For analysis, the building will be subjected to El Centro earthquake. Damping coefficient (C) is calculated for each damper by using the following equation.

$$C = 2\xi m\omega \tag{2}$$

Where ξ is the damping ratio which is taken as 5%, m is the lumped mass on each floor, ω is the fundamental frequency of the structure.

4. Results and Discussion

Base shear and maximum roof top displacement were calculated by using nonlinear time history analysis and the obtained results were compared with results of buildings with and without damper. Fundamental natural frequency of rectangular shaped building without damper is 5.78 rad/sec, L shaped building is obtained as 5.32 rad/sec and that of C shaped building is obtained as 5.61 rad/sec.

Table 3.Natural frequency of the structure

Building type	Natural frequency (Hz)				
	Without damper	With damper			
		DXB	DXF	DYB	DYF
Rectangular	0.921	1.445	1.088	1.059	1.015
L shape	1.176	0.668	0.948	1.050	0.907
C shape	1.236	0.841	1.107	0.898	0.923

From the above table it has been observed that, when dampers are arranged in longer faces (X direction) natural frequency value increases. When dampers are arranged in alternate bays increases due to increase in stiffness. Hence the flexibility of the structure also gets reduced.

Variation of base shear

Variation of base shear values in rectangular, C and L shaped building is shown in table 4. It has been observed that building with dampers arranged in alternative bays on X direction shows less base shear value.

Table 4. Variation of base shear

Building type	Base shear values (kN)				
	Without damper	With damper			
		DXB	DXF	DYB	DYF
Rectangular	1576.95	961.48	1083.93	1555.72	1557.9
L shape	1382.08	788.50	820.24	1357.88	1379.13
C shape	1262.597	764.25	765.53	1238.22	1240.53

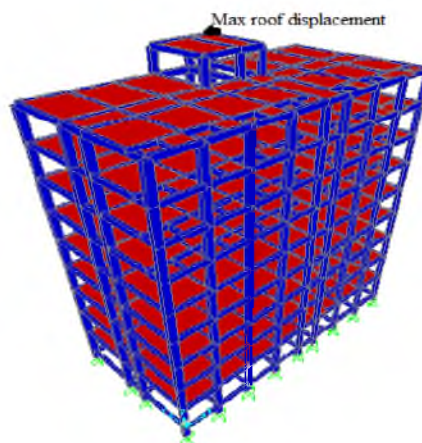


Fig 8. Maximum roof top displacement in rectangular building

Variation of roof top displacement

Table 5. Variation of roof top displacement

Building type	Roof top displacement values (m)				
	Without damper	With damper			
		DXB	DXF	DYB	DYF
Rectangular	0.0168	0.0095	0.0110	0.0162	0.0166
L shape	0.0225	0.0116	0.0127	0.0196	0.0205
C shape	0.0139	0.0086	0.0092	0.0151	0.0154

Table 5 shows the variation of roof top displacement when dampers are arranged in different configuration.

DXB arrangement shows reduction in roof top displacement in case of rectangular, C and L shaped building.

Parametric study

Parametric study is conducted by varying the aspect ratio of the building. Aspect ratio is varied from 1.5, 2.5 and 3.5, ie, number of storeys are increased as G+5, G+8 and G+13.

Table6. Variation of aspect ratio in rectangular shaped building

Aspect ratio	Roof top displacement values (m)				
	Without damper	With damper			
		DXB	DXF	DYB	DYF
1.5	0.00888	0.00467	0.0046	0.0083	0.0086
2.5	0.0139	0.00861	0.00865	0.0121	0.0115
3.5	0.0252	0.0171	0.0191	0.0201	0.01752

Table7. Variation of aspect ratio in C shaped building

Aspect ratio	Roof top displacement values (m)				
	Without damper	With damper			
		DXB	DXF	DYB	DYF
1.5	0.0112	0.0055	0.00551	0.0116	0.0117
2.5	0.0167	0.0095	0.0110	0.0162	0.0166
3.5	0.0225	0.0126	0.0134	0.0203	0.0173

Table8. Variation of aspect ratio in L shaped building

Aspect ratio	Roof top displacement values (m)				
	Without damper	With damper			
		DXB	DXF	DYB	DYF
1.5	0.0143	0.00524	0.01371	0.0135	0.0135
2.5	0.0225	0.0116	0.0127	0.0196	0.0205
3.5	0.0292	0.0127	0.0197	0.0234	0.0263

From parametric study of aspect ratio, it has been observed that when the height of the structure increases the flexibility of the structure also increases. Also, it has been observed that frequency of the structure increases when height of the building decreases. Building with 6 storeys shows higher frequency due to its lesser mass. From the above table, it has been noted that lateral displacement is more in case of building with aspect ratio 3.5 for rectangular, L and C shaped buildings.

5. Conclusions

From the results obtained from the nonlinear time history analysis it has been observed that when viscous dampers are arranged in longer sides (X direction) the base shear value and roof top displacement values decreases.

- DXB arrangement shows better seismic performance in terms of lateral displacement in case of L, C and rectangular shaped building
- DXB arrangement shows 40% reduction in base shear in case of rectangular building, 43% reduction in case of L shaped building and 39% reduction in case of C shaped building
- DXB gives 48% reduction in lateral displacement in case of rectangular, L shaped building and 38% reduction in case of C shaped building.
- Seismic response of the structure increases with increase in height of the structure

References

1. Banazadeha, M., Ghanbaria, A., and Ghanbarib, R. "Seismic performance assessment of steel moment-resisting frames equipped with linear and nonlinear fluid viscous dampers with the same damping ratio", *Journal of Constructional and Steel Research*, Vol.136, pp.215–228, 2017.
2. Ras, A. and Boumechra, N. "Seismic energy dissipation study of linear fluid viscous dampers in steel structure design", *Journal of Constructional and Steel Research*, Elsevier, Vol.4, pp. 189–249, 2017.
3. Momen, M., Ahmed, M., Raheem, A.E., Ahmed, M.M., and Aly, G. "Irregularity effects on the seismic performance of L shaped multi-story buildings", *Journal of Engineering Science*, Vol. 44, pp. 513–536, 2016.
4. Deng, P., Li, X., Dong, W., and Tai, L. "Seismic Analysis of L shaped Irregular Plane Frame Structure with Viscous Dampers", *Applied Mechanics and Materials*, Vol. 501-504, pp.1547-1550, 2014.
5. Goel, K.R., and Rai, D.C. "Seismic response control of irregular structures using nonlinear dampers", *Engineering Structures*, Vol. 2, pp.701-723, 2013.
6. Miyamoto, K.H., and Gilani, S.J. "The effectiveness of viscous dampers for structures subjected to large earthquakes", *Journal of Engineering Science*, Vol.5, pp .389-493, 2012.
7. Whittle, K.J., Williams, S.M., Karavasilis, L.T., and Blakeborough, A. "A Comparison of Viscous Damper Placement Methods for Improving Seismic Building Design", *Journal of Earthquake Engineering*, Vol.4, pp.78-95, 2012.
8. Chukwuma, S.E., and Herrera, A. "Analytical investigation of the response of a building with added viscous dampers" *Journal of Earthquake Engineering*, Vol.39, pp.381-402, 2009.
9. Jinijie, M.S., and Qingxuan, Z. "Performance based evaluation of irregular plane framed RC structures" 14th World conference on Earthquake engineering, Beijing and China, 2008.
10. IS 1893 (Part I): 2016, "Code of practice for criteria for earthquake resistant design of structures", *Bureau of Indian Standards*, New Delhi
11. IS 875 (Part I & II): 1987, "Code of practice for design loads (other than earthquake) for buildings and structures", *Bureau of Indian Standards*, New Delhi.
12. IS 456: 2000, "Code of practice for Plain and reinforced concrete", *Bureau of Indian Standards*, New Delhi.

Flexural Behaviour of RCC Beams Retrofitted with Engineered Cementitious Composite (ECC)

Jackson Vincent¹ and Jean Molly Simon²

¹PG Research Scholar, Structural Engineering, Mar Baselios College of Engineering and Technology, Thiruvananthapuram, Kerala, India

jacksonvincentb@gmail.com

²Asst. Professor, Department of Civil Engineering, Mar Baselios College of Engineering and Technology, Thiruvananthapuram, Kerala, India

jeanms17@gmail.com

Abstract. Reinforced concrete structures often have to face modifications and improvement of their performance during their service life. The main contributing factors are change in their use, new design standards, deterioration due to corrosion in the steel. In such circumstances there are two possible solutions: replacement or retrofitting. It is often better to repair or upgrade the structure by retrofitting. Out of various techniques, engineering cementitious composite is widely used nowadays. In this study, flexural failed beams specimens are retrofitted using engineering cementitious composite. The specimens are tested under two point loading for flexure specimens. The effectiveness of using engineering cementitious composite for retrofitting is studied under load- deflection graph, crack pattern and ultimate load carrying capacity of beams that are pre- loaded to 67% of ultimate load of control specimen. Increase in ultimate load of ECC-PVA retrofitted beams was 57% where as with ECC-PP retrofitted beams 54%. Increase in energy absorption capacity of ECC-PVA retrofitted beams was 126% where as with ECC-PP retrofitted beams 106% when compared with control beams.

Keywords: Engineered Cementitious Composite, Energy absorption, Ultimate load carrying capacity.

1. Introduction

Reinforced concrete structures often have to face modification and improvement of their performance during their service life. Concrete has limited ductility, low resistance to crack propagation and is weak in tension. The inherent microstructure and volumetric changes during manufacturing results in the formation of micro cracks in the material even before loading. These pre-existing cracks lead to brittle failure of the material in tension. The main contributing factors are change in their use, deterioration due to corrosion in the steel caused by exposure to an aggressive environment and accident events such as earthquakes. It is often better to repair or upgrade the structure by retrofitting. Different methods of structural strengthening or retrofitting techniques that have been developed over the years include external bonding of steel plates, glass fibre reinforced plastic (GFRP), fibre reinforced polymer (FRP) sheets, external pre- stressing, carbon fibre wrapping, external bar reinforcement and very recently improved external (bars) reinforcement techniques. The request of an increase of the bearing capacity of the existing structures due to an increase of the live loads is a typical issue in designer. This study focuses towards the development of a retrofitting system using the addition of a thin overlay of Engineered Cementitious Composite (ECC) to reinforced concrete (RC) members of M20 grade.

1.1 Engineered Cementitious Composite (ECC)

Development of FRC's started in 1970s. During the past 10 years, polyvinyl alcohol (PVA) fibre has been introduced in the production of FRC, resulting to a new composite, which exhibits a pseudo ductile behaviour similar to that of steel and is called "Engineered Cementitious Composites (ECC)" or simply bendable concrete. It was developed in 2001 by Dr. Victor Li at the University of Michigan.

However, Engineered Cementitious Composite is no longer confined to the academic research laboratory; it is finding its way into precast plants, construction sites, and repair and retrofitting jobs in countries including Japan, South Korea, Australia, Switzerland, Canada, and the United States. The new kind of material is very effective in transferring stress across the cracks and fractures and occurred with the formation of multiple cracks.

The most distinctive characteristic separating ECC from conventional concrete and fibre-reinforced concrete (FRC) is an ultimate tensile strain capacity of 3% to 5%, depending on the specific ECC mixture. This strain capacity is realized through the formation of many closely spaced micro cracks, allowing for a strain capacity over 300 times that of normal concrete. These

cracks, which carry increasing load after formation, allow the material to exhibit strain hardening, similar to many ductile metals.

Fracture properties of the cementitious matrix are carefully controlled through mix proportions. Fibre properties, such as strength, modulus of elasticity, and aspect ratio have been customized for use in ECC. The interfacial properties between fibre and matrix have also been optimized in cooperation with the manufacturer for use in this material.

2. Experimental Program

The experimental work consisted of casting and testing of beams of length 1000 mm and cross section 100 mm x 150 mm. The beams were designed according to IS 456-2000 [28]. The reinforcement details are shown in Fig.1. Two 10 mm diameter bars were used as tension reinforcement; two 8 mm bars were used as compression reinforcement 2 legged 6 mm stirrups were used at a spacing of 90 mm center to center were provided at flexural span . Strain gauges were provided on one of the two bars of each diameter. The rebars were leveled smooth on the portion where strain gauge was to be attached and then is attached using suitable adhesive. The lead wires were then soldered to the stain gauge and proper insulation were provided in order to avoid damaging of the gauge.

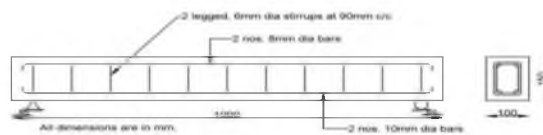


Fig.1 Reinforcement detailing for flexure and shear beam [9]

2.1 Materials Used

Materials used include Portland Pozzolanic Cement, fine aggregate and Coarse aggregate conforming to IS: 2366 (Part III) 1963, fly ash, steel reinforcements and super plasticizer were used for the investigation. The basic philosophy lies in complete elimination of coarse aggregate to impart greater homogeneity, with mineral and chemical admixture to get stronger gel formation during hydration. Poly Vinyl Alcohol and Poly Propylene fibres were used in the study with aspect ratio 100 (length 12mm, diameter 0.12mm). The mix proportion was selected from the optimum mix obtained from the trial mixes conducted in previous study. The mechanical properties were also determined for finding the optimum mixes.



Fig 2. Poly Vinyl Alcohol and Poly Propylene fiber

Table 1. Properties of fiber

Type of fibre	PVA fiber	PP fiber
Length, mm	12	12
Diameter, mm	0.12	0.12
Aspect ratio	100	100

Table 2. Mix proportion of M20

Mix	Cement (kg/m ³)	Fine aggregate (kg/m ³)	Coarse aggregate (kg/m ³)	Compressive strength (MPa)
M20	340	666.4	1326	28.50

Table 3. Mix proportion of UHPFRC Mixes

Mix	Cement	Fine Aggregate	Fly Ash	SP	Water	28 th day strength		
						Fiber PVA	ECC-PVA	ECC-PP
		Kg/m ³		l/m ³		Percentage volume		
Mix 1	587	470	704	17	300	1.25	46.70	48.10
Mix 2	587	470	704	17	300	1.50	47.90	50.20
Mix 3	587	470	704	17	300	1.75	49.90	46.90
Mix 4	587	470	704	17	300	2.00	47.50	41.30
Mix 5	587	470	704	17	300	2.25	45.40	40.80

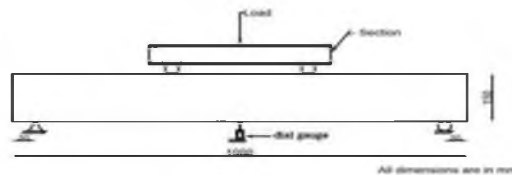
Optimum fibre content was found out and retrofitting was carried out only with the optimum mix.

2.2 Preparation of specimens

Three specimens each were prepared for control and flexural retrofitting with M20 grade concrete. The specimens were prepared and cured for 28 days. After 28 days, the specimens were tested.

2.3 Test Procedure

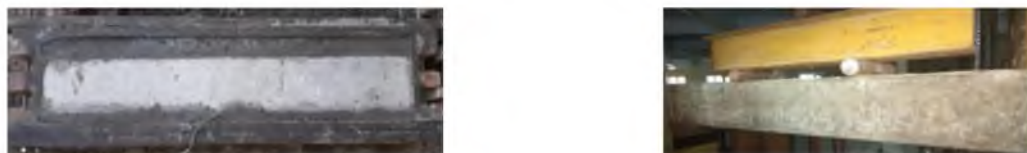
The beams were tested under two point loading. The values obtained from the dial gauge at the mid span were used to plot the load deflection curve. Strain gauges were used to measure the strains. These strain values were used for plotting the moment curvature relationship. The moment was obtained from the loading configuration. The loading configuration for two points loading is shown in Fig.3

**Fig.3** Loading configuration

2.4 Distressing and retrofitting of beam specimen

The three control beams (CB) were loaded up to failure and their ultimate loads were determined. The remaining six beams were then distressed up to 67% of the ultimate load.

The preloaded beams are then U- wrapped with ECC-PVA and ECC-PP, 2.5cm was adopted as overlay thickness and was done over the full span. Retrofitting was made easily with the help of moulds and they were demoulded and kept for curing.

**Fig.4** Preloaded and retrofitted beams

2.5 Flexural Test on Retrofitted Beams

After the completion of curing period, the beams were then tested in the universal testing machine with the same test procedure as mentioned earlier. The beams were tested in a 1000 kN universal testing machine. The flexure behaviour of the ECC-PVA retrofitted and ECC-PP retrofitted beams were compared to that of the control beams. Fig.5 shows the test setup used for the study.



Fig. 5 Test setup

3. Results and Discussion

3.1 Crack Pattern and Failure

The crack pattern for all the retrofitted and normal beams were shown in Fig.6 Cracks was not observed at the beginning of the test. After some time, cracks initiated at the flexural span of the beam. As the load increased, the existing cracks started to propagate and new cracks were also developed. At the ultimate stage most of the cracks travelled up to the mid of the beam, even though the number and size of the cracks were different in normal and retrofitted beam. The control specimen had the more number of wide cracks were noticed. During testing, the crack widths were measured using crack detection microscope of 50x magnification at load increment of 2.5kN. Crack formations in retrofitted beams were of reduced width compared to retrofitted beams as the fibers played a lead role in arresting cracks. Fig. 7 shows the crack propagation graph of all the retrofitted and normal beams. The crack width pattern was different in normal and retrofitted beam. The maximum crack width value was observed in normal beam which was 0.64 mm.



Fig. 6 Crack pattern

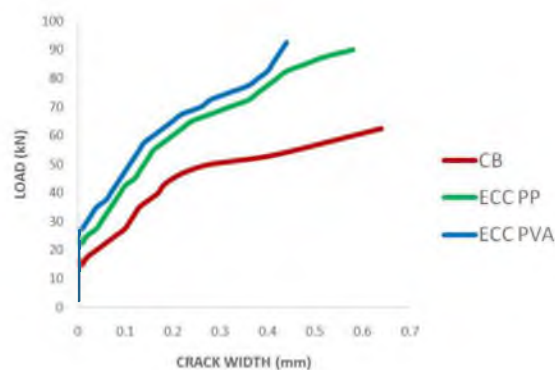


Fig. 7 Crack propagation graph

3.2 Load- Deflection Behaviour at mid span

The load and deflection values recorded during the two point loading test of beams were used to draw the load deflection graphs. Fig.8 shows the load- deflection plot of the control beam specimen and retrofitted specimens. From the load deflection

plot of shear beams, it was observed that initially the curve was linear up to certain load for the control as well as for the retrofitted specimens. For the CB, it was observed that the linearity was up to the first crack load. Further application of load causes the curve to deviate from linearity. In case of the retrofitted beams, the load carrying capacity was increased than the control beam. The fibres in ECC-PVA arrested the micro cracks developed thus improved the load carrying capacity than ECC-PP. Also the initial, yield and ultimate load was given in Table 4. Energy absorption was also found by calculating the area under the load deflection plot. Due to the limitations in the experimental set up, the load deflection graph could be plotted only up to 80 % of the peak load, in the descending portion of the curve. Thus, the energy absorption was calculated as the area under the curve up to the peak load and under the descending portion up to 80 % of the peak load. The energy absorption of beams is shown in Table 5.

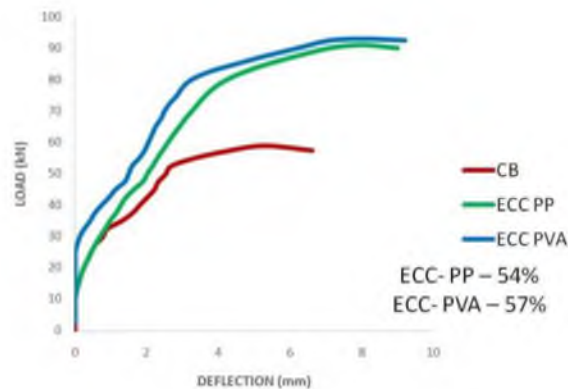


Fig. 8 Load vs deflection Plot for Flexure retrofitted beams

Table 4. Initial Yield and ultimate load values

Beam ID	Initial Crack load (kN)	Yield load (kN)	Ultimate Load (kN)	
			Absolute	Relative
CB	13	52.5	59	1
ECC- PVA	28	80	93	1.57
ECC- PP	22	77.5	91	1.54

Table 5. Energy absorption

Specimen	Energy absorption (kNmm)
CB	310.79
ECC- PVA	641.72
ECC- PP	702.71

3.3 Moment curvature relationship

Fig. 9 shows the moment curvature plot for the control and retrofitted beams. The moment curvature can be said to have three stages.

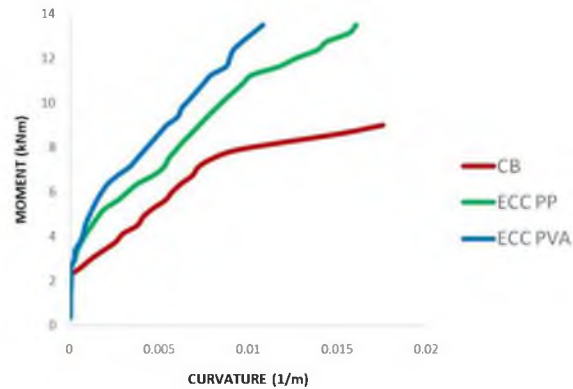


Fig.9 Moment curvature relationship

First stage is till initial cracking, second stage till yielding of tension steel and the third stage to limit of useful strain in concrete. The curve is linear up to first crack moment. Further when the moment increases, the curve shifts from linearity. When the moment reaches yield moment, the curves become flat. When steel yields, a large increase in curvature occurs with a small change in moment.

3.4. Ductility indices

Displacement ductility was calculated as the ratio between the displacements at ultimate load to the displacement at yield load. The ductility could be considered at 80% of the peak load, because this takes into account, the softening part of load deflection curve. Hence for calculating ultimate deflection, 80% of peak load is considered. Softening ductility consideration is important in seismic design and where large deformations are involved. Failure of an under reinforced beam is called tension failure.

Table 6. Ductility indices of the beams

Beam ID	Displacement ductility		Curvature ductility	
	Absolute	Relative	Absolute	Relative
CB	2.11	1	2.27	1.00
ECC- PVA	2.90	1.37	2.07	0.91
ECC- PP	2.40	1.13	2.16	0.95

This is because the primary reason of failure is the yielding of steel bars. The large increase in curvature, before collapse of the beam is an indication of ductile failure of beam. Curvature ductility was calculated as the ratio of curvature at ultimate load to that of curvature at yield load. The ductility index of the beams is shown in Table 8.

4. Conclusions

The Load deflection behaviour, crack width, energy absorption, ultimate load carrying capacity, moment curvature relationship and ductility indices mixes were studied in this work. An optimum poly vinyl alcohol fibre and polypropylene fibre volume fractions were found out based on the basis of compressive strength. Based on the results of this study, the following conclusions were made:

- An Engineering cementitious composite of strength 40 MPa was developed with an optimum of 1.5% for polypropylene fiber and 1.75% for poly vinyl alcohol fiber
- Increase in ultimate load of ECC-PVA retrofitted beams was 57% for flexure where as with ECC-PP retrofitted beams 54% for flexure
- Increase in energy absorption capacity of ECC-PVA retrofitted beams was 126% for flexure where as with ECC-PP retrofitted beams 106% for flexure

References

1. Zuanfeng, P., Chang, W. and Wei, W.: Study on Mechanical Properties of Cost- Effective Polyvinyl Alcohol Engineered Cementitious Composites, *Construction and Building Materials*,78, 397-404. (2015)
2. Zhu, Y., Zhaocai, Z. and Yan, Y.: Effect of Water-Curing Time on the Mechanical Properties of Engineered Cementitious Composites, *ASCE Materials, Civil Engineering*, 28, 123-129, (2016)
3. Jian, Z., Shunzhi, Q., Guang, Y. and Victor, C, L.: Improved Fibre distribution and Mechanical properties of Engineered Cementitious Composites by Adjusting the Mixing Sequence, *Journal of Cement & Concrete Composites*, 34, 342-348, (2012)
4. Qian, S., Zhou, J. and Schlangen, E.: Influence of Curing condition and Precracking time on the Self-Healing behaviour of Engineered Cementitious Composites, *Journal of Cement & Concrete Composites*, 32, 686-693, (2013)
5. Yu, Z., Zhaocai, Z., Yingzi, Y. and Yan, Y.: Measurement and Correlation of Ductility and Compressive strength for Engineered Cementitious Composites (ECC) produced by binary and ternary systems of binder materials: Fly ash, slag, Silica fume and Cement, *Journal of Construction and Building Materials*, 68, 192-198, (2014)
6. Mustafa, S., Zafer, B., Erdogan, O., Tahir, K., Hasan, E. and Mohamed, L.: Improving the workability and rheological properties of Engineered Cementitious Composites using factorial experimental design, *Journal of Composites: Part B*, 45, 356-368, (2016)
7. Li, V.C. "Engineered Cementitious Composites (ECC) – Material, Structural, and Durability Performance", *Concrete Construction Engineering Handbook*, Chapter 24, Ed. E. Nawy, published by CRC Press, (2015)
8. Chethan, V., Ramegowda, M. and Manohara, H. "ENGINEERED CEMENTITIOUS COMPOSITES-A REVIEW" , *International Research Journal of Engineering and Technology*, 2, 144-149, (2015)
9. Biju, B. and Krishnan, H. "Development of Ultra High Performance Concrete by Normal Curing Method" *Proceedings of National Conference on Recent Trends in Computer Science & Engineering and Sustainability in Civil Engineering* , 3, 116-118, (2016)
10. IS 2386 (Part III) - 1983 (Reaffirmed 2002), Methods of test for aggregates for concrete, *Bureau of Indian Standards*, New Delhi, India, 1983.
11. IS 10262-2009, Concrete mix proportioning- Guidelines, *Bureau of Indian Standards*, New Delhi, India, 2009.
12. ASTM C-109, Standard Test Method for Compressive Strength of Hydraulic Cement Mortars, *American Society for Testing and Materials Standard Practice*, Philadelphia, Pennsylvania, 2016.
13. ASTM C-469, Standard Test Method for Modulus of elasticity of Hydraulic Cement Mortars, *American Society for Testing and Materials Standard Practice*, Philadelphia, Pennsylvania, 2013.
14. ASTM C-1609, Standard Test Method for Modulus of rupture of Hydraulic Cement Mortars, *American Society for Testing and Materials Standard Practice*, Philadelphia, Pennsylvania, 2013.
15. ASTM C 642, Standard Test Method for Density, Absorption, and Voids in Hardened Concrete, American Society for Testing and Material Standard Practice, Pennsylvania, 2006.
16. BS-1881-1983, Method for determination of tensile splitting strength, British standards Institute, London, U.K.

Numerical Study on the Flexural Behaviour of Concrete Filled Steel Tube Beam Strengthened with CFRP

Neethu Prakash¹ and Jisha S. V.²

¹PG Research Scholar, Structural Engineering, Mar Baselios College of Engineering and Technology, Thiruvananthapuram, Kerala, India
neethusprakash94@gmail.com

²Assistant. Professor, Department of Civil Engineering, Mar Baselios College of Engineering and Technology, Thiruvananthapuram, Kerala, India

jpn.nitk@gmail.com

Abstract. Concrete filled steel tubular (CFST) beams are composite structural members with high strength and ductility than the conventional concrete and steel members. In this study the flexural behaviour of CFST beams strengthened with carbon fibre reinforced polymer (CFRP) were investigated. CFST beam of dimensions $91.5 \times 91.5 \times 3.6$ mm strengthened with CFRP of 0.5 mm thickness have been considered. Flexural behaviour was investigated by considering the effect of single layer, two layers and three layers of CFRP with different wrapping length. The study concluded that flexural strength increases with the multilayer wrapping of CFRP up to 75% length of beam and effect of wrapping length of single layer CFRP is not significant in the strength enhancement.

Keywords: CFST beam, CFRP sheet, Flexural strengthening, Finite element analysis

1. Introduction

Composite steel-concrete structural members have been widely used in the design and construction of modern steel framed buildings. Concrete Filled Steel Tubes (CFST) are one of the recently used composite structure in bridges [1], electrical power transmission structures, underground structures, heavy industrial buildings as well as in high-rise structures. It consists of a steel tube infilled with concrete and whose combined action resists the load acting on them. The composite action is developed due to the interface stresses between steel and concrete. The structure offers numerous benefits, including high strength and fire resistances, favourable ductility and large energy absorption capacity.

Compared to conventional reinforced concrete or structural steel, CFSTs have many advantages. Steel tube confines the concrete infill due to which a triaxial state of compression is developed, that increases the strength and strain capacity of the infill. Local and global buckling of steel tube is restrained by concrete infill, and hence the deformation capacity of a CFST member compared to hollow tube is increased and the steel and concrete combined action efficiently improves the stiffness and load carrying capacity. Fig.1 shows CFST beam used in a bridge at Shinkansen – Japan [1].



Fig.1. CFST beam in Bridge of Shinkansen –Japan [1]

Commonly used CFST cross sections are concrete filled in Circular Hollow Section (CHS), Square Hollow Section (SHS) and Rectangular Hollow Section (RHS), which are given in Fig.2 where B and D are the outer dimensions and t is the thickness of steel tube [2]. Circular cross section is better than the other two cross sections, since it provides more confinement to the concrete. But square and rectangular cross sections are widely used due to the easiness of construction and because of the aesthetic reasons.

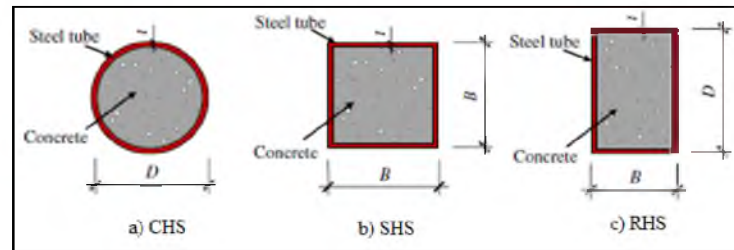


Fig.2. Typical CFST sections [2]

There are some other members included in the CFST family such as Concrete Filled Double skin Steel Tubes (CFDST), Concrete-encased CFST, CFST with additional reinforcement and Stiffened CFST.

The behaviour of CFST beam mainly depends on the interaction between steel and grout, difference in the Poisson's ratio of steel and concrete and load condition [3]. In order to work as a structural composite element, the load has to be transferred across the contact surface. The load will be transferred as shear stresses. Four mechanisms involved in the transferring of shear stresses are adhesion, micro interlocking, friction and binding. Binding mechanism is the dominant shear transfer mechanism for CFST subjected to pure bending and it is inactive in pure axial compressive loading. Micro interlocking mechanism is obtained due to the surface irregularities in the steel tube and it will assist to the shear transfer until crushing of grout is taken place. Adhesion is due to the vacuum generated in the capillaries due to the chemical process in the concrete. When two surfaces come into contact, the resistance of their internal tangential slip is expressed as friction. Buckling or plastic hinge formation is the main failure mechanism in the CFST [3]. This mechanism is generally affected by the way in which load is applied, width to thickness ratio and material strength.

2. Strengthening of CFST beam

CFST beam may require strengthening like other conventional structural members due to several reasons. They may require upgrading so that they can carry extra loads or need to be repaired due to degradation attributed to aging, fire and fatigue. Commonly used strengthening are section enlargement and external bonding of steel plate and fibres. Strengthening by replacing or adding new steel part is not economical because it needs heavy equipments and it is very time consuming. Therefore external bonding of Fibre Reinforced Polymer (FRP) had been proposed as an efficient and cost effective method. One of the popular types of FRP is the Carbon Fibre Reinforced Polymer (CFRP) fabric sheet. They are perfect for resisting environmental degradation.

Several researchers have extensively investigated the efficiency of using the CFRP material to strengthen CFST beam. Experimental investigation [4,5] on flexural behaviour of CFRP reinforced CHS, SHS and RHS tubes subjected to in-plane bending showed that strengthening effect of CFRP improved with the increase in strength ratio (β) of CFRP. The effect of CFRP strengthening on flexural behaviour of Concrete Filled Aluminium alloy circular hollow section Tubes (CFAT) is also carried out [6]. The results showed that the ultimate strength enhanced by reinforcing with the CFRP, but the ductility is deteriorated. Increase in number of CFRP layer has little influence on the ultimate strength, flexural stiffness and ductility for CFAT specimens. Strengthening of CFST beam depends on various parameters such as depth to thickness ratio, compressive strength of concrete, shear span to depth ratio, depth to width ratio, yield strength of steel tube [7]. It was found that the depth to thickness ratio, yield strength of steel tube and depth to width ratio has significant effect on ultimate moment carrying capacity of CFST beam. The performance of circular CFST beam externally reinforced by CFRP sheets under the combined actions of tension and bending were studied [8]. The main parameters considered in this study are fibre orientation, load eccentricity, number of CFRP layer. They obtained efficient increasing strength for CFRP with fibre oriented in the longitudinal direction. From literature studies, the importance for more studies to investigate the flexural behaviour of CFST beam with CFRP wrapping was identified. The effect of multiple layers and different length of CFRP sheet were investigated and is being outlined.

3. Idealisation of the beam

3.1 Concrete

Linear and non linear properties assigned for concrete. For linear properties, modulus of elasticity and Poisson's ratio were given. Poisson's ratio was given a value of 0.2 and modulus of elasticity was determined with 28 days compressive strength of concrete strength [12]. The average compressive strength of concrete was taken as 38.5 N/mm² and density is 2500 kg/m³ [13].

$$E_c = 5000 \sqrt{f_{ck}} \tag{1}$$

Where E_c is the elastic modulus of concrete and f_{ck} is the 28 days cube compressive strength of concrete.

The uniaxial stress-strain relationship [14] for concrete was constructed by compression using the following relations.

$$\epsilon_0 = \frac{2f_{ck}}{E_c} \tag{2}$$

$$f = E_c \frac{\epsilon}{1 + \frac{\epsilon^2}{\epsilon_0^2}} \tag{3}$$

Where f is the stress at any strain ϵ and ϵ_0 is the strain at ultimate compressive strength. Simplified stress strain relationship for concrete in compression is obtained and is shown in Fig.3.

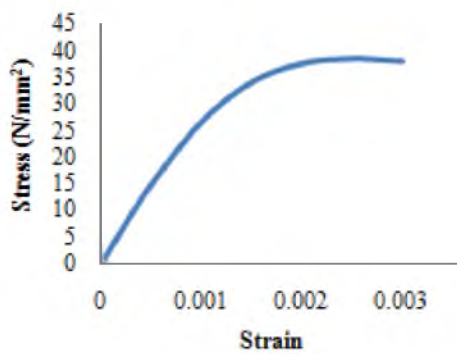


Fig.3. Stress strain relationship for concrete in compression

3.2 Steel

Cold Formed Square Hollow Section with outside dimensions of 91.5 mm square and 3.6 mm thickness [13] (91.5 x 91.5 x 3.6CF SHS) and grade YSt 240 @ 9.67 kg/m conforming to IS 4923 – 1997 and IS 1161 – 1998 [9, 10] was used in this study. Non-linear behaviour of steel was considered by specifying yield stress and tangent modulus. The tangent modulus of the steel was assumed as 0.5 percentage of its Young’s modulus and the yield stress was 240 MPa. Elastic properties such as Young’s Modulus and Poisson’s ratio were given as 200000 N/mm² and 0.3 respectively for all the specimens [11]. Density of the steel is 7500 kg/m³.

3.3 CFRP

Unidirectional CFRP sheet with thickness 0.5 mm was used in this study. Since the properties of CFRP composite are not same in all the directions, they were considered as an orthotropic material. The tensile strength and density of CFRP was 3800 N/mm² and 1720 kg/m³ respectively. Orthotropic properties of CFRP are shown in Table 1.

Table 1. Properties of CFRP [13]

Property		Value
Modulus of Elasticity (MPa)	E_x	230000
	E_y	17900
	E_z	17900
Poisson’s ratio	ν_{xy}	0.22
	ν_{yz}	0.30
	ν_{xz}	0.22
Shear modulus (MPa)	G_{xy}	11790
	G_{yz}	6880
	G_{xz}	11790

The effect of CFRP on flexural behaviour of CFST beam was evaluated for multiple layers CFRP with different wrapping length. Different wrapping lengths of CFRP sheet were applied in 50%, 75% and 100% of the effective length of beam. Details of CFST beam specimens are shown in Table 2.

Table 2. Specimen details of CFST beam

Parameter	Specimen's designation	No. of CFRP layer
Beam without CFRP	S0	—
Beam with CFRP in 50% effective length	S50-1	1
	S50-2	2
	S50-3	3
Beam with CFRP in 75% effective length	S75-1	1
	S75-2	2
	S75-3	3
Beam with CFRP in 100% effective length	S100-1	1
	S100-2	2
	S100-3	3

3.4 Adhesive

The adhesive material used in the study was MBrace saturant. It is a two part system, a resin and a hardener. The Young's modulus and Poisson's ratio of the material was 17 MPa and 0.4. It had an ultimate tensile strength of 1138 MPa. The average thickness of each adhesive layer was about 0.8 – 1.0 mm. For the present study adhesive layer of 0.8 mm was considered.

3.5 CFST beam

The simply supported CFST beam had a cross sectional dimension and total length of 91.5x 91.5 x 3.6 mm and 1500 mm respectively. CFRP is provided in the bottom flange of beam for an effective length of 1400 mm. The dimensions of beam are illustrated in Fig.4.

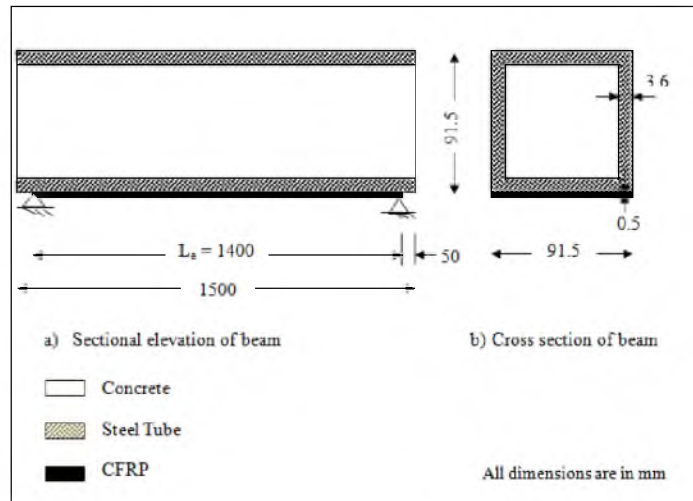


Fig.4. Dimensions of CFST beam [13]

The CFRP patch technique [15] was proposed to represent the multiple CFRP layer, including the adhesive layer in between them and transferring them to one equivalent layer. Here total three numbers of layers was considered. The present study assumed that all of the adhesive layers which are located in between CFRP layers have constant thickness and width. The total thickness of CFRP patch was evaluated as follows:

$$t_{cfpr,patch} = (n t_{cfpr}) + (n - 1) t_{ad} \tag{4}$$

Where $t_{\text{cfrp,patch}}$, t_{cfrp} and t_{ad} are the equivalent thickness of CFRP patch, thickness of single CFRP sheet and thickness of single adhesive layer respectively, and n is the number of CFRP layer used in CFRP patch.

4. Finite Element Analysis

The structural behaviour of square CFST beam with CFRP strengthening was investigated by finite element method using ANSYS software.

Concrete, steel tube and CFRP was modelled using eight noded brick elements having three translation degrees of freedom at each node. For concrete Solid 65 element was used. It has special cracking and crushing capabilities along with the ability of creep and plastic deformation. For steel tube and CFRP Solid 185 element was used. It has plasticity, creep, swelling, stress stiffening, large deflection, and large strain capabilities. Concentrated loads were applied at one third span of the steel tube from both the ends. For simply supported beam condition, the vertical displacement of bottom flange of steel tube was restrained and also all the rotational degree of freedom were released to allow rotation. The whole beam was discretised longitudinally with elements of 20 mm size.

5. Validation of CFST beam

The CFST beam was validated by comparing the numerical study presented here with the experimental investigation of Sundarraja and Prabhu (2011). The comparison of load – midspan deflection of CFST beam with and without CFRP is depicted in Fig.5 and Fig.6 respectively.

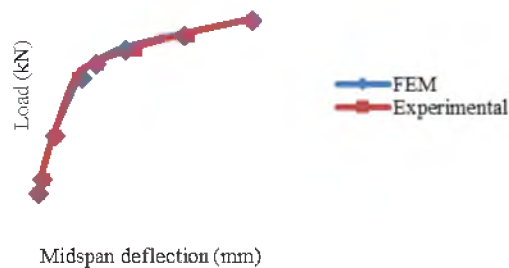


Fig.5. Load- Midspan deflection of validated beam without CFRP

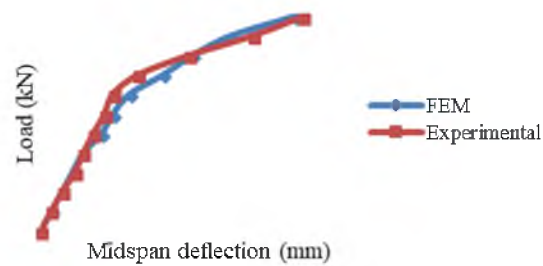


Fig.6. Load- Midspan deflection of validated beam with single layer of CFRP

The pattern of load – midspan deflection is almost same for numerical and experimental investigation [13] in both the cases. Thus the developed CFST beam is capable of showing the response under similar loading conditions.

6. Results and Discussion

6.1. Effect of retrofitting with CFRP

The flexural behaviour of CFST beam with and without CFRP layer was analysed. The deflection behaviour of S0 and S100-1 under same loading of 120 kN is shown in Fig.7. Maximum deflection was occurring at the midspan of the beam. Comparison of load- midspan deflection curve of S0 and S100-1 is shown in Fig.8. From that there was a maximum reduction of 21% for S100-1 from S0 due to external bonding of CFRP.

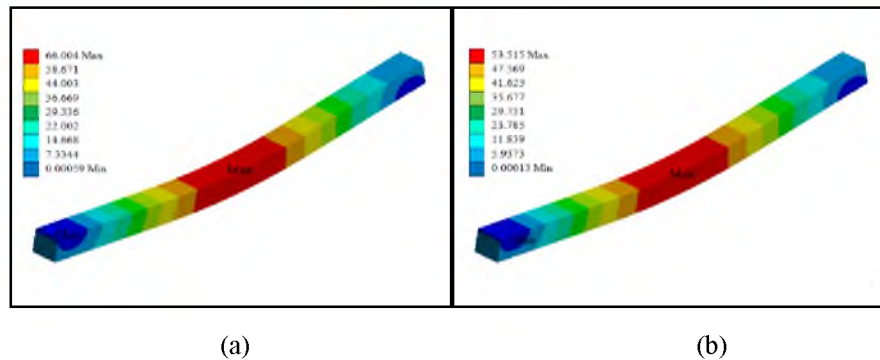


Fig.7. Deflection behaviour of (a) S0 and (b) S100-1

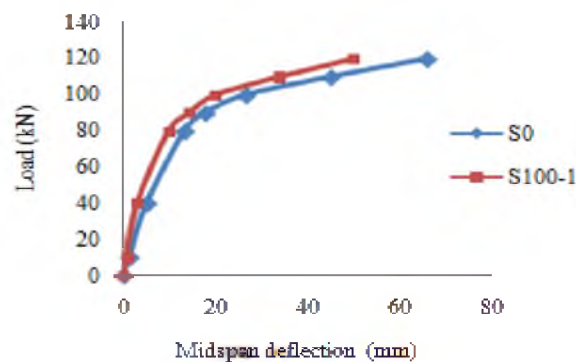


Fig.8. Comparison of load- midspan deflection behaviour of beam S0 and S100-1

6.2. Effect of length and multiple layer of CFRP

The variations in midspan deflection of the beams with increase in number of CFRP layer for 50%, 75% and 100% wrapping length were compared with CFST beam without any CFRP layer.

The load- midspan deflection of beam with multiple layers CFRP in 50% beam length is illustrated in Fig.9. It can be seen that there is a gradual reduction in the midspan deflection of beam by increasing the number of layers. The results showed that the midspan deflection was reduced by 17.75%, 34.3% and 42.27% for beam with one, two and three layer of CFRP respectively from beam without CFRP strengthening. During the initial loading stage, no changes were observed in the deflection until they achieved the ultimate capacities. For 50% wrapping of CFRP the slight change in the reduction of deflection is due delamination failure. This failure may be attributed to the enormous amount of peeling stress, which occurred along the bonding surfaces between steel and CFRP sheet. Because CFRP sheet with 50% strengthening lengths were located within the high peeling stress zone and large bending stress at the peeling points result in delamination failure. Generally the peeling stress is proportional to bending stress.

The load- midspan deflection of beam with multiple layers CFRP in 75% and 100% beam length are shown in Fig.10 and Fig.11.



Fig.9. Comparison of load – midspan deflection for beam with CFRP in 50% length

For 75% strengthening lengths, the peeling stress could be overcome by the bonding strength between the CFRP sheet and steel tube, thus preventing the delamination failure. Thus there is an enhancement in the reduction of midspan deflection for beam with CFRP in 75% length. It can be observed that midspan deflection was reduced by 18% for single layer of CFRP and the percentage reduction was increases to 42.47% and 67.23% when strengthened with two and three layer respectively.

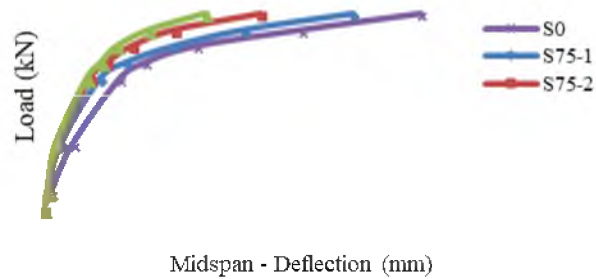


Fig.10. Comparison of load – midspan deflection for beam with CFRP in 75% length

Similar load – midspan deflection behaviour were observed for 100% wrapping length. It can be observed that midspan deflection was reduced by 21% for single layer of CFRP and the percentage reduction was 25.67% and 46.6% higher the value of 1 layer CFRP strengthening for two and three layer respectively.

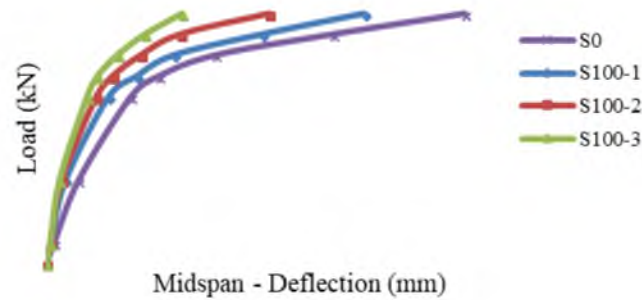


Fig.11. Comparison of load – midspan deflection for beam with CFRP in 100% length

A comparative study of percentage reduction of midspan deflection for different wrapping length with multiple layers CFRP listed in Table 3. The midspan deflection of the CFST beam was decreased with strengthening using CFRP. But there was no significant enhancement in the reduction of midspan deflection for CFST beam wrapped in 50%, 75% and 100% of their effective lengths when applied with one layer of CFRP sheet. It is also observed that there was not much difference between the midspan deflection values of the beam wrapped with 75% and 100% of their lengths when the CFRP patch was increased up to three layers.

Table 3. Percentage reduction of midspan deflection from CFST beam without CFRP

Wrapping length (%)	% reduction of midspan deflection for		
	1 layer	2 layer	3 layer
50	17.75	34.30	42.27
75	18.00	42.47	67.23
100	21.00	46.47	67.60

The load carrying capacity of the strengthened CFST beams with three number of CFRP layer increased by 7%, 21% and 23.5% for 50%, 75% and 100% wrapping length respectively when compared with CFST beam without any CFRP strengthening.

7. Conclusions

The numerical analysis of CFST beam strengthened with CFRP was conducted and the flexural behaviour was studied. Based on the investigation the following conclusions were arrived.

- The effect of CFRP retrofitting in CFST beam shows an improvement in flexural strength.
- Effect of wrapping length of single layer of CFRP is not significant in the strength enhancement. Because almost same percentage reduction in deflection was obtained for 50%, 75% and 100% wrapping length.
- Flexural strength increases with the multiple layers wrapping of CFRP up to 75% length of beam. That is, almost same percentage reduction of midspan deflection was achieved for 75% and 100% wrapping length. Hence, CFRP strengthening up to 75% length can be consider as an effective method for retrofitting CFST beam

References

1. https://en.wikipedia.org/wiki/Bridge_of_Shinkansen-Japan, downloaded on 06/01/2018.
2. Han, L. H., Li, W., Bjorhovde, R.: Developments and advanced applications of concrete-filled steel tubular (CFST) structures: Members, Journal of Constructional Steel Research, 100, 211-228 (2014).
3. Hansen, H.: Numerical and experimental study of partially concrete filled circular steel sections, Master's Thesis, Aalborg University (2011).

4. Feng, R., Wei, W., Huang, J., Huangd, J.: Experimental and numerical investigations on flexural behaviour of CFRP reinforced concrete-filled stainless steel CHS tubes, *Engineering Structures*, 156, 305-321 (2018).
5. Chen, Y., Feng, F., He, K., Chen, X., Huangd, J.: Flexural behaviour of concrete-filled stainless steel SHS and RHS tubes strengthened by CFRP, *Thin-Walled Structures*, 122, 208-229 (2018)
6. Chen, Y., Feng, R., Xu, J.: Flexural behaviour of CFRP strengthened concrete-filled aluminium alloy CHS tubes, *Construction and Building Materials*, 142, 395-319 (2017).
7. Javed, M. F., Sulong, R. N. H., Menon, S. A., Rehman, S. K., Khan, N. B.: Finite element modelling of the flexural behaviour of square and rectangular steel tubes filled with normal and high strength concrete, *Thin walled structures*, 119, 470-481 (2017).
8. Wang, Z. B., Yu, Q., Tao, Z.: Behaviour of CFRP externally reinforced circular CFST member under combined tension and bending, *Journal of Construction Steel Research*, 106, 122-137 (2014).
9. IS 4923: 1997, Hollow steel section for structural use – specification, Bureau of Indian Standards, New Delhi, India.
10. IS 1161: 1998, Steel tubes for structural purposes – specification, Bureau of Indian Standards, New Delhi, India.
11. IS 800: 2007, General construction in Steel – code of practice, Bureau of Indian Standards, New Delhi, India.
12. IS 456: 2000, Plain and reinforced concrete code of practice, Bureau of Indian Standards, New Delhi, India.
13. Sundarraja, M. C., Prabhu, G. G.: Finite element modelling of CFRP jacketed CFST members under flexural loading, *Thin-Walled Structures*, 49, 1483-1491 (2011).
14. Zand, A. A. W., Badaruzzaman, W. H., Mtalib, A. A., Hilo, S. J.: Finite element analysis of square CFST beam strengthened by CFRP composite material, *Thin -walled structures*, 96, 348-358 (2015).
15. Zand, A. A. W., Badaruzzaman, W. H., Mtalib, A. A., Hilo, S. J.: The enhanced performance of CFST beams using different strengthening schemes involving unidirectional CFRP sheet: An experimental study, *Engineering Structures*, 108, 184-198 (2016).

Flexural Behaviour of Hybrid Fibre Reinforced High Strength Concrete

Kalyani Laxman¹ and Akhil Raj S. R.²

¹PG Research Scholar, Structural Engineering, Mar Baselios College of Engineering and Technology, Thiruvananthapuram, Kerala, India

kalyaniprasadlaxman@gmail.com

²Asst. Professor, Department of Civil Engineering, Mar Baselios College of Engineering and Technology, Thiruvananthapuram, Kerala, India

akhil.raj@mbcet.ac.in

Abstract. Hybrid Fibre Reinforced Concrete is a type of concrete in which more than one type of small closely spaced and uniformly dispersed fibres are added to concrete to act as crack resistor and to substantially improve its properties. The use of two or more types of fibres in a suitable combination may potentially not only improve the overall properties of concrete, but may also result in performance synergy. In this study steel fibres and polyester fibres were used as hybrid fibres. They were used in different proportions (0.25%, 0.5%, 0.75%, 1% and 1.25% volume of concrete for steel fibre and 0.2%, 0.4%, 0.6% weight of concrete for polyester fibre). Experiments were conducted to study the effect of steel fibre and polyester fibre in different proportions in hardened concrete. Reinforced concrete beams were tested under two point loading to determine the flexural strength. From the study it was concluded that 0.75% volume fraction of steel fibre and 0.4% volume fraction of polyester fibre gave better performance with respect to hardened tests and hence their flexural characteristics were studied. 16% increase in ultimate load for hybrid beam specimen was observed. Improvements in different characteristics were accounted due to the bridging effect of the fibre.

Keywords: Hybrid Fibre Reinforced Concrete, Steel Fibre Reinforced Concrete, Polyester Fibre Reinforced Concrete, Flexural Behaviour, Two Point Loading

1. Introduction

Concrete is not able to resist direct tension (in comparison of its ability to resist direct compression) because of its low tensile strength and brittle nature. Plain concrete is weak in tension because it develops numerous microcracks when loading is applied. These micro cracks propagate in the concrete matrix under constant applied load. Consequently, plain concrete members cannot sustain tensile stresses developed due to the applied force without the addition of reinforcing elements that are able to withstand these stresses. The addition of randomly distributed discrete fibres to the structural concrete increases its stiffness, ductility and load carrying capacity, while at the same time reduced crack development and propagation. Positive synergy of different fibres can complement each other to make a new composite material with high performance and good economic benefits [1]. A composite can be termed as hybrid, if two or more types of fibres are rationally combined in a common matrix to produce a composite that drives benefits from each of the individual's fibres and exhibits a synergetic response.

Due to the rapid development in Hybrid Fibre Reinforced Concrete (HFRC) and its extensive applications, HFRC is becoming increasingly popular. HFRC has higher strength, deformation ability and energy dissipation ability than Plain Concrete (PC), it can improve the hysteretic behaviour of columns [2] and decrease the surface cracks in road pavement which consequently improves its service life. HFRC can also be used to retrofit the reinforced concrete members after an earthquake or long service life and mitigate the spread of cracks in concrete structures. Applications of HFRC include any kind of construction because of its unique properties and its high range of strength values. Some of the pioneering applications are in bridges, tunnel linings, building components like column, sandwich structure like steel concrete structure, industrial flooring, machine foundation etc. Addition of short discontinuous fibres plays an important role in the improvement of mechanical properties of concrete. It increases elastic modulus, decreases brittleness; controls crack initiation and its subsequent growth and propagation. Debonding and pull out of the fibre require more energy absorption, resulting in a substantial increase in the toughness and fracture resistance of the materials to the cyclic and dynamic loads [3].

The main advantage of hybrid fibre reinforced concrete is to impart strength and toughness by providing a system in which one type of fibre stronger and stiffer, improves the first cracks stress and ultimate strength, and the second types of fibre, which is more flexible, and ductile leads to improved toughness and strain in the past cracking zone[4].

1.1 Steel Fibre Reinforced Concrete

Steel Fibre Reinforced Concrete (SFRC) maybe termed as concrete containing cement, water, fine or fine and coarse aggregates, and discontinuous discrete steel fibres. It may also contain pozzolanaos and other admixtures commonly used in conventional concrete. Steel fibres are added to concrete to improve the structural properties, particularly tensile and flexural strength. The extent of improvement in the mechanical properties achieved with SFRC over those of plain concrete depends on several factors, such as shape, size, volume, percentage and distribution of fibres [5].

1.2. Polyester Fibre Reinforced Concrete

Polyester fibre has improved impact strength as they have higher modulus of elasticity. These are defined as polymers containing -CO-O- groups in the main chain. This definition excludes polymers of esters such as vinyl acetate and methyl/ methacrylate since in these polymers the ester groups reside in the side-chains and not in the polymer backbone. [7]. Polyester fibre prevents the micro shrinkage cracks developed during hydration, making the structure/plaster/component inherently stronger. The modulus of elasticity of this fibre is high with respect to the modulus of elasticity of the concrete or mortar binder. Hence it helps in increasing flexural strength [8].

2. Experimental Program

The experimental work consisted of casting and testing of beams of length 1000 mm and cross section 100 mm x 150 mm. Two numbers of 10mm diameter bars were provided as tension reinforcement and two numbers of 8mm diameter bars were provided as compression reinforcements. 6mm diameter bars at 90mm centre to centre spacing were provided as stirrups. Fig.1 shows reinforcement details. Strain gauges were provided on one of the two bars of each diameter. The rebars were levelled smooth on the portion where strain gauge was to be attached and then is attached using suitable adhesive. The lead wires were then soldered to the stain gauge and proper insulation were provided in order to avoid damaging of the gauge. The strain readings were measured using strain indicator and for measuring the central deflection dial gauges were used. Testing of beams were carries out using an Universal testing machine of 1000kN capacity and delection, strain readings and crack propogation were measured at each 2.5kN increment of loading.

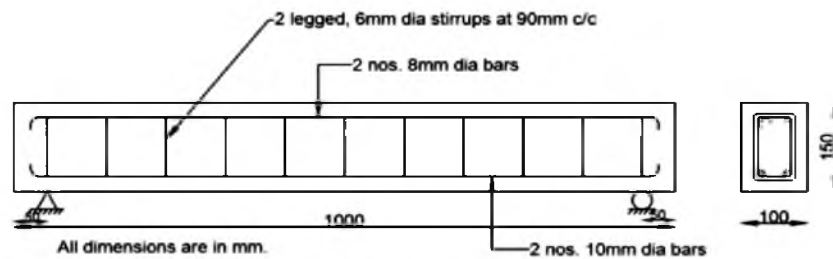


Fig.1. Reinforcement detailing [2]

2.1 Materials Used

Portland Pozzolano cement conforming to IS: 4031(part 5) 1988, aggregate conforming to IS 383-2016. Two types of fibres were used in the study of aspect ratio 60 (crimped steel fibre 30mm length and 0.5mm diameter) and polyester fibre of aspect ratio 340. The mix proportion for M50 concrete(NHSC) was selected from the optimum mix obtained from the trial mixes. The mechanical properties were also determined for finding the optimum mixes. The optimum percentage by volume of steel fibre to be added to steel fibre reinforced high strength concrete (SFRHSC) was selected from the optimum compressive strength of trial mixes. Optimum percentage of polyester fibre by weight of concrete to be added to the hybrid fibre reinforced high strength concrete (HFRHSC) was also selected from the optimum compressive strength of trial mixes.



Fig. 2. Crimped steel fibres



Fig. 3. Polyester fibres

Table 1. Properties of fibres

Type of fibre	Crimped steel fibre	Polyester fibre
Aspect ratio	60	340
Density (kg/m ³)	7810	1360

Table 2. Mix proportion of M50 mix

Mix	Cement (kg/m ³)	Fine aggregate (kg/m ³)	Coarse aggregate (kg/m ³)	w/c ratio	Water (kg)	Slump (mm)	Compressive strength	w/c ratio
M50	420	719	1382	0.35	147	85	58.10	0.35

2.2 Preparation of specimens

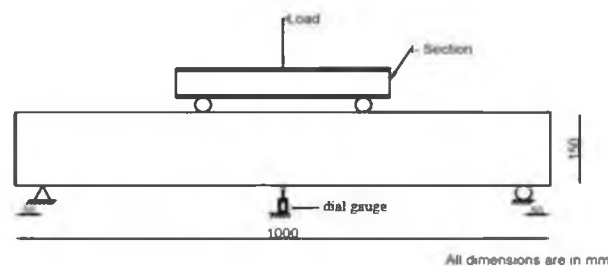
Total of 9 beam specimens were prepared with M50 grade concrete. The specimens were prepared and cured for 28 days. After 28 days, the specimens were tested.

Table 3. Specimen details

Specimen ID	Size	No. of specimens
NHSC		3
SFRHSC	100mm x 150mm x 1000mm	3
HFRHSC		3

2.3 Test Procedure

The beams were tested under two point loading. The values obtained from the dial gauge at the mid span were used to plot the load deflection curve. Strain gauges were used to measure the strains. These strain values were used for plotting the moment curvature relationship. The moment was obtained from the loading configuration. The loading configuration for two points loading is shown in Fig.4.

**Fig.4.** Loading configuration

2.6 Flexural Test on Retrofitted Beams

The flexural behaviour of RC beams of and their respective control mixes were compared and results obtained are shown below. After the completion of curing period, the beams were tested in the Universal Testing Machine (UTM). The beams were tested in a 1000 kN UTM. The flexural behaviour of the SFRHSC and HFRHSC beams were compared to that of the control beam. Fig.5 shows the test setup used for the study.



Fig.5. Test setup

3. Results and Discussion

3.1 Compressive strength and slump values of SFRHSC and HFRHSC mixes

Compressive strength and slump values of trial mixes were given in Table 5 and from the results optimum fibre content for crimped steel were found out as 0.75 % and that for polyester fibre were found out as 0.4%. Tests were conducted based on IS code.

Table 5. Compressive strength and slump values of UHPC and UHPFRC mixes

Mix designation	Compressive strength (N/mm ²)
SFRHSC-0.25	53.33
SFRHSC-0.50	57.37
SFRHSC-0.75	58.99
SFRHSC-1.00	52.00
SFRHSC-1.25	48.88
SFRHSC-0.25	53.33
SFRHSC-0.75, HFRHSC-0.2	59.6
SFRHSC-0.75, HFRHSC-0.4	62.1
SFRHSC-0.75, HFRHSC-0.6	55.5

3.2 Hardened properties of NHSC, SFRHSC and HFRHSC mixes

Some of the hardened properties were also studied and the results were given in Table 6. All the tests were done according to IS codes.

Table 3. Mechanical Properties of NHSC, SFRHSC and HFRHSC

Mix	Cylinder compressive strength (N/mm ²)	Split tensile strength (N/mm ²)	Modulus of elasticity (N/mm ²)	Modulus of rupture/ flexural strength (N/mm ²)
NHSC	47.06	5.2	3.57x10 ⁴	6.2
SFRHSC	48.9	5.7	3.67x10 ⁴	6.8
HFRHSC	49.6	5.8	3.92x10 ⁴	6.9

From the results it was clear that the addition of steel fibre and polyester hybrid had improved the mechanical properties of the mix

3.3 Crack Pattern and Failure

The crack pattern for control beam, SFRHSC and HFRHSC beams were shown in Fig.8. Cracks were not observed at the beginning of the test. After some time, shear cracks initiated at shear zone. As the load increased, the existing cracks started to propagate and new cracks were also developed.

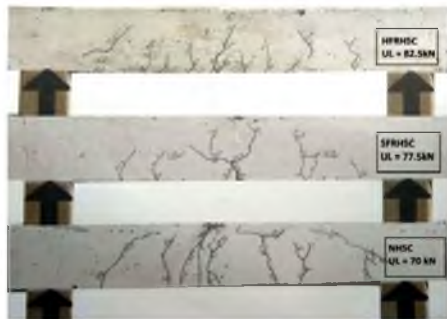


Fig. 8. Crack pattern

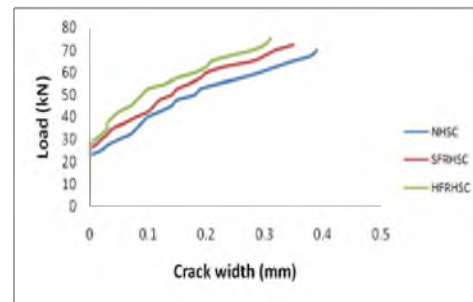


Fig.9. Crack propagation graph

After the initial crack developed in the specimen, with each increment in the load the width of the initial crack was observed using crack detecting microscope and width was noted. The crack width propagation of various optimum mix is shown in Fig.9. The crack width propagation of both HFRHSC and SFRHSC beams were slightly lower than control specimens and the final crack width was also reduced.

3.4 Load-Deflection Behaviour at mid span

The load-deflection curve for beam specimens were plotted as shown in Fig.10.

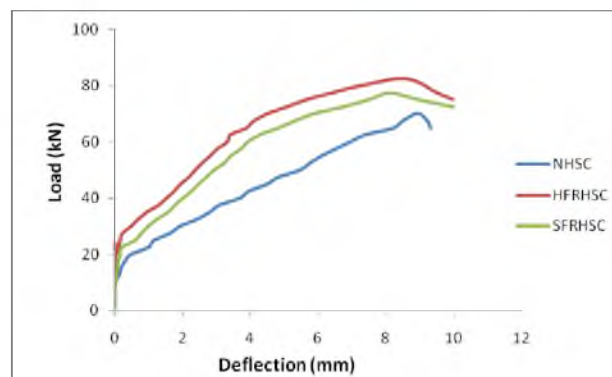


Fig. 10. Load-deflection plot for shear retrofitted beams

It was observed that the curves for HFRHSC and SFRHSC specimens showed similar load-deflection behaviour with control specimens. There is a linear portion till initial cracking and thereafter, non-linearly varying curve till the yield load. Beyond the yield point, the deflection of the beams increased until the ultimate load was reached. It was observed that by the addition of fiber the load carrying capacity of the beams increased. Deflection was more in HFRHSC and SFRHSC after yielding compared to control beams. This shows the improved ductility behaviour of HFRHSC and SFRHSC beam specimens. This is due to the tensile properties of steel fibre.

The initial, yield and ultimate loads are given in Table 7. Energy absorption was also found by calculating the area under the load deflection plot. Due to the limitations in the experimental set up, the load deflection graph could be plotted only up to 80 % of the peak load, in the descending portion of the curve. Thus, the energy absorption was calculated as the area under the curve up to the peak load and under the descending portion up to 80 % of the peak load. The energy absorption of beams is shown in Table 8.

Table 7 Initial, yield and ultimate load values

Beam ID	Initial Crack load (kN)	Yield load (kN)	Ultimate Load (kN)	
			Absolute	Relative
NHSC	22	58	71	1
SFRHSC	26	65	77.5	1.09
HFRHSC	28	67.5	82.5	1.16

Displacement ductility could be calculated as the ratio between the displacements at ultimate load to the displacement at yield load. The ductility could be considered at 80% of the peak load, because this takes into account, the softening part of load deflection curve. Hence for calculating ultimate deflection, 80% of peak load is considered. Softening ductility consideration is important in seismic design and where large deformations are involved. Failure of an under reinforced beam is called tension failure.

Table 8. Energy absorption capacity and ductility indices of beams

Specimen	Energy Absorption Capacity (kNmm)	Displacement Ductility		Curvature Ductility	
		Absolute	Relative	Absolute	Relative
NHSC	423.25	1.37	1	1.64	1
SFRHSC	587.28	1.69	1.23	2.20	1.34
HFRHSC	642.85	2.09	1.52	2.42	1.47

This is because the primary reason of failure is the yielding of steel bars. The large increase in curvature, before collapse of the beam is an indication of ductile failure of beam. Curvature ductility was calculated as the ratio of curvature at ultimate load to that of curvature at yield load. The ductility index of the beams is shown in Table 8.

3.5 Moment curvature relationship

Moment curvature plot for the control, SFRHSC, HFRHSC beams were given in Fig.11. The moment curvature can be said to have three stages.

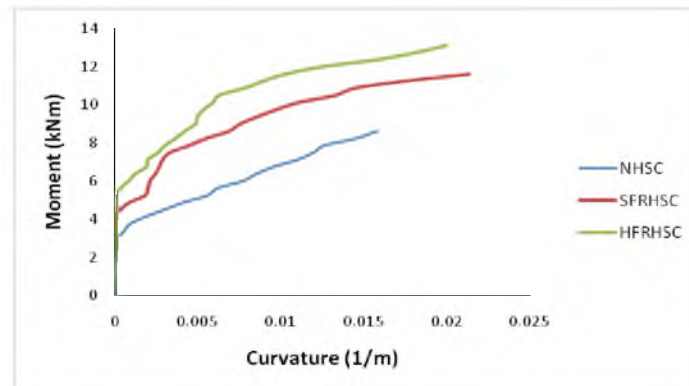


Fig. 11. Moment curvature relationship

First stage is till initial cracking, second stage till yielding of tension steel and the third stage to limit of useful strain in concrete. The curve is linear up to first crack moment. Further when the moment increases, the curve shifts from linearity. When the moment reaches yield moment, the curves become flat. When steel yields, a large increase in curvature occurs with a small change in moment.

4. Conclusions

From the experimental investigation conducted, the load deflection behaviour, crack width, energy absorption, ultimate load carrying capacity, moment curvature relationship and ductility indices of the mixes were studied and based on the results obtained, the following conclusions were made:

- The failure of the beams of both the mixes was in flexural mode.
- Deflection is more for SFRHSC and HFRHSC beam specimens. This proves the improved ductility characteristics of SFRHSC and HFRHSC mix.
- The energy absorption value obtained from the load deflection graph in SFRHSC and HFRHSC beams was greater than that of NHSC beams by 38% and 51% respectively. The displacement ductility and curvature ductility index obtained was highest in the HFRHSC specimens.
- An improvement in the flexural properties maybe due to the bridging effect of fibres in hybrid fibre reinforced concrete.

References

1. Zhong,X.L., Chang,H.L., Yun,D.S and Xiao,J.Z. (2017) Experimental investigation on mechanical properties of Hybrid Fibre Reinforced Concrete, *Construction and Building Materials*, 157, 930-942
2. Banthia,N and Gupta,R. (2004) Hybrid Fibre Reinforced Concrete(HyFRC): fibre synergy in high strength matrices, *Materials and Structures*, 37, 707-716
3. Ganesan,N., Indira,P.V and Sabeena,M.V. (2014) Bond stress slip response of bars embedded in hybrid fibre reinforced high performance concrete, *Construction and Building Materials*, 50, 108-115
4. Mohankar,R.H., Pidurkar,M.D. , Thakre,P.V and Pakhare,S.S. (2016) Hybrid Fibre Reinforced Concrete, *International Journal of Science, Engineering and Technology Research*,5, 1-4
5. Yifei,H and Hong,H. (2017) Pull-out behaviour of spiral-shaped steel fibres from normal-strength concrete matrix, *Construction and Building Materials*, 139, 34-44
6. Chanh,N.V. (2014) Steel Fiber Reinforced Concrete, *Concrete International Design and Construction*, 22,108-116
7. Zhihong,Z and Dorel,F. (1995) Synthetic Fibre Reinforced Concrete, *Polymer Science*, 20, 185-210
8. Ansari,S and Sharma,H.S. (2017), Comparison of properties of Fiber Mix Reinforced Concrete & Conventional Concrete, *International Journal of Engineering Science and Computing*, 7, 12202-12205
9. Wan,A.W.J., Ibrahim,I.S and Abdul,R.M.S (2013) Flexural behaviour of reinforced concrete beams with discrete steel – polypropylene fibres, *SICEST*, 101, 1-6
10. Soulioti,D.V., Barkoula,N.M., Paipetis,A and Matikas,T.E (2009) Effects of Fibre Geometry and Volume Fraction on the Flexural Behaviour of Steel-Fibre Reinforced Concrete, *International Journal for Experimental Mechanics*, 47, 535-541
11. Gao,J., Wei,S and Morino,K (1997), Mechanical Properties of Steel Fiber-reinforced, High-strength, Lightweight Concrete, *Cement and Concrete Composites*, 307-313
12. Mathda,V.S and Khair,H.K (2016) Study of Effects of Polyester Fibers on Compressive Strength of Concrete, *International Journal for Research in Applied Science & Engineering Technology*, 4, 53-56
13. Yun,H.D., Yang,I.D., Kim,S.W., Jeon,E.W., Choi,C.S and Fukuyama,H (2007) Mechanical properties of high-performance hybrid-fibre-reinforced cementitious composites (HPHFRCCs), *Magazine of Concrete Research*,59, 257-271
14. Huang,L., Yin,C., Lihua,X., Ping,C and Aoli,Z (2016) Local bond performance of rebar embedded in steel-polypropylene hybrid fiber reinforced concrete under monotonic and cyclic loading, *Construction and Building Materials*, 103, 77-92
15. Yoo,D.Y and Banthia,N (2016) Experimental and numerical analysis of the flexural response of amorphous metallic fiber reinforced concrete, *Materials and structures*, 1, 50-64
16. Ali,E and Gökhan,K (2016) The effects of material properties on bond strength between reinforcing bar and concrete exposed to high temperature, *Construction and Building materials*, 112, 691-698
17. Al-Shannag,M.J and Charif,A (2017) Bond behavior of steel bars embedded in concretes made with natural lightweight aggregates, *Elsevier Journal of King Saud University - Engineering Sciences*, 29, 365 - 372
18. Shen,D., Shi,X., Zhang,H., Duan,X and Jiang,G(2016) Experimental study of early-age bond behavior between high strength concrete and steel bars using a pull-out test, *Elsevier Construction and Building Materials*, 113, 653 - 663
19. Garcia-Taengua,E., Marti-Vargas,J.R and Serna,P (2016) Bond of reinforcing bars to steel fiber reinforced concrete, *Elsevier Construction and Building Materials*, 105, 275 - 284
20. Arul,R.C and Baskar,K (2017) Experimental Investigation on Flexural Behaviour of Steel Fibre and Nylon Fibre Reinforced Concrete Beam, *International Conference on Recent Trends in Civil Engineering, Technology and Management*, 82-91

21. Pravin,B.S., Sangita,V.P and Kulkarni,V.P (2015) Flexural Behavior of Hybrid Fiber Reinforced Concrete Deep Beam and Effect of Steel & Polypropylene Fiber on Mechanical Properties of Concrete, *International Journal of Advance Research In Science And Engineering*, 4, 63-73
22. Seara-Paza,S., Gonzalez-Fonteboab,B., Martinez-Abellab,F and Eiras-Lopez,J (2018) Flexural performance of reinforced concrete beams made with recycled concrete coarse aggregate, *Elsevier Engineering Structures*,156, 32 - 45
23. Mohammed,T.U., Das,H.K., Mahmood,A.H., Rahman,M.N and Awal,M.A (2017) Flexural performance of RC beams made with recycled brick aggregate, *Elsevier Construction and Building Materials*, 134, 67-74
24. Hawileh,R.A., Abdalla,J.A., Fardmanesh,F., Shahsana,P and Khalili,A (2017) Performance of reinforced concrete beams cast with different percentages of GGBS replacement to cement, *Elsevier Archives of Civil and Mechanical Engineering*, 17, 511 -519
25. Qeshta,I.M.I., Shafiqh,P and Jumaat,M.Z (2015) Flexural behaviour of RC beams strengthened with wire mesh-epoxy composite, *Elsevier Construction and Building Materials*, 79, 104 - 114
26. IS 1489 (Part I) -1991 IS 1489 (Part I) (Reaffirmed 2005), Specification for Portland pozzolana cement, Part 1: Flyash based, *Bureau of Indian Standards*, New Delhi, India
27. IS 383- 2016 (Reaffirmed 2002) Specification for Coarse and Fine Aggregates From Natural Sources For Concrete, *Bureau of Indian Standards*, New Delhi, India, 2016
28. IS 2386 (Part III) - 1983 (Reaffirmed 2002) Methods of test for aggregates for concrete, *Bureau of Indian Standards*, New Delhi, India, 1983
29. IS 1608-2005 (ISO 6892- 1998), Metallic Materials- Tensile Testing at Ambient Temperature, *Bureau of Indian Standards*, New Delhi, India
30. IS 10262-2009, Concrete mix proportioning- Guidelines, *Bureau of Indian Standards*, New Delhi, India
31. IS 516-1959 (Reaffirmed 2004), Methods of test for strength of concrete, *Bureau of Indian Standards*, New Delhi, India
32. IS 5816 (1999): Method of Test Splitting Tensile Strength of Concrete, , *Bureau of Indian Standards*, New Delhi, India
33. IS 2770 (Part I)-1967 (Reaffirmed 2007) Method of Testing Bond in reinforced concrete, *Bureau of Indian Standards*, New Delhi, India, 1970
34. IS 456 - 2000 (Reaffirmed 2005) Plain and reinforced concrete - code of practice, *Bureau of Indian Standards*, New Delhi, India, 2000
35. Park,R. and Thomas,P.T Reinforced Concrete Structures, Wiley India, Third Edition, 2009.

Strength and Behaviour of RCC Beams Retrofitted by Textile Reinforced Concrete

Sunoj J.S.¹ and Jayasree S.²

¹PG Research Scholar, Structural Engineering, Mar Baselios College of Engineering and Technology, Thiruvananthapuram, Kerala, India
sunojuseelan@gmail.com

²Associate Professor, Department of Civil Engineering, Mar Baselios College of Engineering and Technology, Thiruvananthapuram, Kerala, India
jayasree.s@mbcet.ac.in

Abstract. The need for strengthening structural elements in structures arises, when the capacity of an existing structure is no longer adequate to resist the current design loads or due to the larger ultimate loads. There are several methods for strengthening reinforced concrete beams. Textile Reinforced Concrete (TRC) is considered to be an environmentally sustainable concrete which can be used to retrofit the reinforced concrete beams and columns. The use of Alkali Resistant Glass Fibre mesh (AR Glass) as the reinforcing material in concrete is one of the innovative and cost-effective technique in the field of structural retrofitting. In this paper the strength and behaviour of reinforced concrete beams retrofitted by TRC with AR glass mesh as reinforcing material was investigated and it was found that all the flexural properties can be improved.

Keywords: Textile Reinforced Concrete, AR glass mesh, flexural properties

1. Introduction

Moment Resisting Frames (MRF) are the rectilinear assemblages of structural elements such as beams and columns, with beams rigidly connected to the column. When the importance of earthquake was unknown, the buildings were designed only for gravity loads. Such buildings are in a safe zone until it is affected by an earthquake. Earthquake is a destructive phenomenon which causes severe damage to structures. In most of the structures, failure occurs either in beams, columns or at joints. Retrofitting is a suitable method to reinstate the strength of damaged members, in order to meet the strength requirements posed due to increased load, deflection or corrosion. There are global and local techniques for retrofitting of structures. Global techniques include the addition of members and local techniques include strengthening of individual members. A number of techniques have been developed for increasing the strength and deformation capacity of existing Reinforced Cement Concrete (RCC) structures. These include the use of shotcrete overlays, steel jacketing, externally bonded Fibre-Reinforced Polymers (FRP) [1] etc.

FRP-based strengthening or seismic retrofitting techniques have been well-established in the civil engineering community due to favorable properties offered by these materials. Due to the excellent material properties, most notably freedom from corrosion but lightness and flexibility, textile reinforcements have made their entrance into the modern concrete construction market [2]. These technological transformations will take reinforced concrete construction in entirely new directions.

Textile reinforced concrete (TRC) is a type of reinforced concrete in which the usual steel reinforcing bars are replaced by textile materials. Instead of using a metal cage inside the concrete, this technique uses a fabric cage inside the same. Materials with high tensile strengths with negligible elongation properties are reinforced with woven or nonwoven fabrics. The fibres used for making the fabrics are of high tenacity like Jute, Glass Fibre, Kevlar, Polypropylene, Polyamides (Nylon) etc [2]. A typical TRC is shown in Fig.1. Some of commonly used TRC reinforcements are Alkali Resistant glass mesh (AR glass), Carbon fibre mesh, Basalt fibre mesh, Aramid fibre mesh and Polyvinyl Alcohol fibre mesh (PVA).



Fig 1. Textile-reinforced concrete

Kong et al. experimentally investigated the mechanical and durability behaviour of TRC subjected to tensile and bending loads. The effects of the reinforcement ratio in TRC was also investigated. Increase in the number of layers of AR glass mesh increased both the tensile and bending strength. The ultimate strength value of the TRC composite obtained from the tensile test is lower than that from the bending test [3]. Du et al. conducted a study on the influences of textile layers and short steel fibres on the tensile behaviour of basalt TRC. The tensile behaviour of basalt TRC is considerably influenced by the number of textile layers. The TRC specimens with three to five textile layers exhibit pronounced strain-hardening behaviour and consequently, prominent enhancement of tensile behaviour [4]. Hashemi et al. conducted a study to strengthen the RCC beams with cementitious mineral-based material for bonding instead of epoxy adhesives and found that there is a considerable improvement in flexural performance of beams by using cementitious material. Retrofitting of RCC structures using TRC has a great scope in future due to various properties like strength, durability, corrosion resistance etc.

The objective of this study:

- To find the flexural behavior of RCC beams retrofitted with textile concrete with AR glass mesh as reinforcing material.

2. Material Properties and Mix Proportions

The concrete used in this investigation was of M30 grade. For retrofitting of beams, high performance cement mortar of strength 50 N/mm² (HPC 50) was prepared. Portland Pozzolana Cement, crushed stones of 20 mm coarse aggregate, manufactured sand passing through sieve of size 4.75 mm and conforming to zone II of IS 383-2016 as fine aggregates were used [6,7]. The mix design was done as per IS 10262-2009 [8], to obtain a M30 grade concrete. The mix proportion thus obtained was 1:2.1:4.13. Fig. 2 shows AR glass mesh of size 4×4 mm which is used for this work. Table. 1 shows the mechanical properties of AR glass mesh.



Fig 2. AR glass mesh

Table 1. Mechanical properties of AR glass mesh*

Properties	
Structure of textile	Biaxial 0/90
Tensile strength (MPa)	2100
Surface weight (g/cm ²)	95.0± 5%
Mesh size (mm)	4x4
Appearance	Roll

* Provided by the manufacturer

3. Experimental Investigations

3.1. Specimen Preparation

Twelve RCC beams of size 100x150x1000 mm were prepared. Among them three were control beams (CB) and the remaining nine beams were retrofitted using TRC with AR glass mesh as reinforcing material (TRC-ARG mesh). After 24 hours of casting, these specimens were demoulded and kept immersed in water for 28 days. Fig. 3 shows the cross section and reinforcement details of the specimen.

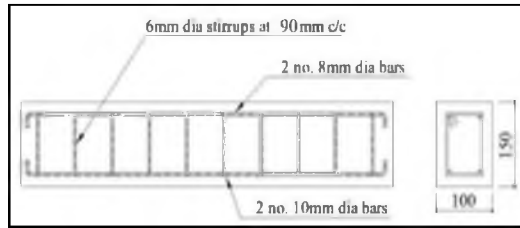


Fig 3. Reinforcement details of the specimens [9]

3.2. Testing of Control Specimens

All the beams were tested under two point loading in a Universal Testing Machine of 1000 kN capacity and the experimental setup is shown in Fig.4. Central deflections were measured using a dial gauge. Two strain gauges were fixed at the top and bottom reinforcements to measure the strains as shown in Fig.5. Ultimate loads were noted for the control specimens CB.



Fig4. Test setup



Fig 5. Connection of strain gauge

3.3. Preloading of Specimens

The remaining nine beams were preloaded to 67, 80 and 90% of ultimate loads of CB (three in each group and were designated as PB-67, PB-80 and PB-90 corresponding to their preloading conditions.

3.4. Retrofitting of RCC Beams

After preloading beams were retrofitted with TRC-ARG meshof two layers and U-wrapping technique was adopted. Retrofitted beams were designated as RB-67, RB-80and RB-90 respective of their preloading conditions which is shown in Table 2.

Table 2. Specimen details.

Specimen ID	Specification	No. of specimens
RB-67	Retrofitted after preloading of 67% of Ultimate Load	3
RB-80	Retrofitted after preloading of 80% of Ultimate Load	3
RB-90	Retrofitted after preloading of 90% of Ultimate Load	3

Various steps involved in retrofitting the beam are discussed below:

(i) Surface preparation:

The surface of the RC beams to be retrofitted were prepared for receiving the HPC mortar. Light blows were given to the surface of the beams by means of a chisel. The white wash left on the surface was also thoroughly scraped using sand paper. The surface was kept dry. Fig 6 shows the surface preparation.

(ii) Surface coat:

A thin layer approximately 2 to 3 mm thick HPC mortar to the old concrete was applied throughout the span of the beam. Fig 7 shows the application of surface coat of HPC.

(iii) Wrapping of AR glass mesh:

After the application of surface coat, glass mesh of size 4×4 mm was wrapped around the beam in one layer as shown in Fig 8. The mesh was impregnated into the concrete by using float.

(iv) Application of second coat:

After the wrapping of the glass mesh around the beam, another thin layer of HPC mortar was applied over the surface using a trowel and is shown in Fig. 9. The same procedure is repeated for the second wrapping and the surface was finely finished.



Fig6. Surface Preparation

Fig 7. Application of Mortar



Fig8. Application of AR glass mesh Fig 9. Application of mortar over the layer

3.5. Testing of Retrofitted Beams

Beams were tested same as that of CB. The ultimate load, crack pattern, crack width, first crack load, ductility indices, load-deflection characteristics, energy absorption capacity and moment curvature relationship were then compared between retrofitted specimens and control specimens.

4. Results and discussion

4.1. Crack Width and Crack Propagation

At each 5 kN increment of loading, crack width was noted. Crack pattern of preloaded specimens is shown in Fig.10 and for control and retrofitted specimens is shown in Fig.11. More number of finer cracks were found in retrofitted beams compared to the control beams. This may be due to the effect of uniformly distributed AR glass mesh.

Fig 12 and Fig 13 shows the crack width in preloaded and retrofitted beams. It was found that the width of cracks reduced significantly due to retrofitting in all the three cases of retrofitted beams.

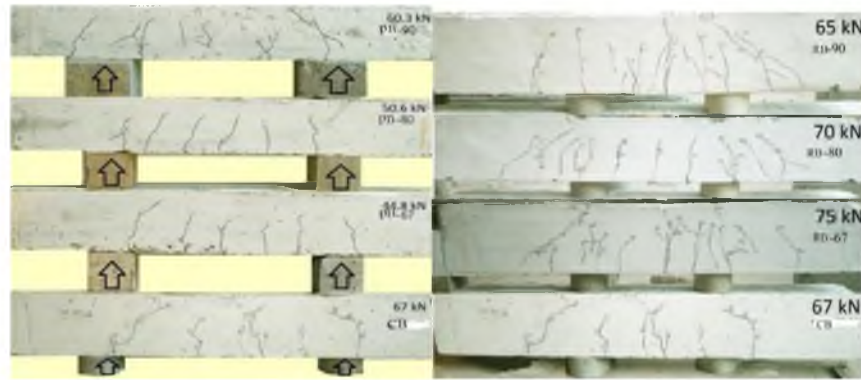


Fig 10. Crack propagation of preloaded beams Fig 11. Crack propagation of retrofitted beams

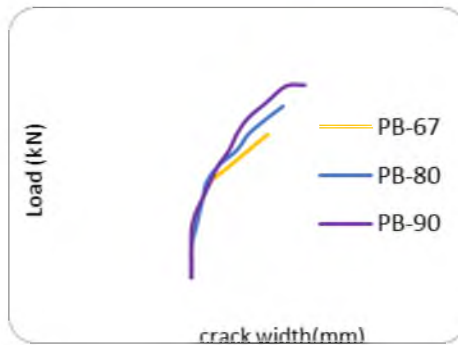


Fig 12. Crack propagation of preloaded specimens

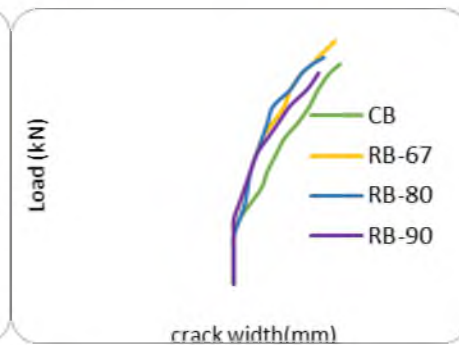


Fig 13. Crack propagation of retrofitted specimens

4.2. Load Deflection Plot

Load deflection plot for the control and retrofitted beams are shown in Fig.14. The curve was linear up to the first crack load for all the specimens. Further application of load makes the curve deviate from linearity. This is due to the formation of multiple cracks. Deflections of retrofitted beams were increased compared to the control beams up to 65 kN and thereafter decreased.

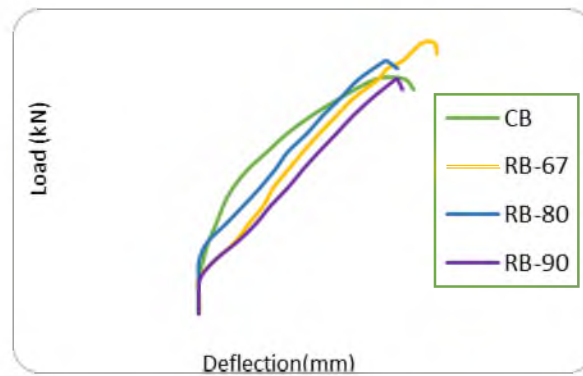


Fig 14. Load deflection graph for retrofitted specimens

4.3. First Crack Load and Ultimate Load

Table 3 shows the First crack, Yield and Ultimate loads of all the beams. All the loads were found to increase in retrofitted beams, may be due to the additional strength provided by AR glass fibre mesh. There is a considerable increase in ultimate load for RB-67 and RB-80. In RB-90 it was slightly less than that of CB.

Table 3. First crack, yield and ultimate load details of specimens

Specimen	First crack load(kN)	Yield load (kN)	Ultimate load (kN)
CB	10.20	47.00	67.00
RB-67	20.00	52.00	75.00
RB-80	18.00	50.00	70.00
RB-90	20.00	50.00	65.00

4.4. Energy Absorption Capacity and Stiffness

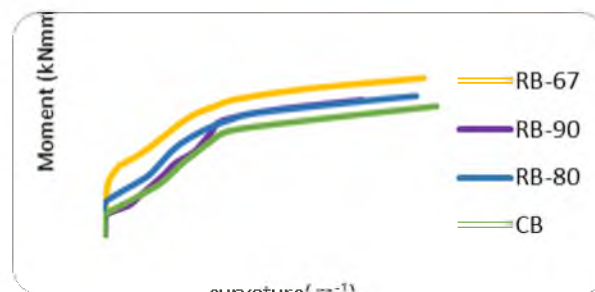
The area under the load deflection plot gives the Energy Absorption Capacity (EAC). Due to the limitations in the experimental setup, the load deflection graph could be plotted only up to 80 % of the peak load, in the descending portion of the curve. Stiffness of the beams was estimated by the slope of the initial linear portion of the load deflection curve [10]. Table 4 shows the energy absorption and stiffness of the all the beams. RB-67 shows greater increase in the energy absorption capacity, whereas RB-80 and RB-90 not reached up to that of CB. It is also found that the stiffness of all the retrofitted beams was increased. This may be due to the confining effect of AR glass mesh.

Table 4. Energy absorption and stiffness of RCC beams

Specimen	Energy Absorption Capacity (kNmm)	Stiffness (kN/mm)
CB	217.12	13.00
RB-67	224.79	15.01
RB-80	185.50	14.82
RB-90	158.95	14.62

4.5. Moment Curvature Relationship

The moment curvature plot for the beams were shown in Fig.15. From the plot it is clear that the retrofitted beams show greater curvature than the control beams. When it reaches yield moment, the curves become more or less flat. When steel yields, large increase in curvature occurs with a small change in moment [10].

**Fig 15.** Moment curvature relationship of retrofitted beams

4.6. Ductility Indices

Displacement ductility was calculated as the ratio of the displacement at ultimate load to the displacement at yield load. Failure of an under reinforced beam is called tension failure. This is because the primary reason of failure is the yielding of steel bars. The large increase in curvature, before collapse of the beam is an indication of ductile failure of beam. Curvature ductility was calculated as the ratio of curvature at ultimate load to that of curvature at yield load. High value of ductility shows the ability to undergo large inelastic deformation without any reduction in strength [10]. The absolute values of displacement and curvature ductility were presented in Table 5. There was an increase of ductility by 2% for RB-67 and a decrease of ductility by 1 and 3% for RB-80 and RB-90 than control specimen.

Table 5. Values of displacement and curvature ductility

Specimen	Displacement Ductility	Curvature Ductility
CB	1.32	2.60
RB-67	1.40	2.63
RB-80	1.30	2.57
RB-90	1.27	2.52

5. Conclusions

Based on the experimental investigation the following conclusions were arrived.

- Compared to CB, the width of cracks were reduced and spacing of cracks increased in retrofitted specimens.
- Retrofitting of RCC beams by TRC-ARG mesh increased the flexural strength by 12% for RB-67 and 5 % for RB-80 while a decrease in strength by 3% is found in RB-90 when compared to that of CB.
- Energy absorption capacity was increased by 4 % for RB-67 and for RB-80 and RB-90 there was a decrease in strength by 14 and 26 % when compared to CB.
- There was an increase of stiffness by 16, 14 and 13 % for RB-67, RB-80 and RB-90 respectively.
- There was an increase of ductility by 2% for RB-67 and a decrease of 1% and 3% for RB-80 and RB-90 when compared to CB.

Hence it can be concluded that TRC-ARG is an effective tool for retrofitting RCC beams.

References

1. Titiksh, A., and Gupta, M. K.: A Study of the Various Structural Framing Systems Subjected to Seismic Loads, *SSRG International Journal of Civil Engineering (SSRG-IJCE)*, 2(4), 23-30,(2015)
2. [https://www.sglgroup.com/TextileFibreCompositesinCivilEngineerings/sustainable construction/index.html](https://www.sglgroup.com/TextileFibreCompositesinCivilEngineerings/sustainable%20construction/index.html)
3. Kong, K., Mesticou, Z., Michel, M., Si Larbi, A and Junes, A (2017) Comparative characterization of the durability behaviour of textile-reinforced concrete (TRC) under tension and bending, *Composite Structures*.
4. Du, Y., Zhang, M., Zhou, F and Zhu D (2017) Experimental study on basalt textile reinforced concrete under uniaxial tensile loading, *Elsevier Procedia Engineering*, Vol. 138, 88-100.
5. Hashemi, S and Mahaidi, R (2012) Flexural performance of CFRP textile retrofitted RC beams using cement-based adhesive at high temperature, *Construction and Building Materials* 28,791-798.
6. IS 1489 (Part 1) - 1991 (Reaffirmed 2005), Specification for Portland pozzolana Cement, Bureau of Indian Standards, New Delhi, India, 1991.
7. IS 383 - 1970 (Reaffirmed 1997), Specifications for coarse and fine aggregate from natural sources for concrete, Bureau of Indian Standards, New Delhi, India, 197
8. IS10262:2009, Concrete mix proportioning-Guidelines, Bureau of Indian Standards, New Delhi, India, 2009
9. Jayasree, S., Ganesan, N and Ruby Abraham (2016) Effect of Ferrocement Jacketing on Flexural Behaviour of Beams with Corroded Reinforcements, *Construction and Building Materials* 121(2016)92-99
10. Hari Krishnan, K. R. and Bindu Biju, (2017) A Review Paper on Development of Ultra High Performance Fibre Reinforced Concrete, *Proceedings of National Conference On Advances In Structural Engineering (NASE-2017)* pp. 136-138, (ISBN 978-81-933590-0-6)
11. Al Osta, M. A., Isa, M. N., Baluch, M. H and Rahman, M. K (2017), Flexural behavior of reinforced concrete beams strengthened with ultra-high-performance fiber reinforced concrete, *Journal of Engineering Structures* Vol.106, pp. 374-384.
12. Signorinia, C., Nobilic, A., Gonzálezb, C. E and Siligardic, C (2018) Silica Coating For Interphase Bond Enhancement Of Carbon And AR-Glass Textile Reinforced Mortar (TRM) , *Composites Part B* 141 (2018) 191–202.
13. Holčapeka, O., Vogel, F. and Reitermana, P (2016) Using of Textile Reinforced Concrete Wrapping for Strengthening of Masonry Columns with Modified Crosssection Shape, *Procedia Engineering* 195 (2017) 62 – 66.
14. Hartig, J., Combe, H.U., and Schicktanz, K.,(2008) Influence of bond properties on the tensile behaviour of Textile Reinforced Concrete, *Cement and Concrete composites* 30,898-906.

USE OF RECYCLED PREMIX CHIPPING CARPET (RPCC) FOR RURAL ROAD CONSTRUCTION

JESH JAYAKUMAR, Dr ANIL R

ABSTRACT

The major factor affecting cost of road construction is cost of aggregates and binder materials. The study determines the suitability of recycled material in road construction. This will help in achieving economy in road construction as well as saving on environment degradation in term of reduced mining and less pollution. Construction and maintenance of roads and highways involve use of specified gradation of aggregates and properties of the binder. Replacing a part of the virgin mix with recycled aggregate is an optimal solution provided the recycled mix retains desirable strength and durable functions of the mix. This paper deals with use of recycled premix chipping carpet for rural road construction.

Key Words: Premix chipping carpet, Recycled mix;

1 PREAMBLE

Rural roads in India form a substantial portion of the Indian road network. The roads are poor in shape and specifications affecting the rural life quality and mobility. These roads include other district roads (ODR) and village roads (VR). The premix chipping is an important layer in construction of rural roads. Open graded premix chipping carpet consists of coarse aggregates of 12.5 mm and 10 mm sieve sizes, premixed with bitumen binder are compacted to a thickness of 20mm to serve as a surface course of the pavement. Being open graded construction the PMC is to be invariably covered by a suitable seal coat such as premixed sand bituminous mix. The roads undertaken for the study are PMGSY proposed rural roads.

The Pradhan Mantri Gram Sadak Yojana (PMGSY) (IAST: Pradhan Mantri Gram Sadak Yojana) is a nationwide plan in India to provide good all-weather road connectivity to unconnected villages.

The Recycling of aggregate is a process in which used aggregate is reused for new road construction. Recycled aggregate used in the present study is obtained from the debris of dismantled roads. The major function of the pavement is to transfer wheel load to the sub grade. In

this load transfer mechanism aggregates have to bear stresses occurring due to the wheel loads on the pavement and on the surface course, they also have to resist wear due to abrasive action of traffic. Therefore the properties of aggregate are of considerable significance to the highway engineers. The aggregates are categorized based on their size, shape, texture and gradation for different pavement mixes by various agencies like ASTM, BIS, ISI and IRC.

Recycling is driven by increasing customer demand for sustainable products, aggregates companies are now competing in the field of sustainability in order to maintain their market share. An additional driver for increased use of recycled materials is the reduction of embodied carbon used in extraction and processing of primary aggregates [3]. This can lead to significant long term cost savings in fuel efficiency and transportation charges.

2 OBJECTIVES

The main objective of the study is:

To identify the maximum allowable percentage of RAP
That can be added to Pre-mix chipping carpet.

To identify the strength variations of the Recycled Mix
for the selection of optimum proportion of recycled aggregates.

3 SCOPE OF THE STUDY

The scope of the study is limited to pre-mix chipping carpet rural road construction under PMGSY, India

4 LITERATURE STUDY

The use of recycled aggregates not only reduced cost of road construction but also improved eco-friendly environment.

Aravind K (2011) [1] studied the various hot mix recycling rehabilitation techniques intended for recycling and combined with required quantity of virgin asphalt binder and new aggregates in a hot mix plant. It deals with comparable performance to that of conventional mixes and better quality control. It studies the variation in properties of virgin mix and recycled mix like stiffness modulus, indirect tensile strength, fatigue and rutting performance by varying the percentage of RAP content.

Dr. Praveen Aggarwal (2014) [2] studied to suitability of recycled material in GSB layer for road construction. The study deals comparison of CBR, permeability and dry density tests results of virgin and recycled mix of various RAP content. The suitable percentage of RAP was found to be 15% of the recycled mix.

M. Abukhattala (2012) [3] Studied the rate of utilizing reclaimed asphalt pavement in HMA and base material in Ontario as low as 8% of the total recycled material used in year between 2008 and 2010.

The study also specifies the modification to the binder grade in the asphalt mixture, especially the low temperature grade, does not need much concern when RAP is used in less than 15% of the total weight of the mixtures.

The effect of introducing RAP into the binder course mix was evaluated through a series of laboratory tests including the Marshall Test, Indirect Tensile Stiffness Modulus Test, Indirect Tensile Fatigue Test and Water Sensitivity Test.

5 METHODOLOGY

Methodology adopted for the present study consists of

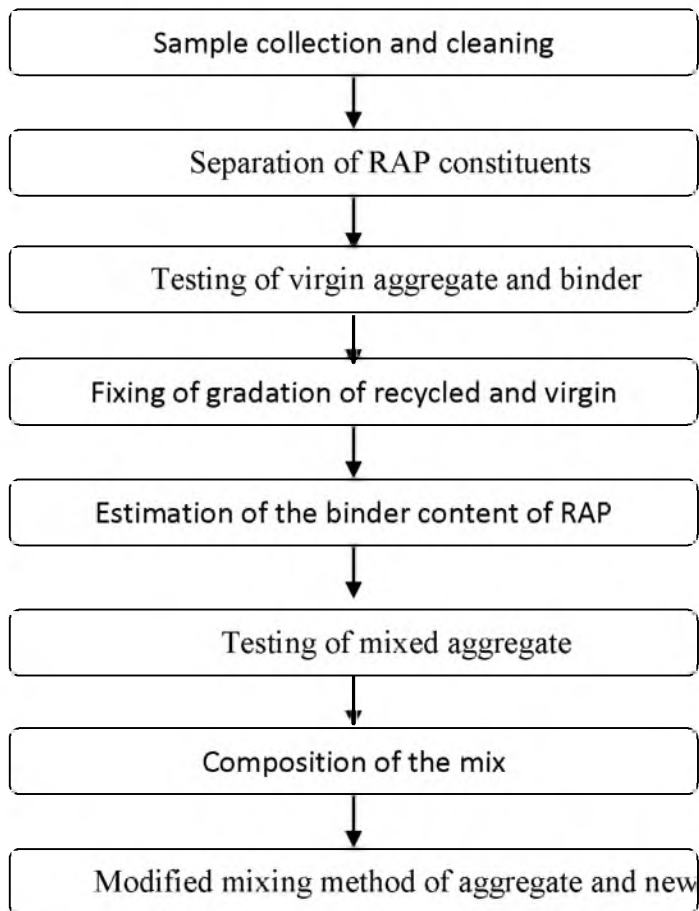


Fig. 1 Flow chart of methodology

5.1 SAMPLE COLLECTION AND CLEANING

The site selected for the study is PMGSY road Alanthara, Venjaramoodu Thiruvananthapuram. The road taken under the study is estimated for reconstruction and the raw materials including RAP and virgin aggregate are selected for study from the site. The aggregate is cleaned with cotton plug. The it is cleaned with high pressure water jetting and it is dried in oven.



Fig. 2 PMGSY road Alanthara Venjaramoodu

5.2 SEPERATION OF RAP CONSTITUENTS

The bituminous mix is selected from the rural road site is taken for study. The mix is thoroughly washed by action of jet power washing. Relatively high pressure power washing units are commonly available. This high velocity water is great enough to dislodge dirt and debris. The chances of flakes and wear from accelerated washing should be taken care during washing. The poor washing techniques will accelerate the water absorption. The washed aggregate mix is thoroughly cleaned with cotton plug. It is then oven dried for 24 hrs at 105 to 110°C. The process of separation of old aggregate binder mix is done mostly by heating and using CBE (centrifuge bitumen extractor). The bitumen is first treated with rejuvenators and aggregate mix is heated to around 175°C where most of the bitumen is separated and remaining is treated in CBE. The bitumen mix after heating is mixed with Trichloroethylene and rotated at specific speed and mix is separated.

5.3 TESTING OF VIRGIN AGGREGATE AND BINDER

The aggregate properties of the virgin mix are evaluated. The various laboratory tests were done to evaluate the strength properties of the RAP. The gradation of RAP used is as per 14-2004 (Table 3 gives gradation of RAP used).

Table1. Physical properties of virgin aggregate (IRC 14-2004)

Test Description	Value	Range	Method of test
Abrasion Value	24%	Max 40%	IS:2386 (Part 4)
Impact Value	26%	Max 30%	IS:2386 (Part 2)
Stripping Value	.5%	Max 10%	IS :2386 (Part 7)
Water absorption	.2%	Max 2%	IS :2386 (Part 10)
Soundness (magnesium sulphate-5 cycles)	4.6%	Max 18 %	IS: 2386 (Part 9)
Bulk density	1786 kg/m ³	Min 1120 kg/m ³	IS:2386(Part 3)
Combined flakiness and elongation index	28	Max 30	IS: 2386 (Part 5)
Angularity	10	0-11	IS: 2386(Part 5)
Specific Gravity	2.76	2.6-2.9	IS :2386(Part 5)

The binder considered for the study is NRMB (Natural rubber modified bitumen). The following properties of the binder were tested.

Table2. Physical properties of virgin binder (ASTM)

Test Description	Value	Range	Method of test
Softening point	58°C	Min 50	ASTM D 36
Elastic Recovery ratio	39%	Min 35%	ASTM D 6085
Penetration	52 cm	50-90 cm	ASTM D 5
Viscosity	425 centipoise	2-6 poise	ASTM D 2170/ D4402
Specific Gravity	.99	.97-1	ASTM D 92

5.4 GRADATION OF AGGREGATES

A sieve analysis (or gradation test) is a practice or procedure used to assess the particle size distribution of a granular material. The size distribution is often of critical importance to the way the material performs in use. A sieve analysis can be performed on any type of non-organic or organic granular materials including sands, crushed rock, clays, granite, feldspars, coal, soil a wide range of manufactured powders, grain and seeds, down to a minimum size depending on the exact method. The Combined gradation is obtained by mixing a known fraction of RAP with remaining fraction of virgin aggregates. The combined gradation should satisfy the gradation range as per IRC 14-2004. The combined gradation of the aggregates can go up to 40% of the RAP which confirms to specified gradation.

Table 3 Gradation of virgin aggregate and RAP (IRC 14-2004 part 2)

Sieve size	Percentage finer (%) (virgin aggregate)	Percentage finer (%) (RAP aggregate)	Combined Gradation (40%RAP)	Range
22.4	93.572	99.30	95.86	66-100
13.2	45.572	71.367	55.86	33-66
11.2	23.75	14.71	20.13	20-33
5.6	0.25	1	0.55	0-15

5.5 TESTING OF MIXED AGGREGATES

Various tests are performed to evaluate the strength of mixed aggregate. The test done in the study is impact test and Los Angeles abrasion test.

5.5.1 IMPACT TEST OF MIXED AGGREGATE

The property of a material to resist impact is known as toughness. Due to movement of vehicle on road, the aggregates are subjected to impact resulting in a breakdown in to smaller pieces. The aggregates should therefore have sufficient toughness to resist their disintegration due to impact. This characteristic is measured by impact value test. The aggregate impact value is a measure of resistance to sudden impact or shock, which may differ from its resistance to gradually applied compressive load. The chief advantage of aggregate impact test is that the test equipment and the test procedure are quite simple and it determines the resistance to impact of stones simulating field condition. The test can be performed in a short time even at a construction site or at a quarry, as the apparatus is simple and portable. The maximum impact strength is obtained for the gradation containing 15% of RAP aggregate

Table 4 Variation of Impact value wrt RAP(%)

Percentage RAP	Impact value
5	28
10	27
15	26
20	28
25	29
30	29
35	30
40	31

5.5.2 ABRASION TEST ON MIXED AGGREGATES

When vehicles move on the road, the soil particles present between the pneumatic tires and road surface causes abrasion of road aggregates. The steel rimmed wheels of animal driven vehicles also cause considerable abrasion of road surface. Therefore, the aggregate should be hard enough to resist the abrasion. In order to test the suitability of road stones do resist the abrading action due to traffic, tests are carried out in the laboratory using Los Angeles Abrasion test.

Percentage RAP	Abrasion value (%)
5	25
10	26
15	27
20	26
25	27
30	28
35	29
40	29

5.6 DETERMINATION OF BINDER CONTENT OF RAP

The bitumen content of the paving mixture can be found out using centrifugal bitumen extractor or annual centrifuge. Bitumen extractor is used for quantitative determination of bitumen paving mixes. This involves heating of bituminous sample until it starts crumbling and place it in extractors rotating bowl and add solvent. It uses the rotation of the rotor inside a centrifuge to separate bitumen and aggregate. The extractors centrifugal action forces liquid through a filter paper ring at bowls periphery and the process is repeated until the solvent expelled is clear in color. The remaining are weighted and graded before and after extractions. The binder content is determined.

The binder content is given by

$$b = \frac{W_1 - (W_2 + W_3 + W_4)}{W_1} * 100$$

Where b - bitumen content (%)

W1 - weight of sample of RAP

W2- increase in weight of filter paper

W3- weight of residue filtered from trichloroethylene solution

W4- weight of RAP after extraction

We get the value of b = 4.5%

5.7 COMPOSTION OF THE RPCC

From the previous results the various percentages of the composition of the RPCC is given by

% of virgin aggregates = 57.3

% of RAP aggregates = 38.2

% of virgin binder = 2.7

% of RAP binder = 1.8

5.8 MODIFICATIONS IN MIXING OF RPCC

Conventional mixing involves heating of virgin and recycled aggregates in a rotating drum mixer where they are heated and mixed thoroughly and transferred to next mixing chamber where they are coated with bitumen. This chamber involves heating of binder and mixing with recycled mix through rotating drum action. This is not an effective method of mixing as in the case of mixing of old and new aggregates. The modification involves an additional mixing chamber for mixing and pre heating of the old aggregates. This hot mix of old aggregates is then transferred to mixer drum where they are mixed with preheated virgin aggregates and mixing process is continued like conventional mixing. This concept allows RAP to be preconditioned flashing of moisture in the drum also eliminate problems associated with scavenger system.

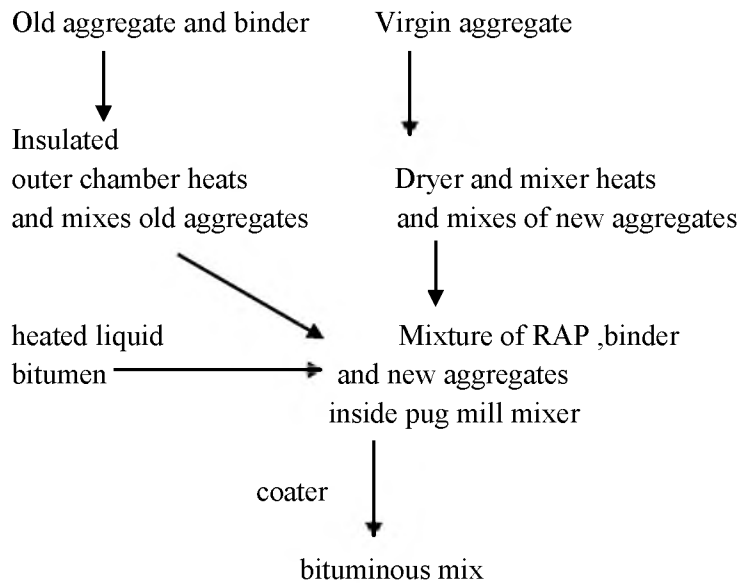


Fig 5. Modifications done in Conventional mixer

Many years of research has led to the development of theories and methodologies in roadway capacity analysis in the developed countries. For example, the Highway Capacity Manual (*HCM*) developed in the United States of America describes roadway capacity

6 CONCLUSION

The premix chipping carpet used in village roads can be recycled. The RAP for the site selected village road, Alanthara Venjaramoodu Thiruvananthapuram can be recycled.

The maximum percentage of RAP that can be added to the mix is 40% of the proportion. Any proportion beyond this RAP percentage does not satisfy the standard gradation.

In the study the maximum percentage of RAP added is 35% of the proportion. The proportion beyond this RAP percentage does not satisfy the strength criteria.

The conventional mixing of RAP with Virgin aggregates can be made more effective using modified RAP mixer.

7 REFERENCES

- [1] Constituent Proportioning in recycled asphalt mix with multiple RAP sources by Aravind K, Science direct Vol 104 December 2011
- [2] Use of recycled aggregates in Granular sub base by Dr Praveen IJIRSET Vol3 Issue 10, 2014.
- [3] Investigation on use of recycled asphalt shingles in Ontario hot mix asphalt: A Canadian case study. By M. Abukhettalacanadian journal of civil engineering, 2014
- [4] Specifications for Highway works, Dept of transportation HMSO 1960
- [5] Specifications of Materials used for Unbound Aggregate by Penning A UNBAR3 University of Nottingham 2009
- [6] Japan Road association "Technical Guide line for recycling and utilizing waste pavement materials" 1984
- [7] IRC 14 – 2004 Premix chipping carpet construction techniques and practices

Accurate Identification of Pavement Materials that are Susceptible to Moisture Damage with the use of Advanced Conditioning and Test Methods and the use of Machine Learning Techniques

Ram Kumar Veeraragavan, Nivedya, M. K., Rajib B. Mallick
Worcester Polytechnic Institute, Worcester, Massachusetts, 01609, USA

ABSTRACT: In order to prevent premature failure in hot mix asphalt (HMA) pavements due to moisture ingress, it is necessary to identify mixes that are susceptible to moisture damage during the mix design stage. The objective of this paper is to present a method that utilizes a conditioning process along with suitable destructive and nondestructive tests and machine learning techniques to accurately assess the moisture damage potential of HMA mixtures. The scope of work included conditioning with the Moisture Induced Stress Tester (MiST) and testing of a set of HMA mixes with known field performance, and analysis of the data using machine learning techniques. Input variables obtained from a destructive test, the indirect tensile strength test and a non-destructive test, the ultrasonic pulse velocity test, were used to identify the good and poor performing mixes. Various machine learning models were used and it was found that the Support Vector Machine and the Naïve Bayes methods were able to classify the mixes with high accuracy. Use of indirect tensile strength, ultrasonic pulse velocity test and classification based machine learning technique are recommended for the development of accurate models and research in pavement engineering.

1 Introduction

Moisture in any form combined with traffic and environmental conditions can cause significant loss in asphalt pavement strength and durability. Moisture related damage in pavements has been observed since the late 1920's [1]. Extensive research conducted by Hicks [2] showed that about half of the states in United States had experienced moisture-related distresses. Moisture induced damage has been regarded as one of the leading causes of premature failures in asphalt pavements and a major concern to the paving industry.

Over the years, extensive research has been conducted to develop a reliable and practical laboratory test procedure that can simulate field moisture damage condition and which can give predictions that correlate well with field performance. From the literature, it can be concluded that no single laboratory test method can be used to accurately predict the performance of a given hot mix asphalt (HMA) mixture due to various potential mechanisms of moisture damage. Research conducted by the Maine Department of Transportation (MDOT) and other agencies have found the moisture conditioning of HMA samples with the Moisture Induced Stress Tester (MiST) and the use of Indirect Tensile Strength test (ITS) to be effective in screening moisture susceptible HMA mixtures [3]. However, the results of tests were not found to be sufficiently accurate to justify the use of the MiST plus ITS procedure on a regular basis.

This paper presents a study that utilized the MiST and the ITS along with a suitable non-destructive test, the Ultrasonic Pulse Velocity (UPV) test and machine learning techniques to accurately assess the moisture damage potential of HMA mixtures.

2 Literature review

Moisture in liquid or vapor can infiltrate an asphalt pavement through various sources like rain water from the surface through cracks, or by capillary action from underground water through interconnecting air-voids or can exist from the mixing process as a result of improper drying of aggregates during mixing process [4, 5]. Moisture damage in asphalt pavement has been studied extensively for the past several decades and is defined as the loss in structural strength and durability of an HMA mixture due to the deteriorating effects of moisture [6]. It is a complex phenomenon involving many factors resulting in loss of stiffness and structural strength of the pavement [7]. The moisture by itself does not cause much damage to an asphalt pavement but it is the moisture along with traffic and environmental conditions that accelerates the pavement deterioration process [8, 9].

Moisture damage mechanism in HMA can be broadly classified into cohesive failure (within binder or mastic) or adhesive failure (between binder/mastic and aggregate) or combination of both in HMA. Some of the major damage mechanism as reported in previous research studies [10-15] include detachment, displacement, spontaneous emulsification, pore pressure-induced damage, hydraulic scour, and effects of environment on aggregate-asphalt system. Some of the theories that have been developed to explain the adhesion of binder to aggregates include surface energy theory [16], chemical bond theory [17] and mechanical interlock theory [2, 18]. Some of the other significant factors include binder rheology [19], source, their adsorption, polarity, functional groups present and the affinity of asphalt binders to water [20-22], aggregate characteristics [19, 23, 24] (such as mineralogy, texture, gradation) and mixture properties [5] (such as air voids, film thickness, permeability). Despite understanding the various types of moisture damage mechanism, researchers all around the world are still trying to find a reliable laboratory test and evaluation procedure to screen HMA mixes that are susceptible to moisture damage [1, 25].

Over the past several decades many laboratory testing and conditioning process have been developed, but none of them have been widely accepted by state agencies till date. Most of laboratory test methods are performed on loose mixtures or on compacted samples. The earlier loose mixture tests include boiling water test and static immersion test, which were both qualitative tests, and involved subjecting the loose mixtures at elevated and room temperatures for specific time and observing visually for stripping potential. Some of the compacted mix sample test include Indirect Tensile Strength (ITS) and the dynamic modulus, as well as wheel tracking tests (Hamburg). At present, one of the most widely used mix design test procedure to evaluate moisture damage is the AASHTO T283 test [26], which was developed on the basis of the work conducted by Lottman [27]. However, this test method has been reported to have poor correlation with field performance and has been found to be inconsistent with respect to saturation of the samples. In addition, the AASHTO T283 test process does not simulate the pore pressure that is generated under traffic in the presence of moisture. Researchers have also found that the AAHTO T283 test combined with Hamburg test had difficulties in predicting the field performance of pavement that are moderately resistant to moisture (NCHRP 9-34) [28].

Field observation of HMA mixes in areas of pavement with high water saturation and traffic loading have indicated localized and severe stripping of pavement [14, 29, 30]. Traffic loading in the presence of moisture induces pore water pressure, which contributes to premature failures in asphalt pavements [31]. One of the major drawbacks of many laboratory conditioning systems is that they cannot simulate the damage caused by the generation of pore water pressures. To overcome such a problem, the Moisture Induced Stress Tester (MiST) was developed (2003) [32, 33] on the basis of work that was originally conducted by Jimenez [34]. MiST is an accelerated moisture conditioning device that simulates the action of repeated traffic loading on a saturated asphalt pavement by applying cyclic pore water pressure on a HMA sample. It has been found in a study that high pore water pressure does exist in the upper layers of HMA in the field [35] and that the MiST is capable of simulating that condition.

In the MiST conditioning process, a sample is placed inside a chamber with a bladder. The chamber is filled with water and then sealed to prevent the presence of any air inside it. The water is then heated to the desired temperature and the bladder is then pressurized and depressurized sequentially over the desired number of cycles to force water through and out of the sample. The sample subjected to this pressurized cycles is then tested, and the results of tests conducted on the conditioned and the unconditioned samples are compared to evaluate the moisture damage potential of the mix.

Traditional statistical models such as linear regression models or significance tests are normally used to relate mix properties to performance or screen poor performing mixes. The main disadvantage of such traditional statistical methods is that they cannot estimate nonlinear and complex relationships accurately. Recent advances in the area of statistics and data science have led to the development of Machine Learning (ML) techniques [36]. ML techniques can be used to predict HMA mix properties more accurately than traditional statistical approaches [37]. There is a need for research on accurate prediction of mix performance using ML techniques.

Machine learning techniques can be broadly classified into two categories on the basis of technique that are used to train the model: supervised and unsupervised [36]. Supervised learning is the process of training the machine

learning model with inputs/features and corresponding targets. In unsupervised learning, there is no target data, and the process is used for clustering data on the basis of their features alone. Supervised machine learning can be further divided into classification and regression techniques. In cases where the response variable (target variable to be predicted) is discrete/categorical, classification techniques are normally used. Regression techniques are used in cases where the response variable is continuous. There are various classification machine learning techniques such as:

- Support vector machines: These models are used for high dimensional and non-linearly separable data. They separate the data by a subspace such as hyperplane capable of separating the observations into two sets.
- Naïve Bayes: These models are used for small data set with a higher number of parameters. The process assumes that the features in a class are not related to each other.
- K-Nearest neighbor: These models are used to establish benchmarks and categorize data based on the classes of their nearest neighbor.
- Decision tree: These models predict the target class by learning some simple decision rules inferred from the features of the entire data.

3 Materials and methodology

Twenty-three plant produced loose HMA mixtures of known field performances (by field observation and experience) were utilized in this study. Thirteen loose HMA mixtures, which were provided by one department of transportation (DOT) were compacted with a Superpave gyratory compactor at $5\pm 1\%$ voids, and the remaining ten HMA mixtures, which were provided by another DOT were compacted at $7\pm 1\%$ voids, each according to their standard construction practice. Table 1 presents the different properties of each mix. A minimum of three samples were used for each test, for each mix.

Table 1. Mix information.

Mix No. /Performance	NMAS (mm)	Target construction voids, %	Binder type	Percentage of binder	Percentage of RAP	Additive
1/good	12.5	5±1	PG 64-28	5.6	20	No
2/good	12.5	5±1	PG 64-28	5.5	20	No
3/poor	9.5	5±1	PG 64-28	6.2	10	No
4/good	9.5	5±1	PG 64-28	6.4	20	No
5/good	9.5	5±1	PG 64-28	6.5	20	Lime
6/good	12.5	5±1	PG 64-28	5.3	20	No
7/poor	9.5	5±1	PG 64-28	6.5	0	No
8/poor	9.5	7±1	PG 58-28	6	20	Commercial
9/good	12.5	7±1	PG 70-28*	4.9	15	No
10/good	12.5	5±1	PG 64-28	5.6	20	No
11/poor	9.5	7±1	PG 58-28	6.0	20	No
12/good	9.5	5±1	PG 64-28	6.6	20	No
13/poor	12.5	5±1	PG 64-28	5.8	0	Lime
14/good	12.5	5±1	PG 64-28	5.8	20	No
15/good	12.5	5±1	PG 64-28	6.0	10	No
16/good	12.5	5±1	PG 64-28	5.7	20	No
17/good	12.5	5±1	PG 64-28	5.0	20	No
18/poor	12.5	7±1	PG 64-28	5.7	20	No
19/poor	12.5	7±1	PG 64-28	5.4	10	No
20/good	12.5	7±1	PG 64-28	4.9	20	No
21/poor	12.5	7±1	PG 64-28	4.6	20	No
22/poor	12.5	7±1	PG 64-22	5.0	0	No
23/good	12.5	7±1	PG 64-28	5.4	10	No

* Polymer modified

The compacted samples were then subjected to moisture conditioning using the MiST. MiST conditioning was conducted according to the ASTM D7870 standard, which specifies 3,500 cycles at 275 kPa, and at 60°C for PG 64-28 and PG 70-28 mixes, and 50°C for PG 58-28 mixes. In addition to this ASTM protocol the samples were subjected to a 20-hour dwell period (saturation) prior to the application of cyclic pore pressure. The dwell period

simulated the soaking period of water immediately after construction before the passage of traffic and allowed the diffusion of water into the asphalt-aggregate interface.

To evaluate the performance of HMA sample before and after MiST conditioning, a non-destructive testing, the Ultrasonic Pulse Velocity test (UPV), and a destructive testing, the Indirect Tensile Strength (ITS) test were used. The UPV testing, which is based on surface wave propagation techniques was conducted according to the ASTM C597-09 standard. The UPV testing works by converting the electrical pulse from a piezoelectric crystal to ultrasonic shock waves (p-waves), which travel from the transducer through the specimen and are then collected by the receiver on the other side of the specimen (direct transmission position). The shock waves received from receiving transducer are converted back to an electrical pulse. The seismic modulus is then calculated from the ultrasonic pulse velocity or the p-wave travel time, according to the following equation.

$$V_p = H/t_v; M_v = \rho \times V_p^2; E_s = M_v \times \frac{[(1+\mu) \times (1-2\mu)]}{(1-\mu)}$$

$E_d = (E_s/3.2) \times$ Temperature correction factor;

Temperature correction factor = 0.95 (for a test temperature of 21.1 °C)

Where, V_p = velocity of wave; t_v = time of travel; ρ = density; μ = Poisson's ratio; E_s = seismic modulus, E_d = design modulus

Hence, any change in the material property after MiST testing would be reflected in the ultrasonic travel time. The ITS testing was conducted according to the ASTM D6931 procedure. The results from UPV and ITS testing are shown in Figures 1 and 2 respectively. In Figure 1, it can be seen that seismic modulus of moisture conditioned samples were lower than unconditioned samples for all mixes, except for mixes 9 and 15 which are the better performing mixes. This shows that UPV testing is sensitive to the effects of moisture damage. The indirect tensile strength was reduced after moisture conditioning, as can be seen in Figure 2, irrespective of good or poor performance in the field. A conventional statistical analysis of the data, as shown in Table 2, showed inaccurate identification of good and poor performing mixes – note that some good mixes show significant reduction in modulus/strength. Although some poor mixes showed significant reduction, the overall accuracy of prediction was 82.6% for E_s and 73.9% for ITS.

Based on the collected laboratory test data, supervised machine learning classification techniques were used to predict the performance (good or poor) of the HMA mixes. Here, post-MiST seismic modulus values and post-MiST ITS values were used as input variables. The K-NN, Naïve Bayes, Support Vector Machines (SVM) and decision tree methods of ML were used in this study. The data consisted of test properties of each sample, and the samples were labelled according to the observed performance (good or poor) of the mix from which the samples were prepared. Therefore, the total dataset consisted of 58 observations. The training and validation data consisted of 65 % and test data consisted of 35% of the total data. K-fold cross validation was carried out in order to avoid overfitting and the value of k used was five. A confusion matrix is a representation of the error matrix that is generally used to visualize the performance of the machine learning classification models. Confusion matrix was constructed to evaluate the prediction accuracy of the different models. It can be seen in Figure 3 that Naïve Bayes and SVM based models have the highest accuracy (95%), much higher than that from the statistical analysis.

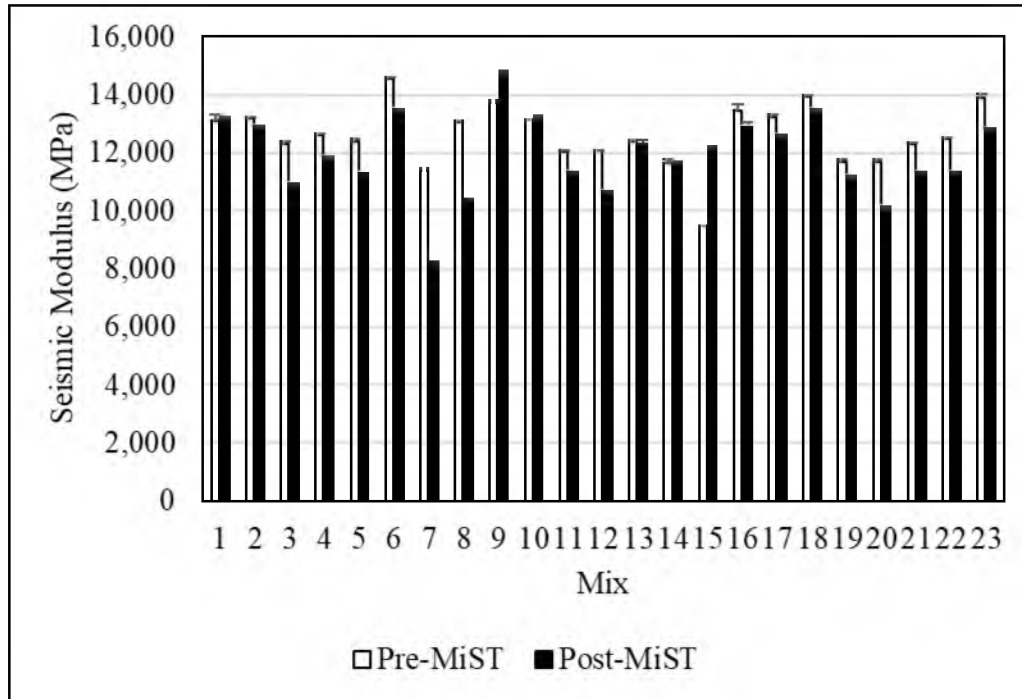


Figure 1. Seismic modulus values before and after MiST conditioning
 Note: The error bars indicate the standard deviation of the data.

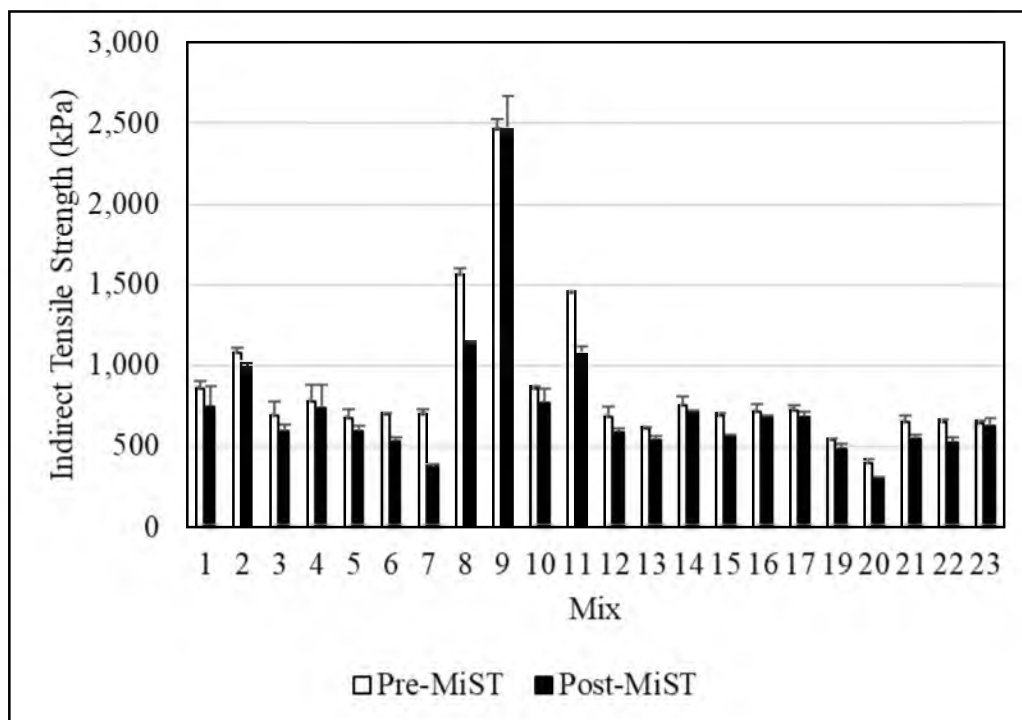


Figure 2. Indirect Tensile Strength before and after MiST conditioning
 Note: The error bars indicate the standard deviation of the data

Table 2 Summary of statistical analysis

Mix	Performance	Additive	Siesmic modulus difference Significant or not?	ITS difference Significant or not?
1	Good	No	No	No
2	Good	No	No	Yes
3	Poor	No	Yes	No
4	Good	No	No	No
5	Good	Lime	Yes	No
6	Good	No	No	No
7	Poor	No	Yes	Yes
8	Poor	Commercial	Yes	Yes
9	Good	No	No	No
10	Good	No	No	No
11	Poor	No	Yes	Yes
12	Good	No	No	No
13	Poor	Lime	No	No
14	Good	No	No	No
15	Good	No	No	No
16	Good	No	No	No
17	Good	No	No	No
18	Poor	No	Yes	No
19	Poor	No	Yes	No
20	Good	No	Yes	Yes
21	Poor	No	Yes	Yes
22	Poor	No	No	Yes
23	Good	No	No	No

Note: True positive (TP) identifies the good mixes as good mixes and true negative (TN) identifies the poor mixes as poor mixes and accuracy is calculated as,

$$\text{Accuracy} = \frac{TP+TN}{\text{Total observation (n)}}$$

The accuracy for E_s is calculated below :

$$\text{TP}=12; \text{TN}=7;$$

$$\text{Accuracy} = \frac{12+7}{23} = 82.6\%$$

Accuracy for ITS is calculated below:

$$\text{TP}=12; \text{TN}=5;$$

$$\text{Accuracy} = \frac{12+5}{23} = 73.9\%$$

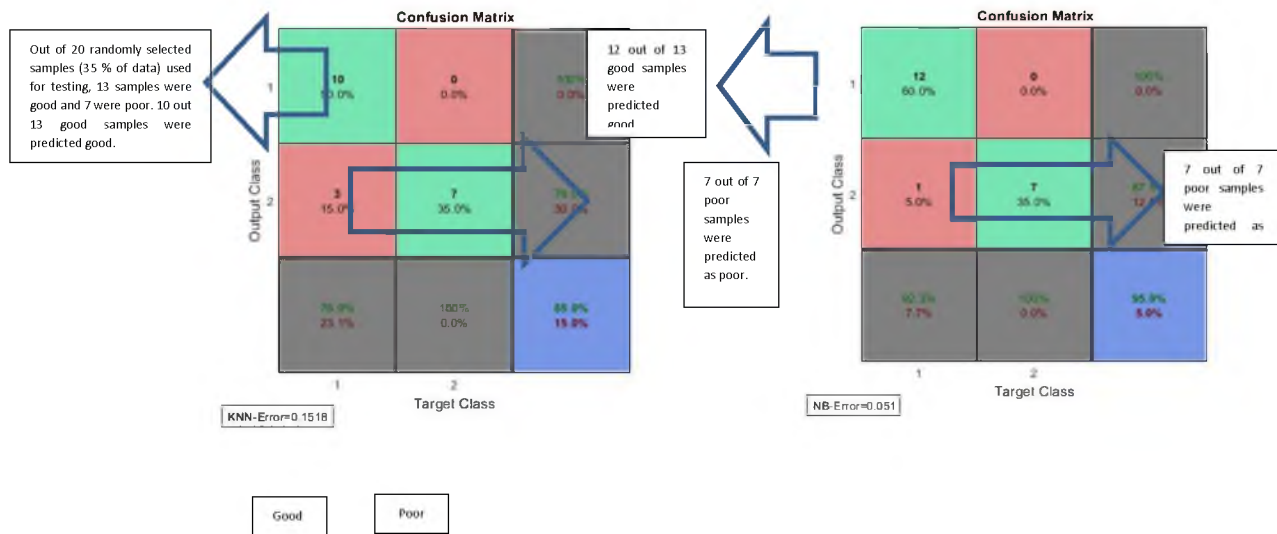


Fig. 3a. Confusion matrix for K-NN classification; Accuracy = 85% Fig. 3b. Confusion matrix for Naïve Bayes classification; Accuracy = 95%

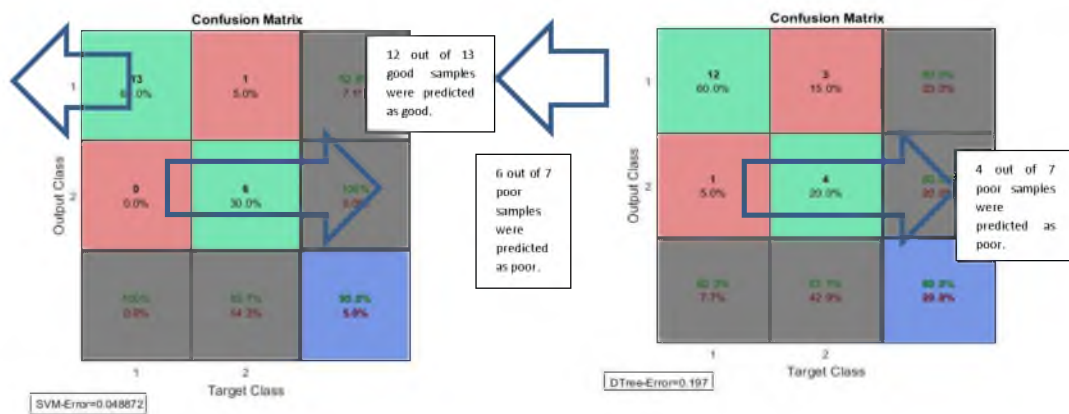


Figure 3c. Confusion matrix for SVM classification; Accuracy = 95% Fig. 3d. Confusion matrix for Decision tree classification; Accuracy = 80%

Figure 3 Confusion matrix for different machine learning models with an example calculation of accuracy of K-NN classification model

		Actual		
		GOOD	POOR	
Predicted	GOOD	True good (10)	False poor (0)	100%
	POOR	False good (3)	True poor (7)	70%
		13	7	85%

$$\text{Accuracy} = \frac{TP+TN}{\text{Total observation } (n)} = \frac{17}{20} = 85\%$$

Fig. 3e. Example calculation of accuracy of K-NN model

Figure 3 Confusion matrix for different machine learning models with an example calculation of accuracy of K-NN classification model (continued)

4 Conclusions and Recommendations

The following conclusions and recommendations can be made from the study.

1. MiST conditioning process with the 20-hour dwell period prior to 3,500 pressure cycling at 275 kPa was able to simulate field moisture damage conditions in the laboratory.
2. Non-destructive testing using ultrasonic pulse velocity was able to identify moisture susceptible mixes.
3. The test properties such as seismic modulus and indirect tensile strength after moisture conditioning can be used by agencies to predict the moisture damage potential of HMA.
4. Models developed with two machine learning techniques, the Support Vector Machine and Naïve Bayes (NB) method show excellent accuracy for classification of mixes into good and poor performing in terms of potential of moisture damage.
5. The use of the indirect tensile strength test along with the ultrasonic pulse velocity test is recommended.
6. Machine learning models should be developed and utilized for accurate classification of HMA mixes according to their moisture damage potential.
7. The use of machine learning methods should be explored for other areas of research in pavement engineering.

References:

- [1] Hamzah, M.O., Kakar, M.R., Hainin, M.R., An overview of moisture damage in asphalt mixtures, *Jurnal Teknologi (Sciences & Engineering)* 73(4), 125-131 (2015).
- [2] Hicks, R.G., Moisture damage in asphalt concrete, Transportation Research Board (1991).
- [3] Arepalli, U. M. A study of moisture induced material loss of hot mix asphalt (HMA), Ph.D. Dissertation, Dept. of Civil And Environmental Engineering, Worcester Polytechnic Institute, MA, (2018).
- [4] Kringos, N., Scarpas, A., Physical and mechanical moisture susceptibility of asphaltic mixtures, *International Journal of Solids and Structures* 45(9), 2671-2685 (2008).
- [5] Behiry, A.E.A.E.-M., Laboratory evaluation of resistance to moisture damage in asphalt mixtures, *Ain Shams Engineering Journal* 4(3), 351-363 (2013).
- [6] Santucci, L., Moisture sensitivity of asphalt pavements, *Tech Topics* (2002).
- [7] Yi, J., Shen, S., Wang, D., Feng, D., Huang, Y., Effect of Testing Conditions on Laboratory Moisture Test for Asphalt Mixtures, *Journal of Testing and Evaluation* 44(2), 856-867 (2016).
- [8] Grenfell, J., Ahmad, N., Liu, Y., Apeagyei, A., Large, D., Airey, G., Assessing asphalt mixture moisture susceptibility through intrinsic adhesion, bitumen stripping and mechanical damage, *Road Materials and Pavement Design* 15(1), 131-152 (2014).

- [9] Zhang, J., Apeageyi, A.K., Airey, G.D., Grenfell, J.R., Influence of aggregate mineralogical composition on water resistance of aggregate-bitumen adhesion, *International Journal of Adhesion and Adhesives* 62, 45-54 (2015).
- [10] Kiggundu, B.M., Roberts, F.L., Stripping in HMA mixtures: State-of-the-art and critical review of test methods, National Center for Asphalt Technology Auburn, AL. (1988)
- [11] Taylor, M.A., Khosla, N.P., Stripping of asphalt pavements: State of the art (discussion, closure), (1983).
- [12] Al-Swailmi, S., Terrel, R., Water Sensitivity of Asphalt-Aggregate Mixtures: Test Selection, SHRP-A. (1994)
- [13] Choubane, B., Page, G., Musselman, J., Effects of water saturation level on resistance of compacted hot-mix asphalt samples to moisture-induced damage, *Transportation Research Record: Journal of the Transportation Research Board* (1723), 97-106 (2000).
- [14] Kandhal, P., Rickards, I., Premature failure of asphalt overlays from stripping: Case histories, *Asphalt Paving Technology* 70, 301-351 (2001).
- [15] Little, D.N., Petersen, J.C., Unique effects of hydrated lime filler on the performance-related properties of asphalt cements: physical and chemical interactions revisited, *Journal of Materials in Civil Engineering* 17(2), 207-218 (2005).
- [16] Read, J., Whiteoak, D., *The shell bitumen handbook*, Thomas Telford (2003).
- [17] Syunyaev, R., Balabin, R., Akhatov, I., Safieva, J., Adsorption of petroleum asphaltenes onto reservoir rock sands studied by near-infrared (NIR) spectroscopy, *Energy & Fuels* 23(3), 1230-1236 (2009).
- [18] Masad, E., Castelblanco, A., Birgisson, B., Effects of air void size distribution, pore pressure, and bond energy on moisture damage, *Journal of testing and evaluation* 34(1), 1-9 (2005).
- [19] Curtis, C.W., Ensley, K., Epps, J., *Fundamental properties of asphalt-aggregate interactions including adhesion and absorption*, National Research Council Washington, DC, USA. (1993)
- [20] Caro, S., Masad, E., Bhasin, A., Little, D.N., Moisture susceptibility of asphalt mixtures, Part 1: mechanisms, *International Journal of Pavement Engineering* 9(2), 81-98 (2008).
- [21] Plancher, H., Dorrence, S., Petersen, J., Identification of chemical types in asphalts strongly adsorbed at the asphalt-aggregate interface and their relative displacement by water.[Moisture damage to roads], Energy Research and Development Administration, Laramie, WY (USA). Laramie Energy Research Center. (1977)
- [22] Petersen, J., Plancher, H., Ensley, E., Venable, R., Miyake, G., Chemistry of asphalt-aggregate interaction: relationship with pavement moisture-damage prediction test, *Transportation Research Record* (843) (1982).
- [23] Bagampadde, U., Isacson, U., Kiggundu, B., Influence of aggregate chemical and mineralogical composition on stripping in bituminous mixtures, *The international journal of pavement engineering* 6(4), 229-239 (2005).
- [24] Airey, G., Masad, E., Bhasin, A., Caro, S., Little, D., Asphalt mixture moisture damage assessment combined with surface energy characterization, *Proceedings of a conference on advanced characterization of pavement and soil engineering materials*, pp., 739-748. (2007)
- [25] Solaimanian, M., Harvey, J., Tahmoressi, M., Tandon, V., Test methods to predict moisture sensitivity of hot-mix asphalt pavements, *Moisture Sensitivity of Asphalt Pavements-A National Seminar* California Department of Transportation; Federal Highway Administration; National Asphalt Pavement Association; California Asphalt Pavement Alliance; and Transportation Research Board. (2003)
- [26] AASHTO, T., 283.(2014), Standard method of test for resistance of compacted asphalt mixtures to moisture-induced damage
- [27] Lottman, R.P., *Laboratory test methods for predicting moisture-induced damage to asphalt concrete*, (1982).
- [28] Solaimanian, M., Harrigan, E., Improved conditioning procedure for predicting the moisture susceptibility of HMA pavements, *Proceedings of Moisture Damage Symposium*, Laramie, Wyoming, USA. (2002)
- [29] Kandhal, P.S., Lubold, C.W., Roberts, F.L., Water damage to asphalt overlays: case histories, National Center for Asphalt Technology Nashville, Tennessee. (1989)
- [30] Shakiba, M., Darabi, M.K., Little, D.N., Effect of Pore Water Pressure on Response of Asphalt Concrete, *Transportation Research Record: Journal of the Transportation Research Board* (2631), 114-122 (2017).
- [31] Dawson, A., *Water in road structures: movement, drainage & effects*, Springer Science & Business Media (2008).
- [32] Regimand, A., James, L.H., Muse, P.D., Landreth, K., He, T., System and method for conditioning and detection of susceptibility to moisture damage in asphalt mixes, Google Patents. (2012)
- [33] Regimand, A., James, L.H., Muse, P.D., He, T., System and method for conditioning and detection of moisture damage in asphalt mixes, Google Patents. (2004)
- [34] Jimenez, R., *Testing for debonding of asphalt from aggregates* (1974).
- [35] Mallick, R.B., Gould, J.S., Bhattacharjee, S., Regimand, A., James, L.H., Brown, E.R., Development of a rational procedure for evaluation of moisture susceptibility of asphalt paving mixes, *Transportation Research Board*, Washington, DC (2003).
- [36] Bishop, C. M. *Pattern Recognition and Machine Learning*. Springer, New York, (2006).
- [37] Nivedya, M. K., Mallick, R. B., Accurate Prediction of Laboratory Permeability of Hot Mix Asphalt using Machine Learning Techniques, *Advances in Materials and Pavement Performance Prediction*, Doha, Qatar (2018).

COMPARING THE PROPERTIES OF HMA WITH WARM ASPHALT MIXES BY VARYING TEMPERATURES USING SASOBIT & STEARIC ACID AS ADDITIVES

K.Govind Goud¹, Dr. P. Sravana², A. Nitish³

¹ Asst.Professor, MGIT college, Hyderabad. govind247307@gmail.com

² Professor and Coordinator, Center for Transportation Engineering JNTUH college of Engineering, Hyderabad, sravana.jntu@gmail.com

³ Assistant Quality cum Material Engineer, BSVL Construction, Mahaboobnagar, nitish.amerneni@gmail.com

Abstract. Warm mix asphalt (WMA) is a recent technology used to reduce the mixing and compaction temperatures without affecting the quality of pavement. The Warm Mix Asphalts (WMA) is modified Hot Mix Asphalt (HMA) which is produced, laid and compacted in temperature which is lower than conventional HMA. The WMA is produced by mixing chemical additives to the conventional mix to improve the pavement performance.

In this study an attempt is made to compare the Marshall properties of WMA produced with the inorganic additive: “SASOBIT” and chemical additive “STEARIC ACID” with HMA for Dense Grade Bituminous Macadam (DBM). The adopted mixing temperature for HMA was 160°C and the mixing temperatures for WMA was 110°C - 140°C, with an additive dosage rate of 3% by weight of the binder respectively.

The optimum binder content was to be found out individually for the mixture for different mixing temperatures and additive dosage rate. The Laboratory study Concludes that volumetric properties (VA, VMA and VFB), stability, flow value were improved for WMA mix by the addition of the additive.

Keywords: Sasobit, Stearic Acid, Warm mix asphalt, Marshal Stability.

1. Introduction

Warm Mix Asphalt is the manufacturing and paving of asphalt mixes at significantly lower temperatures than Hot Mixed Asphalt (HMA), while maintaining or even exceeding the quality of equivalent conventional HMA mixes. WMA can be conveniently classified by the degree of temperature reduction compared to that of conventional HMA. This is illustrated in Figure 1, which shows the typical ranges in mix temperature, from cold mixes to conventional hot mix asphalt (HMA). It also shows how the consumption of fuel increases in order to produce mixes at higher temperatures. If the production temperature is less than 100°C (212°F) it is considered as a “half-warm” mix. Generally WMA is regarded to have production temperatures at least 20°C below those of HMA, and above 100°C. While HMA is generally manufactured at temperatures between 140°C and 160°C, WMA is typically produced at temperatures between 100°C and 140°C.

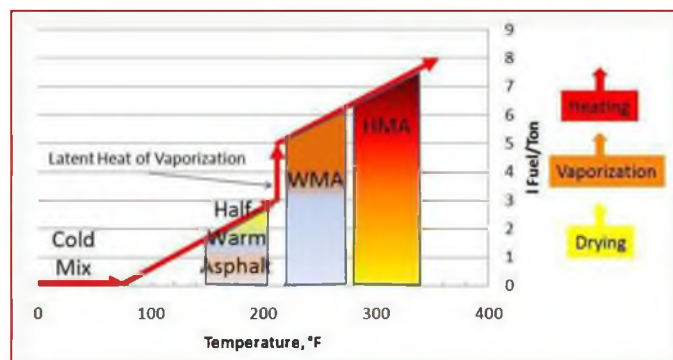


Figure 1: Typical temperature ranges for mixes, from cold mixes to conventional

2. Objectives

The following are the primary objectives of this research:

- To determine the physical properties of VG 30 and WMA samples (3% of Sasobit and Stearic acid as additive).
- Designing aggregate gradation and determining the optimum bitumen content for Dense Graded Bitumen mixes.
- To study the variation in various Marshall Properties like Stability, Flow, Air voids, Voids in Mineral Aggregate (VMA), Voids Filled with Bitumen (VFB) with the Change in temperature of aggregates with warm mix asphalt (Sasobit & Stearic Acid) when compared to VG30 bitumen.
- To determine the Suitable temperature for paving of WMA.

o Experimental Work and Results

Table 3.1: Physical Requirements for Coarse Aggregate for DBM.

S. No	Property	Test	Specification	Test Result
1	Cleanliness (dust)	Grain size analysis	Max 5 % passing 0.075 IS-Sieve	20mm - 0.333
				10mm - 0.389
2	Particle shape	Flakiness Index	15 % Max	13.03%
		Elongation Index	20% Max	17.50%
3	Strength	Aggregate Crushing Value(ACV)	30 % Max	13.02%
		Aggregate Impact Value(AIV)	27 % Max	14.30%
		Los Angeles Abrasion Value	35 % Max	24.32%
4	Durability	Soundness		
		Sodium Sulphate	Max 12 %	16.76%

		Magnesium Sulphate - 2	Max 18 %	
5	Water absorption value	Water absorption value	2 % Max	Average :- 0.12%

Table 3.2 Properties of Bitumen

Property	Test Method	Value	Requirement as per IS-73
Penetration at 25°C (mm)	IS : 1203 – 1978	50.02	50-70 mm
Softening Point (°C)	IS : 1203 – 1978	53°C	Min 47°C
Specific gravity	IS : 1203 – 1978	1.03	

Table 3.3: Results of tests for Sasobit & Stearic Acid WMA mix

Property Tested	Test Method	Sasobit	Stearic Acid
Penetration (100 gram, 5seconds at 250C) (1/10th of mm)	IS 1203-1978	39 mm	98 mm
Softening Point 0°C (Ring & Ball Apparatus)	IS 1205-1978	52.4°C	47.1°C

Table 3.4: Composition of Dense bituminous macadam mix

IS Sieve size (mm)	Job Mix Formula (JMF)	Aggregate (%)	Weight of aggregate (gms)	Cumulative weight (gm)
37.5	100	4.32	51.84	51.84
26.5	95.68	8.32	99.84	151.68
19	87.36	10.25	123	274.68
13.2	77.11	34.59	415.08	689.76
4.75	42.52	10.7	128.4	818.16
2.36	31.82	22.09	265.08	1083.24
0.300	9.73	6.1	73.2	1156.44
0.075	3.63	2.63	31.56	1188
FILLER	1	1	12	TOTAL = 1200

Table 3.5: Dense bituminous macadam Gradation as per MORT & H specification

Grading	1	2
Nominal aggregate size mm	40mm	25mm
Layer Thickness	80 - 100mm	50 - 75mm
IS Sieve (mm)	Cumulative % by weight of total aggregate	
45	100	-
37.5	95-100	100
26.5	63-93	90-100
19	-	71-95
13.2	55-75	56-80
4.75	38-75	38-54
2.36	28-42	28-42
0.3	7--21	7--21
0.075	2--8	2--8
Bitumen content by mass of total mix %	Min 4.0	Min 4.5
Bitumen Grade pen	65 or 90	65 or 90

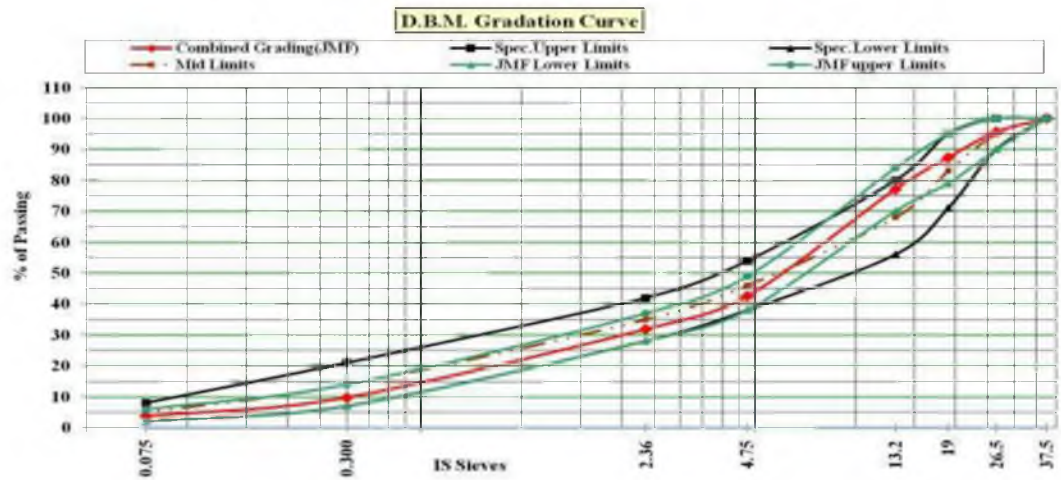


Fig 3.1: DBM Gradation Curve



Fig 3.2 shows the Marshall samples that are prepared for the test of stability and flow for VG 30 samples of different Bitumen content



Fig 3.3 shows Marshall Samples for Sasobit WMA for Different aggregate temperatures



Fig 3.4 shows Marshall Samples for Stearic Acid WMA for Different aggregate temperatures

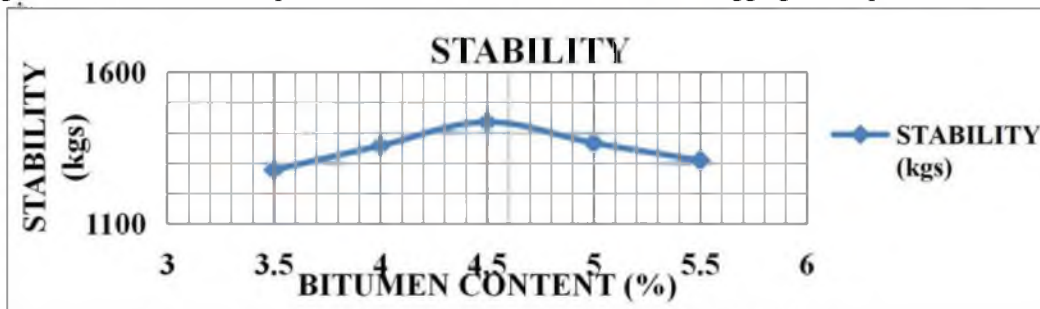


Fig3.5 Variation of Marshall Stability of DBM

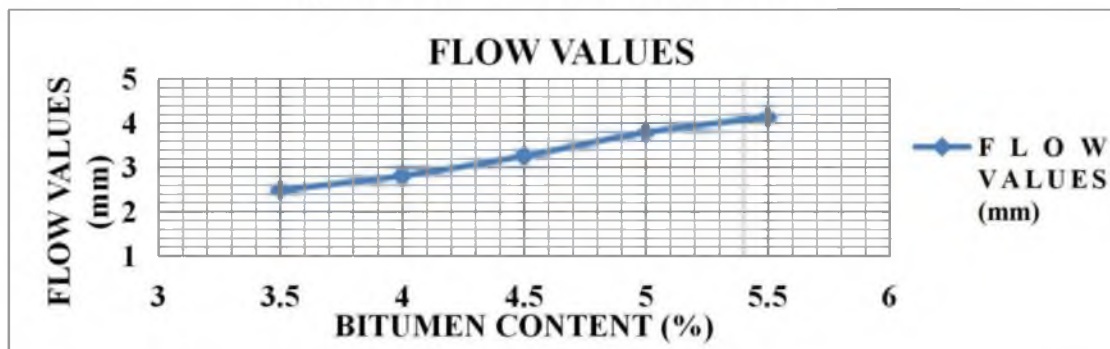


Fig 3.6 Variation of Flow Value of DBM

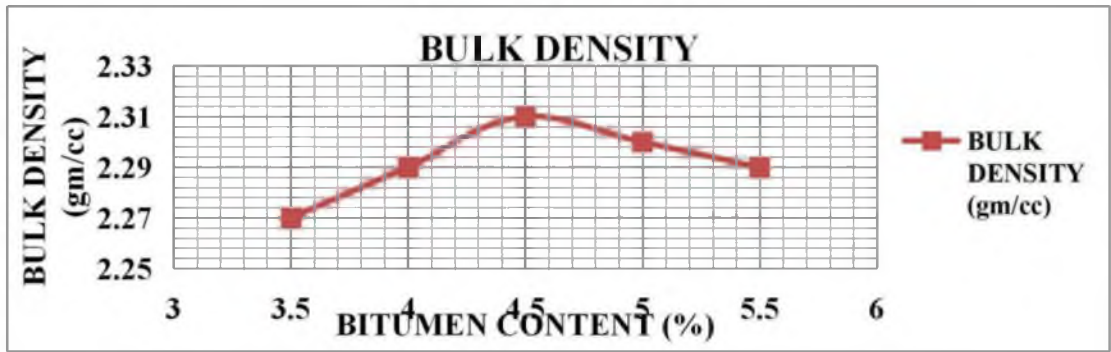


Fig 3.7 Variation of bulk density Value of DBM

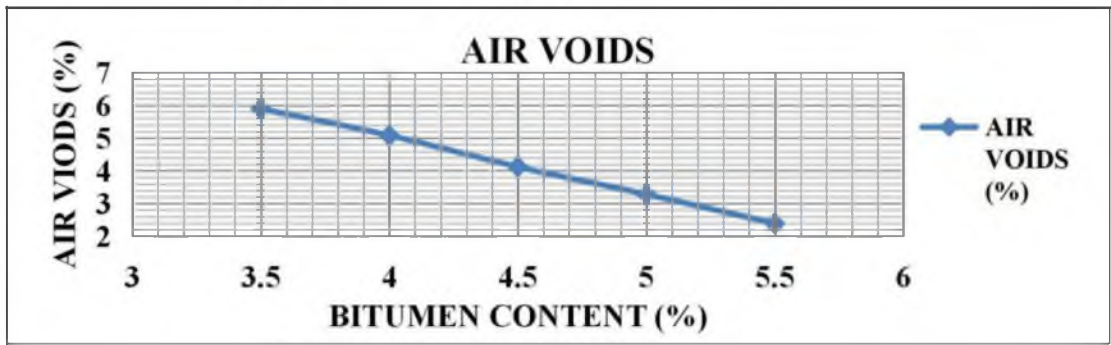


Fig 3.8 Variation of air voids of DBM

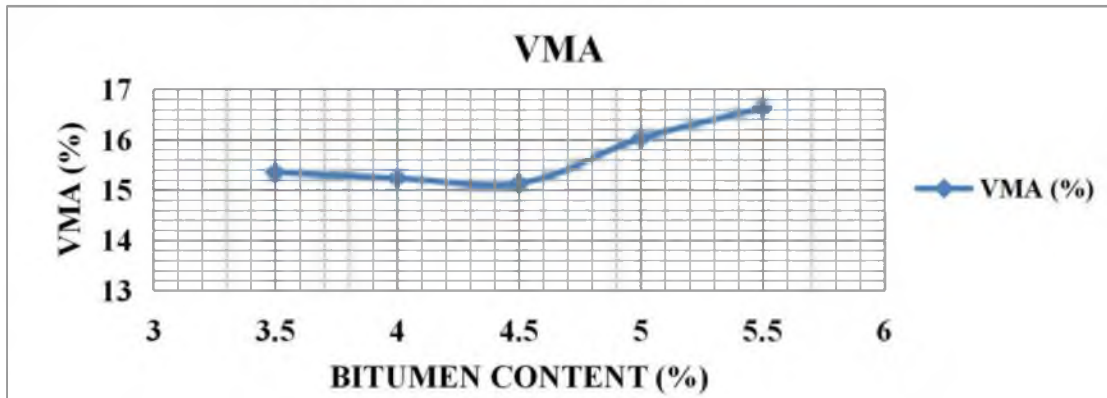


Fig 3.9 Variation of VMA of DBM

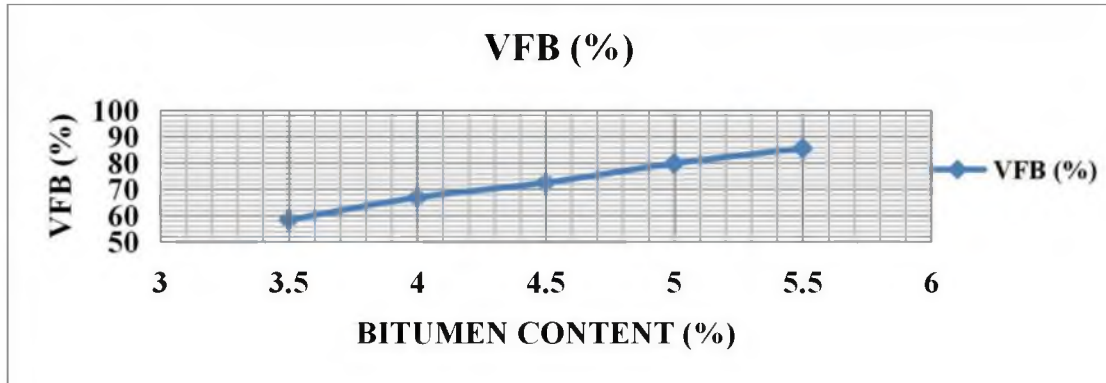


Fig 3.10 Variation of VFB of DBM

3.1 OPTIMUM BINDER CONTENT

Optimum Binder Content is found out by taking average value of following three bitumen Contents found from above graph i.e.

- I. Bitumen content corresponds to maximum stability
- II. Bitumen content correspond to maximum unit weight
- III. Bitumen content corresponding to the median of designed limits of percentage air voids in total mix.

It is suggested by the MORTH that at the target composition the air voids should be within the range 4%. So, the optimum aggregate temperature (OBC) of the present DBM mixes was decided to be estimated based on the average aggregate temperature for maximum density, maximum stability and specified percent air voids in the total mix. Here **LIME** has been selected as filler material for further investigation considering its wide availability, low cost price and environment protection. From the looking into the above graphs the **OBC** is taken as **4.5%**.

3.2 EFFECT OF SASOBIT ON DBM

For preparation of mix, binder content at 4.5% and Sasobit content is opted as 3% by weight of bitumen content varying the aggregate temperatures. Here suitable temperature and other Marshall properties are calculated by Marshall Method.

Table 3.6. Stability value for different Aggregate Temperatures.

AGGREGATE TEMPERATURE (°C)	STABILTY (kgs)
110	1303.67
120	1359.24
130	1429.85
140	1371.25

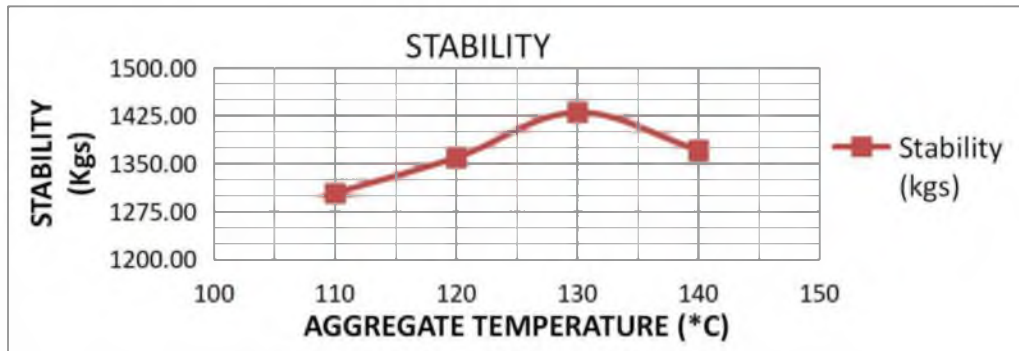


Fig 3.11 Variation of Marshall Stability of WMA With different temperatures

Table 3.7 Flow value for different Aggregate Temperatures

AGGREGATE TEMPERATURE (°C)	FLOW (mm)
110	2.93
120	3.23
130	3.57
140	3.77

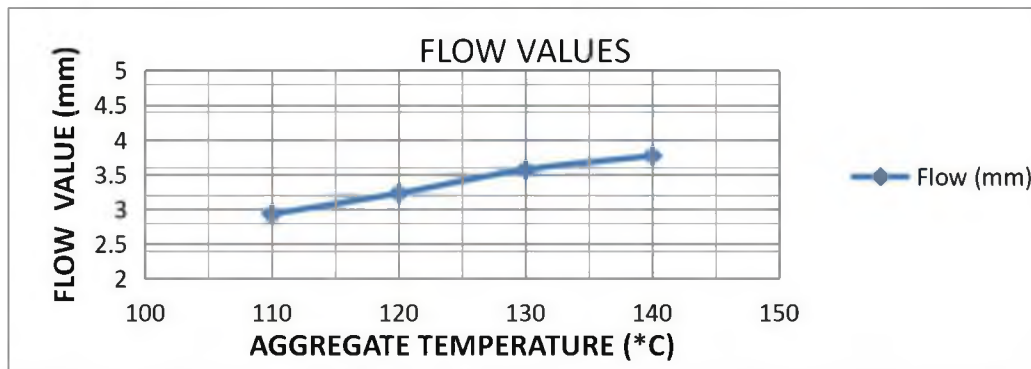


Fig 3.12 Variation of Flow value of WMA with different Aggregate Temperatures.

Table 3.8 Bulk density for different Aggregate temperatures

AGGREGATE TEMPERATURE (°C)	BULK DENSITY
110	2.29
120	2.31
130	2.32
140	2.31

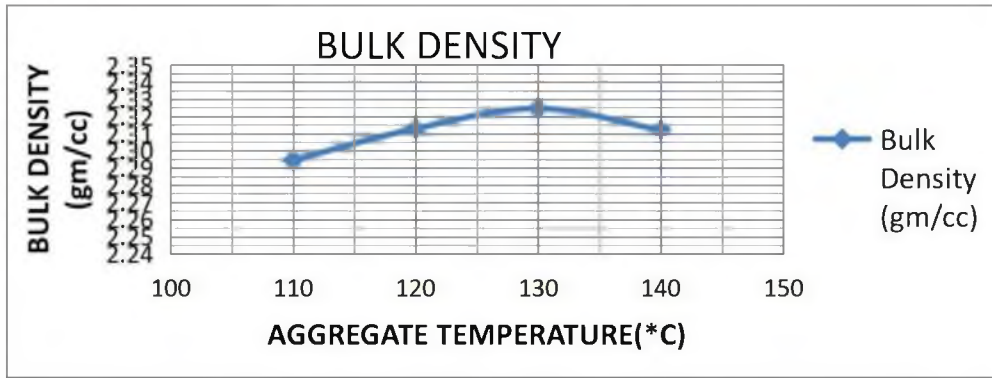


Fig 3.13 Variation of Bulk Density of WMA With different Aggregate Temperatures

Table 3.9 % Air voids for different Aggregate temperature

AGGREGATE TEMPERATURE (°C)	AIR VOIDS (Va)
110	5.37
120	4.94
130	4.59
140	4.49

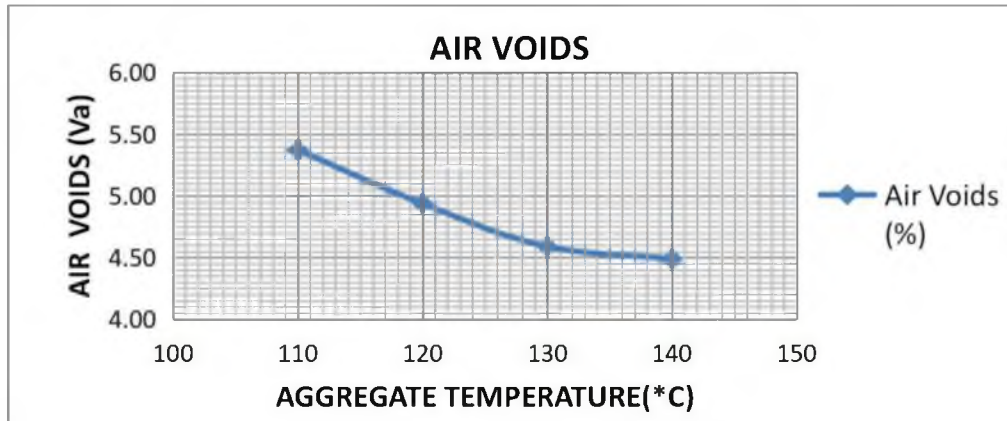


Fig 3.14 Variation of Air Void of WMA With different aggregate temperature

Table 3.10 VMA for different Aggregate temperature

AGGREGATE TEMPERATURE (°C)	VMA
110	15.69
120	14.96
130	14.59
140	14.81

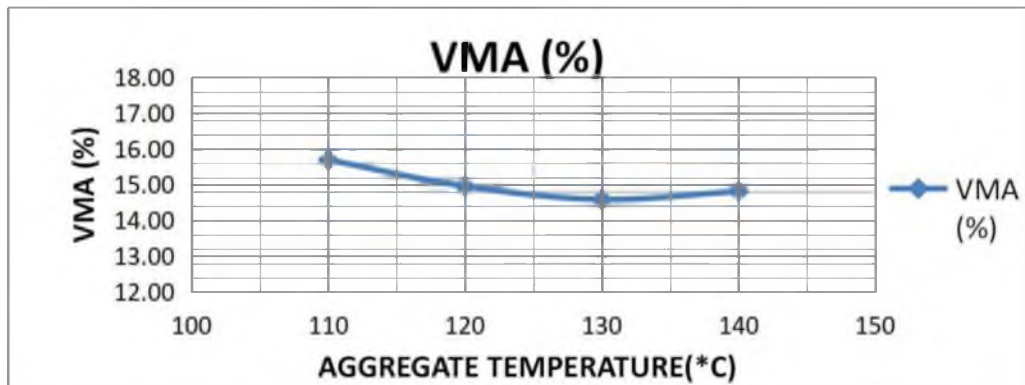


Fig 3.15 Variation of VMA of WMA With different aggregate temperature

Table 3.11 %VFB for different Aggregate temperature

AGGREGATE TEMPERATURE (°C)	VFB
110	67.37
120	67.85
130	68.95
140	70.25

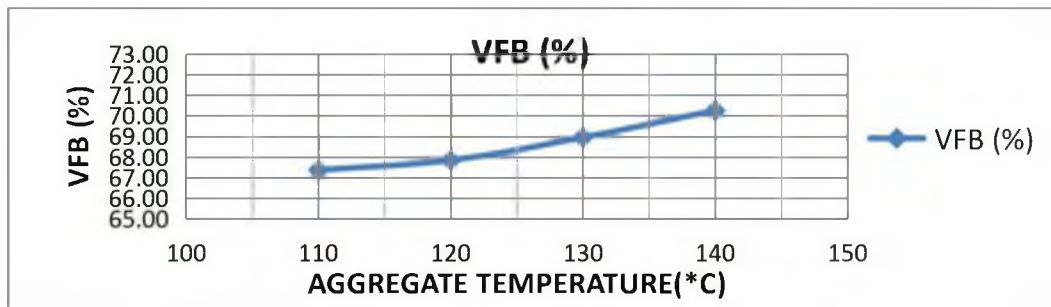


Fig 3.16 Variation of VFB of WMA With different aggregate temperature

3.3 EFFECT OF STEARIC ACID ON DBM

For preparation of mix, binder content at 4.5% and Stearic Acid content is opted as 3% by weight of bitumen content varying the aggregate temperatures. Here suitable temperature and other Marshall properties are calculated by Marshall Method.

Table 3.12 Stability value for different Aggregate Temperatures

AGGREGATE TEMPERATURE (°C)	CORRECTED STABILTY (kgs)
110	1323.25
120	1412.67
130	1318.91
140	1287.67

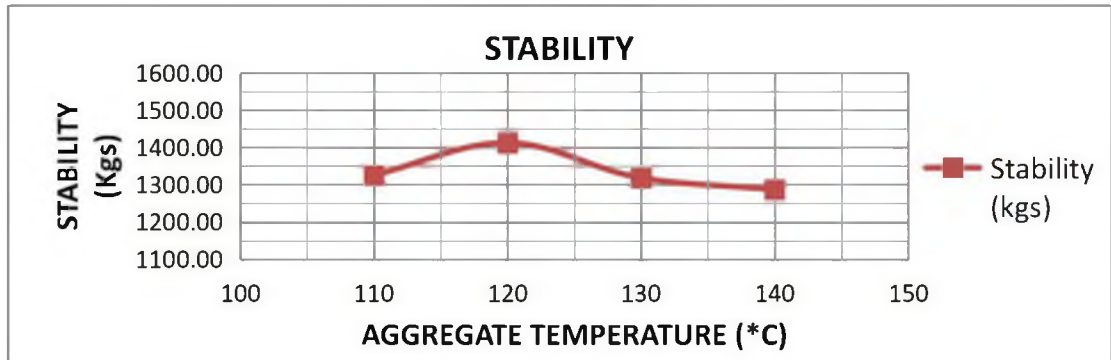


Fig 3.17 Variation of Marshall Stability of WMA With different temperatures

Table 3.13 Flow value for different Aggregate Temperature

AGGREGATE TEMPERATURE (°C)	FLOW (mm)
110	2.77
120	2.94
130	3.24
140	3.59

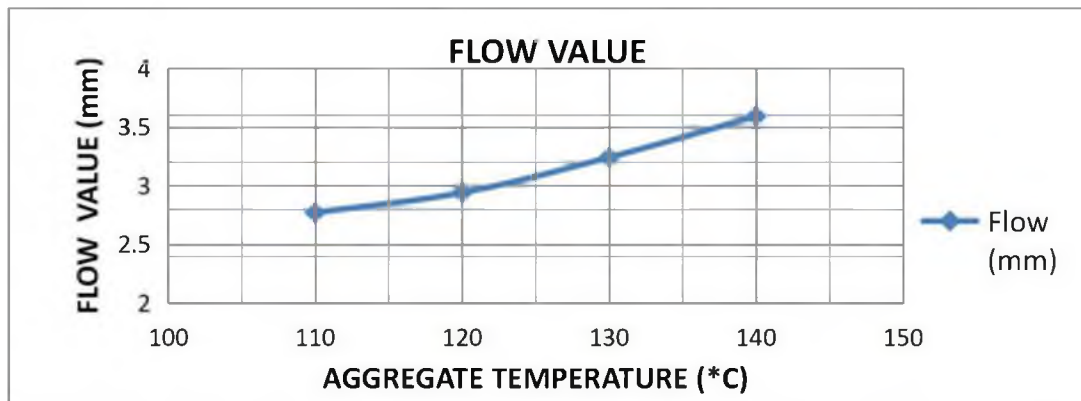


Fig 3.18 Variation of Flow value of WMA with different Aggregate Temperature.

Table 3.14 Bulk density for different aggregate temperatures

AGGREGATE TEMPERATURE (°C)	BULK DENSITY
110	2.32
120	2.34
130	2.33
140	2.32

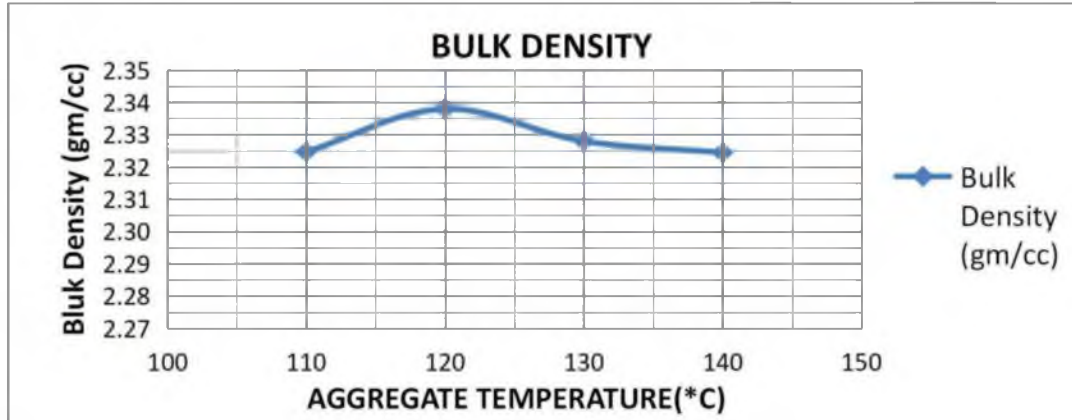


Fig 3.19 Variation of Bulk Density of WMA With different Aggregate Temperature.

Table 3.15 % Air voids for different aggregate temperature

AGGREGATE TEMPERATURE (°C)	AIR VOIDS (Va)
110	4.73
120	4.36
130	4.02
140	3.78

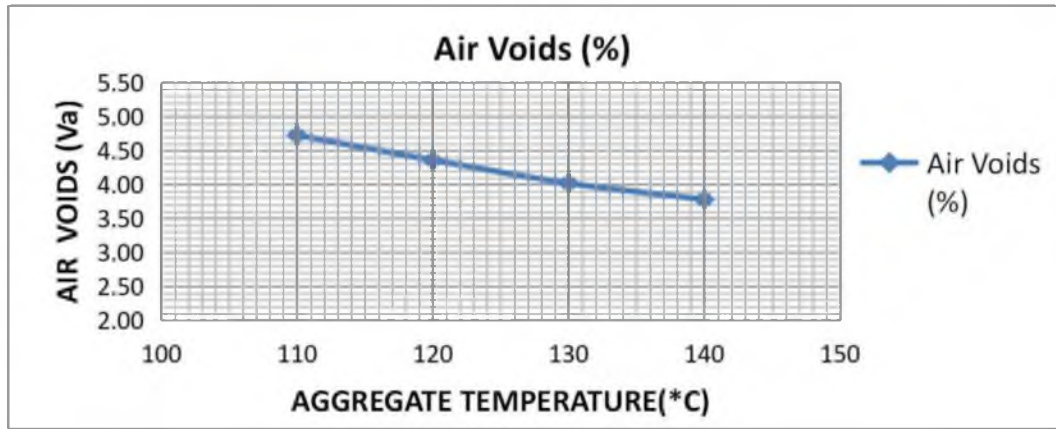


Fig 3.20 Variation of Air Void of VMA With different aggregate temperature

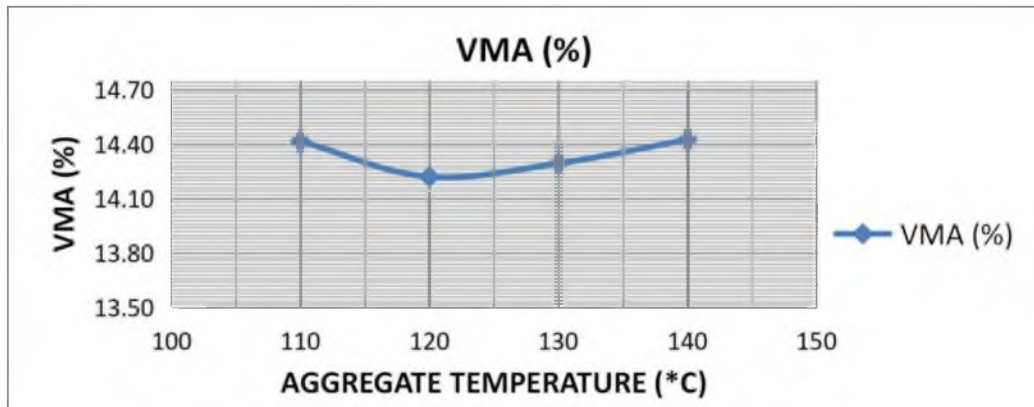


Fig 3.21 Variation of VMA of DMA With different aggregate temperature

Table 3.17%VFB for different aggregate temperature

AGGREGATE TEMPERATURE (°C)	VFB
110	67.18
120	69.34
130	71.87
140	73.79

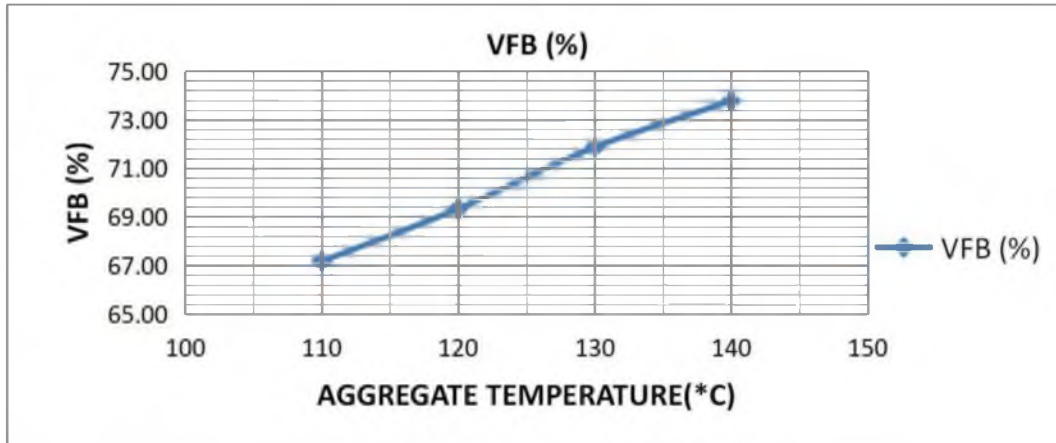


Fig 3.22 Variation of VFB of WMA With different aggregate temperature

3.4 OPTIMUM AGGREGATE TEMPERATURE (OAT)

Optimum Aggregate temperature is found out by taking average value of following three aggregate temperatures found from above graph's i.e.

- I. Optimum Aggregate temperature correspond to maximum stability
- II. Optimum Aggregate temperature correspond to maximum unit weight
- III. Optimum Aggregate temperature corresponding to the median of designed limits of percentage air voids in total mix

Table 3.19 Optimum Aggregate temperature Values of WMA Sasobit Mixes

Property	Aggregate Temperature (°C)			
	110	120	130	140
Nominal aggregate size of 25 mm			130	
Marshall stability (Kgs)	1303.67	1359.24	1429.85	1371.25
Flow Value (mm)	2.93	3.23	3.57	3.77
Bulk density (gm/cc)	2.29	2.31	2.32	2.31
Air Voids (%)	5.37	4.94	4.59	4.49
Voids in Mineral Aggregate VMA (%)	15.69	14.96	14.59	14.81
Void filled with bitumen VFB (%)	67.37	67.85	68.95	70.25

Table 3.20 Optimum Aggregate temperature Values of WMA Stearic Acid Mixes

Property	Aggregate Temperature (°C)			
	110	120	130	140
Nominal aggregate size of 25 mm		120	130	140
Marshall stability (Kgs)	1326.25	1412.67	1318.91	1287.67
Flow Value (mm)	2.77	2.94	3.24	3.59
Bulk density (gm/cc)	2.32	2.34	2.33	2.32
Air Voids (%)	4.73	4.36	4.02	3.78
Voids in Mineral Aggregate VMA (%)	14.41	14.22	14.29	14.42

3.5 COMPARISON BETWEEN HMA AND WMA SASOBIT & STEARIC ACID

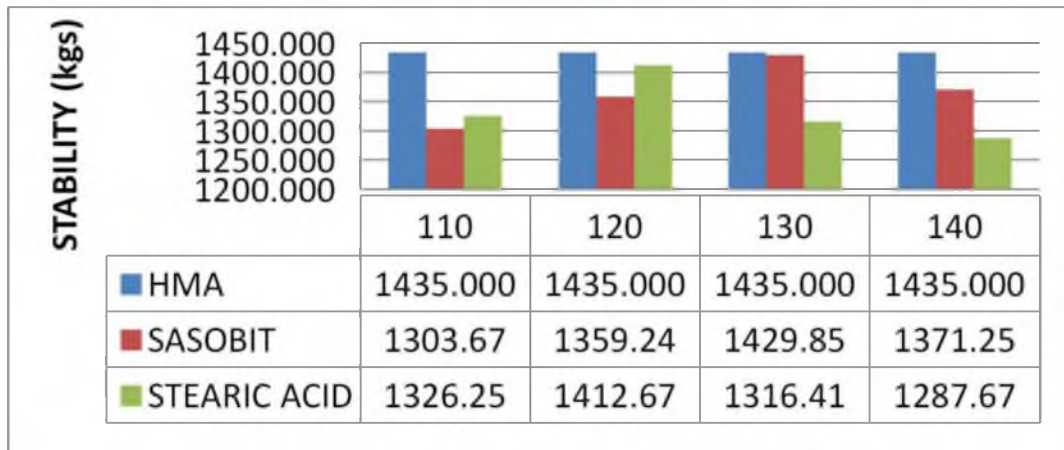


Fig 3.23 Marshall Stability value comparison on HMA & WMA mixes

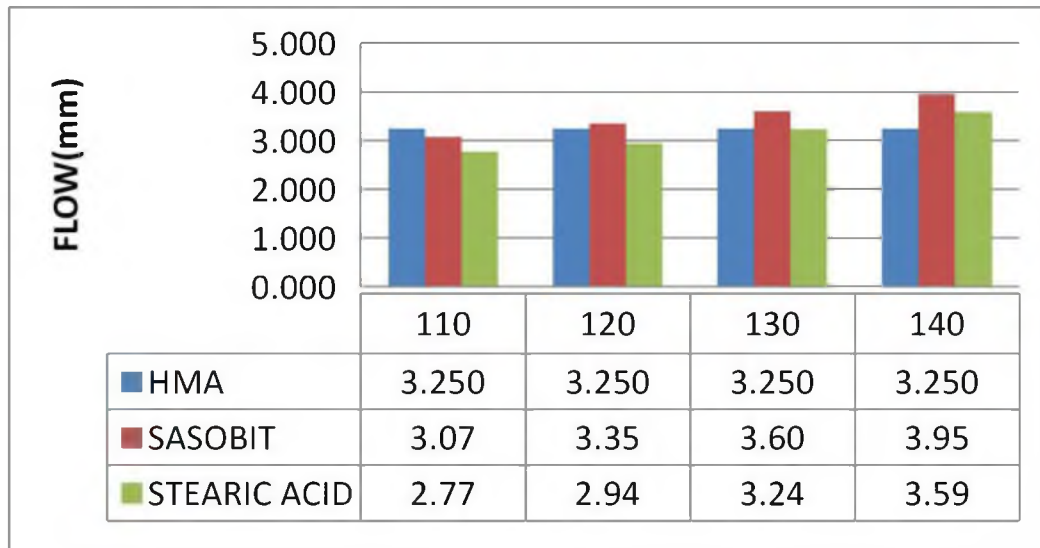


Fig 3.24 Flow value comparison on HMA & WMA mixes

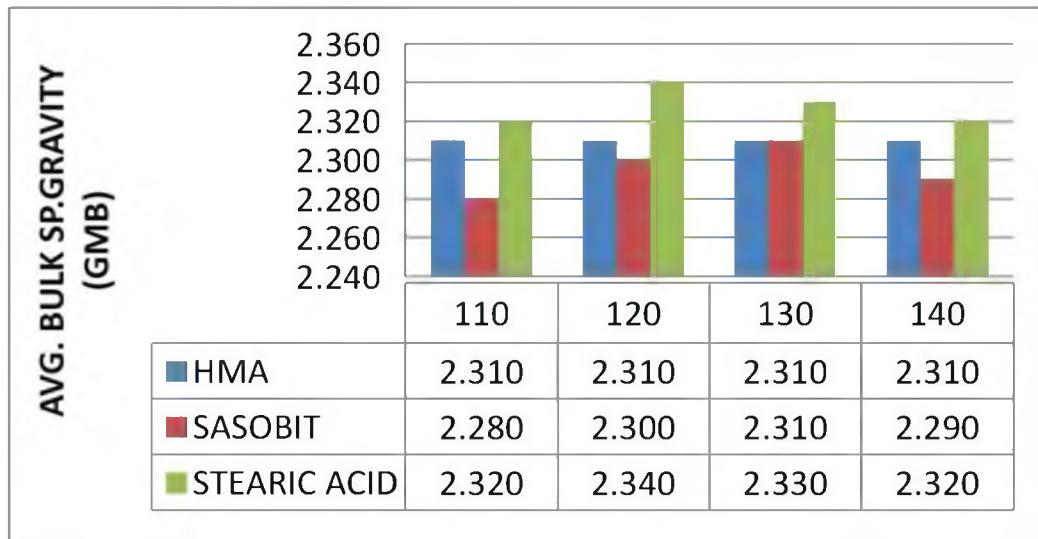


Fig 3.25 Bulk density value comparison on HMA & WMA mixes

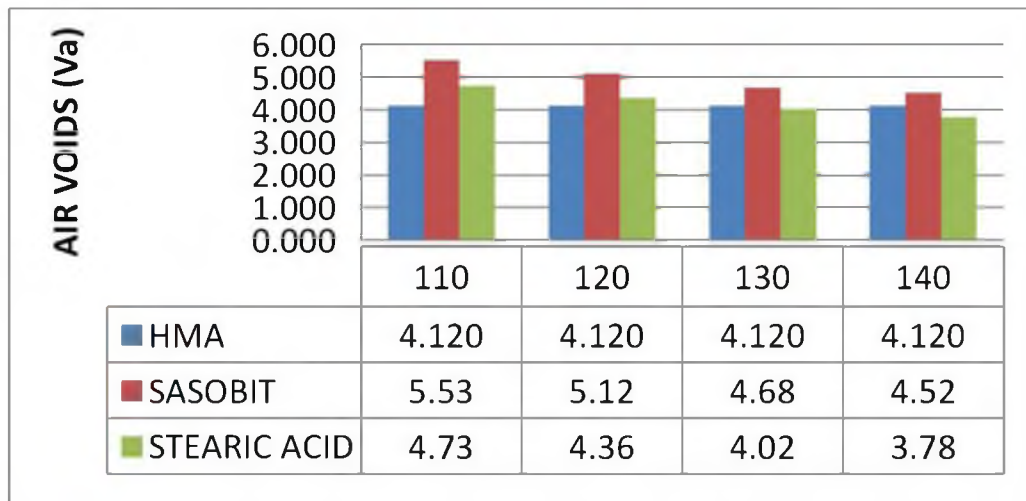


Fig 3.26 Air Voids (%) value comparison on HMA & WMA mixes

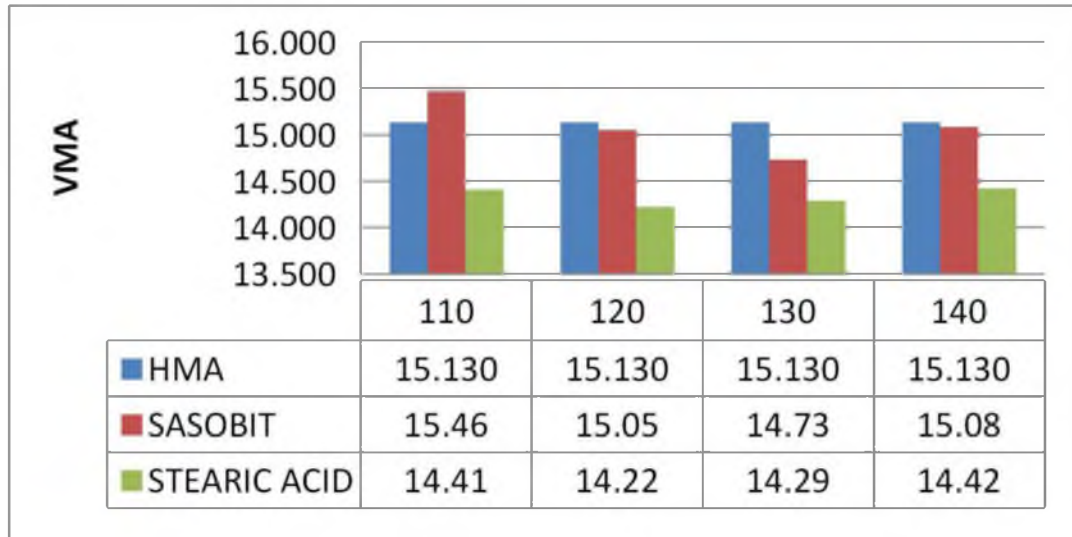


Fig 3.27 VMA (%) value comparison on HMA & WMA mixes

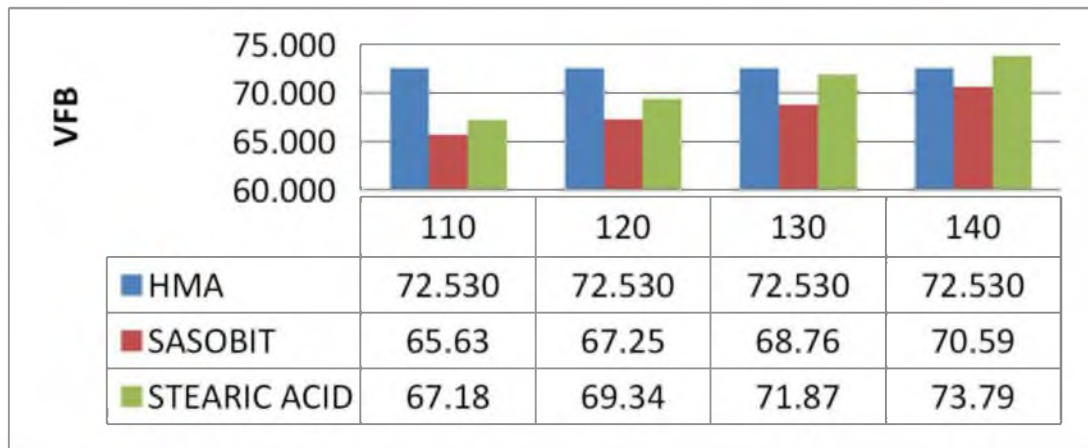


Fig 3.28 VFB (%) value comparison on HMA & WMA mixes

3.5 COST ANALYSIS CALCULATIONS

Table 3.21 SASOBIT- COST ANALYSIS PER MT OF ASPHALT MIX (DBM) - with 3 % SASOBIT and 25% Fuel Saving

SASOBIT- COST ANALYSIS PER MT OF ASPHALT MIX (DBM) - with 3% Sasobit and 25% Fuel Saving

A	Cost Increase	Value	Unit	Total (Rs/ MT)
a	Sasobit - Required per MT of hot mix			
	Cost of Sasobit per Kg	70	Rs	
	With 3% dosage (Binder content considered as 4.5%)			
	Increase in the cost of Hot Mix	1.35	Kg	95
B	Savings	Value	Unit	Total (Rs/ MT)
a	Savings in Fuel			
	Consumption per MT for Normal hot mix - (Aggregate heating, production and laying)	5.5	lts	
	Savings for Sasobit Mix- with minimum 25% savings	1.375	lts	
	Savings in Fuel (cost @ Rs 55/ ltr, deisel)			76
b	Savings in bitumen due to addition of Sasobit			
	Binder cost- Rs 45000/ MT			
	Bitumen saved (0.1%)	0.9	Kg	45
c	Reduction in Anti-Strip Usage			
	Cost per Kg	150	Rs	
	Dosage per MT of binder	0.5%		
	Qty required per MT of Hot Mix	0.225	Kg	
	Savings			34
	Total Minimum Assured Savings (a + b + c)			154
	Direct Cash Benefit (B -A)			60

Table 3.22 showing Project Economics (1 lane , 1 KM Project)

Cost of Sasobit	Value	Units
A)DBM Layer		
Width of Lane	3.5	Mts
Length	1000	Mts
Thickness (110mm)	0.11	Mts
Total Volume of Mix Required	385.0	Cub Mts
Weight of the Mix Required	924.4	MT
Bitumen Required (4.5%)	41.6	MT
Sasobit Required (3% of Bitumen)	1247.9	Kgs
Total Sasobit Required per Lane Km	1247.9	Kgs
Total Kms of Project	1	Kms
Lanes	1	Nos

Total Sasobit Required for the Project	1247.91975	Kgs
Price of Sasobit	70	Rs/ Kg
Total Cost of Sasobit for the project	87,354	Rs

3.23 Direct Cash Savings of Sasobit Usage

DIRECT CASH SAVINGS ON ACCOUNT OF SASOBIT USAGE	
	INR
FUEL SAVINGS	69,906.62
SAVINGS OF BITUMEN	41,597.33
SAVINGS OF LIME	31,197.99
TOTAL SAVINGS	142,701.93
NET REVENUE (in INR)	55,347.55

4 CONCLUSION

It is observed that the penetration value of Neat / VG30 Bitumen drops down from 62.7 to 58 for WMA Sasobit and there is a increase in penetration value from 62.7 to 98 for Stearic Acid.

It is observed that the softening point value of Neat / VG30 Bitumen & drops down from 49.8 to 38 for WMA Sasobit and 47.1 for Stearic Acid.

The Bulk density value for VG30 bitumen mixes at OBC 4.5% in HMA at 160°C was equal to that of WMA Sasobit & Stearic acid at 130°C and 120°C, Thereby attaining better density at much lower temperatures than HMA.

The Marshall properties of Sasobit WMA at 130°C and Stearic Acid WMA 120°C are comparable to HMA at 160°C.

Reduction in emissions as compared to HMA Mixtures.

It is economical to use WMA at site over HMA as it enhances Direct and Indirect cost savings.

REFERENCES

1. Ministry of Road Transport and Highways (MORT & H), “*Specifications for road and bridge works*”.
2. Bureau of Indian Standards, Paving Bitumen- Specification (Third Revision) IS 73:2006, July 2006.
3. Mix Design Methods for Asphalt Concrete and Other Hot- Mix Types, Asphalt Institute Manual Series NO.2 (MS-2), 6.
4. S.K. Khanna and C.E.G Justo “*Highway Engineering*” 2008.
5. Marshall Procedures for Design and Quality Control of Asphalt Mixtures. Asphalt Paving Technology: Proceedings vol. 54. Association of Asphalt Paving Technologists Technical Sessions, 11-13 February 1985. San Antonio, TX. pp. 265-284.
6. MeadWestvaco (2003) “laboratory study to determine applicability of Sasobit & Stearic Acid for typical paving operation”
7. Graham C. Hurley and Brain D Prowell (2006) “Evaluation of Sasobit & Stearic Acid for use in Warm Mix Asphalt” NCAT, Auburn University, Alabama
8. Oke Oluwaseyi ‘Lanre (2010) “A study on development of guidelines for the production of Bitumen Emulsion stabilized RAP for roads in the Tropics” Ph.D. Thesis, University of Nottingham.

9. Maria del Mar Colas Victoria (2010) "Update of Emulsion based mixes (cold & warm)".
10. Zun jhang (2010) "Effects of Warm Mix Asphalts Additives on Asphalt Mixture Characteristics and Pavement performance" Civil Engineering Theses, Student Research, University of Nebraska-Lincoln.
11. Prithvi Singh Kandhal (2010) "Warm Mix Asphalt Technologies: an overview" Journal of Indian Road Congress.
12. Narayan Panda (2010) "Laboratory investigations of stone matrix asphalt using sisal fibre for Indian roads" B.tech project, NIT Rourkela.
13. J. Oliveira, H. Silva, P. Fonseca et al., "Laboratory and field study of a WMA mixture produced with a new temperature reduction additive," in Proceedings of the 2nd International Conference on Warm Mix Asphalt, St. Louis, Mo, USA, 2011.
14. D. Jones, R. Wu, T. Bor-Wen, Q. Lu, and J. T. Harvey, "Warm-mix asphalt study: test track construction and first-level analysis of phase 1 HVS and laboratory testing," Research Report UCPRC-RR-2008-11, 2008.
15. Y. Kim, C. Baek, J. Lee, et al., "Evaluation of LEADCAP WMA additive for use in PSMA mixture in China," in Proceedings of the International Conference on Highway Engineering for Sustainable Innovations toward Green Highways, Bangkok, Thailand, 2012.
16. J. Lee, Y. Kim, D. Cho, S. Yang, J. Lim, and S. Kwon, "Evaluation of moisture susceptibility of warm-mix asphalt with MMLS," in Proceedings of the 24th World Road Congress, Mexico City, Mexico, 2011.

Environmental Impact Assessment of Thrissur-Vadanapally Road Project

Rosmy Sebastian¹, Vincy Verghese² and M. G. Cyriac³

PG Scholar,

²Assistant Professor

³Associate Professor,

Department of Civil Engineering,

Jyothi Engineering College, Cheruthuruthy, Thrissur, Kerala 679 531.

Abstract. Environmental impact assessment (EIA) for transportation projects has an integral role in environmental management schemes. All the road works and other transportation infrastructure development programs creates significant impact on various aspects of life. Impacts can be positive or negative. Here an EIA is conducted to study the socio-economic impacts and bio-physical impacts of widening of Thrissur - Vadanapally road project and evaluation of the same. The impact prediction is done by means of good fit models for the existing conditions. Gaussian air dispersion model, CRTN Model for traffic noise, Mass Balance and Streeter- Phelps Equation for water quality analysis were used. With the help of these models, the prediction is done accurately. The predicted impact includes the meteorological and climatic impacts, noise quality, water quality, air quality and social impacts. Water quality changes rises only when there is change in drainage pattern occurs. These change is modelled using the Streeter Phelps equation and the mass balance equations. Air quality modelling was done using the Gaussian dispersion model and the impact of traffic noise was done using the CRTN Models. The air and noise values at the present condition was greater than the prescribed norms of pollution control board. The air quality issues are predominant at distances nearer to the source, as the distance increases the effect of air pollution also decreases. Various mitigation measures are suggested for reducing the impacts predicted or to avoid the impact in each stage of construction.

Keywords: Environmental impact assessment, impact prediction, impact modelling, mitigation measures

1 Introduction

Recent environmental issues that has developed due to Urbanization with special effects on the environment has led to the process called Environmental Impact Assessment (EIA) which can be defined as “the need to identify and predict impacts on the environment and on man's wellbeing of legislative proposals, policies, programs, projects and procedures and to interpreter and communicate information about the impacts”. Since the introduction of EIA over 30 years ago, the possible profits has been widely recognized and it has been adopted and implemented in more than 100 countries by numerous aid and funding agencies .In essence, EIA is a process that assesses the impact of developments on the environment in a efficient, universal and multidisciplinary way taking into consideration all environmental components. EIA as a process involves a number of steps which are as follows: [3]

- Description of project
- Screening
- Scoping/consideration of alternatives
- Baseline studies public consultation and participation
- Impact prediction
- Preparation of Environmental Impact Statement(EIS)
- Decision making
- Post decision making and monitoring

1.1 Objectives

The main objective of the study is identified as to predict and evaluate impacts of a road project.

To achieve the main objective of predicting and evaluating the impacts of a road project involves following subtasks:

- Impact prediction using good fit models
- Suggesting mitigation measures for impacts predicted

2 Literature Review

Environmental impact assessment (EIA) is a planning instrument for predicting the effects on the environment from altering or building a new establishment. For the purposes of EIA, the meaning of environment incorporates physical, biological, cultural, economic and social factors. Over the last three decades, environmental impact assessment (EIA) or environmental assessment (EA) has become a major tool for effective environmental management. Over the years, the focus of EA has changed towards making it a useful tool for environmental sustainability, which can be very effectively put to use to ensure that all important factors are included and unnecessary factors are revealed and dropped. This contributes towards ensuring that the environmental sinks and resources are not so excessively stressed as to cause any reduction in the assimilative capacity of the environment.

Highway projects are generally undertaken to improve the economic and social welfare of the people. At the same time, they may also create an adverse impact on the surrounding environment. People and property in the direct path of the road works are affected. The environmental and social impact of highway projects include damage to sensitive eco-systems, soil erosion, changes to drainage pattern and thereby groundwater, interference with animal and plant life, loss of productive agricultural lands, resettlement of people, disruption of local economic activities, demographic changes, accelerated urbanization and increase in air pollution. Highway development and operation should, therefore, be planned with careful consideration of the environmental impact. To minimize these adverse effects that may be created by highway development projects, the techniques of EIA become necessary. Identification and assessment of potential environmental impact should be an integral part of the project cycle. It should commence early in the planning process to enable a full consideration of alternatives and to avoid later delays and complications. [3]

Impacts of the project on various environmental components were identified at preconstruction, construction and operation phases of the project on the basis of assessment of proposed project activities and analytical review of baseline environmental status of the project impact zone. Further, the impacts were categorized into permanent or temporary and highly significant, moderately significant, less significant and no significant based on the character and magnitude of impacts. Various impact on air, noise and water quality were identified using the models available.

2.1 Air Dispersion Model

Gaussian plume model uses a realistic description of dispersion, where it represents an analytical solution to the diffusion equation for idealized circumstances. The model assumes that the atmospheric turbulence is both stationary and homogeneous. In reality, none of these conditions is fully satisfied. However, Gaussian plume model has been successfully used for rural configurations. [1] The Gaussian dispersion equation can be written as:

$$C(x, y, z) = \frac{Q}{2\pi\sigma_y\sigma_z u} \exp\left(\frac{-y^2}{2\sigma_y^2}\right) \left[\exp\left(\frac{-(z-h)^2}{2\sigma_z^2}\right) + \exp\left(\frac{-(z+h)^2}{2\sigma_z^2}\right) \right] \quad (1)$$

Where C is the concentration, Q is the emission rate of the pollutant from the source, u is the wind speed which defines the direction x. y is the horizontal distance perpendicular to the wind direction, z is the vertical direction, H is the effective height of the plume (considering the additional height Δh to which the hot gases rise above the physical height of the source h); i.e., H = h + Δh, and σ_y and σ_z are the parameters of the normal distributions in y and z directions, usually called the dispersion coefficients in y and z directions respectively.

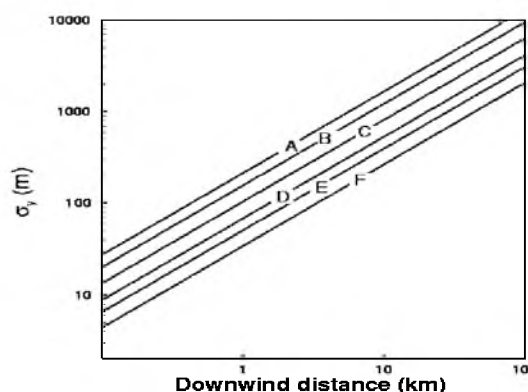


Fig.1. Pasquill-Gifford (P-G) curve for σ_y

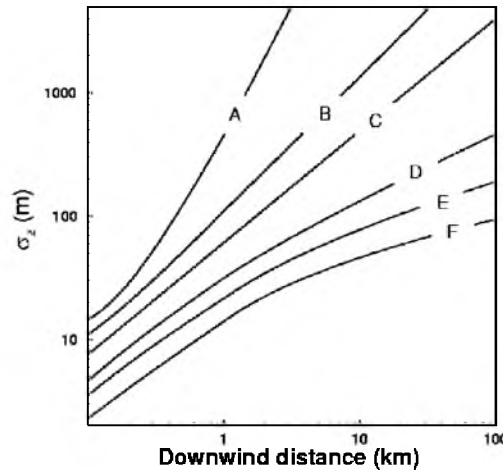


Fig.2. Pasquill-Gifford (P-G) curve for σ_z

Pasquill assigned a letter value to each of the curves ranging from A through F, where A represents highly turbulent conditions resulting in vigorous diffusion and F represents conditions with relatively little turbulence and weak diffusion. Furthermore, he specified practical criteria needed to identify the atmospheric conditions represented by each of the curves that were based on routine observations of wind speed, cloud cover and solar insolation. Gifford subsequently reformulated Pasquill’s method of defining h and θ to produce the now well-known and widely used curves for σ_y and σ_z , given in figure 1 and 2. In the graphs each curve represents the following:

- A: strongly unstable
- B: moderately unstable
- C: slightly unstable
- D: neutral
- E: slightly stable
- F: moderately stable

2.2 CRTN Model for Traffic Noise

A motor traffic noise model based on the perpendicular propagation analysis technique (direction perpendicular to the center line of motorways carriageway) is found performed well in a statistical goodness-of-fit test against the field data. For each type of vehicle, regression analysis of noise level (dB A) on speed was carried out based on Logarithmic relationship. [4]

A traffic noise model was applied for the basic noise level study. The equation being used in practice for predicting the basic traffic noise is the calculation of road traffic noise (CRTN) model. The main equation for predicting the noise level is given by,

$$L = 10 \log Q + 33 \log (V + 40 + 500 / V) + 10 \log (1 + 5P / V) - 26.6 \tag{2}$$

Where:

L= Predicted noise level in dB

Q= Traffic flow

P = Percentage of heavy vehicle;

V = Average speed of vehicles.

2.3 Mass Balance and Streeter- Phelps Equation for Water Quality Modelling

The Streeter–Phelps equation is used in the study of water pollution as a water quality modelling tool. The model describes how dissolved oxygen (DO) decreases in a river or stream along a certain distance by degradation of biochemical oxygen demand (BOD). The equation is also known as the DO sag equation. [1]

$$D_t = \frac{K_D L}{K_R - K_D} [10^{-K_D t} - 10^{-K_R t}] + [D_0 10^{-K_R t}] \tag{3}$$

Where.

D_t = Dissolved oxygen (DO) deficit, mg/l

K_R = Re oxygenation coefficient

$$= K_{R(20)} [1.016]^{T-20}$$

$K_{R(20)}$ = Re oxygenation coefficient at 20°C, generally taken 0.15-0.2

$$K_D = \text{De oxygenation coefficient}$$

$$= K_{D(20)} [1.047]^{T-20}$$

$K_{R(20)}$ = De oxygenation coefficient at 20°C, generally taken 0.1

L = Ultimate BOD of the mix at the point of discharge, mg/l

D_0 = Initial DO deficit, mg/l

When two streams or rivers merge or water is discharged to a stream it is possible to determine the BOD and DO after mixing assuming steady state conditions and instantaneous mixing. The two streams are considered as dilutions of each other thus the initial BOD of the mix,

$$C = \frac{C_S Q_S + C_R Q_R}{Q_S + Q_R} \tag{4}$$

Where,

C = Initial concentration of BOD in the river downstream of the mixing

C_S = BOD of the content of the merging river

C_R = Background BOD of the concentration in the river

Q_S = Flow in the merging river upstream from the mixing point

Q_R = Flow in the river upstream from the mixing point

3 Project Description

The Project road Thrissur- Vadanapally is situated in the Thrissur district of Kerala State in the state highway 75 (SH-75). Thrissur- Vadanapally section of length 16.12 km which starts at Chungam Kanjani bus stop (Chain age -0+000) and ends at Eravu (Chain age - 8+980), the total length of the stretch being 8.980 km. The project road lies in the Thrissur District in Kerala and passes through Olarikkara - Elthuruth - Kannapuram -Manakody - Kunnathangadi -Arimbur - Kanjany -kandassankadavu- Vadanapally - Joins NH 17.

Various surveys including those for environmental and social impacts have been carried out for the project roads. These were conducted during the Feasibility Study and updated during the revision of EIA. The carriageway is throughout 10m for the project road, two lane divided carriage way with shoulders. The calculated traffic along the road way at present is 1547 vehicles/hour.

The improvement alternatives considered by the consultants have generally been

- Improve to a wide carriageway of 17m with more shoulders and lined drains with M15 concrete.
- Widening of the carriageway and associated land acquisition to expand the highway to two lanes or to the required width.
- Most of the available corridors widths vary within each link and could not accommodate the widening to two lanes without additional acquisition of land. The available corridor width is not consistent.

4 Data Collection

Primary information regarding the road project like the alignment, cost were collected from the Public works department (PWD), Thrissur. Secondary information was collected from District Planning Maps and District Census Handbooks. Base line information were collected from Thrissur cooperation and Water quality testing laboratory, Thrissur.

The base traffic count was also determined using the video graphic survey technique. Composition of each vehicle in the traffic stream identified for finding out the air quality details. Fresh environmental monitoring was carried out for determination of ambient air quality, water quality, and noise level at various locations along the proposed alignment to establish the baseline status of these environmental parameters along the project area. The important sources of air pollution in the region are vehicular traffic and domestic fuel burning activities. Details of monitoring results are presented in Table 1 and 2.

Table 1. Emission rate for different modes

Mode	CO ₂	CO	No _x	CH ₄	SO ₂	PM	HC	Total
Bicycle	0	0	0	0	0	0	0	0
Two wheeler	26.6	2.2	0.19	0.18	0.013	0.05	0.2	29.433

Three wheeler	60.3	5.1	1.28	0.18	0.029	0.2	0.14	67.229
Car	223.6	1.98	0.2	0.17	0.05	0.03	0.25	226.28
Bus	515.2	3.6	12	0.09	1.42	0.56	0.87	533.74
LMV	515.2	3.6	12	0.09	1.42	0.56	0.87	533.74
HMV	515.2	5.1	1.28	0.09	1.42	0.2	0.14	523.43

Table 2. Emission rate

Mode	Speed of vehicle (m/s)	Emission at entry (Olarikkara) (g/s)	Emission at exit (Eravu)(g/s)
Bicycle	0	0	0
Two Wheeler	42	2468.547	1816.193
Three Wheeler	40	30.532	30.525
Car	45	1937.522	1903.58
Bus	40	533.739	462.571
LMV	50	445.951	280.488
HMV	35	583.754	583.754

Emissions from the vehicle at entry and exit depends on the number of vehicles and its speed. As the speed of the vehicles increases the emission rate decreases. Also emission rate depends on the road way characteristics.

Noise level monitoring was carried out at each location in a peak hour traffic time using sound level meter capable of measuring the Sound Pressure Level (SPL) in dB. The calculated noise levels at locations in the project road are presented in Table 3. The values are compared with the standards prescribed by CPCB for various zones.

Table 3. Ambient noise level along the project road

Sl no	Place	Category of zone	Sound level(dB)	Applicable CPCB values at day time (dB)
1	Waiting Shed	Commercial cum Residential	70.5	55
2	Kalhara Apartments	Residential	60	55
3	Mother Hospital	Silent zone	70.5	50
4	Olarikkara Temple	Silent zone	70.5	50
5	Olarikkara Church	Silent zone and commercial zone	72.5	60
6	Elthuruth Junction	Commercial	69	65
7	Somany Fittings , Chettupuzha	Commercial	71.5	65
8	Saraswathi Vilasam School, Chettupuzha	Silent zone	69	50
9	St. Gemma's L. P School	Silent zone	72	50
10	Niya Collections , Kunnathangnadi	Commercial	73	65
11	Govt U. P. School Arimbur	Silent zone	69	50
12	Kerala Agro Industries Cooperation	Commercial	60	65
13	St Joseph's H.S. S Eravu	Silent zone	70	50
14	Karali Engineering Works	Commercial cum Residential	72	55

5 Modelling of Potential Impacts

5.1 Air Quality Impacts

Obtained emission rates are used for modelling in the Gaussian plume model. Defining the study area conditions the equation 1 reduces to,

$$C(x, 0, 0) = \frac{Q}{2\pi\sigma_y\sigma_z u}$$

Since the emission is at ground level, height of the plume H is taken as zero and the horizontal direction perpendicular to the direction of wind y and the vertical z is also taken as zero. The results of this study is tabulated in the table 3 and 4. The concentration are tabulated for each 110m x distance at the entry and exit points of the road stretch. Concentration of vehicular emission at various distances from the point of its origin was plotted.

Table 4. Concentration of pollutants at entry point (Olarikkara)

Entry Q=5347.697*10 ⁶ µg/s	
x (m)	C (µg/m ³)
100	14055067.35
210	7649016.245
320	3123348.3
430	2248810.776
540	1115481.536
650	937004.49
760	638866.698
870	449762.155
1000	267715.568

Table 5. Concentration of Pollutants at exit point (Eravu)

Exit Q=5432.79*10 ⁶ µg/s	
x (m)	C (µg/m ³)
100	14278712.75
210	7770728.028
320	3173047.278
430	2284594.04
540	1133231.171
650	951914.183
760	649032.398
870	456978.808
1000	271975.481

The concentration of the emission will be higher at its origin point. As the distance from the source increases its concentration level decreases and reduces up to a negligible level. This means that zones nearer to the road project suffer more than that at the far end. The vehicular emissions have damaging effects on both human health and ecology. There is a wide range of adverse health/environmental effects of the pollutants released from vehicles. The effects may be direct as well as indirect including right from reduced visibility to cancers and death in some cases of acute exposure of pollutants specially carbon monoxide. These pollutants are believed to directly affect the respiratory and cardiovascular systems. In particular, high levels of sulphur dioxide and Suspended Particulate Matter are associated with increased mortality, morbidity and impaired pulmonary function. At Olarikkara there we have sensitive areas like hospitals, religious places with the impact zones and

also we have residential cum commercial zones. So special care should be taken for that zones. At the exit point of our project corridor, i.e. at Eravu, we have residential cum commercial zones with in the effected distance

5.2 Water Quality Impacts

Water quality issues are considered only due to the drainage pattern. When it rains the rain water reaches the nearby water body i.e. to the Puzhakkal River nearer to the project corridor. The changes in the give water quality conditions are checked. The change in dissolved oxygen is only calculated using the Streeter–Phelps equation and mass balance equations. The present and predicted water quality changes are given in the table 5 given below.

Table 6. Water quality of Puzhakkal River

Parameters observed	Present water quality	Predicted water quality change	Permissible limits IS 10500(2012)
Nitrate	2.340 mg/l	30 mg/l	45 mg/l
Iron	0.234 mg/l	0.8 mg/l	0.3 mg/l
Chloride	24.000mg/l	40.000mg/l	1000 mg/l
pH	6.3	6.4	6.5-8.5
COD	13.6 mg/l	47.16 mg/l	
BOD	8.5 mg/l	30 mg/l	
DO	4.8	5.2	

Using the mass balance equation initial BOD of the river- effluent mixture will be equal to 10 mg/l corresponding to a flow of 27 m³/s for river water and 1.55 m³/s drainage water. The ultimate BOD of the river is taken as 14.62 mg/l and it is assumed that river is flowing at a velocity of 0.2 m/s. Using the equation 3 and 4 the DO deficit was calculated for the entire river length i.e. for 30 Km. saturation DO is taken to be 7.6 mg/l corresponding to 5000mg/l chlorine at 30°C. The results are given in the table 6.

Table 7. DO deficiency at Puzhakkal River

Distance (Km)	Number of days	DO deficit (mg/l)
5	0.28	3.92
10	0.57	3.42
15	0.86	2.83
20	1.15	2.55
25	1.44	2.41
30	1.73	2.36

Due to the re-oxygenation process the DO deficit value decreases. The oxygen deficiency in the water will affect the biotic life present in the river.

5.3 Noise Quality Impacts

The major source of noise pollution is due to the noise generated from the vehicles. The noise level at the entry and exit points are calculated by considering the vehicular traffic present there using the equation 2

Table 8. Noise level due to traffic

	At entry	At exit
Total number of vehicles	3362	2321
Percentage of heavy vehicles	2.85%	3.61%
Average speed of vehicles	42 Km/h	42 Km/h
Traffic flow	2241.33 veh/h	1547.33 veh/h
Noise level	72.01 dB	70.41 dB

The ambient noise level calculated is above the permissible limits i.e., greater than 55dB in the residential cum commercial areas. Also we have to take attention towards the sensitive areas like hospitals and religious places in the entry point. The increased noise level will effect badly on these areas.

6 Mitigation Measures

The increased runoff due to widening of the roadway will be negligibly small. Water quality in roadside ponds adjacent to the right of way may show slight improvement after road upgrading due to reduced erosion from improved roadside berms and embankment slopes stabilized or protected by rip trap or other material including planting to prevent soil erosion. The water quality impacts will be controlled, mitigated or minimized by the enforcement of all applicable laws and regulations. This is built in to the Environmental Management Plan. The upgrading of the project road link will reduce erosion from the roadway and result in minor improvements in water quality (i.e. reduced silt loads). Care has been taken in the design to provide side drainage.

The net air quality impact during the operational phase of the project road is expected to be beneficial. Improvements in road surface condition and traffic capacity will alleviate local congestion and improve traffic flow, thereby reducing engine idling and the contribution it makes to local air quality degradation. With improved vehicle performance on a better road surface, the air pollution should actually be reduced. Provision for designated parking areas for auto rickshaws, cars, jeeps etc will improve the road safety conditions and traffic management situations decongesting the traffic corridor thereby positively contributing to air quality improvements. Paving and provision of adequate side drainage in villages will significantly reduce human exposure to air pollution, including both vehicular emissions and roadside dust.

Confining construction activities of the project road links to social working hours and employing noise controlled construction equipment of international standards will mitigate noise impacts during the construction phase for the local population. Measures will include:

- Source Controls, i.e. requirements that all exhaust systems be maintained in good working order; properly designed engine enclosures and silencers will be employed; and regular equipment maintenance will be undertaken.
- Site Controls, i.e. requirements that stationary equipment will be placed as far away from sensitive receptors as possible (i.e. aggregate crushers, etc.); disposal sites and haul routes will be selected to minimize objectionable noise impacts; and shielding mechanisms will be employed where possible.
- Time and Activity Constraints, i.e. operations will be scheduled to coincide with periods when people are least likely to be affected; work hours and work days will be limited to less noise sensitive times as far as possible.
- Community Awareness, i.e. public notification of construction operations will incorporate noise considerations and methods to handle complaints should be included.

It is anticipated that there will be 'measurable' decrease in noise levels as the measured values indicate high noise levels in the region. Estimated noise levels due to road use following which noise levels may exceed the ambient noise standards specified by the Noise Pollution (prevention and control) Rules 2000 of the Ministry of Environment and Forests, Government of India. Mitigation at these locations may include the posting of signs prohibiting the use of horns and, to the extent possible, landscape planting to serve as noise barriers. The effect of noise can be reduced considerably by the combined effect of sound insulating walls and green barriers. [6]

7 Conclusions

The predicted impact includes the noise quality, water quality and air quality. Water quality changes rises only when there is change in drainage pattern occurs. These change is modelled using the Streeter Phelps equation and the mass balance equations. Air quality modelling was done using the Gaussian dispersion model and the impact of traffic noise was done using the CRTN Models.

- The results shows that there will be reduction in water quality mainly at the point of discharge especially reduction in DO level and increased turbidity. The water quality issues raised in other stages of construction should be properly checked.
- The air and noise values at the present condition are greater than the prescribed norms of pollution control board. According to the project details, the improved road conditions reduces these air quality and noise quality issues as the riding characteristics get improved.

As a future work, more realistic models for modelling the environmental issues can be used. With the emergence of satellite remote sensing technology and Geographic Information Systems (GIS), research presents a new framework for the analysis phase of the Environmental Impact Assessment (EIA) for transportation projects based on the integration between remote sensing technology, geographic information systems, and spatial modeling.

Acknowledgement

The authors express heartfelt gratitude to all my data sources especially to PWD Section Office, Water Quality Testing Laboratory and Cooperation Office, Thrissur for their support that made this mini project valuable. Authors also would like to express sincere gratitude to staff, students and management of Jyothi Engineering College for the priceless assistance in accomplishing the work.

References

1. Adel A. A., "On the Atmospheric Dispersion and Gaussian Plume Model", 2nd International Conference on Waste Management, Water Pollution, Air Pollution, Indoor Climate (WWAI'08), (2008).
2. Joyce E. F., and Williams H. E, "On assessing the environmental impact of urban road traffic", International Journal of Environmental Studies, 3:1-4, 201-207, DOI: 10.1080/00207237208709516, (1972).
3. Lenzen, M., Christopher, J. D, "Environmental impact assessment including indirect effects—a case study using input–output analysis", Elsevier -Environmental Impact Assessment Review -23, 263–282, (2003).
4. Ramachandra, T. V., and Shwetmala, "Emissions from India's transport sector: Statewise synthesis", Elsevier- Atmospheric Environment, 1-8, (2009).s
5. Rawat, K. etal. "Mathematical Modeling of Environmental Noise Impact", Indian Journal of Biomechanics: Special Issue. (2009).
6. EIA and EMP for Kasargod – Kanhangad Road, Pilathara – Pappinisseri Road and Thalassery – Valavupara Road Public Works Department , Government of Kerala

DEVELOPMENT OF A RELATION BETWEEN STRUCTURAL AND FUNCTIONAL CHARACTERISTICS OF THE PAVEMENT

Janani L. ¹, Ph.D. Student, National Institute of Technology, Tiruchirappalli

Raunak Dixit ², M. Tech Student, National Institute of Technology, Tiruchirappalli

Sunitha V. ³, Assistant Professor, National Institute of Technology, Tiruchirappalli

Samson Mathew. ⁴, Professor, National Institute of Technology, Tiruchirappalli

Abstract:

This study endeavors in developing a relationship between functional and structural characteristics of a pavement. Eighteen rural roads of total length (37.88 KM) with different traffic, subgrade characteristics and climatic conditions in seven districts of Tamil Nadu were selected. Considering advantages of modern high-performance survey devices in the acquisition of road pavement functional parameters, it would be of practically significant if the structural state of a pavement could be estimated from its functional conditions. Linear regression model, Non-linear regression models and Artificial Neural Network (ANN) models were used to obtain the relationship between structural and functional characteristics of the pavements.

Keywords: *Functional characteristics, Structural Characteristics, linear regression, nonlinear regression, ANN*

1. Introduction

India owns the second largest network of roads in the world, next to USA. As per statistics of year 2009, the total road length in the country is over 3.3 million km, which gives the spatial road density of about 1 km/km² of area. Assuring good conditions to the pavement allows users to drive with acceptable comfort and safety levels. However, in order to guarantee high quality standard, road agencies have to monitor the performance parameters of the entire network frequently and to adopt the most proper maintenance operations where needed. Indeed, continuous collection of new data regarding pavement conditions is a strategic operation to update Pavement Management Systems (PMSs) and optimize network maintenance and agency funds. Pavement performance parameters are also very numerous and diversified (structural and functional parameters). It is relatively economical to perform roughness or distress measurements through high-speed Profilometers or Roughometer. However, deflection data collection by means of Falling Weight Deflectometer (FWD) or Benkelman Beam Deflection (BBD) is slow, with high unit costs, and adverse effects on traffic due to the stop-and-go procedure. To overpass this limitation, many researchers have tried to analyse various performance indicator (roughness, distresses, structural capacity, etc.) and to identify some useful correlation among them. In this way, it would be possible to estimate the value of some indices performing other surveys, reducing then the frequency of the slowest and most expensive ones.

The most interesting and remarkable relationship should exist between roughness measurements and the pavement structural performance. It is known that roughness and irregularities are related to deterioration of the pavement structural capacity and, if a pavement structure is not designed adequately, roughness would increase quickly. However, despite some research attempts, it is not easy to analytically develop this relationship. So, results are very interesting and prove that the ANN represents an adequate model to evidence this relation. The papers show the effectiveness of the adoption of a large Coir data for the analysis of the correlation. ANN provides also better results in comparison with Linear Regression. **Jain et al.** (2017) used Artificial Neural Network Based Development of Pavement Depreciation Models for Urban Roads. **Sollazzo et al.** (2017) developed an ANN model to correlate roughness and structural performance in asphalt pavements in terms of International Roughness Index (IRI) and Effective Structural Number (SN_{eff}). **Murillo** (2013) gave the correlation between deflections measurements on flexible pavements obtained under static and dynamic load techniques. The major goal of this study was to find the relationship between the structural and functional characteristics of the pavement.

2. Study Area

The study area comprises of 18 low volume roads with a total length of 37.88 km constructed as part of Bharat Nirman Phase III project in Coimbatore, Dharmapuri, Dindigul, Krishnagiri, Ramanathapuram, Tiruppur and Tiruchirappalli districts. Figure 1 is a map showing the study area.



Fig. 1.Study area

Table 1 shows the list of 18 low volume roads identified for this study.

Table 1 List of Roads identified for this Study

2. Project Approach

Sl.No	District	Block	From	To	Length (km)
1	Coimbatore	Thondamuthur	Narasipuram	Poondi	3.786
2	Coimbatore	Thondamuthur	Vaithegi falls road	Javvukadu via Panchanvayal	3.75
3	Dharmapuri	Nallampalli	Mittareddihalli	Komathampattipudur	0.8
4	Dindigul	Guziliamparai	Chatrapatty Mallapuram road	Seethapatty	1.505
5	Krishnagiri	Thally	Thallykothanur	B.B.Palayam	0.6
6	Ramanathapuram	Kadaladi	KamuthiSayalkudi road	Perumal Thalaivanendal	2.21
7	Ramanathapuram	Kadaladi	ThanjavurSayalkudi road	Malatar road	0.915
8	Ramanathapuram	Kadaladi	Chithirangudi	Ponthampuli road	1.755
9	Tiruppur	Avinashi	CheyurKuttagam	Salaipalayam	1.25
10	Tiruppur	Pongalur	Kandiyankoil	Thayampalayam	3.4
11	Tiruppur	Udumelpet	Kolumam Kallapuram Road	Navalodai Colony	1.0
12	Tiruppur	Udumelpet	Sugar mill road	Kalliyapuram road	1.8
13	Tiruppur	Udumelpet	Erisinampatty	Thirumurthi Settlement	2.85
14	Tiruppur	Udumelpet	Udumalpet-Chinnar road	Etthikalmedu Attumalai Settlement	2.8
15	Tiruppur	Udumelpet	Elayamuthur Poochimedu Road	Athithurai.	0.96
16	Tiruppur	Udumelpet	Elayamuthur	Poonikattuthurai Road	2.15
17	Tiruchirappalli	Uppiliyapuram	Maradi	Kattapalli	2.85
18	Tiruchirappalli	Uppiliyapuram	Sobanapuram	Gandhipuram	3.5
TOTAL					37.88

This study endeavors in developing a relationship between functional and structural characteristics of a pavement along with formulating a Pavement Deterioration Model and Maintenance Management Model. The steps involved in this process are shown in figure 2.



Fig 2. Project Approach

The delineation of study area was done in such a manner that it consists of roads having enough dynamics to achieve the goals of this research. An extensive data collection was performed on all the selected roads. Various tests were adopted for studying the material properties and pavement performance of the pavements. The details of these tests are explained below.

Pavement Material Properties

Pavement material properties were studied using both laboratory as well as field tests.

a) Standard Proctor compaction test: The Proctor compaction test is a laboratory method for experimentally determining the optimal moisture content at which a given soil type will become most dense and achieve its maximum dry density. This test is done as per IS 2720 (Part 7) -1980.

b) Laboratory CBR test: The California bearing ratio (CBR) test is a penetration test meant for the evaluation of subgrade strength of roads and pavements. The results obtained by these tests are used with the empirical curves to determine the thickness of pavement and its component layers.

Pavement Performance Study

Pavement performance study comprises of the analysis of both functional and structural performance of the pavement.

a) Functional Performance: Functional performance of the pavements was evaluated by conducting distress surveys and roughness measurement.

Distress Survey: The various distresses in the pavement namely Rutting, Raveling, Potholes, Depression, Cracking Area, and Edge Drop were measured. Visual Survey for judging the condition of the drainage and Shoulder was also performed in order to depict the distress more precisely.

Roughness Measurement: Roughness of the study roads have been measured with MERLIN and Roughometer.

i) MERLIN: MERLIN (Machine for Evaluating Roughness using Low-cost Instrumentation) is used either for calibrating response type instruments or for direct measurement of roughness. The machine is made to rest on the road with the wheel, rear foot and probe in contact with the road surface. The vertical displacement between the road surface under the probe and the centre point of an imaginary line is marked on a chart. Each new measurement is taken by moving the MERLIN forward to a new position on the road and recording the corresponding new position of the pointer on the chart so that a histogram distribution of markings is gradually built up. The spacing between the two marks, D is measured in millimeters. As per IRC: SP 72 – 2007 the range of IRI ranges from 2.4 to 15.9 Road roughness can be determined using equation 1.

$$IRI = 0.593 + 0.0471D \dots\dots\dots (1)$$

Where, D is measured in mm and IRI in m/km

i) Roughometer: It is a portable type equipment and consists of an accelerometer sensor which is installed at the rear axle of survey vehicle, a distance measuring instrument, interface module and a controller. The pavement roughness measurements using this equipment should be done preferably at a speed between 40 to 60 km/hr, in order to obtain most reliable and accurate data. The output is in the units of International Roughness Index (IRI).

b) Structural Performance

The structural characteristics of the pavement were measured using Benkelman beam Deflection Test. *Benkelman Beam Deflection (BBD) Test:* The deflection of flexible pavements under moving wheel loads was determined by Benkelman Beam Apparatus. The test was conducted as per IRC 81-1997 at sub sections of the roads. A Truck loaded with 12 tons such that the rear axle load is 8170 kg, equally distributed over the two sets of dual wheels is used. The spacing between the tyres should be 30-40 mm; the tyre is 10x20 ply inflated to a pressure of 5.60 kg/sq. cm. The rebound deflection value D at any point is given by equation 2.

$$D = 2(D_o - D_f) + 2K(D_i - D_f) \dots \dots \dots (2)$$

where,

D_o = The Initial Dial gauge reading under and in between the gap of the back dual wheel of Truck normally it is adjusted to zero

D_i = Intermediate Dial gauge reading at a distance 2.7m after running of Truck

D_f = Final Dial gauge reading at a distance 9m after running of Truck.

The allowable limit of deflection, for which no need of improvement is required as per IRC: 81 – 1997 is 0.45mm.

The collected data was consolidated and Pavement performance parameters like IRI, characteristics deflections etc. were calculated. An attempt was made to establish a relationship between the functional parameters and deflection of the pavement. A pavement prediction model was developed by dint of this relation and the IRI and Deflection for the next season were predicted. From these predicted values, a Maintenance Priority Index was formulated to prioritize the pavement for the Maintenance and Rehabilitation work.

3. Models to Correlate Structural and Functional Characteristics of Pavement

Linear regression model, Non-linear regression models and Artificial Neural Network (ANN) models were used to obtain the relationship between structural and functional characteristics of the pavements. A large database of pavement material properties of the selected roads played the key role in improving the accuracy of the models. This database contains records on structural characteristics, functional characteristics, climatic features, and traffic details for nine test sections located in Tamilnadu. The test sections selected to study the correlation of functional and structural characteristics of the pavement are listed in table 2.

Table 2 Selected Roads to Analyse the Correlation of Structural and Functional Properties of Pavement

Sl.No.	District	Block	From	To	Length (km)
1	Coimbatore	Thondamuthur	Narasipuram	Poondi	3.786
2	Coimbatore	Thondamuthur	Vaithegi Road	Javvukadu(Via) Panchanvayal	3.75
3	Dindigul	Guziliamparai	Chatrapatty	Seethapatty	1.505
4	Ramanatha Purn	Kadaladi	Sayalkudi road	Malatar road	0.915
5	Tiruchirappalli	Uppiliyapuram	Maradi	Kattapalli	2.85
6	Tiruchirappalli	Uppiliyapuram	Sobanapuram	Gandhipuram	3.5
7	Tiruppur	Udumelpet	Elayamuthur	Poonikattuthurai road	2.15
8	Tiruppur	Avinashi	Kuttagam	Salaipalayam	1.25
9	Tiruppur	Pongalur	KandiyanKoil	Thayampalayam	3.4

The following data were collected for all the nine test sections.

- Length of the section(L)
- Pavement Temperature (temp)
- Average Daily Traffic Volume of roads in PCU(T)
- CBR of Natural Subgrade
- Maximum Dry Density of the soil subgrade(MDD)
- Rutting data for different sections
- International Roughness Index for different section(IRI)
- Deflection data for different sections(D)

The Table 3 shows the sample data for one road.

Table 3 Sample data for one test section

Road Name	Length (km)	Length of section (km)	Average Daily Traffic	CBR (%)	MDD (g/cc)	Rutting Data (mm)	IRI (m/km)	Deflection (mm)
Narasipuram to Poondi	3.786	0.386	106	2.92	1.77	7.06	6.66	1.02
		0.45		1.82	1.69	7.00	7.14	0.48
		0.45		3.65	1.68	7.38	6.98	0.68
		0.45		1.46	1.78	6.72	6.75	0.53
		0.45		1.82	1.81	6.94	5.55	0.52
		0.4		2.19	1.66	7.35	6.46	0.34
		0.4		3.28	1.76	7.11	6.85	0.47
		0.4		2.92	1.80	6.88	7.03	0.31
		0.4		2.92	1.81	7.50	6.84	0.00

Length of section, Average Daily Traffic, CBR value, Pavement Temperature, MDD, Rutting data and IRI were considered as the independent variables. Deflection for different section and Effective Structural number were considered as dependent variables for all the models.

Linear Regression Analysis

Linear regression attempts to find the relationship between the variables by fitting a linear equation to observed data. The regression statistics of Linear Regression Analysis are shown in Table 4.

Table 4 Regression Statistics of Linear Regression Analysis

R ² - Value	0.31
Mean Square of Errors	0.64
DOF	7

Nonlinear Regression Analysis

Exponential Regression Analysis and Logarithmic Regression Analysis was performed.

a) Exponential Regression Analysis

It is the process of finding the equation of a best fitting exponential function for this set of data. The regression statistics of Exponential Regression Analysis are shown in Table 5.

Table 5 Regression Statistics of Exponential Regression Analysis

R ² - Value	0.43
Mean Square of Errors	0.56
DOF	7

b) Logarithmic Regression

Analysis

It is a method of regression that is used to predict a continuous quantity which can take any positive value for the given set of data. The regression statistics of Logarithmic Regression Analysis are shown in Table 6.

Table 6 Regression Statistics of Logarithmic Regression Analysis

R ² - Value	0.204
Mean Square of Errors	0.44
DOF	7

Artificial Neural Network (ANN)

ANNs are recent computational models defined in analogy with the biological characteristics to simulate the decision process in the brain. They are useful to approximate and estimate unknown functions depending on various and numerous input values.

Multilayer Feed-forward Neural Network (MFNN) is the most widely used type of ANN. An MFNN is characterized by three kinds of layers of interconnected neurons: input, hidden, and output layers. Each neuron processes the received inputs and, according to a properly defined activation function, produces an output that is transmitted to neurons in the following layer through specific connections defining the network topology. Each connection is associated to a specific weight (w_i) that amplifies or reduces the input. For the single neuron, the relationship existing between inputs (x_i) and output (y_i) is defined using a specific transfer function that usually has the logistic sigmoidal shape.

$$f(I) = \frac{1}{1 + e^{-I}}$$

Where, $I = \sum w_i x_i$ is the sum of the weighted inputs x_i produced by the previous neurons.

In a “supervised approach” – such as MFNN -, given a large set of input and output data, the training procedure consists in the modulation of the various weights to produce acceptable output. The results should be very similar to the output provided for training. Usually, the training phase is performed using a back propagation, model that allows the network to adjust the weights in a reverse direction, distributing the error among the various neurons and minimizing it after each iteration.

Levenberg-Marquardt is the most used training algorithm and, generally, the error is evaluated in terms of Mean Square Error (MSE). (Sollazzo et. al, 2017). Figure3 shows the internal skeleton of the ANN model Building phase. ANN works on the principle of predicting the output value by analysing the trends of input data. Then Statistical Fitting curve are obtained by comparing output value given by ANN and Target value.

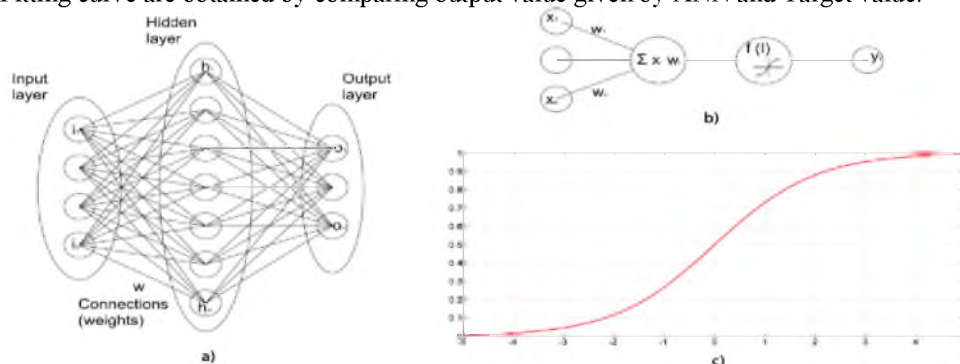


Fig. 3 a) Layers of a MLP ANN and Network topology. b) Perceptron structure. c) Sigmoidal transfer function.

The Prime objective was to estimate the Deflection of the asphalt pavement from different attributes of the pavement using ANN model.

Each ANN created had 25 hidden neurons, and the related records were randomly divided in the training (70 %), validation (15 %), and test (15 %) groups. Trainings were performed using the Levenberg- Marquardt algorithm, measuring performance by means of MSE. Figure 4 depicts the different layers in the constructed ANN.

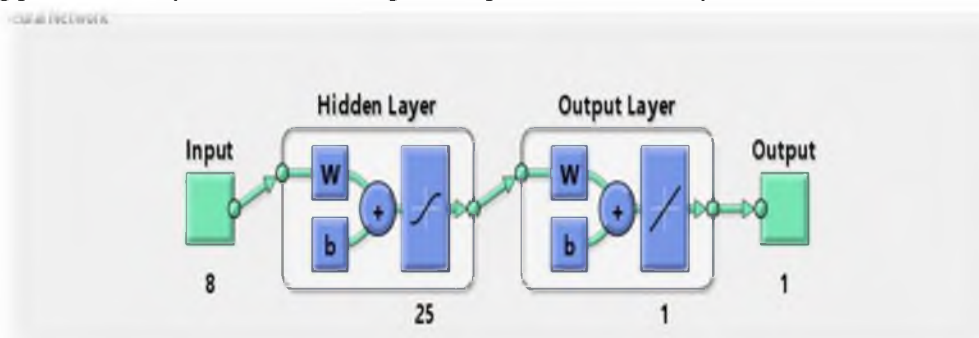


Fig. 4 Different layers in ANN

The consolidated data was fed as the input of ANN model.

Table 7 shown below, are the consolidated output of the ANN for all phases (Training, validation, Test and All Sample phase)

Table 7 Consolidated ANN output

Phase	Sample Size	MSE	Regression Value
Training	54	0.06	0.95
Validation	12	0.11	0.89
Test	12	0.08	0.92
All	78	0.094	0.91

4. Results and Discussions

Table 8 compares the Statistical analysis provided by all the approaches.

Table 8 ANN vs. Linear and Nonlinear Regression Analysis

Model	Phase	Sample Size	MSE	R-value
ANN	Training	54	0.06	0.95
	Validation		0.11	0.89
	Test		0.08	0.92
	All		0.094	0.91
LR	Total		0.52	0.56
Nonlinear-Exponential	Total		0.56	0.66
Nonlinear-logarithmic	Total		0.44	0.45

ANN can assure better results in terms of both R-values and MSE values. Although some of the records have been used only for testing in the ANN approach, LR provides an R-value 60% lower than ANN, while the MSE for LR is larger than ANN

Thus the numerical application assess that ANN can effectively be used as a powerful tool for predicting deflection performance using different attribute of the pavement.

5. Conclusions

The numerical application (R^2 -value and SSE) assess that ANN can effectively be used as a powerful tool for estimating structural performance using roughness data, especially if compared to Linear and nonlinear Regression models. With the above relation, it would be possible to estimate the value of some indices like deflection data, by perform other surveys (like IRI and CBR), thus reducing the frequency for the use BBD and FWD which are slowest and most expensive ones. Statistical parameter like R-value for ANN model comes out to be above 0.91 thus shows strong relation between the Predicted output value and the target value. For further validation, LR model value compared with the ANN parameters in terms of R-value, R-value for ANN obtained as 0.91 which is 60% more than that of LR, from that it can be concluded that ANN is the better tool for predicting the Deflection using IRI and other parameters.

REFERENCES

1. **Chopraa, T., ManoranjanParida, Naveen Kwatra and JyotiMandhanid** (2017) Development of Pavement Maintenance Management System (PMMS) of Urban Road Network Using HDM-4 Model. *International Journal of Engineering & Applied Sciences (IJEAS)*, **9**, 14-31
2. **Dattatreya, J.K., A Veeraragavan, K Murthy and C.E.G Justo** (1992) A suggested simplified system for pavement maintenance management of road network. *Journal of Indian Roads Congress*, **53(2)**, 217-273
3. **Gupta, A., Praveen Kumar and RajatRastogi** (2011) Pavement Deterioration and Maintenance Model for Low Volume Roads. *International Journal of Pavement Research and Technology*, **4**, 195-202
4. **Gupta, P.K. and R Kumar** (2015) Development of optimum maintenance and rehabilitation strategies for urban bituminous concrete surfaced roads. *International Journal of Scientific and Technology Research*, **4(2)**, 56-66.
5. **Jain, K., S S Jain and M.S Chauhan** (2013) Selection of Optimum Maintenance and Rehabilitation. *International Journal for Traffic and Transportation Engineering*, **3(3)**, 269-278.

6. **Jain, S. S., S Aggarwal and M Parida** (2015) HDM-4 pavement deterioration models for Indian national highway network. *Journal of Transportation Engineering*, **131(8)**, 623–631.
7. **Murillo Feo C.A.** (2013) Correlation between deflections measurements on flexible pavements obtained under static and dynamic load techniques. *18th International Conference on Soil Mechanics and Geotechnical Engineering, Paris*.
8. **Reddy, B.B. and A Veeraragavan** (2002) Priority ranking model for managing flexible pavements at network level, *Technical Paper Published in 62nd annual session of Indian Roads Congress(IRC)*, Kochi, India
9. **Reddy, B.B. and A Veeraragavan** (2001) Priority ranking model for managing flexible pavement at management level, *Centre for Transportation Engineering, Bangalore University, Bangalore*, 378–394.
10. **Shah, Y U., S.S. Jain and DeveshTiwari** (2016) Adaptation of HDM-4 Tool for Strategic Analysis of Urban Roads Network. *Transportation Research Procedia*, **17**, 71 – 80
11. **Shaha , Y.U., S.S. Jain, DeveshTiwari and M.K. Jain** (2013) Development of Overall Pavement Condition Index for Urban Road Network. 2nd Conference of Transportation Research Group of India ,**104**,332 – 341
12. **Sollazzo, G., T.F. Fwa and G. Bosurgi** (2017) An ANN Model to Correlate Roughness and Structural Performance in Asphalt Pavements. *Construction and Building Materials*, **134**,684–693
13. **IRC: 81-1997**Guidelines for strengthening of flexible road pavements using benkelman beam deflection technique.: Indian Roads Congress, New Delhi.
14. **IRC: SP 72 – 2007**Guidelines for the design of flexible pavements for Low volume Rural Road.: Indian Roads Congress, New Delhi.
15. **IRC: 37**Guidelines for the design of flexible pavements.: Indian Roads Congress,NewDelhi,2001

Effect of Accessibility on Potential Tourist Destinations –A Case Study of Kozhikode District in Kerala

V S Sanjay Kumar¹, Saleel K², Teena John³

¹ Senior Scientist, ^{2,3} Project Engineer
National Transportation Planning and Research Centre (NATPAC), Kerala

Abstract. Kerala is well renowned for being one among the perfect tourist locations in India. Even though many of the locations in Kerala have high tourism potential, they are not projected out in to the sight of people as what it demands and subsequently may result in the decrease in proportion of the tourists. The paper tries to find out such types of unexplored locations and the reasons behind, taking Kozhikode district in the state of Kerala, India, as the study area. All the known and unknown tourist places in the district were analyzed and an attempt is made to explore those unexplored tourist locations. Data were collected on the basis of questionnaire survey including how many of them were already aware of each tourist places, how many of them had visited, not visited and the reason(s) behind. Along with this, data pertaining to existing condition and connectivity pattern of each of these locations were identified. It has been inferred that the identified unexplored locations will attract more tourists provided improvements in connectivity are made.

Keywords: Accessibility, Tourism, Unexplored, Questionnaire

Introduction

Tourism is considered as a key sector which ensures socio-economic development of the country. Transport accessibility is most often the factor that influences the choice of tourist destination. Transport is a key enabler of tourism and plays a vital role in moving tourists from their place of residence to their final destination and on to various attractions. It is a matter of fact that, in order to have better coverage and visibility, the tourism destinations should be accessible. There are a lot of tourist destinations in the state of Kerala, which lacks visibility/accessibility and hence only limited number of tourists visit the place. In order to increase the accessibility, the destination should be connected well with the major transport network by suitable mode. This paper tries to find out such types of unexplored locations and the reasons behind, taking Kozhikode district in the state of Kerala, India, as the study area, with an objective to develop a transport network connecting major tourist destinations and also to improve the existing transport facilities for promoting tourism, which will provide employment, increase business and earn foreign exchange for the country.

Scope and Objectives

The scope of the study was to identify the effect of transport network connecting the major tourist destinations in a region. The major objective was to identify the connectivity issues of various potential tourist destinations and to evaluate how these issues are affecting the tourist inflow and to examine the role of transport and quality of serviceable infrastructure in development of tourism.

Study area and methodology

Kozhikode district is in south west shore of Indian landmass with a long recorded history as a commercial hub from antiquated time travel records. The whiff of history keeps on saturating the paths, bazaars and business centres of Kozhikode. Lavish green, wide open quiet shorelines, historic sites, wildlife sanctuaries, rivers and hills make Kozhikode a popular destination.

The methodology of the study included a reconnaissance survey to identify the major and unexplored tourist destinations in the selected area. A detailed questionnaire survey was conducted to identify the tourist inflow and connectivity issues of all identified potential tourist destinations. Various data pertaining to existing connectivity were collected. Major connectivity issues were identified from the data analysis. The forecasting of number of tourists and corresponding traffic volume were made if all the connectivity issues are rectified.

2. Data Collection

2.1 Reconnaissance survey

A reconnaissance survey was conducted to identify the various tourist locations in the study area. As part of reconnaissance survey, a total of 54 tourist attractions were recognized. Out of this, excluding all religious places and already explored tourist locations, 15 locations were found to be unexplored potential tourist destinations and are listed in table 1. These locations were categorized as refreshment, Dam/ Trekking/ Waterfall and beaches/Light house.

Table 1. Identified unexplored and potential tourist destinations

Refreshment	
1	Janakikkad
2	Kakkad Eco Tourism
3	Vanaparvam
4	Kanayamkode
5	Vallikotukavu
6	Payamkuttimala
Dam/ Trekking/ Water fall	
7	Arippara waterfalls
8	Peruvannamuzhi dam
9	Nambikkulam
10	Kakkayam dam
11	Vayalada
Beaches/ Light house	
12	Kadalur light house
13	Sand banks beach
14	Thikoti drive in beach
15	Vellivamkallu inscriptions

2.2 Questionnaire survey

A detailed questionnaire survey was conducted on both explored and unexplored tourist locations. A total of 2025 samples were taken which give an accuracy level of 95% confidence interval at 1% significant level for an infinite population. Preliminary analysis was done to obtain gender wise classification, age group distribution and mode split. Mode split emerged from the results is shown in Fig.1.

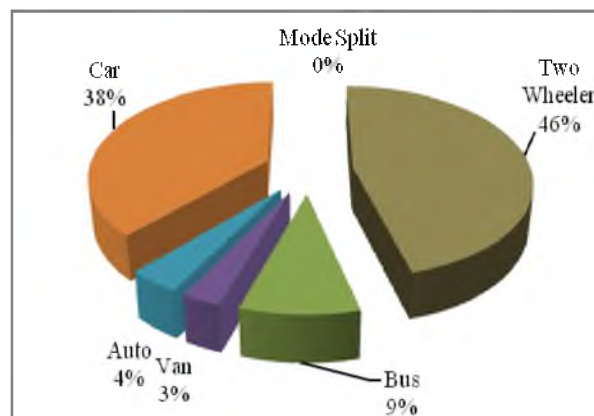


Fig.1. Mode split

3. Results and Discussions

3.1 Data Analysis

An analysis was done which indicates the number of total tourists who have heard and who have visited each of these unexplored locations. From table 2, which details the proportion of sample who has visited/heard of the

potential locations, it can be seen that most of the locations are remaining unexplored. From the questionnaire survey, it was found that most of the tourists who already have visited these locations are not interested to visit the places again after their first visit. The main reasons for not visiting and the responses given by tourists are tabulated in table 3.

Table 2. Awareness Results from questionnaire survey

Location	% heard	% visited	% prefer to visit again	% not prefer to visit again
Janakikkad	32	9	71	29
Kanayamkode	28	15	61	39
Kakkad Eco Tourism	40	13	52	48
Vanaparvam	19	8	67	33
Vallikkatukavu	27	15	49	51
Peruvannamuzhi Dam	62	33	59	41
Nambikkulam	13	1	33	67
Arippara Waterfalls	49	27	38	62
Kakkayam Dam	70	48	70	30
Vayalada	46	29	48	52
Thikkoti Beach	51	27	47	53
Sand Banks Beach	22	14	53	47
Kadalur Light House	27	16	49	51
Velliyamkallu	17	3	55	45
Payamkuttimala	35	17	87	13

It was observed that most of the tourists who visited these unexplored tourist centres demand improvement on road conditions along with basic amenities, placing sign boards at major intersections and proper accessibility. So by rectifying all these identified issues, tourist inflow to each of these locations will enhance.

Table 3. Reasons for not visiting again

Location	Poor accessibility (%)	Inadequate signs & information (%)	Far from other tourist places (%)	Security/safety issues (%)	Lack of basic amenities (%)	Not of interest (%)	Others (%)
Janakikkad	53.4	8.8	5.8	3.5	5.2	3.7	8.4
Kanayamkode	54.1	2.5	3.4	1.0	2.5	8.6	6.9
Kakkad	48.9	3.9	6.0	1.9	2.7	2.4	9.4
Vanaparvam	58.4	2.7	4.1	1.4	2.3	3.4	7.3
Vallikkatukavu	51.9	2.4	3.2	2.5	3.6	3.5	8.7
Peruvannamuzhi	37.3	6.9	5.2	6.3	8.9	1.9	8.0
Nambikkulam	58.7	2.2	1.7	0.7	1.1	1.8	7.0
Arippara	44.0	12.9	3.6	8.5	7.2	0.3	6.5
Kakkayam	32.5	7.4	4.0	4.8	6.1	0.6	7.1
Vayalada	41.4	9.6	4.2	6.8	6.6	1.4	7.4
Thikodi beach	42.7	2.7	3.6	2.6	6.0	1.4	9.6
Sand banks	53.0	7.0	2.6	1.8	5.0	1.7	9.7
Kadalur	50.7	2.7	2.2	1.7	1.5	1.4	8.3
Velliyamkallu	57.6	16.9	4.0	5.8	4.0	2.8	8.4

3.2 Estimation of tourist demand if improvements are made

It is anticipated that the tourist inflow to the identified unexplored destinations will increase manifold provided improvements to the location are made, particularly the connectivity aspect. The potential tourist demand is calculated based on three aspects as follows,

1. Base year tourists: This corresponds to the existing condition and considers the number of tourists who visit the places in the base year

2. Recurring tourists: This category considers, those tourists, who have heard about these locations and who have already visited the location, but are not interested to visit again due to the reasons as per table 3. It is assumed that this proportion of tourists will visit the location again with the rectification measures demanded.

3. Induced demand: It is clear from the questionnaire survey that most of the tourists were not aware about the unexplored tourist centres. Proportion of people who are interested in the type of tourist location but were not aware of the existence of such places were determined. Based on the preference made by the corresponding sample, the induced tourist traffic to the unexplored places is found out.

Total Demand

Total anticipated demand of tourists is obtained by adding these three categories for the base year. This demand is forecasted for the year 2030. Tourist inflow towards individual unexplored tourist centres can be obtained by multiplying the total demand with corresponding percentage of tourists obtained as per the preceding paragraphs. The obtained values are converted to vehicular traffic based on the base year mode split. Table 4 shows the existing percentage share of tourists for each locations, corresponding number of tourists in the base year, increased percentage share after improvements and the corresponding number of tourists and the forecasted traffic volume.

Table 4. Estimated number of tourists and traffic

Location	% share of tourists	Demand in base year	% share of tourists after improvement	Estimated demand in base year	Tourist demand in 2030	Estimated Traffic in 2030 (PCU/day)
Janakkad	9.1	74377	31.5	257202	343096	643
Kanayamkode	14.8	120687	59.4	485332	647411	1212
Kakkad	12.6	102911	38.0	309995	413519	774
Vanaparvam	7.8	64086	44.3	362190	483144	905
Vallikkatukavu	15.3	124897	64.6	527598	703790	1318
Peruvannamuzhi Dam	33.1	270377	67.1	547848	730803	1369
Nambikkulam	1.3	10291	19.7	160540	214153	401
Arippara Waterfalls	27.2	222195	72.1	589219	785991	1472
Kakkayam Dam	48.0	391999	82.7	675249	900750	1687
Vayalada	29.4	239971	79.5	649478	866374	1623
Thikkoti Beach	27.4	224066	68.0	555487	740993	1388
Sand Banks Beach	14.4	117413	72.2	589526	786401	1473
Kadalur Light House	16.5	134720	70.5	576175	768591	1439
Velliyamkallu	3.4	28067	22.0	179881	239953	449
Payamkuttimala	17.2	140480	51.5	420959	561539	1052

It can be inferred from the table that the number of tourists that will visit the unexplored destination will increase to the tune of 3 to 7 times. The result will be an overall economic development of the area and in turn increasing the state's revenue.

4. Conclusion

Eventhough many of the locations in our country have high tourism potential, they are not projected out in to the sight of people as what it demands. There will be many reasons for the same. This paper examined such a scenario taking one of the districts in Kerala, as a case study. It was observed that the tourists who visited these unexplored locations were worried about proper transport connectivity and signs and information. The analysis

of data revealed that the tourist inflow will increase to the tune of 3 to 7 times to these locations once proper connectivity is made. The result will be an overall economic development of the area and in turn increasing the state's revenue.

Acknowledgement

The authors express their sincere gratitude to the Kerala State Council for Science Technology and Environment, Government of Kerala for providing necessary financial assistance for the project.

References

- Byung-Wook Wil, Dexter J.L. (1993), "Traffic Impact analysis of Tourism development", Annals of Tourism Research, Volume 20, Issue 3.
- IRC 64-1990, Guidelines for Capacity of Roads in Rural Areas
- John Mangmuan Lian Zou, Dr. G.P. Prasain (2017), "North-Eastern states tourism : Exploring the unexplored on earth", IOSR Journal of Humanities and Social Sciences, Volume 22, Issue 8, Ver 14, PP 35-40
- Chowdhary S (2014), "An overview of tourism circuits- A Case study of Jammu region", International Journal of Interdisciplinary Research, Volume 1, Issue 1

Activity Based Transportation Modeling for Chelakottukara ward of Thrissur District

Midhun. Tand Dr. Anitha Jacob²

PG Scholar,

² Associate Professor,

Department of Civil Engineering,

Jyothi Engineering College, Cheruthuruthy, Thrissur, Kerala 679 531.

(anithajacob@jecc.ac.in)

Abstract. An Activity-based model is the one that generally replaces the conventional trip-based model, which is usually represented to as the four-step model. With the variations in the transportation system attributes and changes in socio-demographics of the individuals, the transportation planners and engineers' need to have the ability to estimate the variations in transportation demand so as to make a well-versed transportation infrastructure planning decision possible. Activity-based models are used for this purpose; these models are used to forecast travel characteristics and usage of transport services under different socio-economic scenarios. An activity-based travel pattern model has been developed for the individuals of the study area. This activity-travel pattern model will take different input parameters such as various land-use, socio-demographic, activity system, and transportation level-of-service attributes. Thus it will provide the activity-travel pattern of each individual in the study area as the output, within the continuous time domain.

Keywords: Activity-Based Travel Pattern, Four-Step Model, Socio-Economic, Travel Demand.

1 Introduction

Transportation plays an important role in the growth and economy of a nation. For a country like India, transportation planning is becoming unavoidable due to the fast-growing population and travel demand. Transportation planners and engineers have to be able to forecast the response of transportation demand for the changes in the attributes of the transportation system and changes in the socio-demographics of the people using the transportation system in order to make informed transportation infrastructure planning decisions. Travel-demand models are used for this purpose. It is used to predict the travel characteristics and the use of transport services under various socioeconomic scenarios and for various transport service and land-use configurations.

The mathematical relationship between travel demand and traveler and system characteristics can be achieved with the help of travel demand modeling. Earlier travel demand modeling is done with the help of trip based four-step modeling – as the trip generation, trip distribution, mode choice and route choice. This four-step modeling is said to be conventional modeling. Later on, new generation models such as tour based and activity based models emerged overcoming most of the drawbacks of the conventional method. The tour based approach considers a chain of trips starting and ending at the same location as the individual unit of analysis whereas activity-based travel demand model considers travel as a derived demand to satisfy the need of the individual [1].

The objective of this paper is to develop an activity-based travel demand model for Chelakottukara, the 22nd ward of the Thrissur City of Kerala, taking into consideration of the socio-economic factors and travel pattern, validating the generated model and suggesting how it can be made beneficial in the planning process. It includes a tour generation model for both single and complex activities.

2 Literature Review

2.1 Trip-Based Models

Trip-based travel models have evolved over many decades. As their name suggests, trip-based models use the individual person trip as the fundamental unit of analysis. Trip-based models are widely used in practice to support regional, sub-regional, and project-level transportation analysis and decision making. Trip-based models are often referred to as “4-step” models because they commonly include four primary components. The first trip generation components estimate the numbers of trips produced by and attracted to each zone (these zones

collectively represent the geography of the modelled area). The second trip distribution step connects where trips are produced and where they are attracted to. The third mode choice step determines the travel mode, such as automobile or transit, used for each trip, while the fourth assignment step predicts the specific network facilities or routes used for each trip[2].

2.2 Activity-Based Models

Activity-based models are having some similarities to traditional 4-step models: activities are generated, destinations for the activities are identified, travel modes are determined, and the specific network facilities or routes used for each trip are predicted. However, activity-based models incorporate some remarkable advances over 4-step trip-based models, such as the clear representation of realistic constraints of time and space and the linkages among activities and travel, for an individual person as well as across multiple persons in a household. These linkages enable them to more sensibly represent the effect of travel conditions on activity and travel choices. Activity-based models also have the ability to integrate the influence of very detailed person-level and household-level attributes and the ability to create detailed information across a broader set of performance metrics. These abilities are possible because activity-based models work at disaggregate person-level rather than a more aggregate zone-level like most trip-based models [2, 3].

2.3 Econometric Modeling Approach

It involves systems of equations to capture relationships among macroscopic indicators of activity and travel, and to predict the probability of decision outcomes. These models explore how activity and travel patterns are related to land use and socio-demographic characteristics of the traveler. The main criticism of the econometric approach is that it does not explicitly model the behavioral mechanisms underlying activity engagement and travel. This limits the richness of the behavior theories that can be incorporated into the model system. Nevertheless, the family of econometric models - ranging from discrete choice models, hazard duration models and limited-dependent variable models - remains strong approach to activity-travel analysis. Its strength lies in allowing the examination of alternative hypotheses about the unconcerned relationships among behavioral indicator [4, 5].

3 Study Area

The study area selected is Chelakottukara, the 22nd ward of Thrissur Corporation which is shown in figure 1. The study area consists of total population of 5627 individuals as of 2011 census, 1599 dwelling units and 580 other building comprising a total of 2179 units.

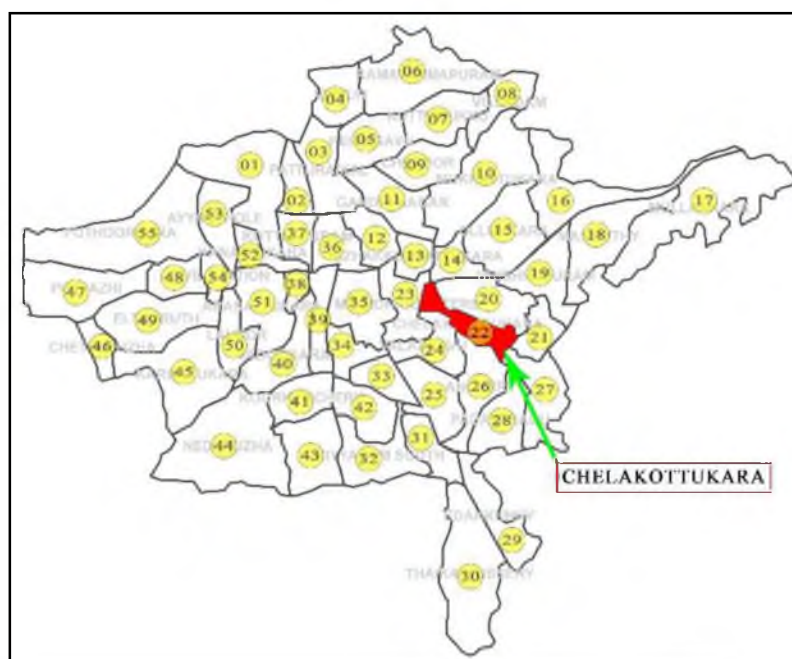


Fig.1. Thrissur Corporation Map

4 Methodology

The study area selected was Chelakottukara, 22nd ward of Thrissur Corporation. The primary data, i.e. socio-economic and travel characteristics were collected using household questionnaire survey. The secondary data, i.e. population data were obtained from Thrissur Corporation. After compiling, sorting and coding, the activity-travel pattern model was developed using SPSS software.

4.1 Data Collection

Data need to be collected can be divided into two - primary data and secondary data. Primary data is the data obtained from the household questionnaire survey. For this survey, an activity travel diary is mandatory, which can incorporate personal information and travel information of whole members of the selected household. On the other hand, secondary data includes population data. The sample size of the study area is estimated with the help of current population and building details of the study area [6]. The guideline suggested by Bruton [7] is adopted and a sample size of 160 households is selected in a random manner.

4.2 Preliminary Analysis

The data collected from the household questionnaire survey is sorted and coded as a different group of similar characteristics. These coded data is later used as the variables for model generation. Summary of the data collected is given in table 1.

Table 1. Summary of Household Survey Data

Details	Item	Value	(in %)
Household	Average Household size	3.55	-
	Average Household income per month (in Rs.)	29228.00	-
Trip	Average tour rate per household	2.09	-
	Average tour rate per person	0.59	-
Sample	Workers	198	35.74
	Students	128	23.10
	Homemakers	154	27.80
	Retirees	63	11.37
	Employment Seeking Group	10	1.81
Total	Female	288	51.99
	Male	266	48.01
	Individuals	554	-

Distribution Based on Occupation. From the chart plotted (Figure 2) based on occupation share of people, it can be identified that in the sample collected, 28% of total population are Home Makers. By conducting the preliminary study one can also find that the female percentage is slightly higher than that of the male. That would be the reason for this increase in Home Makers. Also, it can be found that by combining the working groups (government employee, private employee, self-employed and daily wages) together it is noted that about 36% (1+17+16+2) in the study area are employed. This indicates that the average income obtained from the survey is appropriate.

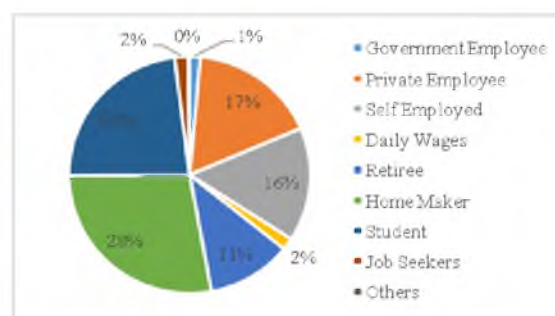


Fig.2. Distribution of Occupation

Distribution Based on Age. A chart has been generated for the distribution on age, which is given in figure 3. It can be observed that in the sample collected, there is an equal distribution of ages in all age category of people. But among them also majority of the people are in the age limit of 45 to 60 years. This implies that the age cross section of the sample is good.

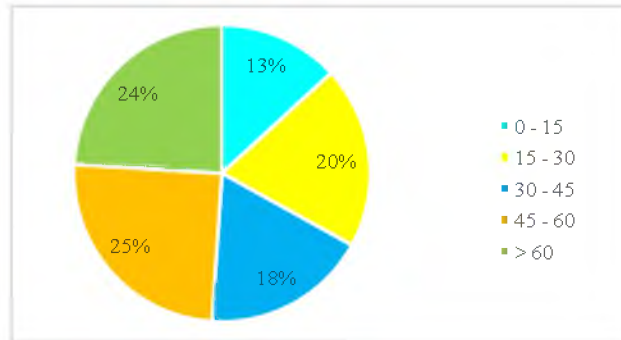


Fig.3. Distribution of Age

Distribution of Household Size. A graph has been plotted with household size along the x-axis and percentage household size along the y-axis, which is shown in figure 4. From this graph, it can be identified that for a household size of 4, the percentage household size is maximum, which is 30.57%. As it is mentioned earlier that the average household size of the study area is 3.55, this graph is giving the clear picture regarding how the average household reached that value.

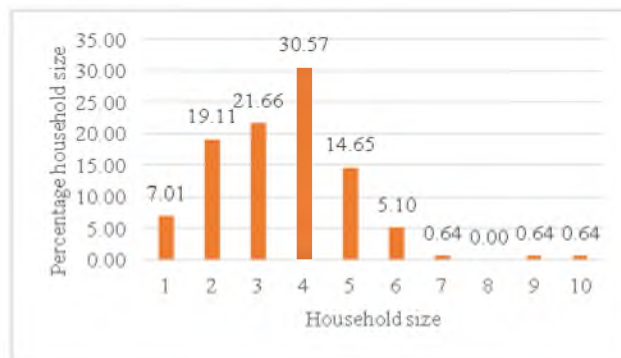


Fig.4. Distribution of Household Size

Distribution of Person’s Education Level. Person's education level is illustrated in figure 5. It can be seen that of the sample collected, 72% of people are below graduate. That can be the reason behind the increase in self-employment and private employment compared to that of the government employment. That is also reflecting directly on their income too as it has already seen that the average income of the study area is Rs. 29288.00 per month.

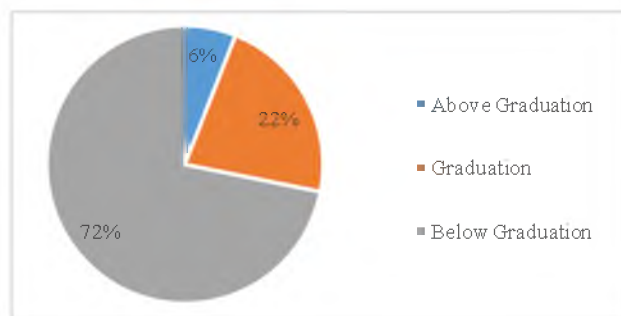


Fig.5. Distribution of Education Level

Distribution of Vehicle Ownership. The chart (Figure 6) is plotted with the ownership of vehicles. It can be seen that for about 64% of the sample is owning one or two automobiles. This may increase the tours that can be generated.

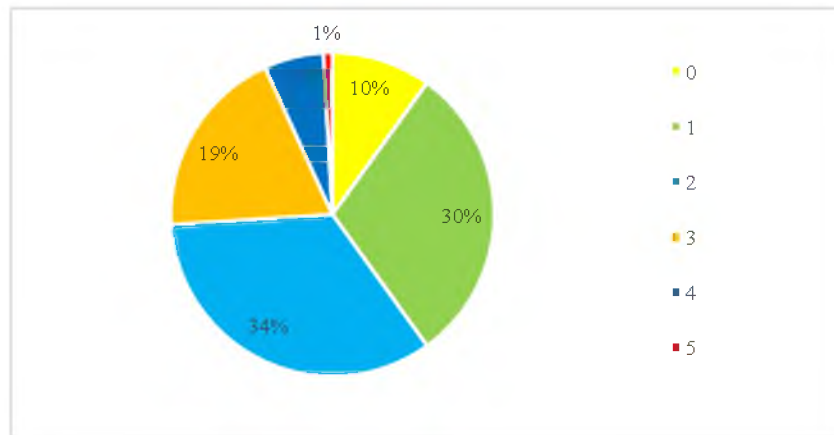


Fig. 6. Distribution of Vehicle Ownership

Distribution of Tour Rate. In order to find a relationship between household tour rate and vehicle ownership, a graph has been plotted with the number of automobiles in a household along the x-axis with tours per household along the y-axis, as shown in figure 7. It can be seen that with the increase in the automobile ownership there is an increase in the number of tours generated per household. Hence, that it can be said that both the automobile ownership and numbers of tours made are directly proportional to each other as the automobile increases the number of tours also increases.

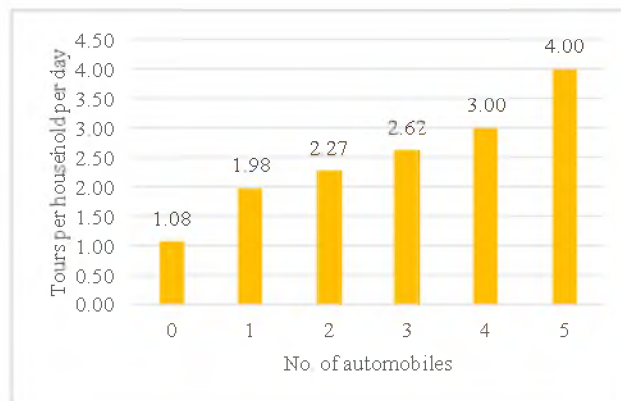


Fig.7. Distribution of Tour Rates

Activity-Travel Patterns. The activity-travel patterns that are identified from the sample taken are of two types, namely simple activity pattern and complex activity pattern. In simple activity pattern, there will be only two number of trips. In complex activity pattern there will be a minimum of three number of trips. The simple activity patterns obtained are, HWH (Home-Work-Home), HEH (Home-Education-Home), HSH (Home-Shop-Home) and HOH (Home-Others-Home). While the different complex activity patterns observed are HWH+ and HOH+ [8].

Distribution of Activities. It has been already found from figure 2 that 37% of total population are workers. Thus there is a chance of having more work activities in the study area, and from the figure 8, it can be found that 46% of total activities are of working activity.

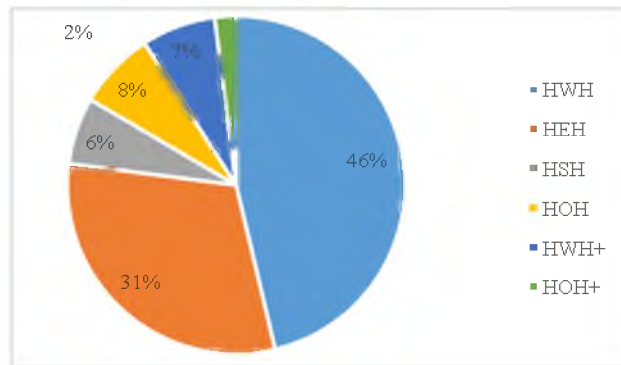


Fig.8. Distribution of Activities

4.3 Modeling

The modeling was done using SPSS (Statistical Package for Social Science) statistical software package. The utility maximization theory described by multinomial logit model is used as the modeling approach. Multinomial logistic (MNL) regression, which is the simplest model, is used to predict categorical placement or the probability of category membership on a dependent variable based on multiple independent variables. The variables used for modeling the activity-travel patterns are gender, age, education, type of employment, monthly income, vehicle ownership, mode of travel, distance of travel, cost of travel, duration of travel, activity duration and time of day. Before going for the model development the first task is to find the correlation between different variables. That has been found out with the help of SPSS by using Spearman's rank correlation technique, which is given in table 2.

Table 2. Correlation study of activity pattern

Variables	Code	Type of Correlation
Gender	G	Negative
Age	A	Positive
Education	Ed	Negative
Employment	Em	Positive
Income	I	Negative
License	Li	Negative
Vehicle	V	Negative
Mode	M	Positive
Travel Distance	TD _i	Negative
Travel Cost	TC	Negative
Travel Duration	Tdu	Negative
Activity Duration	Adu	Negative
Time of Day	Ti	Positive

The final output is to generate a model and thereby estimate the total number of different activities occurring in the study area. To reach the desired output it is necessary to go through three different steps. The first step is to obtain the score of each activity by the help of equations generated. After that the next step is to calculate the probability of occurrence of each activity by the help of score of each activity pattern. Then the last step is to find the total number of activity with the help of probability of occurrence of each activity and the total population of the study area.

Model Formulation. Multinomial logistic (MNL) regression model is used to predict categorical placement or the probability of category membership on a dependent variable based on multiple independent variables. As an outcome of multinomial logit modeling, the different equations that can be used for predicting the utility score of various activity patterns are as given below:

$$\begin{aligned}
 HWH = & -3.693 + 0.127V - 0.025TD_i + 0.003TC + 0.003TD_u + 0.002AD_u + 0.105G_0 + 0.827A_1 + 0.241A_2 \\
 & + 0.179A_3 + 0.031A_4 - 0.045Ed_0 + 2.370Em_0 + 1.516Em_1 + 1.213Em_2 + 1.827Em_3 \\
 & - 0.152Em_4 + 0.073Em_5 - 1.733Em_6 + 0.332I_1 + 0.282I_2 - 0.073I_3 - 0.024Li_0 \\
 & + 3.412M_0 + 3.646M_1 + 3.369M_2 + 3.584M_3 + 3.562M_4 + 3.092M_5 + 0.028Ti_1 \\
 & - 0.218Ti_2 + 5.457Ti_3
 \end{aligned}$$

$$\begin{aligned}
 HEH = & -3.183 - 0.036V + 0.009TD_i - 0.011TC - 0.005TD_u - 0.001AD_u - 0.156G_0 - 1.204A_1 - 0.138A_2 \\
 & - 0.125A_3 + 0.070A_4 - 0.025Ed_0 - 2.231Em_0 - 1.776Em_1 - 1.715Em_2 - 2.075Em_3 \\
 & - 0.649Em_4 - 0.112Em_5 + 2.813Em_6 + 0.160I_1 - 0.107I_2 + 0.638I_3 - 0.150Li_0 \\
 & + 3.737M_0 + 3.549M_1 + 4.971M_2 + 4.564M_3 + 4.717M_4 + 4.953M_5 + 1.191Ti_1 \\
 & + 1.374Ti_2 + 16.107Ti_3
 \end{aligned}$$

$$\begin{aligned}
 HSH = & -5.424 - 0.169V + 0.030TD_i - 0.008TC - 0.014TD_u - 0.015AD_u - 0.636G_0 - 0.059A_1 - 0.504A_2 \\
 & - 0.276A_3 - 0.341A_4 + 1.468Ed_0 - 2.391Em_0 + 0.543Em_1 - 0.299Em_2 + 0.242Em_3 \\
 & + 1.039Em_4 - 0.219Em_5 - 1.659Em_6 + 0.526I_1 + 0.677I_2 + 0.676I_3 - 0.270Li_0 \\
 & + 13.389M_0 + 14.252M_1 + 13.650M_2 + 13.024M_3 + 13.239M_4 + 13.079M_5 - 2.904Ti_1 \\
 & - 1.804Ti_2 + 19.225Ti_3
 \end{aligned}$$

$$\begin{aligned}
 HOH = & -4.225 - 0.087V - 0.025TD_i + 0.006TC + 0.021TD_u - 0.001AD_u + 0.727G_0 + 0.088A_1 - 1.140A_2 \\
 & - 1.843A_3 - 0.636A_4 + 0.135Ed_0 - 5.986Em_0 - 3.443Em_1 - 2.895Em_2 - 3.868Em_3 \\
 & - 0.144Em_4 - 0.376Em_5 - 2.642Em_6 + 1.092I_1 + 2.600I_2 + 3.047I_3 - 0.708Li_0 \\
 & + 10.653M_0 + 9.465M_1 + 10.151M_2 + 10.233M_3 + 8.769M_4 + 8.999M_5 - 4.159Ti_1 \\
 & - 5.096Ti_2 + 2.791Ti_3
 \end{aligned}$$

$$\begin{aligned}
 HWH = & -1.794 - 0.286V - 0.038TD_i + 0.071TC + 0.004TD_u + 0.002AD_u - 0.115G_0 + 0.383A_1 \\
 & + 0.360A_2 - 0.290A_3 - 0.294A_4 - 0.145Ed_0 - 0.273Em_0 + 0.024Em_1 + 2.639Em_2 \\
 & + 1.440Em_3 + 1.361Em_4 - 0.045Em_5 - 0.235Em_6 - 4.016I_1 - 4.663I_2 - 4.044I_3 \\
 & + 1.512Li_0 + 5.532M_0 + 5.457M_1 - 0.794M_2 + 0.675M_3 + 3.825M_4 + 3.789M_5 \\
 & - 2.738Ti_1 - 0.885Ti_2 + 0.024Ti_3
 \end{aligned}$$

$$\begin{aligned}
 HOH = & -9.473 - 0.250V + 0.066TD_i + 0.017TC - 0.032TD_u - 0.001AD_u + 0.131G_0 + 3.424A_1 \\
 & + 4.253A_2 + 2.803A_3 + 0.837A_4 - 1.066Ed_0 - 2.196Em_0 + 1.894Em_1 - 0.125Em_2 \\
 & + 3.359Em_3 + 5.253Em_4 + 3.346Em_5 + 1.640Em_6 + 0.375I_1 + 2.219I_2 + 4.187I_3 \\
 & + 0.660Li_0 + 2.489M_0 + 3.934M_1 + 0.660M_2 + 2.122M_3 - 0.652M_4 + 3.856M_5 \\
 & + 2.439Ti_1 + 3.755Ti_2 + 8.863Ti_3
 \end{aligned}$$

From these equations, the score of each type of activity pattern can be found out by inputting the values corresponding to each independent variables.

The probability of occurrence of each activity pattern can be calculated by using the equation (1).

$$\Pr(Y_i = 1) = \frac{e^{score(X_i,1)}}{1 + \sum_{k=1}^{K-1} e^{score(X_i,k)}} \tag{1}$$

Where X_i is the vector of explanatory variables describing observation i to k .

The total number of activity pattern can be calculated by multiplying these probabilities by the total population of the study area which is 5627.

Model Characteristics. The overall test of the relationship between the independent variables and dependent variables is given by the likelihood ratio test. Here the model with independent variables has a significance of 0.000 which is less than the level of significance 0.05. Hence, it is concluded that the dependent variables are related to independent variables. The significance of the model is obtained with the help of knowing the Chi-Square value of the model which is 433.94 and degrees of freedom 186. The tabled Chi-Square value is 239.428 corresponding to the same degrees of freedom. From this two Chi-Square values it can be seen that the tabled value is less than the obtained value. This means that the coefficients of independent variables have a significant role in the equations generated. Also, the significance of each independent variables is given in table 3.

Table 3. Model statistic

Variables	Chi-Square	df	Sig.
Intercept	0.000	0	
Vehicle	2146.848	6	0.000
Travel Distance	3386.861	6	0.000
Travel Duration	7364.159	6	0.000
Gender	6.234	6	0.398
Age	8935.943	24	0.000
Education	1838.605	6	0.000
Income	26159.825	18	0.000
Mode	6248.857	30	0.000

*the values for travel cost, activity duration, employment, license and time can't be estimated by SPSS

The model that has developed is having a McFadden's coefficient of determination (R^2) value of 0.409. Generally R^2 values will range from 0 to 1 [9]. 0 indicates that the model explains that, there is no variability of the response data around its mean. And 1 indicates that the significant variability of the response data around its mean.

The accuracy of the model has been checked by the help of substituting 1/3rd of the data which is not used for the model creation. As an outcome, the accuracy of the model generated is 82%, which can be considered as a good model.

5 Conclusions

An activity tour generation model was developed on six different aspects using activity-based approach. The multinomial logit model was used as the modeling tool. For every activity-based tour generation model, activity tour chains were considered as the dependent variable and different independent variables (gender, age, educational qualification, employment, income, license, vehicle ownership, mode used for travel, travel distance, travel cost, travel duration, activity duration and time of day) were identified significant in the model. The utility functions developed from the model is used for generating the probability functions which predicts the occurrence of activity tour chains. The activity tour chains considered in the model were home-based work tours, home-based educational tours, home-based shopping tours, home-based other tours, home-based complex work tours and home-based complex other tours.

The model was developed to predict the score of each activity. Using multinomial logit model, the probability of each activity was calculated. The models can serve as a platform for predicting the number of tours generated for a given socioeconomic group and accordingly transportation and land use plans can be formulated in a long-term perspective.

The extension of the study area from a single ward of the Thrissur city to entire Thrissur city can be considered as the future scope of this mini project. By implementing it in such a manner a decent and good model can be made that can make so many advantages to the Thrissur Corporation to analyze what will be the possible outcome by making any significant changes in that area. Also, a micro-simulation model creation can also enhance the importance of the extension of this mini project.

ACKNOWLEDGEMENT

Authors would like to express sincere gratitude to the staff, students, and management of Jyothi Engineering College for the priceless assistance in accomplishing the work.

REFERENCES

- [1] B. G. Hutchinson, "Principles of Urban Transport Systems Planning." Scripta Book Company, University of Michigan, 320-400, 1974.
- [2] R. B. Chandra, S. Srinivasan, Y. G. Jessica and S. Aruna, "Activity-Based Travel-Demand Modeling for Metropolitan Areas in Texas." Center for Transportation Research, The University of Texas at Austin, Paper No. 0-4080, 2003.
- [3] G. M. Michael, "An Activity-Based Microsimulation Model for Travel Demand Forecasting" Conference on Activity-based Approaches, Netherlands, 1996.
- [4] J. Castiglione, M. Bradley and J. Gliebe, "Activity-Based Travel Demand Models: A Primer." Resource Systems Group, Inc., SHRP 2 Report S2-C46-RR-1. Transportation Research Board, Washington D.C, 2015.
- [5] S. V. S. Saladi and K. V. Krishnarao, "Activity-Based Approach to Travel Demand Modeling: An Overview." *TransportiEuropei*, 61(6), 2016.
- [6] G. R. L. Amrutha, V. S. Landge and K. V. S. Sanjay, "Activity-Based Travel Demand Modeling of Thiruvananthapuram Urban Area." *Transportation Research Procedia* 17, ELSEVIER, 498-505, 2016.
- [7] M. J. Bruton, "Introduction to Transportation Planning." Hutchinson Technical Education, London, 99-150, 1971.
- [8] Y. Sadayuki and M. Abolfazl, "An Activity-Based Microsimulation Model of Travel Demand in the Jakarta Metropolitan Area" *Journal of Choice Modeling*, 3(1), 32-57, 2010.
- [9] D. Salgado, D. Jolovic, T. M. Peter and M. A. Rafael, "Traffic Microsimulation Models Assessment – A Case Study of International Land Port of Entry" *Procedia Computer Science* 83, ELSEVIER, 441-448, 2016.

URBAN RESIDENT'S AWARENESS AND READYNESS FOR SUSTAINABLE TRANSPORTATION A CASE STUDY

Leejiya Jose and Vincy Verghese

Abstract-The present course of transport development in Kerala marked by over-dependence on motor vehicles pushing the main cities of the state into a major transportation crisis. Increased use of motor vehicles, especially in areas unable to afford proper facilities comes at both a heavy economic and environmental cost. With the number of vehicles on its roads increasing to unmanageable levels, Kerala is already in the grip of transportation crisis. Unless imaginative measures and innovative practices are adopted, the State might find it is impossible to provide an efficient transport system.

A sustainable transportation system besides controlling air emissions, traffic congestion or excessive fuel use, must balance the present and long term needs for the environment, economic growth and equity. Walking and bicycling have negligible environmental effects. However, they are affected by the environmental impact of motorized transport. Walkers and cyclist are turning to be a rare sight in the cities. The union government has claimed that it has taken many important steps to make public transportation system sustainable and environment friendly. Many projects aimed for more sustainable mobility are either not or only partly successful. Sustainable mobility requires considerable changes in individual travel behavior.

This paper studies the willingness of an urban population to use sustainable vehicles and their readiness to reduce car usage and also the barriers and motivations to using sustainable transportation for daily trips by conducting a survey of vehicle users. Modes of sustainable transportation considered in this project are pedestrians, bicycle and public transportation. Distribution of the questionnaire will make from house to house and also approaching respondent at the recreation center, shopping centers etc., for the selected area.

KEYWORDS: Sustainable transportation, Questionnaire, Car sharing, Cycle tracks, Household survey

Leejiya Jose, PG Scholar, Department of civil Engineering, Jyothi engineering college, Cheruthuruthy (email: leejyakjose@gmail.com).

Vincy Verghese, Assistant professor, Department of civil engineering, Jyothi engineering college, Cheruthuruthy (email: vincyverghese@jecc.ac.in).

I. INTRODUCTION

Development of road infrastructure has not kept pace with the rapid increase in the number of vehicles in Kerala. The number of all class vehicles in the State went up from 1,19,720 in 1975 to 36 lakhs in 2006. This was accompanied by increase in road length from 14,870 km to 21,347 km. Energy intensity of various transport modes is a key factor in determining transport related environmental impacts. Energy consumption per passenger km by bus is the least and is highest for cars among road based personalized vehicles. Public transportation provides more sustainable travel compared to other transport modes. But the sustainable mobility requires considerable changes in individual travel behavior.

Road traffic has increased significantly over the years because most households today have access to two or more cars. In Kerala the average number of vehicles owned per family is two, and the average number of family members with driving license is also two. These figures indicate that virtually every family has a car and every family has more than one member with a driving license. The union government has claimed that it has taken many important steps to make public transportation system sustainable and environment friendly. Many projects aimed for more sustainable mobility are either not or only partly successful. Sustainable mobility requires considerable changes in individual travel behavior. Nevertheless, travel by private car remains the predominant mode of choice in major city centers. A number of studies have shown that some people might not always drive

out of need, but because of choice. Car features provide a psycho-social value, which influences everyone to use a car rather than other modes of transportation. Therefore, the government should enhance transport policies that reduce the dependency and need to drive a car by providing alternatives other than driving.

Sustainable Transport is sometimes known as Green Transport and it is any form of transport that does not use or rely on dwindling natural resources. Instead it relies on renewable or regenerated energy rather than fossil fuels that have a finite life expectancy. For this reason, it is said to have a low or a negative effect on the environment since it makes use of energy sources that are sustainable. Walking, cycling and sailing are excellent examples of sustainable transport.

The sustainable transportation means any sort of transportation vehicle or transportation habit that is environmentally friendly and doesn't emit toxic gases that could impact the environment and human health. A sustainable transportation system, besides controlling air emissions, traffic congestion or excessive fuel use, must balance the present and long-term needs for the environment and economic growth.

II .LITERATURE REVIEW

Although no common accepted definition of sustainability, sustainable development or sustainable transport is available, it is generally accepted that sustainable development are, and more specifically, sustainable transport, implies finding a proper balance between environmental, social and economic qualities. A popular definition for sustainable transport was developed by the European Conference of Ministers of Transport (ECMT 2004), which stated that a sustainable transportation system is one that is accessible, safe, environmentally-friendly, and affordable.

This chapter provides an overview of previous research on sustainable transportation projects. It introduces the framework for the case study that comprises the main focus of the research described in this thesis.

Many projects aimed for more sustainable mobility are either not or partly successful. Sustainable mobility requires considerable changes in individual travel behavior. One of the main reason of unsuccessful sustainable mobility project is the habitual character of individual travel behavior. The reduction of car use is a specific problem because the attractiveness of car is based on many variables associated with comfort, such as convenience, independence, flexibility, safety or privacy. These factors are studied by Nasrudin et al.[1]. They found that most of the respondents are considered driving a car as relaxing and safe and also stated that driving a car gave them freedom. This study examined willingness of people to switch to more sustainable vehicles, willingness to reduce car usage, willingness to switch to public transport etc.,

A modification for this study is done by Nasrudin et al[2]. This study examined how transport policy measures have influenced travel behavior to promote sustainable transportation and the readiness of an urban population to reduce car usage. And they measured the respondent's readiness to reduce car use, readiness to reduce car speed and readiness to walk and cycle.

Different variables tested in this survey includes the role of road pricing in travel behavior, role of parking fees in shopping venue selection, readiness to practice sustainable modes of travel and reasons why respondents do not like to walk or cycle. The results showed that increase in petrol prices would be a key factor to reduce travel and car usage and more provisions on public transport and affordable public transport fares would also encourage them to reduce car usage and opt for public transport.

Nasrudin et al.[3] conducted a study on "Barriers and motivations for sustainable travel behavior" in order to understand the barriers and motivations to using sustainable transportation for daily trips. The reasons for respondents are not motivated to use public transport are inefficient services and expensive fares. And the findings in this study are barriers and motivations to walk and cycle, Percentage of reasons why respondent do not like to walk or cycle, barriers and motivations to use public transportation and level of willingness to use public transport if the services are improved. And the main barriers and motivations to use public transport found in this study are punctuality problem, inefficient public transport services, expensive fares etc.

Abdullah, Y.A., et al[4] are studied the willingness of an urban population to use sustainable vehicles and their readiness to reduce car usage. The number of cars owned and number of licenses held in the family, the emotion and perception of owning and driving a car, the level of readiness to reduce car usage are evaluated in this study. Results of the survey suggested that the majority were not ready to consider cycling and walking as alternative. Every family has a car and every family has more than one member with a driving license. And also they found that a car is seen as something that provides security from unwanted people and events, as well as providing convenience, reliability and capability to provide access to more destinations than public transport.

III.METHODOLOGY

Methodology is the systematic, theoretical analysis of the methods applied to a field of study. It comprises the theoretical analysis of the body of methods and principles associated with a branch of knowledge. The methods section describes action to be taken to investigate a research problem and the rationale for the application of specific procedures or technique used to identify, select, process, and analyze in the formation applied to understanding the problem, thereby, allowing the reader to critically evaluate a study’s overall validity and reliability. And this section describes how was the data collected or generated, and how was it analyzed.

Data collection is done by household survey. Household surveys collect information by sampling the homes where people live and then interviewing one or more persons at each home. Household surveys are the most common type because they offer a standard way of collecting information.

A total of 384 respondents were selected for this survey, as a sample representing the total population of Thrissur city by using stratified random sampling method. Selected of the sample were calculated based on the total population which is of 315957 peoples, with 95% degree of confidence limit, and 5% of the margin of error. Survey is conducted by approaching respondent at their home for different sections in the city. Here for this survey, the sampling is done by using a survey software known as sample size calculator.

A. Sample Size Calculator

This Sample Size Calculator is presented as a public service of Creative Research Systems survey software. We can use it to determine how many people you need to interview in order to get results that reflect the target population as precisely as needed. We can also find the level of precision we have in an existing sample.

Before using the sample size calculator, there are two terms that we need to know. These are: confidence interval and confidence level

B. Sample Size Calculator Terms: Confidence Interval & Confidence Level

The confidence interval (also called margin of error) is the plus-or-minus figure usually reported in newspaper or television opinion poll results.

The confidence level tells you how sure you can be. It is expressed as a percentage and represents how often the true percentage of the population who would pick an answer lies within the confidence interval. The 95% confidence level means you can be 95% certain; the 99% confidence level means you can be 99% certain. Most researchers use the 95% confidence level.

The data used for the sampling are:

- Total population =315957 persons (From census data 2011)
- Confidence level =95%
- Margin of error =5%
- Sample size needed =384

Results obtained from the sample calculator for the given population is as shown in the Fig3.2.

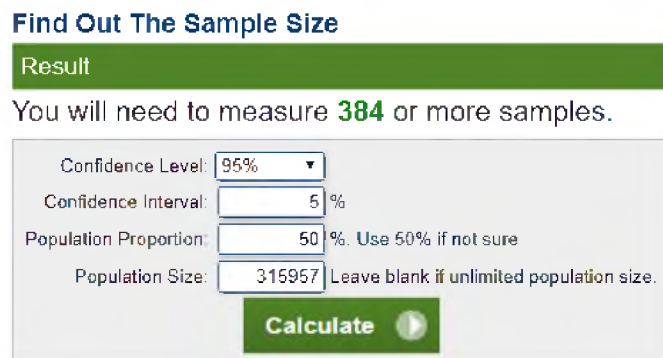


Fig. 1 Sample size calculator

The following table (Table.1) also represents sample size required for different population ranges

TABLE 1
SAMPLE SIZE FOR VARIOUS POPULATION RANGES

Population size	Confidence level=95%			Confidence level=99%		
	Margin of error			Margin of error		
	5%	2.5%	1%	5%	2.5%	1%
100	80	94	99	87	96	99
500	217	377	475	285	421	485
1,000	278	606	906	399	727	943
10,000	370	1332	4899	622	2098	6239
100,000	383	4513		659	2585	14227
500,000	8762			663	2640	16055
1,000,000	384	1532		663	2647	16317
	9423					
	384	1534				
	9512					

From this table sample size required for a population of 315957 and 95% confidence level with margin of error 5% is 384.

IV. DATA ANALYSIS

After data has been collected, it needs to be presented in a way that communicates the information and enables conclusions to be drawn. Clear, accurate and appropriate ways of presenting data were chosen out of the several ways of data presentation. The several ways of presenting data include tables, pie charts, bar graphs and line graphs, only tables, pie charts and bar graphs were used in this research.

The purpose of the discussion is to interpret and describe the significance of our findings in light of what was already known about the research problem being investigated, and to explain any new understanding about the problem after taken the findings into consideration. This chapter presents the results of the data analysis and discussion of the results.

A. Car Ownership and Driving Licenses Held in A Family

Table 2 shows that, the average number of vehicles owned per family was two and the average number of driving licenses belonging to a family was also two. These numbers show that virtually every family has a car and every family has more than one member with a driving license.

TABLE 2
NUMBER OF VEHICLES OWNED AND DRIVING LICENSES HELD IN A FAMILY

Number of vehicles owned in the family	Total	Percentage (%)	Number of driving licenses held in the family	Total	Percentage (%)
0	28	7	0	26	7
1	108	27	1	111	28
2	158	40	2	149	37
3	70	18	3	81	20
4	26	6	4	22	5
5	8	2	5	7	2
			6	2	1
Total	398	100		398	100

B. Emotions and Perceptions Toward Car

From the conducted interviews with car owners and non-car owners to investigate the psycho-social benefits to people which is obtained by using cars, it is found that a car is seen as something that provides convenience, reliability, and capability to provide access to more destinations than public transport. In the current study, when asked how they generally felt while driving their cars, the majority of the respondents provided positive feedback. Most considered driving a car gave them freedom and they considered driving a car as safe and relaxing than other public transportations.

TABLE 3
PERCENTAGE OF VARIOUS EMOTIONS FELT WHEN DRIVING A CAR

Statements	Total	Percentage (%)
Freedom	186	33
Relaxing	164	29
Safety	115	21
Stressful	39	7
Tiring	40	7
Troublesome	17	3

From table 3 and fig 3 respondents stated that driving a car gave them freedom and considered driving a car as relaxing and saf



Fig.2 Percentage of various emotions felt when driving a car

C. Willingness to Switch to More Sustainable Vehicles

Lensink (2005) concluded that obtaining a more sustainable transport system requires that more attention should be paid to the interaction between infrastructure planning and traveler’s decision behavior. The research of Boarnet and Sarmiento and Cao et al. suggested that residents of a new urbanist area were more willing and able to take public transport, walk, or cycle to their destinations, due to their own personal beliefs and philosophies on transport and the environment.

D. Willingness to switch to walking or cycling

Walking and cycling are the two modes of transport which are available to nearly everyone, produces almost no emissions, promote fitness and health and make the minimum impact on the local environment..

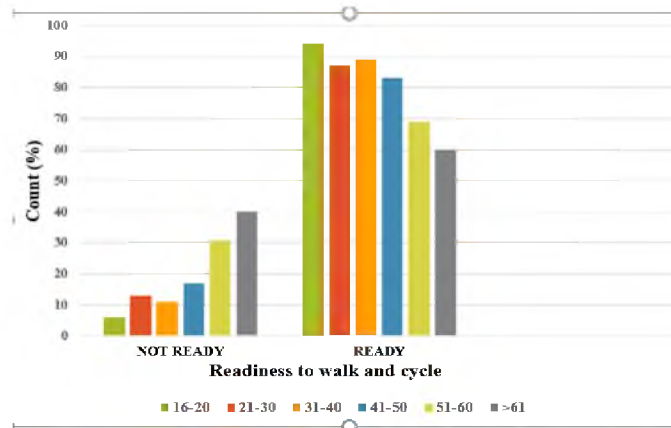


Fig.3 Willingness to switch to walking or cycling

The study found that majority are willing to cycle or walk as alternatives to using a motor vehicle.

In general, younger generations tend to be more concerned about environmental quality than older generations. Hence the younger generations are considered more open to environmental issues than older generations. In this study, the results show that the younger age group (16-20) recorded the highest result in showing ready to walk or cycle. And the older age group (greater than 61) recorded the highest in showing not ready to walk or cycle.

E. Level of willingness to switch to use public transport by gender

The current study examined the level of willingness to use public transport by gender. Table represents willingness of people to use public transport.

TABLE 4
LEVEL OF WILLINGNESS TO SWITCH TO USE PUBLIC TRANSPORT BY GENDER

Gender	Willingness to use public transport		Total
	Not ready	Ready	
Male	20	185	205
	9.8%	90.2%	100%
Female	12	181	193
	6.2%	93.8%	100%
Total	32	366	398
	8%	92%	100%

From this table we can see that female respondents were shown to be more ready to use public transport compared to males. And overall 92% respondents are ready to use public transport and 8% of respondents are not ready. Which means that women were found to be more willing to reduce their car usage, more positive towards reducing the environmental impact of travel modes, and more positive towards ecological issues than men.

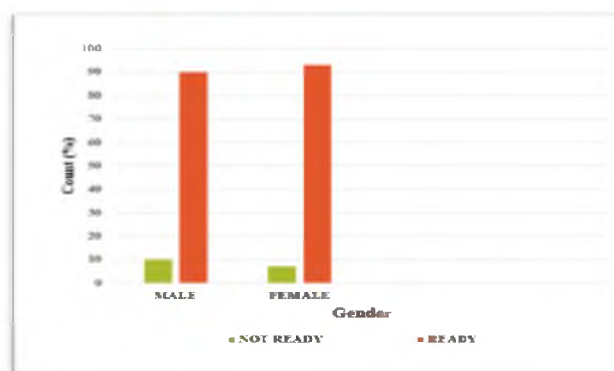


Fig.4 Level of willingness to use public transport by gender

F.Mode of Travel to Work

The objective of this stage of the analysis was to identify association between different modes of travel to work. The Figure 4.4 reveal the main modes of transport by which residents get to work.

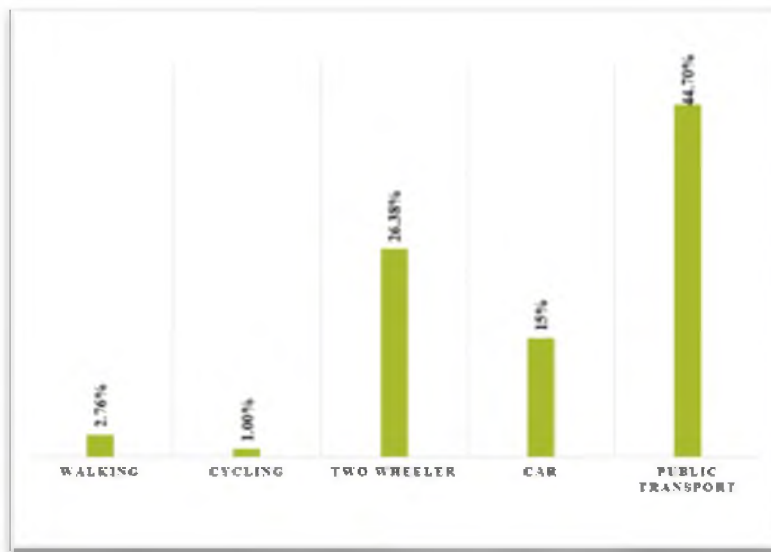


Fig.5 Mode of travel to work

The results of this study showed that 44.70% of respondents use public transportation to commute to work compared with 26.38% who use car and 15% who use two wheelers. To encourage residents to support a sustainable transportation program, the respondents were asked to provide an opinion on the factors that would reduce the use of cars. The respondents were given several statements on options would motivate them to reduce car use.

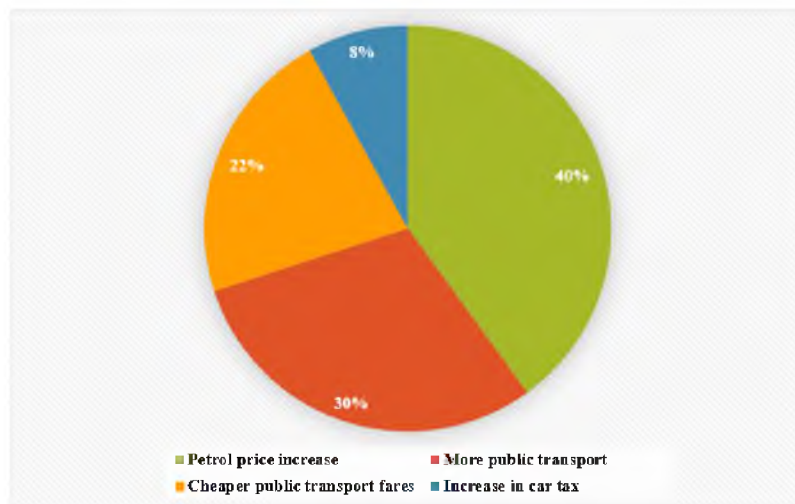


Fig.6 Reasons causing car use reduction

Majority stated that the increase in petrol prices would be a key factor to reduce travel and car use. Other than that, more provisions on public transport and affordable public transport fares would also encourage them to reduce car use and opt for public transport as the main mode of travel.

G.Mode of travel to personal trips

The objective of this stage of the analysis was to identify association between different modes of travel to personal trips. The Figure 4.6 reveal the main modes of transport by which residents get to personal trips.

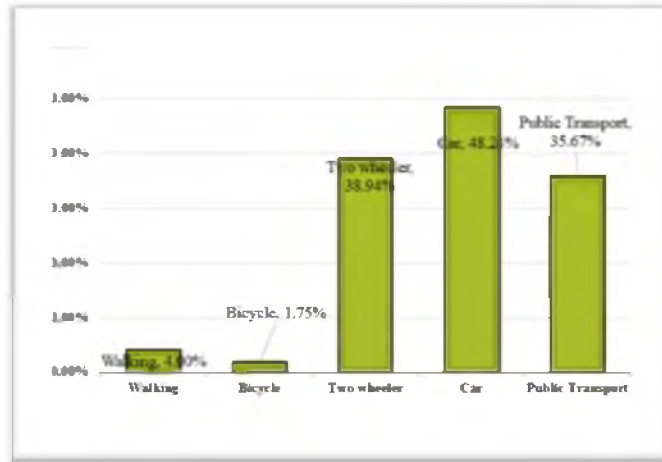


Fig.7 Mode of travel to personal trips

From the figure () most of the respondents use car (48.24%) to commute to personal trips compared to 38.94% who uses two wheelers and 35.67% who uses public transport.

H.Reasons for not using public transportation

Public transportation is transport of passengers by group travel systems available for use by the general public, typically managed on a schedule, operated on established routes, and that charge a posted fee for each trip. Example of public transport include city buses, passenger trains etc. But the use public transport decreasing day by day and the reason for this decrease in use of public transport is analyzed in this section and the percentage of various reasons are provided in the table 4.4.

TABLE 5
REASONS FOR NOT USING PUBLIC TRANSPORTATION

Reasons for not using public transportation	Total	Percentage(%)
More comfortable using the car	168	42
Loss of time waiting for public transport	94	24
Public transport is not efficient	50	13
Expensive fares	35	9
Others	26	7

Table 3 shows that, 42% of respondents stated that they were “more comfortable using the car”. This was followed by the second highest reason, “loss of time waiting for public transport”. Among the reasons respondents refuse to use public transport are punctuality problem, inefficient public transport services, and expensive fares.

In this study, we have identified several barriers in using public transport. When respondents were asked their reason for not using public transport, 42% of respondents stated that they were “more comfortable using the car”. This was followed by the second highest reason, “loss of time waiting for public transport”. Among other reasons included inefficient public transport and expensive fares.

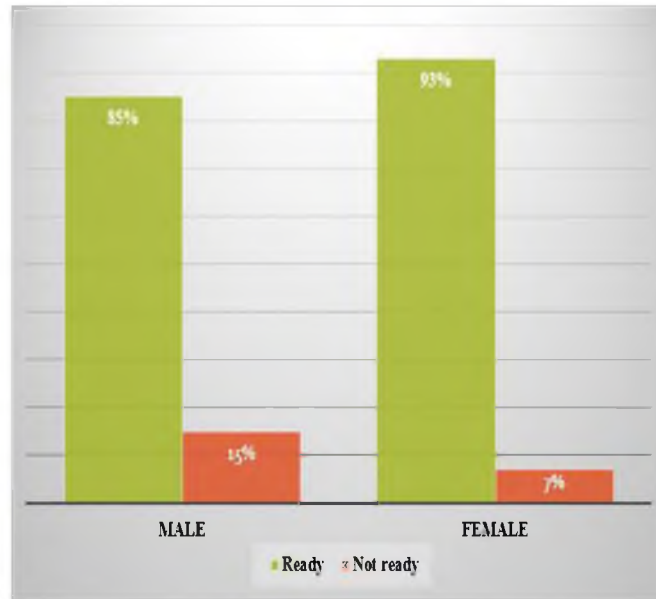


Fig.8 Willingness to use public transportation if the services are improved

However, the current study also found that the majority of respondents are willingness to use public transport if the services are improved. The improvement in public transport system would motivate them to use public transport as alternative to using a private vehicle.

I. Readiness to adopt cycling

Walking and cycling are the two modes of transport which are available to nearly everyone, produces almost no emissions, promote fitness and health and make the minimum impact on the local environment. This section analyzes the readiness of urban population to adopt cycling if exclusive cycle tracks are provided. And the percentage of readiness of people to adopt cycling is presented in the following Figure (Fig 4.8).

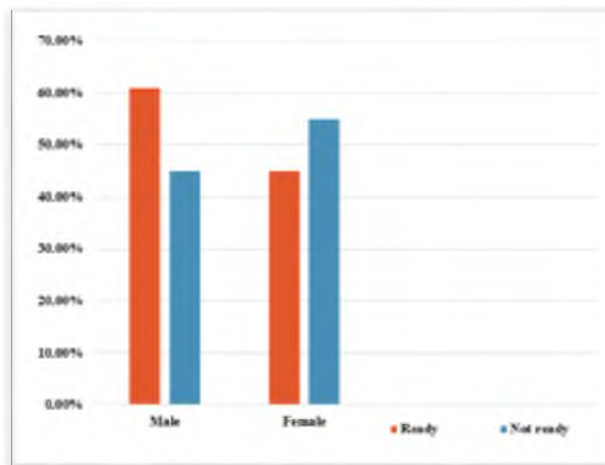


Fig.9 Readiness to adopt cycling, if exclusive cycle tracks are provided

From the Fig 4.8, it is clear that most of the respondent are ready to use cycling, if exclusive cycle tracks are provided. This analyzes shows that male respondents are more ready to adopt cycling compared to that of females. About 60% of male and 45% of females are ready to adopt cycling.

J. Readiness to use car sharing

Car sharing is the practice of sharing a car for regular travelling especially for commuting.

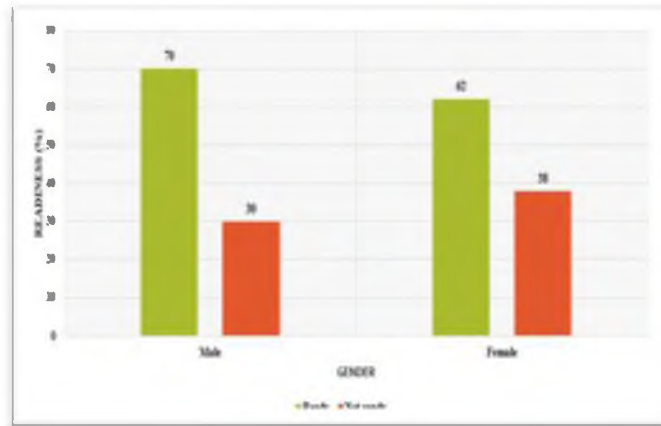


Fig.10 Readiness to use car sharing

The study found that the majority are willing to use car sharing. Male are more ready to use car sharing (70%) compared to females (62%).

K.Readiness to use share auto services (at least up to 7km)

Share auto is the practice of sharing auto rickshaws for regular travelling especially for commuting. This study tested the readiness of respondents for using share auto services and the results shows that majority are ready to adopt share auto services. In which females are more ready to use share auto services compared to males. About 82 % of females are ready to use this services compared to 67% males. About 33% males are not ready to use share auto services as a mode of travel.

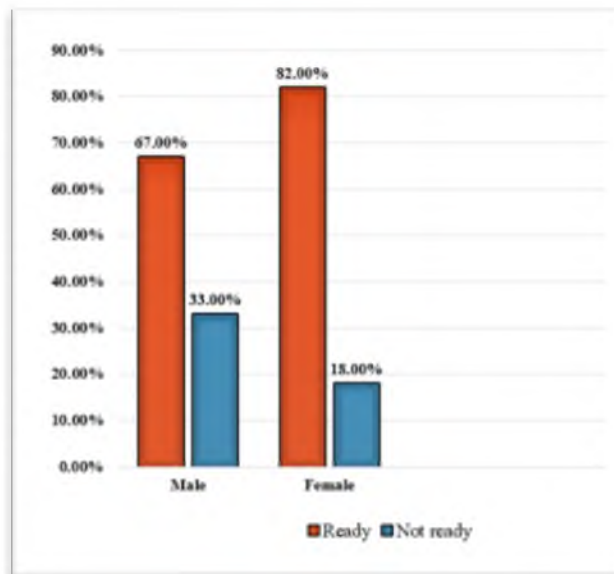


Fig.11 Readiness to use share auto service

V.SUMMARY

The willingness of an urban population to use sustainable vehicles and their readiness to reduce car usage and the barriers and motivations to using sustainable transportation for daily trips are studied in this project by conducting a household survey of urban population. This study indicates that the majority of the respondents are ready to consider cycling or walking as alternative modes of travel and most of the residents are depend on their car and two wheelers. The habitual character of daily mobility is seen to be a major barrier for changes towards a more sustainable behavior. Other general conclusions obtained from the study are

- The average number of vehicles owned per family was two and the average number of driving licenses belonging to a family was also two. These numbers show that virtually every family has a car and every family has more than one member with a driving license.

- Most considered driving a car gave them freedom and they considered driving a car as safe and relaxing than other public transportations.
- The study found that majority are willing to cycle or walk as alternatives to using a motor vehicle. Younger age group (16-20) recorded the highest result in showing ready to walk or cycle
- Petrol price increase is the main factor which causes car use reduction and provision of more public transport facilities also reduces car use
- If proper cycle tracks are provided, it will encourage people to use bicycles as a convenient mode of transport, especially for short trips
- Most of the respondents are ready to use public transportation, if services are improved
- Willingness to use sustainable modes of travel is depending up on age, gender, vehicle ownership etc.,

VI.CONCLUSION

Road traffic has increased significantly over the years because most households today have access to two or more cars. A number of studies have shown that some people might not always drive out of need, but because of choice. Car features provide a psycho-social value, which influences everyone to use a car rather than other modes of transportation. The willingness of an urban population to use sustainable vehicles and their readiness to reduce car usage and the barriers and motivations to using sustainable transportation for daily trips are studied in this project by conducting a household survey of urban population. This study indicates that the majority of the respondents are ready to consider cycling or walking as alternative modes of travel and most of the residents are depend on their car and two wheelers. The habitual character of daily mobility is seen to be a major barrier for changes towards a more sustainable behavior.

REFERENCES

- [1]Nasrudin, N.,Abdullah, Y.A.,Leh, O.L.H.,(2017). “Promoting Sustainable Travel Behavior Through Transport Policy Measures”.Journal of the Malaysian Institute of Planners 15(2),85-96
- [2] Perra, V.M., Sdoukopoulos, A., Latinopoulou, M.P., (2017). “Evaluation of sustainable urban mobility in the city of Thessaloniki”.Transportation Research Procedia 24, 329-336
- [3] Nasruudin, N., Rostam, K.,Noor, H.M.,(2014). “Barriers and Motivations for Sustainable Travel Behaviour: Shah Alam resident’s perspectives”.Procedia –Social and Behavioral Sciences 153,510-519
- [4] Nasrudin, N.,Nor, A.R.M.,Noor, H.M.,Abdullah, Y.A.,(2013). “Urban Resident’s Awareness and Readiness for Sustainable Transportation Case Study: Shah Alam,Malaysia”.Procedia –Social and Behavioral Sciences 105,632-643
- [5] Zayed, M.A., (2016). “Towards an index of city readiness for cycling”.International Journal of Transportation Science and Technology 5,210-225

Use of Data Mining Technique for Systematic Road Safety Audit of Non-urban Highways

Bincy B.J.¹ and Dr. Anitha Jacob²

PG Scholar,

² Associate Professor,

Department of Civil Engineering,

Jyothi Engineering College, Cheruthuruthy, Thrissur, Kerala 679 531.

(anithajacob@jecc.ac.in)

Abstract. The number of road crashes is increasing at an alarming rate in India. Hence, there is an urgent need for a systematic approach to improve road safety. A Road Safety Audit (RSA) is the formal safety performance examination of an existing or future road or intersection by an independent, multidisciplinary team. It qualitatively estimates and reports on potential road safety issues and identifies opportunities for improvements in safety for all road users. Budgetary constraints limit many developing countries from performing the audit on regular basis. This will eventually delay any rehabilitation or repair process making the road conditions the worst and risky. This paper proposes a systematic approach to do the road safety audit on a highway and to do effective and efficient data mining, for deriving knowledge driven decisions in the classification of highway sections. The approach will help to perform safety evaluation of sections and to identify the crash potential locations. Further output of the work is the development of a mathematical model for classification of highway sections based on road safety audit.

Keywords: Data mining, Weka, Road Safety Audit, Road safety model

Introduction

Road Safety Audit (RSA) is a systematic process for examining the safety performance of an existing or future road by an independent team or trained specialties. Qualitative estimation on potential road safety issues, identification of opportunities for improvements and ensure safety for all road users are the basic objectives of RSA. Government integrates RSAs into the project development process for new roads and intersections, and also encourages RSAs on existing roads and intersections. Public agencies with a desire to improve the overall safety performance of roadways under their jurisdiction should be excited about the concept of RSAs. All new and reconstructed roads should be as safe as possible. Since RSA is done based on a clearly defined procedure it can be used at any phase of project development from planning stage to construction. RSAs can also be used on any sized project from minor intersection and roadway retrofits to mega-projects. Through the systematic application of RSA, it can ensure a growing awareness about road safety principles which can be applied throughout the highway planning, design, construction and maintenance organization. Traffic control devices provide safe and secure journey for the road users. These are devices used to inform, guide and control the traffic. Maintenance of traffic control devices is one of the most important aspects of highway management systems. Scientific and well-timed installation of the traffic control devices increases safety as well as significantly decreasing accident rates. For a safer driving environment, timely maintenance of the traffic signs is very important and incorporating these activities makes a viable economic sense. The specialized units of highway authorities, that is the Road Safety Authority (RSA) frequently check the safety requirements of the traffic control devices.

Road Safety Audit can minimize the risk and severity of road accidents by the road project and also can minimize the need of remedial work after construction. Road safety inspection based on (IRC SP – 88, 2010) [1] is conducted on an existing road, from Kunnankulam to Peramangalam, since it is identified as one of the accident black spot.

Background

This section, describe a short survey about Road Safety Audit, and classification of road by means of Weka software and analysis

Road Safety Audit (RSA)

Road safety audit is done to ensure the operational safety performance of a road. Hence, it has the potential for improving safety when it is applied to a road or traffic design before the project is implemented. Through RSA the identification of potential safety hazards on new road projects at the appropriate stage can be done and so that it can minimize the adverse effects at minimum cost. It can be conducted on any design proposal, which involves changes to the ways road users will interact, either with each other or with their physical environment. Purpose of the audit is to identify hazardous features on existing road so that it can be eliminated or otherwise treated before they become an accident prone location.

Mehar and Agarwal [2] present some basic concepts for a systematic approach for formulation of a road safety improvement program in India. They developed an accident record system, for ranking of safety hazardous locations, and also for identification of safety improvement measures and to determine priorities of safety measures. It also describes the difficulties faced in the safety audits and analysis of accidents. Their study highlights the system of accident data collection in India is inconsistent and irregular. This study presented a frame work for development of road safety improvement program in India. They also stressed the need for developing a comprehensive methodology that should be capable of identifying the remedial measures based on the analysis of accident records as well as detailed engineering studies.

Griselda Lopez and Jaun de Ona [3] conducted analysis on the deficiency of traffic control devices with regard to crashes on rural highways. They adopted variables related to geometric and environmental road characteristics and found that the road which is improperly or poorly signaled can lead to incorrect placement or maneuvers of vehicles and ambiguous situations that can increase the risk of crashes. They analyze the relationship between road crashes in two-lane rural highways and certain deficiencies in signaling.

They also found out that the human error is most often related to the perception and processing of information presented by the road or traffic environment. There are situations that cause problems with road user perception, interpretation or judgment stages may lead to driver to loss of control. Driver will get distracted due to crashes derive from diverse sources outside the vehicle. Hence, it is crucial to maintain the road features in optimal conditions so that they have the least possible impact on the drivers performance. They had done the analysis using CART method.

Arun S Bagi, Dheeraj N Kumar [4] explained that for each accident there is a need of systematic study in a scientific manner and detailed investigation of the accident spot. This type of investigation will help to identify some of the causative factors responsible for accidents and to give relative importance. The results of the study could be employed advantageously to take up preventive measures to reduce the accidents. They studied accident prone areas on the Bannerghatta road and studied the effect of roadway geometrics and traffic conditions on the road stretch. Pedestrian safety analysis is also done. Accident prone locations are identified by the analysis. The study focuses on is the identification of accident prone areas on the road from FIR, to study the effect of roadway geometrics and traffic conditions on the road stretch and development of statistical relationship between accident rates and various factors causing accidents.

Saffarzadeh and Farshad [5] studied the maintenance of highway traffic control device and the problems faced, they found that in many developing countries, due to budget limits and lack of regular maintenance activities and many deficiencies related to signs, guardrails road markings increased. They also tried to propose an appropriate management system for the maintenance of traffic control devices, along with the development of computer software for control devices, which can identifying the necessary time for maintenance. With those mathematical models it can increasingly lead to the efficiency of operational systems for the maintenance of traffic control devices with in the limitation of the allocated budgets. These models are essentially flexible like any other mathematical model, regarding the alternatives.

Farzaneh Moradkhani, Somayya Ebrahimkhani [6] identified the factors behind road traffic accidents using data mining algorithms including and keep controlling on it. They have done the research, evaluation and implementation by using Weka software. The results of data mining will help organizations such as

transportation, to explore the accidents data recorded by the police information system, and discover patterns and predict future behaviors and effective decisions to be taken to reduce accidents.

Majid Khalilikhah, Kevin Heaslip [7] studied the effects of damage on sign visibility. Traffic signs are provided to convey information to the drivers. So it is necessary to ensure visibility in night time or low light conditions, traffic signs must be in compliance with the minimum retro reflectivity standards outlined by the road safety manual. They studied about the aging of sign and also other contributing factors affect sign retro reflective performance and are determined the effects of various damage forms on sign retro reflectivity, through statistical methods, including regression models, chi-square test, t-test, and odds ratio were employed to analyze traffic sign data.

Data Understanding

The first stage of data mining process is to select the related data from many available data source and to correctly describe the data. Data sources can vary based on the purpose of analysis. The data was collected from two sources

A. Road inventory data

The selected study area is a 15 Km road stretch. The study area is divided into 200m sections for the convenience of study.

B. Traffic collision data

Past five year (2013-2017) accident data of Kunnankulam and Peramangalam police station is collected from the FIR, and it includes information such as Location, Time Driver, Passenger, Pedestrian data related to (age, sex, alcohol influence) and also severity of crashes (Fatal crashes, Grievous injury crashes and Minor injury crashes)

The data type can be quantitative or qualitative data. Quantitative data is measurable using numerical values. Qualitative data also known as categorical data contains both nominal and ordinal data. Nominal data has finite non-ordered values, such as terrain data has two values: flat and rolling. Once relevant data are selected, data pre-processing should be done.

Data Pre-Processing

Data pre-processing involves converting the collected raw data into an understandable form. Real-world data is sometimes insufficient, unpredictable and/or lacking in certain performance or trends and is likely to contain many errors. Data pre-processing is the best method for resolving such errors. Data pre-processing prepares the unprocessed data for further processing.

A. Data Field Selection

Data gathered from various sources were combined, classified and examined. Some of the data which are not relevant for the data mining technique was ignored.

B. Data classification

Data classification process can improve the quality of the data collected by correcting the errors detected. Generally data classification reduces errors and improves the data quality. Data classification can correct the errors such as the entries which are clearly invalid occurred due to human error and error on the problem reporting system can be identified and those which are correctable were corrected.

C. Data Transformation

Data transformation is the process of transforming the data into appropriate forms which are able for data mining. The data set used in the study contained integer values for the entire attributes. The attribute considered in the training dataset are presented in Table 1. The table shows the classification values for the corresponding attributes.

Table 1. Classification table

Attribute	Classification values
Width of road	1:Proper 2:Not sufficient
Shoulder width	1:Proper 2:Not sufficient
Terrain	1:Flat 2:Rolling
Veh/3 min	1: Vehicle count with in limit 2:Exceeds limit
Passing Zone width	1:Sufficient 2:Not sufficient
Warning Sign	1:Properly provided 2:Provided -not clear 3:Not provided
Regulatory Sign	1:Properly provided 2:Provided -not clear 3:Not provided
Informatory Sign	1:Properly provided 2:Provided -not clear 3:Not provided
Pavement Markings	1:Properly provided 2:Partially removed 3:Completely removed
Position of sign board	1:proper sight distance 2:Less sight distance
Post Mounted Delineators	1:Properly provided 2:Very less in number 3:Not provided
Crash Severity	0:No crash 1:Minor injury 2:Major injury 3:Fatal

Data Mining

Data mining, is an emerging technique for data analysis hence it has the ability to collect, store and can extract the hidden predictive information from large databases. With the increased volume of database it is very difficult to understand the data without any powerful tool. Data mining is a new powerful technology with great potential to help user to derive decision from the data collected hence it is a typical tool for decision supporting system. Data mining tool is very useful to solve questions quickly in which by traditional method were too time consuming to solve. Through data mining the collected data can be organized, explored and can discover patterns for predicting the future behavior. Data mining techniques can be implemented in existing software and also can enhance the value of existing information resources, which can be integrated with new products and systems.

Weka Analysis

Weka (Waikato Environment for Knowledge Analysis) is software developed by the University of Waikato, New Zealand which is popular suite for machine learning. Weka is freely available software and is licensed under the GNU General Public License. It is a collection of machine learning algorithms mainly useful for solving real-world data mining problems. It is Java based software and runs on almost any platform and the algorithms can either be applied directly to a dataset or it can be called from the Java code. Weka supports

several standard data mining tasks, more specifically, data preprocessing, pattern extraction, and clustering, classification, regression, visualization, evaluating and interpreting results.

Experimentation

To predict the classes of road in the study area various classification models were built using Weka software. In Weka, decision trees are easy to build and understand, and it can manage both continuous and categorical variables, and can perform classification as well as regression. They automatically handle interactions between variables and identify important variables. Since WEKA's explorer generally chooses reasonable defaults, the J48 decision tree algorithm, Simple CART, Navie Bayes, SMO, Multi-layer perceptron were used to perform the classification analysis. Training and testing were done using ten-fold cross-validation.

J48. It is the implementation of ID3 algorithm developed by Weka project team and it is used to generate univariate decision trees. [8]

Naive Bayes. It is a probabilistic classifiers based on applying Bayes' theorem with strong (naive) independence assumptions between the features.[8]

SMO (Sequentially minimal optimization). It implements sequential minimal algorithm for training a support vector classifier. It replaces all missing values and transforms all nominal attribute into binary one. [9]

Multi-layer perceptron. It is a neural network system, and it can be used for difficult to complex problems. They are very good for approximation.[9]

Simple CART. This decision tree is normally applicable in data mining to produce a frame work that predicts the value of its dependent variable.[3]

Results

For the analysis there are 66 sections of road. All the five classifiers performed similarly well with respect to the number of correctly classified instances. Accuracy measure represents how far the set of data are being classified correctly. The error rates and accuracies of each classifier are analyzed and are shown in Table 2.

Table 2.Accuracy measurement

Sl no	Classifiers	No: of correctly classified instances	Accuracy in %	Error rate
1	Classification tree(J48)	62	93.93	0.06
2	Navie Bayes	64	96.96	0.26
3	SMO	66	100.00	0.27
4	Multi-layer perceptron	66	100.00	0.02
5	Simple CART	62	93.93	0.16

Among them Multi layer perceptron classifier sounds better with 0.0268 error rate and 100% accuracy even though SMO classifier also give 100% accuracy but the error rate is slightly greater than Multi-layer perceptron. Hence, out of all classifiers Multi layer perceptron suits best for predicting classes of roads.

However, accuracy alone does not completely describe the prediction efficiency, and other means of evaluating the predictive models are necessary. The receiver operating characteristics (ROC) curve, the relative operating characteristic curve, gives the comparison of two operating characteristics based on the changes in the criterion. ROC curve is a plot between the fraction of (TPR) true positive rate versus the fraction of false positives FPR (false positive rate). In an entirely random test has an AUC of 0.5, while a perfect test (i.e., one with zero false positives or negatives) has an AUC of 1.00.

Here in all cases, the AUCs values obtained were greater than 0.5, with the Multi-layer perceptron model displaying AUCs equals to 1. These results indicate that Multi layer perceptron suits best for predicting classes of roads. After the prediction of type of road the top correlated independent parameters which affects the classification of the road has to be find out.

Exploration

Data Exploration is done to predict future trends and irregularities are searched in order to achieve a better understanding of the data set. After sampling the data, it is to be explored numerically for grouping the data. The classification and analysis process can be made more accurate through Data Exploration.

Correlation

Correlation analysis is done with two third of the data in order to identify top correlated attributes. Correlation is done to measure the degree of association between two variables, hence it is a non parametric test and is done based on the assumption that data must be ordinal and the score of one variable must be monotonically related to other variable. The relevant features can be obtained by conducting correlation analysis i.e., the (variables, predictors) they are the independent and dependent variables for the model construction. The top 5 attribute obtained are:

- Regulatory sign
- Pavement markings
- Position of sign board
- Post mounted delineators
- Crash

Data Modelling

Through modeling it can formulate models that explain patterns in the data. Data Modeling is done to construct mathematical equations by combining variables that reliably predicts a desired outcome. Modeling is done by using SPSS software.

7.1 Model calibration

Model calibration is the reverse process to regression, where instead of a future dependent variable being predicted from known explanatory variables, a known observation of the dependent variables is used to predict a corresponding explanatory variable. The calibration in regression is the use of known data on the observed relationship between a dependent variable and an independent variable to make estimates of other values of the independent variable from new observations of the dependent variable.

7.2 Coefficient of Determination (R^2)

It represents the variation of dependent variable explained by the independent variable included in the model. A value of R^2 is between 0 and 1. The coefficient of determination, R^2 , is used to analyze how differences in one variable can be explained by a difference in a second variable. The coefficient of determination, R^2 , is similar to the correlation coefficient, R. The correlation coefficient formula will show how strong linear relationship is existing there is between two variables.

Table 3 shows the summary of R^2 values. Higher the value of R^2 , the model will be better. The obtained value of R^2 is 0.88 it means 88 % of the points should fall within the regression.

Table 3. Summary of R Square

Model	R	R^2	Adjusted R^2	Std. Error of estimate
1	0.94	0.88	0.86	0.26

7.3 Regression analysis

Linear regression is an approach for modeling a relationship between a scalar dependent variable with one or more independent variables. In linear regression, the relationships are modeled using linear predictor functions whose values are unknown model parameters are estimated from the data. Such models are called linear models. Regression analysis is a statistical process for estimating the relationships among variables.

7.4 Model validity

Remaining one third data is checked for validity. Then the average root mean square error is calculated. Model with minimum root mean square is selected. Regression validation is the process of deciding whether the numerical results satisfying contemplate relationships between variables, obtained from regression analysis, are

acceptable as descriptions of the data. In this case, dependent variable is the class of road and independent variables are Regulatory sign, pavement markings, position of sign board, post mounted delineators, accident. The coefficients of these dependant variable obtained by conducting regression analysis is shown in table 4

Table 4. Regression coefficients

Model	Unstandardized B	Coefficients Std. Error	Standardized Coefficients Beta	T	Sig.
Constant	-0.394	0.160		-2.455	0.02
Regulatory sign	0.159	0.049	0.197	3.249	0.02
Pavement Markings	0.354	0.067	0.401	5.308	0.00
Position of sign board	0.401	0.199	0.242	3.385	0.02
Post mounted delineators	0.135	0.055	0.151	2.438	0.02
Crashes	0.257	0.049	0.365	5.505	0.00

By substituting the corresponding values of these road sections into the road safety model the rank of the road will obtain as:

$$\text{Class of road} = -0.394 + 0.159 * \text{regulatory sign} + 0.354 * \text{pavement markings} + 0.401 * \text{position of sign board} + 0.135 * \text{post mounted delineators} + 0.257 * \text{accident}$$

(1)

Table 5 shows the ranking of road based on the RSA model. Based on these value ranking of each section of road in the study stretch are found out.

Table 5. Ranking of highway sections

Classification	Rank
Good	1
Fair	2
Poor	3

Application of RSM

Consider a road section with No regulatory sign, Completely removed pavement markings, Sign board kept with less sight distance, Delineators less in number, Occurrence of major accident

Table.4 shows the classification values corresponding to the conditions of road as obtained by road safety audit. By substituting the corresponding values of these road sections into the road safety model the rank of the road will obtain i.e.

$$\begin{aligned} \text{Class of road} &= -0.394 + 0.159 * 3 + 0.354 * 3 + 0.401 * 2 + 0.135 * 2 + 0.257 * 2 \\ &= 2.736 \approx 3 \end{aligned}$$

(2)

Hence road is classified as Poor

Table 6. Road classification

Condition of road	Classification values
No regulatory sign	3
Completely removed pavement markings	3
Sign board kept with less sight distance	2
Occurrence of major accident	2
Delineators less in number	2

Conclusions

The outcome of a road safety audit is the identification of any road safety deficiencies and formulation of recommendations aimed at removing or reducing the deficiencies. Thus, an audit will help to identify the accident potential locations and perform safety evaluation of highway sections. In this study, a model for the classification of different sections could be developed. It helps to identify the condition of each road section, hence can make out the section which needs to be improved. Out of the total 66 sections of Kunnankulam - Peramangalam highway, 33 sections are in good condition with adequate traffic control devices, 25 road sections are in fair condition and 8 sections are in poor conditions. These sections can be improved by providing proper treatments as identified from the audit.

Acknowledgement

Authors heartily thank Dr. Elangovan T., Executive Director, Kerala Road Safety Authority and Former director of NATPAC for his guidance and suggestions during this project work. The help rendered by Prof. Divya Menon of Department of Computer Science Engineering of Jyothi Engineering College, Cheruthuruthy is gratefully acknowledged.

References

1. Manual on Road Safety Audit, Indian Roads Congress SP-088, 2010.
2. Mehar M. and Agarwal P. "A methodology for ranking road safety hazardous locations using analytical hierarchy process" in Social and behavioral science 2010 Vol.104, Issue 8, pp.1030-1037.
3. Griselda L. and Juan de. O., "Influence of deficiencies in traffic control devices in crashes on two-lane rural" in Accident analysis and prevention 2016, Vol.96, Issue.2, pp.130-139.
4. Arun B. and Dheeraj K. "Road Safe2ty and Accident Prevention in India: A Review", in International Journal of Advanced Engineering Technology, 2014 vol.5, Issue 2, pp.64-68.
5. Saffrzadeh M. and Farshad S. "Repair and maintenance for highway traffic control devices" in Journal for science and technology 2011, Vol. 29, Issue 11, pp.156-164.
6. Farzaneh M. and Somayya E. "Analysis of the traffic injury severity on two -lane two way rural roads based on classification tree model" in Safety Science 2011, Vol.49, Issue.10, pp.1314-1320.
7. Majid K. and Heaslip K. "The effects of damage on sign visibility: An assist in traffic sign replacement" in Journal for traffic and transportation engineering 2016 Vol.3, Issue.6, pp. 571-581.
8. Ramya V. "Analysis and prediction of Bangalore traffic south road accidents" in International Journal on recent and innovation trends in computing and communication 2016, Vol.4, Issue.7, pp. 69-75.
9. Pal. S.K. and Mithra S.K. "Multi Layer Perceptorn, Fuzzy sets and classification" in IEEE transactions on neural network 1993, Vol.3, Issue.5, pp.683-692.

A STUDY ON PROFIT OPTIMISATION OF KERALA STATE ROAD TRANSPORT CORPORATION

Anusree P.P.^[1] and Jomy Thomas^[2]

^[1]PG Student, Department of Civil Engineering, Rajiv Gandhi Institute of Technology, Kottayam, India

^[2]Assistant Professor, Department of Civil Engineering, Rajiv Gandhi Institute of Technology, Kottayam, India

Abstract-Growth of transportation needs has increased the need of better transportation facilities. In a developing country like India public transport systems plays an important role in providing passenger transportation. Most of the Indian states have Government owned public transport companies. These days most of these State Road Transport Corporations are facing severe financial crisis. Though the main objective of SRTU is public service, it should work on a self-sustaining basis. So profitability of public transport undertaking is gaining significance, also profit making is a measure of efficiency of such a system.

Kerala State Road Transport Corporation is one among the State Road Transport Undertakings. Recent year's data shows that KSRTC is in loss. So this study focuses on the various financial and physical performance measures that are to be optimized to increase the profitability of KSRTC. Correlation and regression analysis done and a prediction model for profitability of KSRTC is developed by using a software SPSS. The result of the study shows that the variables load factor, effective kilometers, schedules operated and staff per schedule have significant effect on profitability.

Keywords: Profitability, KSRTC

1. INTRODUCTION

As living standards increase, the demand for transportation also rises. In developing countries and emerging economics, the solution seems to be to increase on-road transport. Public transport is a solution for the problem. Public transport systems are an essential part of safe, clean and affordable transport for development. From a social perspective, public transport is often the only means of transport for the common man. It gives them greater access to education, health care, recreation and improves their livelihood opportunities. Also public transport is efficient than personal motor vehicles in terms of the road space it uses up and the energy it consumes.

Public transport remains the primary mode of transport for most of the population in India. India's public transport systems are among the most heavily used in the world. It provides the vital connectivity to far flung areas in a developing society. There are several modes of public transport. Buses take up over 90% of public transport in Indian cities, and serve as a cheap and convenient mode of transport for all classes of society. Also it helps to reduce the traffic congestion during peak hours and helps to carry more number of passengers. State Road Transport Corporations are the government companies which provide public transportation. The Road Transport Act 1950 gave a boost to rural mobility. The promulgation of RTC Act enabled States and Central Governments to take initiative to form the Road Transport Corporations. Now there are 67 STUs in India, of which 21 were functioning as statutory corporations, 27 were incorporated as government companies, eight were run as departmental enterprises and 11 were being run as municipal undertakings. State Road Transport Undertakings provides public transport facilities in every state with the help of a number of buses. After the economic liberalization, all these government state transport corporations have introduced various facilities like low-floor buses for the disabled and air-conditioned buses to attract private car owners to help decongest roads. Kerala State Road Transport Corporation or KSRTC is the state-run bus company in the state of Kerala. It is one of the oldest state run public bus transport services in India. KSRTC is a Public Sector Corporation under the

Ministry of Transport of the State Government of Kerala. This Kerala Public transport bus service was started in 1938 with headquarters in Thiruvananthapuram. It is one of the oldest state run public bus transport services in India. The Kerala State Road Transport Corporation began as the Travancore State Transport Department, constituted by the former Travancore Government with the intent of reorganizing the transportation services of the state, but later it changed on the state's name i.e. Kerala. The acting of the Road Transport Corporation Act in 1950, the Government of Kerala formulated KSRTC rules in 1965. The Kerala State Road Transport Corporation was formally established by the government of Kerala by the notification dated, 15 March 1965. The Transport Department was converted into an autonomous corporation on 1 April 1965.

The main objective of the study is to find the factors affecting profitability of KSRTC and to optimize the profit. This can be done by fulfilling the following objectives

- To find the parameters affecting profitability of KSRTC by using correlation and regression analysis.
- To make a multiple linear regression model to predict the future profit.

2. LITERATURE REVIEW

2.1 General

To begin with the project first it is essential to have an idea about the different approaches and researches in the subject area. So for that a detailed review of literature is conducted. There are different methods used for the analysis of profitability of a firm. A large variety of studies were conducted in different part of the world for different organizations. The transport sector need to continuously review their capacity in order to make sure that they give better services to the society and the users. Even though profit making is not a motto for public transport it should not be in loss. There were a lot of studies conducted worldwide to analyze the profitability of organizations. A brief detail of case studies used for the analysis of profitability of organizations is described below.

2.2 Research Papers

Multiple Linear Regression

Multiple linear regression attempts to model the relationship between two or more explanatory variables and a response. Variable by fitting a linear equation to observed data. It quantifies the impact of various simultaneous influences upon a single dependent variable. It is capable of dealing with an arbitrarily large number of explanatory variables. Multiple regression analysis will estimate the equation of a hyper plane in n Space such that the sum of squared error has been minimized. Its intercept implies the constant term, and its slope in each dimension implies one of the regression coefficients.

A study has been conducted by **Woremi et.al.,(2009)** at Niger state of Nigeria to evaluate the performance of public transport company. The study evaluates the variables that tend to determine the level of performance of public transport companies in Niger state. This study was carried out in Minna, the administrative seat of Niger State, Nigeria. The purpose of this study is the entire management and/or operators of public transport company in Niger State. Structured questionnaires and interview techniques were adopted for data collection. The collected data is analyzed using multiple linear regression technique to identify the factors affecting performance of public transport companies in Niger. The research involved working with the independent variables of years of establishment of the corporation, Cost of maintenance, government policies on importation of spare parts, total number functioning vehicles, state of the roads and its networks, effect of exchange rate, effect of paratransit, staff strength, and organizational structure/managerial factors. The performance function model was estimated using three functional forms of linear, semi log and exponential equations. Then linear function was chosen as the lead equation based on R^2 , t and f values. The result shows that cost of maintenance is significant at 5% level and organizational structure is significant at 10% level. So it was concluded that cost of maintenance and organizational structure play prominent role in performance of public transport companies in Niger

Soumen Mitra and Dr.Jayita Guha Niyogi (2012) conducted a study on A quick assessment technique to determine profitability in private city bus services – case study Kolkata-Howrah urban area, India. This study has been conducted in Kolkata-Howrah urban area which incorporates data on route, operation and financial system. A multiple linear regression is used. This indicates that five attributes, namely route-length, number of days a bus operates in a month, average passenger per day, average fare, legal cost involved.

3. STUDY AREA AND DATA COLLECTION

3.1 Study area

KSRTC is having 28 depots covering the entire Kerala state. This study is conducted for all depots of KSRTC. Data required for this study is collected from Transport Bhavan Trivandrum for the years 2011 to 2016. The data regarding physical performance and financial performance are collected. The study area is shown in figure 1.



Fig.1. Location of KSRTC Depots

3.2 Data Collection

Data collection is the first and foremost important phases of transport study. Since final results and conclusions depend on the accuracy of the data collected, care should be taken in this phase. The study is based on the data, which is collected from Transport Bhavan, Thiruvananthapuram. For conducting correlation and regression analysis monthly data of average kilometer per liter, Total Fuel used, Staff per schedule, accidents, schedules, effective kilometer, average vehicle utilization, load factor, EPKM and CPKM for years 2011 to 2016 is extracted from the obtained data set.

4. METHODOLOGY

4.1. General

There are different methods used for the evaluation of performance and efficiency of an organization. Literature review gives an idea about those methods.

4.2. Correlation

There are a number of physical and financial performance parameters that affect the profitability of a public transport company. Physical performance measures includes parameters like number of divisions, number of depots, number of bus stations, number of schedules, schedules added, new vehicles added, vehicles scrapped, number of routes, route kilometers, load factor, effective kilometers, vehicle utilization, fleet utilization, kmpl, tyre life, staff per schedule, number of break-downs, number of accidents etc. Financial performance parameters includes revenue, cost of operation, CPKM, EPKM etc.

Correlation is a statistical technique that can show whether and how strongly pairs of variables are related. So to find the effect of these parameters on profitability, the correlation between these parameters and profitability is found out. The variables that are used for the correlation analysis are average kilometer per liter, Total Fuel used, Staff per schedule, accidents, schedules, effective kilometer, average vehicle utilization, load factor and profitability which is taken as the ratio of EPKM to CPKM.

Correlation between two variables is expressed based on correlation coefficient (r). It ranges from -1.0 to $+1.0$. The closer r is to $+1$ or -1 , the more closely the two variables are related. If r is close to 0 , it means there is no relationship between the variables. If r is positive, it means that as one variable gets larger the other gets larger. If r is negative it means that as one gets larger, the other gets smaller which is often called an "inverse" correlation. Correlation coefficients are normally reported as a value between -1 and $+1$. The square of the coefficient is equal to the percent of the variation in one variable that is related to the variation in the other.

Correlation between two variables can be found out using SPSS. Correlation between two variables is said to be significant if the significance value is less than .05 for a confidence level of 95%, and is significant if the significance value is less than .01 for a confidence level of 99%.

4.3. Regression

Regression analysis is a statistical process for estimating the relationship among variables. It is widely used for prediction and forecasting. In this project regression analysis is used to find the relationship between the parameters and profitability and to develop a prediction model.

A multiple linear regression model can be expressed as follows

$$Y=A_0+B_1X_1 + B_2 X_2+ B_3 X_3+ + B_n X_n \quad (1)$$

Where,

Y = Dependent variable

A₀.Constant

B₁, B₂, B₃,B_n- Coefficients to be estimated.

X₁, X₂, X₃,.....X_n -Independent variables

Regression analysis is done by taking profitability as dependent variable and staff per schedule, load factor, vehicle utilization, effective kilometer and number of schedules operated as independent variables. It is done using monthly data for the years 2011-2016. The regression equation can be used to forecast the future profitability of KSRTC.

3. DATA ANALYSIS AND RESULT

5.1. General

Data collected from the depot is analyzed using different methods. First the relationship between different financial and physical parameters is analyzed using correlation. Then depending on the correlation of parameters with the profitability regression analysis is done and a multiple linear regression model for forecasting the future profit using those parameters is made.

5.2. Descriptive Statistics

Descriptive statistics are brief description coefficients that summarize a given data set, which can be either a representation of the entire population or a sample of it. It is used to describe the basic features of the variables in the study.

Table1. Descriptive statistics

	Profitability	Load Factor	Avg Vehicle Utilization	Effective KM	Total Fuel Used	Schedules Operator	Staff Per Schedule	Accident	Avg KMPL
N Valid	60	60	60	60	60	60	60	60	60
Missing	0	0	0	0	0	0	0	0	0
Mean	1.012242	82.1898	92.9788	1472475.33	7658958.12	4521.62	9.2498	.1755	3.6895
Median	1.007050	84.5450	92.9200	1472531.50	11350364.00	4523.00	9.2650	.1650	4.1400
Mode	.9602 ^a	86.02 ^a	91.50 ^a	1304953 ^a	562015 ^a	4510 ^a	9.15 ^a	.00 ^a	4.16
Std. Deviation	.0572438	5.12266	1.91347	78973.591	5634471.371	154.542	.33713	.11616	.60101
Minimum	.8831	72.92	87.96	1304953	562015	4129	8.41	.00	2.84
Maximum	1.1270	88.97	97.36	1592829	13343616	4892	9.78	.65	4.24
Sum	60.7345	4931.39	5578.73	88348520	459537487	271297	554.99	10.53	221.37

a. Multiple modes exist. The smallest value is shown.

5.3. Normality check

An assessment of the normality of data is a prerequisite for many statistical tests as normal data is an underlying assumption in parametric testing. There are two main methods of assessing normality – graphically and numerically. A histogram is a graphical representation of numerical data and was first introduced by Karl Pearson.

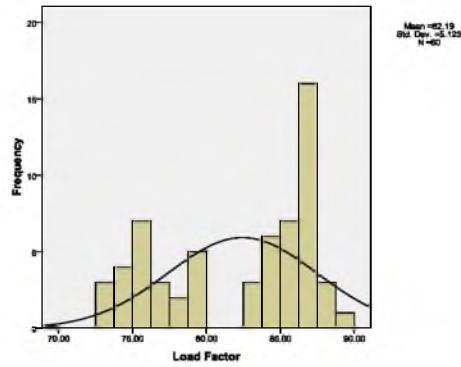


Fig.2. Load factor

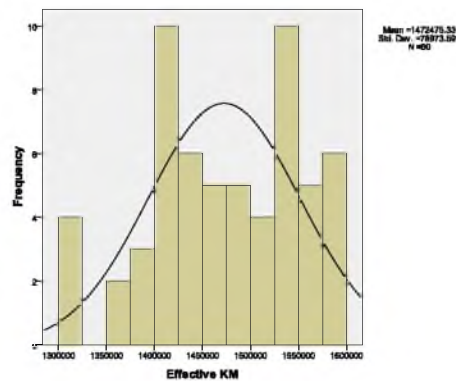


Fig.3. Effective KM

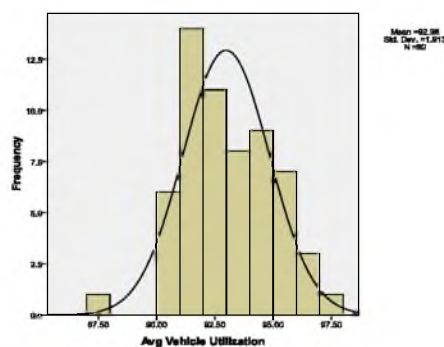


Fig.4. Avg. Vehicle Utilization

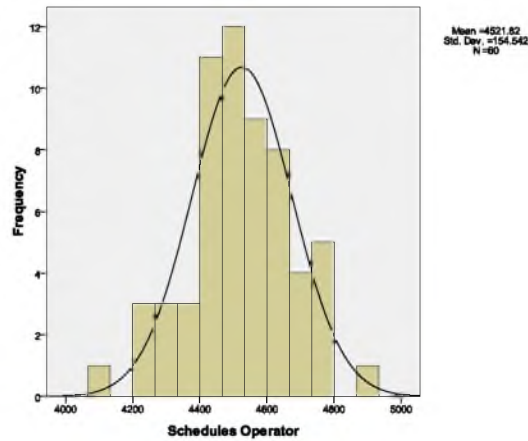


Fig.5. Schedules Operated

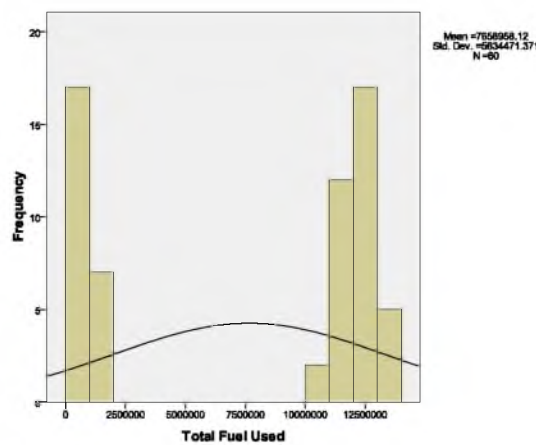


Fig.6. Total Fuel Used

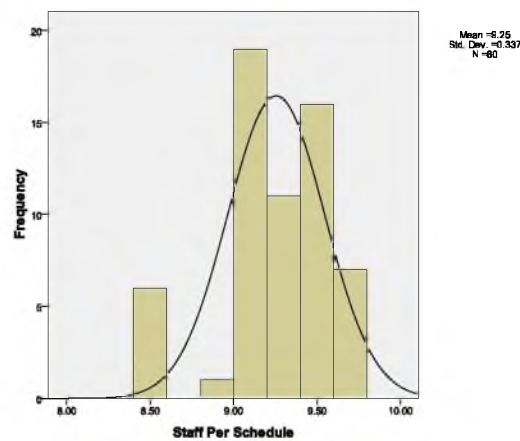


Fig .7. Staff per Schedule

From these histograms we can see that all variables are normally distributed. Hence parametric test can be employed for analysis of variables.

5.4. Correlation

The data collected shows that physical and financial performance measures are varying every year and every month and profit also varying along with that. To analyze the effect of these variables on profitability of depot,

correlation between these variables is found using SPSS. The variables used to find correlation are average kilometer per liter, total fuel used, staff per schedule, accident total, schedules, effective kilometer, average Vehicle utilization, load factor, EPKM, CPKM, and profitability.

The correlation matrix shows the Carl Pearson correlation between two variables. The correlation matrix shows that load factor, average vehicle utilization, effective kilometer, total fuel used and number of schedules are positively correlated to profitability, whereas staff per schedule is negatively correlated to profitability. So increase in load factor, average vehicle utilization, effective kilometer and total fuel used will increase the profitability and increase in staff per schedule will decrease the profitability.

5.5. Scatter plots

A scatter plot or scatter gram illustrates the scores or data that we wish to correlate, where the axes are the two variables. If the scores on one variable increase and so do the scores on the second variable, this is known as a positive correlation. If scores on one variable increase while the scores on the other variable decrease this is known as a negative correlation. When the points are randomly scattered there is generally no correlation between the two variables.

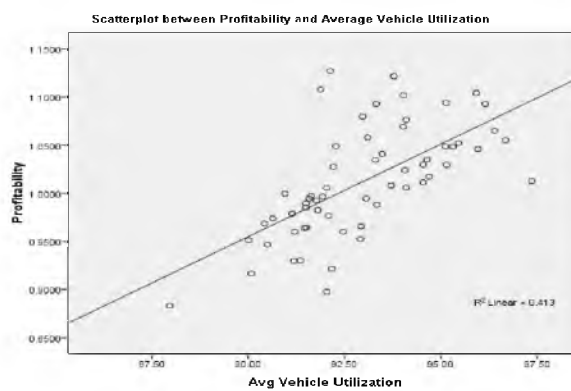


Fig.8. Scatterplot between Profitability and Avg. Vehicle Utilization

The scatter plot clearly illustrates that there is a positive correlation between ‘Average vehicle utilization’ and ‘Profitability’.

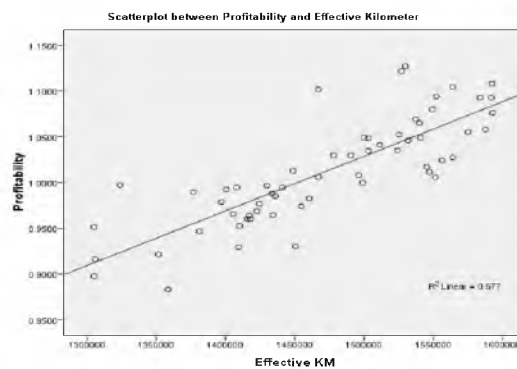


Fig.9. Scatterplot between Profitability and Effective KM

The scatter plot clearly shows that there is a positive correlation between ‘Effective Kilometer’ and ‘Profitability’.

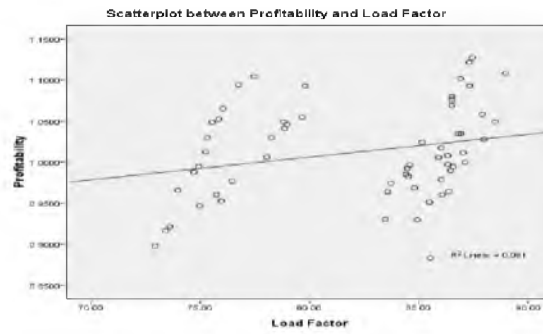


Fig.10. Scatterplot between Profitability and Load Factor

Scatterplot shows that there is a positive correlation between ‘Load Factor’ and the ‘Profitability’.

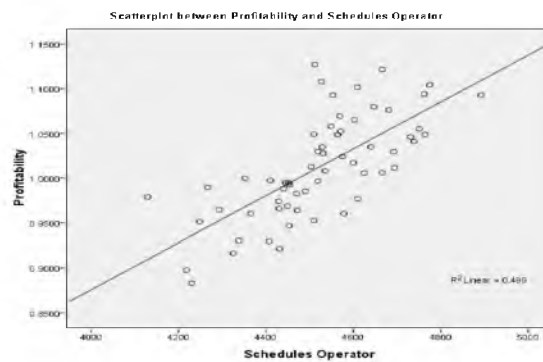


Fig.11. Scatterplot between Profitability and Schedules Operated

The scatter plot clearly illustrates that there is a positive correlation between ‘number of Schedules Operator’ and ‘Profitability’.

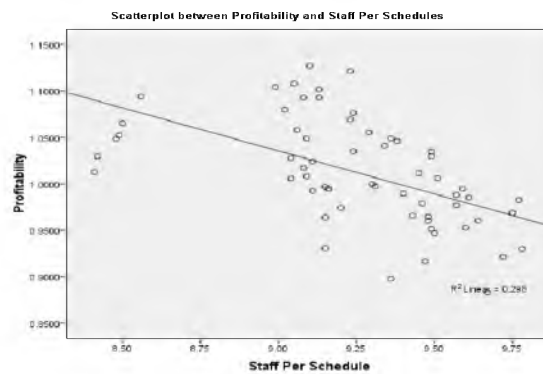


Fig.12. Scatterplot between Profitability and Staff per Schedule

The scatter plot clearly illustrates that there is a negative correlation between ‘number of Schedules Operator’ and ‘Profitability’.

5.6. Regression Analysis

Correlation analysis shows that there are several parameters that affect the profitability of bus services. The variation in these parameters controls the profitability. Regression analysis is done to make a prediction model for profitability. Profitability is taken as dependent variable and staff per schedule, load factor, average vehicle utilization, effective kilometer, and number of schedules is taken as dependent variables. The analysis is done using monthly data for the years 2011 to 2016. Regression is done for different combination of variables and the

regression equation is selected for the highest R square value (From Table 2). The regression results are given in tables below.

Table2. Regression Model Summary

Model	R	R Square	Adjusted R Square	Std. Error of the Estimate
1	.844 ^a	.712	.669	.0368687

a. Predictors: (Constant), Schedules Operator, Load Factor, Staff Per Schedule, Avg. Vehicle Utilization, Effective KM

Table3. Regression Coefficients

Model	Unstandardized Coefficients		Standardized Coefficients	t	Sig.
	B	Std. Error	Beta		
Constant	1.298	.609		2.131	.042
Staff Per Schedule	-.199	.034	-.344	-5.85	.040
Load Factor	.013	.002	.800	6.5	.050
Avg Vehicle Utilization	.002	.006	.066	.338	.538
Effective KM	4.3E-7	.000	.460	4.31	.038
Schedules Operated	6E-9	.000	.383	2.115	.042

From the coefficients obtained from regression (Table 3) the multiple linear regression equation is,

$$\text{Profitability} = 1.298 - .199 \times \text{Staff per Schedule} + 0.013 \times \text{Load Factor} + 0.00000043 \times \text{Effective Kilometer} + 0.00000006 \times \text{Schedules Operated}$$

The result shows that if staff per schedule is increased by one unit profitability of depot decreases by 0.199 units. An increase of load factor by one unit increases the profitability by 0.013 units. Unit increase in effective kilometer increases the profitability by 0.00000043 units and unit increase in schedules operator increases the profitability by 0.00000006 units. The result shows that vehicle utilization does not have an influence on profitability. All variable except vehicle utilization are significant.

Validation of regression model

Various coefficients are estimated by regression model using SPSS software. After obtaining the model, it is validated using 30% data which was not used in the model development. Model validation was done by estimating the error in predicting using Mean Absolute Percentage Error (MAPE).

$$MAPE = \frac{1}{n} \sum \left| \frac{O_i - E_i}{O_i} \right| \times 100$$

Where,

n = Number of observations

O_i = Observed value

E_i = Model predicted value (Estimated value)

According to Lewi’s scale of interpretation of estimated accuracy any forecast with a MAPE value less than 10% can be considered highly accurate, 11%-20% as good, 21%-50% as reasonable and 51% or more as inaccurate.

The obtained average MAPE value is 13.969, which lies between 11% and 20%. Hence the developed model can be regarded as Good.

6. CONCLUSIONS AND RECCOMENDATIONS

6.1. Conclusions

- Correlation analysis shows that load factor, average vehicle utilization, effective kilometer, total fuel used and number of schedules are positively correlated to profitability, whereas staff per schedule is negatively correlated to profitability.
- Using the variables correlated to profitability, multiple linear regression equation is formulated. Regression analysis shows that load factor, staffs per schedule, effective kilometer, and number of schedules have significant effect on profitability.
- The regression equation thus formulated can be used for predicting the profitability of the depot in future
- Load factor is having the highest significance on profitability

6.2. Recommendations

This study considers the different parameters that affect the profitability of public transport. To maximize the profit and to enhance efficiency the significant variables are to be altered accordingly. Load factor is increasing with year and is in the range of 70 to 90%. Staff per schedule has to be reduced to optimize the profit. Increase in effective km results in increase in profitability.

4. REFERENCES

- [1]. A Woremi& Joshua Remi, "A Study of the Performance of Public Transport Company in Niger state, Nigeria", *International Journal of Business and Management*, Vol.4, No.11 ,November 2009
- [2]. Soumen Mitra & Dr.Jayita Guha Niyogi, "A Quick Assessment Technique to Determine Profitability in private City bus services- Case study Kolkata-Howrah Urban area, India", *International Journal of Research in Management & Technology (IJRMT)*, Vol. 2, No. 4, August 2012.
- [3]. Perry R. Hinton, Charlotte Brownlow, Isabella McMurray & Bob Cozens, ""SPSS Explained"

Estimation of PCU and Saturation Flow for Mixed Traffic Condition at Urban Signalized Intersections

Minu Mol Raju¹, Subhash Chand² and Jomy Thomas³

¹PG Scholar, Civil Engineering Department, RIT, Kottayam

²Principal Scientist, Traffic Engineering and Safety Division, CRRRI, Delhi

³Assistant Professor, Civil Engineering Department, RIT, Kottayam

Abstract. Heterogeneous traffic pattern prevails in India. The traffic stream behaves differently in a heterogeneous traffic condition as compared to that of a homogeneous condition prevailing in developed countries. Most of the existing analytical approaches based on the field data have the limitation of an underlying assumption of homogeneity, which is a long way from the high variations of driver vehicle characteristics in mixed traffic condition. Hence it is necessary to convert heterogeneous traffic to homogeneous traffic by applying appropriate factors (PCU) for different types of vehicles while designing or evaluating any signalized intersection. The purpose of this project is to estimate appropriate PCU values for different classes of vehicles at signalized intersections with mixed traffic in Delhi. PCU values are estimated using two methods based on space occupancy - time occupancy ratio method. Estimated values are then compared with standard IRC values. Using these PCU values, base saturation flow is estimated for analysis of traffic flow at the intersection. The reliability of PCU values can be validated against the field saturation flow. The effect of influencing parameters such as approach width, vehicle composition, turning movements is also studied. The estimated PCU and saturation flow values find extensive application in design, capacity and operation of a signalized intersection.

Keywords: Passenger Car Unit, Saturation Flow, Signalized Intersection, Mixed traffic, Projected Area, Clearance time

Introduction

The road traffic in India is highly heterogeneous comprising vehicles like Cars, Buses, Trucks, Auto-Rickshaws, Bikes/Scooters, Cycles, and Rickshaws etc. which have wide ranging static and dynamic characteristics. Due to the highly varying physical dimensions and speeds, it becomes difficult to make these vehicles to follow traffic lanes and the vehicles occupy any convenient lateral position on the road depending on the availability of road space at a given instant of time. Hence, expressing traffic volume as number of vehicles passing a given section of road or traffic lane per unit time will be inappropriate when several types of vehicles with widely varying static and dynamic characteristics are comprised in the traffic. The problem of measuring volume of such heterogeneous traffic has been addressed by converting the different types of vehicles into equivalent passenger cars and expressing the volume in terms of Passenger Car Unit (PCU) per hour. PCU values for the different types of vehicles on Indian roads have been suggested by IRC (SP 41-1994). These PCU values are in the form of single set of constant values. However, the PCU value of a vehicle category may not be constant, because it may vary, based on not only the vehicle factors but also with several other factors associated with roadway and traffic conditions. This paper focuses on the determination of the dynamic PCU values for different vehicle categories at signalized intersections under mixed traffic conditions by adopting a concept of space and time occupancy. It considers the horizontal projected area of the vehicle, without any restriction on the length of detection zone and width of road.

Objectives

- To estimate appropriate PCU values for different classes of vehicles at signalized intersections with mixed traffic in Delhi.
- To compare the PCU values obtained by current studies with IRC values.
- To estimate saturation flow at the intersections using the estimated PCU values.
- To study the impact of various influencing parameters such as road width, traffic composition, turning movements etc. on the saturation flow.

Literature Review

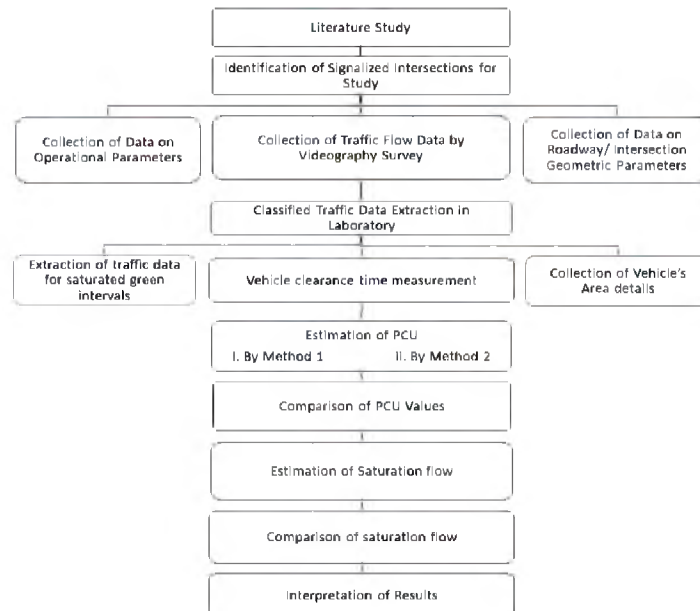
Indian Roads Congress Special Publication (IRC SP-411994) had recommended PCU values for two wheelers as 0.5, three wheelers as 1 and bus/lorry as 3 at signalized intersection for conversion of different types of vehicles into equivalent PCU. Dynamic PCU model concept developed by Chandra and Sikdar (1993) considered the intersection clearing speed of each category of vehicles. Mavani et. al. (2016) determined Dynamic PCU values at signalized intersections on urban corridor of Ahmedabad city. In the study, relative project area and actual traveltime of the vehicle category were considered to decide the dynamic PCU of vehicle category. It was observed that dynamic PCU value of 2W and 3W are quite lower than suggested static PCU values.

Parvathyet. al. (2013) developed new set of PCU values for mixed flow at signalized intersections. PCU of different vehicle classes were estimated using headway ratio method and regression method. Also, an attempt was made to find the effect of length of passenger cars on PCU. It was found that the estimated PCU values are different from those being used in India, and they are inversely related to the length of passenger car. A study by Alex et. al. (2015) focused on the determination of the dynamic PCU values for different vehicle categories at signalized intersections under mixed traffic conditions by adopting a modified concept of area occupancy. For this, the authors have developed a microscopic traffic simulation model, TRAFFICSIM, which was reported elsewhere. The paper explains the variation of dynamic PCU with traffic composition, width, stream speed and flow ratio. Using the obtained dynamic PCU values, a saturation flow model was also developed.

From the literature study, different methods have been identified to estimate the PCU values. Most of the existing analytical approaches for PCU estimation based on the field data have the limitation of an underlying assumption of homogeneity, which is a long way from the high variations of driver vehicle characteristics in mixed traffic condition. This paper focuses on the determination of the dynamic PCU values for different vehicle categories at signalized intersections under mixed traffic conditions by adopting a concept of space and time occupancy.

Methodology

In the present study attempt has been made to estimate values of PCU and saturation flow in the field by actually measuring the flow at the stop line during saturated green phase and to study the impact of various influencing parameters such as road widths, traffic composition etc. based on actual field studies/experiments of the typical Indian traffic conditions.



1.1 Selection of Study Area

The project work is undertaken at CRRI, Delhi. Hence signalized intersections are selected in the urban corridor of Delhi. Intersections selected for this study are right angle intersections and have level gradient on all

approaches and least interference to entry or exit traffic due to pedestrians, bus stops, parked vehicles, etc. All the approaches of the intersections reach saturated stage for whole or majority of the green interval during almost each phase during peak hour as traffic flow is very heavy. That is, intersections represent ideal base conditions.

1.2 Field survey

Field surveys were done in order to collect the following parameters:

- Roadway/Approach conditions and operational parameters
- Traffic conditions
- Vehicular dimension

1.3 Methods for Estimation of PCU Values

Proposed Method 1. PCU factors for different classes of vehicles are estimated for saturated flow condition separately for through (TH) and Right turn (RT) movements of different approaches (with exclusive through and right turn movements) using the concept of space and time occupancy and using these values saturation flow was estimated in PCU per hour for each approach. The basic concept used to estimate the PCU is that it is directly proportional to the space occupancy ratio and time occupancy ratio with respect to the standard design vehicle, a car.

$$PCU_i = \frac{A_i}{A_c} \tag{1}$$

PCU_i = Passenger Car Unit of vehicle type i, A_i= Area of ith vehicle, A_c= Area of passenger car, t_c= Average clearing time of car in sec, t_i= Average clearing time of vehicle type i in sec

Proposed Method 2. Another approach is also considered for estimating PCU values. In the previous method, it is observed that length of vehicle is double counted that is, length is considered both in area ratio and clearance time ratio. Clearance time is taken as time of vehicle (area) occupying the intersection common space/area from entry of front bumper at entry line to exit of rear bumper at exit line. Thus, length of vehicle is taken in the time occupancy factor. Also, area of vehicle is given by the product of length and width which accounts to the space occupancy factor. Hence to eliminate double counting of length factor, the equation is modified as given below,

$$PCU_i = \frac{W_i}{W_c} \tag{2}$$

PCU_i = Passenger Car Unit of vehicle type i, W_i= Width of ith vehicle, W_c = Width of passenger car

1.4 Estimation of Field Saturation Flow

Saturation flow in PCU was calculated based on PCU values obtained by Method 1 and Method 2. Classified average saturation flow for exclusive through (TH) and exclusive right turning (RT) movements of different approaches of the selected intersections were converted into Passenger car unit (PCU) by multiplying the respective PCU factors estimated in this study with the number of vehicles of the category in order to derive average saturation flow in PCU per hour green.

$$s = \frac{\text{Total volume during saturated period (PCU)}}{\text{Total saturated green time in sec}} \times 36 \tag{3}$$

Data Collection And Analysis

1.5 Study Area

In the present study, exclusive through and right turning movements are considered. Hence, four approaches of two T- intersections with fixed signal time were selected for the study. Approach width ranges from 11.3m to 15.2m. Selected intersections are 1) Bhairon Marg – Mathura Road intersection and 2) Bhairon Marg - Ring road intersection.

1.6 Data Collection

Roadway condition and operational data are collected from the field and location map. Traffic turning movement data of the subject approaches of the intersections are collected by videographic survey. To make the analysis meaningful, the vehicles were divided into eight different categories as shown in Table. Since car traffic is predominant in the study area, it is further classified into standard car and big car. Average dimensions and projected rectangular areas of each type of vehicle category are also given in Table 1.

Table 1. Vehicle categories and their average dimensions

Sl. No:	Category of vehicle	Average Dimension, m		Projected area on ground, m ²
		Length	Width	
1	Standard Car (SC)	3.82	1.45	5.55
2	Big car (BC)	4.58	1.77	8.11
3	Two-wheeler (2W)	1.87	0.64	1.2
4	Three-wheeler (3W)	3.2	1.4	4.48
5	Light Commercial Vehicles (LCV)	6.1	2.1	12.81
6	Heavy Commercial Vehicles (HCV)	10.1	2.43	24.54
7	Bicycles	1.9	0.45	0.86
8	Cycle Rickshaws	2.66	1.16	3.09

1.7 Estimated PCU Values

In Method 1, space occupancy ratio is obtained in terms of projected area for each class of vehicle. PCU values suggested by IRC-SP 41 are also given for comparison. It is observed that, PCU values for smaller vehicles are underestimated and that for bigger vehicles are overestimated in comparison with IRC PCU values. In Method 2, space occupancy ratio is obtained in terms of width of each class of vehicle. PCU values suggested by IRC-SP 41 are also given. It is observed that the PCU values obtained by Method 2 are comparable with IRC values. The vales obtained are almost same as that of IRC values. The results obtained are shown in Table 2.

Table 2PCU values of different vehicles at different approaches for exclusive through(TH) and right turn(RT) movements estimated by Method 1 and Method 2

Vehicle class	Method 1				Method 2				IRC values
	Intersection 1		Intersection 2		Intersection 1		Intersection 2		
	TH	RT	TH	RT	TH	RT	TH	RT	
Standard Car	1.00	1.00	1.00	1.00	1.00	1.00	1.00	1.00	1.00
Big car	1.51	1.54	1.54	1.56	1.26	1.29	1.29	1.28	1.00
2 - wheeler	0.20	0.20	0.20	0.20	0.40	0.38	0.40	0.41	0.50
3 - wheeler	0.84	0.92	0.84	0.80	1.01	1.10	1.01	1.08	1.00
LCV	2.45	2.64	2.58	2.59	1.54	1.66	1.52	1.59	1.50
HCV	5.69	6.10	5.96	6.09	2.16	2.32	2.20	2.24	3.00
Bicycle	0.31	0.24	0.29	0.25	0.28	0.24	0.29	0.25	0.50
Cycle rickshaw	1.32	-	1.48	-	1.17	-	1.48	-	

1.8 Estimation of Saturation flow

Field estimated Saturation flow. Saturation flow in PCU was calculated based on PCU values obtained by Method 1 and Method 2.

Using IRC SP-41 formula.A generalized formula is given in IRC SP-41 for direct calculation of saturation flow on the basis of road width. The saturation flow expressed in terms of Passenger Car Units (PCUs) per hr and with no parked vehicles present is given by

$$s = 525 \times w \text{ PCU/hr} \tag{4}$$

where, w = width of approach road in m.

This expression is valid for widths from 5.5 m to 18 m. Using this formula, unit base saturation flow for different approaches was also estimated for comparison purpose only

Using IRC PCU values.PCU values for the different types of vehicles at signalized intersection on Indian roads are suggested by IRC SP 41. These PCU values are in the form of single set of constant values. Unit saturation flow is estimated using these PCU values. Same methodology for field estimation of saturation flow is followed here.

Using Indo-HCM formula.As per Indo – HCM study (2012-2017), unit base saturation flow rate for a typical base signalized intersection is obtained from following equation.

$$USF_0 = \begin{cases} 630; w < 7.0 \\ 1140 - 60w; 7.0 \leq w \leq 10 \\ 500; w > 10 \end{cases} \tag{5}$$

where, USF₀ = Unit base saturation flow rate in PCU/hr/m, w = effective width approach in meters

Using PCU values by Justo and Tuladhar. PCU values for different classes of vehicles in signalized intersections for mixed traffic condition suggested by Justo & Tuladhar is given in Table. Saturation flow is estimated using these values also.

Using US HCM . The US-HCM 2000, developed by Transportation Research Board (TRB), includes a model to calculate saturation flow rate considering the effect of various factors like width, gradient, parking activity, heavy vehicles, area type, turning movements, and pedestrian blockage (TRB 2000). The base saturation flow s_0 , is considered to be 1,900 passenger cars (pc) per hour of green time per lane for a signalized intersection. In US HCM standard lane width is taken as 3.66m. Hence base unit saturation flow for the study intersections can be estimated as follows:

$$s_0 = 1900/3.66 = 519 \text{ PCU/hr/m} \tag{6}$$

Table 3 Unit saturation flow of different approaches of intersections as calculated by different methods (PCU) as compared to standard value

Intersec tion	Appro ach	Width (m)	Base Saturation Flow (PCU/hr/m)						
			Method 1	Method 2	As per Justo & Tuladhar	IRC PCU values	IRC Formula	Indo- HCM	US HCM
1	TH	11.29	660	587	424	584	525	500	519
	RT	12.23	542	530	473	490			
2	TH	15.57	625	585	507	603	525	500	519
	RT	13.81	528	527	483	482			

Results And Discussions

1.9 Comparison of PCU Values Obtained by Two Methods with IRC PCU values

In order to compare PCU values obtained by different methods, bar diagram was plotted as shown in Figure 1. In the case of vehicles that are larger than standard car, PCU values obtained by Method 1 gives higher value than that estimated by Method 2. For those vehicles that are smaller than standard car, PCU values obtained by Method 1 gives lower value than that estimated by Method 2. It is observed that, big car LCVs and HCVs shows higher variation in PCU values. In the method 2, estimation of PCU is done such that double counting of vehicle length is eliminated. Since length of LCVs and HCVs compared to standard car is much higher, their PCU value shows higher variation.

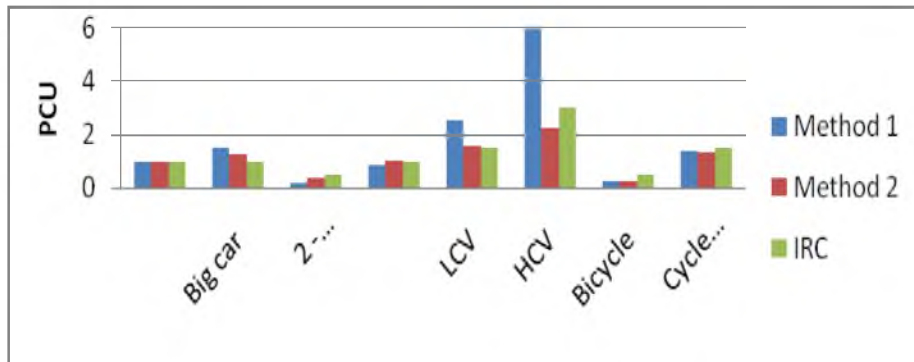


Figure 1 PCU values obtained by two methods

1.10 Comparison Of Unit Saturation Flow Estimated By Different Methods

Saturation flow is estimated using different PCU values and standard formulas. It is worth to further mention here that the saturation flow per meter width obtained from field estimation of PCU values is quite high as compared to other methods based on IRC SP-41, Indo-HCM and US HCM for all the approaches of the selected intersections as shown in **Error! Reference source not found.**. This may be attributed to (a) appreciable higher percentage of car and (b) higher percentage of two-wheeler filling the gaps between the larger vehicles during saturated flow. Saturation flow obtained by Method 2 is closer to the IRC values. Hence it can be concluded that Method 2 gives more realistic PCU values compared to Method 1.

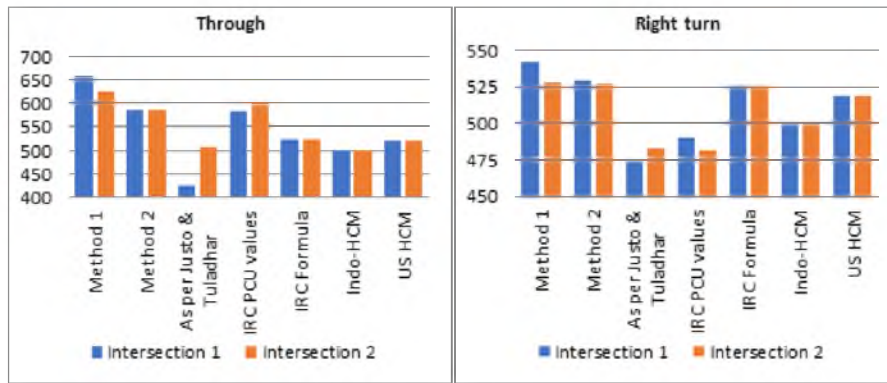


Figure 2 Variation of Saturation flow with approach width for through and right turn movements obtained by different methods

1.11 Variation in Unit Saturation flow with vehicle composition

It is observed that percentage composition of each category of vehicle influences the saturation flow. Increase in the percent of standard car and big car causes a reduction in saturation flow. As the percent of standard car increases from 20% to 60%, saturation flow gets decreased by 18%. Also 14% increase in big car causes 16% decrease in saturation flow. Effect of two wheelers is well reflected from the analysis. 13% increase in two-wheeler composition causes an increase of 18% in saturation flow. Due to lack of lane discipline and the fact that motorcycles arrange themselves in front and between vehicles in a non-uniform way. Thus, the available space is fully utilized which increases the saturation flow rate. It is also noted that the increase in percentage of LCVs and HCVs leads to an increased flow rate. It can be due to bigger size of vehicle which increases the area occupancy.

For both through movement and right turn movement, trend of variation remains same for each class of vehicle. Only standard car and big car shows an inverse relation with the percentage composition. All other classes of vehicle show a direct relation with their percentage composition. It cannot be concluded that the variation is due to the composition only; many other factors can have influence on the saturation flow such as approach width, headway etc.

Conclusions

1.12 Conclusions

The following are the important conclusions drawn based on this study

1. Method 1 and Method 2 give consistent PCU values for each vehicle class across different approaches. Method 2 gives more realistic PCU values compared to Method 1. The reliability of PCU values are validated against the field saturation flow.
2. In the case of vehicles that are larger than standard car, PCU values obtained by Method 1 gives higher value than that estimated by Method 2. For those vehicles that are smaller than standard car, PCU values obtained by Method 1 gives lower value than that estimated by Method 2.
3. The study shows that, saturation flow holds a strong relation with the percentage composition of different vehicle classes. Saturation flow increases with increase in two wheelers, three wheelers, LCVs and HCVs while it decreases with increase in standard car and big car.
4. The saturation flow analyzed for different approaches shows that it does not depend only on approach width; therefore, the empirical formula 525w suggested for Indian conditions in Special Publication (SP)-41 (IRC 1994) of the Indian Roads Congress is inappropriate for obtaining saturation flow.

1.13 Limitations of The Study

1. Effect of combined through and right turn movement could not be studied.
2. The driver behaviour, which depends on physical, mental, psychological and environmental factors, could not be incorporated in the research due to difficulties in measurement and quantification of the influencing factors.

1.14 Future Scope

In this study, the effects of approach width and vehicle composition on PCU values of different vehicle categories and saturation flow have been analysed. There is further scope for the study of the effect of headway on saturation flow. Also, the effect of combined through and right turn movement can be studied.

References

- Indian Roads Congress (IRC), Guidelines for design of at-grade intersections in rural and urban areas, IRC Special Publication, No. 41, Indian Roads Congress, New Delhi, India(1994)
- Highway Capacity Manual, Highway Research Board, National Research Council. Department of Traffic and Operations, Special Report 87, Committee on Highway Capacity, Washington, DC(1965)
- Highway Capacity Manual, Washington, D.C. Transportation Research Board, National Research Council (2000)
- A. J. Mavani, D. R. Sisodiya, D. K. Kadiya, P. M. Shah, Dr. H. R. Varia: Determination of Dynamic PCU values at Signalized Intersection on Urban Corridor of Ahmedabad City, International Journal of Advance Engineering and Research Development, Volume 3, Issue 5 (2016)
- ParvathyR, Sreelatha T, Reebu Z Koshy : Development of new PCU values and effect of length of passenger cars on PCU, International Journal of Innovative Research in Science, Engineering and Technology, Volume 2, Special Issue 1 (2013)
- Sheela Alex, Kuncheria P. Isaac: Dynamic PCU values at signalised intersections in India for mixed traffic, International Journal for Traffic and Transport Engineering, 5(2): 197 – 209 (2015)
- Pinakin N. Patel, AshishDhamaniya, B. K. Katti: Effect of mixed traffic characteristics on Saturation flow and Passenger Car Units at signalized intersections, European Transport, Issue 59, 1825-3997(2015)
- Anusha C. S., Verma, A., Kavitha, G.: Effects of two-wheelers on saturation flow at signalized intersections in developing countries, Journal of Transportation Engineering, 139 (5), pp. 448-457 (2013)
- C. E. G Justo, S. B. S. Tuladhar: Passenger car unit values for urban roads, Journal of the Indian Road Congress, 45, 183-238 (1984)
- Chandra, S. and Kumar, U.: Effect of Lane Width on Capacity under Mixed Traffic Conditions in India, ASCE Journal of Transportation, 129(2), pp 155-160 (2003)
- Basu, D., Maitra, S.R, Maitra, B.:Modelling passenger car equivalency at an urban midblock using stream speed as measure of equivalence(2006)
- Arasan V. T. and Shriniwas S. Arkatkar: Micro-simulation Study of Effect of Volume and Road Width on PCU of Vehicles under Heterogeneous Traffic Journal of Transportation Engineering, ASCE, vol.136, No.12, pp1110-1119, December (2010)

Analysis and Development of Traffic Speed-Flow-Density Relationships for Urban Roadway

Thasneem Nadirsha³ and Archana S.⁴

PG Scholar,

² Assistant Professor,

Department of Civil Engineering,

Jyothi Engineering College, Cheruthuruthy, Thrissur, Kerala 679 531.

(thasneemnadir786@gmail.com, archanas@jecc.ac.in)

Abstract. India is a developing country containing heterogeneous traffic, which is characterized by wide variations in traffic characteristics. The new technologies offer the greatest challenge and hope for improving the quality of traffic system. The ability to apply traffic flow fundamentals is an essential ingredient in working toward improving the transportation system. The present study is concerned with macroscopic traffic flow characteristics observed on 4-lane divided carriageway [Thrissur-Kunnankulam (SH-69)]. The intention of this paper was to analyse traffic flow, density, and speed for developing a model that provide the exact character of traffic flow. Traffic flow fundamental diagrams are used to characterize the relationship between these parameters. Study of traffic flow involves selection of location, videographic survey, analysis of video recordings, statistical analysis and calculation of basic parameters of traffic flow. Data extracted are compiled for each direction. Scatter diagrams were plotted by using the collected data. The relationship between parameters was developed based on regression analysis using statistical software SPSS 21. The speed-density function obtained was compared to macroscopic models such as Greenshield's model and Greenberg's model. By using speed-density model, flow-density and speed-flow relationships are predicted for the given highway. Further validation of the predicted model is done using graphical residual analysis. This succeeded to develop new models enabling theoretical determination traffic parameters for a given urban roadway.

Keywords: Heterogeneous traffic, Macroscopic parameters, Scatter diagrams.

1 Introduction

Traffic flow represents the traffic load on the transportation system and the interaction between these loadings and the facility capacity determines the operational performance of the system. Hence it is extremely important to know the flow rates, their temporal, spatial and modal variations, and the composition of the traffic stream. Speed and travel time are the fundamental measurements of traffic performance of the existing highway system, and speed is a key variable in the redesign or design of new facilities. Density is an important characteristic that can be used in assessing traffic performance from the point of view of users and system operators.

The traffic stream models determine the fundamental relationships among macroscopic parameters for uninterrupted flow conditions. The traffic stream characteristics include flow, speed, and density. The relationships are for free-flow and congested-flow conditions away from flow interruptions such as at intersections.

2 Literature Review

J Roux [1] tested the significance of foreign models to South African conditions, by using data obtained from South African freeways. He evaluated speed-flow relationships for individual lanes. Different curves are used to explain congested and flow uncongested flow. P. Balaji [2] established speed-flow model for urban road for different vehicle composition. He concluded that multi-class speed-flow models are more adequate than single-class speed-flow models. D. Ashish [3] developed speed density relations for various vehicle composition on urban arterial roads under mix traffic conditions in states using a set of equations and constructed speed

prediction models. R.S. Dhapudkar [4] developed a macroscopic model at signalized intersection in order to develop new models for Indian roads which consist of traffic with various operating characteristics. XU Cheng [5] generated ten speed-density models. The models are evaluated by parameter calibrations and fitting errors by using non-linear least square method. Saurav B. [6] predicted density from speed-density models by measuring the vehicular density from moving observer method. Parameters of traffic stream were calculated and fitted in graphs using single regime models and corresponding parameters were determined using SPSS software. Hashim and Wahidah [7] developed model on the basis functional relationships between traffic parameters for three major highways in Malaysia. The density-speed model developed was compared to the classical single regime models.

3 Data Collection and Extraction

3.1 Determination of Study Section

The initial step was the selection of the road stretch, from which the data were collected. The road selected was Thrissur-Kunnankulam road (see Fig. 1). The next step was the selection of the study section on the selected road in which the entry point and exit point are marked. A pilot study was organized on the selected road which covers both free-flow and congested-flow conditions in order to determine the place were predictable to get the data more precisely. The distance enclosed by the entry and exit point is noted as 1.4 km. The data were collected by videographic survey conducted on typical weekdays over peak and off-peak hour.

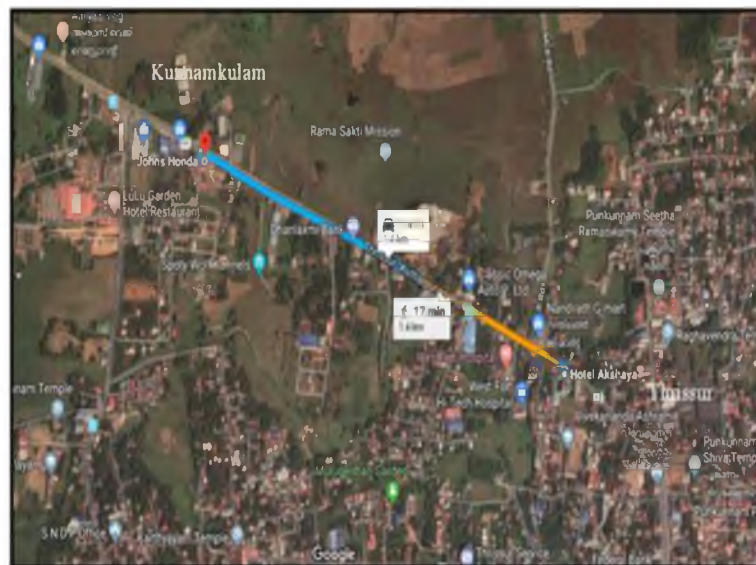


Fig.9. Study Section (Thrissur-Kunnankulam Road)

3.2 Data Processing

Video recordings were processed by tracing vehicle movement crossing the specified study section. The flow data is calculated at entry and exit points in such a way that the vehicles which are passing through the section in every five-minute interval. The speed data is done by calculating the time by which vehicle which enters and exit the rectangular section. Initial density is determined using photographic technique along the entire section. By using initial density, the density is calculated at every five-minute interval using Eqn. 1 as follows:

$$k_t = k_{t-1} + N_{\text{entry}} - N_{\text{exit}} \quad (1)$$

Where,

k_t is the density at time t

N_{entry} is the number of vehicles entered the stretch during the time from $t-1$ to t

N_{exit} is the number of vehicles going out the stretch during the time from $t-1$ to t

The collected data from the video recordings were gathered in Excel sheets, and then processed in order to obtain the macroscopic traffic stream parameters such as flow, speed, and density.

4 Data Analysis

4.1 Determination of Speed-Density Relationship

The speed-density curve is plotted using Greenshield's, Greenberg's and Exponential models, where density is independent variable and speed is dependent variable (see Fig. 2 and Fig. 4 towards Thrissur and Fig. 3 and Fig. 5 towards Kunnankulam). Greenshield's and Greenberg's models could predict the traffic condition when velocity equals zero ($v=0$). The Greenshield's model is linear while the Greenberg's model non-linear. Both of them have the highest point of traffic congestion when velocity is zero. These highest points cannot represent the maximum congestion levels because the classical functions are either linear or exponential.

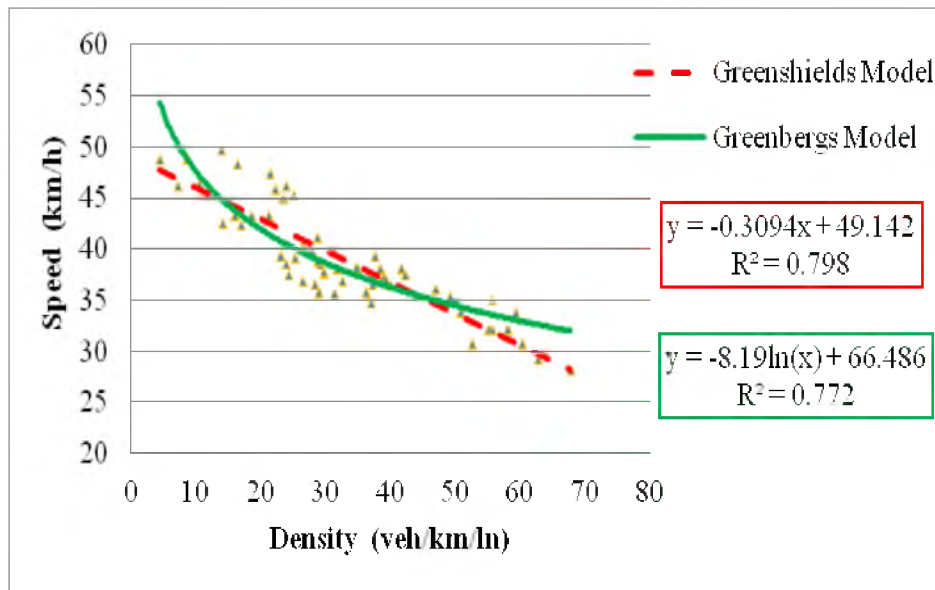


Fig.2. Speed-Density Relationship using Greenshield's and Greenberg's Models (Towards Thrissur)

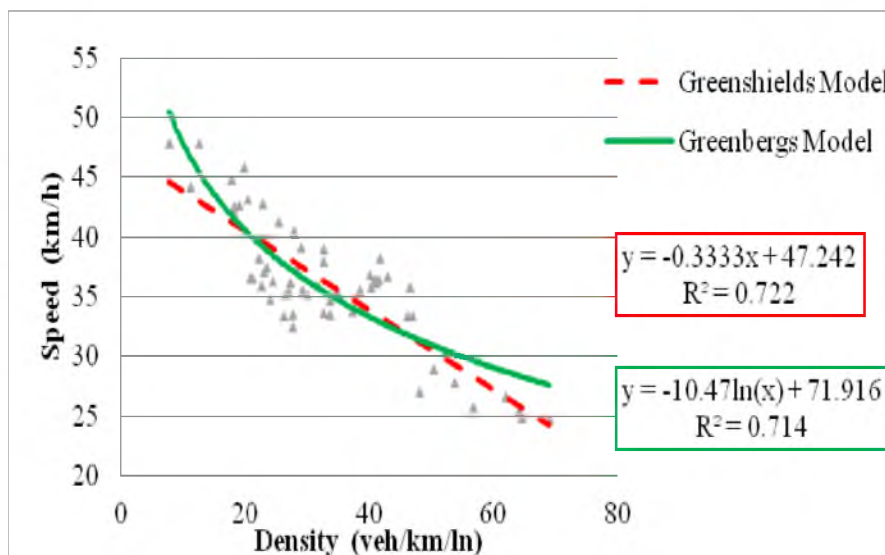


Fig.3. Speed-Density Relationship using Greenshield's and Greenberg's Models (Towards Kunnankulam)

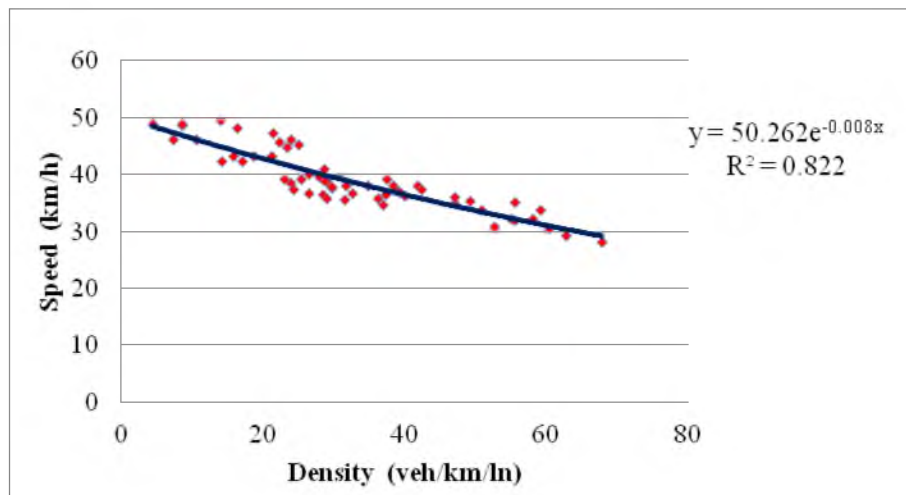


Fig.4. Speed-Density Relationship in Exponential Scale (Towards Thrissur)

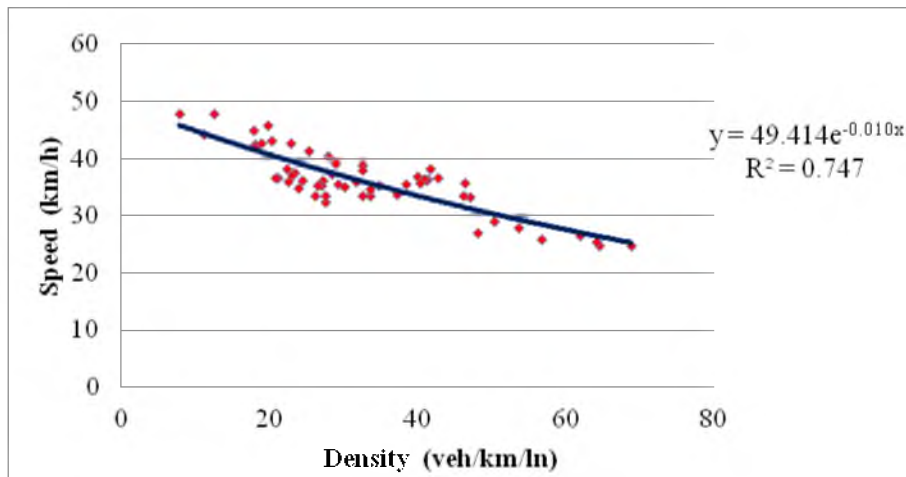


Fig.5. Speed-Density Relationship in Exponential Scale (Towards Kunnankulam)

4.2 Speed-Density Model

The final form of speed-density relationship model is presented as follows:

Towards Thrissur:

$$u = 50.262 e^{-0.008k} \tag{2}$$

Towards Kunnankulam:

$$u = 49.414 e^{-0.010k} \tag{3}$$

Where,

u is the speed (km/h) and k is the density (veh/km)

4.3 Flow-Density Model

The flow density relationship can be derived as follows:

$$q = u * k \tag{4}$$

Towards Thrissur:

$$q = (50.262e^{-0.008k})k \tag{5}$$

Towards Kunnankulam:

$$q = (49.414e^{-0.010k})k \tag{6}$$

Then obtained flow-density model are plotted, where density is independent variable and flow is the dependent variable. The best fit logarithmic curve is drawn over the observed data for two lanes (see Fig. 6 and Fig. 7).

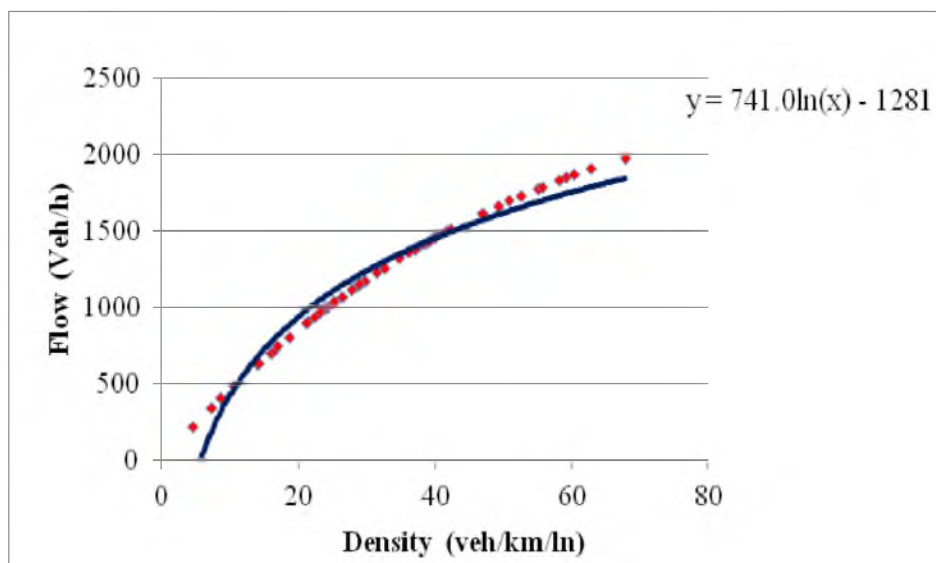


Fig.6. Flow-Density Relationship (Towards Thrissur)

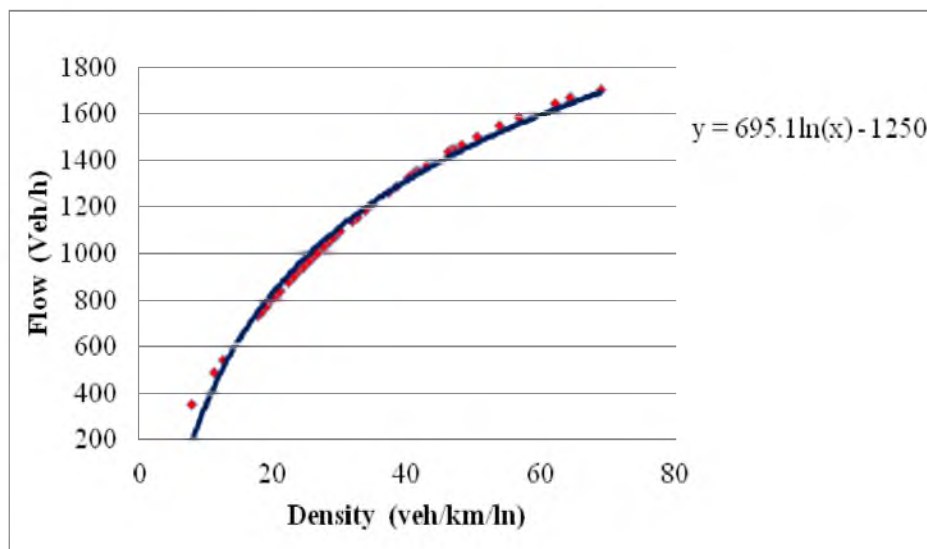


Fig.7. Flow-Density Relationship (Towards Kunnankulam)

4.4 Speed-Flow Model

Flow is chosen as the dependent variable and speed as the independent variable because a variation in vehicle's speed is responsible for the variations in flow. The flow-speed function can be mathematically illustrated by the exponential function.

Towards Thrissur:

From Eqn. 2

$$u = 50.262e^{-0.009k}$$

Therefore

$$k = -\frac{1}{0.009} \log \frac{u}{50.262} \tag{7}$$

Substituting value of k in Eqn.5

$$q = (50.262e^{-0.009(-2.870 \log u)})(-2.4870 \log u) \tag{8}$$

Towards Kunnankulam:

From Eqn. 3

$$u = 49.414e^{-0.010k}$$

Therefore

$$k = -\frac{1}{0.010} \log \frac{u}{49.414} \tag{9}$$

Substituting value of k in Eqn.6

$$q = (49.414e^{-0.010(-2.0237 \log u)})(-2.0237 \log u) \tag{10}$$

Then obtained speed-flow model curve are plotted. The best fit linear curve is drawn over the observed data for two lanes (see Fig. 8 and Fig. 9).

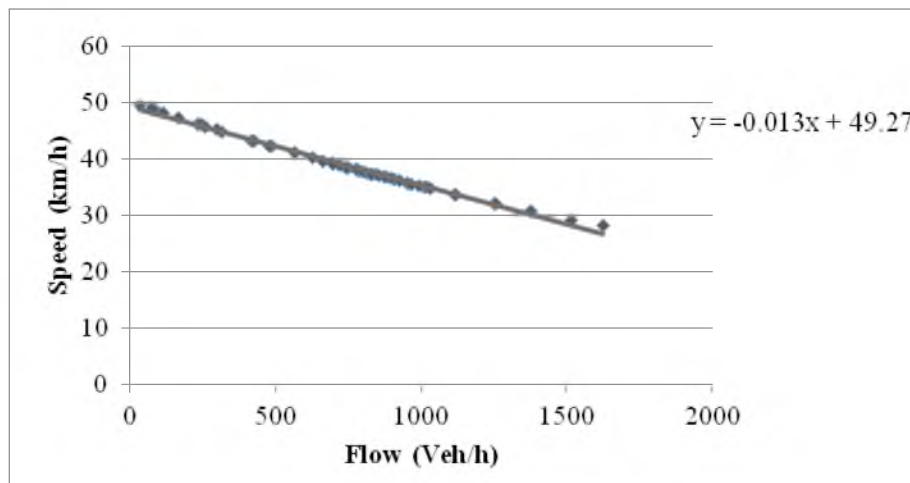


Fig.8. Speed-Flow Relationship (Towards Thrissur)

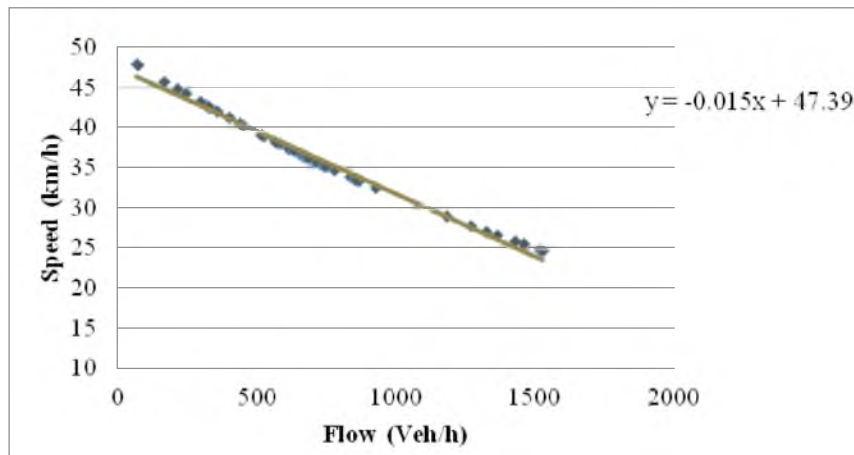


Fig.9. Speed v/s Flow Relationship (Towards Kunnankulam)

5 Model Validation

Graphical Residual Analysis: The basic tool for statistical modeling is graphical residual analysis. The acceptability of various phases of the model is provided by different plots of the residuals from a fitted model. Numerical methods like R^2 statistic for model validation are also useful, but usually to a small extent than graphical methods. Graphical Residual Analysis for the given lanes (see Fig. 10 and Fig. 11).

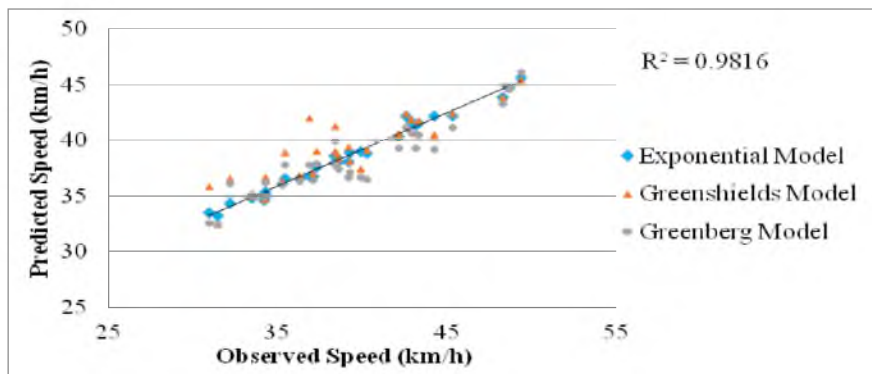


Fig.10. Graphical Residual Analysis (Towards Thrissur)

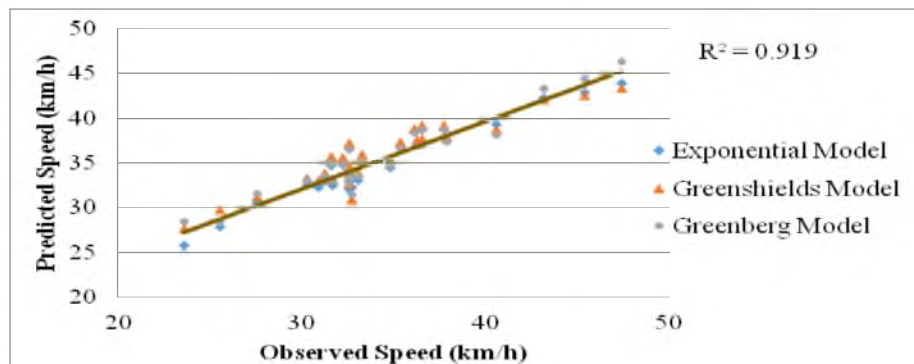


Fig.11. Graphical Residual Analysis (Towards Kunnankulam)

6 Results and Discussions

In the field, it is hard to find the linear relationship between speed and density as proposed by Greenshield. Greenberg's model is inadequate to predict the speed at lower densities. Because when density attains zero, speed readily increases to infinity. Traffic parameters obtained from Greenshield's and Greenberg's models are shown in Table 1.

Results of regression analysis of traffic speed against density are shown Figure 4 and Figure 5. Doubtless, the exponential models are statistically adequate in determining speed-density relationships for the given road in the uncongested regime. The higher R^2 coefficient for different lanes shows the best goodness of fit. The main drawback of the model is speed becomes zero only when density approaches infinity. Hence this cannot be used for predicting speeds at high densities. The model shows a better fit than Greenshield's and Greenberg's models for the uncongested condition. But it does not present a good fit to the congested condition. The density at maximum flow rate obtained is 125 veh/km and 100 veh/km towards Thrissur and Kunnankulam. The free-flow speed obtained is 50.26 km/h and 49.41 km/h towards Thrissur and Kunnankulam.

The characteristics of the relationship between traffic flow and density in logarithm scale begin at the origin is shown in Figure 6 and Figure 7. At the initial section of the graph, traffic congestion accumulates at the highest level as exhibited by minimum flow and density. As the density rapidly increases, flow also begins to steadily increase. The speed-flow curves of different lanes for the given road are shown in Fig.8 and Fig.9. As the speed rapidly increases, the flow begins to steadily decrease. Therefore, the characteristics of the speed-flow relationship are determined by linear regression technique.

The regression analysis was used to statistically evaluate the mathematical models. The obtained values of R^2 are 0.982 and 0.919 for the Exponential model in both lanes which implies the validity of the predicted model. Predicted Greenshield's model slightly overestimated and Greenberg's model slightly underestimates density for the lane towards Thrissur and the predicted Greenshield's and Greenberg's model slightly overestimated density for the lane towards Kunnankulam.

Table 1. Traffic parameters obtained from Greenshield's and Greenberg's models

Traffic Parameters	Towards Thrissur		Towards Kunnankulam	
	Greenshield's Model	Greenberg's Model	Greenshield's Model	Greenberg's model
A	49.14	66.48	47.24	71.91
B	-0.309	-8.19	-0.333	-10.4
u_f (kmph)	49.14	-	47.24	-
u_f/k_j	0.309	-	0.333	-
k_j (vph)	159	3352	142	1007
C	-	8.19	-	10.4
$Clnk_j$	-	66.48	-	71.91
u_0	24.57	-	23.62	-
k_0	79.5	1233	71	370
q_{max}	1953	10099	1677	3853
R^2	0.798	0.772	0.722	0.714

7 Conclusions

By conducting this research on the urban road, the basic traffic flow parameters have obtained. The obtained parameters were used to develop diagrams for relations between flow, speed, and density in the un-congested regime. This helped to develop model equations, which can be used for theoretical determination of characteristics of the road in an urban road network in uncongested traffic conditions.

Further research should be done to incorporate heterogeneity and non-lane disciplined characteristics of Indian traffic and including more road types within different environments and cross-sections in order to attain exact relationship between basic traffic flow parameters. Automatic counters and measuring tools should be adopted in order to abate field work and measuring error possible extent.

Acknowledgment

Authors owe a great debt of gratitude to teaching and non-teaching staffs, students, and management of Jyothi Engineering College for their valuable suggestions and support for the completion of the project.

References

1. Roux, J. and Bester, C. J. Speed-Flow-Density Relationships on Cape Town Freeways. University of Stellenbosch, Dept of Civil Engineering, Private Bag X1, Matieland, 7602, (2011).
2. Balaji P. and Karthik, K. S. Vehicle Class-wise Speed Volume Model for Tree-lane Undivided Urban Roads. *Procedia – Social and Behavioral Sciences*, Vol.104, pp.468-476, (2013).
3. Ashish D. and Satish, C. Speed Prediction Models for Urban Arterials Under Mixed Traffic Conditions. *Procedia – Social and Behavioral Sciences*, Vol.104, pp.342-351, (2013).
4. Dhapudkar, R. S. Analysis and Development of Traffic Stream Parameters of Heterogeneous Traffic at Signalized Intersection. *The International Journal of Engineering and Science*, Vol.3, No.5, pp.33-89, (2014).
5. Cheng, XU., Zhao-wei, QU. and Xiao-ming, C. Analysis of Traffic Flow Speed-density Relation Model Characteristics. *Journal of Highway and Transportation Research and Development*, Vol.8, No.4, pp.104, (2014).
6. Saurav, B., Anik D. and Julfiker, H. Estimation of Traffic Density to Compare Speed Density Models With Moving Observer Data. *International Journal of Research in Engineering and Technology*, Vol.4, No.8, (2015).
7. Hashim N. M. and Wahidah, N. H. Outflow of traffic from the national capital Kuala Lumpur to the north, south and east coast highways using flow, speed and density relationships. *Journal of traffic and transportation engineering*, Vol.3, No.6, pp.540-548, (2016).

MANAGING TRAFFIC CONGESTION USING GIS – A CASE STUDY IN ATTINGAL TOWN

Anjana U, Ashtami Hari, Ayana Asok G, Greeshma M J & Riya Sreekumar
Department of Civil Engineering
LBS Institute of Technology for Women, Trivandrum, India
 Anoja B V
Department of Civil Engineering, LBS Institute of Technology for Women

ABSTRACT: Traffic congestion is one of the major problem faced by most of the developing towns and cities. Various factors influence the speed of vehicles on the road. Mapping out these factors can help in the assessment and management of traffic congestion. *In this paper, QGIS software has been used to determine roadside friction points that impact the vehicle speed on Attingal town in Trivandrum district. Allotting a new parking space is found out to be the solution for the studies conducted.*

Keywords: Congestion Management, QGIS, friction points, parking survey, GPS tracking

1. INTRODUCTION

Geographic Information System (GIS), over the years, has emerged as one of the efficient technological tools in the field of transportation engineering. It has shown great applications in a number of fields including transportation. The various advantages of GIS make it an attractive option to be used to face the emerging traffic problems. The advantage of GIS can be attributed to its capability to cope with the large volume of data with geographic spatial characteristics. GIS has a large database storage capacity, which can integrate data from disparate sources. While working with traffic speed, integrating spatial and non-spatial data from different sources becomes a prime concern. Moreover, along with great data integration capabilities, it is also a great visualization tool as it produces relevant maps assisting in decision making process.

There are various influencing factors that affect the speed of vehicles on the road, such as width of road, structure of the road, construction work on roads (e.g. work undertaken for Metro Rail construction); various land uses that attract motorized / pedestrian traffic bound to hospitals, institutional, commercial area etc. Mapping out these factors using GIS capabilities can help in the assessment and management of traffic congestion.

Attingal is a municipality in the Trivandrum district in Kerala state, India. It is the headquarters of Chirayankeezhu taluk and the important government institution of the taluk such as the taluk office and treasuries are situated in Attingal town. It is in the suburb of the extended metro polytan region of Trivandrum.

Located 30 km north of Trivandrum it is the largest and the most important town in Trivandrum district after the capital. The Attingal junction is the major bottle neck on the national Highway between Kochin and Trivandrum the people are affected by the lack of parking space and demand expansion.

2. OBJECTIVES OF THE STUDY

The present study was done with the following objective:

- To identify the roadside friction locations on varying widths of urban, arterials and sub-arterials in Attingal Trivandrum region.
- To predict influence of the friction points on the vehicular speed on urban roads.

3. LITERATURE REVIEW

The literatures review was done to find the various key parameters of congestion at traffic, existing methodologies that were adopted for congestion modelling and the existing GIS application in the area of management.

Kalaga Rao and Mohan Rao (2009) studied the application of GPS for traffic data such as travel time and traffic speed and they validated the GPS data by conventional methods and statistically validated the results of these parameters and found that the GPS data can be used for traffic studies without compromising the accuracy of the data.

Anitha selva sofia et. al., (2013) talks about traffic congestion, which is a condition on road networks that occurs by slower, and increased vehicular queuing. To study the effect of the Transportation System Management (TSM) measures, one needs to have a clear view of the flow patterns, location as well as existing road network. GIS can be effectively used to analyse the problems associated with transportation.

Amudapuram Mohan Rao, S. Velmurugan, and Arpita Chakraborty (2014) studied about Various factors influence the speed of vehicles on the road. Mapping out these factors can help in the assessment and management of traffic congestion. In this article, GIS has been used to identify various roadside friction points that impact vehicle speed on some of the urban arterials in Delhi.

STUDY AREA

Attingal has one of the highest road densities in Trivandrum. The major road include Kanyakumari-Panvel Highway (NH66) along with SH46 and SH47 connecting the town to Klimanur and Venjarammodu, passes through the town. SH 46 joins the town at Alamcode and SH 47 at Munumukku, which had a high traffic density. Owing to improper development of rail based modes in Delhi, the city is heavily dependent on road based modes of transportation (87 per cent of the total trips performed in the city are made using road based transport systems). In the present study, one locations was selected at Attingal area, the locations are shown in Figure 1.

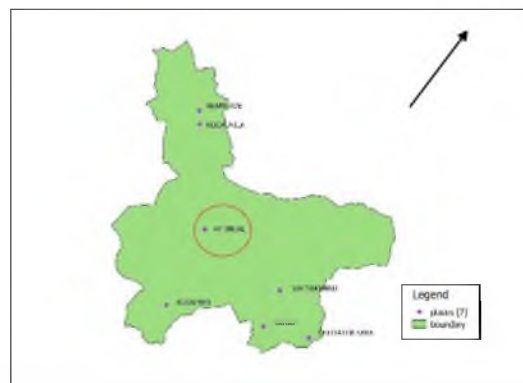


Figure 1: Study Area Map

Friction points

Friction factors are defined as all those actions related to the activities taking place by the side of the road and sometimes within the travelled way (like bus stops, unauthorized parking), which interfere with the traffic flow on the travelled way. They include but not limited to pedestrians, bicycles, non-motorized vehicles, parked and stopping vehicles, bus stops, petrol pumps on the side roads etc. These factors are normally very frequent in densely populated areas in the developing economies. In this study, initially friction point locations were identified on the selected road corridors and subsequently the influence of these factors on traffic performance measures were assessed. These friction points were identified by using GPS tracker and located by using graphical method. These points were plotted on map created using the QGIS software shown Figure 2.

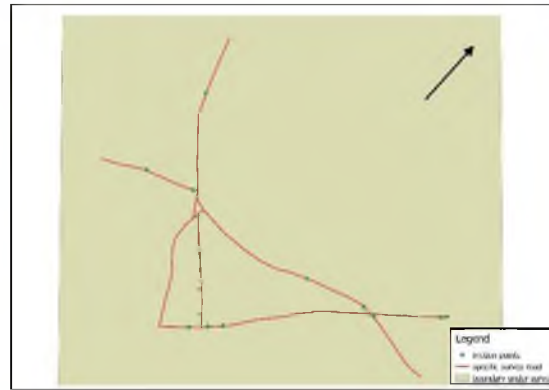


Figure 2: Map of friction points

4. METHODOLOGY

1. Identification of parameters which affect traffic congestion.
2. Selection of study corridor.
3. Collection of data
4. Map creation and analysis

5. DATA COLLECTION

1. Using Manual counters: It is the most traditional method. In this case trained observers gather traffic data that cannot be efficiently obtained through automated counts e.g.: vehicle occupancy rate, pedestrians and vehicle classifications. The most common equipment used are tally sheet, mechanical count boards and electronic count board systems. This was parking count was collected.

Table1: Parking Survey Data Monday (peak day one)

VEHICLE	9:30 AM	10:30 AM	5:00 PM	6:00 PM
CAR	117	143	211	242
TWO WHEELER	235	285	293	236
THREE WHEELER	22	32	35	23
HEAVY	11	7	18	3

Table 2: Parking Survey Data Friday (peak day two)

VEHICLE	8:30 AM	9:30 AM	10:30 AM	4:00 PM	5:30 PM
CAR	204	248	212	186	253
TWO WHEELER	351	397	324	347	406
THREE WHEELER	53	49	35	55	32
HEAVY	14	9	12	3	8

Table 3: Parking Duration

VEHICLE	LONG TERM PARKING
CAR	65-85
TWO WHEELER	180-220

2. Attribute Data: Non-spatial data has no specific location in space. It can however, have a geographic component and can be linked to a geographic location. The data on traffic speed was collected using the Performance Box wherein the probe vehicle fitted with GPS was deployed.



Figure 3: Path Map

Table 4: Typical Probe Vehicle GPS Data Path 1

LATITUDE	LONGITUDE	LENGTH	SPEED
8.69967	76.810963	78	19
8.69948	76.811784	167	20
8.69915	76.812585	266	22
8.69886	76.813339	352	20
8.69899	76.813518	391	14
8.69986	76.813586	484	21
8.70086	76.813627	600	24
8.70176	76.813804	703	21
8.70259	76.814216	806	28

Table 5: Typical Probe Vehicle GPS Data Path 2

LATITUDE	LONGITUDE	LENGTH	SPEED
8.69499	76.812544	81	23
8.69569	76.812644	172	24
8.69667	76.812878	353	27
8.69755	76.813105	384	26
8.69807	76.813632	410	10
8.69744	76.81367	501	18
8.69684	76.813693	539	9
8.69601	76.813741	590	2.84
8.69589	76.81374	646	2.38
8.69536	76.81373	711	17
8.69491	76.813721	736	3.1
8.69485	76.813714	768	0
8.6945	76.813366	821	5
8.69406	76.812682	899	15

Table 6: Typical Probe Vehicle GPS Data Path 3

LATITUDE	LONGITUDE	LENGTH	SPEED
8.69734	76.814629	87	26
8.69686	76.815293	177	28
8.69637	76.816531	326	38
8.69604	76.817392	425	0
8.69586	76.817858	483	23
8.69535	76.818647	583	5.98
8.6953	76.818224	636	22
8.6953	76.817418	730	14
8.6953	76.816959	780	26
8.69513	76.815979	790	25
8.69489	76.814808	1020	32
8.69479	76.814099	1100	16
8.69479	76.813589	1160	20
8.69482	76.812806	1240	14
8.69486	76.812592	1260	10

Table 7: Typical Probe Vehicle GPS Data Path 4

LATITUDE	LONGITUDE	LENGTH	SPEED
8.69314	76.820008	27	15
8.69311	76.82057	87	15
8.69343	76.820107	153	15
8.69391	76.819688	220	15
8.69433	76.81942	279	8.39
8.6945	76.8193	300	11
8.69496	76.819015	360	4.93
8.69502	76.818927	372	1.84
8.69511	76.818955	382	1.33
8.69513	76.818055	424	13
8.69512	76.81968	465	10
8.69513	76.820037	505	10
8.6951	76.820623	572	11
8.69513	76.820983	612	10
8.69506	76.82138	656	9

Map creation and analysis

The maps needed for the needed study was created using QGIS software. The base map was collected from the website of the land use board of Kerala. The boundary map of Attingal municipality, The major and other road of Attingal municipality map, Major location of Attingal municipality map and The map of specific study area was created.

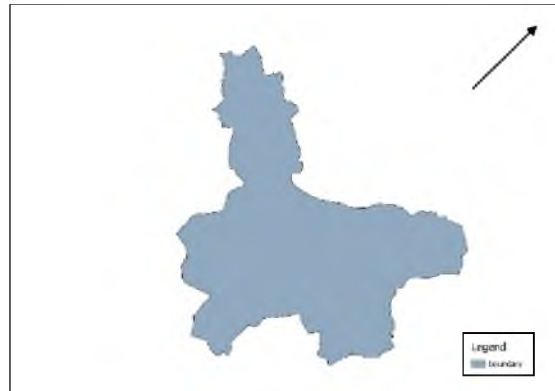


Figure 4: Boundary Map



Figure 5: Major Location Map

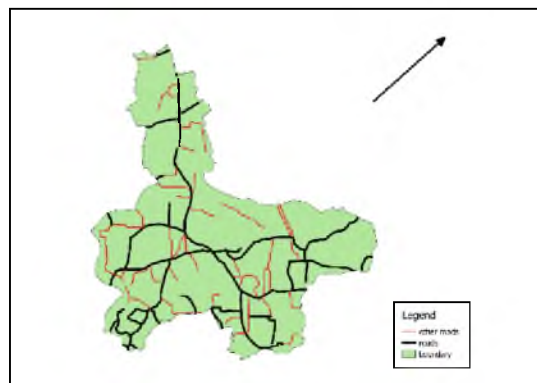


Figure 6: Major roads and Other roads Map

Traffic speed data analysis

The traffic speed data analysis was done using data bases and the speed – length graphs plotted using the traffic speed data collected. This traffic speed data was collected as 4 parts. This was again transferred as points called friction points on the specific study area map.

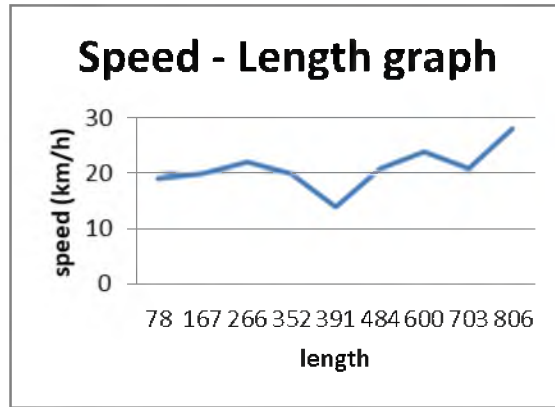


Figure7: Speed – Length graph Path 1

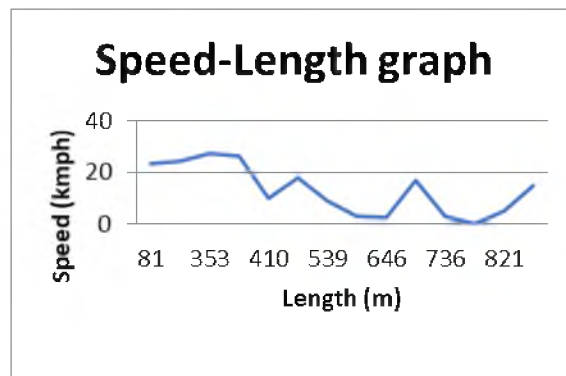


Figure 8: Speed – Length graph Path 2

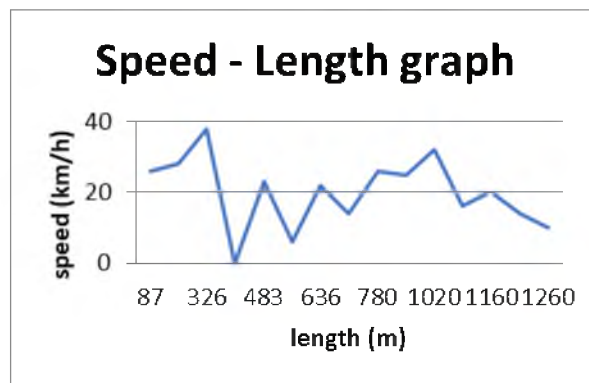


Figure 9: Speed – Length graph Path 3

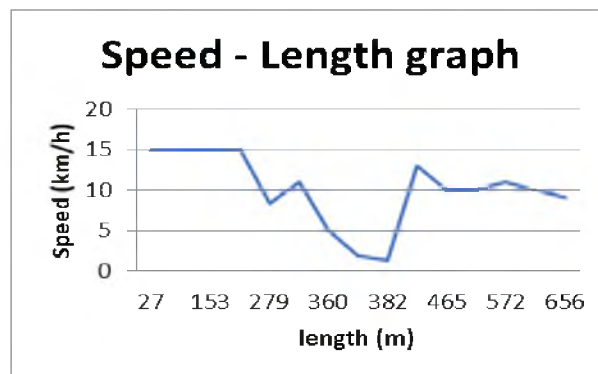


Figure 10: Speed – Length graph Path 4

Identification of influence of friction points

One run on the study path at a peak period of time was plotted on a graph using the GPS tracker data to understand the variation in speed. The speed profile plot was plotted by depicting the absolute distance on the x-axis and variable speed on the y-axis.

The friction points are the points of minimum speed on the travel path taken at one run. These points are again plotted to the specific study area map to identify the point of friction and to make the reasons for the speed reduction.

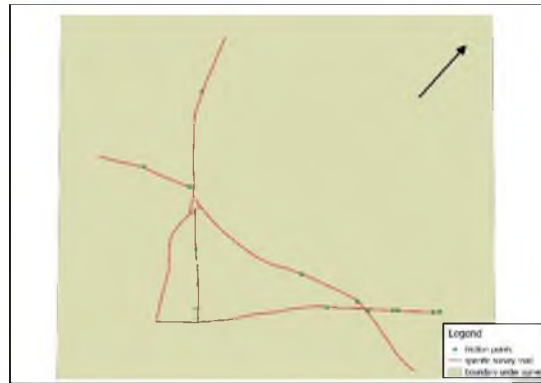


Figure 11: Friction Points Map

6. CONCLUSION

- The influence of the friction points on the traffic speed shows that the influence of the bus stops, school zone and junctions is up to 95% .
- This study observed that the impacts of the pedestrian crossing roads and parking of vehicles on the roads would have a negative influence on speed varying from 20% to 65% whereas the bus stops located without the proper provision of bus bays would reduce the speed of the vehicle to the tune of 25% to 40%.
- Parking was one of the major cause for the traffic congestion in the study area, so we suggest an effective parking system like multi-level parking system on a convincing space with in the traffic congestion zone .

REFERENCES

- [1] Amudapuram Mohan Rao,S. Velmurugan,Arpita Chakraborty(2014) “Managing traffic congestion with GIS” in Geospatial World, June 16 2014
- [2] Anitha Selva Sofia Sd., Nithyaa.R, Prince Arulraj,G (2013) “Minimizing the Traffic Congestion Using GIS” IJREAT International Journal of Research in Engineering & Advanced Technology, Volume 1, Issue 1, March, 2013.
- [3] Kalaga Ramachandra Rao and Mohan Rao (2009) “Application of GPS for Traffic studies” in Journal of Urban Transport Volume-8 No.1, December 2009.

Overtaking Behaviour of Vehicles on Undivided Roads Under Heterogeneous Traffic

Ameera V U* and Vincy Verghese**

Abstract— Traffic on Indian roads is highly mixed in nature with wide variations in the static and dynamic characteristics of vehicles. These vehicles do not follow strict lane discipline and occupy any available lateral position on the road space. Overtaking is one of many important behaviour considered in the analysis of road traffic accidents and performance on undivided roads where the vehicles use the opposing lane to overtake the slower vehicles with the presence of oncoming vehicles from opposite direction. Overtaking process involves lane-changing manoeuvres, acceleration and deceleration actions and estimation of relative speed of overtaking and overtaken vehicles, and also, estimation of speed and distance of the oncoming vehicle. The main objective of the present study is to study the overtaking characteristics of vehicles on undivided roads under heterogeneous traffic conditions. For this purpose, details of overtaking data were collected on a single-lane two-way undivided road using moving car observer method and registration plate method. The data extracted and analysed were the acceleration characteristics, speeds of the overtaking vehicles, overtaking time, overtaking distances, safe opposing gap required for overtaking, flow rates, overtaking frequencies and types of overtaking and overtaken vehicles. The results obtained from this study will be useful to understand the overtaking behaviour of vehicles in mixed and non-lane discipline traffic conditions. These parameters will be useful in the development of traffic simulations models for undivided roads and thereby for estimation of capacity.

Keywords— *lane-changing manoeuvres; ~~safe opposing gap~~; moving car observer method; registration plate method*

INTRODUCTION

Traffic is highly mixed in nature with lack of lane discipline on Indian roads. Traffic compositions mostly comprises of motorized vehicles such as two-wheelers, three-wheelers, cars, trucks, buses and non-motorized vehicles like bicycles, etc. Overtaking in two lane highways is a frequent phenomenon and a major consideration in traffic operations and safety. Characteristics like the dimensions, speed, acceleration, deceleration, clearances and manoeuvrability of these vehicles vary widely and hence, traffic speed is the most important factor affecting the safe movement of vehicles. In mixed traffic, vehicles use the road space more effectively and their movement depends on lateral and longitudinal gaps. The willingness to overtake mainly stems from the speed difference between the subject vehicle and the rest of traffic on the same or opposing travel lane and the tendency of each driver to maintain a desired speed during driving.

*Ameera V U**, PG Scholar, Department of Civil Engineering, Jyothi Engineering College (email: ameerausman94@gmail.com)

*Vincy verghese***, Assistant Professor, Department of Civil Engineering, Jyothi Engineering College, Cheruthuruthy (email: vincyverghese@jecc.ac.in) They are unavoidable especially in the case of mixed traffic conditions where a speed differential always exists between the fast and slow moving vehicles. Also, overtaking is one of the most complex and important manoeuvre on undivided roads where the vehicles use the opposing lane to overtake the slower vehicles with the presence of oncoming vehicles from opposite direction. The ability to pass is influenced by a variety of parameters including the volumes of through and opposing traffic, speed differential between the overtaking and overtaken vehicles, highway geometry particularly available sight distance, and human factors. Hence, the knowledge of overtaking and lane-changing behaviour of vehicles is essential in understanding of traffic behaviour on undivided roads. The aim of the study is to evaluate the overtaking behaviour of vehicles on undivided roads with the following specific objectives:

- To determine the acceleration and overtaking characteristics of different types of vehicles during overtaking.
- To develop relationships between relative speed of overtaking and overtaken vehicles and the overtaking time for different classes of vehicles.
- To develop relationships between overtaking frequency with traffic flows in the ongoing direction, opposite direction and traffic flows in both the directions.

LITERATURE REVIEW

Studies Related to the Topic

In order to carry out the study, it is necessary to evaluate the overtaking characteristics of different vehicle types on undivided rural road. Various parameters like the total time taken during overtaking operation, Speed of overtaken and overtaking vehicle, acceleration characteristics, opposing gap required for overtaking etc are to be determined. Asaithambi, G. et al. [1] carried out similar study on a two-lane two-way national highway (NH 66) of 1.2 km road section in Mangalore, India. The overtaking characteristics of all types of vehicles under mixed

traffic conditions were observed and mathematically modelled. The data extracted and analysed were the acceleration characteristics, speeds of the overtaking vehicles, overtaking times, overtaking distances, safe opposing gap required for overtaking, flow rates, overtaking frequencies, types of overtaking strategy, and types of overtaking and overtaken vehicles. Chandra, S. et al [2] have studied the acceleration and overtaking characteristics of different types of vehicles using floating car method. The influence of shoulder condition (paved and unpaved) on the acceleration behaviour during overtaking was presented. In the case of highways with paved shoulders, two-wheelers rarely overtook the test vehicle as they mostly used shoulder lane for their movement. The relation between the overtaking speed and the acceleration rates was evaluated. The relation between the relative speed of the overtaking and overtaken vehicles against the overtaking time for flying overtaking was also studied and found that the overtaking time depends upon the speed differential between the overtaking and overtaken vehicles. Mocsari, T. [3] analysed the overtaking behaviour of vehicles on two-lane rural roads in Hungary using the data collected by an instrumented vehicle. Out of 230 overtaking cases, 55% were accelerative overtaking, 20% were continuous (flying) overtaking and the rest were multiple vehicle overtaking. In case of continuous overtaking, there was a higher difference in average speed of vehicles compared to accelerative overtaking. In accelerating overtaking and in continuous overtaking the average difference between the average speed of the vehicle that is overtaking and the vehicle to be overtaken is 15.4 km/h and 26.4 km/h respectively. Mawjoud, A. et al. [4] has obtained a relation between passing manoeuvres and flow rate for each and both directions and found that the number of passing manoeuvre increases as the flow rate for both directions increase up to 1500 veh/h flow rate. Llorca, C. et al. [5] carried out a comprehensive comparison between two databases of passing manoeuvres. The first one obtained from a field study and the second one used a driving simulator. The results showed similarities between passing time and passing distance of completed manoeuvres.

METHODOLOGY FOR DATA COLLECTION

The data for this study was collected on a two-lane two-way state highway (SH22) on three stretches of 1km each on Thrissur- Shornur road in Kerala. Satellite image of the study area is shown in fig.1. The traffic data were collected for 1 hour during off-peak hours on weekdays using moving car method and registration plate method.

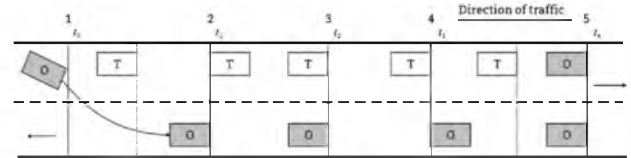


Fig. 2. Events during overtaking process

Moving Car Method

Moving car method was chosen for the collection of data on overtaking manoeuvre. The schematic picture of an overtaking manoeuvre which was observed on the study section is shown in the fig.2. In this method, test car (T) was driven with a uniform speed of 40 km/h to make other vehicles to overtake the test car. The acceleration and overtaking characteristics of different types of vehicles were evaluated. The data was collected for six categories of vehicles such as Cars, Heavy Vehicles (HV), Buses, Two Wheelers (TW), Auto and Light Motor Vehicles (LMV). The entire process of the overtaking operation was divided into five events and the time taken for each event was recorded with a help of a stop watch.

- Event 1: when the overtaking vehicle (O) moves to the opposing lane for initiating the manoeuvre.
- Event 2: when the front tyre of the overtaking vehicle is in line with the rear tyre of the test vehicle.
- Event 3: when the front tyre of the overtaking vehicle is in line with the front tyre of the test vehicle.
- Event 4: when the rear tyre of the overtaking vehicle is in line with the front tyre of the test vehicle.
- Event 5: when the overtaking vehicle either comes back to its original lane or continues to travel in the opposing lane after overtaking the test vehicle.

Registration Plate Method

This method was employed to get the traffic flows, composition and number of overtaking and overtaken vehicles on the study stretch in both lanes. Video cameras were placed at each end of the section to record the passage of vehicles. The following data were extracted from the video recorded, simultaneously for every 5 min: vehicle registration number and type of vehicle. The overtaking vehicles were not observed directly, but obtained through the difference in entry and exit orders at both the ends of the study section. If the order of a vehicle at the exit differs from the order at the entry, then that vehicle had performed an overtaking manoeuvre. The number of overtaking for every 5 minute was noted down by checking the order of vehicles at entry and exit. The flow rate of vehicles in on-going direction and opposing direction was also obtained from the collected data.

DATA EXTRACTION AND ANALYSIS

The data obtained through moving observer method and registration plate method was analysed to study the

acceleration and overtaking characteristics of different types of vehicles, Estimation of safe opposing gap required for overtaking vehicle, Type of overtaking performed by different category of vehicles, Total distance and total time required for overtaking and effect of flow rate on overtaking frequencies.

Estimation of Acceleration Rate and Speed

Certain assumptions were made in order to calculate the overtaking distances. A is the overtaking vehicle assumed to be originally travelling at design speed at the time of initiation of overtaking process, v_a (m/s or km/h); B is the test vehicle (slow moving vehicle) travelling with uniform speed, v_b (m/s or km/h); C is the vehicle coming from opposite direction assumed to be travelling at design speed, v_c (m/s or km/h) as shown in fig. 2.

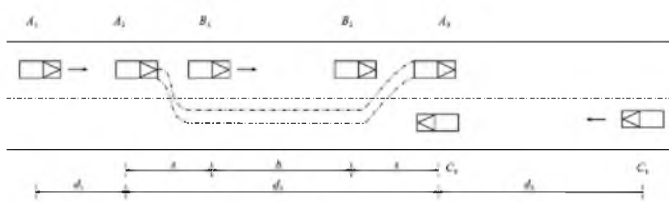


Fig. 3. Overtaking manoeuvre

It is assumed that when the vehicle is at position A1, it is forced to reduce its speed to the speed of the slow moving vehicle, B. From the position A2, the vehicle A starts accelerating and shifts to the adjoining lane, overtaking the vehicle B, and shifts back to its original lane ahead of B in position A3 in time T. During the overtaking manoeuvre d_2 is the distance travelled by the vehicle A from A2 to A3 during the actual overtaking operation in time T and d_3 is the distance travelled by the vehicle C from C1 to C2 during the overtaking operation of A, i.e., in time T. The minimum distance between position A2 and B1 may be taken as the minimum spacing s of the two vehicles while moving with the speed, v_b . The minimum spacing between the vehicles depends on their speed and is given by empirical formula:

$$s = 0.7v_b + 6 \tag{1}$$

The minimum distance between B2 and A3 may be assumed equal to s as mentioned above. If the time taken by the vehicle A for the overtaking operation from position A2 to A3 is T, the distance covered b by the slow moving vehicle B travelling at a speed of v_b is calculated by the following equation:

$$b = v_b T \tag{2}$$

Thus, for the distance d_2 ,

$$d_2 = b + 2s \tag{3}$$

However, the time T depends on the speed of overtaken vehicle B and the acceleration of overtaking vehicle A. This time T can also be calculated by equating the distance d_2 to the general

formula used to calculate the distance travelled by a uniformly accelerating body with initial speed, v_b and acceleration a .

$$d_2 = b + 2s = v_b T + \frac{aT^2}{2} \tag{4}$$

$$T = \sqrt{\frac{4s}{a}} \tag{5}$$

$$d_2 = v_b T + 2s \tag{6}$$

The total time taken for overtaking is obtained from the data collected using moving car method. If the spacing s is known, then the acceleration is calculated as:

$$a = \frac{4s}{T^2} \tag{7}$$

From the distance travelled d_2 and time taken T by the vehicle to complete the overtaking, the speed of overtaking vehicle v_a can be calculated as:

$$v_a = \frac{d_2}{T} \tag{8}$$

Effect of Speed on Acceleration

The rate of acceleration achieved by all categories of vehicles during overtaking was estimated. A Positive linear relationship is observed between the speed and acceleration showing higher overtaking speed associated with higher rate of acceleration as shown in fig.4.

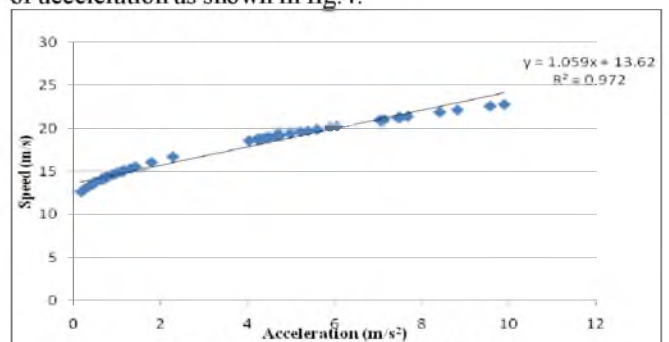


Fig. 4. Plot between Speed and Acceleration

Opposing Gap Required for Safe Overtaking

The safe buffer distance plays an important role when drivers choose gaps in the opposing adjacent lane in order to overtake a slow moving vehicle. To complete the overtaking manoeuvre, a vehicle needs certain obstacle-free distance in the opposing lane, in reality a vehicle initiates an overtaking manoeuvre only if the distance gap between the vehicle and the oncoming vehicle is much greater than this distance. . Most of the overtaking manoeuvres involve estimation of distance gaps in the opposite stream. It is seen that the mean

safe opposing distance for overtaking is 190.3 m with minimum safe opposing distance of 103 m and maximum of 448 m.

Proportion of Flying and accelerative Type of Overtaking

Two types of overtaking were observed from the analysis which are flying and accelerative. Flying overtaking is performed by 45.45% of drivers and accelerative by 54.55% of drivers as shown in fig.5. It was seen that cars (69%) are performing higher number of flying overtaking compared to other category of vehicles. This may be due to higher operating characteristics of cars. Buses, light motor vehicles and Heavy vehicles are performing higher number of accelerative overtaking compared to other vehicle types. This may be attributed due to their lower operating characteristics and larger size of vehicles. In the case of two-wheelers, both types of overtaking are almost equal which is believed to be due to their higher manoeuvrability and smaller size.

Total Distance Covered During Overtaking

The total distance covered by the overtaking vehicle depends on the speeds of overtaking and overtaken vehicles. It was found that the mean values of overtaking distances for accelerative overtaking (129 m) is higher compared to flying overtaking (69.5m). This is believed to be due to the fact that a vehicle performing accelerative overtaking has to follow the vehicle ahead for some time and reduce its speed in order to find gaps in the opposing lane which increases the overtaking distance. Total distance for each category of vehicle is shown in Table 1. The mean overtaking distance for buses (171.2 m) and heavy vehicles (194.2 m) are longer compared to other categories of vehicles. This is believed to be due to their lower operating characteristics and larger size. The overtaking distance for two-wheelers (89.5 m) is shorter which may be due to their smaller size and higher manoeuvrability.

TABLE 1. TOTAL OVERTAKING DISTANCE FOR DIFFERENT TYPES OF VEHICLES

Vehicle Type	Total overtaking distance (m)			
	Mean	Min	Max	Std. Dev.
TW	89.5	57.3	149.8	29.9
Auto	120.3	104.1	129.8	9.8
Car	79.6	54.2	126.8	22.8
LMV	111.1	62.3	144.8	30.2
HMV	194.2	165.7	226.6	25.0
Bus	171.2	152.2	190.3	15.6

Total Time Required During Overtaking

The time taken for the flying overtaking (3.3 s) is lesser when compared to the accelerative type of overtaking (8.1 s). As discussed earlier, for performing accelerative overtaking the vehicle has to follow the vehicle ahead for some time in order to perform the overtaking and hence, it is higher. The total overtaking time for all categories of vehicles is shown in the table 2.

TABLE 2.

TOTAL OVERTAKING TIME FOR DIFFERENT TYPES OF VEHICLES

Vehicle Type	Total overtaking time (s)			
	Mean	Min	Max	Std. Dev.
TW	5.6	2.7	11	2.7
Auto	8.3	6.9	9.2	0.9
Car	4.7	2.4	8.9	2.1
LMV	7.5	3.1	10.6	2.7
HMV	15	12.4	17.9	2.3
Bus	12.9	11.2	14.7	1.4

The total time taken for overtaking by cars (4.5 s) and two-wheelers (5.6 s) are lesser compared to other vehicle types. The reason may be due to the fact that these vehicles have higher manoeuvrability and higher operating characteristics. For heavy vehicles, the total overtaking time is higher (15 s) which may be due to lower operating characteristics and larger size of vehicles.

Effect of Speed Difference on Overtaking

Speed of the overtaken vehicle is a controlling element in the determination of overtaking time and distance. Hence, it is worthwhile to determine the effect of speeds of both overtaking and overtaken (test) vehicles. The speed difference of all categories of vehicle with respect to test vehicle (i.e., car) was determined and plotted against the time taken by the overtaking vehicle as shown in fig.5. The possible explanation for this is when two vehicles are moving with more or less similar speed it becomes difficult for the overtaking driver to perform the overtaking immediately as the driver has to maintain a minimum gap with the leader in order to avoid collision. In the case of higher speed difference (i.e., one vehicle moving with a lesser speed compared to other vehicle), the fast moving vehicle can easily overtake the slow moving vehicle within a short period of time.

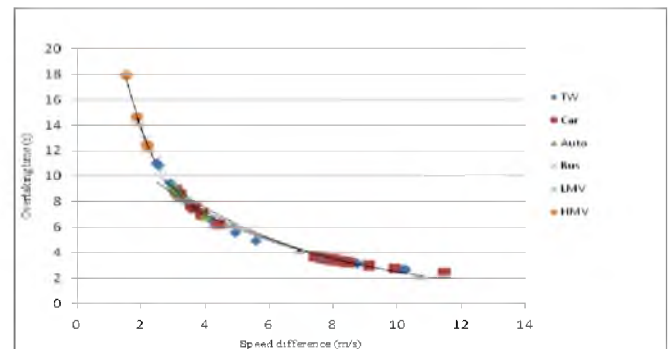


Fig. 5. Effect of Speed Difference on Overtaking Time

TABLE 3. R² VALUE FOR DIFFERENT CATEGORIES OF VEHICLES

Type of Vehicle	TW	Car	Auto	Bus	LMV	HMV
R ² value	0.973	0.980	0.999	0.998	0.992	0.997

Effect of Flow Rate on Overtaking Frequencies

The number of vehicles performing overtaking operation, the flow of vehicles in the opposite direction and flow of

vehicles in the same direction were obtained from extracting the video record. The number of overtaking decreases with increase in flow rate in the opposing direction as shown in fig.6. This may be due to the lesser number of gaps in the opposing direction due to increase in flow.

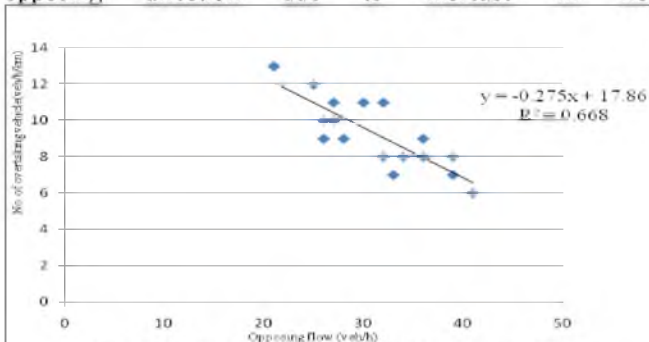


Fig. 6. Number of Overtaking Vehicle vs Opposing Flow

Similarly, number of overtaking manoeuvres increases in the undivided road as the inflow rate increases as shown in Fig.7. Possible explanation for this is as the number of vehicles moving in the on-going direction of traffic increases, the tendency to overtake will increase. This might be attributed due to the fact that the drivers desire to travel at higher speed and often they overtake the leader vehicle to achieve higher speed.

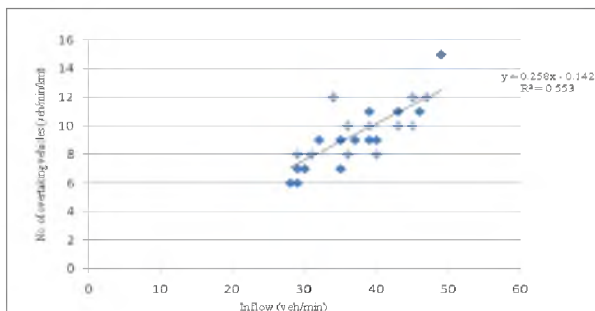


Fig. 7. Number of Overtaking Vehicle vs Inflow

CONCLUSIONS

Although the proportion of each type of overtaking is almost the same, there is an increase in the proportion of accelerative overtaking. This may be due to the geometric conditions of the road surface. Presence of horizontal curves and vertical curves and by roads hinders the sight distance. As a result drivers were forced to reduce their speed while overtaking. It was found that the mean values of overtaking distances for accelerative overtaking is higher compared to flying overtaking. This is believed to be due to the fact that a vehicle performing accelerative overtaking has to follow the vehicle ahead for some time and reduce its speed in order to find gaps in the opposing lane which increases the overtaking distance. Mean overtaking time was more for heavy vehicles due to their lower manoeuvrability and larger size. The results obtained from this study will be useful to understand the overtaking behaviour of vehicles in mixed and non-lane discipline traffic conditions. These parameters will be useful

in the development of traffic simulations models for undivided roads and thereby for estimation of capacity. The findings from the study can also be used to estimate potential collision times which will be helpful to improve the road safety. The study also finds implications on estimation of overtaking sight distance and designing of overtaking zones.

ACKNOWLEDGMENT

First of all I would like to thank God, the almighty for the divine grace bestowed on me to complete this seminar successfully. I would also like to express my thanks to the Management and Principal Fr. Jaison Paul Mulerikkal CMI of Jyothi Engineering College, Prof. S Rathish, Head of the Department of Civil Engineering, my seminar guide Asst.Prof. Ms. Vincy Verghese, seminar coordinators Prof. Dr. Anitha Jacob and Asst. Prof. Ms Archana. S for their valuable guidance, timely corrections and scholarly guidance. I am indebted to my parents and for their constant encouragement and all my friends who have helped me a lot during the initial stages of this project.

REFERENCES

- G. Asaithambi and G. Shravani , "Overtaking behaviour of vehicles on undivided roads in non-lane based mixed traffic conditions" Journal of Traffic and Transportation Engineering, vol. 4, pp. 252-261, 2017.
- S. Chandraa and S. Shuklab, "Overtaking behavior on divided highways under mixed traffic conditions" Procedia - Social and Behavioral Sciences, pp.313 – 322, 2012.
- T. Mocsari, "Analysis of the overtaking behaviour of motor vehicle drivers" Acta Technica Jaurinensis, vol 2, pp. 97-106, 2009.
- A. Abul Mawjoud and G. Sofia, "Passing Behavior on Rural Two-lane Highways" Al-Rafidain Engineering, vol 22, pp. 123-134, 2014.
- C. Llorca and H. Farah, "Passing Behavior on Two-Lane Roads in Real and Simulated Environments" Transportation Research Board, Washington, D.C, pp. 29-38, 2016.

QUANTIFICATION AND ANALYSIS OF BLINDSPOTS FOR LIGHT MOTOR VEHICLES

Aleena Mathew*, E. S. Krishna Ram*, Elizabeth Maria Alex *, Gokul G. Kumar*, Jeslin Elizabeth* and M. Satyakumar**

*B. Tech Students, Department of Civil Engineering, Mar Baselios College of Engineering and Technology, Nalanchira, Thiruvananthapuram, Kerala – 695 015

^aE S Krishna Ram, Email- krestvm@gmail.com

** Professor and Head of the Department of Civil Engineering, Mar Baselios College of Engineering and Technology, Nalanchira, Thiruvananthapuram, Kerala - 695015, Email -satyan5262@yahoo.co.in

Abstract. In recent years, the rapidly increasing vehicular population, deteriorating road conditions, driving environment and human factors has led to a lot of traffic accidents and casualties. If, there exist a mechanism to detect obstructions in the road, and then relay the processed information back to the driver, he may be alerted about the impending danger. The lack of visual stimuli due to blind spots, both vehicular and external is often a leading contributor of road accidents. This paper outlines procedures for calculating and analysing the factors affecting blind spots for light motor vehicles by quantifying blind spot of the test vehicle with respect to suitable parameters. An opinion survey was conducted to understand driver needs and various opinions were collected and analysed. An ultrasonic sensor system was developed with the collected blind spot data which maps physical environment around the car, with special care given to blind spots and relay it back to the driver in real time.

Keywords: Blind spots, Ultrasonic sensor, Arduino

1. Introduction

Road accidents, which are normally not forecasted and avoidable, are general risks in day to day life. Statistics reveal that inadequate visual data is one of the major reasons for the increasing number of road accidents. Drivers are being involved in accidents, with other vehicles which are not exactly due to his/her faults, but due to the presence of certain hidden areas around the vehicle in which the driver has no visibility. These hidden areas around the vehicle are known as blind spots. Blind spot is an obscuration of the visual field, they are associated with vision as well as in vehicles. With respect to a vehicle, a blind spot is that area around the vehicle that cannot be directly observed by the driver while at the controls, under normal driving conditions either directly or through any of the mirrors. The issue whether an object is visible to a driver depends on many variables, the basic one being line-of-sight, or in other words, is the object geometrically visible to the driver with no obstructions getting in the way [1]. Various vehicular and human characteristics also affect blind spots. These factors include passenger height, age, A and B pillar geometries etc. Fig. 1.1 shows the location of two cars on the road, the driver's view from side and rear mirror highlighting the issue of blind spot.

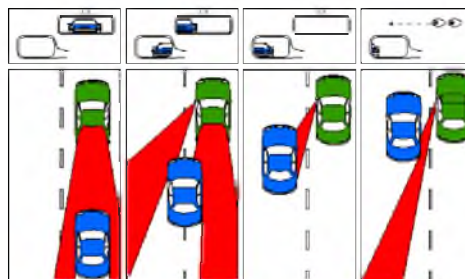


Fig. 1.1: Example of vehicular blind spot. [2]

It is necessary to monitor blind spot areas and the obstacles in the area need to be detected and reported to the driver in real time. Drivers nowadays are getting more and more concerned about safety and safety features in their cars and are also willing to pay the cost of acquiring safer vehicles and such safety equipment [3]. Blind

spots can be monitored using technologies of two different categories which are Active and Passive Blind Spot Monitoring. Active blind spot monitoring uses cameras and radars for monitoring whereas passive blind spot monitoring uses convex mirrors or lenses for obtaining a wider view of the surrounding. Conducting a proper study on vehicular blind spot and developing a proper blind spot detection system can bring down the accidents caused due to driver negligence in this regard.

1.1 Objective

- i. To prepare baseline for vehicular blind spots in LMV's of leading categories and use it for further studies
- ii. To conduct a user opinion survey to collect data on various human factors affecting blind spots
- iii. To analyze the collected data and bring out the causes and to suggest remedies to prevent accidents due to blind spots
- iv. To develop a cost-effective sensor to detect blind spots and relay the information back to the driver

1.2 Literature Review

Kula Sekhar A. et.al. [4] developed a method for detecting blind spot by using ultrasonic sensor and controlling the direction of car by automatic steering by providing partial braking to the individual wheels and reported that the accidents caused due to driver negligence while overtaking and lane changing can be brought down by a great extent. Tigadi A et.al. [5] proposes a driver assistance system to improve a driver's safety while changing lanes on the highway in intelligent vehicle applications which uses radar based technology and camera based technology. Hassan M. et.al. [6] developed a blind spot system known as ZRT Vehicle Blind Spot System (ZRT-VBSS) using Arduino and ultrasonic sensors to overcome the problems due to blind spot which is capable to detect a moving vehicle in blind spot area under static and dynamic conditions. The results from the investigation show that ZRT-VBSS is capable to perform at various operating condition that make it reliable to provide solution for driver to overcome the blind spot phenomenon.

2. Methodology

A test vehicle which is significant, relevant and one which caters to a large number of people is to be selected. The study population consisted of a spectrum of drivers with characteristics such as age, gender, driving experience and physical structure. The strategy for data collection was adopted based on this. A sample selection tree has been developed based on the above-mentioned population characteristics. Subject wise categorisation of sample has been done, in which age, gender, physical characteristics and driving experience was considered. The actual and theoretical blind spots of test vehicle was identified and the actual spectrum is to be mapped above theoretical spectrum for comparison.

3. Data collection

3.1 Selection of test subject and vehicle

Maruti Suzuki Alto was selected as the test vehicle based on the monthly sales data as of November 2017, as it emerged as the Best Selling Car. Then the number of subjects to be tested for blind spots around the vehicle was fixed as 50, after considering various factors such as time taken to complete the test for a person and whether it can effectively accommodate the heterogeneity of the actual population of drivers (age and gender). Data was collected from Regional Transport Office (R.T.O), Thiruvananthapuram, Kerala regarding the number of Active Light Motor Vehicle Licensees in the region, age and gender-wise split up of the population was also obtained. The sample population was stratified in such a way that the percentage of people of various categories were kept as same as that obtained from the R.T.O data to obtain the most accurate result as shown in Fig 3.1.

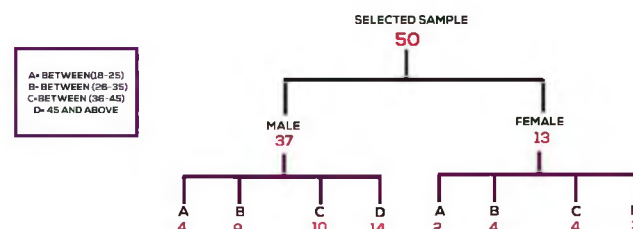


Fig 3.1: Strategy of data collection

3.2 Identification of practical blind spots

To identify the practical blind spots, initially a 2 m boundary around the car was cleared and arrows were erected at the same distance around the car. A Total station was setup at a position where the car and the driver is visible. The test subject, that is drivers of different age categories was seated on the driver’s seat and was instructed to adjust the seat and the mirrors as per requirement to simulate actual driving conditions. He/she was told to observe the reflective prism that one of the team member was moving with along the 2m boundary and was instructed to acknowledge when the prism was not visible to him. Driver’s response was recorded and area around the car which was not visible to the subject was marked on the ground and reading was taken with the Total Station. The Subject’s eye position was also measured with the prism kept at the subjects’ eye level.

The points plotted in site using the total station was opened in AutoCAD software. The respective angles subtended by the blind spot regions at the eye of the driver was noted, added and expressed as a percentage. Fig 3.2 shows schematic representation of the theoretical blind spot of the vehicle.

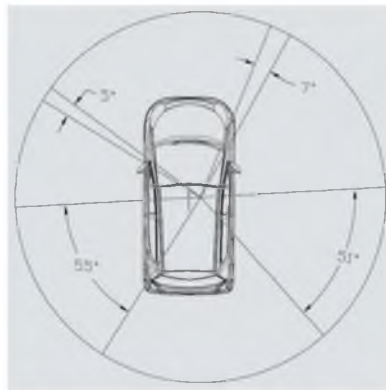


Fig 3.2 Schematic representation of the practical blind spot around a vehicle.

3.3 Identification of theoretical blind spots

The theoretical blind spots are those caused by the geometric design of the test vehicle around the vehicle which is independent of various human characteristics. A powerful laser pointer kept at 120cm from ground level was used to replace the test subject to provide data that are independent of human factors and the data collection was finished as per the previous method.

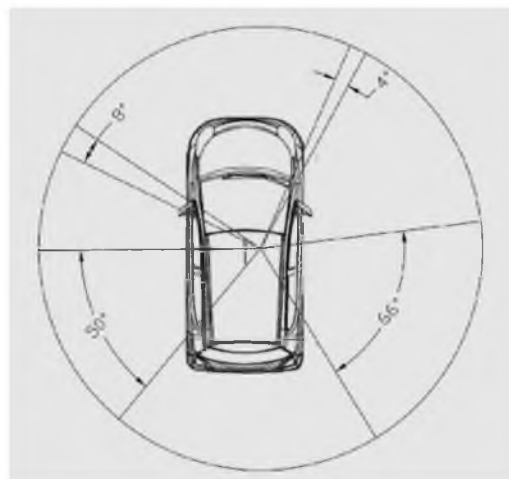


Fig 3.3 Schematic representation of the theoretical blind spot around a vehicle

3.4 Conducting questionnaire survey

A questionnaire survey was prepared using questions regarding awareness of blind spot. Responses to the survey questions were recorded and suggestion towards blind spot reduction according to them was also noted.

1. Data analysis

The primary results of the collected data is described below:

4.1 Variation in age-wise classification

The percentage blind spots for each of the selected age category are observed as:

- for age group A (18-25), the observed percentage blind spot was 30.41%
- for age group B (26-35), it was 31.64%
- for age group C (36-45), it was 32.6%
- for age group D (>45), it was 33.74%

It is clear from the obtained data that age and blind spot percentage has a directly proportional relationship.

4.2 Variation in height-wise classification

The percentage blind spots for each of the selected height category are observed as:

- for height, up to 160cm, the observed percentage blind spot was 32.06%
- for height between 161-170 cm, it was 33.84%
- for height >170cm, it was 30.57%

It was observed that there is an increase in the percentage blind spot up to 170cm and then this trend began to decrease as height further increased.

4.3 Variation with gender

The percentage blind spots for males and females of the selected age category are observed as:

- for age group 18-25 years, blind spots were 28.75% for males and 33.75% for females
- for age group 26-35 years, blind spots were 31.35% for males and 32.29% for females
- for age group 36-45 years, blind spots were 33.11% for males and 33.31% for females
- for age group >45 years, blind spots were 34.01% for males and 32.03% for females

It can be concluded that females had higher degree of blind spots for ages up to 45 years and the trend reversed contrary to what was expected for ages greater than 45 when compared to male counterparts.

2. Discussion of test results based on collected data and questionnaire survey

5.1 Discussion based on human characteristics.

The outcomes of the study of blind-spots with respect to person's physical characteristics are discussed below.

a) Age

As expected, blind spots were found maximum in age category D i.e. greater than 45, and in younger's blind spots were comparatively lower than older counterparts. This can be accounted by a fact that as the age of a person increases, the ability of the ciliary muscles which controls our pupil size to function effectively decrease which causes reduction in sight. Peripheral vision also deteriorates as a person ages leading to increased blind spots around the car.

b) Gender

It is seen that female drivers have higher percentage of blind spots than their male counterparts. Such a variation based on gender might be due to increased peripheral vision in men which is contrary to popular belief that women has higher peripheral vision. However, in female drivers aged above 45, a slight variation in this trend was observed as percentage blind spots for male drivers were more than female drivers. The result obtained might not be an actual representation of the true data as number of test subjects were 3 and a conclusive statement can only be made after conducting further test.

c) Corrected vision

Drivers using spectacles, even though have corrected vision was found to have a higher percentage blind spot as most of the such drivers complained of the blocking of view by the spectacle frame, which can be the reason.

d) Height

The variation of percentage blind spot with height of the person was similar to that of a bell curve i.e. the percentage blind spot was low for height up to 160cm and for height greater than 170cm in general. However, for drivers having height in between 160-170cm the data clearly shows an increased blind spot percentage.

e) Vehicle

The geometric design of car determines to a large extent the degree of blind spot in the vehicle. It is generally accepted that the degree of blind spot and size of the vehicle under consideration follows a directly proportional relationship.

5.2 Comparison of Average Blind spot with Theoretical Blind spot

The average value of degree of blind spot around the vehicle after taking into consideration the values obtained from 50 test subjects was 116° which was very much similar to the obtained degree of theoretical blind spot which was 118° . This similarity between the obtained values and theoretical values indicates geometric similarity in design of the vehicle that suits to the need of the drivers.

3. Model Development

Effective blind spot monitoring can only be achieved by providing a complete 360° coverage using sensors and cameras around the vehicle. It's very helpful to the drivers, if he is able to view the obstacles around his car while at the controls in an effective and economic manner. The system can reduce the number of accidents and casualties by a huge amount and provide a proper assistance to the driver in his or her blind spots. A model based on the concept studied has been prototyped in the form of a device incorporating ultrasonic sensors, Arduino mega microprocessors, power supply boards, vibration motor, etc. which can provide a complete 360° coverage around the vehicle.

6.1 Working

Two ultrasonic sensors were used at right and left side of the car. These sensors were rotated at 180° using a servo motor to achieve a complete 360° coverage around the car. In actual case, more number of sensors can be accommodated around the vehicle, which can eliminate the use of servo motors. Ultrasonic sensors emit ultrasonic radiations, these radiations propagate through the medium strike the obstacle and reflect back to the sensors. Receiver captures the signal and transfers it to Arduino microprocessor. Two microprocessors (Arduino Mega) were used to process the data received from the sensors. Fig 6.1 shows the arrangement of the various components.

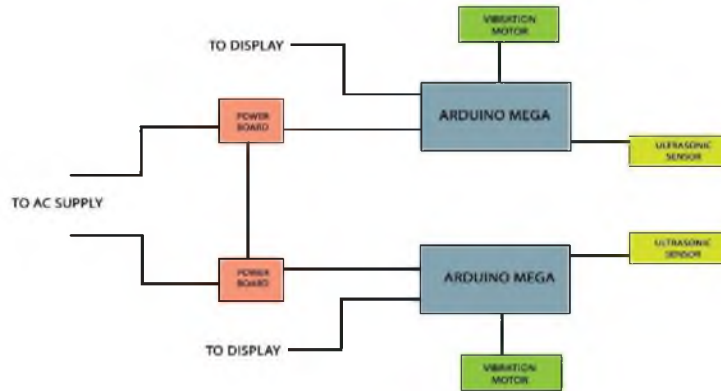


Fig 6.1: Arrangement of various components

The received data consist of the position of the obstacle and the distance between the car and the obstacle. The data is processed by the microprocessor and the processed data was plotted on a screen using MATLAB software. Two additional power supply boards were used to power the circuit. These power circuit boards were connected to AC mains. Blind spot data of the driver obtained from the survey was transferred to the Arduino microprocessor. A vibration motor was set up to the chip to give a slight vibration to the steering wheel when there is an obstacle or a vehicle approaching through the blind spot region. The advantage of the system is that it provides a 360° coverage around the car in real time.

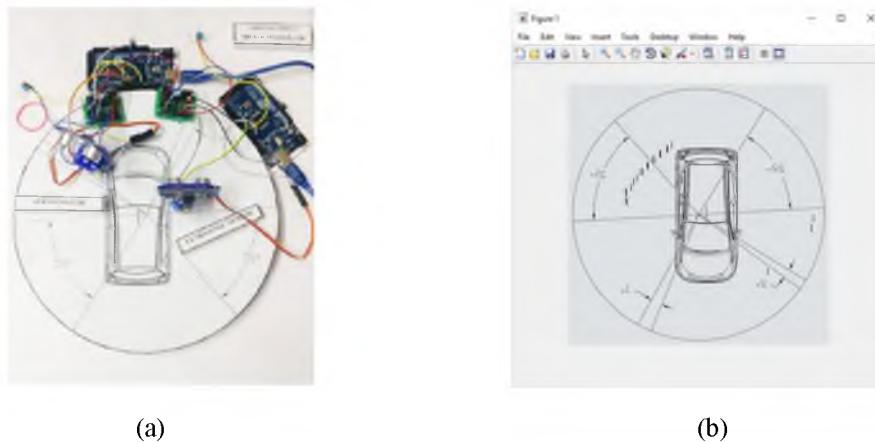


Fig 6.2 (a): Photograph of the prototype developed

(b): Sample output from MATLAB

4. Conclusion

The following specific conclusions can be drawn based on this study:

- There exist conical pillar shaped portions which hinders vision of drivers named as A, B and C Pillars.
- These pillars create obstruction to the visibility of drivers which depends on the design of vehicle and characteristics of the driver.
- Proper side mirror adjustment and additional fittings on side mirror can eliminate the problems occurring due to blind spot to a certain extent.
- Scientific studies on blind spots may lead to changes in vehicular manufacturing, effective placing of the pillars and reducing the area of pillars can lead to reduction in accidents related to blind spots.
- Awareness among drivers on blind spots varies with respect to their age, gender and driving experience.

- Prototype model which senses the driver's blind spots and alerts him has been developed which helps the driver to understand his/her driving behavior with respect to blind spot and act accordingly.
- Pedagogical tools such as videos and other driver training methods may help to bring in importance of this concept and make necessary changes in the driving behavior.

5. Limitations of the study

The following could be pointed out as the limitations of the study.

1. The sample population was limited to 50
2. Only one car was analyzed
3. Theoretical blind spot was taken as the average of only 3 trials.
4. The number of variables accounted were limited
5. Only static conditions were observed and dynamic conditions while driving were ignored
6. Driver perception was not considered
7. Test was only carried out during day time
8. Only a single weather condition was tested
9. Physical properties of the obstructions were not considered

Different assumptions had to be made over the course of the paper such as:

1. Eye level of the driver was assumed as 1.20m for theoretical blind spot determination
2. The vehicle was assumed to be on a flat area
3. A circular area with radius 2m around the car was considered as significant for the project

6. Scope for further study

The primary objective of this project work was to determine and analyze the geometrical blind spots around light motor vehicles. Many areas of future research have arisen from the experimental work and the most significant of them are outlined below.

- The project Quantification and Analysis of Blind spots for Light Motor Vehicles can further be expanded into various categories of vehicles such as buses, trucks, and to different cars in the future.
- The data obtained from the project can be used to create a Blind Spot Detection and Awareness Sensor which can be implemented on a large scale in commercial vehicles.
- The project can be expanded for dynamic conditions also, considering the various conditions prevailing under driving.

References

1. Owsley C. and McGwin G., "Vision and driving", *British Journal of Ophthalmology*, 6(20), pp. 2368-2361 (2010).
2. "A Method for Determining and Presenting Driver Visibility in Commercial Vehicles", <<https://doi.org/10.4271/2007-01-4232>> (accessed on December 14, 2017).
3. Souders D., Ryan B. and Charness N., "Valuation of active blind spot detection systems by younger and older adults", *Accident Analysis and Prevention*, 7(106), pp. 504-514 (2017).
4. Sekhar A. and Nazar N., "Blind-spot detection with automatic steering", *International Journal of Research in Engineering and Technology*, 5(4), pp. 326-327 (2015).
5. Tigadi A., Gujanatti R., Patil G., "Survey on Blind Spot Detection and Lane Departure Warning Systems", *International Journal of Advance Research in Engineering, Science & Technology*, 2(5), pp. 2394-24449 (2015).
6. Hassan. and Irfan H., "Development of Vehicle Blind Spot System for Passenger Car", *Applied Mechanics and Materials*, 10(393), pp. 350-353(2013).

Comparative Study on Cell Filled and Whitetopped Concrete Overlay with Human Hair as Pavement Rehabilitation Methods

Gokul.K.L¹ and Satyakumar M.²

¹PG Student, Structural Engineering, Mar Baselios College of Engineering and Technology, Thiruvananthapuram, Kerala, India

gokulkltvm@gmail.com

²Professor and Head, Department of Civil Engineering, Mar Baselios College of Engineering and Technology, Thiruvananthapuram, Kerala, India

satyan5262@yahoo.co.in

Abstract. During the past two decades, the issue of rehabilitation of the existing pavements using various techniques is gaining momentum. The use of fibre reinforced concrete for rehabilitation purposes is becoming popular. Fibre reinforced concrete is an economical method to overcome flexural failure, micro cracks etc. Human hair is a non-degradable fibre which can be used as a reinforcement material in concrete overlays. Human hair fibre added concrete can be used as a concrete for cell filling and whitetopping concrete pavement rehabilitation methods to overcome the functional deficiencies of existing bituminous pavements. In whitetopping a concrete overlay is provided over the existing deteriorated bituminous pavement. In Cell Filled concrete overlay a mesh of cell is provided and is filled with concrete. In this study the mechanical properties of whitetopped and cell filled concrete overlays incorporated with human hair is being investigated. A field trial of Cell Filled and Whitetopped concrete with and without hair fibre was tried. Conclusions were drawn based on these laboratory and field studies.

Keywords: Whitetopping, Cell Filling, Human hair, Pavement rehabilitation, Mechanical properties

1. Introduction

Road traffic is increasing steadily over the years. This is an international phenomenon. An international forecast predicts that such increase will continue in near future. Even in case of developed countries, there is an unavailability of funds essential for new infrastructure ventures, both for constructing them and more meaningfully towards their conservation and repairs. The position in the context of a developing country like India is visibly far inferior. As a result, more and more roads are deteriorating and the standing pavement structure as a whole is often found to be insufficient to survive up with the present traffic. Appropriate firming and conservation of roads is immediately essential to certify well-adjusted regional development and mitigation of deficiency as they connect the villages and other small town centres harbouring backwardness. A majority of these roads do not have traffic well-intentioned pavement. [1] The cost of firming and restoration by predictable method of this large network will need enormous resources both physical and financial which are pretty occasional.

Most of the prevailing flexible pavements in the network typically have thin bituminous layers. These bituminous pavements, in overall, have a problem that they get deteriorated with time. Most of our roads exhibit, in general deficiencies like alligator cracking, upheaval, rutting, fatigue cracking, and thermo cracking.

Under the rehabilitation plans, typically the overlays are being placed over such cracked or rutted bituminous stratum without making any significant energies to seal these cracks properly [2]. Occasionally the cracks are so extensive also widespread that it is not even conceivable to fully seal them, with the effect that such recently overlaid surfaces yet again exhibit rutting/cracks in a very squat time. Reflection cracks are one example regularly come across with such overlay repairs. Such conservations do not improve their predictable life and bring avoidable disparagement from the public. Such practices of strengthening by overlaying thus essential to be discarded.

Any alternative technique of strengthening or fixing of roads should, therefore, be based on their permanency reasonably purely by initial cost. The cost assessment for such alternative strengthening/repair methods should be based on the concept of life-cycle cost. Substitute approaches of strengthening/repairs should take maintenance of the deficiencies of current bituminous layers. Rutting and cracking are prodigiously witnessed to be common nature type of distress on furthestmost of bituminous pavements. This could be remedied by milling the existing faces. Milling expressively de-stresses the cracked/rutted section. White topping and Cell filled concrete overlay were investigated as rehabilitation methods of moderately distressed bituminous concrete pavements and intersections. Now a day these have much import role for pavement preservation. In this cement concrete overlays over current bituminous pavements have been used as a rehabilitation option for more than 80 years [3]. A cross-section of a pavement displaying concrete overlay over bituminous layer is revealed in fig. 1.



Fig.1 Cross-section of a pavement shows the concrete overlay over bituminous layer [3]

2. Whitetopping concrete overlay

White topping (WT) is a technique of strengthening or rehabilitating weakened asphalt pavements by Plain Cement Concrete (PCC) overlay with or without fibers (fig 2). Ultra-Thin White topping (UTWT) and Thin White topping (TWT) are being progressively accomplished in USA and West Europe. Thickness up to 100 mm, it is labelled as UTWT and for thickness more than 100 mm but up to 200 mm; it is called Thin White Topping (TWT) (fig 3). Beyond 200 mm thickness, it is called Conventional White topping identical to our regular PCC pavements. The prevailing design standards are somewhat dissimilar than those of normal concrete pavements. In case of UTWT, the bond between the existing asphalt pavement and Plain Cement Concrete (PCC) overlay is considered compulsory. However, in case of TWT the bonding is necessary but not compulsory. Another alteration is that for these overlays joints are spaced near. Usual spacing of joints is at 0.6 m to 1.2 m besides in some cases it is up to 1.5 m. These joints are generally not dowelled. No tie rods are also provided in the longitudinal joints. The thickness of UTWT is between 75 to 100 mm. [4]

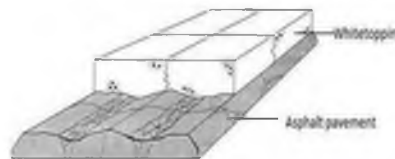


Fig.2 Schematic diagram of a pavement structure with whitetopping [5]



Fig.3 Finished TWT pavement

3. Cell Filling Concrete Overlay

As a substitute, for improved structural performance and low preservation, an innovative pavement technology termed Plastic Cell Filled Concrete Block Pavement (PCCBP) was developed in South Africa. Plastic cell formwork has been effectively used for canal lining, reinforced earth treatment, etc. The cells are tensioned and spread across the foundation stratum and concrete is filled and compacted into the cells. (fig.4). Upon compaction, the cell walls get deformed, resulting in interlocking of neighbouring individual concrete blocks. Cell Filled Concrete (CFC) overlay is one of cast-in-situ block pavement Deformed walls of plastic sheet behave like a hinge

and the blocks can undergo limited rotation. Thus, flexibility is introduced into the cement bound (rigid) surfacing. Cell filled concrete overlay is also a better choice for the rehabilitation of village roads [6].



Fig.4 Cell filled pavement under construction and compaction of concrete [6]

4. Human Hair Fibre

Human Hair Fibre (HHF) (fig.5) is considered as a waste material in most parts of the world and is a collective fundamental found in municipal waste streams which cause massive environmental difficulties.. It is also accessible in plenty and at a very little cost. Human hair fibre reinforced concrete can avoid the spalling of concrete. The belongings like high tensile strength, unique chemical composition, thermal insulation etc. makes it seemly to be used as a reinforcing material. [7]



Fig.5 Human hair fibre

5 Research significance

The work carried out to study the performance of Cell filled and Whitetopped overlays, represent a new rehabilitation choice to address pavements with surface distress problems and also the use of human hair fibre in concrete overlay to utilize the waste material as a resource.

6 Experimental investigations

The first stage is to find the mechanical properties of Cell filled and Thin whitetopped concrete with and without human hair fibre. Second stage include casting field trails of Cell filled and Thin whitetopped concrete overlay with and without human hair fibre.

6.1 Test on Mechanical Properties

The mechanical properties of CFC and TWT concrete with and without human hair fibre were conducted in laboratory. Test include cube compressive strength, cylinder splitting tensile strength and flexural strength test. In Cube compressive strength test, cube strength were evaluated according to IS 516-1959 [9] The test were conducted on a 2000 kN compression testing machine. In the case of flexural strength one measure of the tensile of concrete, it is measure of an unreinforced beam to resist failure in bending. The flexural strength is expressed as modulus of rupture in Mpa and is determined by standard third point loading and center point loading according to IS 516 – 1959[9]. For find split tensile strength, cylinder strength were evaluated according to ASTM C496 / C496M – 11 [10], the test were conducted in a 2000 kN compression testing machine.

6.2 Field casting of overlay

Field trail were done to evaluate the performance of CFC and TWT concrete overlays with and without hair fibre.

6.2.1 Rehabilitation by CFC and TWT concrete overlays

For the present work 6 potholes with a depth greater than 10mm were selected and they are relaid with CFC and TWTC overlays with and without hair fibre.

6.2.2 Construction of Cell Filling Concrete overlay

The Constructing region is cleaned after the milling operation. The form work is placed over the surface, to be rehabilitated. It is recommended that a good profile correction were need for CFC overlays. After the placing of

form works, the cells are filled with concrete and compacted well. The construction of CFC overlay were shown in fig.7



Fig.7 Construction of CFC overlay

6.2.3 Construction of Thin whitetopping concrete overlay

The damaged pothole is rehabilitated by placing the Thin concrete overlays as shown in fig.8



Fig.8 Construction of WTC overlay

7 Results and Discussion

The result obtained from each experiments and a detailed discussion on it is presented:

7.1 Cube compressive strength test results

The compressive strength results were shown in table 1

Table 1 Compressive strength of CFC and WTC specimens without HHF

SL.NO	Compressive strength 28 th day (N/mm ²)			
	CFC	Average	WTC	Average
1	48.5	48.46	49.6	49.7
2	48.2		49.5	
3	48.7		50	

Table 2 Compressive strength of CFC and WTC specimens with HHF

SL.NO	Percentage of HHF by weight of cement	Compressive strength 28 th day (N/mm ²)	
		CFC with HHF	WTC with HHF
1	0	48.46	49.7
2	0.5	48.48	50.13
3	1	49.51	53.2
4	1.5	52.7	56.8
5	2	49.3	50.2
6	2.5	48.6	49.6
7	3	47.8	48.3

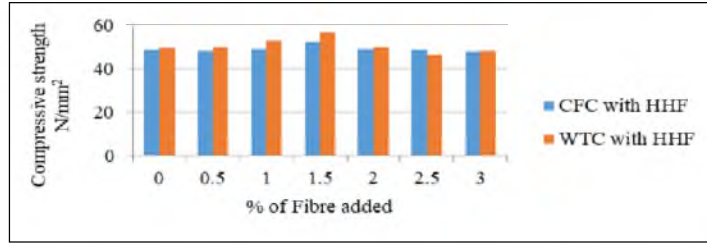


Fig.9 Compressive strength VS. % addition of HHF on CFC and WTC specimens with HHF

From table 1 and 2 it is clear that WTC specimens achieved higher compressive strength than CFC specimens. The maximum compressive strength value obtained for CFC and WTC specimen at a fibre content of 1.5 %, the value obtained were 52.7 and 56.8 N/mm² respectively. It is seen that the compressive strength of CFC and WTC with fibre were higher than that without. Also the characteristic compressive strength achieves a value more than 50 N/mm² at 1.5 % of fibre (fig.9).

7.2 Split strength test results

Table 3 Split tensile strength of CFC and WTC specimens without fibre

SL.NO	Split tensile strength 28 th day (N/mm ²)			
	CFC	Average	WTC	Average
1	3.73		4.22	
2	3.75	3.89	4.52	4.41
3	4.2		4.49	

Table 3 shows the split tensile strength of CFC and WTC without HHF. It is clear that average split tensile strength is higher for WTC than CFC.

Table 4 Split tensile strength of CFC and WTC specimens with HHF

SL.NO	Percentage of HHF by weight of cement	Split tensile strength 28 th day (N/mm ²)	
		CFC with HHF	WTC with HHF
1	0	3.89	4.41
2	0.5	3.9	4.43
3	1	4.0	4.45
4	1.5	4.3	4.68
5	2	3.8	4.2
6	2.5	3.73	3.84
7	3	3.3	3.76

Table 4 Shows in the results of split tensile strength of CFC and WTC with HHF. Here also it can be seen that the split tensile strength of WTC is higher for a percentage fibre content of 1.5 by weight of cement. The above results are shown in fig.10

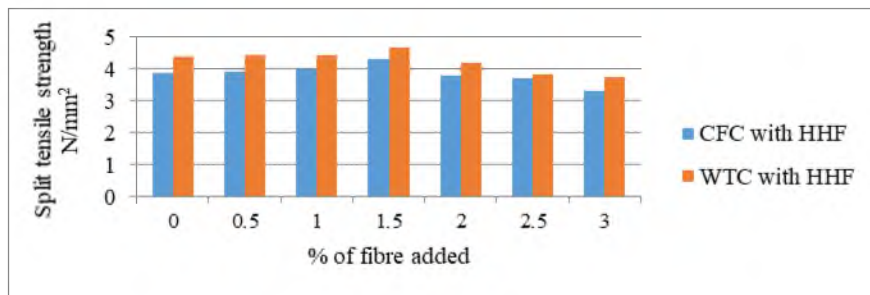


Fig.10 Split tensile strength of CFC and WTC specimens with HHF

7.3 Flexural strength test results

Flexural strength results of CFC and WTC specimens are shown in table 5 below

Table 5 Flexural strength of CFC and WTC specimens without HHF

Specimen	Flexural strength 28 th day (N/mm ²)			
	CFC	Average	WTC	Average
1	4.51		4.67	
2	4.52	4.51	4.65	4.67
3	4.50		4.69	

Table 5 shows the flexural strength results of CFC and WTC without HHF. From this table it is clear that WTC specimen gives better results than CFC specimen.

Table 6 Flexural strength of CFC and WTC specimens with HHF

SL.NO	Percentage of HHF by weight of cement	Flexural strength 28 th day (N/mm ²)	
		CFC with HHF	WTC with HHF
1	0	4.51	4.67
2	0.5	4.54	4.73
3	1	4.63	5.11
4	1.5	4.83	5.23
5	2	5.22	5.45
6	2.5	4.51	4.9
7	3	4.21	4.4

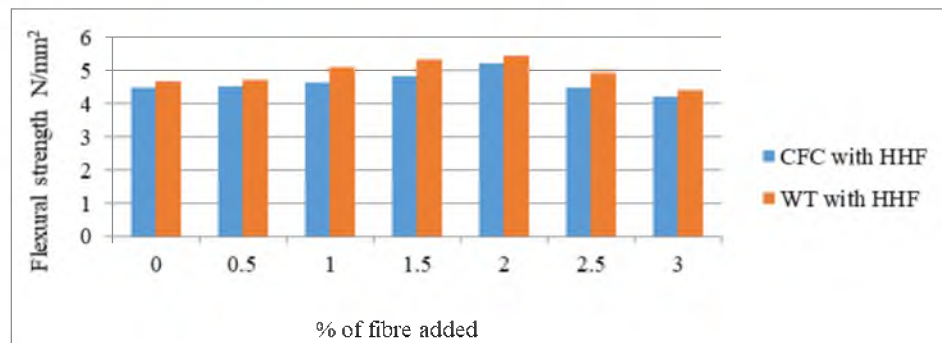


Fig.11 Flexural strength Vs % addition of HHF on CFC and WTC specimens with HHF

Table 6 shows the results of flexural strength of CFC and WTC with HHF. From the table it is clear that 2% of HHF shows a higher flexural strength for both CFC and WTC. Here also WTC with 2% HHF shows higher value than CFC. The results are shown in fig.11.

As a whole it is understood that WTC with HHF is performing better than CFC. Hence WTC with hair fibre can be recommended for pavement rehabilitation works.

7.4 Field observation results

Figures 12 to 15 shows the observation made on field on a particular day of WTC and CFC with and without HHF on the Date- 5.03.18 and figures 16 to 19 on the Date-07.04.18



Fig.12 WTC overlay without hair fibre **Fig.13** WTC overlay with hair fibre



Fig.14 CFC overlay without hair fibre **Fig.15** CFC overlay with hair fibre



Fig.16 WTC overlay without hair fibre **Fig.17** WTC overlay with hair fibre

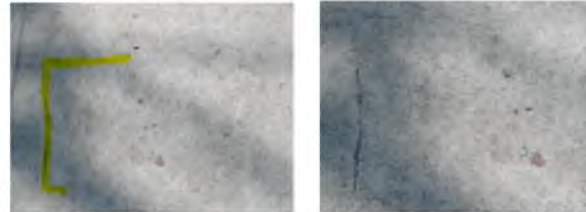


Fig.18 CFC overlay without hair fibre



Fig.19 CFC overlay with hair fibre

From these figures it is clear that field performance of WTC with HHHF was better than CFC. The observation done on 05.03.18, (fig.12 to 15), shows no visible distress for WTC with HHHF. However the specimen that is WTC without HHHF, CFC with and without HHHF observed on 07.04.18 shows mild defects. In the case of WTC without HHHF (fig.16) the transverse cracks were observed, which may be due to temperature stress, loading etc. But in the case of WTC with HHHF there were no such defects observed. (fig.17). So it can summarised that performance of WTC with HHHF is better than CFC specimens.

8 Conclusions

Following conclusions were drawn:

- Cell filled and Whitetopped overlays represent a new rehabilitation choice to address pavements with surface distress problems
- Addition of 1.5 percentage dosage of human Hair fibre gained an optimum value in the compressive strength for CFC and WT concrete
- Addition of 1.5 percentage of hair fibre in concrete achieves an characteristic strength greater than 50N/mm²
- Whitetopping concrete overlays shows a superior mechanical performance in the lab than that of Cell Filled concrete overlays
- Human hair fibre can reduce the risk of spalling of concrete
- The White Topping pavements show great potential to be a viable rehabilitation method due to easiness of construction

References

- 1 Modarres.A., Rahimzadeh.M and Zarrabi.M: Field investigation of pavement rehabilitation utilizing cold in-place Resources, *Conservation and Recycling, ELSEVIER* Volume 83 Pages 112-120.(2014)
- 2 Karlaftis, A.G. and Badr.A: Predicting asphalt pavement crack initiation following rehabilitation treatments, *Transportation Research Part C, ELSEVIER*, Volume 55 Pages 510-517, (2015)
- 3 Kambale.A., Jadhav.A., Gaikar.U., Gadade.S, and Chavan.A.D : Experimental Study on Ultra-Thin White Topping Use in Village Road, *International Journal of Scientific Research in Science, Engineering and Technology (IJSRSET)* ISSN : 2394-4099, Volume 4, Issue 6, pages.01-06, (2018)
- 4 Ankush .K and Sachdeva S.N.: A review of using thin whitetopping overlays for rehabilitation of asphalt pavements, *Journal of Basic and Applied Engineering Research* ISSN: 2350-0077. Volume 2, pages.182-252, (2015)
- 5 SinhaV.K., Tia and Kumar.S : Whitetopping A cost-effective rehabilitation alternative for preserving bituminous pavement on long term basic, *Journal of Indian Road Congress India* Volume 6, No 3. pages.223-240, (2007)
- 6 Subrat,R.,Reddy.K and Pandey B.B : An Investigation on Cell-filled Pavements, *International Journal of Pavement Engineering*. Volume 12, pages.21-55, (2010)
- 7 Kaushik.S., Reddy R.C and Mahendar, R.V: An Experimental Study on Mechanical Properties of Human Hair Fibre Reinforced Concrete, *IOSR Journal of Mechanical and Civil Engineering* Volume 12, Issue 4 pages 65-75, (2011)
- 8 IS 516 – 1959, Method of Tests for Strength of Concrete, *Bureau of Indian Standards*, New Delhi, India.
- 9 ASTM C496 / C496M – 11, Standard Test Method for Splitting Tensile Strength of Cylindrical Concrete Specimens, American Society for Testing and Materials, Philadelphia, Pennsylvania, 2006.
- 10 IRC: Sp-76: Tentative Guidelines for Conventional, Thin and Ultra-Thin Whietopping *Indian Road Congress*, New Delhi, (2008)

Influence of Gauge Length on the Measurement of Resilient Modulus of Bituminous Mixtures

Arbin Raj¹ and J. M. Krishnan²

^{1,2} IIT Madras, Chennai, 600 036, India
jmk@iitm.ac.in

Abstract. This paper investigates the influence of gauge length on the measurement of resilient modulus of bituminous mixtures with modified and unmodified binders tested at 25 °C. From this investigation, it is clear that for the tests carried out using a quarter-gauge length, the cumulative vertical deformations at the end of 200 preconditioning load cycles stays within 0.025 mm as stipulated in ASTM D7369 – 11. In the case of half-gauge length, the cumulative vertical deformation exceeds 0.025 mm after the application of 200 preconditioning load cycles. It was seen that the resilient modulus and Poisson's ratio computed from the deformations measured using quarter-gauge length exhibited better repeatability when compared to half-gauge length.

Keywords: Resilient modulus, Gauge length, Preconditioning, Poisson's ratio.

Introduction

Majority of the Indian highway network is constructed with bituminous materials. As per IRC: 37 – 2012 design procedures for bituminous pavements, the input material property for bituminous mixtures is resilient modulus. Resilient modulus is a material property which is used for characterising the stiffness of bituminous mixtures for use in mechanistic-empirical pavement design. The basic premise of resilient modulus is that within the linear regime when the applied load is considerably small when compared to the failure load, the material shows recoverable and irrecoverable deformations which are in the steady state (Fig. 1). The corresponding recoverable strain is defined as a resilient strain which is used in the calculation of resilient modulus. In a sense, resilient modulus can be considered as the elastic modulus based on the recoverable strain under repeated loads [3]. The various factors that affect the resilient modulus are diameter and thickness of the specimen, gauge length, temperature, magnitude and duration of loading, type of waveform, and the axis of loading [4].

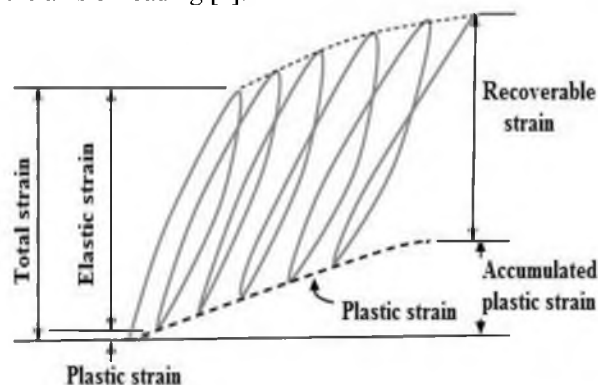


Fig. 1. Strains under repeated loading [3]

Earlier resilient modulus testing was carried out using ASTM test protocol [2] in which deformation is measured only in the horizontal direction, and the Poisson's ratio is assumed for finding the modulus value. Later this ASTM standard was withdrawn in 2003 and replaced with the new ASTM protocol (ASTM D7369-11, 2011) in which both the horizontal and vertical deformations are measured. In a heterogeneous material such as asphalt mixture, the

gauge length plays a critical role in the measurement of deformations. At this point, no clarity exists on the influence of gauge length on the computed resilient modulus. The present study is mainly focused on the influence of gauge length on the computation of resilient modulus values for unmodified and modified bituminous mixtures. In the following, a brief outline of the ASTM D7369-11 is provided.

Determination of Resilient Modulus as per ASTM D7369 – 11

The first step in the test procedure for estimating the resilient modulus value of bituminous mixtures is to compute the indirect tensile strength value of the specimen. Based on the indirect tensile strength value, the load to be applied to the specimen is selected for conducting the resilient modulus test. The load level selected for the test is limited to 10 – 20 % of indirect tensile strength value of the specimen for any given temperature.

This test can be carried out on cylindrical bituminous mixture samples with two different diameters of 101.6 mm and 152.4 mm and a thickness of 63.5 mm. As per the test protocol, one can use three different gauge lengths for computing resilient modulus value for bituminous mixtures (Fig. 2). The three different gauge lengths in relation to the diameter of the test specimens are ¼ of the diameter (25.4 mm for a 101.6 mm diameter of the specimen or 38.1 mm for a 152.4 mm diameter of the specimen), ½ of the diameter (50.8 mm for a 101.6 mm diameter of the specimen or 76.2 mm for a 152.4 mm diameter of the specimen) and one diameter. It should be noted that both the sides of the samples are fixed with LVDT's for an identical gauge length.

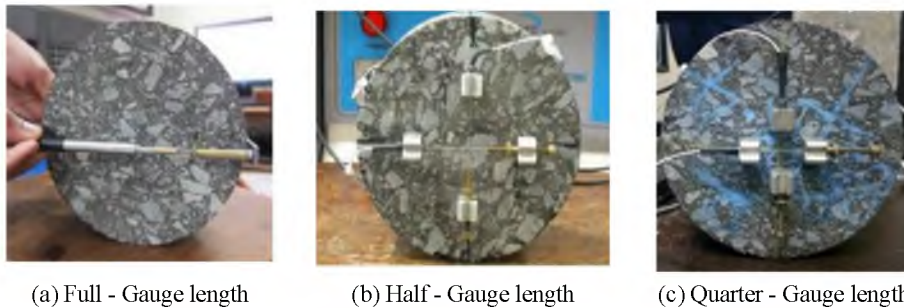


Fig. 2. Specimens fixed with various gauge lengths

As per test protocol [1], a split cylindrical sample is subjected to vertical compressive haversine loading of 1 Hz frequency at 25 °C. The sample shall be preconditioned along the axis of testing by applying a minimum 100 load cycles in the form of haversine pulse of 0.1 s loading and 0.9 s rest period. The next five cycles after preconditioning period are used for the computation of Poisson's ratio and resilient modulus. Both the preconditioning cycles and test load cycles constitute one sequence of loading. After one sequence of loading, the sample is rotated 90 degrees, and the sample is again subjected to the same sequence of loading. Thus, one sample is subjected to test at two different orientations, and the deformations are measured along the horizontal and vertical direction using the sensors mounted on the surface of the sample. Using a curve fitting technique specified in the test protocol, the total and instantaneous recoverable horizontal and vertical deformations are determined. The post-processing procedure involves computing Poisson's ratio (Equation 1) and the resilient modulus (Equation 2).

$$\mu = \frac{I_4 - I_1 \times \left(\frac{\delta_v}{\delta_h}\right)}{I_3 - I_2 \times \left(\frac{\delta_v}{\delta_h}\right)} \quad (1)$$

$$M_R = \frac{P_{cyclic}}{\delta_h \times t} (I_1 - I_2 \times \mu). \quad (2)$$

Here μ is the Poisson's ratio, M_R is the resilient modulus in MPa, δ_v and δ_h are the measured recoverable vertical deformation and horizontal deformation in mm respectively, t is the thickness of specimen in mm, P_{cyclic} is the cyclic load applied to the specimen in N, and I_1, I_2, I_3, I_4 are the constants which vary according to the gauge length positions as shown in Table 1.

Table 1. Constant values for M_R and μ calculation [1]

Gauge length as a fraction of diameter of specimen	I_1	I_2	I_3	I_4
0.25	0.144357	-0.450802	0.155789	-0.488592
0.50	0.233936	-0.780056	0.307445	-1.069463

As per the test protocol [1], one needs to test a minimum of 3 samples from each type for checking the repeatability of resilient modulus values within the laboratory, and the allowable standard deviation is stipulated as 7 %. Therefore, after testing one type of sample, one thus has 24 resilient modulus values, (3 trials \times 2 orientation \times 2 planes \times 2 deformations) and the required standard deviation is computed from such data set.

Experimental Investigation

In this study, bituminous concrete grade-2 with median grading and a binder content of 5 % was used. This investigation was carried out using one unmodified binder (VG30) which confirms to IS 73 (2013) and a modified binder (PMB40 (E)) which confirms to IS 15462 (2004). Samples with 150 mm diameter and 160 mm height were prepared using gyratory compactor, with 205 gyrations for the compaction process. The gyratory compacted samples were sliced into small cylindrical samples of 150 mm diameter and 63.5 mm thickness, and the sliced samples with an air void of 4 ± 0.5 % were used for this investigation. All the tests were carried out at 25 ± 0.5 °C with half - gauge length and quarter-gauge length.

The sample selected for conducting resilient modulus test was marked on both sides along the horizontal and vertical diametric axis. Depending upon the selected gauge length, the gauge points were glued on both sides of the sample surface along the horizontal and vertical axis using an alignment device. Finally, the LVDT's were mounted on top of the gauge points. The stepwise procedure for LVDT fixing is shown in Fig. 3.

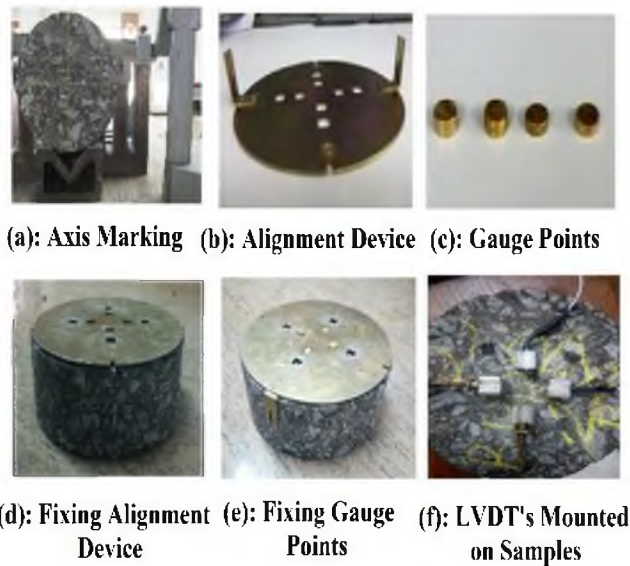


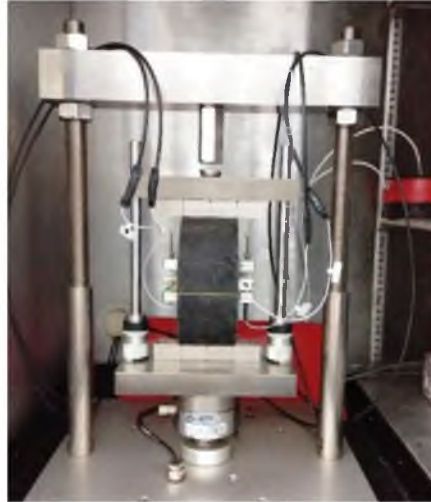
Fig. 3. Stepwise procedure for LVDT fixing

Before the conduct of resilient modulus test, the indirect tensile test was carried out to determine the indirect tensile failure load. As per the test protocol, one can use 10 – 20 % of the failure load for conducting resilient modulus test. The indirect tensile test was carried out for samples prepared with each binder at 25 °C followed by the procedure outlined in ASTM D6931 – 17 (2017). The maximum load at which the sample fails is taken as the indirect tensile failure load of the sample. In this investigation, 10 % of indirect tensile failure load was used for testing unmodified and modified binders. The indirect tensile failure load at 25 °C and the load level (10 %) used for this study is tabulated in Table 2.

Table 2. Indirect Tensile strength load of bituminous samples at 25 °C

Binder	IDT failure load (kN)	Load level used for testing (10 %)
VG30	24.32	2.432
PMB40 (E)	21.10	2.110

Before conducting the resilient modulus test, the sample is placed inside the temperature controlled cabin kept at test temperature for a minimum duration of 6 hours for conditioning. Then the sample is placed on the test device for testing in such a way that it is sandwiched between the top and bottom loading strips as shown in Fig.4. The bottom loading strip is a fixed one while the top one is free to move.

**Fig. 4.** Alignment of the sample inside the loading strips

Instead of 100 preconditioning cycles as stipulated in ASTM D7369 – 11, 200 preconditioning load cycles were applied such that the sample exhibits a constant strain rate [8]. After 200 preconditioning cycles, the next five cycles were used for the post-processing analysis. The deformations in both horizontal and vertical directions for zero and 90-degree orientations were measured using the sensors mounted on the surface of the sample and recorded for all the 205 load cycles at every 0.001-second interval using UTS 003 software [5]. The deformation was analysed to calculate the total horizontal recoverable deformation and total vertical recoverable deformations for each cycle following the curve fitting procedure mentioned in the test protocol [1]. Using the total horizontal and vertical recoverable deformations, both Poisson's ratio and the resilient modulus values were computed

Results and Discussion

As per test protocol [1], one can conduct the test for all the three different gauge lengths before selecting the resilient modulus value. In this investigation, half-gauge length and quarter-gauge length was selected, and the influence of gauge length is discussed below.

Influence of Gauge Length

From the Fig. 5, it is observed that the cumulative vertical deformation for the VG30 sample at the end of 100 preconditioning cycles using half-gauge length and quarter-gauge length was found to be less than 25 μm . When the sample is subjected to 200 preconditioning cycles with half-gauge length, the cumulative vertical deformation exceeded 25 μm . However, for quarter-gauge length, the cumulative vertical deformation for VG30 sample stayed within 25 μm without much variability between different planes (Fig. 6). Similar observations were seen in the case of modified binder (PMB40 (E)) tested at same load levels and same testing temperature for both the gauge lengths (Fig. 7 and Fig. 8).

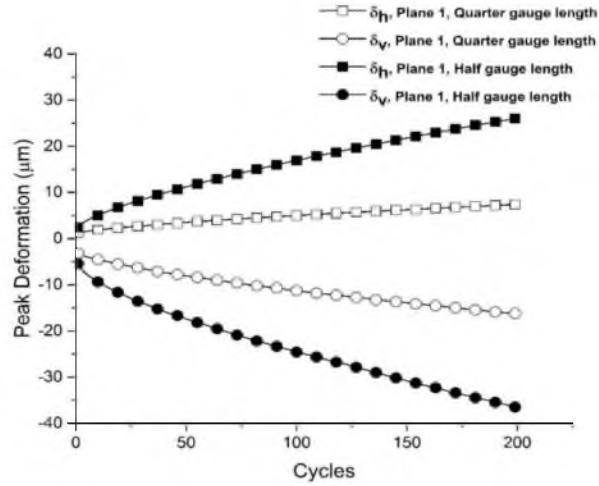


Fig. 5. VG30 with 200 preconditioning cycles

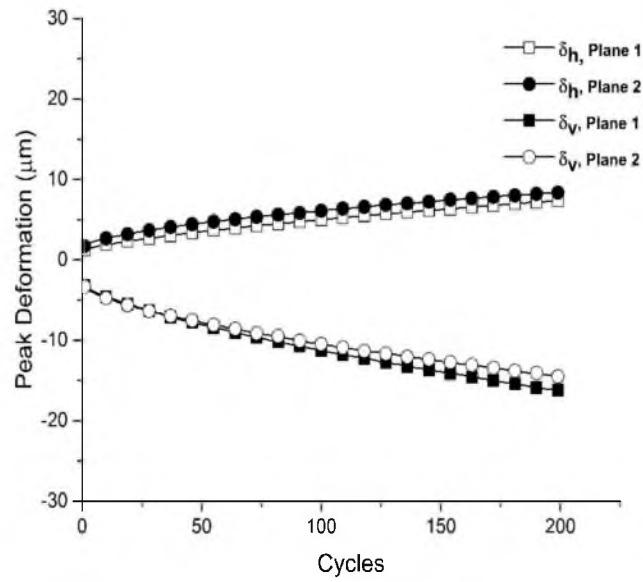


Fig. 6. VG30 with 200 preconditioning cycles (Quarter-gauge length)

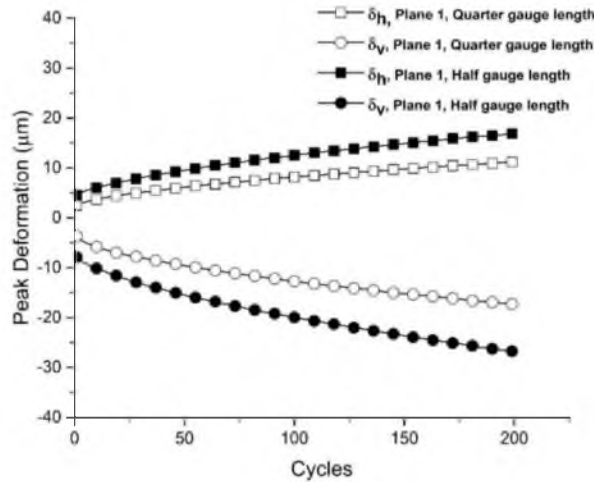


Fig. 7. PMB40 (E) with 200 preconditioning cycles

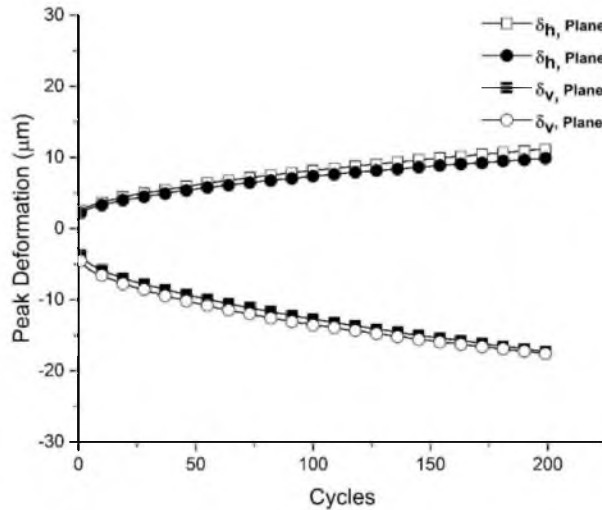


Fig. 8. PMB40 (E) with 200 preconditioning cycles (Quarter-gauge length)

The preconditioning load cycles are provided to ensure that the sample reaches a steady state. If the sample deformation exhibits steady state, the variability in the computed resilient modulus values can be reduced. From observing the above test results, if one uses a quarter-gauge length, the number of preconditioning cycles required is 200, and steady state can be reached. However, in the case of samples tested using half-gauge length, with 200 preconditioning cycles, it is difficult to reach steady state.

Effect of Gauge Length on Resilient Modulus

Table 2 and 3 shows the computed resilient modulus and Poisson’s ratio corresponding to instantaneous and total recoverable deformations for unmodified and modified binders tested using half and quarter-gauge length at 25 °C.

Table 3. Test results for unmodified binder (VG30) at 25 °C

Plane	Quarter-Gauge Length				Half-Gauge Length			
	Instantaneous		Total		Instantaneous		Total	
	μ	M_R	μ	M_R	μ	M_R	μ	M_R

0 Degree	1	0.22	10637	0.21	7510	0.36	11565	0.35	7282
	2	0.24	11110	0.26	8729	0.42	11892	0.30	7948
90 Degree	1	0.23	11410	0.24	8231	0.25	10054	0.35	6574
	2	0.25	10726	0.27	8272	0.27	11010	0.26	7040

Table 4. Test results for modified binder (PMB40 (E)) at 25 °C

Plane		Quarter-Gauge Length				Half-Gauge Length			
		Instantaneous		Total		Instantaneous		Total	
		μ	M_R	μ	M_R	μ	M_R	μ	M_R
0 Degree	1	0.29	8777	0.30	5958	0.33	9668	0.30	6363
	2	0.30	8908	0.32	6379	0.31	9818	0.25	7081
90 Degree	1	0.30	9082	0.33	6981	0.40	9358	0.35	6512
	2	0.26	8645	0.27	6137	0.24	8987	0.13	6179

From the above data, it is seen that the resilient modulus values computed using instantaneous recoverable deformations are high when compared to the resilient modulus computed using total recoverable deformations. If one compares the resilient modulus values estimated using quarter-gauge length, unmodified binder shows higher modulus value than the modified binder at 25 °C. In the case of half gauge length, it is difficult to point out the variation in the resilient modulus values between unmodified and modified binders. Analyzing the test results from the perspective of gauge length, the variation in the estimated resilient modulus values are less for the quarter-gauge length and half-gauge length. However, the variability in the estimated values for Poisson's ratio and resilient modulus between different planes and orientation were observed as less (standard deviation is less than 7 %) for quarter-gauge length.

Summary

In this paper, the influence of two different gauge lengths on the measurement of resilient modulus for bituminous mixtures with modified and unmodified binders was studied. This study was carried out as per the ASTM D7369 – 11 test protocol. The following conclusions derived from this investigation are as follows;

- It is possible to achieve steady state for a sample tested with $\frac{1}{4}$ th diameter of the specimen as gauge length (quarter) when subjected to 200 preconditioning cycles. In the case of gauge length, the sample may reach a steady state when subjected to more number of preconditioning cycles.
- Since the sample reaches a steady state when subjected to 200 preconditioning cycles, the variability was found to be less in the computed resilient modulus and Poisson's ratio for quarter-gauge length testing. This implies that the test results obtained from quarter-gauge length show more precision when compared to half-gauge length.
- For quarter-gauge length, the computed instantaneous and total resilient modulus value for unmodified binder was higher than the modified binder. Since the variability in the test results is more, comparison of the resilient modulus values for different binders with half-gauge length was not well established

Acknowledgements

The authors thank Department of Science and Technology, Govt. of India [grant number DST/TSG/STS/2011/46] for the funding and IPC Global, Australia for the technical support provided during the experimental investigation.

References

1. ASTM D7369-11, Standard Test Method for Determining the Resilient Modulus of Bituminous Mixtures by Indirect Tension Test, ASTM International, West Conshohocken, PA, (2011).
2. ASTM D4123-82, Standard Test Method for Indirect Tension Test for Resilient Modulus of Bituminous Mixtures (Withdrawn 2003), ASTM International, West Conshohocken, PA, (1995).
3. Huang, Y.H.: Pavement analysis and design, 2nd edition, Englewood Cliffs, New Jersey, Prentice Hall,(2004).
4. Fairhurst, C. E., Kim, Y. R., and Khosla, N. P.: Resilient modulus for testing of asphalt specimens in accordance with ASTM D4123 – 82, Fourth International RILEM Symposium, Hungary, 402-408, (1992).
5. IPC Global, Resilient modulus testing UTS 003 - Technical reference manual, IPC Global, Victoria, Australia, (2017).
6. ASTM D6931-17, Standard Test Method for Indirect Tensile (IDT) Strength of Asphalt Mixtures, ASTM International, West Conshohocken, PA, (2017).
7. IRC: 37-2012, Guidelines for the design of flexible pavements, Indian Roads Congress, New Delhi, India, (2012).
8. Arbin Raj, and J. M. Krishnan.: Inconsistencies in the measurement of resilient modulus of bituminous mixtures, ASTM Journal of Testing and Evaluation (To be communicated, 2018).

Influence of Rest Period and Confinement Pressure on the Measurement of Dynamic Modulus of Bituminous Mixtures

Devika. R¹, Sriram. V², J. Murali Krishnan³

¹ Project Associate, Dept. of Civil Engineering, IIT Madras, Chennai, 600036, India

² Final Year B.Tech. Student, Dept. of Civil Engineering, SASTRA University, Thanjavur, 613401, India

³ Professor, Dept. of Civil Engineering, IIT Madras, Chennai, 600036, India
jmk@iitm.ac.in

Abstract. This paper investigates the variation of dynamic modulus and phase lag with confinement pressure and rest period. In this investigation, bituminous mixtures fabricated with unmodified VG30 binder were used and tested as per AASHTO: TP-79 (2010) protocol incorporating confinement pressure and rest period between successive frequencies. The analysis of the data showed that there is a considerable change in the modulus of the material with the application of confinement pressure. The phase lag at higher temperature exhibited decreasing values at lower frequencies similar to what is seen in test procedure without any rest period.

Keywords: Dynamic modulus, phase lag, confinement pressure, rest period.

Introduction

Majority of the Indian highways are bituminous. A robust design procedure is to be followed to achieve the full advantage of the pavement during its design life. Currently, the Mechanistic-Empirical Pavement Design Guide (M-EPDG) [7] recommends dynamic modulus as a parameter for the mechanical characterisation of the bituminous mixtures.

Determination of dynamic modulus is carried out using an Asphalt Mixture Performance Tester (AMPT). The AASHTO: TP-79 (2010) [1] test method for the determination of dynamic modulus as a function of frequency is carried out in AMPT. Ten different frequencies (25, 20, 10, 5, 2, 1, 0.5, 0.2, 0.1 and 0.01 Hz) are suggested, and the test is conducted from the highest to the lowest frequency without any rest period between subsequent frequencies. The UTS 006 [8] software calculates the required load to be applied in such a way that the targeted strain lies between 75 and 125 micro-strain. It is assumed that in this strain range the response of the material is linear. Considerable issues exist in the computation of dynamic modulus and phase lag when using this test protocol.

Since only dynamic modulus and the associated master curve are used in pavement design, not much attention is focused on the variation of phase lag as a function of frequency. Deepa et al. (2017) [3] has shown from a careful analysis of the dynamic modulus data that a phase lag can decrease as the frequency decreases especially for temperatures above 35°C. While this is considered as an ‘anomalous’ behavior in many literatures [2 and 5], Deepa et al. (2017) have shown that it is indeed the characteristic trait of a viscoelastic material when subjected to loading without rest periods. It is expected that such variation of phase lag will influence the dynamic modulus computed. Also, it is not clear how the application of confinement pressure during testing can change the dynamic modulus and phase lag.

This paper aims at determining whether the inclusion of rest periods will lead to a decrease of phase angle for a decrease in frequency. Also, in these test protocol, the influence of confinement pressure during testing was investigated.

Experimental Investigation

Test Matrix

A total of 4 set of testing conditions were used, and the associated results were collected. These correspond to a) without rest period and confinement condition (NCNRP) (control sample), b) with a rest period and without confinement condition (NCRP), c) without rest period and with confinement condition (CNRP) and d) with a rest period and confinement condition (CRP). The test matrix followed for carrying out the experimental investigation is given in Table 1. A total of 24 samples were tested. Some of the trials were repeated for checking the repeatability and was found to be well within limits.

Table 1. Test Matrix – dynamic modulus

Sample	Pressure applied (kPa)	Rest Period (minute)	Temperature (°C)	Total number of samples
VG 30	0 , 200	0,2	5, 15, 25, 35, 45, 55	2×2×6 = 24

1.1. Material Properties

As a part of this study, an unmodified VG30 binder was used to fabricate samples. The binder was tested as per IS: 73-13(2013) [4]. The binder test results are tabulated in Table 2. The bituminous mixture chosen was Bituminous concrete (BC – Grade 2) with a nominal maximum aggregate size of 13.2 mm. The current study employed mid-gradation with a binder content of 5.2%. The gradation as per MORTH (2013) [6] is shown in Figure 1.

Table 2. Material properties of unmodified binder (IS: 73-13 2013)

Characteristics	Result
Penetration at 25°C, 100g, 5s, 0.1mm	40
Absolute viscosity at 60°C, Poises	3438
Kinematic viscosity at 135°C, cSt	544
Softening Point, (R&B), (°C)	51
Viscosity ratio at 60°C	2
Ductility at 25°C after rolling thin film oven test, cm	100+

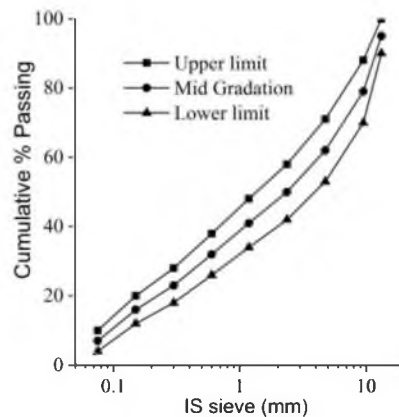


Fig. 1. Aggregate Gradation

1.2. Sample Preparation

The batching of aggregate was done as per the mid-gradation. The mixing and compaction temperature for the binder was determined using the viscosity-temperature relationship. Based on this, the binder was heated to a temperature of 165°C. The mixing of aggregate and binder was carried out in an automatic mixer machine. After mixing, the mixture was short-term aged for 4 hours at 135°C and 0.5 hours at 155°C

for compaction. At the end of 4.5 hours, cylindrical samples were cast using a Superpave gyratory compactor. A vertical pressure of 600 kPa and 205 gyrations were applied to the sample at an angle of 1.25° to produce specimens of 165 mm height and 150 mm diameter. The samples were then cored and sliced to 150 mm height and 100 mm diameter specimen for testing. The samples used for carrying out the test had air voids in the range of $4 \pm 0.5\%$.

The test specimens were then fixed with hexagonal studs to which the LVDT's were clamped before the test. The studs were glued to the specimens using a stud fixing jig maintaining a gauge length of $70 \pm 1\text{mm}$. Three axial LVDT's were mounted on the specimen at an angle of 120°. Figure 2 shows the procedure followed for the stud fixing.



Fig. 2. Stud fixing

2. Test Results and Analysis

2.1. Test protocol

Figure 3 depicts the load application with a rest period and confinement pressure. The UTS006 software records the axial deformation using the three displacement transducers as a function of time for all the twenty cycles. This data is used to calculate the dynamic modulus and phase lag.

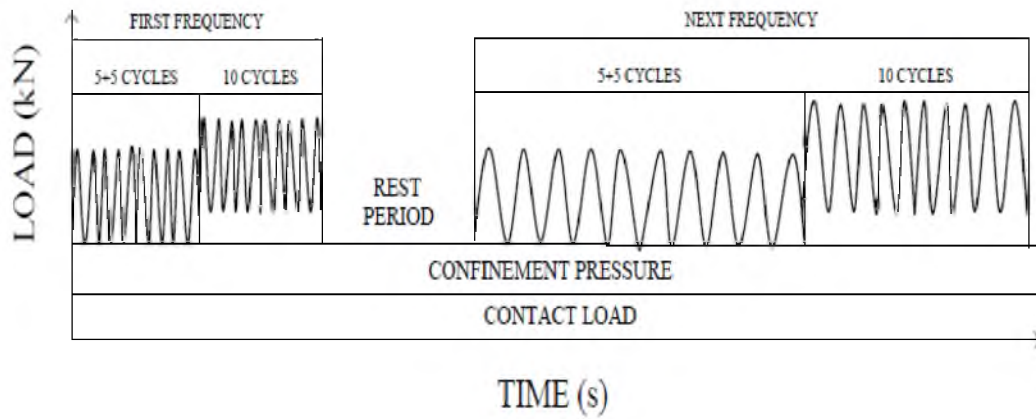


Fig.3. Schematic representation of the modified protocol

2.2. Variation of dynamic modulus with confinement

The variation of dynamic modulus with frequency for three different temperatures is shown in figure 4(a)-(c). It can be observed from the plots that the dynamic modulus increases considerably with the application of confinement pressure, especially at higher temperatures.

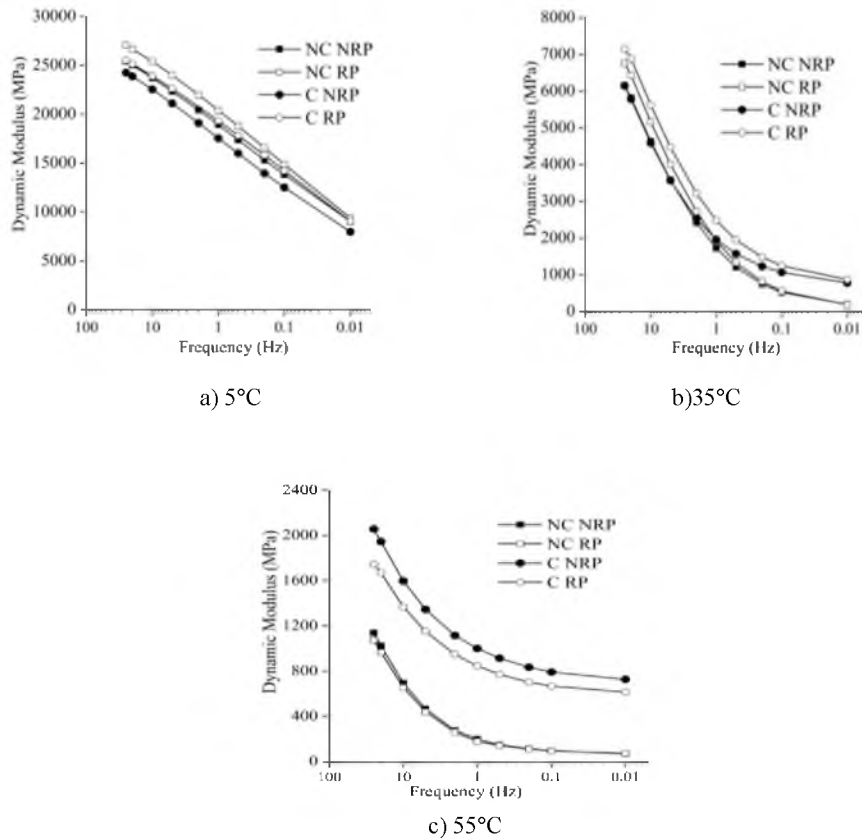


Fig.4. Dynamic modulus vs frequency for different temperatures

At low temperatures and high frequency (for instance 5°C and 25 Hz), the dynamic modulus at confined conditions is almost 6% less than the unconfined conditions. At intermediate conditions (for instance 35°C and 1 Hz), the dynamic modulus at confined conditions is nearly 17% more than of the unconfined conditions. At the very high temperature and low frequency (for instance 55°C and 0.01 Hz), the dynamic modulus at confined conditions is 90% more than that at unconfined conditions.

2.3. Trends in phase lag data

The variation of phase lag with the frequency at different temperatures for all the four conditions is shown in figure 5 and 6. It can be seen from the plots that the phase lag increases with decreasing frequency at a lower temperature for all the conditions. A reverse trend in phase lag was observed at a higher temperature that is the phase lag was seen decreasing with a decrease in frequency even when tested using the modified protocol, by providing confinement and rest period.

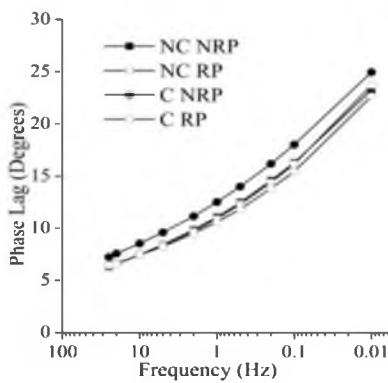


Fig.5. Phase lag vs frequency for 5°C

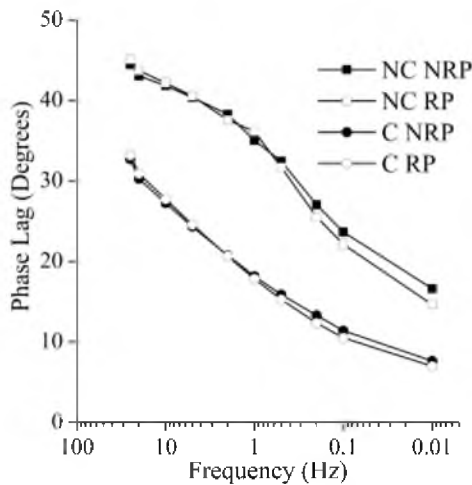


Fig.6. Phase lag vs frequency for 55°C

Conclusion

This paper looked into modifying the existing AASHTO: TP-79 (2010) protocol to determine the dynamic modulus and phase lag. From the analysis of the data, it was seen that there is an appreciable increase in the dynamic modulus

with the application of the 200kPa confinement pressure at higher temperatures. This may be attributed to the fact that the mastic in the bituminous mixtures exhibits considerable pressure sensitive nature at high temperature (45, and 55°C) and all frequencies. One of the possible reasons for the decrease in phase lag with decreasing frequency at high temperatures even with the application of confinement and rest period may be due to the increase in strain after the initial decrease in strain when the sample is subjected to a hydrostatic state of stress.

Acknowledgements

The authors thank Department of Science and Technology, Govt. of India [grant number DST/TSG/STS/2011/46] for the funding and IPC Global, Australia for the technical support provided during the experimental investigation.

References

- AASHTO: TP-79, 2010. Standard method of test for determining the dynamic modulus and flow number for hot mix asphalt using the asphalt mixture performance tester (AMPT). American Association of State Highway and Transportation Officials, Washington, DC (2010).
- Bonaquist, R.: NCHRP Report – 629, ruggedness testing of the dynamic modulus and flow number tests with the simple performance tester. Washington, DC: Transportation Research Board (2008).
- Deepa, S., Saravanan, U., and Murali Krishnan, J.: On measurement of dynamic modulus for bituminous mixtures. International Journal of Pavement Engineering, DOI:10.1080/10298436.2017.1380809 (2017).
- IS: 73-13, 2013. Paving bitumen – specification, Bureau of Indian Standards, New Delhi, India (2013).
- Lee, K., et al.: Dynamic modulus of asphalt mixtures for development of Korean pavement design guide. Journal of Testing and evaluation, 35 (2), 143-150 (2007).
- MORTH, 2013. Specification for roads and bridge works, 4th revision, Ministry of Shipping, Road Transport and Highways, New Delhi, India (2013)
- NCHRP: 1-37A, ed. Guidelines for the mechanistic-empirical design for new and rehabilitated pavement structures. Washington, DC: Transportation Research Board (2004).
- UTS006, 2017. SPT dynamic modulus test software reference. Australia: IPC Global (2017).

How to consistently collect rheological data for bitumen in a Dynamic Shear Rheometer?

P.S.Divya¹ and J. Murali Krishnan²

¹Project Officer, Dept. Of Civil Engineering, IIT Madras, Chennai-600036.

²Professor (Corresponding Author), Dept. Of Civil Engineering, IIT Madras, Chennai-600036.

E-mail: jmk@iitmadras.ac.in

Abstract. The measurement of rheological properties of binders is dependent on various factors such as time, temperature as well as on aging. The common causes of erroneous measurements that occur during the rheological tests are related to the sample conditioning and sample loading. Bituminous binders are subjected to steric hardening while stored at room temperatures and thus can cause increased stiffness during measurement. Gap setting and sample loading also play a key role in obtaining consistent data using a Dynamic Shear Rheometer (DSR). In this article, the issues one should understand to collect rheological data for bitumen in a DSR consistently are addressed.

Keywords: Dynamic Shear Rheometer (DSR), Rheology, Steric Hardening.

1. Introduction

Rheological properties of binders are of utmost importance for characterizing the fundamental and performance-based properties. The rheological characterization is influenced by various factors such as aging, time and temperature. These factors have to be taken into account to obtain a consistent data from rheological tests. Preconditioning measures have to be taken to avoid erroneous measurements due to the influence of these factors.

Steric hardening of binders is a common cause of increased stiffness in binders which estimates up to 50% increase in modulus (ASTM D7175, 2015). It is a reversible aging which occurs when bituminous binders are stored at ambient temperatures (Little et al., 2018). This reversible aging can be removed by conditioning the sample at temperatures near to the softening point before any rheological test.

Sample loading, gap setting and the quantity of the sample used while testing in DSR is also crucial parameters which decide on the reliability of the data obtained. Gap setting of the measuring systems in DSR is dependent on the sample loading temperatures. As bituminous binders are loaded near to softening point temperatures, the gaps are subjected to change due to thermal expansion of the measuring geometries. This variation in gaps can alter the sample thickness which can lead to the variation in the modulus values. The DSR measures the torque and the deflection angle made by the top plate with respect to the bottom plate at the periphery. As per ASTM D7175 (2015), after trimming of the sample, a bulge should be produced at the sample's outer surface. Hence it should be ensured that sufficient amount of the sample is placed on the plate so that it is completely covered for the accurate data measurements.

The objective of this paper is to emphasize the various issues encountered based on the above factors while performing rheological tests and the measures to be taken to overcome these issues for obtaining consistent data.

2. Experimental Plan

The main issues associated with the performance of rheological experiments using a DSR are explained in the following section. For this purpose, steady shear and frequency sweep experiments (Table 1) were conducted using Anton Paar make DSR (Modular Compact Rheometer 302). Table 2 shows the properties of VG30 used for testing as per IS73:2013.

Table 5 Test Matrix

Temperature (°C)	Test	Frequency Range (Hz)	Shear rate (1/s)	Strain (%)	Computed Parameters	Data Acquisition
35	Frequency Sweep	50 to 1	-	0.05	G' , G'' and δ	Data collected for every 1 s, a total of 490 data points were collected.
	Steady Shear	-	1 and 5	-	$\dot{\gamma}$ and η	Data collected for every 1s, a total of 300 data points were collected.

Table 6 Material Properties

Tests (As per IS73:2013)	Measurements
Penetration at 25°C, 0.1 mm, 100g, 5s (Spec. value = 45 min.)	50
Softening Point, (R&B),°C (Spec. value = 47 min.)	52
Absolute viscosity at 60°C, Poises (Spec. value =2400-3600)	3022
Viscosity ratio at 60°C (Spec. value = 4.0 max.)	1
Kinematic viscosity at 135°C, cSt (Spec. value = 350 min.)	595

3. Results And Discussions

3.1 Steric Hardening

Bituminous binders undergo steric hardening when stored at ambient temperatures. Steric hardening also referred to as reversible aging is a time-dependent behaviour in which one sees secondary molecular associations which result in increased stiffness of the binders. This increase in stiffness can overestimate the modulus approximately up to 50%. ASTM D7175 (2015) recommends annealing of the samples stored at ambient temperatures before testing. It is suggested that one should heat the sample in an oven to a temperature of not more than 163°C so that it is sufficiently fluid with occasional stirring such that the entrapped air bubbles are removed. The reversible aging can also be removed by conditioning the sample in a water bath maintained at a temperature near to the softening point of the binder. In such procedure, the required amount of the sample to be tested is taken in a sealed steel container and maintained in the water bath at the required temperature for 1 hour.

To illustrate the influence of steric hardening and the necessity to condition the samples, frequency sweep tests were carried out (Table 1) with and without conditioning for a VG30 binder and the results are shown in Figure 1 and 2.

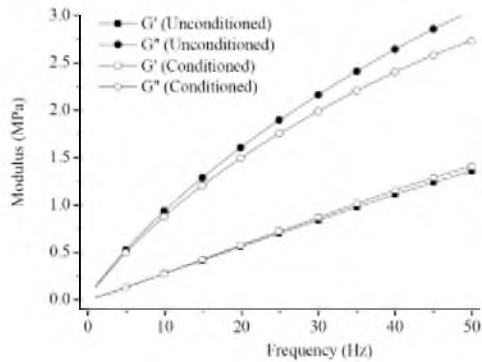


Fig.2 Modulus vs Frequency

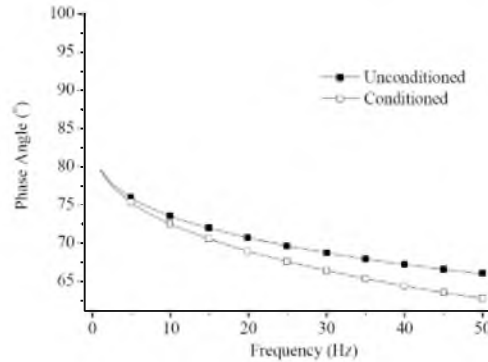


Fig.3 Phase lag vs Frequency

3.2 Gap Setting

One of the crucial steps for obtaining reliable results from DSR is the gap setting of the measurement geometry. ASTM D7175 (2015) does not provide enough details on the steps for overcoming this issue. When the tests are carried out at temperatures in the range of 20–40°C, the loading of samples is carried out at temperatures at least 10°C higher than the softening point of the binders (preferably 60°C). Due to such temperature change, the top and bottom plates in a parallel plate arrangement can undergo thermal changes which can lead to erroneous measurements. Hence it is recommended that a gap setting is performed at the test temperature, loading temperature as well as at an intermediate temperature between the test and loading temperature.

To emphasize the above issue, the frequency sweep test results are shown for two cases. In the first case, the gap setting was carried out at 60 and 35°C and in the second case, the gap setting was done only at 60°C. Figures 3 and 4 show the difference in modulus and phase lag obtained related to the same. The significant difference in the loss modulus (G'') and phase angle can be clearly seen.

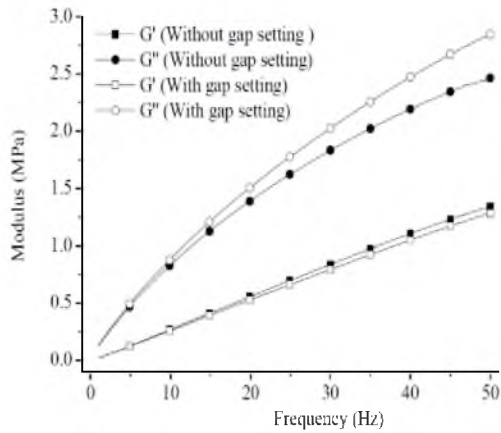


Fig.4 Modulus vs Frequency

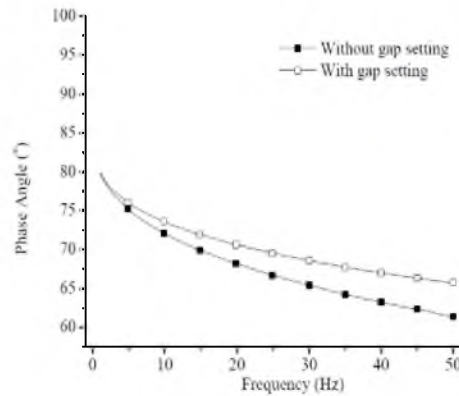


Fig.5 Phase lag vs Frequency

3.3 Sample Filling

The amount of sample taken for performing the test is an important parameter for the correct measurement of the parameters. It should be ensured that the measuring plates should be covered with the sample completely. As per ASTM D7175 (2015), sufficient sample should be placed so that while the trimming of the excess sample is complete and the required gap is attained, a slight bulge is created. However, ASTM D7175 (2015) does not clearly specify the additional amount of sample to be provided in the bulge. Such care is required when one is carrying out temperature sweep experiment (higher to lower) wherein a significant contraction in the sample is expected in all the directions. In the DSR for testing a sample at a gap of 1mm, the sample is trimmed at a gap of 1.05mm. At a gap of 1.05mm, the volume of sample is 0.515ml which are retained in the actual volume of 0.490 ml at 1mm thus causing the sample to slightly bulging out. Figure 5 shows how sample filling should be carried out for a cone and plate assembly.

In this investigation, testing was carried out for two cases, with underfilled and with correct filling. In figure 6, the gap between the top and bottom plate can be observed due to insufficient sample. Figure 7 shows a properly trimmed sample with a bulge at the outer face of the plates. Figures 8 and 9 shows the results obtained for an underfilled and a correctly trimmed sample. It can be noted that the modulus values obtained from an underfilled sample are very much lesser than that obtained from a properly trimmed sample.

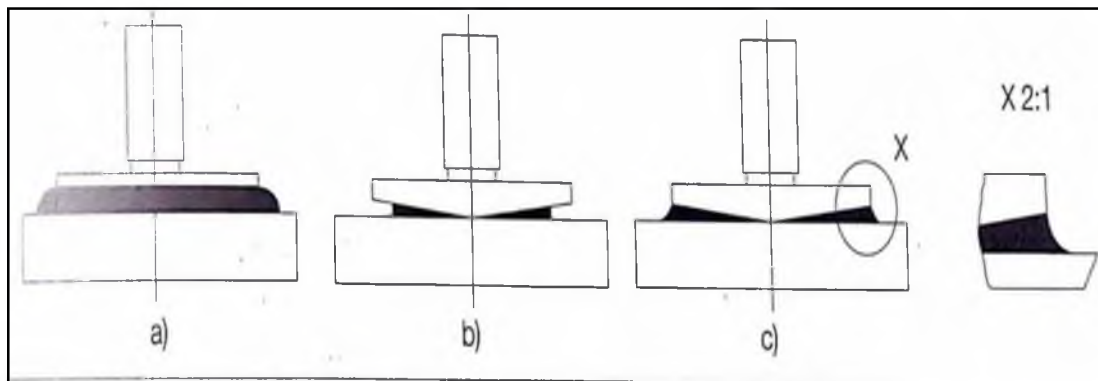


Fig.6 Overfilled, underfilled and correctly filled sample (Mezger, 2015)



Fig.7 Underfilled Sample



Fig.8 Correctly filled Sample

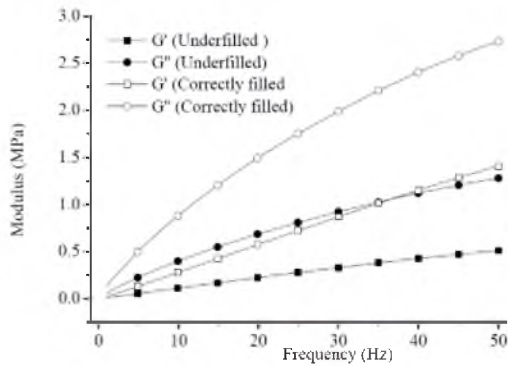


Fig.9 Modulus vs Frequency

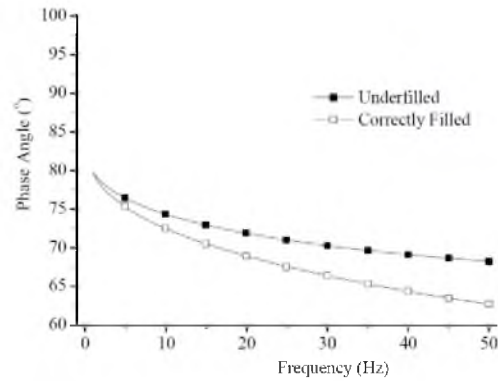


Fig.10 Phase lag vs Frequency

3.4 Torque limit

The DSR motor has a minimum and maximum torque capacity (0.05mNm and 200mNm respectively for MCR302) within which it can measure the data accurately. The torque limit varies with the capacity of the motor used. Hence all the input test parameters should be such that the measured torque is within limits for obtaining consistent data. Figure 10, 11 and 12 show the data for a steady shear experiment.

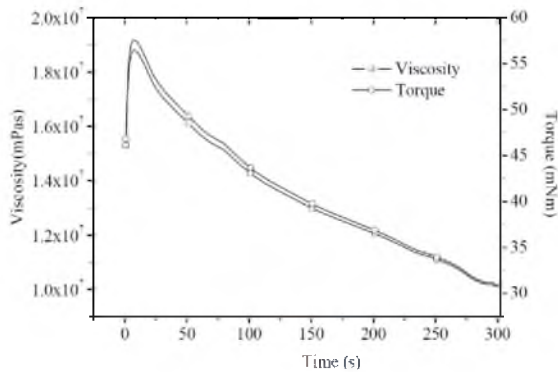


Fig.11 Within Torque Limit

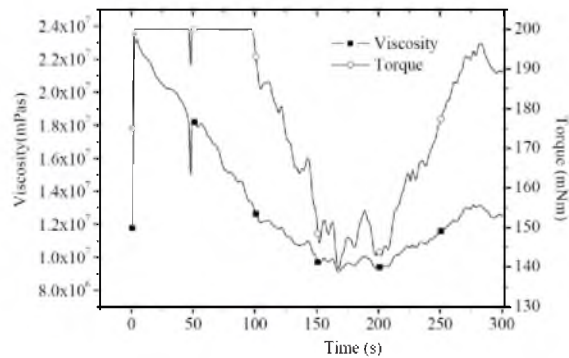


Fig.12 Torque Limit Exceeded

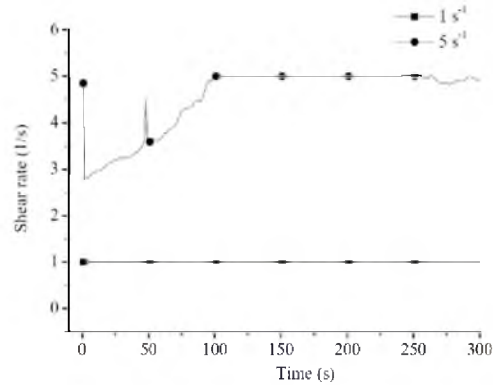


Fig.13 Comparison of shear rate

Figure 10 shows the data for a shear rate of 1 s^{-1} in which the peak torque obtained is 55 m-Nm which is within limits. Figure 11 shows the data for a shear rate of 5 s^{-1} for which the peak torque is 200 m-Nm which is the maximum torque capacity for MCR302 series. As this shear rate has exceeded the torque limit, it can be observed that the viscosity data is inconsistent and erroneous. Figure 12 shows the steady shear variation with time. For a shear rate of 1 s^{-1} , it can be observed that the shear rate is maintained throughout the test duration. For a shear rate of 5 s^{-1} as the torque limit has exceeded, the shear rate has reduced and was not maintained constant during the test duration.

4. Conclusions

- The effect of steric hardening plays an important role in the rheological measurement of binders. Proper conditioning of the samples is required to overcome such effect to obtain consistent data.
- The gap setting at the loading and testing temperature is necessary to get consistent data. The temperature compensation of the measurement geometry plays a critical role.
- During the measurement, the loading of a precise volume of the sample is of utmost importance since computation of the strain is carried out close to the periphery of the parallel plates in the DSR.
- The sensitivity of the equipment to record torque within the tolerances prescribed should be strictly adhered to.

5. Acknowledgements

The authors thank Department of Science and Technology, Government of India for providing funding for the purchase of binders. The grant number is DST/TSG/STS/2011/46. The authors would like to acknowledge Anton-Paar, India for the useful technical discussion.

References

1. Anton Paar (2014). "Instruction Manual for Peltier Systems and MCR series." Anton Paar GmbH, Graz, Austria.
2. ASTM D7175 (2015). Standard Test Method for Determining the Rheological Properties of Asphalt Binder Using a Dynamic Shear Rheometer. ASTM International, West Conshohocken, PA.
3. Little, D.N., Allen, D.H. and Bhasin A. Modeling and Design of Flexible Pavements and Materials. Springer, 2018.
4. Mezger, T.G., Applied Rheology: with Joe Flow on Rheology Road. Graz, Austria: Anton Paar, 2015.
5. Origin Pro 8. Origin laboratory, Northampton, MA, 2010

Moisture Conditioning Process for Large-Sized Prismatic Straight Beam Specimens of Bituminous Concrete

Utsav Vishal¹, Venkaiah Chowdary¹, J. Murali Krishnan²

¹National Institute of Technology, Warangal - 506004, Telangana, India

²Indian Institute of Technology Madras, Chennai - 600036, Tamil Nadu, India. jmk@iitm.ac.in

Abstract. This study proposes a moisture conditioning process for large-sized prismatic beam specimens of bituminous concrete. Such beams are required for evaluating the fatigue characteristics of bituminous mixtures in a four-point beam bending test. The current moisture conditioning protocols are aimed at cylindrical specimen only, and no guidelines are available for prismatic beams; especially when these beams are compacted to lower air voids content. In this study, prismatic beam specimens of bituminous concrete mixed with VG-30 and CRMB-60 binder were prepared. In addition to the control samples, warm mix asphalt and lime additive added samples were also produced. Warm mix asphalt was produced using a surfactant based warm mix additive. Lime was added to both hot mix and warm bituminous mixtures. Prismatic beams with target air voids of $4 \pm 0.5\%$ and with dimensions of 0.38 ± 0.006 m (length) \times 0.050 ± 0.002 m (width) \times 0.063 ± 0.002 m (height) were produced. These specimens were subjected to partial vacuum saturation by submerging completely in water. The vacuum pressures and durations were adjusted such that the desired saturation could be achieved. The saturated bituminous concrete beam specimens were mechanically weakened through the freeze-thaw conditioning. It is observed that the binder type plays a significant role in the degree of saturation whereas the influence of additives is negligible on the degree of saturation.

Keywords: Air Voids, Degree of Saturation, Lime, Moisture Conditioning, Prismatic Straight Beam, Vacuum Saturation, WMA Additive.

1 Introduction

Most of the bituminous roads fail prematurely due to poor drainage. Moisture accelerates the rate of distresses in bituminous pavements. Very limited information is available on how to understand and quantify the effects of moisture induced damage in bituminous mixtures. Determination of moisture sensitivity of bituminous mixtures is one of the most critical aspects to be considered for evaluating the performance of bituminous pavements as the high moisture susceptible bituminous mixtures will deteriorate at a much rapid rate. Hence, simulation of field moisture damage conditions in the laboratory is required such that bituminous mixtures that are more resistant towards the moisture damage could be identified.

Traditionally, AASHTO T283 [2] test protocol is practised to simulate the moisture damage conditions in the laboratory. This protocol is prescribed for cylindrical specimen geometries. A moisture-conditioned sample is subjected to indirect tension testing, and the ratio of the failure load with a control sample is used as a criterion to rank bituminous mixtures. In such procedures, the sample is compacted to in-place air voids after construction ($\approx 6-8\%$) and hence the saturation of the sample to the required level (70-80%) is fairly straightforward and the whole process can be finished in 15 to 20 minutes. It is not clear whether such procedure could be adapted to quantify the moisture damage of beam specimen, where one is interested in characterising the influence of moisture damage on the fatigue characteristics. Such samples are compacted to 4% air voids and hence subjecting the samples to the required degree of saturation is not straightforward. It is also not clear how to saturate prismatic beam at 4% air voids and what effect will the addition of additive will have on the degree of saturation. It is also not well known that what effect binder type will have on the degree of saturation.

The fatigue performance of bituminous mixtures is evaluated in the laboratory using a four-point beam bending test setup under controlled conditions. This test setup utilises large-sized prismatic beam specimens. As the moisture damage accelerates the distresses in bituminous mixtures, quantification of such mechanisms requires moisture conditioning of the specimens. Post moisture conditioning, these specimens can be further evaluated for fatigue response. As there is no standard test protocol available for moisture conditioning of these specimens, this study focuses on the development of moisture conditioning process for large-sized prismatic beam specimens.

2 Literature review

Moisture sensitivity tests such as boil test, immersion-compression test, retained Marshall stability test and submerged wheel tracking test are practised to assess the bituminous mixtures susceptibility to moisture [7]. In the boil test, the loose bituminous mixtures are immersed in boiling water for 10 minutes, and the mix is visually inspected for stripping after removing the loose bitumen [3]. Moisture sensitivity is also measured as the number of freeze-thaw cycles required to induce crack on sample [9] where multiple freeze-thaw cycles are performed with freezing at $-12\text{ }^{\circ}\text{C}$ for 24 hours and thawing at $60\text{ }^{\circ}\text{C}$ for 24 hours. Immersion-compression test involves axial compression test on a 100 mm diameter cylindrical specimen at $25\text{ }^{\circ}\text{C}$ without lateral support after the specimen is conditioned underwater at $60\text{ }^{\circ}\text{C}$ for 24 hours. Here, the moisture sensitivity is determined as the ratio of the wet specimen to the dry specimen [1, 5]. Marshall immersion test follows similar conditioning process as immersion compression test, where Marshall stability is used to determine the strength of the compacted bituminous mixtures. Original Lottman [10] method recommends to vacuum saturate the specimen in water for 30 minutes, freeze at $-18\text{ }^{\circ}\text{C}$ for 15 hours and thaw at $60\text{ }^{\circ}\text{C}$ for 24 hours. Resilient modulus and tensile strength tests are conducted to evaluate the intensity of moisture damage. Modified Lottman and Tunnicliff and Root [4] conditioning process suggests, 55 to 80% saturation for cylindrical specimen compacted to $7 \pm 0.5\%$ air voids. Modified Lottman test conditioning follow a freeze-thaw conditioning process whereas Tunnicliff and Root conditioning eliminated the freezing process [10, 12]. It is reported that bituminous mixtures that were known as moisture susceptible mixtures were accepted by modified Lottman and ASTM D4867 test procedures [7]. AASHTO T283 [2] test procedure recommends indirect tensile strength test on a cylindrical specimen of 100 mm or 150 mm diameter compacted to $7 \pm 0.5\%$ air voids. The specimens are vacuum saturated between 70 to 80 %, and these specimens are further considered for the freeze-thaw process. The current guideline suggests application of partial vacuum between 254-660 mm Hg continuously for 10 minutes for a cylindrical specimen [2].

IRC:111-2009 [8] recommends to vacuum saturate the specimens for 30 minutes without clearly stipulating the degree of saturation. It is important to note here that IRC:111-2009 [8] saturation may not be applicable across different bituminous mixtures prepared using different binder types as the specific time duration may not result in the desired degree of saturation. It is to note here that, one of the focus points of the current study is to identify various saturation parameters. Various conditioning processes are used to condition bituminous mixtures to quantify its moisture susceptibility depending upon the location of construction. Freeze-thaw conditioning is applicable where the pavements experience sub-zero temperatures. Similarly, bituminous mixtures can also be conditioned at $60\text{ }^{\circ}\text{C}$ for 24 hours, neglecting the freezing process. This study reports the experimental investigation conducted to moisture condition a prismatic beam specimen.

3 Experimental Investigation

3.1 Materials

A total of eight combinations of the bituminous mixture was considered for the study. Unmodified, VG-30 and crumb rubber modified, CRMB-60 binders following guidelines IS 73: 2013 and IS 15462: 2004 respectively were selected. The bituminous mixture specimens were prepared using locally available aggregates selected from a single source with two types of binders. Aggregates were batched to satisfy the target bituminous concrete gradation-II [11]. A surfactant based dark brown coloured warm mix additive was used to produce warm mix asphalt (WMA). Addition of warm mix additive provides improved workability during the production of the bituminous mixture at reduced temperature. WMA additive was added to the binder at $160\text{ }^{\circ}\text{C}$ and $180\text{ }^{\circ}\text{C}$ for VG-30 and CRMB-60 respectively at the proportion of 0.4% and 0.5% by the weight of the binder. The above dosage rates are fixed such that the desired characteristics of WMA, i.e., the desired workability could be achieved even at reduced mixing temperatures. Thorough mixing of WMA additive was achieved by mixing at 500 rpm for 15 minutes using a mechanical stirrer. Hydrated lime was introduced to the aggregate, replacing 2% of filler (passing 75- μm sieve) by the weight of total aggregate as an anti-stripping agent. The batched aggregates and binder were heated to mixing temperature and were mixed in an automated bituminous mixer. Both the unmodified and crumb rubber modified

binders selected for the study were blended with aggregate to produce hot mix asphalt (HMA) and WMA bituminous mixture. Both the HMA and WMA bituminous mixture were also produced with the addition of lime to generate beam specimen. Theoretical maximum specific gravity (G_{mm}) was determined to be 2.604 for specimen prepared using VG-30 and 2.606 for specimen prepared using CRMB-60.

A shear box compactor, as shown in Fig. 1(a) following ASTM D7981 [6] specification was used to compact the bituminous mixtures to produce beams of size $0.45\text{ m} \times 0.15\text{ m} \times 0.169\text{ m}$. These beams were further sliced to $0.38 \pm 0.006\text{ m} \times 0.050 \pm 0.002\text{ m} \times 0.063 \pm 0.002\text{ m}$ as shown in Fig. 1(b), using a saw cutter. Overall, 16 shear box beams were fabricated and 44 samples having air voids between $4 \pm 0.5\%$ were selected for the study (Fig. 1b). Four fatigue beams were extracted from one shear box compacted large beam, and the entire slicing process is depicted pictorially in Fig. 2 in four steps.

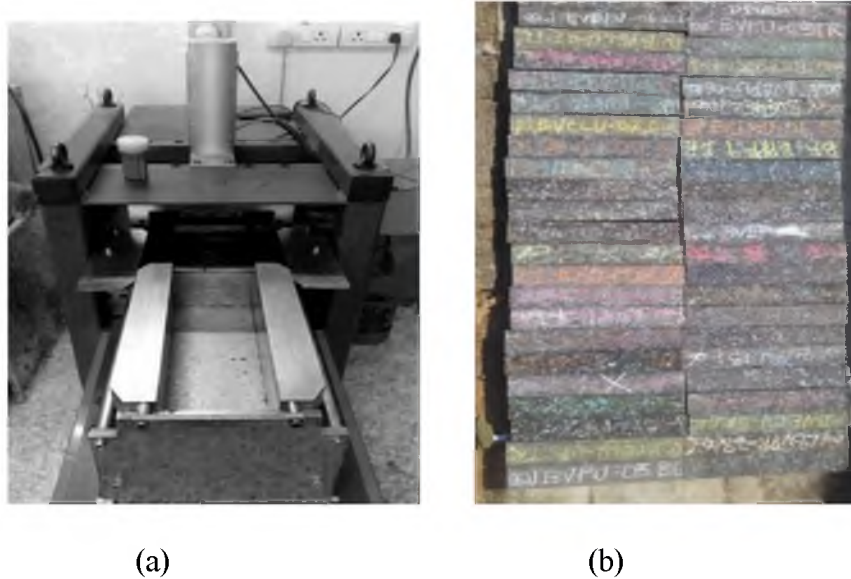


Fig. 1. a) Shear-box compactor, (b) sliced beams considered for the study

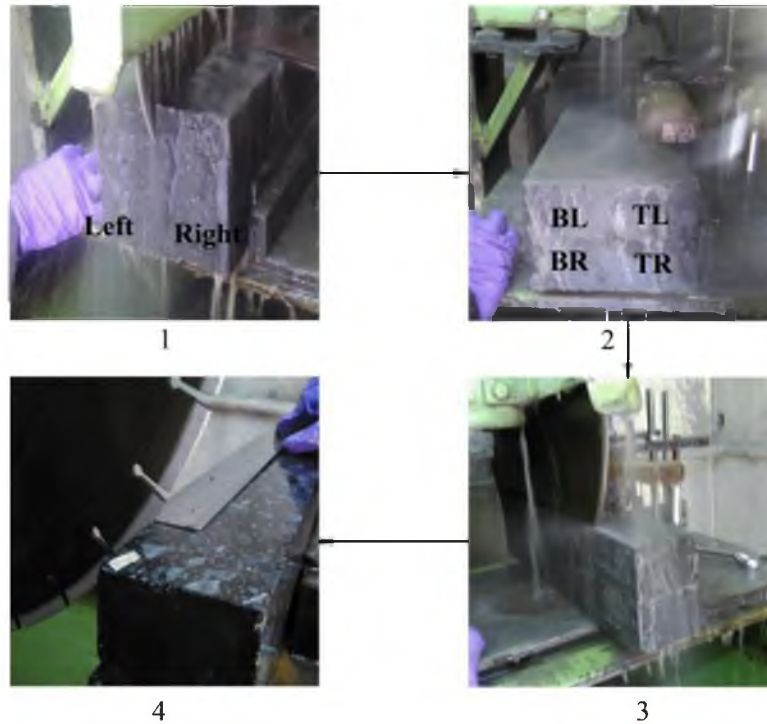


Fig. 2. Slicing of the shear box beam using a saw cutter

3.2 Moisture Conditioning Process

The vacuum system consists of a vacuum pump, a non-return valve, a vacuum dial gauge, a vacuum controller, a moisture trap and a glass vacuum chamber (Fig. 3). The high capacity vacuum pump used in this study is capable of applying vacuum up to 760 mm Hg. The non-return valve ensures that once the vacuum was created in the vacuum chamber, no leakage of air occurs from vacuum pump that in turn can affect the vacuum created in the chamber. It was also checked and ensured that there was no leakage of air from any joints and the push-in pipe. A calibrated dial gauge was installed to measure the applied vacuum accurately. A trial and error approach was adopted to determine the intensity of partial vacuum for saturating a prismatic beam specimen. It was ascertained to apply a vacuum in the range of 700 to 740 mm of Hg. The vacuum controller, directly connected to a power supply of vacuum pump was used to maintain the selected vacuum. A moisture trap was installed to filter any moisture from the air flowing from vacuum chamber towards vacuum pump during the process of saturation. A cylindrical glass vacuum chamber of 100 mm inner diameter and 550 mm height with a glass flange on top was used for moisture conditioning of the specimen. The thickness of the wall of the glass cylinder is 5 mm. The top flange is connected to an outlet, through which vacuum is applied. The chamber is used to submerge the sliced fatigue beam in water during the saturation process.

The fatigue beam specimen was placed inside the airtight glass chamber and was submerged completely in water. A partial vacuum was applied, and as the vacuum reached 740 mm Hg, the controller stops the vacuum pump, and the vacuum was maintained. On the development of vacuum, the air present in the voids of the fatigue beam specimen was subjected to pressure gradient, and the air bubbles coming out of the submerged beam specimen could be seen clearly in Fig. 4. When the vacuum reduces to 700 mm Hg, the controller triggers the pump to start and stops it again when 740 mm Hg vacuum is attained. Following partial vacuum application, the beam was then allowed to remain submerged in water after the release of vacuum, to permit the water to enter the empty voids in the beam under atmospheric pressure. Multiple trials were carried out to achieve the specified degree of saturation. To fix the time of saturation based on the preliminary trials, each specimen was allowed to saturate for 3 hours. It was perceived that specimen prepared with VG-30 saturated for 3 hours attained the degree of saturation between 70-80 %. However, beams prepared using CRMB-60 binder at equivalent air voids achieved 40-50 % degree of saturation after 5 hours at the similar application of partial vacuum. The influence of modified binder was evident on attainment of a degree of saturation when compared with unmodified bituminous mixtures. It is therefore not

necessary that the degree of saturation shall be identical for unmodified and modified bituminous mixture at 4 % air voids, subject to similar partial vacuum and time. The internal microstructure is completely different for crumb rubber modified bituminous mixtures. The degree of saturation depends on the interconnectivity of the air voids, in other words, the internal structure created by the aggregate matrix and the asphalt mastic. Even though the bituminous mixtures with unmodified and modified binders were compacted to equivalent air voids of 4 %, it is hypothesized in this study that the resulting variation in degree of saturation of both these bituminous mixtures is mainly due to the difference in terms of the connectivity of the air voids. Higher the interconnectivity of the air voids, the degree of saturation is likely to be higher.



Fig. 3. Vacuum system

The degree of saturation is calculated using the difference in air weight of fatigue beam before and after saturation as shown in Equation (1) and the volume of air voids is computed using Equation (2).

$$S = \frac{100 \times (W_{sat} - W_d)}{V_{air}} \quad (1)$$

$$V_{air} = \frac{V_a \times V_{beam}}{100} \quad (2)$$

where, S – degree of saturation (%), W_{sat} – saturated surface dry weight of beam after saturation (g), W_d – weight of dry beam in air (g), V_{air} – volume of air voids (cm^3), V_a – air voids (%), and V_{beam} – volume of beam (cm^3).

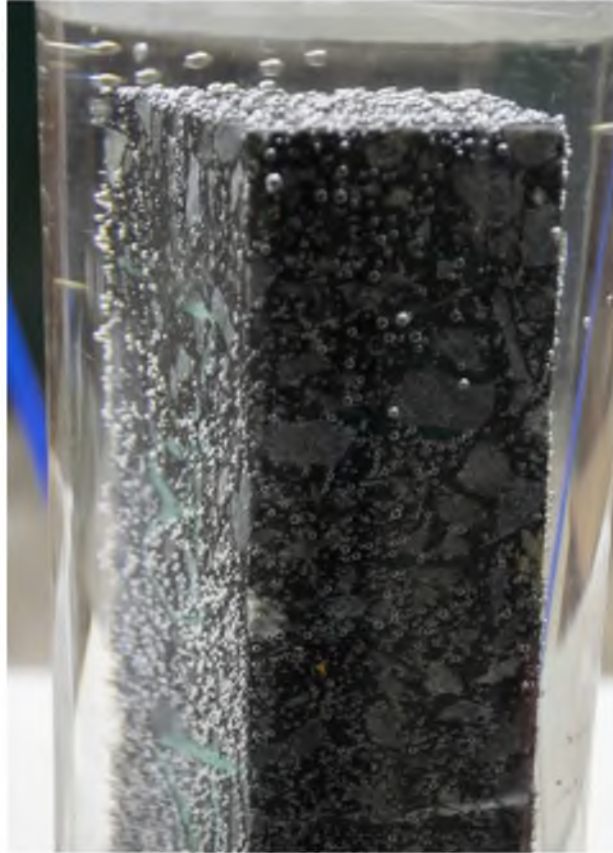


Fig. 4. Saturation of fatigue beam

3.3 ANOVA

Analysis of Variance (ANOVA) was carried out to find the influence of various parameters on the degree of saturation. One-way ANOVA was performed at 95% confidence interval. In the first set, within a given binder the influence of additive (WMA additive, lime, and WMA additive with lime) used was assessed. Secondly, the effect of binder type (unmodified and modified) on the degree of saturation was evaluated. The fixed variable in the first set is the type of additive used in the study and response variable is the degree of saturation. In the second set, the fixed variables are the types of binder used in the study. The null hypothesis for the study is no statistical difference in the means between the variables exist. Also, the alternative hypothesis states that there is a statistical difference in the means between the variables. The null hypothesis was accepted if the tabulated p-value was greater than p-critical (0.05) value, else the null hypothesis was rejected, and alternative hypothesis was accepted.

4 Results and Discussion

The optimum time required to saturate fatigue beam was found to be 3 hours for VG-30 binder and 5 hours for CRMB-60 binder. Though all eight mixtures were compacted at 4 ± 0.5 % air voids, the degree of saturation was found to be very different across the binders. The difference in the degree of saturation between unmodified and modified bituminous mixtures can be hypothesised due to the change in the internal structure at comparable air voids. The air voids range, duration of saturation and degree of saturation details for the test conducted to address the study objective are specified in Table 1.

Table 1. Details of the collected data for the study

Binder	Bituminous Mix	Air Voids Range (%)	Duration (hrs)	No. of samples	Degree of saturation (%)
--------	----------------	---------------------	----------------	----------------	--------------------------

VG-30	HMA	4.1-4.5	3	3	68-82
	WMA	3.8-4.5		8	75-82
	HMA with Lime	3.9-4.3		4	68-74
	WMA with Lime	3.5-4.6		8	67-81
CRMB-60	HMA	4.0-4.8	5	4	51-66
	WMA	4.5-4.9		4	41-51
	HMA with Lime	3.8-4.9		10	30-65
	WMA with Lime	4.4-4.7		3	35-46

One-way ANOVA shows that there is no significant effect of the addition of additives on the degree of saturation as shown in Table 2 for a given binder. One way ANOVA was carried out with 23 samples of VG-30 and 21 samples of CRMB-60. As the p-value (Table 2) for both VG-30 and CRMB-60 is greater than 0.05 (p-critical), the null hypothesis was accepted which signifies that the means for all the four variables are equal. Thus, it can be implied that use of additive has a negligible effect on the variation of the degree of saturation for a given binder.

Table2. Effect of additive on the degree of saturation (%)

Additive	VG-30					CRMB-60				
	Mean	SD	F*	F	P	Mean	SD	F*	F	P
Control	76	7.9	3.1	2.1	0.12	52	1.7	3.3	2.8	0.08
WMA additive	78	4.0				46	4.1			
Lime	71	2.7				41	5.5			
WMA additive and Lime	74	5.8				43	3.1			

SD- standard deviation, F* - F critical, F – F calculated, P - P value

Whereas, the degree of saturation was significantly affected by the type of binder as shown in Table 3. All 44 samples of VG-30 and CRMB-60 were examined for the one-way ANOVA. As p-value (Table 3) is smaller than p-critical, the null hypothesis is rejected, and alternative hypothesis was accepted. It can be said that the means of two variables are not equal. Therefore, it can be inferred that degree of saturation is binder dependent.

Table 3. Effect of binder on the degree of saturation (%)

Binder	Mean	SD	F*	F	P
VG-30	75	5.5	4.1	286.8	0.000
CRMB-60	42	6.8			

5 Conclusions

A new process is developed in this study for moisture conditioning of the large-sized prismatic straight beam specimens of bituminous concrete. The study shows that VG-30 mixtures achieved 70 - 80 % degree of saturation in 3 hours, whereas CRMB-60 mixtures were saturated between 40 - 50 % in 5 hours, although both the mixtures were identically compacted. It was also observed that the degree of saturation is dependent on the type of binder governing variability in the internal microstructure, and is independent of the addition of additives within a

particular binder. Specific guidelines related to the parameters to be considered during the moisture conditioning process were provided, and the relative effects of additives and binder type were quantified. Statistically, the effect of additives had no significant effect on the degree of saturation for a particular binder. It was also verified statistically that the degree of saturation is very much binder dependent within the given range of air voids considered in this study.

References

1. AASHTO, T165.: Standard Method of Test for Effect of Water on Compressive Strength of Compacted Bituminous Mixtures. Standard Specification, American Association of State Highway and Transportation Officials, Washington, DC (2002).
2. AASHTO, T283.: Resistance of Compacted Asphalt Mixtures to Moisture-Induced Damage. Standard Specification, American Association of State Highway and Transportation Officials, Washington, DC (2014).
3. American Society for Testing and Materials (ASTM).: Effect of Water on Compressive Strength of Compacted Bituminous Mixtures. ASTM D1075, West Conshohocken, PA (1994).
4. American Society for Testing and Materials (ASTM).: Standard practice for effect of water on bituminous-coated aggregate using boiling water. ASTM D3625, West Conshohocken, PA (2005).
5. American Society for Testing and Materials (ASTM).: Standard Test Method for Effect of Moisture on Asphalt Concrete Paving Mixtures. ASTM D4867, West Conshohocken, PA (2014).
6. American Society for Testing and Materials (ASTM).: ASTM D7981, Standard Practice for Compaction of Prismatic Asphalt Specimens by Means of the Shear Box Compactor. West Conshohocken, PA (2015).
7. Asphalt Institute.: Best practices to minimize moisture sensitivity in asphalt mixtures. Manual Series No. 24 (MS-24). 1sted, Asphalt Institute, Lexington, KY (2007).
8. IRC: 111.: Specifications for Dense Graded Bituminous Mixes. The Indian Roads Congress, New Delhi, India (2009).
9. Kennedy, T. W., Freddy L. R., and Kang W. L.: Evaluation of moisture susceptibility of asphalt mixtures using the Texas freeze-thaw pedestal test. Association of Asphalt Paving Technologists Proceedings. Vol. 51, pp. 327-341. St Paul, MN (1982).
10. Lottman, R.P.: Predicting Moisture-Induced Damage to Asphaltic Concrete -Field Evaluation. NCHRP Report 246, Transportation Research Board, Washington DC (1982).
11. Ministry of Road Transport & Highways (MoRTH).: Specifications for Road & Bridge Works. Fifth Revision, IRC publications, New Delhi, India (2013).
12. Tunnicliff D.G., Root R.E.: Use of antistripping additives in asphaltic concrete mixtures. NCHRP Report 274, Transportation Research Board, Washington, D.C (1984).

Surrogate Safety Assessment Models for Interurban Corridors

Bhamini B.¹, Mohan Rao², S. Velmurugan³ and Jomy Thomas⁴

¹PG Scholar, Civil Engineering Department, RIT, Kottayam

²Principal Scientist, Traffic Engineering and Safety Division, CRRI, Delhi

³Senior Principal Scientist, Traffic Engineering and Safety Division, CRRI, Delhi

⁴Assistant Professor, Civil Engineering Department, RIT, Kottayam

Abstract. 1, 35,000 people were killed on road accidents in India in 2016. Statistics indicate that accidents prove to be a socioeconomic burden to the society. Even though crash data is a true representation of safety, its use in safety studies has many disadvantages. The major disadvantage is that for analyzing the traffic safety aspect of a new facility, one has to wait till considerable number of accidents occurs. Another disadvantage is that from crash data, we may obtain the severity of crash, fatality, damage etc. But more relevant data useful for safety analysis, which includes the causal factors behind the crash such as driver response to a threatening situation, speed of the vehicles, etc. cannot be obtained from this data. Another disadvantage is that not all accidents are reported and this might lead to incorrect and biased conclusions. Surrogate measures to determine traffic safety mean to substitute the need for crash data with another factor which would represent traffic safety. This project aims to identify the accident black spots on the study stretch and develop the surrogate safety assessment models for the identified black spots for assessing safety.

Keywords: Surrogate safety assessment model, black spots

Introduction

Throughout the world more than one million people lose their lives in road traffic crashes each year. It has been estimated that India currently accounts for nearly 10% of road accident fatalities worldwide. In addition, over 1.3 million people are seriously injured on the Indian roads every year. Hence, traffic safety has become a major area of concern for the authorities. The development of urban transport system has not kept pace with the traffic demand both in terms of quality and quantity. As a result, the use of personalized transport mainly two wheelers and intermediate public transport is growing at a rapid speed. World Health Organization (WHO) has mentioned that, accidents are the second most important cause of death for young people having age 9 to 29.

This project aims to clarify the concept of Surrogate measures of safety; summarize the past research in the area and to investigate how simulation can be used in assessing the safety of intersections.

Objectives

The objectives of the thesis are as follows,

- To identify the black spots in the stretch of road between Gurgaon and Faridabad districts in Haryana.
- Application of micro simulation and SSAM for the assessment of intersection safety.
- To develop surrogate safety assessment models.

Literature Review

The study of Liyamol Isen et al. (2013) includes collection of secondary accident data and prioritizing the accident-prone locations by using Weighted Severity Index (WSI) method. WSI method follows a system of assigning scores based on the number and severity of accidents in that particular location in the last five years. Siddharth and Gitakrishnan (2013) introduced a method of sensitivity analysis and automatic calibration of VISSIM model of an intersection in Chennai. VISSIM parameters affecting driver behavior in Indian heterogeneous conditions were found using sensitivity analysis. ANOVA and elementary effects method were used in sensitivity analysis. Mathew and Radhakrishnan (2010) proposed a methodology for calibrating a micro simulation model for highly heterogeneous traffic at signalized intersection. Calibration parameters were identified using sensitivity

analysis, and the optimum values for these parameters were obtained by minimizing the error between the simulated and field delay.

Huang et al. (2013) developed a traffic safety evaluation method based on simulated conflicts at signalized intersections. The selected intersection was simulated in VISSIM simulation system according to the field traffic information. Then the output vehicle trajectory file was analyzed by Surrogate Safety Assessment Model (SSAM) in order to identify simulated conflicts. Simulated conflicts generated by the VISSIM simulation and SSAM were compared to the traffic conflicts measured in the field. After calibration and validation, the remedial measure for this intersection, reducing the speed limit from 60 km/h to 50 km/h, were applied in the VISSIM simulation model. Comparing the simulated conflicts under different speed limits, it was found that the safety performance of this intersection was improved after reducing the speed limit. Vasconcelos et al. (2014) introduced two methods for validation of SSAM as a tool for accident prediction at urban intersections. The first method compared the simulated number of conflicts from the use of SSAM and the predicted number of injury accidents from analytic models in three reference intersection layouts (four-leg priority intersection, four-leg staggered intersection, and single-lane roundabout). The second method compared SSAM results with conflicts observed on site in four-real intersections: two priority ones and two roundabouts.

Methodology

The study area was selected for the stretch of road between Gurgaon and Faridabad districts having length 24.3 Km in Haryana. The accident data for the study stretch were collected from the police stations for the year 2008 to 2014. Accident black spots were identified by using the weighted severity index method. The identified black spots include two intersections. The intersections were simulated in VISSIM 7 and calibration was done by changing the driver behavior parameters. The first one-hour data was used for calibration and rest used for validation. The trajectory data from the calibrated model was extracted and imported to SSAM (Surrogate safety assessment model) software. Calibration of this surrogate safety assessment model was done by changing the surrogate measure's default values. Validation of the model was done by comparing the simulated number of crashes with actual accident number. The accident number of the second black spot was forecasted by using the surrogate safety assessment model.

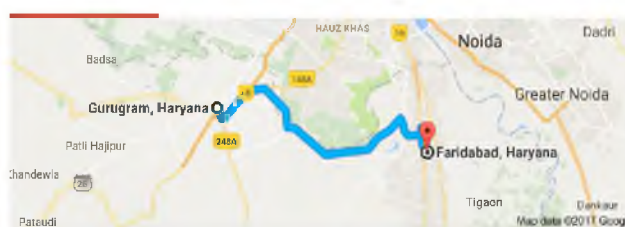


Figure 14 Study stretch – between Gurgaon and Faridabad, Haryana

Data Collection

Accident data was collected for the years 2008 to 2014 from the police stations namely DLF phase I, Surajkund and Sector 55. Accident black spots were identified by using the weighted severity index method. The identified black spots include Silver Oak Chowk intersection and Pali crusher zone intersection. Volume of these intersections was collected by using video graphic method. Total two hours Speed was collected by radar gun at 100 meters away from the intersection. Signal timing was collected manually. The classified vehicle volumes of the intersections were extracted manually from the video with an interval of 5 minutes.

Analysis

Analysis part of the project started with accident data analysis. The primary aim is the identification of black spots. Weighted Severity Index (WSI) method was adopted. Weighted Severity Index (WSI) is a dimensionless value indicating the hazardousness of a spot in the road. The following equation was used. [11]

$$\text{Weighted Severity Index (WSI)} = (41 \times K) + (4 \times GI) + (1 \times MI)$$

Where,

K- Number of persons killed

GI- Number of grievous injuries

MI- Number of minor injuries

WSI of Pali Crusher Zone = $(41 \times 10) + (4 \times 34) + (1 \times 47) = 593$

WSI of Silver Oak Chowk = $(41 \times 3) + (4 \times 35) + (1 \times 11) = 274$

VISSIM Simulation

Satellite images of the intersections were taken from the Google earth. These images are imported in VISSIM as background image and set to the scale. Numbers of lanes, lane width, radius of the curve etc. are inputs as per road inventory details collected from PWD. Indian vehicle types are added to the network, which includes Indian auto, LCV and Delhi Bus.

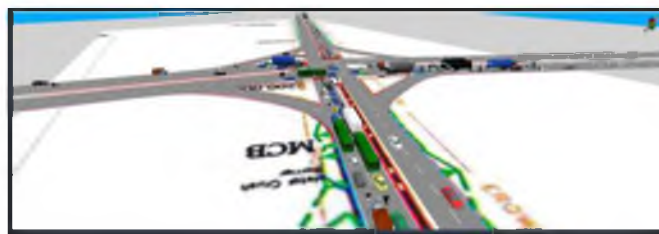


Figure 15 Realistic representation of intersection I - Silver Oak Chowk in VISSIM

2.1 Calibration of VISSIM Model

The first one-hour data was used for calibration. Calibration of the developed model was done by changing the values of the driver behavior parameters. The following table 1 shows the parameters considered for calibration, its default value and calibrated value.

Table 7 Parameters for calibration

Sl.No	Parameters considered	Default value	Calibrated value
1	Average stand Still Distance	2	.25
2	Additive part of safety Distance	2	.1
3	Multiple Part of Safety Distance	3	.1
4	Look ahead distance		
	Minimum	0	50
	Maximum	250	250
5	Observed Vehicles	4	2
6	Look back distance		
	Minimum	0	50
	Maximum	150	100
7	Maximum Deceleration		
	Own	4	7
	Trailing	3	6
8	Accepted deceleration		
	Own	1	3
	Trailing	1	2
9	Waiting Time Before Diffusion	60	150
10	Minimum Headway	.5	.1
11	Safety Distance Reduction Factor	.6	.3
12	Maximum Deceleration for Corporate breaking	3	3
13	Minimum Lateral Distance		

0Km/h	.2	.1
50Km/h	1	.2

2.2 Validation of VISSIM Model

For validating the VISSIM model, next one-hour data of volume was taken as the input and the output volume and speed from the VISSIM is compared with the input values. Geoffrey E. Havers developed a continuous volume tolerance formula while working as a transport planner in London, England in the 1970s. Although its mathematical form is similar to a chi-squared test, is not a true statistical test. Rather, it is an empirical formula that has proven useful for a variety of traffic analysis purposes. GEH values are less than 5 which implies good match between the modeled and observed hourly volumes. [13]

GEH Formula is as follows.

$$G_H = \sqrt{\frac{2(m - c)^2}{m + c}}$$

Where:

m is the values from the traffic model (per hour)

c is the real-world traffic value (per hour)

The following table 2 shows the GH calculation of an approach of the Silver oak chowk intersection.

Table 8GEH of Faridabad approach of Silver Oak Chowk

Data Collection	Time interval	Data Collection Location	Veh(All)	Veh(60)	Veh(90)	Veh(80)	Veh(20)	Veh(10)	Veh(70)
63	200-1100	04:00 FBD	441	64	5	14	2	353	3
63	1100-2000	04:00 FBD	418	57	9	20	1	328	3
63	2000-2900	04:00 FBD	439	66	8	17	4	341	3
63	2900-3800	04:00 FBD	415	52	7	13	2	337	4
O/P			1713	239	29	64	9	1359	13
I/P			1765	271	34	58	12	1380	10
GH			1.2469	2.0039	0.8908	0.7682	0.5674	0.5674	0.8846

Development of Surrogate Safety Assessment Model (SSAM)

Surrogate safety assessment model was developed by importing the trajectory data from the VISSIM simulation into SSAM software developed by FHWA. The surrogate measures include Time to collision (TTC), Post encroachment time (PET), Maximum speed (MaxS) etc.

Time to collision is defined as the time left for collision provided the speed and course of the colliding objects continue to remain the same during a car following scenario. Post Encroachment time has been defined by Cooper (1983) as the difference between the time at which the leading vehicle enters a collision point and the time at which the following vehicle enters the same point. As post encroachment time decreases the chances of collision increases.

The general notion that high speeds (MaxS) lead to accidents in most of the cases have always been a question discussed upon and denied upon by many researchers. But it is quite obvious that higher speed gives the driver less time to react to any incident that might occur and similarly it also does not give time to the other road user involved in conflict to react accordingly which can lead to crashes.

2.3 Calibration and validation of SSAM

- The first step of calibration of the model developed in SSAM software was to determine the sensitive parameters that affect the conflict number.
- The values of surrogate measures are changed and compared the conflict number at each iteration (Trial and Error method).
- The result indicates that TTC, PET and MaxS are the sensitive parameters. Calibrated values of the TTC 1.3 – 1.5 second, PET, MaxS are, 4 – 4.1 second and 10– 20 m/s respectively.

- The average accident number and the predicted accident number hold a good match implying the developed model is validated

2.4 Forecasting of accident number

The value calibrated from Silver oak chowk was 4 to 4.1sec for PET which was not applicable for the Pali crusher zone intersection. In order to calibrate the Pali Crusher zone model, PET has changed to 3.2 - 4.1 sec. Then the predicted number (simulated number) of crashes per year becomes eight, which matches with the actual accident number.

2.5 Assessment of effectiveness of remedial measures

The speed limit reduced from 80 kmph to 70 kmph for Car and Two-wheeler, 65 kmph to 50 kmph for Bus and HGV, 50 kmph to 40 kmph for Auto in VISSIM simulation. Lane discipline is introduced in simulation by changing the driver behaviour parameter, i.e., desired position at free flow has changed from 'any' to 'middle of the lane'. This resembles traffic barriers in the road in order to obtain the lane discipline and to avoid aggressive driving. For both Pali Crusher Zone and Silver Oak Chowk, Crash number is reduced from eight to one.

Results and Conclusions

- The black spots in the study stretch were identified by weighted severity index (WSI) method.
- The identified black spots include two intersections named Silver Oak Chowk (WSI is 274) and Pali crusher zone (WSI is 593).
- VISSIM models developed for the intersections were calibrated by changing the driver behavior parameters.
- The VISSIM models were validated by comparing the speed and volume of simulated model with the actual values. The percentage error between simulated speed and field speed was less than ten. The GEH values for the volume of the two intersections were less than five.
- The surrogate safety assessment model (SSAM) for the Silver oak chowk intersection was created. The sensitive parameters include TTC, PET and MaxS were found out by changing the default values in the model. The calibration of the model was done by changing the range of values of the sensitive surrogate measures. The calibrated values of the TTC, PET, and MaxS are 1.3 – 1.5 second, 4 - 4.1 second and 10 – 20 m/s respectively.
- The average accident number (7) and the predicted accident number (8) hold a good match implying the developed model is appropriate for assessing the safety.
- The value calibrated from Silver oak chowk was 4 to 4.1sec for PET. In order to calibrate the Pali Crusher zone model, PET has changed to 3.2 - 4.1 sec. Then the predicted number (simulated number) of crashes per year becomes eight, matches with the actual accident number which is seven.
- The reduction in the PET value implies, at Pali crusher zone the drivers are aggressive and not adhering to car following. That means vehicles are in over speed. Therefore, chances of collision are more.
- The remedial measure suggested in order to avoid the accidents includes reduce the speed limit and introduce traffic barriers to obtain the lane discipline and to avoid aggressive driving. Speed limit was reduced as 70km/h for car, 50km/h for two wheelers, truck and bus in VISSIM models. After analyzing the trajectory data from the modified VISSIM models in SSAM, it is shown that crashes per year is reduced to one. So reduction in the speed limit will be an effective solution to reduce the accidents at the study stretches.
- For both intersections (Pali Crusher Zone and Silver Oak Chowk), Crash number is reduced from eight to one implying the remedial measure suggested will be effective for reducing the accidents

References

- Luis Vasconcelos, Luis Neto, Alvaro Maia Seco, and Ana Bastos Silva: Validation of the Surrogate Safety Assessment Model for Assessment of Intersection Safety, Journal of the Transportation Research Board Vol: 24, pp. 1-9, (2014)
- Kaan Ozbay, Hong Yang, BekirBartin, Sandeep Mudigonda: Derivation and Validation of a New Simulation-based Surrogate Safety Measure, Journal of Transportation Research Board, pp. 1-19, (2008)

- Fei Huang, Pan Liu, Hao Yu, Wei Wang: Identifying if VISSIM simulation model and SSAM provide reasonable estimates for field measured traffic conflicts at signalized intersections, *Accident Analysis and Prevention*, Vol: 50, pp.1014– 1024, (2013)
- Tom V. Mathew and Padmakumar Radhakrishnan: Calibration of Microsimulation Models for Nonlane-Based Heterogeneous Traffic at Signalized Intersections, *Journal of Urban Planning and Development*, Vol. 136, No. 1, pp. 59-66, (2010)
- P. Siddharth S M and Ramadurai G.: Calibration of VISSIM for Indian Heterogeneous Traffic Conditions, *Procedia - Social and Behavioral Sciences*, Vol: 104, pp. 380-389, (2013)
- Durrani U., Lee C. and Maoh H.: Calibrating the Wiedemann's vehicle-following model using mixed vehicle-pair interactions, *Transportation Research Board*, pp. 227–242, (2016)
- Gettman, D. and Head L.: Surrogate safety assessment model and validation: final report, FHWA-HRT-08-051,(2008)
- Hamid Behbahani and NavidNadimi: A Framework For Applying Surrogate Safety Measures For Sideswipe Conflicts, *International Journal For Traffic And Transport Engineering*, Vol: 5, pp. 371 – 383, (2015)
- Banik B. K, Chowdhury M. A. I., Hossain E. and Mojumdar B.: Road Accident and Safety Study in Sylhet Region of Bangladesh, *Journal of Engineering Science and Technology* Vol. 6, No. 4 493 – 505, (2011)
- Sorate R. R., Kulkarni R. P., Bobade S. U., Patil M. S., Talathi A. M., Sayyad I. Y. and Apte S. V.: Identification of Accident Black Spots on National Highway 4 (New Katraj Tunnel to Chandani Chowk), *IOSR Journal of Mechanical and Civil Engineering (IOSR-JMCE)*, Volume 12, Issue 3 Ver. I, PP 61-67, (2015)
- Liyamol Isen, Shibu A, Saran M. S.: Identification and Analysis of Accident Black spots using Geographic Information System, *International Journal of Innovative Research in Science, Engineering and Technology*, 2, 131-139, (2013)
- Apparao G. and Raju M. S. G.: Identification of Accident Black Spots For National Highway Using GIS, *International journal of scientific & technology research* Volume 2, Issue 2, (2013)
- UK Highways Agency, *Design Manual for Roads and Bridges*, Volume 12, Section 2

Use of Statistical Methods for the Analysis of Axle Load Data for Pavement Design

Donia Savio¹ and J. Murali Krishnan²

¹Ph.D. Scholar, ²Professor

Indian Institute of Technology Madras, Tamil Nadu, India

²jmk@iitm.ac.in

Abstract

One of the major considerations for designing a highway pavement is traffic data in terms of Average Annual Daily Truck Traffic (AADTT) and axle load data. Vehicle Damage Factor (VDF) approach is used in India for calculating the Equivalent Standard Axle Load (ESAL) and Asphalt Institute uses Truck Factor (TF). When ESAL is computed using VDF and TF approaches, a uniform distribution is inherently assumed for representing the axle load data. Most of the Indian highways are heavily overloaded and it is well known that extreme axle loads can damage the pavement more, though the number of such axle load repetitions are less. It is not sure whether the uniform distribution can capture such behavior. Different types of probability density functions are available which can explain such data well. This work involves identification of a specific distribution to explain the axle load data.

In this investigation, the traffic and axle load data for a particular stretch of National Highway 16 was collected and statistical analysis was carried out. Analysis of axle load data indicated overloading. The axle load data were described using mixed probability density functions. ESAL was calculated using Load Spectra Factor (LSF) in addition to VDF and TF approaches.

Keywords: VDF, TF, overloading, ESAL, LSF

Introduction


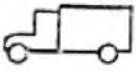
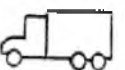
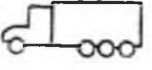
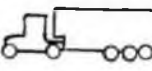
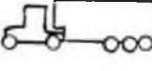
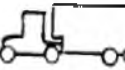


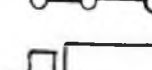
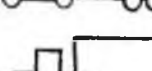
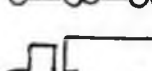
In India, the bituminous pavements are designed as per the guidelines of IRC:37-2012 (2012) and use Vehicle Damage Factor (VDF) method for calculating Equivalent Standard Axle Load (ESAL). Asphalt Institute uses Truck Factor (TF) in calculating ESAL (Huang, 2009). When ESAL is computed using VDF and TF approaches, a uniform distribution is inherently assumed for representing the axle load data. However, statistical analysis of axle load data revealed that the axle load spectra corresponding to each of the axle types did not follow a uniform distribution. Moreover, there exists a considerable amount of overloading in Indian highways and one should ensure that the influence of these overloaded trucks is taken into consideration while designing pavements. From the previous studies (Savio et al., 2016), it was observed that the VDF and TF approaches were less sensitive to overloading. This could lead to inaccurate estimation of the ESAL leading to improper pavement design. For this reason, a different approach called Load Spectra Factor (LSF) is used in this study. LSF is calculated using the moment statistics of the axle load distribution for various types of axles.

Literature Review

Studies performed on overloading have considered the vehicle to be overloaded when at least one of its axles is overloaded (Fuentes et al. 2012; Pais et al. 2013). Mohammadi and Shah (1993) studied overloading of trucks and used probability distribution models to represent different loading patterns on the load spectrum.

The study conducted by Jiang et al. (2008) explained that the Mechanistic-Empirical Pavement Design Guide (MEPDG) uses the entire axle load spectra collected from the field for pavement design. Haider et al. (2007) developed closed-form solutions to extract ESAL directly from axle load spectra. The results of the study conducted by Haider and Harichandran (2007) indicated that axle load distributions can be effectively related to Gross Vehicle Weights (GVW) and truck proportions. Timm et al. (2005) developed a linear combination of lognormal and normal distributions to characterize the complex axle load spectra. Prozzi et al. (2006) explained that if the axle load spectra are fitted with probability density functions, the physical and statistical meanings of load spectra are properly accounted. Thus, they used the concept of moment statistics in investigating load pavement impact based on axle

Table 2. Vehicle classification

Vehicle classification		Legal axle load limits (Tonnes) (FA - Front axle, RA - Rear axle)	
Vehicle identifier	Vehicle type	Tractor	Trailer
1.12		FA: 6 RA:6 +10.2	----
1.2		FA: 6 RA: 10.2	----
1.22		FA: 6 RA: 19	----
1.122		FA: 6	RA: 6 RA: 19
1.1.122		FA: 6 RA:6	RA: 6 RA: 19
1.1.221		FA: 6 RA:6	RA: 19 RA: 6
1.1.22		FA: 6 RA:6	RA: 19
1.2.11		FA: 6 RA: 10.2	RA:6+6
1.2.22		FA: 6 RA: 10.2	RA: 19
1.2.222		FA: 6 RA: 10.2	RA: 24
1.22.222		FA: 6 RA: 18	RA: 24
1.1.222		FA: 6 RA:6	RA: 24

It is seen that some of the vehicle types found in this stretch of highway possess tridem axles, which is not mentioned in IRC 3:1983(1983). Since IRC:3-1983 (1983) does not have the legal axle load limit for tridem, the legal axle load limits for vehicle identifiers 1.2.222,1.22.222 and 1.1.222 have been taken from TRB (2002).

Overloading Analysis

The overloading analysis was carried out in two different ways: axle type and vehicle type. In the axle type overloading analysis, the axles of different vehicle types were partitioned and grouped under different axle categories. Axle loads greater than the respective axles' legal limit (as per Table2) were considered as overloaded. From Fig.2 one can identify that the Tandem and Tridem axles are comparatively more overloaded than SS and SD.

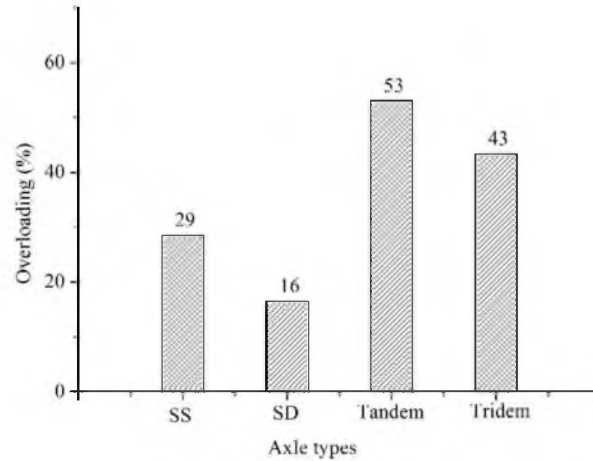


Fig.2. Axle type overloading analysis

Table3. Vehicle type overloading analysis

Vehicle types	Percentage overloading (%)
1.12	100
1.2	13
1.22	35
1.122	61
1.1.122	80
1.1.221	100
1.1.22	100
1.2.22	33
1.2.222	40
1.22.222	33
1.1.222	100

However, in the vehicle type overloading analysis the gross vehicle weight within the legal limits for each of the vehicle types was calculated. Those vehicles with gross vehicle weight exceeding the legal limits were considered as overloaded. From Table 3 it can be seen that all the vehicles belonging to the vehicle types 1.12, 1.1.221, 1.1.22 and 1.1.222 are found to be overloaded. The results from axle type and vehicle type overloading analysis revealed that this highway stretch was significantly overloaded.

Describing axle load data using probability density functions

Due to the high level of uncertainty associated with the axle load data, it is extremely difficult to describe this data with a single probability density function. Hence in this study, multi-modal distributions were used to describe the axle load spectra using the programming language R (R Development Core Team 2011). For this purpose, the data were partitioned based on different axle types. A Mixed-Normal distribution function was used to describe the axle load spectra. Equation 1 shows the density function of Mixed-Normal distribution.

$$f(\mathbf{x}) = p_1 \times \hat{f}_1 + p_2 \times \hat{f}_2, \quad (\text{Haider and Harichandran (2009)}) \quad (1)$$

$$f_1 = \frac{1}{\sqrt{2\pi}\sigma_1} e^{-\frac{(x-\mu_1)^2}{2\sigma_1^2}}, \quad f_2 = \frac{1}{\sqrt{2\pi}\sigma_2} e^{-\frac{(x-\mu_2)^2}{2\sigma_2^2}},$$

where, f_1 and f_2 are the normal distribution density functions with means μ_1 and μ_2 and standard deviations σ_1 and σ_2 respectively. The weight factors for the first and second normal distribution functions are denoted as p_1 and p_2 . The axle load spectra modelled with Mixed-Normal distribution functions are shown in Fig.3. The solid curve indicates first (f_1) and second (f_2) normal distributions used to model the axle load spectrum. The curve with a dotted line shows the combined model of the two normal distributions ($f(x)$) described for the respective axle load spectrum. It can be observed clearly from these figures that the axle load distributions contain well-defined peaks especially for the tandem and tridem axles. These peaks attribute to empty and loaded truck weights respectively. The multi-modal fit parameters obtained for each of the axle types are presented in Table 4. Kolmogorov-Smirnov (K-S) test was carried out and the respective p-values are also given in Table 4. The p-value signifies that one cannot reject the null hypothesis that the sample belongs to fitted distribution at any significance level (α) less than or equal p .

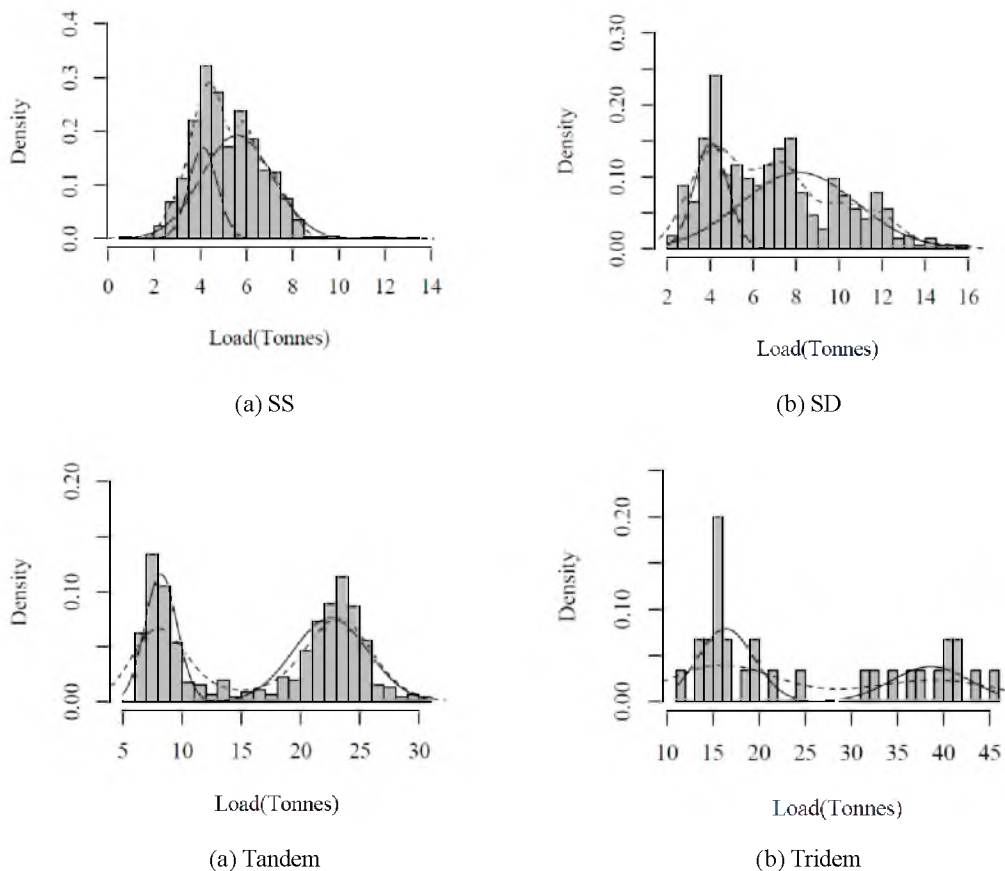


Fig. 3. Axle load spectra described using Mixed-Normal distributions

Table 4. Mixed-Normal fit parameters

Description	Parameters			P- value
Axle type	p	μ (Tonnes)	σ (Tonnes)	

SS	p ₁ =0.262	μ ₁ =4.123	σ ₁ =0.615	0.40
	p ₂ =0.738	μ ₂ =5.592	σ ₂ =1.530	
SD	p ₁ =0.289	μ ₁ =4.052	σ ₁ =0.778	0.09
	p ₂ =0.711	μ ₂ =8.134	σ ₂ =2.672	
Tandem	p ₁ =0.395	μ ₁ =8.216	σ ₁ =1.358	0.06
	p ₂ =0.605	μ ₂ =22.510	σ ₂ =3.165	
Tridem	p ₁ =0.598	μ ₁ =16.391	σ ₁ =3.028	0.54
	p ₂ =0.402	μ ₂ =38.627	σ ₂ =4.243	

Estimation of ESAL

ESAL was calculated using VDF, TF and LSF approaches. The estimation of ESAL using the three approaches are presented in the following paragraphs.

VDF

The entire traffic spectrum collected from the field was first divided based on axle types. Then the frequency distribution (number of axles falling in each load group) of the axle loads were calculated for each of these axle types corresponding to the axle load groups specified in IRC: 37-2012 (2012). Equation (2) shows the Equivalent Axle Load Factor (EALF) formula for SS as per IRC: 37-2012 (2012). Separate equations are available for other axle types as well. Equation (3) shows the formula for VDF.

$$EALF (SS) = \left(\frac{\text{Axle load in kN}}{65} \right)^4 \tag{2}$$

$$VDF = \frac{\sum EAL_i}{\text{Total no. of vehicles}} \tag{3}$$

where, EALF (SS) is the equivalent axle load factor for SS. EAL represents the product of EALF and the frequency corresponding to each load group and $\sum EAL_i$ represents the sum of the Equivalent Axle Load (EAL) of all axle types. The VDF value calculated for the current stretch of highway is 3.20.

Truck Factor (TF)

When compared to VDF, TF was calculated for each of the vehicle types (Table 2) for which axle load survey was carried out. The EALF values for the respective axles of a vehicle were summed up to calculate the TF for that vehicle. The average truck factor is calculated for the respective vehicle types and was used in the calculation of ESAL. Table 5 shows the average truck factor values calculated for each of the vehicle types.

Table 5. TF values

Vehicle types	TF
1.12	4.77
1.2	1.54
1.22	3.10
1.122	7.64
1.1.122	9.08
1.1.221	18.10
1.1.22	6.97
1.2.22	1.26
1.2.11	5.72

1.2.222	5.75
1.22.222	5.47
1.1.222	14.97

LSF

The LSF is determined using the following equation(Prozzi and Hong, 2007).

$$LSF = \int \left(\frac{x}{L_g}\right)^n \times f(x) dx = \frac{M^n}{L_g^n}, \quad (\text{Prozzi and Hong, 2007}) \quad (4)$$

where, $f(x)$ is axle load statistical function for a given axle load type with a standard axle load of ' L_g ' and ' M^n ' is the n^{th} order moment of the distribution. In the current study, the fourth moment of the axle load distribution ($n=4$) was used for calculating LSF as the EALF equation (Equation 2) also uses the power as four. Table 6 shows the LSF values calculated for the different axle types described using the Mixed – Normal distribution functions.

Table 6.LSF values

Axle type	LSF
SS	0.59
SD	1.18
Tandem	3.30
Tridem	3.35

ESAL values

The ESAL values were calculated for an annual growth rate of 5%, design life of 10 years, a directional distribution factor of 50% and a lane distribution factor of 75% using Equation (5)(IRC: 37-2012 (2012))

$$ESAL = \frac{365 \times [(1 + r)^n - 1]}{r} \times A \times D \times F, \quad (5)$$

where, r is the annual growth rate of commercial vehicles in decimal, n is the design life in years, A is AADTT, D is the lane distribution factor and F is the VDF or TF or LSF. ESAL values calculated using the three approaches are shown in Table 7. It is observed that the ESAL values calculated using the three approaches is almost similar. Therefore, one can use LSF method also to calculate ESAL.

Table 7.ESAL values (msa)

Analysis method	ESAL
VDF	50
TF	47
LSF	50

Summary and Conclusion

In this paper, axle load and AADTT data collected from a stretch belonging to National Highway 16 were analysed. The analysis of the axle load data revealed a considerable amount of overloading. The ESAL values were estimated using three different approaches (VDF, TF, LSF). These approaches were found to estimate almost similar ESAL values. Thus, one can use LSF method also to calculate ESAL.

References

- Fuentes, L. G., Macea, L.F., Vergara, A., Flintsch, G. W., Alvarez, A. E., and Reyes, O. J.: Evaluation of Truck Factors for Pavement Design in Developing Countries. *Procedia-Social Behavioral Science*, 53, 1140-1149 (2012).
- Haider, S.W., and Harichandran, R.S.: Characterizing Axle Load Spectra by Using Gross Vehicle Weights and Truck Traffic Volumes. *TRB Annual Meeting CD-ROM*, (2007).
- Haider, S.W., Harichandran, R.S., and Dwaikat, M.B.: Estimating Bimodal Distribution Parameters and Traffic Levels from Axle Load Spectra. *TRB Annual Meeting CD-ROM*, (2007).
- Haider, S.W., and Harichandran, R.S.: Effect of Axle Load Spectrum Characteristics on Flexible Pavement Performance. *Journal of the Transportation Research Board*, 101-114 (2009).
- Huang, Y.H.: *Pavement Analysis and Design*. 2nd edn. Pearson Prentice Hall, New Jersey (2009).
- IRC:3-1983. *Dimensions and Weights of Road Design Vehicles*. Indian Road Congress, New Delhi, India (1983).
- IRC:37-2012. *Guidelines for The Design of Flexible Pavements* Indian Road Congress, New Delhi, India (2012).
- Jiang, Y., Li, S., Nantung, T., and Chen, H.: Analysis and Determination of Axle Load Spectra and Traffic Input for The Mechanistic-Empirical Pavement Design Guide. *JTRP*. (2008).
- Johnson, R. Chapter 5: Probability Densities. *Miller and Freund's Probability and Statistics for Engineers*, 7th edn. Prentice-Hall of India, New Delhi, 166-175 (2005).
- Macea, L., Marquez, L., and Llinas, H.: Improvement of Axle Load Spectra Characterization by a Mixture of Three Distributions. *ASCE Journal of Transportation Engineering*, 141(21) (2015).
- Mohammadi, J., and Shah, N.: Statistical Evaluation of Truck Overloads. *ASCE Journal of Transportation Engineering*, 118(5), 661-665 (1992).
- Pais, J. C., Amorim, S. I. R., and Minhoto, M. J. C.: Impact of Traffic Overload on Road Pavement Performance. *ASCE Journal of Transportation Engineering*, 139(9), 873-879 (2013).
- Prozzi, J. A., Hong, F., and Leidy, J.: Optimum Statistical Characterization of WIM Data Based on Pavement Impact. *TRB Annual Meeting CD-ROM*, (2006).
- Prozzi, J. A. and Hong, F.: Optimum Statistical Characterization of Axle Load Spectra Based on Load- Associated Pavement Damage. *International Journal of Pavement Engineering*, 8(9), 323-330 (2007).
- R Development Core Team. *R: A Language and Environment for Statistical Computing*, R Project for Statistical Computing, <http://www.R-project.org> (2018/4/5)
- Salama, H.K., Chatti, K., and Lyles, R.W.: The Effect of Heavy Multiple Axle Trucks on Flexible Pavement Damage Using In-Service Pavement Performance Data. *ASCE Journal of Transportation Engineering*, 132(10), 763-770 (2006).
- Savio, D., Paul, P., and Krishnan, J.M.: *Statistical Analysis of Axle Load Data and Pavement Damage for a Few National Highways in India*. 4th CEW Delft 2016, CRC Press, Netherlands (2016).
- Timm, D.H., Tisdale, S.M., and Turochy, R.E.: Axle Load Spectra Characterization by Mixed Distribution Modelling. *ASCE Journal of Transportation Engineering*, 131(2), 83-88 (2005).
- TRB. *Regulation of weights, lengths, and widths of commercial motor vehicles*, Committee for the Study of the Regulation of Weights, Lengths, and Widths of Commercial Motor Vehicles Special report 267, USA (2002).
- Weissmann, A. J., Weissmann, J., Papagiannakis, A., and Kunisetty, J. L.: Potential Impacts of Longer and Heavier Vehicles on Texas Pavements. *ASCE Journal of Transportation Engineering*, 139(1), 75-80 (2013).

FEASIBILITY STUDY OF PROVISION FOR EXCLUSIVE BUS LANES ON URBAN ROADS

Arathi A R¹ and Vincy Verghese²

¹ PG Scholar, Department of Civil Engineering, Jyothi Engineering College, Thrissur arathirajkumar@gmail.com

² Assistant Professor, Department of Civil Engineering, Jyothi Engineering College, Thrissur
vincyverghese@jecc.ac.in

Abstract. Optimal use of road transport system is necessary to address the problems like traffic congestion, air pollution and safety. One such way to optimize is by encouraging use of public transport modes (buses) by assigning priority to them. One of the bus preferential treatments is the provision of exclusive lanes for buses on urban roads. The specific aim of this study is mainly to study the feasibility of provision of exclusive bus lanes based on two criteria (1) based on proportion of travellers using different types of road vehicles and (2) based on the total travellers' time savings in terms of money value due to provision of exclusive bus lane on urban roads. The major work element of this study includes vehicle occupancy survey, vehicle volume and composition survey, income survey and estimation of journey time and journey time savings in terms of money value savings. The provision of exclusive bus lanes on urban roads increases the speed of buses, reduces journey time, saves travel cost and reduces road crashes.

Keywords: Exclusive Bus Lane, Vehicle Composition, Windshield Method.

Introduction

Transportation aims at safe and efficient movement of goods and passengers. Faster mobility of goods and passengers is the catalyst for economic growth of a country and this is facilitated by efficient transportation system. In case of road transportation systems, as facility increases, the volume of traffic also increases due to increasing demand for transport, particularly in developing countries like India. Because of the space, financial and material constraints urban road infrastructure cannot be developed beyond a limit and this leads to increase in congestion, pollution and reduction in road safety. Hence, there is a need for an appropriate strategy for optimal use of road transport system to reduce congestion and to increase efficiency of road networks. One way to reduce congestion is by encouraging the travellers to use public transport system (Buses) instead of private transport modes, because public transport system enables mass transit of passengers in fewer vehicles.

To bring about a shift in the passenger preferences, the public transport system should be highly efficient and relatively less expensive to attract the travellers from private modes of transport. This goal can be attained by encouraging public transport modes like buses by assigning priority. One of the methods of assigning priority to public transit are by providing exclusive bus lanes.

Exclusive bus lanes are the lanes restricted only for buses provided in order to speed up the buses, to reduce the interactions between buses and other modes of vehicles and thereby reducing the road crashes.

Objectives

By considering the aim of the study, the main objective formulated is to study the general impact of provision of exclusive bus lanes on traffic flow characteristics under heterogeneous traffic conditions. To achieve this main objective the subtasks formulated was the following.

To develop social criteria based on the proportion of travellers using different modes

To develop economic criteria based on the money value of time of travellers using the different modes.

Literature Review

Arasan and Vedagiri [1] estimated the probable shift of car users to bus due to the increase in level of service (LOS) after providing exclusive bus lanes on Indian city roads carrying heterogeneous traffic. The increase in LOS was determined using a recently developed simulation model. A mode-choice probability curve to depict the

possible modal shift of car users to bus was developed. From the curve, the probability of shift of car users to bus was estimated 0.7 at traffic flow corresponding to level of service C, for an 11 m wide road and 0.28 for 14.5 m wide road.

Arasan and Vedagiri [2] developed and used a heterogeneous traffic flow micro-simulation model to study the impact of provision of reserved bus lanes on urban roads in terms of reduction in speed of other categories of motor vehicles due to the consequent reduction in road space, over a wide range of traffic volume. It has been found that the maximum permissible volume to capacity ratio that will ensure a LOS C was 0.62 for the traffic stream other than buses if the bus lane is provided. Justification of providing exclusive bus lane has also been defined on the basis of number of travellers per unit width of the road.

Cevero [3] developed working paper on Bus Rapid Transit (BRT): An efficient and competitive mode of public transport. This report reviews experiences with designing and implementing BRT systems worldwide. BRT is first defined across a spectrum of service qualities and costs. The report closes with discussions on BRT's likely future given global growth projections and other pressing policy agendas in the foreseeable future.

Chen et al. [4] carried out a study to examine the effect of exclusive bus lanes (XBLs) and transit signal priority (TSP) on bus rapid transit (BRT) in China. A micro-simulation analysis was created based on extensive field data collection. The analysis showed that XBLs and TSP have a significant impact on the operational performance of BRT if both are implemented simultaneously.

Syed et al. [5] studied the Impact of Exclusive Bus Lanes on Traffic Performance in Urban Areas. In this paper, two different transit priority strategies at an intersection are analyzed and their performance impact is evaluated in terms of reduction in delay of the buses and cars, due to the priority given. The main findings of the study are that the bus priorities are more efficient at high volumes. Micro-simulation tool VISSIM is used to carry out the simulation process.

Abdelfatah and Abdulwahid [6] studied the Impact of Exclusive Bus Lanes on Traffic Performance in Urban Areas. This study investigates the impact of XBLs on urban road network performance under different traffic conditions using the micro-simulation software, VISSIM. It considers different parameters such as demand-to-capacity ratio D/C, traffic turning percentages, and bus headway and direction.

Study Area

Study area was selected considering the roadway geometry, traffic movement features and availability of suitable location for mounting the video camera. The area that satisfied the said requirements is Thrissur - Kechery road (17 km), state highway 69, Kerala. In that route Punnamm - Puzhakkal road stretch is selected as study stretch. The selected stretch of road is four lane divided road and 1.8 km long. The available width of the carriageway is 14.5 m (7.0 m in both directions).

Data Collection

The data needed for studying the feasibility of exclusive bus lane includes vehicle composition, vehicle occupancy and monthly income of travellers.

Vehicle Composition

The required traffic data for the study was collected by video recording of the traffic flow on the selected location. A total of 4999veh/hour, 4140veh/hour and 4926veh/hour were observed to pass through the section during the morning peak hour, off peak hour and evening peak hour respectively. The observed vehicle composition was shown in Fig. 1.

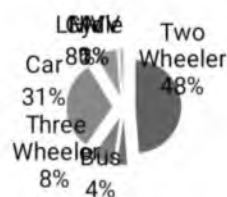


Fig.1. Observed traffic composition.

Vehicle Occupancy

Occupancy of different modes of vehicles is determined using windshield method. Average occupancies of 58.84, 1.36, 2.28, 2.32, 2.76, 1.24 and 1.00 are obtained for bus, two wheeler, three wheeler, car, LMV, HMV and cycle respectively. Proportions of travellers using each mode of vehicles are shown in Fig. 2.

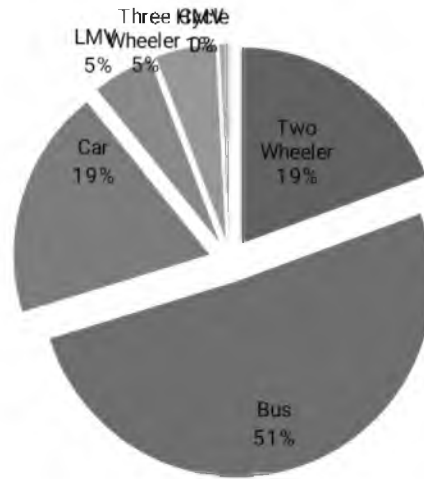


Fig.2. Proportion of travellers.

Speed

The time taken by different modes of vehicle to pass the known distance is retrieved from video and speeds of different modes of vehicles towards Thrissur and Kechery directions are determined. During peak hour the speeds of vehicles are less and their journey time are more compared to off peak hour.

Survey of Income of Travellers

Survey for monthly income of travellers is done at different locations in Thrissur city for different modes of vehicles. Proportion of travellers using different modes of vehicles under each income group is determined. Using (1), the hourly income of the users of different modes was calculated.

$$\text{Hourly Income} = \frac{\text{Monthly Income} \times 12 \left(\begin{matrix} \text{months} \\ \text{in a year} \end{matrix} \right)}{52 \left(\begin{matrix} \text{weeks} \\ \text{in a year} \end{matrix} \right) \times 5 \left(\begin{matrix} \text{working days} \\ \text{in a week} \end{matrix} \right) \times 8 \left(\begin{matrix} \text{working hours} \\ \text{in a day} \end{matrix} \right)} \tag{1}$$

Data Analysis

Journey Time Savings In Terms of Money Value

According to survey, 45% of passengers are ready to shift to bus after the implementation of exclusive bus lane. The reduced traffic volumes after 45% shift of occupants to bus towards Thrissur and towards Kechery are determined. During peak hour and off peak hour, the speeds are determined for different modes of vehicles corresponding to actual traffic volume (without bus lane). Then, the speeds of different modes of vehicles except bus for reduced traffic volume (with exclusive bus lane) is determined using interpolation technique. After the implementation of exclusive bus lane, the bus can flow freely with an increased speed around 70 km/h [6], without any interruption from other vehicles.

Then from this speeds, journey time of all modes of vehicles with and without bus lanes were calculated for travelling a distance of 17km road. While analyzing the journey time, it can be observe that the journey time for all modes are reduced with the implementation of exclusive bus lane. Then, the journey time savings for different modes of vehicles are determined. For bus, a savings of around 11 minute is obtained after the implementation of exclusive bus lane.

The journey time savings are then converted into money value savings by multiplying the journey time savings of each mode with their corresponding hourly incomes and calculated money savings was shown in Table I. A total of ₹ 2777 money savings per hour are obtained with the provision of exclusive bus lane.

Table 1.Money value savings

Vehicle Type	Savings in Journey Time (min)		Average Hourly Income (Rs.)	Money value savings (Rs.)	
	Towards Thrissur	Towards Kechery		Towards Thrissur	Towards Kechery
Two Wheeler	0.37	0.41	159.13	58.88	65.24
Three Wheeler	0.68	0.33	139.13	94.61	44.52
Car	0.21	1.29	195.61	41.08	252.34
LMV	0.03	2.26	187.50	7.50	425.63
Bus	10.49	10.58	73.55	771.54	778.16

Minimum Frequency and Composition of the Buses

There were 51 buses per hour and 62 buses per hour flowing towards Thrissur and Kechery respectively. The minimum frequencies of buses obtained were 1.2 min towards Thrissur and 1.0 min towards Kechery. Minimum composition of the buses is obtained by dividing the total number of buses in that direction by the average occupancy of bus. The minimum composition is obtained as 0.90% towards Thrissur and 1.10% towards Kechery.

Road Space Allocation

Total width of the selected road stretch is 7m (in one direction), extra 3.5m is proposed to be provided exclusively for buses on both directions adjacent to the curb. So that passenger can easily enter to and exit from the buses. A schematic layout of the road stretch with 3.5 meter exclusive bus lane is shown in the Fig. 3.

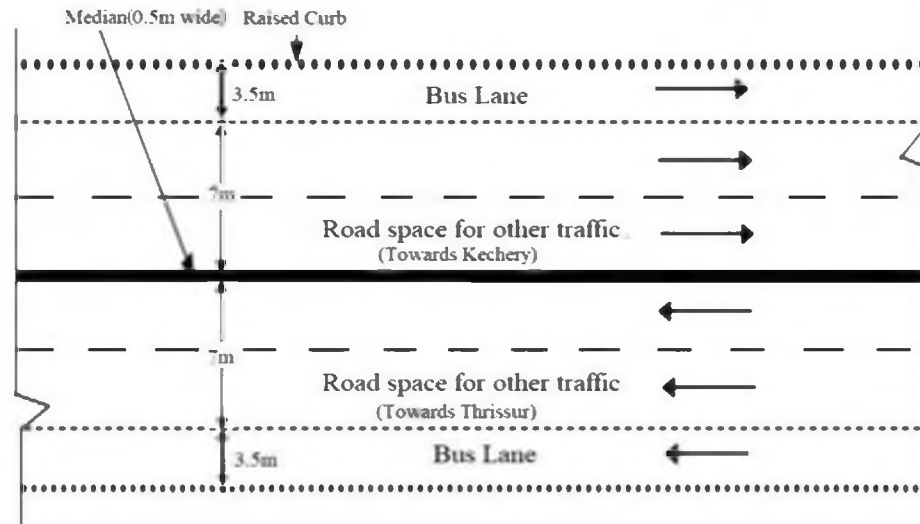


Fig.3. Schematic layout of the road stretch with exclusive bus lane.

Findings

The feasibility study of provision for exclusive bus lane is done based on proportion of travellers using buses and other vehicles and the journey time savings in terms of money value. The following are the findings of this study: The bus travellers, constituting 51% of the total of the travellers, will use only 33 % of the road space, whereas, the users of all the other modes (excluding buses) constituting 49 % of the total of the travellers, will use 67 % of the road space. This shows that the provision of exclusive bus lane is justifiable based on the proportion of travellers using different modes of vehicles.

The money value of total travellers' time savings in one hour, due to the provision of exclusive bus lane on 14.5 m wide and 17 km long urban road stretch was estimated as ₹ 2777 per hour. This shows that the provision of exclusive bus lane is justifiable based money value of journey time savings.

Minimum frequency of bus is determined as 1.2 min towards Thrissur and 1.0 min towards Kechery and the minimum composition of buses were 0.9% and 1.1% towards Thrissur and Kechery respectively.

Features of the Proposed Exclusive Bus Lane

The following are the features of the proposed exclusive bus lane:

- Free flow of buses without any delay
- Proper and systematic scheduling of buses
- Speed = 70 km/h
- Journey time = 14.57 min
- Journey time saved by around 11 min
- Minimum frequency of bus services required = 55s
- Money value savings = ₹ 775 per hour
- Increased proportion of travellers using bus=7%
- Bus headway = 0.85 km
- Width of exclusive bus lane = 3.5m (near curb)
- Length of exclusive bus lane= 17km

Conclusion

By introducing this systematically scheduled and rapid bus service in exclusive bus lanes, more travellers will get attracted towards it and there by the use of public transportation gets enhanced and the private transportation gets reduced. By increasing the frequency of bus services, the demand for bus transit increased. As frequency increases waiting time for the travellers reduced. More travellers get attracted to bus transit. This will reduce the accidents,

pollution and congestion problems. Therefore, it increases the efficiency of the road transportation system and thereby increasing the social and economic background of the country itself.

Future Scope

The obtained results are based on the limited data collected. More extensive data collection and the analytical reasoning are required. Reliable results will be obtained only after the implementation. For getting more reliable results implementation has to be done in a simulation software. Land acquisition problems due to extra widening have to be analysed to make this study more acceptable one.

Acknowledgment

I express my sincere thanks to my colleagues Thasneem Nadirsha, Midhun T. and Leejiya Jose for their help during data collection.

References

- Arasan, V. T., Vedagiri, P.: Simulating heterogeneous traffic flow on roads with and without bus lanes. *Journal of Infrastructure Systems* 15(4), 305-312 (2009).
- Arasan, V. T., Vedagiri, P.: Micro simulation study of the effect of exclusive bus lanes on heterogeneous traffic flow. *Journal of Urban Planning and Development* 136(1), 50-58 (2010).
- Cervero, R.: *Bus Rapid Transit (BRT): An efficient and competitive mode of public transport*. Institute of Urban and Regional Development. Berkeley (2013).
- Chen, Y., Chen, G., Wu, K.: Evaluation of performance of bus lanes on urban expressway using paramics micro-simulation model. In: *Procedia Engineering*, vol. 137, pp. 523 – 530, Beijing (2016).
- Syed, U., Ghodmare, S. D., Khode, B. V.: Performance impact of various bus priority strategies using vissim 7.0. *International Research Journal of Engineering and Technology*. 3(4), 2479 – 2483 (2016).
- Abdelfatah, A., Abdulwahid, A. R.: Impact of exclusive bus lanes on traffic performance in urban areas. In: *Proceedings of the 2nd World Congress on Civil, Structural and Environmental Engineering*, pp. 1 – 10, Spain (2017).

ENVIRONMENTAL ISSUES OF BUILDINGS –GREENSOLUTIONS

Aaliya Azeem

School of Energy and Environmental Engineering, VIT University, Vellore

Email: aaliyaazeem95@gmail.com

ABSTRACT

This paper focuses on the environmental issues caused due to buildings that can be mitigated by green solutions. The green buildings have turned to be a solution for such impacts. Buildings are responsible for 41% of worldwide energy usage, in the form of electricity. Also serves other environmental problems like wastage of water, materials etc. The green techniques adopted in buildings can improve energy efficiency, cost reduction and occupancy comfort.

KEYWORDS: Green buildings, Energy usage, Water consumption, Energy efficiency

1. INTRODUCTION

Buildings have many environmental issues related to its construction, utility, etc. Its impact on humans, resources and the environment is evident. Attaining comfortable as well as healthy indoor environment with minimum consumption of energy is a challenging issue. Inefficient energy use is one of the important problems in buildings. The materials used for the construction of buildings is a significant factor affecting the environment. Usage of non-sustainable materials have negative effect on buildings. Green buildings are now a solution to reduce the negative impact of buildings on environment.

2. ENVIRONMENTAL ISSUES OF BUILDINGS

American building construction contributes to huge percentage of greenhouse gas emissions. Buildings are responsible for majority of CO₂ emissions, which accounts to almost 38%. These emissions has led to climatic changes. It contributes to the rising temperatures and the so process called “global warming”. The extraction of raw materials required for construction during mining process that involves heavy machinery also gives off carbon emissions. Cement industry contributes to 5% of global CO₂ emissions.

During construction process, it makes impact to the local environment, such as chemicals spills waterways pollution on building sites or polluting the aquifer or soil underneath. For constructed buildings, energy usage contributes mainly to environmental impacts.

The raw materials that is used for the construction of buildings usually have environmental impact, especially when non sustainable materials are used for the construction. The transport of

such materials can also possess impact on air quality. The waste that come from building construction as well as demolition are great concerns. The destruction and renovation of buildings generates a huge amount of waste. It includes concrete, glass, aggregates, bricks etc. Large tons of demolition debris wastes creates waste disposal problems. To get rid of the mounting garbage these wastes are likely to be thrown in the landfills. Landfills are the waste disposing sites that designed for collecting different types of wastes. These wastes can pollute the land, air and contaminate the soil.

The environmental issues related to construction can be reduced with the help of many stakeholders, legislators who set regulations for construction waste management and green construction. And now many construction firms emphasis on limiting the environmental impacts arising from construction projects.

The innovation of green materials helped in eliminating or reducing the need for destructive mining practices involving fossil fuels. Green materials can be synthetically produced and helps in lowering the cost. The green materials includes the materials that are highly energy efficient, easily or locally available and that are sustainable. These materials can be recycled or reused in future for other projects, and thus helps significantly in cost savings and reducing the environmental impacts.

2.1 Indoor air quality

Indoor air quality (IEA) indicates the quality of air inside the buildings, also the comfort given to occupants in all terms. It relates to the pollutants, ergonomics, acoustics, lighting and temperature. . Inadequate ventilation can also result in sick building syndrome condition, the condition where the occupants of the building suffer from unhealthy symptoms or diseases. Although usage of air conditioners has improved thermal comfort and health problems related to poor air quality, its energy consumption is taken to consideration. The main aim is to achieve good healthy environment and air quality with proper cooling and ventilation within the buildings.

2.2 Energy and water usage

With the growing population, the energy demand goes on rising, so energy efficiency is a prime objective nowadays. Buildings are the biggest energy consumers which account to 41%, much more than the industrial sector and transportation. The buildings use huge amount of electricity which becomes its major energy usage. It needs energy for lighting, cooling, heating etc. that required for the buildings. In US, buildings consume 73% of the total electricity.

Buildings use a large percentage of water, 13.6% of potable water that is 15 trillion gallons of water. Buildings are responsible not just for consuming large amount of world's water but also responsible for large amount of waste water.

3. GREEN SOLUTIONS

Environmental considerations, sustainability and energy efficiency should be a part of building design. Eco-construction defines the green buildings which involves sustainability not just in construction but also in its materials, techniques, methods and technologies used in it, enhancing environmental performance. Green buildings reduces the environmental impact and also helps in lowering the operating costs of a building.

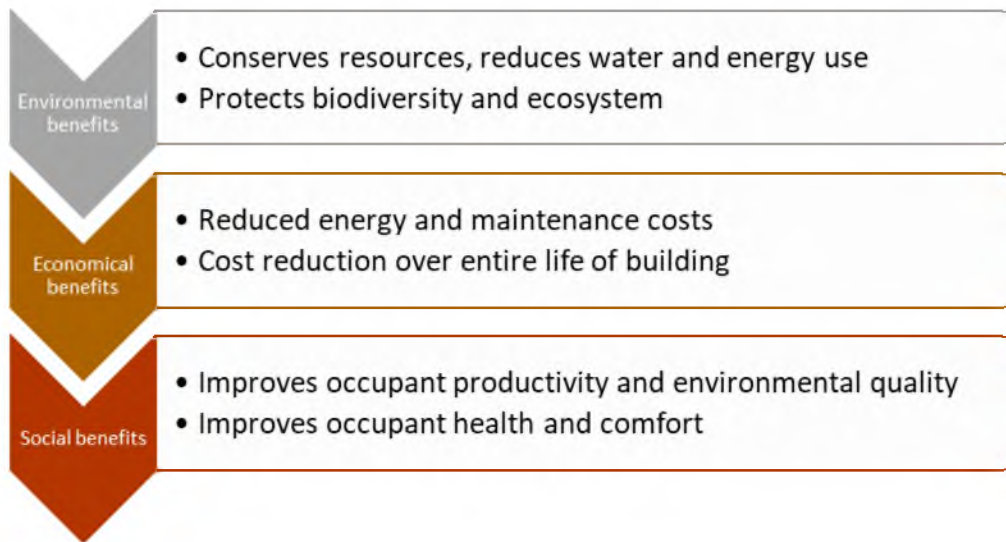
Green buildings consumes less resources. They need less energy, less water requirements as compared to the normal buildings. Less energy and less water usage implies that the monthly utility bills will be reduced. The materials and methods of construction has minimum impact on the environment and climatic changes. The green measures helps in improving the energy efficiency of buildings. These also helps in improving the Indoor Air Quality (IAQ).

Going green is necessary nowadays, to decrease the overall impact of buildings on humans, occupant health and environment. It helps in these motives:

- Reducing pollution, waste, and environmental impact
- Optimized usage of water, energy, other sources of energy
- Protects occupant's health and improves productivity

In going green, though the green materials seems to be costly initially, it saves on energy costs. Going green means conserving energy.

- Environmental benefits: conserves resources, reduces water wastage, efficient energy use, protects biodiversity and ecosystem
- Economical benefits: saves energy costs, less maintenance cost, reduced cost over the lifecycle of building
- Social benefits: improves occupant productivity, health and comfort



Benefits of adopting green measure

4. **GREEN MEASURES**

4.1 Energy efficiency

The usage of high-efficiency windows, insulation of walls, ceilings, floors reduces the energy use. Effective window placement providing natural sunlight through which effective daylighting can be achieved. Solar water heating reduces the energy loads. The energy generation through renewable sources like solar power, hydro power, wind energy and biomass reduces the ecological impact. Buildings consume more energy in the form of electricity, about two thirds of the whole electricity produced. Green building certification emphasis on energy savings.

The main objective is to use energy in an optimal way and to identify energy savings. The choice of equipment should also be energy efficient that controls energy consumption. Some of the ways or measures in which energy savings can be done are:

- Efficient thermal insulation of windows, walls etc.
- Remove energy leaks if any.
- Better airtight seal over the building
- Deduction of thermal losses achieved through proper ventilation
- Optimized electricity management

4.2 Water efficiency

Managing rainwater, irrigation water, wastewater are essentially required as an approach towards sustainability. Green buildings are designed to utilize water effectively. Aerator taps helps to reduce the consumption without getting noticed during its usage. By mixer taps usage, the temperatures can be regulated and controlled. It helps to generate savings. By water efficiency or water savings, there exist prime objectives to be achieved.

The main objectives include:

- to reduce the water consumption
- Protecting the quality of water and
- Efficiently utilizing water

Water conservation over the entire life cycle of the building involves designing a dual plumbing system that recycles water in toilet flushing. Waste water is minimized by utilization of water conservation fixtures such as ultra-low flush toilets, low flow shower heads etc. The grey water which comes from wash basins (or wash rooms), kitchens etc. can be used for lawn, gardening and irrigation.

The rain water that falls over the roof can be collected in storage tanks and can then be used effectively. This can be done by implementing a proper rain water harvesting system on the roof top. The water so collected can be used for gardening, irrigation, other domestic outdoor requirements. Other way of recuperating rain water is green roofs, by which, rain water is collected and serves a green habitat.

4.3 Materials efficiency

Green materials include renewable materials such as bamboo, recycled stone. Products and panels made of compressed earth blocks, rammed earth, clay, coconut, wood fiber plates, calcium sand stone, etc. can be used. Polyurethane blocks which are cheap, reduces carbon emissions and are ecofriendly. The materials should be reusable, recyclable, nontoxic and sustainable. The transportation costs of materials can also be reduced if locally available materials are used. The green materials has the benefit of minimizing the waste by recycling, less dust and noise, better occupational health and safety management.

4.4 Indoor environmental quality

This ensures the occupant health, well-being, their comfort and productivity. The products that emits dust, toxic gases, VOCs should be avoided that increases the IEQ of buildings. The construction materials used and interior finished products should be free of emissions for the occupant health. Adequate ventilation can be provided such as a proper designed HVAC system that helps in indoor air quality. Measures like Green roofs (roofs serving as vegetated surface) provides ecological services like building temperature regulation, enhancement in storm water management, decreased urban heating effects and increase in urban wildlife habitat.

The radiant system is very comfortable type of heating system. Radiant heating exchanges warm specifically from the floor to your body and in addition heating the encompassing air. Radiant heating systems deliver uniform temperatures in all rooms, warmed floor regions and furthermore in all seasons. Radiant heating is likewise a method to keep the transmission of tidy and dust, which are pervasive in warm air heating systems

4.5 Cost savings

Operation and maintenance are part of building planning and development. The addition of new green features also comes into O&M stage. Even though the installation of green features tends to be costlier like the photo voltaics and other modern technologies, its maintenance cost will be less. Also it helps in yielding more over the entire building life than the normal conventional buildings. Sustainable eco-construction also helps in saving costs on usage of resources like in energy and water usage. Energy efficient equipments are used to reduce the energy consumption. For example, using LEDs, solar lights for lightening. The energy efficient utilities and techniques reduces the energy bills significantly.

4.6 Waste reduction

Green construction reduces the wastage of energy and water contributing less wastes into the landfills. Well-designed buildings reduces the amount of waste produced by occupants through proper waste management provision. It provides on-site solutions minimizing the wastes to landfills such as the compost bins. The different types of wastes are separately collected, properly managed and efficiently utilized or disposed. The waste and waste water generated can be used as fertilizers. The biodegradable food waste which can be used in biogas composting units serves as an energy source.

Rainwater instead of simply being wasted as run off, rainwater harvesting system implemented. The rain water collected can be stored for utilities. Even the grey water from dish washing can be used for irrigation and flushing toilets. The waste water, human waste collected at the source can be given to semi-centralized biogas plant producing liquid fertilizer providing soil with nutrients and carbon sinks removing atmospheric carbon dioxide.

4.7 Green techniques using renewable sources

4.7.1 Solar

Solar heating systems when implemented in buildings, it preheats the outside air before it is allowed to enter the building. It helps in reducing the heating costs. Solar heaters can also be used to heat water that required for domestic purposes. Other application of solar walls which require very less maintenance is that, it can be used even in cloudy conditions. Solar electricity produced on a large scale using low cost solar cells is still on research. This proves to be effective both in terms of energy efficiency and in giving high yields.

4.7.2 Geothermal energy

Geothermal energy can be used in places where the geothermal reserves are present abundantly. It can be extracted from under the ground and the obtained energy can be utilized in heating, air conditioning or transformation (conversion) into electricity. A geothermal heat pump system can be implemented which indicates a major investment. It enables its users to utilize an

inexhaustible or renewable energy source which provides 60 to 70% of energy or power that needed to heat a building. It reduces the consumption of fossil fuels that emits lot of greenhouse gases. These resources also has the advantage of not depending on atmospheric conditions.

4.7.3 Wind power

Wind energy is a significant source of energy in green buildings. Wind power is a less expensive clean energy which can be generated. It involves conversion of wind power into other types of energy. The energy conversion include: Wind turbines used for the production of electrical energy, Windmills used for generating mechanical energy or power and Wind pumps can be used for the water extraction and drainage.

4.7.4 Other renewable energy sources

Hydraulic energy generated by displacement of fresh water, sea water, etc. plays an extremely significant role in serving as a source of power (energy).

Biomass is produced by the process called photosynthesis, in which energy from the sun is stored in plants in the form of carbohydrates using carbon dioxide from the atmosphere. Biomass refers to any living material or matter. In energy terms, biomass refers to all organic material which serves energy in different forms like biofuel, biogas, or sometimes used directly for combustion. For example: organic waste, agricultural waste, urban waste, etc. Food waste produced from the buildings can be used as a source of biomass to produce energy.

5. Green building rating benefits:

With the increasing percentage of buildings getting demolished, there is significant impact over climate changes. Therefore there is a need for green construction and the government in US insisted such green programs and LEED came into existence. LEED (Leadership in Energy and Environmental Design) - the rating system designed and developed by USGBC, which evaluates environmental performance of a building and also for promoting sustainable design.

Benefits of Green buildings: LEED certification

LEED Gold certified building:

- Uses 11% less water and 25% less energy than an average non LEED rated building. If a building uses less energy and less water, the monthly utility bills will be lowered.
- Has 19% lower maintenance costs than the normal building
- Produces 34% less greenhouse gas emissions.
- Occupants are more satisfied by average of 27% than the occupants of non-rated buildings. Because, Green buildings helps in increasing comfort and reduces sick building syndrome.

REFERENCES

1. L. Pérez-Lombard, J. Ortiz, *et al*(2008), A review on buildings energy consumption information, *Energy and Buildings* 40 (3) 394–398.
2. A.H. Neto, F.A.S. Fiorelli,(2008). Comparison between detailed model simulation and artificial neural network for forecasting building energy consumption, *Energy and Buildings* 40 (12) 2169–2176.
3. Y. Zhang, J.A. Wright, *et al* (2006). Energy aspects of HVAC system configurations—problem definition and test cases, *HVAC and R Research* 12 (3C) 871–888.
4. J. Morrissey, R.E. Horne,(2011). Life cycle cost implications of energy efficiency measures in new residential buildings, *Energy and Buildings* 43 915–924.
5. A. Joelsson, L. Gustavsson,(2009). District heating and energy efficiency in detached houses of differing size and construction, *Applied Energy* 86 (2) 126–134
6. Sam Kubba, (2010). *Green Construction Project Management and Cost Over site*, Elsevier, USA.
7. Sidney Levy, (2010). *Construction Process, Planning and Management: Green and Sustainable Buildings*, Elsevier, USA.
8. Luis Pérez-Lombard, José Ortiz, *et al*.(2008).“A Review on Buildings Energy Consumption Information”, *Energy and Buildings*, vol. 40, no. 3. pp. 394-398.
9. Ashwin Sabapathy, Santhosh K.V. Ragavan, *et al*,2010. “Energy Efficiency Benchmarks and the Performance of LEED Rated Buildings for Information Technology Facilities in Bangalore, India”, *Energy and Buildings*, vol. 42, no. 11, pp. 2206-2212.
10. Cheng-Li Cheng, (2002) “Study of the Inter-Relationship between Water use and Energy Conservation for a Building”, *Energy and Buildings*, vol. 34, no. 3, pp. 261-266.
11. Prez-Lombard L, Ortiz J, *et al*, (2008). A review on buildings energy consumption information. *Energy and Buildings*, Volume- 40(3), pages-394–398.
12. Jianlei Niu, (2004), Some significant Environmental Issues in High rise buildings in Urban areas, Volume-36, Issue-12, pages 1259-1263.
13. Anne Steinemann, Pawel Wargocki, (2017), Ten Questions concerning Green Buildings and Indoor Air Quality, Volume 112, pages 351-358.
14. Joel Makower, (2008), *The Environmental Impacts of Green Buildings*
15. United States Environmental Protection Agency (EPA). 1991, “Indoor Air Facts No.4 Sick Building Syndrome”.
16. <https://bosscontrols.com/buildings-impact-environment/>

Development of noise map using GIS for Lucknow metropolis

By

Sudhanshu Bhushan*, A.K. Shukla**, Institute of Engineering & Technology, Lucknow

*M.TECH ENVIRONMENTAL STUDENT, **PROFESSOR, DEPARTMENT OF CIVIL ENGINEERING

Email.ID-sudhanshu2508@gmail.com

ABSTRACT

Noise pollution is a problem increasingly acknowledged by authorities and governments around the globe. Geographical Information Systems (GIS 10.1) can conveniently be adapted together to analyse and present noise information. Noise maps can be used to assess and monitor the influence of noise effects. Residents living in high rise buildings are also severely affected by traffic noise. The integration of GIS and noise maps makes it possible to increase the quality of noise effect studies by dealing with uncertainties, by applying standardized methods to study and quantify noise effects. The present work aimed at development of noise map for Lucknow metropolis. In this study, a total of 10 locations were selected for collection of data. Noise pollution can damage physiological and psychological health. The noise levels in terms of L_{10} , L_{90} , L_{AEQ} , L_{NP} and TNI have measured using Sound Level Meter (SPL). The noise levels were observed in the month of September 2017 to November 2017. In the morning time (7AM-9AM) residential zones L_{EQ} was found in the range of 77.89-80.70dB (A), in commercial zones L_{EQ} was in the range of 72.00-82.16dB (A), in industrial zones L_{EQ} was in the range of 68.26-71.62dB (A) and in the silence zones L_{EQ} was in the range of 75.00-78.26dB (A). In the afternoon (12PM-2PM) noise levels were observed for residential zones L_{EQ} was in the range of 64.70-83.72dB(A), for commercial zones L_{EQ} was in the range of 74.90-84.52dB(A), for industrial zones L_{EQ} was in the range of 72.32-75.28dB(A) and for silence zones L_{EQ} was in the range of 73.19-76.49dB(A). In the evening (6PM-8PM) noise levels for residential zones L_{EQ} were found in the range of 76.29-81.03dB (A), for commercial zones L_{EQ} was in the range of 75.16-85.45dB (A), for industrial zones L_{EQ} was in the range of 69.68-81.82 dB (A) and for silence zones was in the range of 68.74-71.78dB (A). Except in industrial zone in all other zones the noise levels are beyond limits.

Keywords– Noise Pollution, GIS, Traffic Noise Maps.

1. Introduction

Noise levels can be researched in different ways: as traffic and transportation; industrial activities, marketing and entertainment facilities [1]. In contrast to other pollutants, the control of environmental noise is interrupted by insufficient knowledge of its effects on humans and lack of defined criteria. Noise pollution is a significant environmental problem in many rapidly urbanizing areas; it is not recognized as serious in many cases, yet it steadily grows in developing and developed countries alike. Among the common negative consequences resulting from urbanization is environmental noise pollution. This is an obvious problem at a time when there is great difficulty in ensuring that urban areas of Lucknow become functional and

aesthetically pleasing. Urbanization is the common primary reason commonly advanced for the present advanced deplorable state of many cities in the country [2]. The World Health Organization [3, 4] promotes actions against noise pollution. Environmental noise management is a part of environmental impact studies and of guidelines for urban development in various countries. Lucknow metropolis, with a population of over 28.2 Lakhs inhabitants, deserves its own noise map. Accordingly, this investigation seeks to develop a noise map of the city based on the noise parameters as L_{AEQ} , TNI (traffic noise index) and L_{NP} .

2. Literature review on noise mapping

Noise maps describe spatial distributions of noise levels. They allow an efficient visualization of the noise distributions in areas where land uses are sensitive to noise. Noise mapping is an efficient assessment method in urban areas [6]. A noise map provides a comprehensive look for the problem of multiple sources and receivers, and thus can improve urban planning. According to Santos [2], the use of noise mapping allows:

- Quantification of noise in the studied location;
- Assessment of population exposure;
- Composition of a database for urban planning with localisation of noisy activities and sensitive zones;
- Modelling of different scenarios for the future;
- Forecast of impact noise of the projected infrastructure and industrial activities.

The most advanced research in noise mapping has been performed in European countries. For example, Germany has conducted relevant research for more than 25 years. Based on the results of previous studies, traffic noise is frequently identified as the main noise source. The UK published the London noise map in 2004, which is the first noise map produced by a national government, as a reference for London citizens to avoid noise nuisances [7]. De Kluijver and Stoter [8] concluded that appropriate use of Geographic Information System (GIS) in mapping noise effects makes it possible to optimize the quality and efficiency of noise effect studies. The GIS is an important tool in spatial analysis and modelling. Sheng and Wa Tang [9] applied a GIS-based traffic noise model system to investigate the influences of existing urban forms on vehicle transport and pedestrian exposure to traffic noise in the Macao Peninsula. Wazir [10] prepared a noise map using ArcGIS 9.3.1 software for better visual information of the noise environment of Guwahati City and its diurnal variations. Interpolation is an effective technique used by various researchers for the purposes of noise mapping. In the interpolation technique, krigging is done to assess the acoustic behaviour of the geographical area. The study highlighted the noise-polluted and vulnerable areas through diurnal noise mapping. It was observed that areas with high traffic congestion, narrow roads, heavy constructional activities and poor traffic management are more vulnerable to high noise levels. Some of the educational institutions, hospitals and nursing homes are within a high-noise environment. Some researchers have developed high temporal/spatial resolution systems for modelling air quality or noise.

3. Materials and methods

3.1. Study area

This research is based on the results of outdoor sound level measurements carried out in September to November 2017 at 10 different locations (2 residential locations, 4 commercial locations, 2 industrial locations, 2 silence locations) in Lucknow metropolis, the capital city of Uttar Pradesh State over the study area; i.e. 80.95°E longitude (Lucknow) and 28.70°N latitude.. Figure 1 is a general view of Lucknow metropolis showing the areas of noise measurements for this study.

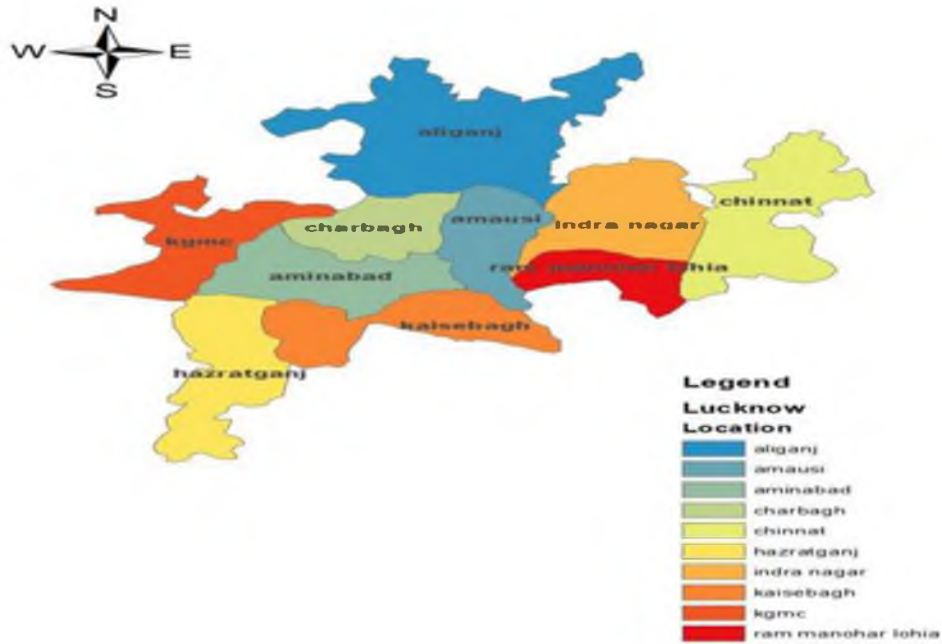


Figure-1 General view of Lucknow metropolis showing the locations of noise measurements

3.2. Experimental Procedure

Instrumentation for the field measurements consisted of a precision-grade sound level meter (Lutron-SL 4010). The instruments were calibrated by the internal sound level calibrator before making measurements at each site. All the instruments comply with the International Electrotechnical Commission (IEC) standards. Monitoring was carried out at a height of 1.5 m and 1 m away from the chest for 60 min. at interval of 15 seconds. L_{Ai} (A-weighted instantaneous sound pressure level) measurements were recorded at intervals of 15 seconds for a period of 60 min, giving 240 readings per sampling location. This procedure was carried out for morning (7AM–9AM), afternoon (12PM–2PM.), evening (6PM–8PM) measurements. From these readings, commonly used community noise evaluation quantities like the exceedence percentiles, L_{10} and L_{90} , the A-weighted equivalent sound pressure level L_{AEQ} , the noise pollution level L_{NP} , and the traffic noise index TNI , were determined. These noise measures are defined as follows [27]:

$$L_{AEQ} = 10 \log_{10} \left[\frac{1}{N} \sum_{i=1}^N \left(\text{anti log} \frac{L_{Ai}}{10} \right) n_i \right] \tag{1}$$

$$L_{NP} = L_{EQ} + (L_{10} - L_{90}) \tag{2}$$

$$TNI = 4(L_{10} - L_{90}) + (L_{90} - 30) \tag{3}$$

where L_{AI} is the i th A-weighted sound pressure level reading dB, n is the total number of readings, L_{Aeq} is the A-weighted equivalent sound pressure level, L_{10} is the noise level that exceeded 10% of the time, L_{90} is the noise level that exceeded 90% of the time (also referred to as background noise level), L_{NP} is the noise pollution level, and TNI is the traffic noise index.

4. Results and discussion

4.1. Assessment of noise parameters:

The average noise parameters were determined at different location. Table 1 shows the daily average values of noise parameters for the study area. At eight locations values of L_{EQ} , L_{NP} , and TNI were exceeded from the permissible limits in the month of September 2017 for time span (7Am to 9AM), (12PM to 2PM) and (6PM-8PM) respectively. The different noise level parameter such as L_{10} , L_{90} , L_{NP} , L_{EQ} and TNI were shown for different locations from 7am to 9am in figure 2. The L_{10} values of noise level varies between 72.83 to 84.68dB, L_{90} values varied between 60.13 to 71.26dB, L_{NP} values varied between 78.28 to 104.18dB, L_{EQ} was in the range of 69.68 to 80.41dB and TNI values varied between 68.63 to 125.9dB and further same the different noise level parameter were showed at different locations for 12pm-2pm. The L_{10} was showed noise level values varies between 76.28 to 86.25dB, L_{90} values varies between 61.02 to 73.25dB, L_{NP} valued varies between 84.25 to 102.77dB and L_{EQ} is in the range of 66.15 to 83.59dB and TNI values were varied between 80.6 to 117.30dB and also same the different noise level parameters were showed at different locations in 6pm-8pm. The L_{10} was showed noise level values varies between 72 to 88.56dB, L_{90} values were varied between 59.00 to 83.00dB, L_{NP} values were varied between 81.57 to 105.8dB, L_{EQ} was in the range of 68.74 to 84.15dB and TNI values were varied between 81 to 119.40dB.

Table 1-Average noise parameters at study locations in the month of September 2017

Time Parameters Locations	7AM-9AM					12PM-2PM					6PM-8PM				
	L10 dBA	L90 dBA	LAeq dBA	LNP dBA	TNI dBA	L10 dBA	L90 dBA	LAeq dBA	LNP dBA	TNI dBA	L10 dBA	L90 dBA	LAeq dBA	LNP dBA	TNI dBA
1. CHINNAT	76.82	65.68	69.72	80.86	80.24	80.00	68.00	72.32	84.32	86.00	83	71	78	91	89
2. RAM MANOHAR LOHIA	78.19	64.19	76.41	90.41	90.19	77.27	66.16	73.20	84.31	80.60	72.83	60	68.74	81.57	81.32
3.INDRA NAGAR	82.93	60.13	79.26	102.06	121.33	76.90	62.00	66.15	85.15	91.60	85	64.2	79.664	100.4	117.4
4.ALIGANJ	81.5	62.53	77.89	96.867	108.41	82.59	61.02	81.20	102.77	117.30	81.48	68.3	76.29	89.47	91.02
5.KGMC	79	64	75.75	90.75	94	78.00	66.00	73.90	85.90	84.00	72	59	68.81	81.81	81
6. AMAUSI	72.83	64.23	69.68	78.28	68.63	78.25	67.00	73.63	84.88	82.00	81.27	69.56	79.77	91.48	86.4
7. CHARBAGH	82.92	64.56	78.92	97.28	108	86.25	73.25	83.59	96.59	95.25	88.56	68.26	82.26	102.5	119.4
8. KAISEBAGH	79.26	71.26	75.55	83.55	73.26	81.26	69.26	79.82	91.82	87.26	84.26	62.53	84.14	105.8	119.4
9.HAZRATGANJ	79	66	72.22	85.22	88	82.00	64.00	74.90	92.90	106.00	81.9	66.1	75.16	90.97	99.3
10.AMINABAD	84.68	60.91	80.41	104.18	125.99 1	82.95	68.21	78.47	93.21	97.17	86.93	70.1	80.32	97.15	107.4

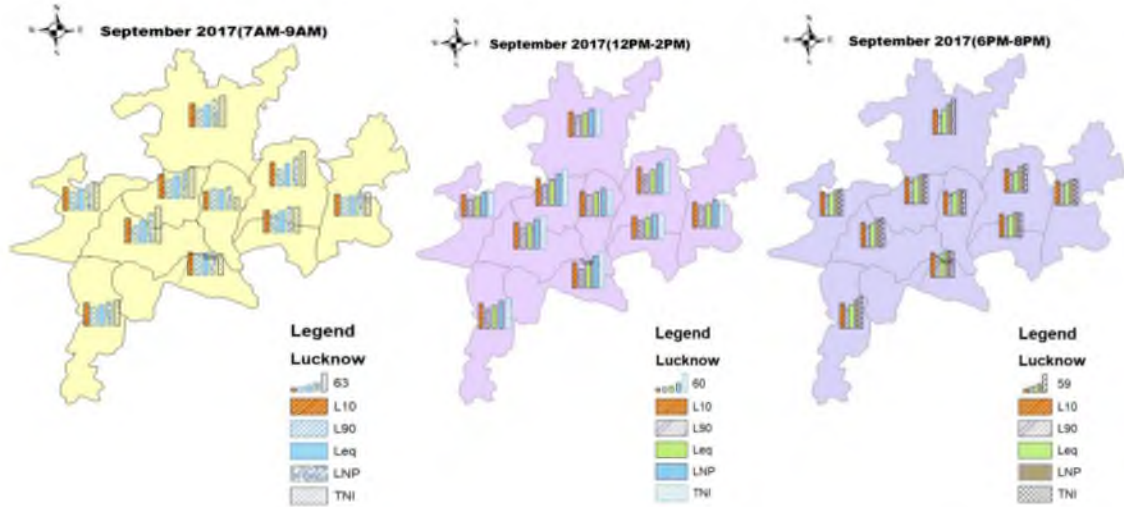


Figure2. Noise map for Lucknow metropolis in the month of September 2017

In the above figure 2, the noise map of all noise parameters show higher values for Aminabad, Indra nagar at the time interval (7AM-9Am), for Charbagh, Kaiserbagh at the time interval (12PM-2PM) and for Aliganj, Amausi at the time interval (6PM-8PM). Now lower values for Kaiserbagh, Hazratganj at the time interval (7AM-9Am), for Aliganj, KGMC at the time interval (12PM-2PM) and for Hazratganj, Chinnhat at the time interval (6PM-8PM).

Table 2 shows the daily average values of noise parameters for the study area. At eight locations values of L_{EQ} , L_{NP} , and TNI were exceeded from the permissible limits in the month of October 2017 for time span (7Am to 9AM), (12PM to 2PM) and (6PM-8PM) respectively. The different noise level parameter such as L_{10} , L_{90} , L_{NP} , L_{EQ} and TNI were shown for different locations from 7am to 9am in figure 3. The L_{10} values of noise level varies between 76.82 to 85.15dB, L_{90} values varied between 61.12 to 71.26dB, L_{NP} values varied between 82.17 to 105.36dB, L_{EQ} was in the range of 69.97 to 81.49dB and TNI values varied between 73.26 to 121.12dB and further same the different noise level parameter were showed at different locations for 12pm-2pm. The L_{10} was showed noise level values varies between 77.62to 86.25dB, L_{90} values varies between 62.53 to 73.25dB, L_{NP} valued varies between 78.50 to 103.98dB and L_{EQ} is in the range of 64.70 to 83.5dB and TNI values were varied between 80.88 to 119.53dB and also same the different noise level parameters were showed at different locations in 6pm-8pm. The L_{10} was showed noise level values varies between 77.62 to 88.25dB, L_{90} values were varied between 62.53 to 74.89dB, L_{NP} values were varied between 70.37 to 105.8dB, L_{EQ} was in the range of 70.37 to 84.14dB and TNI values were varied between 82.75 to 119.40dB.

Table 2-Average noise parameters at study locations in the month of October 2017

Time	7AM-9AM					12PM-2PM					6PM-8PM				
Parameters Locations	L10 dBA	L90 dBA	LAeq dBA	LNP dBA	TNI dBA	L10 dBA	L90 dBA	LAeq dBA	LNP dBA	TNI dBA	L10 dB A	L90 dB A	LAeq dBA	LNP dB A	TNI dB A
1. CHINNAT	77.92	67.72	70.72	82.9	78.52	81.78	70.92	73.62	84.48	84.3	81.7	70.9	79.6	92.6	94.8
2. RAM MANOHAR LOHIA	79.17	65	77.01	91.0	91.32	78.25	67	74.86	85.83	81.1	78.2	67	70.3	82.7	80.3
3.INDRA NAGAR	83.62	61.12	79.69	102	121.1	77.62	63.82	64.70	78.50	89.0	77.6	63.8	79.5	99.9	117
4.ALIGANJ	82.56	66.45	76.88	92.9	100.8	84.28	62.53	82.23	103.9	119	84.2	62.5	77.9	87.9	81.2

5.KGMC	79.58	65	77.48	91.9	92.96	78.18	67	74.84	85.74	80.8	78.1	67	70.5	83.3	81.9
6. AMAUSI	76.82	66.52	69.97	82.1	77.72	81.78	70.92	74.74	85.60	84.3	81.7	70.9	78.9	91.9	94.8
7. CHARBAGH	82.92	64.56	78.92	97.2	108	86.25	73.25	83.59	96.59	95.2	88.2	74.8	82.2	102	119
8. KAISEBAGH	79.26	71.26	76.35	84.35	73.26	81.26	69.26	79.82	91.82	87.2	81.5	70.8	84.1	105	119
9.HAZRATGA NJ	80	67.52	74	86.77	87.04	83.45	66.79	75.82	92.47	103	83.4	66.7	75	93	106
10.AMINABAD	85.15	61.28	81.49	105.3	126.7	83.3	70.2	78.66	91.76	92.6	83.3	70.2	80.9	97.3	107

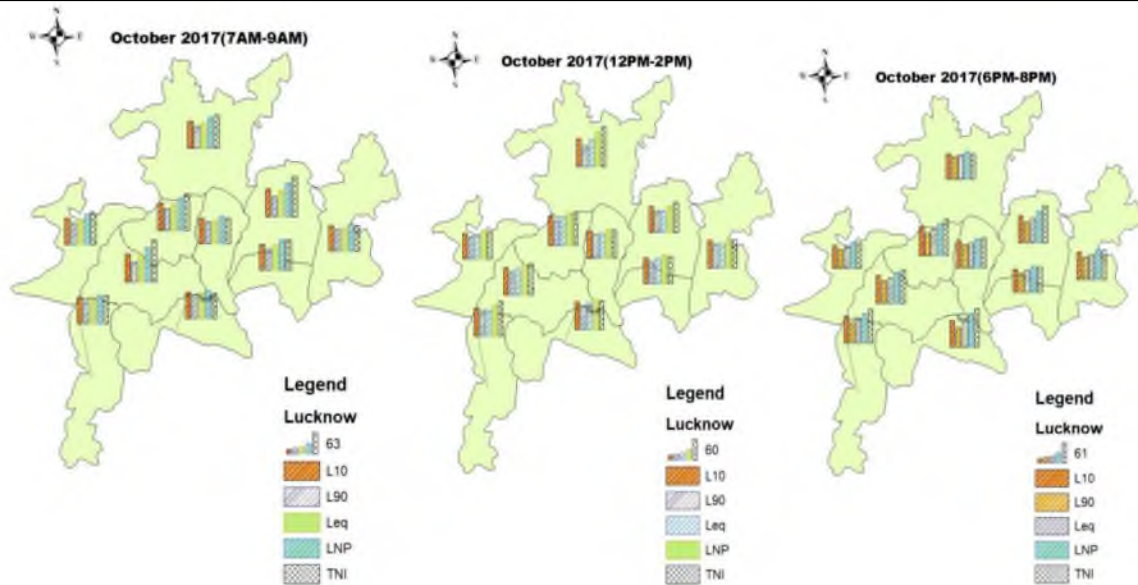


Figure3. Noise map for Lucknow metropolis in the month of October 2017

In the above figure 3, the noise map of all noise parameters show higher values for Aminabad, Indra nagar at the time interval (7AM-9Am), for Aliganj, Amausi at the time interval (12PM-2PM) and for Indra nagar, Kaiserbagh at the time interval (6PM-8PM). Now lower values for Kaiserbagh, Amausi at the time interval (7AM-9Am), for Chinnhat, Hazratganj at the time interval (12PM-2PM) and for Aliganj, KGMC at the time interval (6PM-8PM).

Table 3 shows the daily average values of noise parameters for the study area. At eight locations values of L_{EQ} , L_{NP} , and TNI were exceeded from the permissible limits in the month of November 2017 for time span (7Am to 9AM), (12PM to 2PM) and (6PM-8PM) respectively. The different noise level parameter such as L_{10} , L_{90} , L_{NP} , L_{EQ} and TNI were shown for different locations from 7am to 9am in figure 4. The L_{10} values of noise level varies between 77.67 to 86.17dB, L_{90} values varied between 61.82 to 71.93dB, L_{NP} values varied between 80.77 to 105.55dB, L_{EQ} was in the range of 70.89 to 82.16dB and TNI values varied between 76.73 to 126.34dB and further same the different noise level parameter were showed at different locations for 12pm-2pm. The L_{10} was showed noise level values varies between 78.52 to 86.25dB, L_{90} values varies between 62.92 to 73.25dB, L_{NP} valued varies between 80.13 to 105.64dB and L_{EQ} is in the range of 65.73 to 84.52dB and TNI values were varied between 82.96 to 120.68dB and also same the different noise level parameters were showed at different locations in 6pm-8pm. The L_{10} was showed noise level values varies between 74.12 to 89.26dB, L_{90} values were varied between 62.00 to 73.67dB, L_{NP} values were varied between 83.56 to 102.2dB, L_{EQ} was in the range of 71.44 to 85.44dB and TNI values were varied between 80.14 to 122.4dB.

Table 3-Average noise parameters at study locations in the month of November 2017

Time	7AM-9AM					12PM-2PM					6PM-8PM				
Parameters	L10	L90	LAeq	LNP	TNI	L10	L90	LAeq	LNP	TNI	L10	L90	LAeq	LNP	TNI
Locations	dBA	dBA	dBA	dBA	dBA	dBA	dBA	dBA	dBA	dBA	dBA	dBA	dBA	dBA	dBA
1. CHINNAT	77.69	66.79	71.62	85.3	80.39	82.78	72.72	73.92	85.57	82.96	84.92	73.62	81.82	96.44	88.82
2. RAM MANOHAR LOHIA	80.27	66	78.31	92.41	92.57	79.48	67	76.48	88.68	86.08	74.12	62	71.44	83.56	80.48
3.INDRA NAGAR	84.12	61.82	80.70	103.0	121.02	78.52	64.12	65.73	80.13	91.72	87.56	66.36	81.03	102.2	121.1
4.ALIGANJ	83.29	67.26	77.80	93.83	101.38	84.86	62.92	83.70	105.64	120.68	82.18	72.86	78.42	87.74	80.14
5.KGMC	80.17	66	78.26	92.26	92.17	79.52	67	76.49	88.73	86.24	74.91	62	71.77	84.68	83.64
6. AMAUSI	77.67	67.79	70.89	80.77	77.31	82.78	72.29	75.28	85.77	84.25	84.92	73.67	79.78	91.03	88.67
7. CHARBAGH	83.56	65.23	79.65	97.98	108.55	88.25	74.89	84.52	97.88	98.33	89.26	70.61	83.18	101.8	115.2
8. KAISEBAGH	80.63	71.93	77.95	86.65	76.73	81.95	70.86	80.16	91.25	85.22	85.62	63.35	85.44	107.7	122.4
9.HAZRATGANJ	81	67.52	75	89.07	92.52	83.38	67.81	76.89	92.46	100.09	84.27	67.28	76	93.07	105.2
10.AMINABAD	86.17	62.78	82.16	105.55	126.34	83.68	71.79	78.80	90.69	89.35	89.11	73	81.57	97.68	107.4

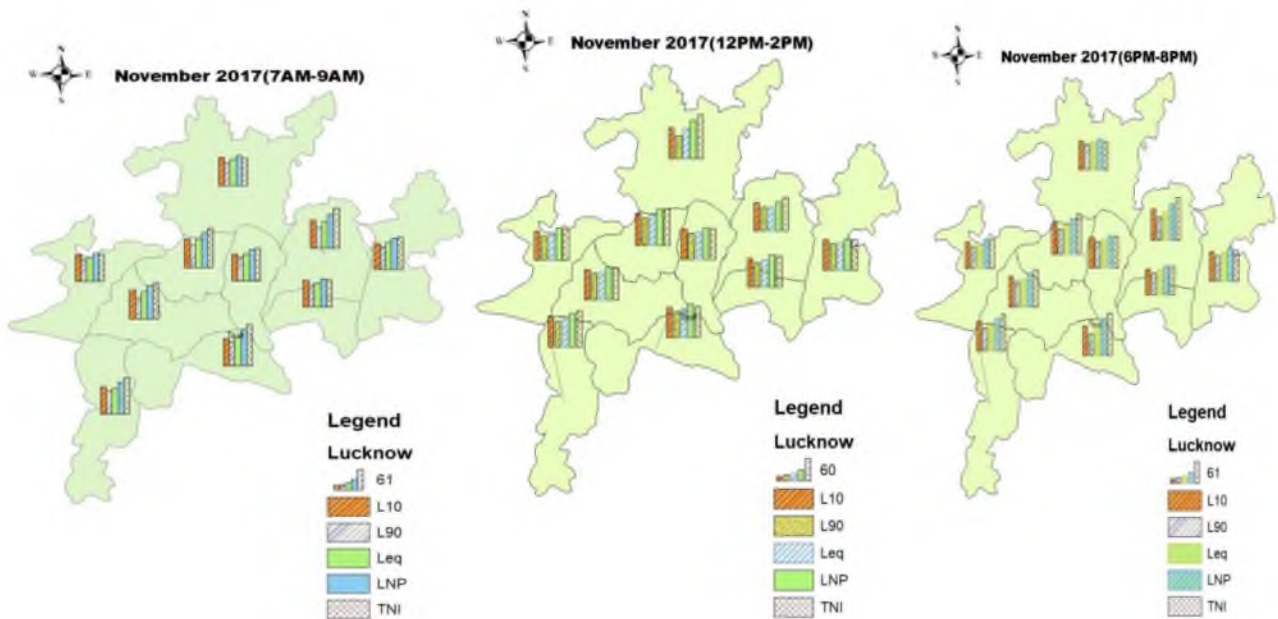


Figure 4. Noise map for Lucknow metropolis in the month of November 2017

In the above figure 4, the noise map of all noise parameters show higher values for Aminabad, Indra nagar at the time interval (7AM-9Am), for Aliganj, Amausi at the time interval (12PM-2PM) and for Indra nagar, Charbagh at the time interval (6PM-8PM). Now lower values for Aliganj, Ram Manohar Lohia at the time interval (7AM-9Am),

for Chinnhat, KGMC at the time interval (12PM-2PM) and for Hazratganj, Ram Manohar Lohia at the time interval (6PM-8PM).

5. Conclusion

In this study, a noise map of Lucknow metropolis has been developed based on the noise parameters: equivalent noise level (LAeq), background noise level (L90), TNI, noise pollution level (LNP), L10. The noise map shows that locations near busy roads/road junctions, commercial places and passengers loading parks have higher background noise level and peak noise level than locations near residential areas. This analysis shows that noise levels at 8 of 10 measurement data exceeded the recommended limit by the standard law of India. Hence, the noise pollution in Lucknow metropolis poses a severe health risk to the residents. Even, discomfort and irritation from the pollution can drastically reduce productivity, both in public service and private sectors. The most valuable step to decrease noise pollution in a big city of Uttar Pradesh like Lucknow is the preparation of noise maps. The noise map itself, with the values of noise parameters, provides baseline data for town planners, engineers and others for planning and execution of their projects. Most of the cities in Uttar Pradesh have not produced noise pollution maps. It is suggested that noise maps should be developed for every big city in Uttar Pradesh to serve as a noise control measure.

References

- [1] Dursun, S., Özdemir, C., Karabörk, H. and Koçak, S., 2006, Noise pollution and map of Konya city in Turkey. *Journal of International Environmental Application and Science*, 1(1-2), 63-72.
- [2] Santos, L.C. and Valado, F., 2004, The municipal noise map as planning tool, *Acústica, Guimarães, Portugal*, Paper ID: 162.
- [3] Zannin, P.H.T. and de Sant'Ana, D.Q., 2011, Noise mapping at different stages of a freeway redevelopment project—A case study in Brazil, *Applied Acoustics*, 72, 479-486.
- [4] World Health Organization (WHO), 1991 Report of the Informal Working Group on Prevention of Deafness and Hearing Impairment Programme Planning, June, (Geneva: WHO/PDH/91.1), pp. 18-21.
- [5] King, E.A. and Rice, H.J., 2009, the development of a practical framework for strategic noise mapping. *Applied Acoustics*, 70, 1116-1127.
- [6] Coelho, J.L.B. and Alarcao, D., 2005, On Noise Mapping and Noise Action Plans for Large Urban Areas, (Budapest: Forum Acusticum), pp. 1039-1044.
- [7] Livingston, Ken (Mayor of London), 2007, Greener London, the Mayor's State of Environment report for London, Greater London Authority, City Hall, London, SE1 2AA., p. 111.
- [8] De Kluijver, H. and Stoter, J., 2003, Noise mapping and GIS: optimizing quality and efficiency of noise studies. *Computers, Environment and Urban Systems*, 27(1), 85-102.
- [9] Sheng, N. and Wa Tang, U., 2011, Spatial analysis of urban form and pedestrian exposure to traffic noise. *International Journal of Environmental Research and Public Health*, 8, 1977-1990.
- [10] Wazir, A., 2011, GIS based assessment of noise pollution in Guwahati City of Assam, India. *International Journal of Environmental Sciences*, 2(2), 731-740.

COMPARITIVE STUDY OF NOISE DESCRIPTORS AND NOISE EXPOSURE LEVEL DUE TO DIWALI NOISE IN METROPOLITAN CITY: LUCKNOW

Ajay Kumar Vasanwal*, A.K.Shukla**, J.B. Srivastava**, Institute of Engineering & Technology, Lucknow

*Student, M.Tech Environment, **Professor, Department Of Civil Engineering Email.Id: ajayce11105@gmail.com

Abstract

Noise is harsh, disagreeable, irritable and unwanted sound which may cause irritation and annoyance to the public as well as to the surroundings. It is a global challenge as it is considered one of the major environmental issues in the present era. In this paper studies have been made for finding variations for noise exposure level, noise descriptors and the comparative study of the noise exposure level (L_{den}), average day night noise level L_{dn} and other noise descriptor such as L_{10} , L_{50} , L_{90} & L_{eq} at four selected location in metropolitan city Lucknow viz. Aliganj, Jankipuram, Indiranagar and Krishnanagar on pre diwali and on diwali day. The sampling was done at four locations on the pre diwali day and the diwali day from 06:00 to 10:00 (daytime), 18:00 to 22:00 (evening time) and 23:00 to 24:00 (night time). Data was taken at an interval of 15 second continuously for the 15 minutes and again for the next 15 minutes with the gap of 15 minutes in successive reading. The results indicates that L_{eq} was from 55.5 dBA on pre diwali to 62 dBA on diwali day at Aliganj while the L_{den} and L_{dn} were 61.7 and 61.1 respectively on pre diwali to 70.5 dBA and 76.3 dBA respectively on the diwali day. At Krishnanagar location, variation was between 59.2 dBA on pre diwali to 84.1 dBA on diwali day while the L_{den} and L_{dn} were 65.8 and 65.2 respectively on pre diwali to 90.6 dBA and 91.6 dBA respectively on the diwali day. Variation at the site of Indiranagar shows L_{eq} 72.1 dBA on pre diwali to 77.8 dBA on diwali day while the L_{den} and L_{dn} are 82 and 81.9 respectively on pre diwali to 87.5 dBA and 87.4 dBA on the diwali day. The variation of L_{eq} at Jankipuram was 56.7 dBA on pre diwali to 76.8 dBA on diwali day while the L_{den} and L_{dn} are 64.2 and 63.5 respectively on pre diwali to 85.8 dBA and 85.4 dBA on the diwali day. It is observed that mostly all the noise parameters at the all study locations are beyond the prescribed limits.

Keywords: Noise pollution, noise exposure level, noise descriptors.

1. Introduction

Noise is considered as an environmental issue and a global challenge. Long-term exposure in the form of unwanted sound significantly imposes environmental problem to humans and animals. The audible range for human ear is 20 Hz to 20 KHz. If the frequency is less than 20 Hz then it is called sub-sonic while more than 20 KHz it is said to ultrasonic range of frequency. Since the sound produced may be liked by one person and may be discarded by other person. Environment (Protection) Act, 1986 recognizes noise as an "environmental pollution" and empowers the Central Government to frame the laws and regulations prescribing the maximum permissible limits for the noise at different locations. **The main sources of noise pollution are the construction activities, traffic emergence, industrialization etc. Noise can affect badly to our environment and threat to humans. Long term exposure may causes permanent hear loss, annoying behaviour, headache, fluctuation in blood pressure, muscular strain and nervous breakdown, lowering of concentration and affect on memory, insomnia, emotional disturbance.** Diwali is a Hindu festival of lighting and full of joy, celebrates using firecracker in the month of October or November every year. **There is huge use of firecrackers in the diwali festival by the young people, children and the fascinated peoples in all over the country. The burning of firecracker induces a lot of air pollution as well as the noise pollution. The pollution produces by this makes the environment more polluted over the existing pollution.**

Undesirable sounds that are emitted by various mechanisms are defined as Noise The acoustic noises are mainly categorised into three types:

- **Steady Noise (industrial machines, transformers, air conditioners and turbines etc.)**
- **Fluctuating Noise (road and rail traffic, aviation, sound and music etc.)**
- **Impulse Noise (land mines, ammunition explosion and crackers etc), so we can say that it is a worst type of noise pollution occurs in the environment.**

2. Literature review

The motor vehicle is the very significant and important sources of noise pollution in the urban environment it contributes to 55% to the total noise pollution (Banerjee et al, 2008). A study based on noise pollution and ordinance, proposed the revision in the noise abatement pollution based on the adequate knowledge followed all over the world, apart from the standards followed in India (Garg et al, 2005) . Study is conducted in Mumbai results that diwali festival creates a lot of noise pollution and there is continuous increment in noise level from the previous year (Patel et al, 2014). In Duhok city (Iraq) during Nawruz festival, results showed measured noise level was 20% higher than the normal days and also beyond the noise standards so we can say that the festivals are the main cause of increase in noise level (Yousif et al, 2014) . In a study held during diwali festival in Chindambaram town (Tamilnadu, India), the recorded noise level on the diwali day for 30 sites it was found that noise level were higher than the prescribed limits (Balashanmugam et al, 2014) . Firecracker uses in enjoying the diwali festival lead to generation of lot of air pollution as well as the noise pollution which affects the human health (Sharma et al, 2016). A review conducted for ambient air and noise quality in India during diwali festival resulted that air quality was degraded and increase in noise level on diwali day than the normal day which is liable to serious health hazard, the study also emphasises on the control on bursting of firecracker to save human health (Chirag et al, 2014) . A study was conducted in Raipur city (Chhattisgarh, India) during the diwali festival which resulted that recorded value at all the sites were higher than the prescribed limit and the main source of increase in noise level were firecracker and traffic emergence after the holidays (Ahirwar et al, 2015). A study was conducted at Mhaswad (Dist. Satara in Maharashtra) where ten different sites were taken and it was found that, the residential zone and silence zone had higher noise level (Sujeet et al, 2016). Study was conducted in Calabar Municipality during pre-carnival, carnival and post carnival indicated that sound level were at a higher edge at morning, afternoon as well as evening. This made adverse effect to all aged humans (Alpan et al, 2015). A lot of efforts had been done to apply the noise exposure management strategies but resulted less improvements (Tickell, 2012). The DNL (day-night average sound level) was selected by EPA as the uniform descriptor of cumulative sound exposure to correlate with health and welfare effects. DNL methodology has given consistent results in the national and international literature under a wide range of noise conditions (including loud and soft noise levels, and frequent and infrequent numbers of discrete aircraft events) (Fidell, 2012). School based study in Italy was done to know the sound exposure effects on students (human being) and formulated; Annoyance Index (AI) score, global noise score (GNS) (Fabrizio et al, 2018).

L_{Aeq} : It is the A-weighted equivalent sound pressure level, **L_{90}** : It is a good measure of background noise and the noise level that exceeded 90% of the time.

L_{50} : It is median noise, which is necessary, the same thing as **L_{eq}** **L_{10}** : It is the noise level that exceeded 10% of the time. It is a good measure of intermittent or intrusive noises, such as traffic, aircraft flyover, barking dogs etc. **L_{den} (Noise exposure)**: is defined in terms of the “average” levels during daytime, evening, and night-time. The **L_{den}** (Day Evening Night Sound Level) or **CNEL** (Community Noise Equivalent Level) is the average sound level over a 24 hour period, with a penalty of 5 dB added for the evening hours or 19:00 to 22:00, and a penalty of 10 dB added for the night time hours of 22:00 to 07:00. **L_{dn}** : The **L_{dn}** is the day night average equivalent sound level over a 24 hour period, with a penalty added for noise during the night time hours of 22:00 to 07:00. During the night time period 10 dB is added to reflect the impact of the noise. **L_{dn}** measurements are useful for assessing the impact that road, rail, air and general industry has on the local population.

Noise exposure is a term which shows the exposure of noise pollution to the population resides in any area in a given time period of noise occurrence. Study of noise exposure easily makes comprehensive about the noise pollution to common people and we can easily educate them about the pollution created by the bursting of firecracker which is harmful to our society and the human health. This can be further a great help in the awareness program, not to burn the huge amount of firecrackers at the festival.

3. Material and Method

3.1 Study area

Lucknow metropolitan city is the capital city of Uttar Pradesh State which is at 80.95°E longitude and 28.70°N latitude, selected as a study area at four site for monitoring the noise level at the site considering as an area source (Aliganj, Indiranagar, Jankipuram and Krishnanagar) in the city on pre-Diwali day and on Diwali day with the help of noise meter (Lutron- SL 4010).

Since noise is considered as a global challenge and it is produced by many anthropogenic activities. In the same way noise pollution created by firecracker in the diwali festival creates a lot of nuisance i.e. psychological and physiological living standard with many health hazard problems. This study is a part of awareness program of noise pollution because of bursting of firecrackers.

The all locations selected for study are residential areas and contains high population density. These highly populated sites taken to study the noise exposure and would give the better idea of exposure condition. Map of study area is shown in figure 1.



Figure 1- Map of Study Area

3.2 Experimental procedures

Instrument was installed at 1.5 m above the ground and instrument set up by proper calibration at several meters from the firecrackers. **The study was carried** in the month of October of year 2017. The interval 15 second was taken for successive reading. L_A (A-weighted instantaneous sound pressure level) measurements was recorded continuously for 15 minutes. There were 120 noise data available for the one hour. **The measurement of noise level for the areas was done at pre diwali day and on the diwali day in the form of A weighted noise level and described in the form of $L_{eq}(A)$. Measurement was taken in an open space using the noise metre from the distance of more than 15 metre from the firecrackers.**

Data was collected in morning (6:00–10:00), evening (18:00–22:00) and night (23:00–24:00). Commonly used community noise evaluation quantities like the exceedance percentiles such as L_{10} , L_{50} and L_{90} , the A-weighted equivalent sound pressure level L_{Aeq} , the noise exposure level L_{den} , and L_{dn} , were determined.

3.3 Exposure limits for noise fireworks

There may be loss of hearing if noise levels exceeds by 90 decibels exposure for long periods and may cause permanent loss of hearing due to 150 decibels or greater even with a single exposure of such intensity (Noise standards for fire-crackers as per Environment (Protection) Act, 2000).

4. Result and Discussion

The results are compared graphically. All the sites which were selected for study indicated the higher noise level than the prescribed limits by the CPCB, 2000.

In figure 2 the L_{eq} for a whole day varies from 55.5dBA on pre diwali to 62dBA on diwali day at Aliganj, **which increases 18.82% on diwali day from the pre diwali day**. Minimum L_{eq} for a pre diwali day was recorded 48 dBA during 06:00-07:00 while the maximum value recorded was 59 dBA during 09:00-10:00. For the diwali day it was seen that the recorded values was minimum during 06:00-07:00 which was 58 dBA and maximum was during 22:00-23:00 i.e.76 dBA, these are presented in Table 1.

TABLE 1: NOISE DESCRIPTORS AT ALIGANJ SITE

ALIGANJ SITE	Leq	L10	L50	L90	Lden	Ldn
PRE DIWALI DAY	55	58	55	48	61.7	62.1
ON DIWALI DAY	67	65	58	53	76.5	76.3

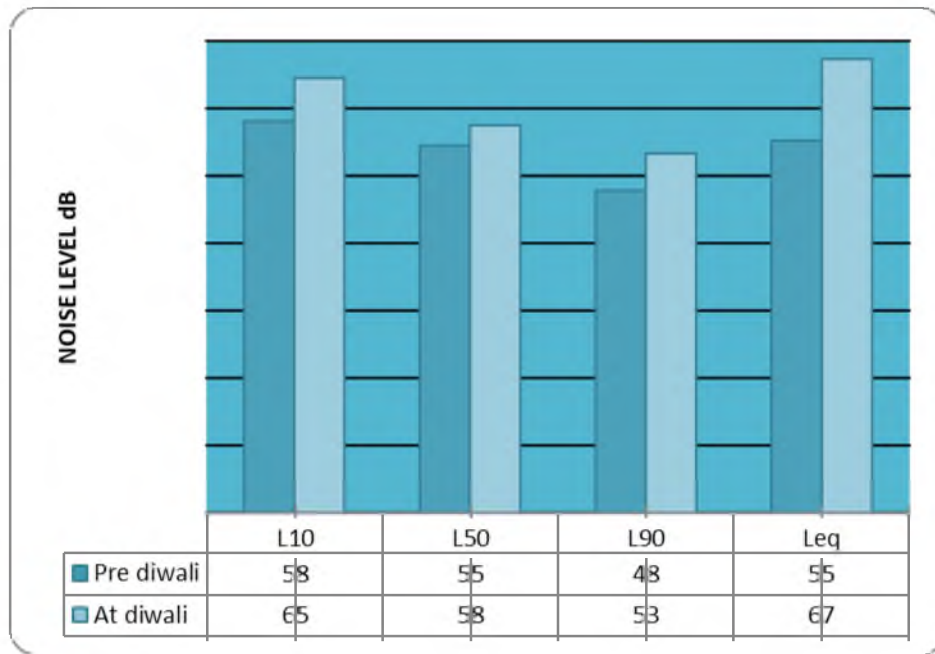


Figure 2: Variation of noise parameters at Aliganj

In the figure 3 atKrishnanagar location, variation in L_{eq} was from 59.2dBA on pre diwali to 84.1 dBA on diwali day **which increases 42% on diwali day from the pre diwali day**. This was more concerning place among all the selected location taken for the study purpose, the enormous volume of traffic and firecracker was the main contributor to increase in noise level. Minimum recorded L_{eq} on pre diwali day was 50 dBA during 06:00-07:00 and the maximum value recorded was 61 dBA during 07:00-09:00. For the diwali day, minimum reading was 50 dBA during 06:00-07:00 and maximum was 89 dBA during 19:00-20:00.

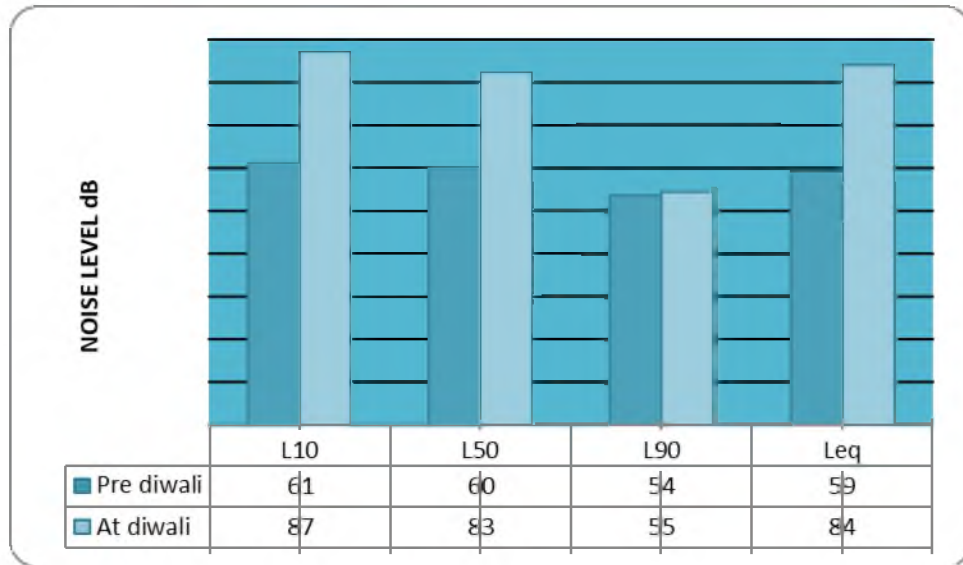


Figure 3: Variation of noise parameters at Krishnanagar

In the figure no 4 the variation at Indiranagar shows L_{eq} 72.1 dBA on pre diwali to 77.8 dBA on diwali day and the noise level are the beyond the prescribed limits. **There was approximately 8 % exceedance in noise level on diwali day from the pre diwali day.** Minimum L_{eq} for a pre diwali day was recorded 51 dBA during 06:00-07:00 and the maximum value recorded was 79 dBA during 22:00-23:00. On diwali day the minimum values recorded during 06:00-07:00 i.e. 50 dBA and maximum value was 86 dBA during 23:00-24:00.

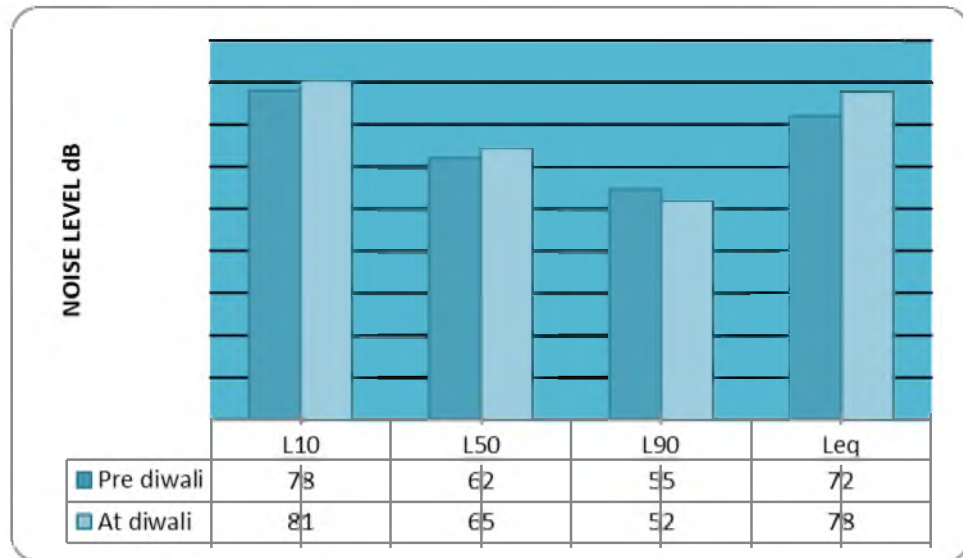


Figure 4: Variation of noise parameters at Indiranagar.

The figure 5 shows the variation of L_{eq} at Jankipuram was 56.7 dBA on pre diwali to 76.8 dBA on diwali day, **this shows that there was increase of 35.50% in noise level at diwali day than the pre diwali day.** The value of noise level at this site was beyond the standard limits. L_{eq} for a pre diwali day was recorded 48 dBA during 23:00-24:00 while it was 62 dBA during 21:00-22:00. For the diwali day the minimum L_{eq} was 50 dBA during 06:00-07:00 and maximum was 81 dBA during 21:00-23:00..

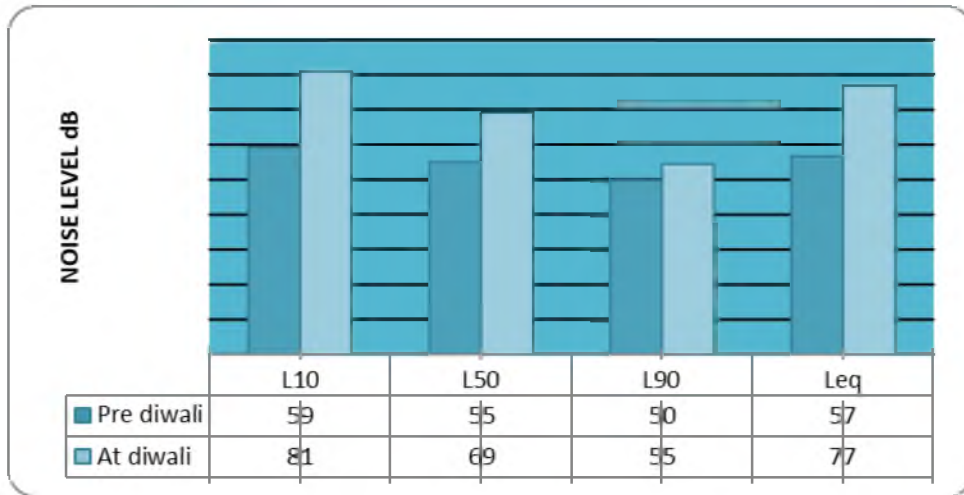


Figure 5: Variation of noise parameters at Jankipuram.

In the figure 6 the values of L_{den} and L_{dn} were 61.7 and 61.1 respectively on pre diwali to 70.5 dBA and 76.3 dBA respectively on the diwali day at Aliganj site. The L_{den} and L_{dn} on Krishnanagar were 65.8 and 65.2 respectively on pre diwali to 90.6 dBA and 91.6 dBA respectively on the diwali day. At Indiranagar the values of L_{den} and L_{dn} are 82 and 81.9 respectively on pre diwali to 87.5 dBA and 87.4 dBA on the diwali day. The L_{den} and L_{dn} at jankipuram are 64.2 and 63.5 respectively on pre diwali to 85.8 dBA and 85.4 dBA on the diwali day. The figure 6 shows the noise exposure variation at all locations.

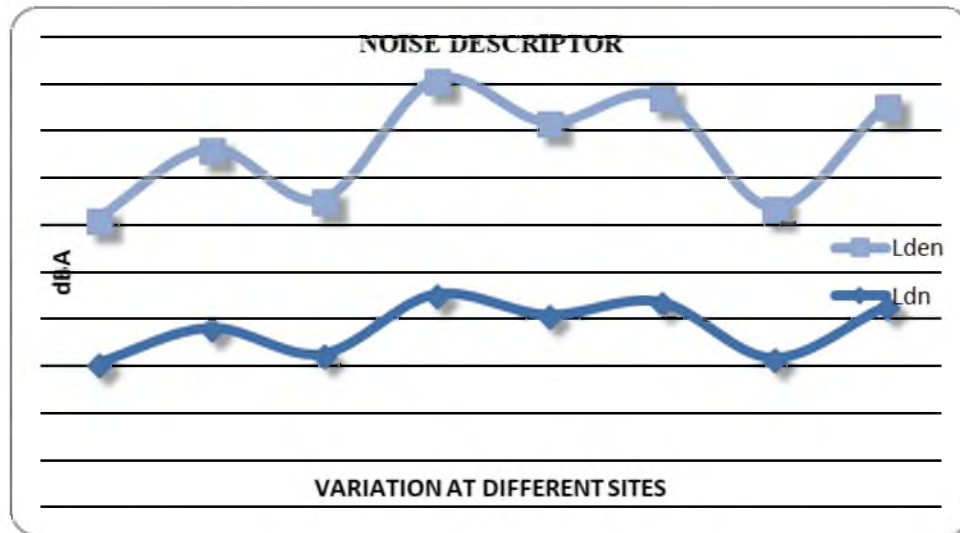


Figure 6: Comparative Variation of L_{den} and L_{dn} at all sites

5. Conclusion

Firecracker used in diwali festival creates a lot of pollution. Burning of firecracker produces impact noise rather than the other type of noise such as continuous and intermittent noise. This impact noise is more harmful for the humans living in nearby place, by the generation of impact noise from the firecrackers it will be more damaging to hearing loss. So this study helps to better understanding of exposure of noise pollution generated by the bursting of firecracker at the diwali festival. This study can be used for making the strategic action plan to better health of peoples living in the residential areas and to curb the noise pollution.

6. Recommendation

From above all discussion we can say that the firecracker used in the festivals creates a lot of nuisance in the form of degraded air quality and noise pollution which is health hazard to all humans as well as to animals. There is need of awareness to the people, not to make such level of high noise pollution because of high decibel producing firecrackers. Platforms like electronic media, print media, governmental body such as CPCB, state pollution control board etc, educational institutes, NGOs and other responsible bodies should make the awareness programme to peoples to curb the such pollution during diwali festival. As per the order based on the Supreme Court, prohibition of use of firecrackers in residential zone should be strictly followed during the time 22:00 to 06:00. Enforcement of legal laws should strictly follow against the unauthorised producers and sellers of firecracker. Play of firecracker should be based on the community or grouped level, not at the individual level so that nuisance can be reduce. Government should forcefully interfere in a way so that it can help to promote the good things to mitigate the problem by legal procedures.

REFERENCES

1. Ahirwar Ajay Vikram, and Bajpai Samir. Assessment of noise pollution during deepawali festival in Raipur city of Chhattisgarh, India. International Conference on Chemical, Environmental and Biological Sciences (CEBS-2015), March 18-19, 2015 Dubai (UAE).
2. Akpan Aniefiok O., Asuquo Ubon E. & Umoh Augustine A. Study of Noise Pollution During Pre-Carnival, Carnival and Post-Carnival Festivals in Calabar Municipality, Calabar, Cross River State, South-South Nigeria. Global Journal of Science Frontier Research Physics and Space Science Volume 13 Issue 1 Version 1.0 Year 2013.
3. Balashanmugam P., Nehrukumar V., Ramanathan AR. and Balasubramanian G. A Study on the influence of Deepawali festival on noise level in Chidambaram town, Tamilnadu, India. International Journal of Current Engineering and Technology, Vol.4, No.1 (February 2014).
4. Banerjee D., Chakroborty S.K., Bhattacharya S., Gangopadhyay A. (2008), Evaluation and analysis of road traffic noise in Asansol: An industrial town town of Eastern India, Internatinal Journal of Environmental Research and Public Health, 5, 3, 165-171.
5. Fidell, S. et al. 1989. Updating a Dosage-Effect Relationship for the Prevalence of Annoyance Due to General Transportation Noise. HSD-TR-89-009. WrightPatterson AFB, Ohio: U.S. Air Force, Noise and Sonic Boom Impact Technology. Cited in FICON 1992
6. Garg, N., Kumar, A., Saini, P. K. and Maji, S. A retrospective view of ambient noise standards in India: status and proposed revision. Noise Control Eng. J., 2005, 63(3), 1-14.
7. Gazalo Guillermo Rey and Juan Miguel Barrigon Morillas, Analysis of sampling methodologies for noise pollution assessment and the impact on the population, International Journal of Environmental Research and public health, 2016, 13(5): 490.
8. Minichilli Fabrizio, Gorini Francesca, Bianchi Fabrizio, Coi Alessio, Manzoli Federica, Mezzasalma Lorena and Cori Liliana, Annoyance Judgment and Measurements of Environmental Noise: A Focus on Italian Secondary Schools, Int. J. Environ. Res. Public Health 2018, 15, 208
9. Patel Nitinkumar L., Bhave Prashant P. Study of noise pollution during deepawali festival. International Journal of Innovative Research in Advanced Engineering (IJIRAE), Volume 1 Issue 6 (July 2014).

10. Sharma M Gupta, Bajaj A, N Bajaj, Mandal. A Study of Temporal Variation in Ambient Air Quality during Diwali Festival in Delhi – A Case Study. International Journal of Advance Research and Innovation, Volume 4, Issue 4 (2016) 591-595.
11. Sujeet Jadhav, Otari Pranav and Mane Akshay. Noise pollution study at mhaswadyatra mahotsav , 2016 Maharashtra, India. International journal of advance research 5(3), 1094-1097.
12. The noise pollution (regulation and control) rules, 2000. CPCB, New Delhi.
13. The Noise standards for fire-crackers were notified by the Environment (Protection) (Second Amendment) Rules, 1999. CPCB, New Delhi.
14. Tickell Colin, Australian Acoustical Society, paper peer reviewed, 2012
15. Verma Chirag and Deshmukh Dhananjay K. The ambient air and noise quality in India during diwali festival: A Review. Recent Research in Science and Technology 2014, 6(1): 203-210.
16. Yousif Kamil M. Study of noise pollution during Nawruz festival in Duhokcity, Iraq. International Journal of Advanced and Applied Sciences, 2(8) 2015, Pages: 23-28.

Treatment of Industrial Effluent with Coir pith and Charcoal Infused Soil Media

Aravind M. A¹ and Rahna L²

¹PG Student, Department of Civil Engineering, Rajadhani Institute of Engineering and Technology, India

²PG Student, Department of Civil Engineering, Rajadhani Institute of Engineering and Technology, India

*Corresponding author email: rahnalailanazar@gmail.com, Tel : +91 9633310787

ABSTRACT

Disposal of industrial waste is one of the major problems for soil pollution. These pollutants can cause threat to both human and the environment. It also affects and alter the chemical and biological properties of soil as well the ground water. Depending on its source, the sewage may also contain a range of chemicals and specialized wastes including industrial chemicals. The effluent collected from one of the major Industries in Trivandrum was used for the study. This paper describes the potential of coir pith and charcoal in eliminating the harmful material from the industrial effluent along with different soil media. The column study was conducted by passing the effluent through coir pith, charcoal, rock sand and well graded soil in isolation and 10 % by total weight of rock sand and well graded soil is replaced by coir pith and charcoal. The quality and properties of the treated effluent water is tested and compared with the original. It has been shown that coir pith and charcoal absorbs the harmful contaminants present in the industrial effluent.

Keywords –Industrial effluent, Coir pith, Charcoal, Rock sand, well graded soil

1. INTRODUCTION

Rapid industrialization has led to the generation of enormous quantity of wastes. These industrial wastes, either solid or liquid pose severe disposal problems. Normally, these wastes are disposed on land and water bodies. As a result, land becomes unfit for any other activity. Severe would be the case where hazardous waste is disposed because the soil in the vicinity becomes environmentally unsafe for human activities. Alternative techniques have been developed in order to conserve the available land and water resources. This industrial waste must be treated before disposing into environment.

Filtration is one of the water treatment processes to ensure water is safe from physical contamination. The present study is to find out the potential of rock sand and well graded soil as a bio filter with addition of natural materials like coconut coir pith and charcoal to reduce harmful contaminants in industrial waste. The focus of this study is to investigate the filtration efficiency of coir pith, charcoal, and rock sand and well graded soil in isolation and also rock sand and well graded soil with 10% of coir pith or charcoal. The parameters analyzed are pH, Conductivity, Biological Oxygen Demand (BOD) & Chemical Oxygen Demand (COD).

The use of natural materials for filtration seems so effective and eco friendly. Studies have been reported on the use of natural materials as a filter media for the filtration of industrial waste water. Shilpa and Nimisha, (2014) has studied the sand filtration process by utilizing activated carbon (AC) derived from coconut shell. It is reported that finer grade activated carbon showed the maximum iron removal (95%). It also reported reduction in COD, BOD and to some extent turbidity compared to traditional sand filtration process.

Azhar et al. (2011) carried out a study on a new composite adsorbent made from rice husk ash. Results indicate that the new composite adsorbent is able to absorb both ammonia and COD compared to commercially activated carbon.

A study was reported by Siong et al. (2013) about the performance of activated carbon in water filtering system. In this paper, two types of granular activated carbon are used. Prototype is being made by using activated carbon and ultraviolet radiation system for water treatment. Surface area and porosity analysis is done on two activated carbons. The results obtained from the water analysis shows that one of the Granular activated carbon will reduce turbidity, total suspended solid, BOD and COD. However the ultraviolet radiation reduced the BOD and COD of the water.

2. OBJECTIVES

The main objectives of the study are;

- To study the effectiveness of coir pith in filtration characteristics in comparison to charcoal.
- To study the effectiveness of Rock sand and well graded soil in filtering industrial waste.
- To evaluate the effectiveness of Rock sand and well graded soil combined with charcoal and coir pith as a filter media for treating industrial waste.

3. EXPERIMENTAL STUDY

3.1 MATERIALS USED

3.1.1 Well graded soil

Well graded soil passing through 4.75mm sieve is used for the initial filtration process. The soil was collected from the campus of Rajadhani College of Engineering and Technology. Gradation curve of the well graded soil is shown in Figure 1.

3.1.2 Rock sand

Rock sand was collected from the campus of Rajadhani College of Engineering and Technology. Rock sand is of uniform sized particles of less than 600 micron.

3.1.3 Charcoal

Charcoal was selected as another suitable natural filter media for the filtration purpose. Charcoal is a highly porous and brittle material whose properties are determined by the condition of the carbonization processes. In this experiment, wooden charcoal is collected by burning wood pieces and crushed them with the help of wooden hammer. The crushed powdered charcoal passing through IS 4.75 mm sieve has been used for the experiment. The physical properties of charcoal are given in Table 1.

3.1.4 Coir pith

Coir pith finds better absorption characteristics and eco friendly. Coir pith has got a blackish brown color. It was collected from District Government Fertilizer store, Trivandrum. The physical properties of coir pith are presented in Table 2.

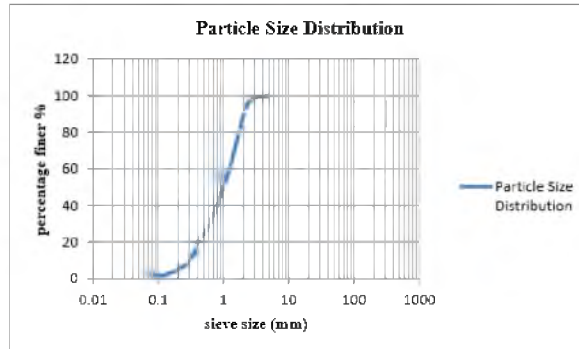


Fig. 1. Gradation curve of well graded soil

Table 1. Physical properties of Coir pith

SI No.	Properties	Values
1	Appearance	Blackish brown
2	Moisture content	10.1-60.2 %
3	Particle size	0.098-0.925 mm
4	Porosity	0.623-0.862
5	Density	0.939-0.605 gm/cc

Table 2. Physical properties of Charcoal

SI No	Property	Values
1	Colour	Dark black
2	Surface area/gm of Charcoal	500-1400 sqm
3	Density	0.2-0.6 t/m ³

3.2 METHODOLOGY

A square column of 0.30 m x 0.30 m x 1.0 m with bottom enclosed using Perspex sheet (Acrolithic tube) was used as the experimental set up. Bottom face is provided with a number of 1cm holes in rectangular arrangement to provide drainage of waste water oozing out from filter media. The apparatus is fixed vertically in a stand with adequate support. A square piece of stitched blanket of coir fibre layer 0.30 m x 0.30 m and 1cm thick is inserted into bottom of tube to prevent runoff of filter media along with filtered industrial waste water. The coir layer is shown in Figure 2.



Fig 2. Stitched coir blanket

3.3 TESTS PERFORMED

3.3.1 Test series 1

The tube is filled with a bed of rock sand or well graded soil up to 0.30 m and weighed accurately to maintain the density of fill. An additional layer of Perspex sheet with 1cm holes in rectangular arrangement is placed on top of rock sand/soil layer in order to distribute effluent or waste evenly throughout tube and to reduce disturbance in rock sand/soil while pouring waste into it. The assembly is shown in Figure 3.



Fig.3. Filter media placed inside column

The industrial waste shown in Figure 5 is evenly poured into the filter column. The waste water coming out from the bottom of the column is collected (Figure 6) and transferred to fresh bottles (Figure 7). Later these samples were tested at the Laboratory of Pollution Control Board, Trivandrum.

3.3.2 Test series 2

Next series of filtration is conducted using rock sand/soil mixed with 10% of coir pith. The total weight of filter bed is kept constant. The volume of the bed is adjusted so as to keep the relative density of the filter media constant. The filter bed is initially soaked well to remove finer impurities. The layer of Perspex sheet was placed on top to distribute waste water evenly.



Fig.5. Industrial waste sample



Fig.6. Filtration and collection



Fig.7. Collected samples

3.3.3 Test series 3

In this series of experiment, the filter media consists of rock sand/soil mixed with 10% charcoal. Here also the relative density kept constant. The filtration took much more time than the previous two cases.

3.3.4 Test series 4

In this series of experiment the filter media consists of coir pith alone, as to know the efficiency of coir pith in isolation to absorb suspended particles from the waste water. The coir pith mainly constitutes of fine organic fibre particles which may supposed to absorb and retain finer particles from the waste water effectively. The coir pith alone consumes more time than the previous tests to get filtered because of the fine organic content.

3.3.5 Test series 5

This series of experiment was using wood charcoal powder in isolation to serve as filter media. This experiment is conducted to compare the effectiveness of charcoal in filtering the harmful contaminants from waste and efficiency of that compared with coir pith. This experiment took greater time in filtration compared to the previous experiments.

4. RESULTS AND DISCUSSION

The following parameters of the filtered sample were studied namely, Biological Oxygen Demand (BOD), Chemical Oxygen Demand (COD), pH and conductivity. The chemical testing are done at the pollution control board (PCB), TVM laboratories. The results from the chemical analyses of filtered water are discussed below.

4.1 pH TEST

All the leachate samples are tested to check the pH of each one with initial sample and are presented in Figures 8 and 9 for rock sand and well graded soil respectively.

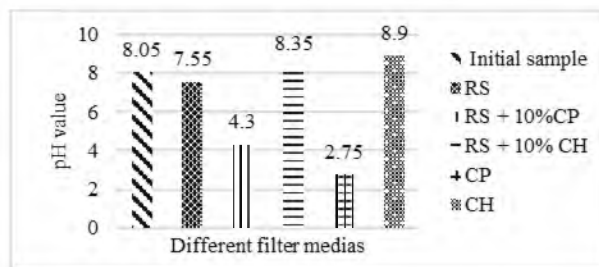


Fig. 8. Variation of pH in filtered water in rock sand media, coir pith and charcoal

The pH of the industrial waste was 8.05 which is alkaline. When the leachate is filtered through rock sand it comes down to 7.55, whereas in well graded soil it is 5.47. Rock sand brings the leachate much nearer to neutral condition. In the case of rock sand/soil along with coir pith and coir pith in isolation, the pH comes to acidic range. Since, charcoal being alkaline, addition of charcoal brought the sample to alkaline condition in rock sand, whereas in soil it comes near to neutral condition. Further treatments are needed to bring the sample to the neutral level.

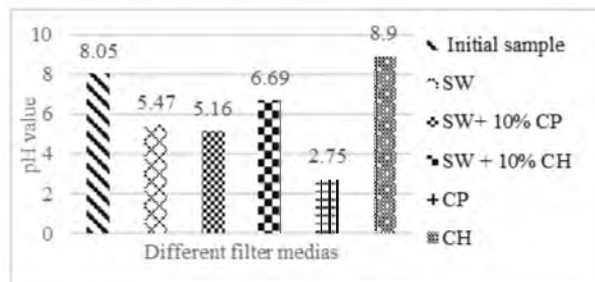


Fig. 9. Variation of pH in filtered water in well graded soil, coir pith and charcoal.

4.2 CONDUCTIVITY TEST

Conductivity of a media/material measures the material's ability to conduct an [electric current](#) through it. The conductivity test results of leachate obtained from each sample are presented in Figures 10 and 11 for rock sand and well graded soil respectively.

The conductivity of initial sample is very high. All the filter medias are effective in reducing the conductivity. Charcoal in-isolation or in combination with rock sand or well graded soil is more effective in reducing the conductivity than coir pith in-isolation or its combination.

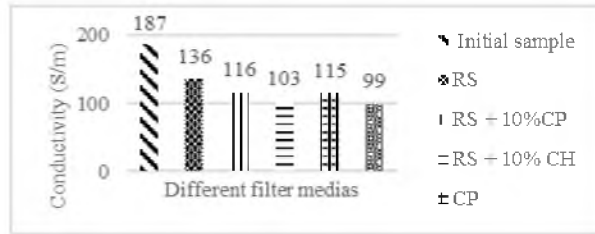


Fig. 10. Variation in conductivity of filtered water in various filter medias with rock sand.

Conductivity is reduced by 27% when the leachate is filtered through rock sand, whereas it was only 11% in well graded soil. Coir pith in-isolation or in combination with rock sand reduced the conductivity by 38% compared to 42% in coir pith mixed soil media. Charcoal in isolation or in combination with rock sand reduces the conductivity by 47%, as against to 49% in soil media. Well graded soil alone is not ideal in reducing the conductivity.

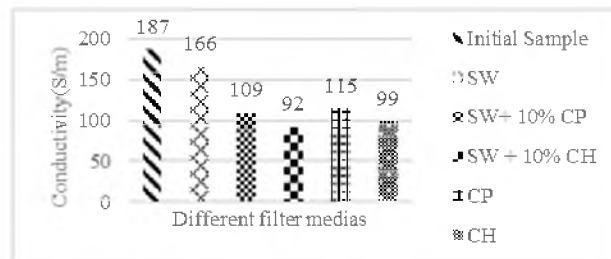


Fig. 11. Variation in conductivity of leachate in various filter medias with soil

4.3 BOD

The BOD value is most commonly expressed in milligrams of oxygen consumed per litre of sample and is used as a surrogate of the degree of [organic pollution of water](#). Most pristine water will have a 5-day carbonaceous BOD below 1 mg/L. Moderately [polluted](#) water may have a BOD value in the range of 2 to 8 mg/L. Water sample may be considered severely polluted when BOD values exceed 8 mg/L. Municipal [sewage](#) that is efficiently treated by a [three-stage process](#) would have a value of about 20 mg/L or more. The BOD of residue of leachate obtained through rock sand and soil are presented in Figures 12 and 13.

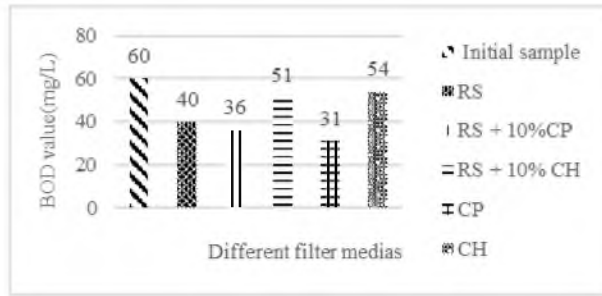


Fig.12. Variation of BOD of filtered water in different filter medias with rock sand

Rock sand is found to be better in reducing the BOD compared to well graded soil. In the additive material, coir pith in isolation is found to be the best compared to other medias in reducing the BOD. Coir pith reduces the BOD by about 48%. Though coir pith in isolation is better, when it is mixed with well graded soil, the reduction in BOD is drastically reduced 48% to 22%. This may be due to the organic materials present in the coir pith. This shows a better performance of coir pith in filtration aspects. The successful removal of BOD by CP is either due to more amount of [oxygen](#) present in the organic fiber content in the coir pith and soil or the abundant presence of aerobic biological organisms in the coir pith.

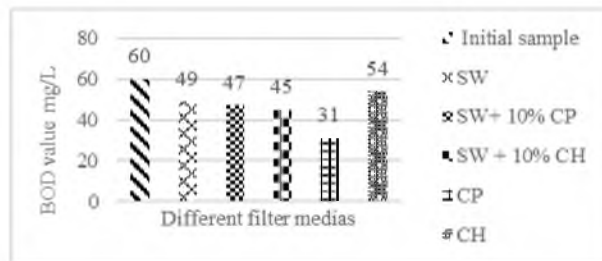


Fig. 13. Variation of BOD of leachate in different filter medias with soil.

3.4 COD

The result of a chemical oxygen demand test indicates the amount of water-dissolved oxygen (expressed as parts per million or milligrams per litre of water) consumed by the contaminants. The most common application of COD is in quantifying the amount of oxidizable [pollutants](#) found in [surface water](#) (e.g. [lake](#) and [rivers](#)) or [wastewater](#). The COD test results are shown in figures 14 and 15.

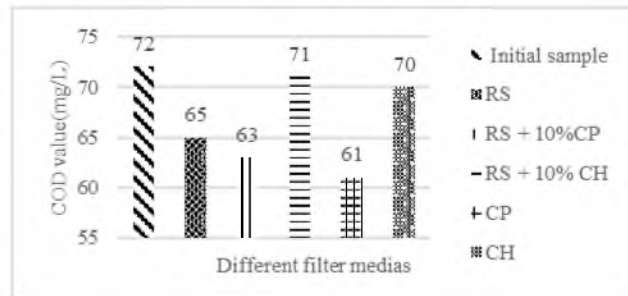


Fig.14. Variation of COD of filtered water in different filter medias with rock sand

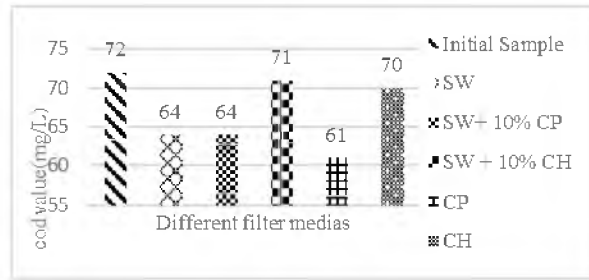


Fig. 15 Variation of COD of leachate in different filter medias with soil

Initial solution had a COD value of 72mg/L. Rock sand and well graded soils in isolation are equally good in reducing the COD. COD has been reduced by 9.7% and 11.1% respectively by rock sand and well graded soil. Rock sand with 10% CP is the ideal combination for reducing COD, and was found to be 12.5%. Addition of coir pith in well graded soil doesn't have any influence in controlling the COD. Coir pith alone is ideal for removing the COD from the effluent, i.e., nearly 15.2%. Charcoal is not at all effective in controlling the COD. The effect of coir pith in removing significant amount of COD might be because of the successive decomposition of organic matter or sufficient oxidation of inorganic chemicals present in the leachate or availability of fibrous coir pith material to consume excess oxygen.

4. CONCLUSION

Based on the chemical analysis of effluent filtered through various medias, the following conclusions were drawn:

- The use of natural materials like coir pith and charcoal as a filtering material introduces an environmental friendly method for filtration and further can reduce the use of chemicals.
- From the column filtration and results obtained, it is observed that Coir pith is very effective in removing the BOD, COD and also brings down the conductivity of waste water to a greater amount.
- The use of charcoal as a filter media is also observed to be very effective. The turbidity and conductivity seems to be less in the filtered samples.
- The results show a new area of application for coir pith as a filter media which is purely eco friendly and very economical.

REFERENCES

1. Shilpa, S. Ratnoji., and Nimishasingh., "A study of coconut shell - activated carbon for filtration and its comparison with sand filtration", IJREEE, 2014, Vol 2, No 3, pp 201-204.
2. Siong, Y., Idris, J., &MazarAtabaki, M., "Performance of activated carbon in water filters" Reseach Gate, 2013.
3. Azhar Abdul Halim., Noor Nazurah Zainal Abidin., Normah Awang., Anuar Ithnin., Mohd. Sham Othman., & Mohd. Ikram Wahab "ammonia and cod removal from synthetic leachate using rice husk composite adsorbent", JUEE, 2011, Vol 5, No 1, pp 24-31.

OPTIMISATION OF PHOSPHATE REMOVAL FROM FERTILISER WASTEWATER USING POLYSULPHONE CHITOSAN NANOSILICA MEMBRANE

Megha M¹, Krishnaveni S¹ and Meera V¹

¹Government Engineering College, Thrissur, India

Abstract. In this research, response surface methodology (RSM) was applied to model the effect of main operational variables including initial pH, contact time and initial phosphate concentration on phosphate removal from fertilizer wastewater by membrane technology. A new membrane was synthesised using Polysulphone, Chitosan and nanosilica. It was found that the decrease of initial pH, contact time and initial phosphate concentration, and their interactions are beneficial for improving phosphate removal efficiency. According to the ANOVA (analysis of variance) results, the model presented high R² value of 99.48% for phosphate removal efficiency which indicates that the accuracy of the polynomial model is acceptable. According to Minitab output, the initial pH of 3, contact time of 1.75 hours and initial phosphate concentration of 30mg/l were obtained as optimum experimental parameter. Phosphate removal efficiency of 67.90% was observed in the experiment at optimum conditions and the treated water can be used for domestic reuse purposes. It can be concluded that RSM is a powerful tool for evaluation and optimization of membrane process for phosphate removal.

Keywords. *Polysulphone Chitosan Nanosilica membrane, Phosphate removal*

1. INTRODUCTION

Eutrophication is one of the most important environmental problems which lead to abundant development of aquatic plants and growth of algae. Eutrophication is the process by which a water body acquires a high concentration of nutrients such as phosphates which promote excess growth of algae. As the algae die and decompose, high levels of organic matter and the decomposing organisms deplete the water of available oxygen, causing the death of other organisms, such as fish. Eutrophication, bringing with it high amounts of phosphates is a main cause in the destruction of ecosystems. Phosphates are largely discharged into environment from waste water from fertilizer industry. Fertilizer industry in India is extremely vital as it manufactures some of the most important raw materials required for crop production. The primary objective of this industry is to manufacture both primary and secondary elements necessary for crop production. As a result, a variety of wastes are discharged from fertilizer plant as water pollutants in the form of processing chemicals such as sulphuric acid, ammonium sulphates, ammonium phosphate etc. Wastewaters from chemical fertilizer industry mainly contain organics, alcohols, ammonia, nitrates, phosphates, heavy metals such as cadmium and suspended solids. In addition to that, oil bearing wastes from compressor houses of ammonia and urea plants, some portion of cooling water and wash water from scrubbing towers for purification of gases also come as waste. The main constituent of fertilizer wastes includes nitrates and phosphates in high amount. Because of this problem phosphate removal from fertilizer industry wastewater is important.

Removal of anions using membranes is an advanced technology. Membrane process is a technique that uses a physical barrier, a porous membrane or filter, to separate particles in a fluid. Particles are separated on the basis of their size and shape with the use of pressure and specially designed membranes with different pore sizes. Membrane processes are versatile. Commercially used membranes for removal purposes are microfiltration membrane, ultrafiltration membrane and nanofiltration membranes. These membranes basically differ according to their pore size. Microfiltration membrane has average pore size of 0.1 microns (0.5-5 microns). Ultrafiltration membrane has average pore size of 0.02 microns (0.001-0.05 microns). Next range of membrane is the nanofiltration membrane

with average pore size 0.001 microns (0.008 to 0.01 microns). Among these membranes, nanosized one is most suitable for removing anions such as nitrate, nitrites and phosphates, sulphates, etc.

Nanotechnology can be defined as the manipulation of materials at atomic level by a combination of engineering, chemical and biological approaches. It is mainly concerned with the synthesis of nanoparticles of variable sizes, shapes and chemical compositions and their potential use for human benefits. Nanomaterials have the potential to improve the environment through the development of new solutions to environmental problems. Nanotechnology holds great potential in advancing water and wastewater treatment to improve treatment efficiency as well as to augment water supply through safe use of unconventional water sources. Nanotechnology-enabled water and wastewater treatment promises to not only overcome major challenges faced by existing treatment technologies, but also to provide new treatment capabilities that could allow economic utilization of unconventional water sources to expand the water supply.

Recently, nanoparticles are widely used for water/wastewater treatment. Nano-based membranes are used conveniently for the removal of pollutants. Nanomembrane possesses pore size of typically 1 nm. These membranes are synthesized by incorporating nanoparticles into the polymeric matrix or modifying traditionally-used materials with different nanocomposites. Nanomembranes are mainly classified into Nano polymer membranes, Inorganic substrate contained nanomembrane and nanofunctionalized membranes. Among them, Thin-film nanocomposite (TFC) membranes are an important subclass which belongs to the nano polymer membranes. The TFC membranes, have a dense, thin, and selective skin layer and a micro- porous support layer prepared from various polymeric materials namely polysulfone (PSF), polyether sulfone, polyurethane, polyacrylonitrile, and polyvinyl difluoride [1]. Polysulfone is the most widely used polymer and are known for their toughness and stability at high temperatures. They contain the subunit $\text{aryl-SO}_2\text{-aryl}$, the defining feature of which is the sulfone group. Mechanically, polysulfone has high compaction resistance, recommending its use under high pressures. It is stable in aqueous acids and bases and many non-polar solvents. Dimensional stability, creep resistance, wide pH limit and good film forming property are certain other properties which make the polysulfone (PSF) more significant among other polymers. Fig. 1 shows the chemical structure of polysulfone [2].

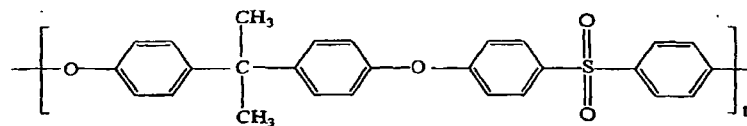


Fig. 1 Structure of polysulfone [2]

Every polymer has its own drawbacks. While in the case of polysulfone, it is its less biodegradability which makes disposal difficult and less hydrophilicity. Since it is a synthetic polymer, the membrane decomposes and degrades slowly in the environment. Hence, it is advantageous to use certain additives that increase the biodegradability of membrane.

Chitosan (CS) is one such additive which is biodegradable as well as biocompatible. It is produced commercially by the deacetylation of chitin and have gained wide attention as effective biosorbent due to low cost and high contents of amino and hydroxyl functional groups which show significant adsorption potential for the removal of various aquatic pollutants [3]. It is the only pseudo-natural cationic polymer which is naturally suitable for film formation [4]. Chitosan is an antifouling agent that has been shown to remove targeting pollutants such as heavy metals, phosphorus, turbidity and natural organic matter[5].

In order to improve the hydrophilicity of the membrane specifically, certain fillers are also added. Nanosilica is one such filler which can improve the membrane's hydrophilicity. Nanosilica particles can improve the strength, hardness, modulus, creep resistance and adhesion within the framework of thermoplastic polymers due to the surface properties of nanoparticles[6][7].

The objective of this study was to fabricate a polysulphone chitosan nanosilica membrane to remove

phosphates from fertilizer wastewater to reuse the water for domestic reuse purposes (phosphate concentration less than 15 mg/l) and to optimize the factors affecting the process by using Response Surface Methodology.

The efficiency of the membrane process is influenced by various factors such as pH, contact time and initial phosphate concentration. Optimization of these factors can be useful in order to achieve better phosphate removal efficiency.

2. MATERIALS AND METHODS

2.1. Fabrication of Polysulphone Nanosilica membrane

For membrane synthesis, chitosan solution was prepared initially by dissolving 1g chitosan (CS) in 50 mL 1% acetic acid solution. Next, 4.2 g polysulfone (PSF) was dissolved in 16.8 mL of N, N-dimethylacetamide (DMAc) solvent at 60°C and stirred for 2 hour. After that, the prepared 1 mL of chitosan solution was added to the PSF solution at 70°C. Then, additional 5 mL of DMAc was added. While chitosan was being added, chitosan gets precipitated. The resultant turbid solution was stirred at 70°C for 1 hour to obtain a homogeneous solution of high viscosity. After that, 0.5 g of SiO₂ nanoparticles was added to the prepared PSF-CS uniform viscous solution and stirring was continued for 1 hour to dissolve the nanoparticles completely. After 1 hour of stirring, the solution was subjected to ultrasonic irradiation for 1 hour. The prepared solution was molded by pouring onto a flat glass rectangular mould. After that, the molded glass surface was immersed in distilled water at 25°C. After 2 hour, the membranes were removed from the water bath and washed with distilled water [5].

2.2. Experimental procedure

Synthetic wastewater having similar characteristics as the fertiliser effluent were prepared using Glucose, Ammonium nitrate, Monopotassium phosphate and Nutrient Solution by trial and error method. Composition of the synthetic wastewater and its characteristics are given in Table 1 and 2 respectively.

Table 1. Composition of Fertilizer synthetic wastewater [8]

Constituents	Concentration
Glucose	200 mg/L
Ammonium nitrate (NH ₄ NO ₃)	735 mg/L
Monopotassium phosphate (KH ₂ PO ₄)	30 mg/L
Dipotassium phosphate (K ₂ HPO ₄)	20 mg/L
Nutrient Solution	10 mL
Composition of Nutrient solution	
Magnesium sulphate heptahydrate (MgSO ₄ .7H ₂ O)	90 g/L
Calcium chloride dihydrate (CaCl ₂ .2H ₂ O)	6 g/L
Iron chloride hexahydrate (FeCl ₃ .6H ₂ O)	1.5 g/L
Manganese chloride tetrahydrate (MnCl ₂ .4H ₂ O)	6.5 g/L
Zinc sulphate heptahydrate (ZnSO ₄ .7H ₂ O)	1.7 g/L
Copper chloride dihydrate (CuCl ₂ .2H ₂ O)	0.1 g/L
Cobalt chloride hexahydrate (CoCl ₂ .6H ₂ O)	1.9 g/L
Nickel sulphate (NiSO ₄ .6H ₂ O)	6.5 g/L
Boric acid (H ₃ BO ₃)	0.1 g/L
Sodium molybdate (Na ₂ MoO ₄ .2H ₂ O)	0.6 g/L
Yeast extract	1 g/L

Table 2 Characteristics of synthetic fertilizer wastewater

Parameters	Concentration
pH	5.87
Conductivity (μ Siemen/cm)	2460.00
TDS (mg/L)	1480.00
COD (mg/L)	248.00
Nitrate (mg/L)	113.50
Phosphate (mg/L)	76.00

2.3. Batch study

The synthesized PSF-CS and PSF-CS-SiO₂ membranes were used as adsorbent materials for the removal of nitrates and phosphates from fertilizer wastes. Experiments were conducted in simple batch mode. Batch mode studies were carried out by dipping membranes of 3 number of area 4×4 cm² each in 1000 mL beaker. The influencing factors which were considered for the batch study include pH, contact time, initial concentrations of phosphate.

Percentage of phosphate removal was calculated by the Eqn.1.

$$\text{Phosphate removal (\%)} = (C_r - C_t) \times 100 / C_r \quad (1)$$

where C_r and C_t are the phosphate concentration in raw and treated solutions, respectively.

2.4. Experimental design and data analysis

The most popular class of second –order designs called Box-Behnken design (BBD) was used for the RSM in the experimental design. The BBD was first introduced by Box and Wilson in 1951, and is well suited for fitting a quadratic surface, which usually works well for the process optimization[9]. Box-Behnken design is a three level design in which all the design points are either at the center of the design or centered on the edges of the cube, equidistant from the center. This process involves three major steps: performing the statistically designed experiments, estimation of coefficients in the proposed model and predicting the response of process and checking the validity of model [10].

In this study, the experimental plan was implemented as a BBD. The effects of three variables including initial pH, contact time and initial phosphate concentration were examined on the membrane process. A total of 15 experiments were done according to the BBD eqn.2.

$$N = 2k(k-1) + cp \quad (2)$$

Where N is the total number of experiments to be repeated, k is the number of factors and cp is the number of centre points. Variables, experimental ranges and levels are shown in Table 3.

Table 3. Experimental levels of the test variables

Variables	Factors	Ranges and levels		
		-1	0	1
pH	X ₁	3	6	9
Contact Time(hours)	X ₂	0.5	1.75	3
Initial Phosphate concentration(mg/l)	X ₃	30	90	150

The experiments repeated at the center of domain lead to calculate an independent estimation of the pure experimental error variance.

3.RESULTS AND DISCUSSIONS

3.1 Development of Regression model equation and validation of the model

Membrane technology is a process which affected by different operational parameters such as initial pH, contact time and initial pollutant concentration. To study the combined effect of the factors, experiments were conducted for different combinations of the parameters using statistically designed experiments. Table 4 presents the observed and predicted phosphate removal efficiencies for the 15 experiments. The coefficients of the response function (Eq. 3); the P and t values for phosphate removal efficiency are also listed in Table 5.

Table 4. RSM design and its observed and predicted values

Run Order	pH	Contact Time	Initial Phosphate concentration	Phosphate removal %	
				Observed	Predicted
1	6	3.00	150	49.33	48.16
2	6	1.75	90	54.88	54.07
3	6	0.5	150	22.93	23.294
4	6	0.5	30	18.66	19.00
5	6	3.00	30	59.70	58.76
6	6	1.75	90	54.55	54.07
7	3	1.75	150	58.93	58.76
8	3	3.00	90	59.32	60.73
9	9	3.00	90	42.56	43.082
10	9	1.75	30	50.50	49.66
11	9	0.5	90	17.66	16.15
12	6	1.75	90	53.78	54.07
13	9	1.75	150	50.20	51.346
14	3	1.75	30	67.90	66.754
15	3	0.5	90	24.56	23.017

Table 5. Estimated regression coefficients for phosphate removal efficiency (%) in coded units

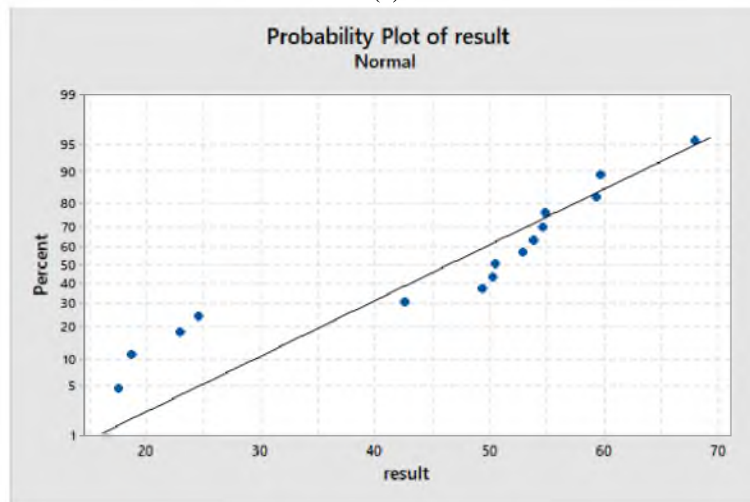
Term	Coefficient	SE coefficient	t	P
Constant	54.403	0.815	66.74	0.000
X ₁	-6.236	0.499	-12.49	0.000
X ₂	15.900	0.499	31.85	0.000
X ₃	-1.921	0.499	-3.85	0.012
X ₁ ²	0.412	0.735	0.56	0.599
X ₂ ²	-18.815	0.735	-25.61	0.000
X ₃ ²	2.067	0.735	2.81	0.037
X ₁ X ₂	-2.440	0.706	-3.46	0.018
X ₁ X ₃	2.168	0.706	3.07	0.028
X ₂ X ₃	-3.660	0.706	-5.18	0.004

The second order polynomial equation for phosphate removal in terms of coded factors is given by the Eq.3

$$Y=54.403-6.236X_1+15.9X_2-1.921X_3+0.412X_1^2-18.815X_2^2+2.067X_3^2-2.440X_1X_2+2.168X_1X_3-3.660X_2X_3 \quad (3)$$

According to Table 5, low P values for all terms except X_1^2 ($P < 0.05$ for all) confirms high significance of these factors. The adequacy of the model was evaluated through ANOVA (analysis of variance). The ANOVA results for phosphate removal are shown in Table 4. In this case, the P value of 0 ($P \leq 0.05$) for regression model equation implies that the second order polynomial model fitted to the experimental results well. Additionally, high R^2 value of (99.48%) for phosphate removal expresses a high correlation between the observed and predicted values. The adequacy of the model was also evaluated by the residuals (difference between the observed and the predicted response value). Residuals are thought as elements of variation unexplained by the fitted model and then it expects that they occur according to the normal distribution. Normal probability plots are a suitable graphical method for judging the normality of the residuals. The observed residuals are plotted against the expected values, given by a normal distribution[11]. The satisfaction of model fit was also examined with the plot of residuals versus fits in Fig. 2. As seen in Fig. 2(a), the normality assumption is confirmed relatively as the points in the plot formed fairly straight line. The satisfaction of model fit was also examined with the plot of residuals versus fits in Fig. 2(b). For a model to be acceptable, no series of increasing or decreasing points, patterns such as increasing residuals with increasing fits and domination of positive or negative residuals should be found. Both of plots in this figure revealed that model is adequate to describe the phosphate removal by response surface methodology.

(a)



(b)

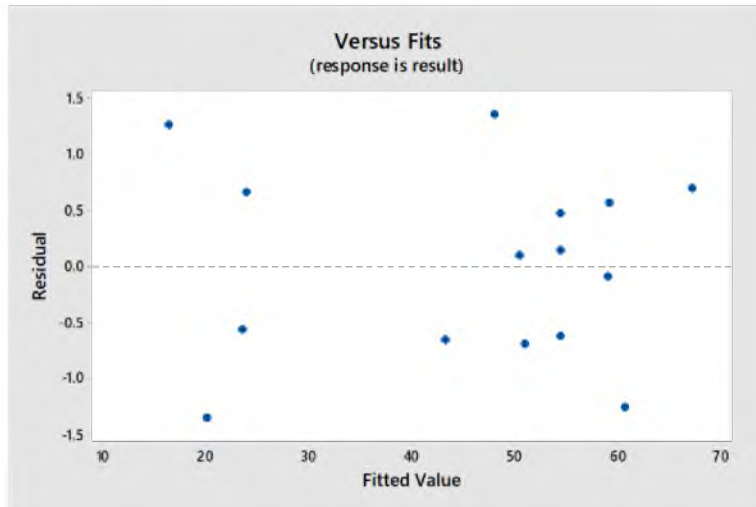


Fig 2.(a) Normal probability plot (b) Residual versus fit plot

3.2. Main effect plots for evaluation of operational parameters

Effect of initial pH on phosphate removal

Initial pH showed a high effect on the phosphate removal. As the pH increased removal efficiency decreased as shown in Fig 3. This is because in acidic medium the membranes were found to be more effective at acidic pH of 3. At pH 3, there are a lot of H⁺ ions in solution and hence, -NH₂ groups which are the backbone of chitosan are protonated in this environment. Protonated -NH₂ groups (-NH₃⁺) adsorb the anions and thus it enhances the electrostatic attraction, thereby results in efficient removal[5].

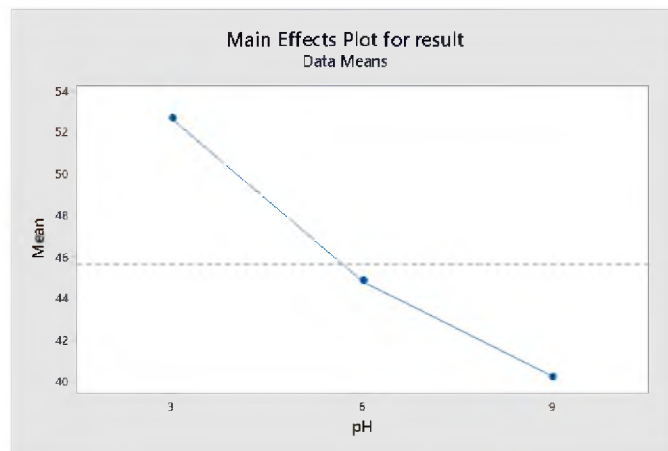


Fig 3. Main effect plot of initial pH for phosphate removal efficiency

Effect of Contact time with phosphate removal

Fig.4 shows the variation of phosphate removal with contact time. As the time increased the removal efficiency increased and then decreased. This is because as the time increases adsorption increases and after a limit saturation occurs.

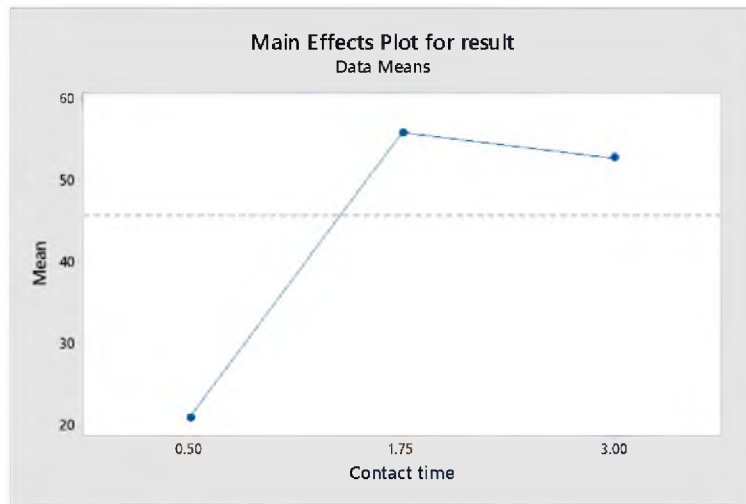


Fig 4. Main effect plot of contact time with Phosphate removal efficiency

Effect of Initial phosphate concentration on the Phosphate removal

At lower initial phosphate concentration, the adequate availability of the active sites of the membranes brings the effective adsorption. On further increase in initial phosphate concentration, the percentage removal gets decreased due to the saturation of the active sites of the membrane towards the solute molecules during adsorption [12].

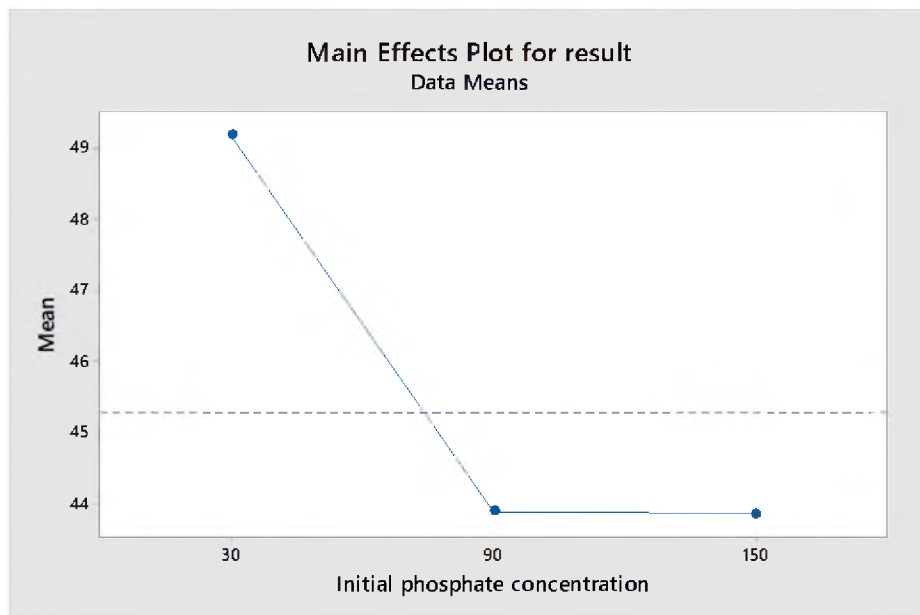


Fig 5. Main effect plot of initial phosphate concentration for phosphate removal efficiency

3.3 Process optimisation

The main objective of the optimization is to determine the optimum values of variables for

phosphate removal with membrane technology using Polysulphone Chitosan Nanocomposite membrane from the model obtained using experimental data. In optimization, the desired aim was defined as target to achieve maximum phosphate removal efficiency. The optimum amounts for factors obtained with consideration of 3, 1.75 hours and 30mg/l as starting values for initial pH, contact time and initial phosphate concentration respectively. The optimization results of the process variables using response optimizer program are shown in Table 6.

Table 6. Optimum values for phosphate removal from fertilizer wastewater

Variable	Unit	Optimum values
Initial pH	-	3
Contact time	Hours	1.75
Initial Phosphate concentration	mg/l	30
Phosphate removal efficiency(observed)	%	67.90
Phosphate removal efficiency(predicted)	%	66.75

4. CONCLUSIONS

In the present study, the effects of three parameters on phosphate removal by membrane technology were investigated using RSM. The results showed that most of the variables as well as the interactions like affected the process performance significantly. According to the ANOVA results, the model presented high R^2 value of 99.48%, which exhibits the good accuracy of the polynomial model. From optimization, 67.90% of phosphate removal obtained at initial pH, contact time and initial phosphate concentration of 3, 1.75 hours and 30mg/l respectively. The final phosphate concentration was 9.63 mg/l and thus the water can be reused for domestic reuse purposes. The experiment done in optimum conditions confirmed that the model and experimental results are in close agreement. Finally, it can be concluded that membrane technology using Polysulphone chitosan Nanosilica membrane is a very useful technology for treatment of highly polluted phosphate fertiliser wastewater to use it for reuse purposes and RSM is a powerful statistical technique for evaluation and optimization of this process.

REFERENCES

- [1] Nayak, V., Jyothi, M. S., Balakrishna, R. G., Padaki, M. and Ismail, A. F. (2014). Preparation and Characterization of Chitosan Thin Films on Mixed-Matrix Membranes for Complete Removal of Chromium, *Chemistry Open*, 4, 278-287.
- [2] Momeni, S. M. and Pakizeh, M. (2013). Preparation, Characterization And Gas Permeation Study of PSF/MgO Nanocomposite Membrane, *Brazilian Journal of Chemical Engineering*, 30(3), 589-597.
- [3] Morghi, M., Abidar, F., Soudani, A., Zerbet, M., Chiban, M., Kabli, H. and Sinan, F. (2015). Removal of Nitrate Ions from Aqueous Solution Using Chitin as Natural Adsorbent, *International Journal of Research in Environmental Studies*, 8-20.
- [4] Tsai, H. A., Chen, H. C., Lee, K. R. and Lai, J. Y. (2006). Study of the Separation Properties of Chitosan/Polysulfone Composite Hollow-Fiber Membranes, *Desalination*, 193, 129-136.
- [5] Saeidi, F. and Zafarmehrabian, R. (2014). Hydrophilic Properties of PSF/SiO₂ Nanocomposite Membranes with Polymeric Additives, *Journal of Basic and Applied Chemistry*, 4(10), 1-7.
- [6] Kumar, R., Isloor, A. M., Rashid, S. A. and Ahmed, A. A. (2013). Permeation, Antifouling and Desalination Performance of TiO₂ Nanotube Incorporated PSF/CS Blend Membranes, *Desalination*, 76-84
- [7] Gharehbash, N. and Shakeri, A. (2015). Preparation and Thermal and Physical Properties of Nano-silica Modified and Unmodified, *Oriental Journal of Chemistry*, 31, 207-212.

- [8] Khurana, M. P. S. and Aulakh, M. S. (2010). Influence of Wastewater Application and Fertilizer use on the Quality of Irrigation Water, Soil and Food Crops: Case Studies from Northwestern India, *Soil Solutions for a Changing World*, 75-78.
- [9] Myers R.H., Montgomery D.C., (2002), Response Surface Methodology: process and product optimization using designed experiments, *John Wiley and Sons*, 2th edition.
- [10] Aleboyeh A., Daneshvar N., Kasiri M.B., (2008), Optimization of C.I. Acid red 14 azo dye removal by electrocoagulation batch process with response surface methodology, *Chemical Engineering and Processing*, 47, 827-832.
- [11] Khataee A.R., Zarei M., Moradkhannejhad L., (2010), Application of response surface methodology for optimization of azo dye removal by oxalate catalysed photoelectron-Fenton process using carbon nanotube- PTFE cathode, *Desalination*, 258, 112-119.
- [12] Saad, R., Belkacemi, K. and Hamoudi, S. (2007). Adsorption of Phosphate and Nitrate Anions on Ammonium-Functionalized MCM-48: Effects of Experimental Conditions, *Journal of Colloid and Interface Science*, 311, 375-381.

Trend and Change point Analysis of Extreme Temperature over India using Non-Parametric Methods and Empirical Mode Decomposition

Drisya S Dharan¹, Anuja PK¹, Govindan Unnithan¹, Anand Vishnu B¹ and Adarsh S²

¹ TKM College of Engineering, Kollam 691005, India

² Assistant Professor TKM College of Engineering, Kollam 691005, India

¹drisyasdharan@gmail.com

Abstract. This paper presents the trend and change point analyses of extreme temperature (T_{max} and T_{min}) datasets of annual and seasonal series of seven homogeneous regions of India for the period 1901-2007. The study used Mann-Kendall (MK) test for detection of trend, Cumulative Sum (CUSUM) test for detection of change point and Empirical Mode Decomposition (EMD) for extracting non-linear trend of all the 70 time series. The results of MK test showed that at all the seven regions except North-West, T_{max} series of winter season showed a significant increase at 5 % significance level. The MK test detected a significantly increasing trend on annual and all seasonal T_{max} series of West Coast (WC) and North East (NE) regions. The CUSUM test detected a change point within 1975-77 for minimum temperature series of East Coast (EC) region for all the seasons except monsoon, which is in agreement with the well debated climate shift of 1976-77 period. The test detected a change point in 1950 for T_{max} series of winter season in all homogeneous regions except northwest (NW). The study also found that change point year estimated in the non linear trend fitting by EMD may differ from that based on statistical estimations.

Keywords: Trend, Change Point, Non-linear, Temperature

Introduction

Temperature is one of the important meteorological variables, which is of direct influence on the hydrological process. The changes in extreme (maximum and minimum) temperature significantly affect the hydrology of the geographical domain of interest. High temperature may affect drought conditions, damage of crops; while low temperature may affect the yield of cereal crops. Many studies have been conducted on the changes in temperature regime of India in the past, out of which some studies focused on extreme temperature. For example, Rupakumar et al. [1] performed linear trend analysis of extreme temperature data of 121 stations over India of the period 1901–1987 and it was found that mean temperature trends over India were similar to the global and hemispheric trends. They showed that the increase in the mean temperatures over India is mainly contributed by the maximum temperatures, with the minimum temperatures were practically trendless. Krishnakumar et al. [2] found the association of extreme temperatures in the pre-monsoon season with Indian summer monsoon rainfall. Kothawale and Rupakumar [3] reported a significant warming trend of 0.05°C per decade during the period 1901–2003, and for 1971–2003 the study noted a relatively accelerated warming of 0.22°C per decade. Kumari et al. [4] analyzed the relation between solar radiation and extreme temperature for twelve different locations in India for the period of 1981-2004 and found that spatial averaged surface extreme air temperatures of India have been increasing, and the change in minimum temperature has been doubled while change in maximum temperature is marginal. Kothawale et al. [5] found trends in extreme temperature events for the pre-monsoon season using daily data on maximum and minimum temperatures from all the seven temperature homogenous regions in India. Pal and Al Tabbaa [6] performed a detailed trend analysis study of extreme temperature dataset from different temperature homogeneous regions in India, at monthly and seasonal scale. It was found that monthly maximum temperature increased over the last century and minimum temperature changes have high variability than maximum temperature changes (both temporally and spatially) with lesser degree of significance. Sonali and Nagesh Kumar [7] performed trend analysis of temperature records from the temperature homogeneous regions of India during 1901-2003 using thirteen different methods.

Eventhough many studies were performed for analyzing the trend (mainly by using Mann-Kendall (MK) and Sen’s slope methods), studies on estimation of change point is rarely attempted by researchers. Due to the changing climate and the induced non-stationarity, it is important to extract the inherent non-linear trend in the datasets [8]. For the extraction of inherent non-linear trend, the techniques like singular spectrum analysis, empirical mode decomposition (EMD) or its variants, wavelet transform etc. have been used by the researchers [9-13]. The next section presents the details of methodologies used, section 3 presents the study area and data details, section 4 presents results and discussion and in the final section important findings are concluded.

2 Methodology

2.1 CUSUM test

CUSUM test originally proposed by E.S. Page (stated in [14]) involves the calculation of cumulative sum of the differences. After computing the mean (\bar{x}) of a time series, the cumulative sum S_i is computed recursively as $S_i = S_{i-1} + (x_i - \bar{x})$ (1)

after assigning $S_0 = 0$. Then $\max(0, S_i)$ is considered as the test statistic. When the values of S exceed a certain threshold value, a change in values has been found. The above formula only detects changes in the positive direction. When the negative changes need to be found as well, the min operation is used and this time a change has been found when the value of S is below the negative value of the threshold value.

2.2 Mann-Kendall Test

Mann-Kendall test [15, 16] is one popular non-parametric test used for the trend analysis and statistical significance. In this method, the test statistics is computed directly based on the values of the random variable and the expression

$$S = \sum_{i=1}^{N-1} \sum_{j=i+1}^N \text{sgn}(x_j - x_i) \tag{2}$$

for the same is

where N is the number of data points, x_j and x_i are data values at time j and i ($j > i$), respectively. This statistics represents the number of positive differences minus the number of negative differences for all the differences considered.

Denoting $(x_j - x_i) = \delta$

$$\text{sgn}(\delta) = \begin{cases} 1 & \text{if } \delta > 0 \\ 0 & \text{if } \delta = 0 \\ -1 & \text{if } \delta < 0 \end{cases} \tag{3}$$

For large samples ($N > 10$), the sampling distribution of S is assumed to be normally distributed with zero mean and variance as follows:

$$\text{Var}(S) = \frac{N(N-1)(2N+5) - \sum_{k=1}^n t_k(t_k-1)(2t_k+5)}{18} \tag{4}$$

where N is the number of tied (zero difference between compared values) groups and t_k the number of data points in the k^{th} tied group.

The Z-statistic or standard normal deviate is then computed by using equation:

$$Z = \begin{cases} \frac{S-1}{\sqrt{\text{Var}(S)}} & \text{if } S > 0 \\ 0 & \text{if } S = 0 \\ \frac{S+1}{\sqrt{\text{Var}(S)}} & \text{if } S < 0 \end{cases} \tag{5}$$

Here, if the computed value of $|Z| > Z_{\alpha/2}$, then the null hypothesis of no trend is rejected at α level of significance in a two-sided test (i.e., the trend is significant). A positive value of Z indicates an increasing trend and a negative value of Z indicates a decreasing trend.

2.3 Empirical Mode Decomposition

Empirical Mode Decomposition (EMD) is a non-parametric signal decomposition method proposed by Huang et al. [17], which decomposes a time series signal $X(t)$ into different oscillatory modes in purely empirical and data adaptive manner. The flow chart of EMD is provided below:

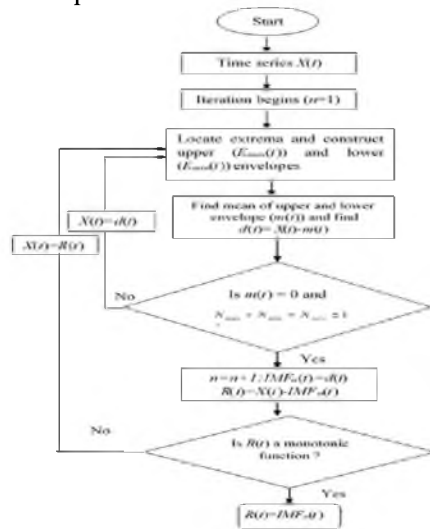


Fig. 1 Flowchart of EMD algorithm [18]

3 Study Area and Data

Indian Institute of Tropical Meteorology (IITM) Pune grouped different parts of India into seven temperature homogenous regions as shown in Fig. 2. The maximum and minimum temperature (T_{max} and T_{min}) data for the period 1901-2007 for the seven regions are collected from IITM Pune (<http://www.tropmet.res.in>) and used for trend and change point analysis.

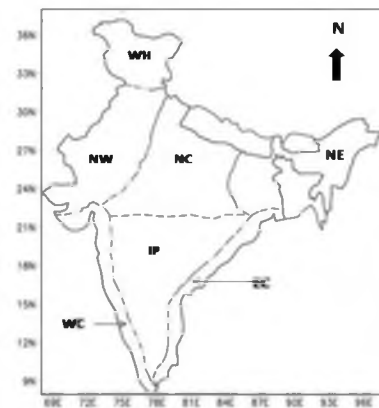


Fig. 2 Map showing temperature homogeneous regions of India. EC-East Coast; WC-West Coast; IP-Interior Peninsula; NE-North East; NC-Noth Central; NW-North West; WH-Western Himalaya

4 Results and Discussion

First the trend analysis of T_{max} and T_{min} series at annual and seasonal temporal scale are performed using MK test by considering significance level of 5 %. The results are presented in Table 1. Then the CUSUM method is used for the detection of change point. The results of CUSUM test are presented in Table 2.

Table 1. Results of MK test of different temperature time series (A-Annual; M-Monsoon PoM-Post Monsoon;W-Winter; PrM-Pre Monsoon) the bold and italic figures show that trend is statistically significant at 5 % level

Region	Maximum Temperature				
	A	M	PoM	W	Pr M
EC	0.791	0.11	1.018	5.586	1.02
IP	1.042	-0.002	1.053	4.554	1.042
NC	0.065	-0.097	2.312	2.711	3.61
NE	2.143	2.377	5.19	4.148	2.121
NW	-1.3	-0.555	1.236	1.734	-0.67
WC	5.75	3.613	6.2	7.551	5.75
WH	-0.371	-0.323	2.337	3.551	0.495
Region	Minimum Temperature				
	A	M	PoM	W	Pr M
EC	2.781	1.922	3.042	1.551	4.046
IP	-0.116	4.294	2.167	1.02	4.216
NC	2.086	-0.783	3.726	0.215	1.976
NE	0.703	-3.268	4.272	0.1	1.195
NW	-1.171	0.027	-0.345	-1.971	0.961
WC	0.215	3.766	1.769	-0.53	1.715
WH	2.983	1.225	2.872	2.42	2.415

Table 2 Change points of extreme temperature datasets by CUSUM method. The bold figures show temperature change happened at climate shift of 1976/77 period

From Table 1 it is noticed that except for few different the temperature series show an increasing trend. Many of the T_{max} series show statistically significant change while a reduction is noted only for monsoon temperature of NE region and winter minimum temperature of NW region. series of NW a significant trend. Annual and all of the four seasonal maximum series showed a statistically

Region	Type	W	PrM	M	PoM	A
EC	Max	1965	1995	1995	1977	1983
	Min	1977	1976	1985	1975	1977
WC	Max	1950	1968	1961	1959	1968
	Min	1992	1919	1991	1956	1991
IP	Max	1950	1982	1963	1963	1982
	Min	1978	1968	1994	1977	2006
WH	Max	1991	1949	1996	1930	1996
	Min	1978	1940	1986	1976	1978
NW	Max	1950	1962	1986	1962	1962
	Min	1932	1983	1994	1999	1932
NC	Max	1950	1933	1969	1962	1962
	Min	1976	2000	1961	1975	1978
NE	Max	1950	1949	1963	1963	1978
	Min	2003	1917	1963	1984	1952

is noticed that the extreme time series show trend. Many of show significant significant noted only for minimum NE region and temperature of None of the T_{max} region displayed trend. Annual four seasonal temperature statistically

significant increasing trend for the WC and NE regions. In the minimum temperature series of WH region annual series and seasonal series except monsoon showed an increasing trend. This study found that winter maximum temperature series of all regions except NW showed a statistically significant increasing trend. The CUSUM method helped in detecting the change point year of different temperature series and Table 2 show that there is no definite pattern or uniqueness in change point years of different series. However it is noted that in winter maximum temperature series, the change point is 1950 for all series except that of EC and WH regions. One can notice the possible harmony of the well debated climate shift year 1976/77[20] (with a deviation of 1 year) in the change point years of certain series. Interestingly, all the regions except NW and NE, the change point year of minimum temperature series coincides with the climate shift year. Also all the four seasonal minimum series and annual minimum series of EC region showed a change point year between 1975 and 1977.

The linear trend fitting is done for all the 70 time series and the non-linear trend of different series is determined by EMD method. The plots of trend analysis of maximum temperature series for winter season of all regions except NW are presented in Fig. 3.

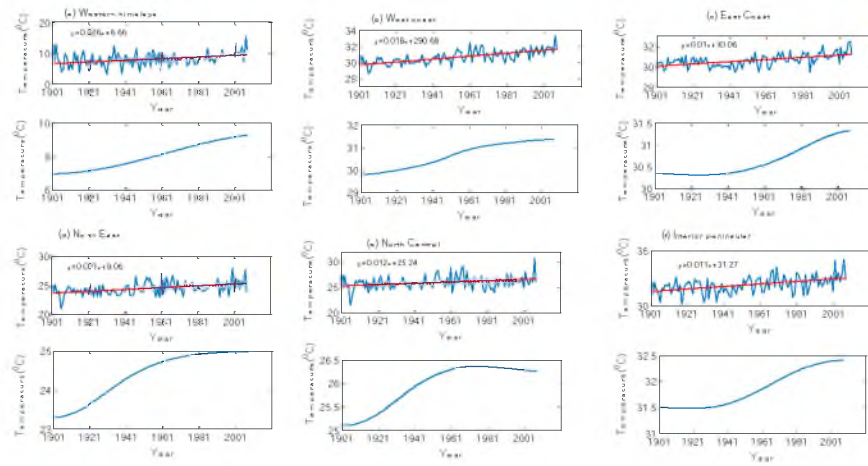


Fig. 3 Linear fitting and EMD of winter maximum temperature series of different homogeneous regions

From Fig.3 it is clear that the non-linear trend is increasing and it resembles with the character noticed by MK test. However on recollecting the fact that the change point year was ~1950s, the change point year is expected around ~1950s in non-linear trend, which is found to be absent in all these series. The non-linear trend of T_{min} series of EC region captured by EMD are presented in Fig. 4. It shows a diametric change in the winter series about 1950s with an increase in the latter half and an opposite nature for monsoon series with a difference in change point years (1950s). For rest of the series the trend is monotonically increasing in practice. Further, the trends of T_{min} series of WH region are presented in Fig. 5. The EMD analysis detected an increasing trend for all the seasonal and annual series. Here the increasing trend starts during the beginning of last century for all of the time series except that of winter season. Thus from different analysis it is noticed that the change point year (in non-linear trend) is not coinciding with the climatic shift year which again signifies the importance of capturing non-linear trends in series. Capturing the true shape of non-linear trend and the changing year by EMD method is helpful in non-stationary modeling of hydrological variables under the changing climate scenario, which eventually help for sustainable management of water resources of the country.

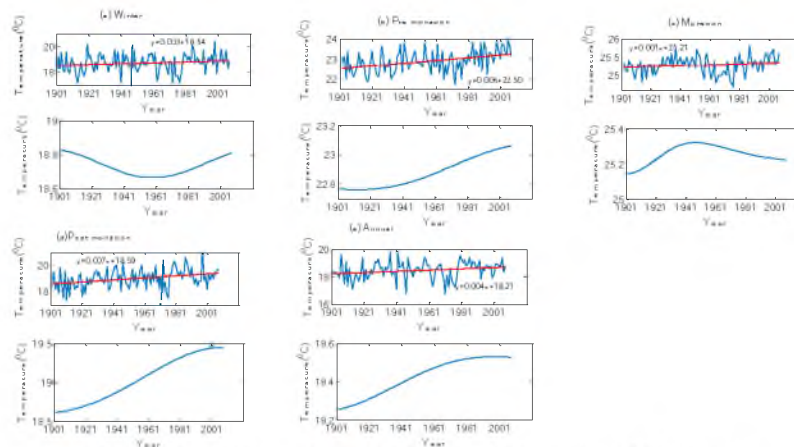


Fig. 4 Linear fitting of annual and seasonal T_{min} series of EC region

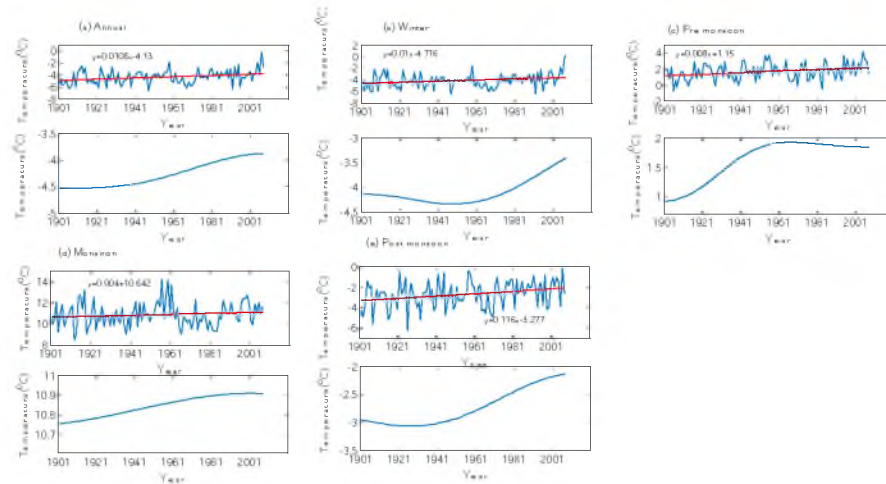


Fig. 5 Linear fitting of annual and seasonal T_{min} series of Western Himalaya

5 Conclusions

This paper performed the trend and change point analyses of extreme temperature (T_{max} and T_{min}) datasets of annual and seasonal temperature of seven homogeneous regions of India for the period 1901-2007. The major conclusions of the study are:

- The results of MK test showed that T_{max} series of WC and NE region displays an increasing trend irrespective of season
- The MK test showed that at all the seven regions except NW, maximum temperature of winter season is significantly increasing
- The CUSUM test detected a change point within 1975-77 for minimum temperature series of East Coast (EC) region for all the seasons except monsoon, which is in agreement with the well debated climate shift of 1976-77 period.
- The CUSUM test detected a change point in 1950s for maximum temperature series of winter season in all homogeneous regions except Western Himalaya (WH)
- The CUSUM test detected a change point during 1975-77 in the T_{min} series of winter season in all regions except the coastal belts of EC, EC and the NE
- The non-linear trend need not be in agreement with the linear trend of the time series and it may comprise a change point year about which an asymmetric change may be present
- The change point year estimated in the non-linear trend fitting may differ from that based on statistical estimations.

References

- Rupa Kumar K., Krishna Kumar K., Pant G.B.: Diurnal asymmetry of surface temperature trends over India. Geophysical Research Letters, 21, 677-680 (1994)
- Krishnakumar K, Rupakumar K Pant G.B.: Pre-monsoon maximum and minimum temperatures over India in relation to the summer monsoon rainfall. International Journal of Climatology, Geophysical. Research Letters, 17, 1115-1127 (1997)
- Kothawale D.R., Rupa Kumar K.: On the recent changes in surface temperature trends over India. Geophysical Research Letters, 32, L18714, DOI: 10.1029/2005GL023528, (2005)
- Kumari P.B., Londhe A.L., Daniel S, Jadhav D.B.: Observational evidence of solar dimming: offsetting surface warming over India. Geophysical Research Letters, 34, DOI:10.1029/2007GL031133 (2007)
- Kothawale D.R., Revadekar J.V., Rupa Kumar K.: Recent trends in pre-monsoon daily temperature extremes over India. Journal of Earth System Science, 119, 51-65 (2010)

- Pal I, Al Tabbaa A.L.: Long-term changes and variability of monthly extreme temperatures in India. *Theoretical and Applied Climatology*, 100, 45–56 (2011)
- Sonali P., Nagesh Kumar D.: Review of trend detection methods and their application to detect temperature change in India. *Journal of Hydrology*, 476, 212–227 (2013)
- Franske C.L.: Non-linear climate change. *Nature of Climate Change* 4, 423–424 (2014)
- Wu Z, Huang N.E., Long S.R., Peng C.K. On the trend, detrending and variability of nonlinear and non-stationary time series. *Proceedings National Academy of Science USA*, 104 (38), 14889–14894 (2007)
- Sang Y-F., Wang Z., Liu C.: Comparison of the MK test and EMD method for trend identification in hydrological time series. *Journal of Hydrology* 510, 293–298 (2014)
- Unnikrishnan P., Jothiprakash V.: Extraction of nonlinear trends using singular spectrum analysis. *Journal of Hydrologic Engineering*, 10.1061/(ASCE)HE.1943-5584.0001237, 05015007, (2015)
- Carmona A.M., Poveda G.: Detection of long-term trends in monthly hydro-climatic series of Colombia through Empirical Mode Decomposition. *Climatic Change* 123(4), 301–31 (2013)
- Sang Y-F., Sun F., Singh V-P., Xie P., Sun J.: A discrete wavelet spectrum approach to identifying non-monotonic trend pattern of hydro-climate data. *Hydrology and Earth. System Science Discussions* doi:10.5194/hess-2017-6 (2017)
- Taylor W.: *Change-Point Analysis: A Powerful Tool for Detecting Changes*. Taylor Enterprises, Libertyville. 2000, <http://www.variation.com/cpa/tech/changepoint.html>
- Mann H.B.: Non-parametric tests against trend. *Econometrica*, 13(3), 245–259 (1945)
- Kendall M.G.: *Rank Correlation Methods*, 4th Ed., Charles Griffin, London, UK, 1975.
- Huang N.E., Shen Z., Long S.R., Wu M.C., Shih H.H., Zheng, Q., Yen N.C., Tung C.C., Liu H.H.: The empirical mode decomposition and the Hilbert spectrum for nonlinear and non-stationary time series analysis. *Proceedings of Royal Society London, Series A*. 454, 903–995 (1998)
- Adarsh S. Multiscale characterization of hydrological time series using mathematical transforms. Ph.D thesis, Indian Institute of Technology Bombay (2017)
- Sahana A.S., Ghosh S., Ganguly A., Murtugudde R.: Shift in Indian summer monsoon onset during 1976/1977. *Environmental Research Letters* 10(5), 10.054006, doi:10.1088/1748-9326/10/5/054006, (2015)

Evaluation of Groundwater Quality at Eloor, Ernakulam District, Kerala Using GIS

Fehmida Fatima S¹ and Bindu A G²

¹ Environmental Engineering, Government Engineering College, Thrissur

² Department of Civil Engineering, Government Engineering College, Thrissur
fehmidaf4@gmail.com

Abstract. Pollution of groundwater resources is one of the major challenges faced by rapidly developing countries like India. Population explosion, large scale industrialization and urbanization have led to rapid decline in groundwater quality. Traditional methods of assessing groundwater quality like random sampling and analysis has become ineffective and obsolete in providing a comprehensive, complete and accurate picture of the pollution levels in large areas. In this paper, groundwater quality in the industrial belt of Eloor in Ernakulam district of Kerala is evaluated using Geographical Information System based geostatistical methods. Ordinary Kriging method based on spatial autocorrelation is used for predicting the groundwater physico-chemical parameters at unmeasured locations.

Keywords: Geostatistical methods, Groundwater pollution, Geographical information system, Ordinary kriging

Introduction

Water is one of the most important natural resources required for sustaining life on Earth. Water in its many forms is required for human health, social and economic well being and development of a nation. It is a vital resource that is becoming increasingly scarce due to rapid increase in population, industrialization, urbanization, climate change and various other anthropogenic activities [9]. Water is present on Earth in many forms; as surface water in rivers, lakes and oceans; as snow and glacial water; as groundwater stored in aquifers and as water vapor in atmosphere. Out of these many sources of water, groundwater is considered as the most dependable source because it is widely available and reliable especially in arid climates and in times of drought and scarcity [6]. About a third of the world's population depends on groundwater for meeting their basic necessities. However, unchecked exposure to large scale pollution and over use has lead to depletion in quality of groundwater resources. This is encountered especially in regions of high population density and industrialization [8].

There are many sources from which groundwater can get polluted. These include natural sources like dissolution of minerals found in soil and rocks and manmade sources like leaching from landfills, application of chemical insecticides and pesticides, industrial discharges and spills etc. The contamination of groundwater leads to ecological degradation, loss of vegetation, pollution of surface water sources and causes adverse effects on human and animal health. Once an aquifer gets contaminated, it is arduous and unfeasible to reverse the effect. Polluted groundwater can cause negative health impacts in humans. Kidney, liver, nerve damages, miscarriages, developmental abnormalities, cancer, poisoning by toxins etc are a few health effects of polluted water. Thus, better management, quality control and monitoring is required to preserve groundwater resources [8].

Conventional methods of monitoring groundwater quality involve construction of monitoring wells and random sampling from bore wells or open wells. These methods are time consuming, expensive and tedious. Alternative methods like spatial mapping of groundwater quality using Geographical Information System has gained momentum in recent years. Since groundwater quality is a spatially varying parameter, mathematical models and spatial analysis can be used to manage groundwater problems. With limited observations or data, manpower, expense and time, GIS based geostatistical methods can be used as an effective tool for obtaining accurate pollution profiles [3][9].

Eloor is a river island formed by the tributaries of Periyar river in Ernakulam District of Kerala in India. It is home to the largest industrial belt in Kerala with over 247 small, medium and large scale industries involved in the production of chemicals, fertilizers, insecticides, leather, rubber, metal plating etc. Most of these industries are several decades old and employ the most polluting manufacturing methods. This has lead to widespread pollution of land, water and air in the area. Eloor is considered as one of the most polluted toxic hotspots in India by Greenpeace. A study conducted by Greenpeace in 2003 found that pollution in Eloor has caused harmful effects in health of local population. Eloor ranks 24th in the list of Critically Polluted Areas (CPA) in the country. There has been a significant

increase in respiratory diseases, birth defects, cancer and many other illnesses in the Eloor community. A study conducted in 2007 on the quality of groundwater in Eloor, found that the groundwater quality was poor [2]. Since the detection of alarming levels of pollutants in the wells of Eloor, a large number of people have abandoned their wells or use it for purposes other than drinking, cooking and bathing.

This study aims to study the status of groundwater pollution in Eloor using GIS based geostatistical methods.

Methods and Data

Study Area

Eloor is a river island occupying an area of 14.21 square kilometers in Ernakulam District of Kerala in India between north latitudes $9^{\circ} 3'$ and $10^{\circ} 6'$ and east longitudes $76^{\circ} 20'$ and $76^{\circ} 28'$. It is formed between two distributaries of the Periyar river [2].

Sample collection and physico-chemical analysis

Thirty groundwater samples were collected from open wells in Eloor from January 2018 to February 2018. Physico-chemical parameters of the collected samples such as pH, temperature, TDS, Chloride, sulphate, iron, nitrate, hardness, COD and lead were analyzed as per APHA methods. Portable pH meter and TDS meter was used to determine pH and TDS respectively. The coordinates of sample points were obtained using handheld GPS.

Geostatistical Analysis

Geostatistical methods such as kriging are widely used in fields such as geology, mining, meteorology and earth sciences for mapping spatial variation of parameters based on spatial autocorrelation. Geostatistics uses both mathematical and geostatistical methods to generate continuous surfaces. It can be used not only to predict values at unmeasured locations, but also to determine the uncertainty in the prediction [2].

A GIS database was created to store the analyzed water quality parameters. Geostatistical wizard tool in GIS was used for interpolation of parameters. Before using kriging for interpolation, exploratory data analysis was done to determine the suitability of data for prediction [1]. Kriging method works best if the data is normally distributed. Histograms and Q-Q plots were used to assess the normality of the data. Parameters which did not show a normal distribution were transformed using transformations such as logarithmic and arcsine transformations to make them conform more closely to a normal distribution. Analysis of normal Q-Q plots and histograms showed that all the parameters exhibited normal distribution. However, logarithmic transformation was applied to parameters that showed a decrease in skewness after transformation. Thus, pH, chloride, nitrate and sulfate data were transformed before predictions.

Ordinary Kriging was used for prediction since it was the easiest and most accurate of all the interpolation methods. Semivariograms were used to study the spatial correlation in data and to fit mathematical models for prediction [7]. The semivariogram parameters such as nugget, sill and range were studied to determine the degree of spatial correlation [6]. Three types of models; spherical, exponential and Gaussian were used to for prediction of parameters at unmeasured locations. The best fitting model was selected after cross-validation based on the lowest root mean square error (RMSE). The smallest RMSE value indicates the most accurate prediction [5]. This model was then used to generate the output surface or thematic map.

Results and Discussions

The results of physico-chemical analysis conducted on thirty groundwater samples are given in Table 3.1. The parameters analyzed include pH, temperature, TDS, chloride, nitrate, hardness, iron, and sulfate.

Table 3.1 Results of physico-chemical analysis

Sample No	pH	TDS (ppm)	Temperature °C	Hardness (mg/L)
1	6.7	200	29.2	186.2
2	6.2	214	28.3	194.3
3	6.0	206	28.8	211.8
4	6.1	211	27.7	205.1
5	6.2	198	27.8	209
6	5.9	185	28.2	214.2
7	6.0	170	28.4	210.8
8	6.9	173	28.7	223.6
9	6.2	198	29	246.6
10	6.3	230	30	243
11	6.2	229	28.1	245.1
12	6.3	225	27.6	268.6
13	6.5	227	29.6	276.5
14	6.9	216	28	267.7
15	7.2	213	26	263.1
16	6.5	205	26.3	269.8
17	6.3	219	26.6	271
18	6.1	223	28	246.4
19	5.7	220	29.2	242.7
20	5.6	236	29.4	255.6
21	5.2	242	28.3	304.2
22	5.6	243	28	311.6
23	5.5	238	28.2	309.9
24	5.4	246	28.2	301.8
25	5.9	242	27.8	283.4
26	5.8	236	28	278.9
27	6.4	227	27.3	248
28	6.1	231	29	251.5
29	6.3	186	28	225
30	6.2	226	29	234.5

Sample No	Cl ⁻ (mg/L)	Fe (mg/L)	NO ₃ ⁻ (mg/L)	SO ₄ ²⁻ (mg/L)
1	198.6	0.23	16.5	134.2
2	202.3	0.15	19.4	136.4
3	200.1	0.32	16.8	139
4	210.4	0.29	15.5	145.6
5	211.9	0.27	19.3	143.2
6	206.6	0.33	20.1	149.6
7	220.8	0.18	24.3	150.3
8	232.5	0.22	23.8	153.6
9	228.6	0.26	25	149.2
10	240.8	0.31	33.3	156.1
11	252.3	0.36	38.6	163.3
12	228	0.33	37.3	166.1
13	226.1	0.3	36.5	168.8
14	228.3	0.28	44.3	177.6
15	225.1	0.23	50.3	173.8
16	211.5	0.25	48.9	174.2
17	213.8	0.32	52.5	176.5

18	224.8	0.36	48.7	173.6
19	230.2	0.35	46.2	186
20	248.4	0.33	39.6	183.8
21	259.8	0.37	36.7	195.6
22	260.1	0.41	29.5	204.2
23	266.5	0.47	26.6	207.8
24	271.8	0.49	24.7	211.9
25	261.2	0.33	27.3	216.6
26	264.8	0.38	28.3	225
27	258.6	0.3	26.6	203.6
28	238.6	0.32	24.2	223.8
29	216.2	0.28	25.6	164.6
30	235.7	0.33	39.9	145.8

Semivariograms were plotted and best fitting model was selected based on lowest RMSE value. Spherical model was found to be best fitting model for TDS, nitrate, hardness and iron. Gaussian model was found to be best fitting model for temperature, chloride and sulphate. Exponential model was found to be best fitting model for pH. The best fitting semivariogram models for the eight groundwater quality parameters are shown in Fig. 3.1 to Fig. 3.8.

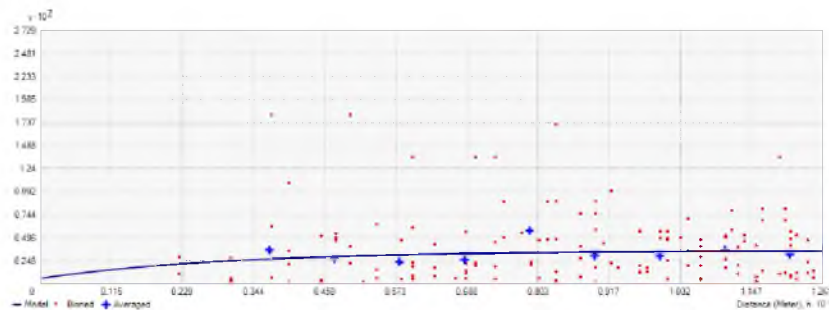


Fig. 3.1 Best fit semivariogram model for pH

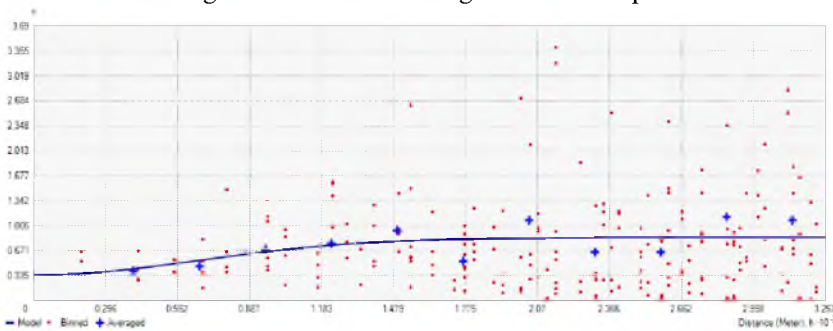


Fig. 3.2 Best fit semivariogram model for temperature

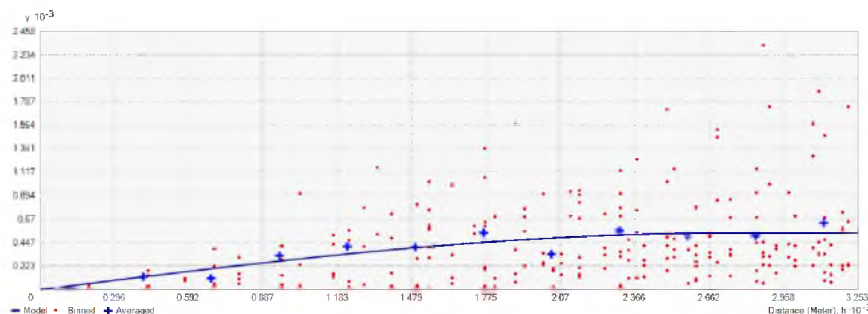


Fig. 3.3 Best fit semivariogram model for TDS

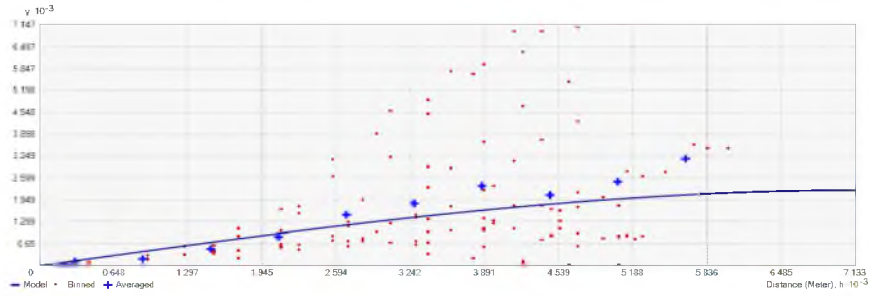


Fig. 3.4 Best fit semivariogram model for hardness

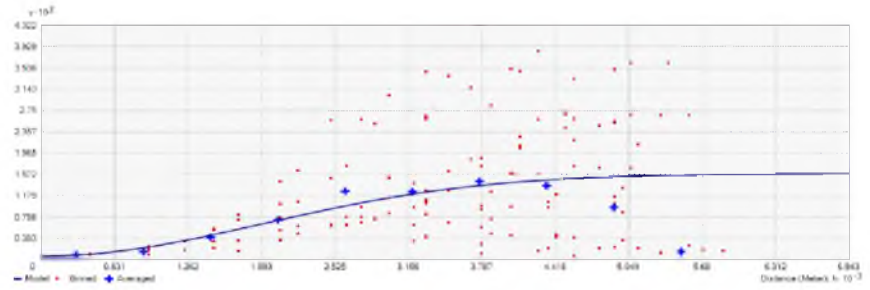


Fig. 3.5 Best fit semivariogram model for chloride

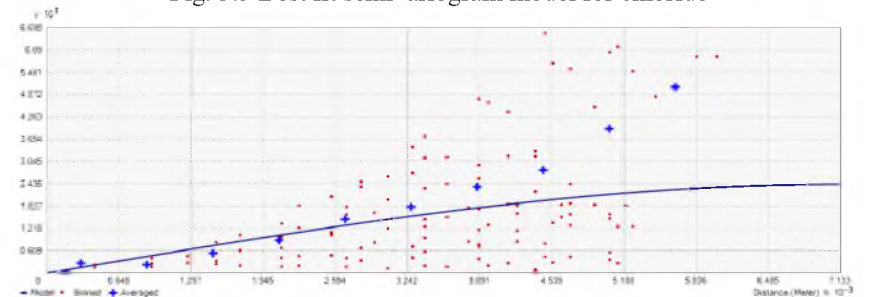


Fig. 3.6 Best fit semivariogram model for nitrate

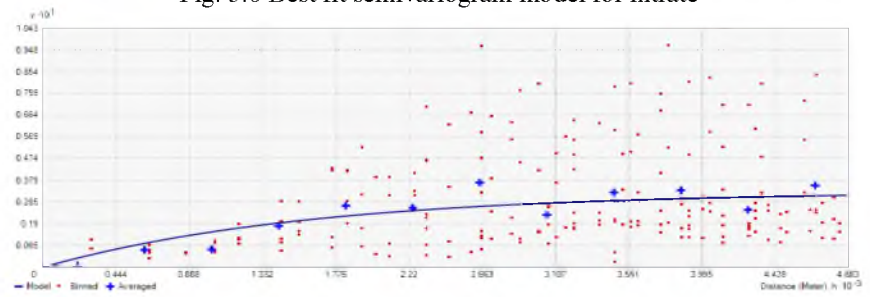


Fig. 3.7 Best fit semivariogram model for sulfate

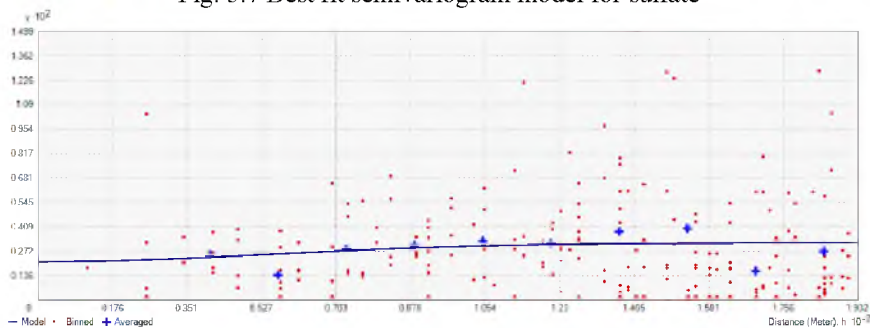


Fig. 3.8 Best fit semivariogram model for iron

The predicted output surface based on the best fitting models for each of the eight parameters is shown in Fig 3.9 to 3.16.

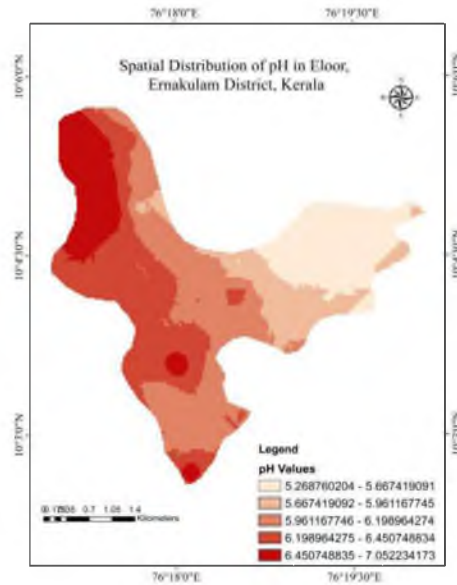


Fig 3.9 Predicted map of spatial variation in pH

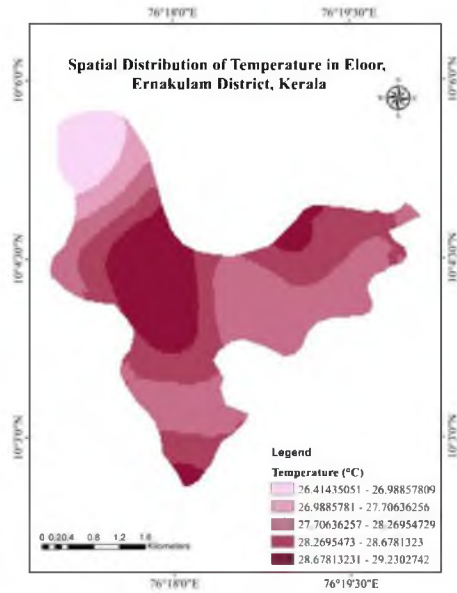


Fig. 3.10 Prediction map of spatial variation in temperature

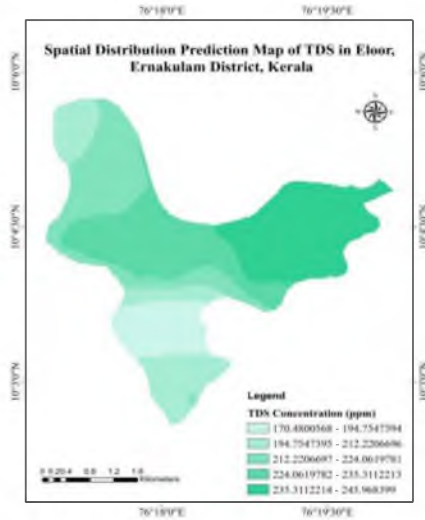


Fig. 3.11 Prediction map of spatial variation in TDS

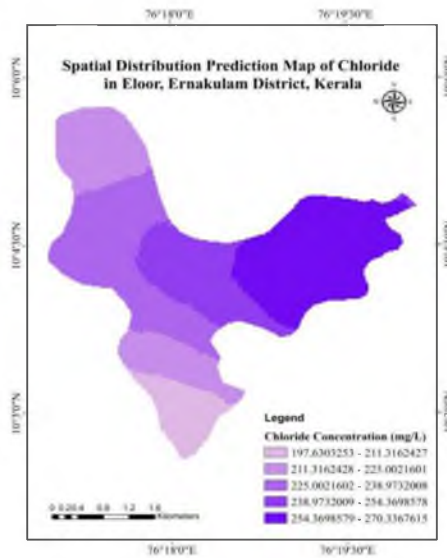


Fig. 3.12 Prediction map of spatial variation in chloride

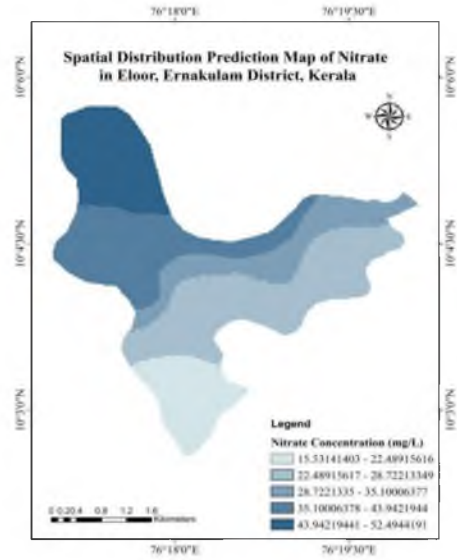


Fig. 3.13 Prediction map of spatial variation in nitrate

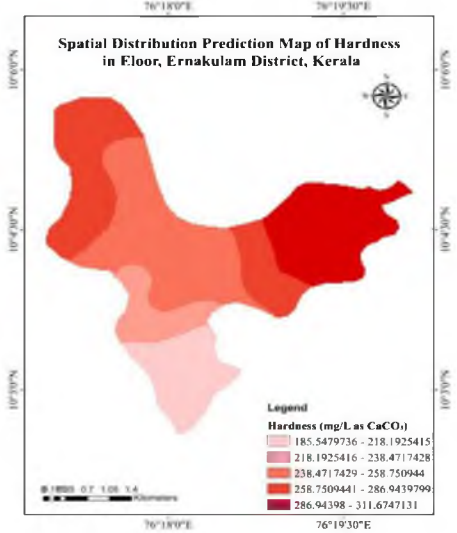


Fig. 3.14 Prediction map of variation in hardness

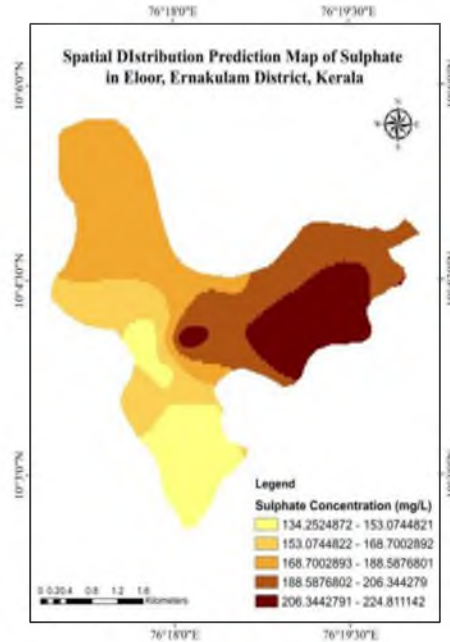


Fig. 3.15 Prediction map of variation in sulfate

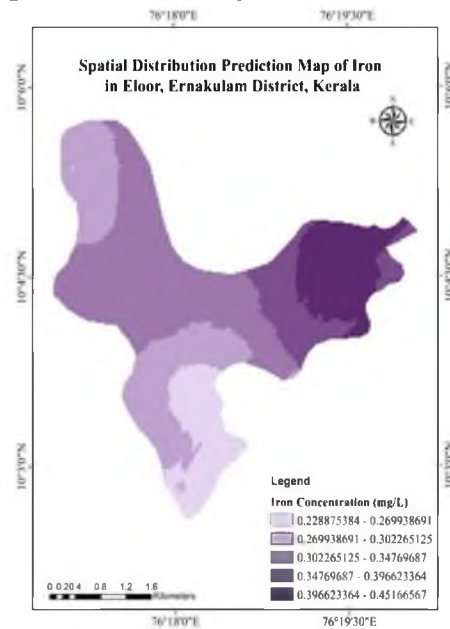


Fig. 3.16 Prediction map of variation in iron

Groundwater showed high acidity in north eastern parts of Eloor and acidity decreases towards the western and southern regions. Temperature shows irregular variations with higher temperature in the central, southern and eastern parts. TDS showed higher values in the eastern region. However, TDS was within limits in the whole area. Chloride concentration exceeded the desirable limit of 250 mg/L in most of the eastern parts of Eloor. Nitrate concentration was found to be high in the north-western regions of Eloor. The desirable limit of 45 mg/L was exceeded in this area. Hardness exceeded the limit of 200 mg/L in almost all the regions with the highest concentration observed in the eastern and northern regions. Sulfate concentration was found to be within limits except in some parts of the eastern region. The concentration of iron exceeded the desirable limit of 0.3 mg/L in almost all regions.

From the above observations, it can be inferred that the groundwater in northern and eastern parts of Eloor are more polluted and unfit for human consumption than the southern regions. This variation may be attributed to the higher density of industries in this region. Using geostatistical methods was found to be a suitable method for predicting concentration of groundwater parameters at unmeasured locations.

References

- Chowdhury, A. (2016). Assessment of spatial groundwater level variations using geostatistics and GIS in Haringhata Block, Nadia district, West Bengal, *International Journal of Research in Engineering and Technology*, 5(5), 276-280.
- Divya R. T., B. Sunil and C. Latha . (2011) Physico- Chemical Analysis of Well Water at Eloor Industrial Area-Seasonal Study. *Current World Environment* Vol. 6(2), 259-264.
- Gharbia, A.S., Gharbia, S.S., Abushbak, T., Wafi, H., Aish, A., Zelenakova, M. and Pilla, F. (2016). Groundwater Quality Evaluation Using GIS Based Geostatistical Algorithms, *Journal of Geoscience and Environment Protection*, 4, 89-103.
- Johnston, K., Ver Hoef, J.M., Krivoruchko, K. and Lucas, N. (2003). Using ArcGIS Geostatistical Analyst, *ESRI*.
- Khosravi, H., Karimi, K., Fard, N.N. and merbahzadeh, T. (2016). Investigation of spatial structure of groundwater quality using geostatistical approach in Mehran Plain, Iran, *Pollution*, 2(1), 57-65.
- Marko, K., Amri, A., Nassir, S. and Elfeki, A.M.M. (2013). Geostatistical analysis using GIS for mapping groundwater quality : a case study in the recharge area of Wadi Usfan, Saudi Arabia, *Arab J Geosci*, 7(12), 5239-5252.
- Oliver, M.A. and Webster, R. (1990). Kriging: a method of interpolation for geographical information systems, *International Journal of Geographical Information System*, 4(3), 313-332.
- Pawari, M.J. and Gawande, S. (2015). Water pollution and its consequences, *International Journal of Engineering Research and General Science*, 3(4), pp 773-776.
- Xiao, Y., GU, X., Yin, S., Shao, J., Cui, Y., Zhang, Q. and Niu, Y. (2016). Geostatistical interpolation model selection based on ArcGIS and spatio-temporal variability analysis of groundwater level in Piedmont Plains, Northwest China, *Springer Plus*, 5, 425-440.

Biodiesel production from waste oil using mussel shell as catalyst

Sona Gloriya Antony¹ and Nithya Kurup²

¹ PG Scholar, Department of Environmental Engineering, UKFCET, Parippally,
glorina.antony@gmail.com

² Assistant Professor, Department of Environmental Engineering, UKFCET, Parippally, nithya.kurup104@gmail.com

Abstract. Waste utilization is an essential component of sustainable development and waste shells are rarely used to generate practical products and processes. Most waste shells are CaCO₃ rich, once calcined at 950 °C for 2 hour and can be employed as inexpensive and green catalysts for the synthesis of biodiesel. Herein, utilization of mussel shell as green catalysts for the transesterification of substrate as feedstock into biodiesel. Waste cooking oil is used in the study which is easily available and sustainable, thus reduces the price of biodiesel to make it competitive with petroleum diesel. Transesterification was done in the presence of waste cooking oil, methanol and the prepared mussel shell catalyst depending on different parameter. The catalysts from waste shells were characterized by Scanning electron microscope (SEM), X-ray diffraction (XRD) and Fourier transformed infrared (FTIR) spectroscopy. The SEM image of catalyst showed the “rod like particle” structures. Different transesterification reaction are done based on the effects of methanol to oil ratio (1:5, 1:10, 1:15), reaction time (1h, 2h) and reaction temperature (55 °C, 60 °C, 65 °C) and catalyst loading (0.1%, 0.2%, 0.3%, 0.4%, 0.5%, 0.6%) and finally being optimized based on density. And then analyzing for Kinematic viscosity, Flash point and Fire point

Keywords:Biodiesel; mussel shell; tranesterification; petroleum diesel

Introduction

The search for alternative energy resources to supplement or replace fossil fuels has been intensifying in the recent years because of the increase in environmental concern, energy security and fast depletion of fossil fuel resources. In this respect, biodiesel is an emerging alternative to diesel fuel derived from renewable and locally available resources which is biodegradable, nontoxic and environmentally friendly.[1]Biodiesel production is carried out through the process of transesterification reaction. The reaction is carried out with a suitable catalyst either homogeneous or heterogeneous. The selection of an appropriate catalyst depends on the amount of free fatty acids in the oil. Recently, homogeneous catalysts are widely chosen for biodiesel production in large scale operation. However, they are toxic, highly flammable and corrosive in nature. Furthermore, the use of homogeneous catalyst produced soaps as by-product and large amount of wastewater that required additional processing technologies and therefore increases the cost for proper disposal. On the other hand, heterogeneous catalysts are capable to overcome the problems faced by the former ones. [2]. Transesterification is the process of converting the vegetable oil or animal fats to biodiesel. Reaction are often carried through an acid or base catalyst. Transesterification of triglyceride using homogeneous and heterogeneous catalyst produces biodiesel[4,5]

The primary aim of the study is to produce biodiesel from raw materials such as waste cooking oil and mussel shell. So as to produce less environment polluting biodiesel as compared to petroleum diesel.

Experimental Details

Materials

Mussel shells were collected from a nearby fishmarket in kollamkerala, India. Waste frying oil was collected from bakeries and restaurants in kollam, India. The collected waste oil from different bakery was filtered using a filter paper to remove the contamination from it. Anhydrous methanol of analytical grade are taken from the laboratory of BIOVENT-Solution for Research, were used in the transesterification reaction.

Catalyst Preparation

Mussel shell was initially rinsed with distilled water to remove any unwanted materials on its surface. The washed mussel shells were then dried in hot air oven at 105 °C for 24 h. The dried mussel shells were calcined in a muffle furnace under static air conditions at 950 °C for 2 h to transform the calcium species in the shell into CaO particle.

1.3 Catalyst Characterisation

- Scanning Electron Microscopy (SEM) analysis was performed to confirm the morphology of the catalyst using a High Resolution Scanning Electron Microscope.
- Fourier Transformed Infrared (FTIR) spectroscopy was used to study the functional groups attached to the catalysts with Nicolet is50FT-IR at wave number 5000-400 cm⁻¹

Optimisation for Biodiesel Production

Biodiesel has been produced by the transesterification of different ratios of waste cooking oil, methanol and catalyst such as 1:5, 1:10, 1:15 methanol to oil ratio and for different catalyst loading rates such as 0.1%, 0.2%, 0.3%, 0.4%, 0.5%, 0.6%. Varying reaction time as 1h, 2h, and reaction temperature as 55 °C, 60 °C, 65 °C was also optimized according to the need.

1.4 Transesterification process

In Fig. 1, Transesterification reaction was done using a reactor at . After reaction the product was transferred to a 1000ml separating funnel for an overnight to produce a clear separation between the layers. In the separating funnel, it appear in 2 layers where bottom layer is glycerol and the top layer is found to be biodiesel as shown in Fig. 2. After separation, biodiesel with density 0.87 is back washed with distilled water to remove any contamination, unreacted methanol content and glycerol. Fig. 3 shows while back washing with distilled water it appears in two layers where bottom layer is water and top layer being biodiesel. Back washing is done 2 to 3 times

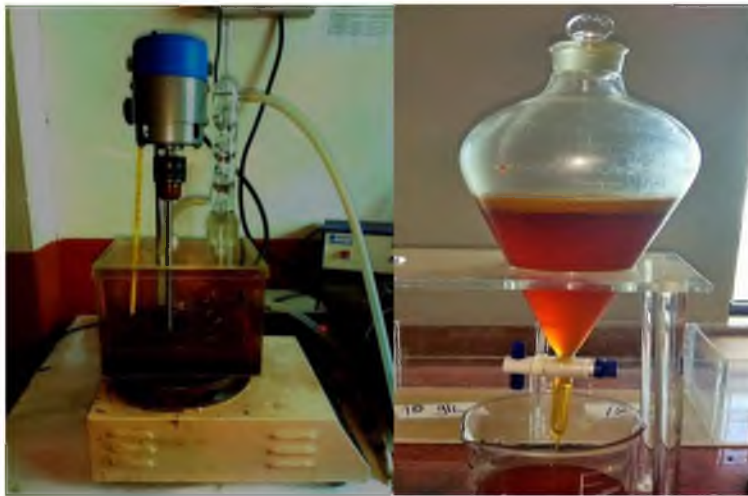


Fig. 1 Transesterification in reactor

Fig. 2 Transesterified product in separating funnel



Fig. 3 Transesterified product backwashed with distilled water

2 Result and Discussion

2.1 Properties of Waste cooking oil

The physicochemical properties of waste cooking oil was analysed and shown in the table 1. From the table it is clear that free fatty acid is the half of acid value. And the biodiesel yield is inversely proportional to the free fatty acid that is as free fatty acid value decreases, biodiesel yield increases.

Table 1. Physicochemical properties of waste frying oil used in the present study.

Properties	
Density at 25 °C (kg/m ³)	912
Acid value (mg of KOH/gm. of oil)	4.488
Free fatty acid (mg of KOH/gm. of oil)	2.244

2.2 Characterization of catalyst using SEM

Fig. 4 shows the SEM image of the catalyst after calcination process for different magnification range. However the calcinated mussel shell shows a rod like particle was observed. It indicated a regular micro morphology of a rod like particle by Nijuet. al [8]

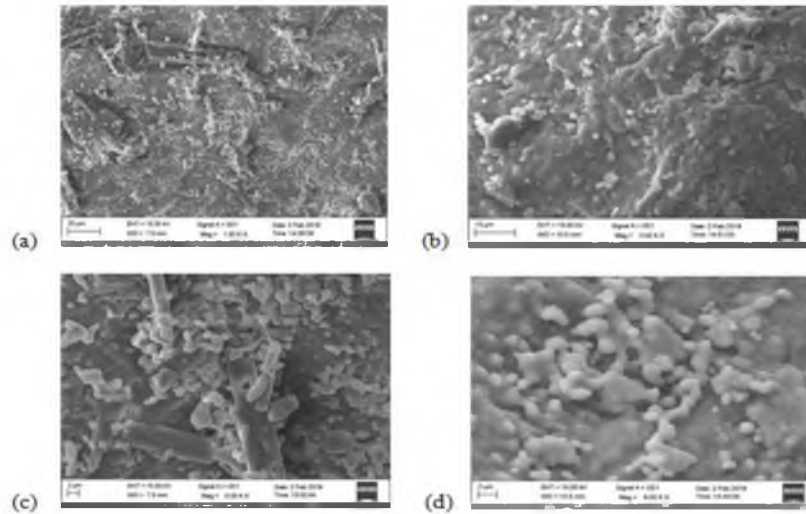


Fig. 4 SEM image at magnification range (a) 1.50KX (b)3.50KX (c)5.00KX (d)8.00KX

2.3 Characterization of catalyst using FTIR

Figure 5 shows the FTIR spectroscopy of the prepared catalyst observed at a range of $500 - 4000\text{cm}^{-1}$. FTIR analysis is carried out to identify the possible functional groups. And it shows that the peaks are in fingerprint portion. Peaks at 1390 cm^{-1} indicates CO bond. Wavenumbers of $873, 1450, 1640\text{ cm}^{-1}$ corresponds to CO_2 and wavenumbers of 3570 and 3420 cm^{-1} are OH groups [1].

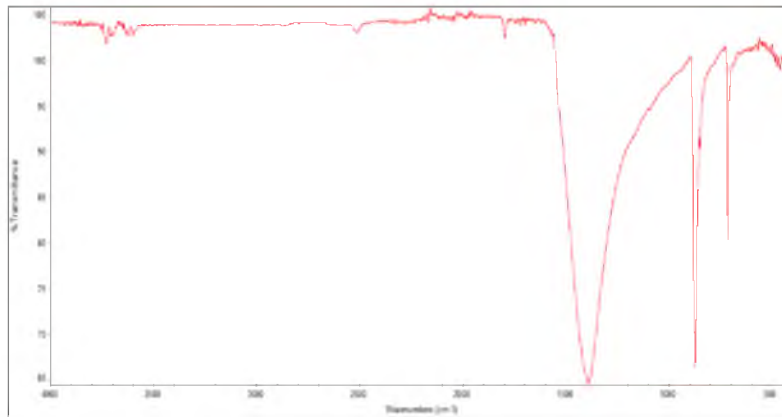


Figure 5: FTIR spectroscopy of prepared catalyst

2.4 Optimization Results

After optimization, it is seen that density was concurrently optimized at the methanol to oil ratio of 1:5. And from that ratio, the catalyst loading was optimized at 0.5% at a temperature of $60\text{ }^\circ\text{C}$ and a reaction time of 1 hour.

3 Conclusions

In this study, waste cooking oil and mussel shell after calcination has been used as the raw material for the production of biodiesel. Thereby enhancing cost effective and green catalyst for the production process. Further characterisation of catalyst such as SEM and FTIR was analysed. Transesterification reaction was carried out with

waste oil, catalyst and methanol at 1:5 methanol to oil ratio, 0.5% catalyst loading at 1 hour and 60°C reaction temperature conditions and optimized based on density.

References

- [1] S. Sulaiman & N. I. F. Ruslan, "A heterogeneous catalyst from a mixture of coconut waste and eggshells for biodiesel production," *Energy sources, part a: recovery, utilization, and environmental effects*, vol. 29, pp. 154–159, 2017
- [2] Vijayalakshmi Shankar & Ranjitha Jambulingam, "Waste crab shell derived CaO impregnated Na-ZSM-5 as a solid base catalyst for the transesterification of neem oil into biodiesel", *Journal of sustainable Environment research*, vol. 27, pp. 273-278
- [3] Yang Liu, Gerhard Knothe, Mingming Lu, "Direct transesterification of spent coffee grounds for biodiesel production," *Journal of Fuel*, vol. 199, pp. 157-161, 2017
- [4] Amanda Laca, Adriana Laca, Mario Diaz, "Eggshell waste as catalyst: A review," *Journal of Environmental Management*, *Journal of Environment Management*, vol. 197, pp. 351-359, 2017
- [5] T. Singhasiri & N. Tantemsapya, "The utilization of waste egg and cockle shell as catalysts for biodiesel production from food processing waste oil using stirring and ultrasonic agitation," *Energy sources, part a: recovery, utilization, and environmental effects*, vol. 38, pp. 3125–3131, 2016
- [6] M.P. Sharma, "Review of process parameters for biodiesel production from different feedstocks," *Journal of Renewable and Sustainable Energy Reviews*, vol. 62, pp. 1063–1071, 2016
- [7] S. Niju, K.M. Meera, S. Begum, N. Anantharaman, "Enhancement of biodiesel synthesis over highly active CaO derived from natural white bivalve clam shell," *Arabian Journal of Chemistry*, vol. 9, pp. 633-639, 2016
- [8] S. Niju, K.M. Meera, S. Begum, N. Anantharaman, "Modification of egg shell and its application in biodiesel production," *Journal of Saudi Chemical Society*, vol. 18, pp. 702–706, 2014
- [9] Buasri, A., Chaiyut, N., Loryuenyong, V., Wongweang, C. and Khamsrisuk, C., "Application of Eggshell Wastes as a Heterogeneous Catalyst for Biodiesel Production," *Journal of Sustainable Energy*, vol. 1, pp. 7-13, 2013
- [10] R.Rezaei, M.Mohadesi, G.R.Moradi, "Optimisation of biodiesel production using mussel shell catalyst," *Energy sources, part a: recovery, utilization, and environmental effects*, vol. 40, pp. 3125–3142, 2013
- [11] N. Viriya-empikul, P. Krasae, B. Puttasawat, B. Yoosuk, K. Faungnawakij, "Waste shells of mollusk and egg as biodiesel production catalysts," *Journal of Bioresource Technology*, vol. 101, pp. 3765-3767, 2010

LANDFILL SITE SELECTION USING GIS AND LANDFILL DESIGN IN TRIVANDRUM DISTRICT

ARATHY NAIR GR, LAKSHMI R VASANTH, NAMRATHA LEKSHMI AJ, SILPA B SANTHOSH

Eighth Semester Civil Engineering Students, LBS Institute of Technology for Women, Poojapura

MINI. M*, ANOJA B V*

**Asst. Professor in Civil Engineering, LBS Institute of Technology for Women*

ABSTRACT:

One of the serious and growing potential problems in Trivandrum is the shortage of lands for waste disposal. An inappropriate landfill site may have negative environmental, economic and ecological impact. Therefore it should be selected carefully by considering both regulations and constraints on the sources. Many criteria like distance from the residential areas, presence of water bodies etc...are taken into consideration while planning for suitable sites. Spatial Analyst Tool like GIS [Geographic Information System] along with AHP [Analytic Hierarchy Process] model is extremely useful in such multi-criteria decision making process.

Keywords: Trivandrum, Landfill site, GIS, AHP.

1. INTRODUCTION

Source reduction, recycling and waste transformation methods are widely used to manage solid waste, however in all of these methods, there is always residual matter even after the recovery process to disposal. The necessity of getting rid of these wastes yields in an economic approach which is called as Land filling.

However, municipal landfill siting is becoming increasingly difficult due to growing environmental awareness, decreased government and municipal funding and extreme political and social opposition. The increasing population densities, public health concerns, and less land available for landfill constructions are also the difficulties to overcome.

Landfill siting is an extremely difficult task to accomplish because the site selection process depends on different factors and regulations. Environmental factors are very important because the landfill may affect the surrounding biophysical environment and the ecology of the area.

Economic factors must be considered in the siting of landfills as well. Economic factors of landfill siting often include the costs associated with acquisition, development, and operation of each site. These costs must be weighed against the amount of capital investment put into the landfill; otherwise the development will not be successful. Social and political opposition to landfill siting has been indicated as the greatest obstacle for successfully locating waste disposal facilities.

It is evident that, many factors must be incorporated into landfill siting decisions and GIS is ideal for this kind of preliminary studies due to its ability to manage large volumes of spatial data from a variety of sources. It efficiently stores, retrieves, analyzes and displays information according to user defined specifications.

Trivandrum is facing a serious problem of solid waste management and its effective disposal. It is the densest district in Kerala with 1,509 inhabitants per square km. It is divided into six taluks: Thiruvananthapuram, Chirayinkeezh, Neyyattinkara, Nedumazhadu, Varkala

and Kattakada. Thiruvananthapuram district is situated between north latitudes 8°17' and 8°54' and east longitudes 76°41' and 77°17'.The district has 3 major rivers, freshwater lakes and more than 300 ponds. Trivandrum district has a reserve forest area of 495.1 square km.About 55% of population resides in urban areas.According to the census of 2011, the Thiruvananthapuram corporation generates about 240 tons per day.

2. SOLID WASTE MANAGEMENT

Solid waste management may be defined as the discipline associated with the control of generation, storage, collection, transfer and transport, processing and disposal of solid wastes. Integrated solid waste management includes theselection and application of suitable techniques, technologies and management programs to achieve specific waste managementobjectives and goals.

Current solid waste management technologies can be summarized as:

- 1) Source reduction
- 2) Recycling
- 3) Waste transformation
- 4) Land filling

2.1 Land filling

It is the process by which the solid wastes that cannot be recycled nor further used; the residual matter remaining after the recovery facility and after therecovery of conversion products and energy is placed in a landfill. Although there is a public opposition to landfills, it is necessary and there is no combination of waste management technique that does not require land filling to make them work. Land filling includes monitoring of the incoming waste stream, placement and environmental the compaction monitoring and of waste, control and facilities.

In the past, the term sanitary landfill is used to describe a landfill in which the waste placed in the landfill was covered at the end of each day. Today, sanitary landfill refers to an engineered facility for

the municipal solid waste designed and operated to minimize public health and environmental impacts

Table 1: Advantages and Disadvantages of Landfill (source: Thesis, Basak Sener)

Advantages	Disadvantages
Independence from other facilities.	Land Depreciation.
Post-closure land development(eg:parks)	Wind borne paper, plastics etc...
Tipping fees from imported wastes.	Imported waste reducing landfill lifespan.
Local employment opportunities.	Public/political opposition.
Potential tax from landfill.	Traffic of large vehicles.
Disposal strategy upto 30 years.	Erosion of waste and/or soil cover.

3. LANDFILL SITE SELECTION

The major goal of the landfill site selection process is to ensure that the disposal facility is located at the best location possible with little negative impact to the environment or to the population. For a sanitary landfill siting, a substantial evaluation process is needed to identify the best available disposal location which meets the requirements of government regulations and best minimizes economic, environmental, health, and social costs. Evaluation processes or methodologies are structured to make the best use of available information and to ensure that the results obtained are reproducible so that outcomes can be verified and defended.

Geographic Information Systems (GIS) are ideal for preliminary site selection studies because it can manage large volumes of spatially distributed data from a variety of sources and efficiently store, retrieve, analyze and display information. Using GIS for site selection not only increases the objectivity and flexibility but also ensures that a large amount of spatial data can be processed in a short time.

Relatively easy presentations of GIS siting results are also one of the advantages.

3.1 Criteria for Landfill Siting

There are a number of criteria for landfill site selection. These are environmental criteria, political criteria, financial and economical criteria, hydrologic and hydro geologic criteria, topographical criteria, geological criteria, availability of construction material and other criteria. The Highways and surface waters should be 200m away from such a site.

4. GIS PHASE

4.1 Map Collection

The Base map of Trivandrum district is collected.

4.2 Analysis by GIS Software

Fig1: Digitized map of study area

Collected maps are georeferenced, digitized and analyzed so as to obtain the suitable candidate sites, as per the criteria given. Here the QGIS Software is used for the aforementioned purpose.

4.2.1 QGIS Software

QGIS (previously known as Quantum GIS) is a free and open-source cross platform desktop Geographic Information System (GIS) application that supports viewing, editing and analysis of geospatial data.



Fig2: Buffer map of study area



5. ENVIRONMENTAL PHASE

5.1 DESIGN PHASE

The following tests are to be carried out to determine the suitability of the candidate sites. Permeability tests, Causes of potential slope failure and probable settlement, Determination of Water table level.

5.2 LANDFILL DESIGN

The site selection of a landfill site depends on the design of a landfill. There are two major types of landfill design: (1) Sanitary landfills (2) Natural attenuation landfills. The main difference between these two types is the control of the entrapment and release of the leachate generated by a landfill. A sanitary landfill uses artificial liners to control the release of leachate while a natural attenuation landfill utilizes the surrounding environmental characteristics in order to decompose released fluids.

5.2.1 Sanitary Landfills

Sanitary landfills are designed to protect humans and the environment from harmful gases and fluids by using methane collection vents and leachate liners and collection pipes. Many landfills are designed for 20 or 30 year lifespan and still require post closure monitoring up to 30 years to ensure the environmental health. The landfill is usually double-lined to trap leachate. Synthetic liners include plastic geomembranes, geomats, geogrids, and geotextiles that commonly contain bentonite clays. In a sanitary landfill, waste is contained in a cell which is covered with a layer of soil and compacted at the end of each working day. The dimensions of the cell depend on the volume of waste received and the availability of cover material. The cell thickness may range from 8 to 30 ft (2.4 – 9.1 m) but typically it is 15 ft (4.6m). The usual slope of the working face is 3horizontal to 1 vertical (3:1) which allows reasonable compaction and easier capping and vegetative growth on the side slopes of the landfill. The width of the working face is usually limited to 2 ft (0.6 m). The first lift of the waste is usually 5 ft (1.5 m) or less with careful removal of the oversize pieces to prevent damage of the underlying leachate collection system. The compaction equipment moves from the bottom to the top of the working face. The thickness of the daily cover is 6-12 in (150- 300 mm). If a lift surface is expected to be exposed over 30 days then an intermediate cover is applied. The intermediate cover is typically 1 ft thick and more resistant to erosion than the daily cover.

5.2.2 Natural Attenuation Landfills

A natural attenuation landfill which allows the liquid wastes to migrate from the landfill uses the natural geological and hydro geological characteristics of the subsurface. It takes the advantage of the natural subsurface processes of biodegradation, filtration, sorption, and ion exchange which help the purification of the groundwater. The other advantages of using natural insitu geological and hydro geological barriers are that natural barriers do not encapsulate waste and inhibit its degradation, and the natural infiltration and percolation characteristics of the subsurface are not disrupted. In addition, this method has relatively minor cost of construction, operation and maintenance compared to the sanitary landfills. Attenuation landfills are based on the dilute and disperse principle of leachate management. Natural low permeability and attenuation characteristics of geological barriers in the subsurface, especially low permeability clay rich overburden and to a lesser extent consolidated mudrocks are preferable for this method to prevent groundwater pollution.

6. RESULTS AND DISCUSSIONS

Site obtained near Neyyattinkara ,Kottamam ward. Preliminary site investigations were carried out.

Soil : Laterite.

Reconnaissance was carried out. Water table depth (measured from near by well) : 18 m.

REFERENCES:

[1] Basak Sener (2004) "Landfill Site Selection Using GIS", Graduate School of Natural and Applied Sciences of Middle East Technical University.

[2] Nadali Alavi, Zeinab Ghaed Rahmat and Mehdi Vosoughi Niri (2016),"LANDFILL SITE SELECTION USING GIS AND AHP", KSCE Journal of Civil Engineering.

Influence of Nano-Silica on Unconfined Compressive Strength of Marine Clay with Curing Time

Joju M R¹ and Dr S Chandrakaran²

1. Joju M R, PG Student, Department of Civil Engineering, National Institute of Technology Calicut, Kerala-673601. Email: jojumariyam@gmail.com
2. Dr. S Chandrakaran, Professor, Department of Civil Engineering, National Institute of Technology Calicut, Kerala-673601. Email: chandra@nitc.ac.in

Abstract. This paper presents the influence of nano-silica on unconfined compressive strength of soft marine clay with curing time. Soft marine clay is highly problematic regarding to engineering projects due to high compressibility, low shear strength and low permeability. Marine clay used for the study was collected from Vypin Island, Cochin. Nanoparticles are one of the recent materials that can be used in soil stabilization. Drastic growths have been taken in the field of nanotechnology, and much nanotechnology-based advancement has been made in geotechnical engineering. Nano-silica possess higher surface area to volume, this enhances cation exchange capacity and reaction with particles of clay. Nano-silica contents varied from 0.5% to 1%. The unconfined compressive strength of treated soil increased with curing time. Curing time taken for the study of variation in UCS were 3, 7, 14, 28 days. Nano-silica gel increased the cohesion between particles there by improvement of unconfined compressive strength. Minute quantity is just sufficient for noticeable changes in properties of soil in the case of nano-silica particles. Nano-silica as recent chemical additive also showed a rapid development in engineering properties of marine clay. So the modifications by chemical additive in marine clay had shown better improvement in UCS of soil.

Keywords: Marine clay, Nanotechnology, Nano-silica, Unconfined Compressive Strength

Introduction

Marine clays are highly compressible fine grained soils. Higher compressibility and lower shear strength are the main engineering problems related to this soil. So modification of properties of soil is necessary for improving the engineering behaviour. Modifications of engineering properties are done by stabilisation technique by different methods.

Cochin marine clay from Vypin Island was taken for study. Cochin industrial capital of Kerala, which is under going rapid industrialization, consists of extremely soft marine clay poses serious problem in the geotechnical engineering practices. Mainly this effect can be observed in the foundation related issues while construction of structures, Bridges, Highways and Dams. Various stabilisation techniques are using to overcome this serious issue regarding engineering practices.

As per researches liquidity index is as high as 0.87, and marine clays are moderately active clays. The compression indices of clay are high for undisturbed samples and are higher than those obtained for remoulded samples. Also shear strength of clay is much lower. [Babu et.al.1988]. Various stabilising agents such as lime, flyash, cement etc... are using for enhancement of properties of marine clay. Nanomaterials are recent in the ground improvement field of geotechnical engineering.

The idea of nanotechnology was first introduced by Richard Feynman in his lecture entitled "There's Plenty of Room at the Bottom" in 1959. Numerous studies have been conducted regarding use of nano particles for improvement of soil strength parameters [Kadaver et.al.2011]. Recently nano-silica, because of its suitable performance compared with micro-silica, has frequently been used in soil improvement projects.

A series of tests on clayey soils by adding nano-silica and found that the addition of nano-silica leads to a reduction in the swelling index of clay. Addition of nano-silica increases the shear strength and Atterberg limits of clay and decreases its permeability [Pham et.al. 2014]. Increase in nano-silica content improved the unconfined compressive strength and elastic modulus of soft clay [Changizi et.al. 2015]. Nano-silica develops a stronger connection by viscous gel leading to an increase in frictional strength and also reduces the distance between clay particles. This improves the shear strength of soft clay [Garcia et.al. 2017].

Moreover, research on pozzolanic activity of silica nanoparticles indicated a high pozzolanic activity of nano-silica compared to micro silica, flyash. Since silica nanoparticles act as an accelerator, structure of cementitious materials becomes denser and more uniform even in a short time of curing [Changizi .et. al. 2017].

This paper evaluates the improvement of unconfined compressive strength (UCS) by nano-silica addition in marine clay with curing time. Study on the effect of nano-silica on marine clay was not performed. Effect of nano-material will change according to the behaviour of clay. The unconfined compressive strength of clay samples was improved with curing time by the increase in nano-silica content.

Materials Used

The main additives used for stabilization of marine clay from Cochin are nano-silica. Marine clay was sampled from Vypin, Ernakulum. Table 1 shows the properties of marine clay. Nano – Silica was obtained from ASTRA chemicals, Chennai. Table 2 shows the chemical composition of nano-silica.

Table 1. Properties of soil sample

Properties	Marine clay
Specific Gravity	2.65
Liquid limit	80%
Plastic limit	34%
Shrinkage limit	14%
Free swell	50%
Clay fraction	49.25%
Soil classification	CH
OMC	32.37%
Dry density	1.42g/cc
UCC	97.07 kPa

Table 2. Chemical Composition of nano-silica

Constituent	%
Silicon dioxide	99.7
Titanium	0.012
Calcium	0.007
Sodium	0.005
Iron	0.002

Methodology

To evaluate the effect of nano-silica on strength of soft clay sample, two groups of specimens need to be taken. One group of natural specimen, next group of three set of specimens stabilised with nano-silica. UCS are tested to find the variation in properties of soil. Soil sample was air dried for a week, pulverized manually using weights, sieved through 425 micron sieve and preserved in large containers in an enclosed room. Soil specimens were mixed with nano-silica in the ranges 0.5%, 0.8%, 1% cured up to four weeks in air-tight bags. A series of unconfined compressive strength tests were conducted on clay treated with different contents of nano-silica. The Optimum nano-silica Content was determined from the test results. The reason for the maximum limit of 1% of nano-silica is due to the fact that tests were performed under constant moisture content and due to the absorption of water by nano-silica, mixing of soil with more than 1% nano-silica content led to a lack of water in the soil /nan-silica mixture; this will results in the bad workability of amended clay [Changizi et al. 2017].

Results & Discussions

Unconfined Compressive Strength of Natural Marine Clay

The results of unconfined compression test of marine clay sample are shown in Figure 1. Three trials are performed to find out the UCS of clay sample. The peak value obtained for the natural clay is 97.07kPa and cohesion is 48.2kPa. Marine clay sample belongs to the medium strength class based on UCS.

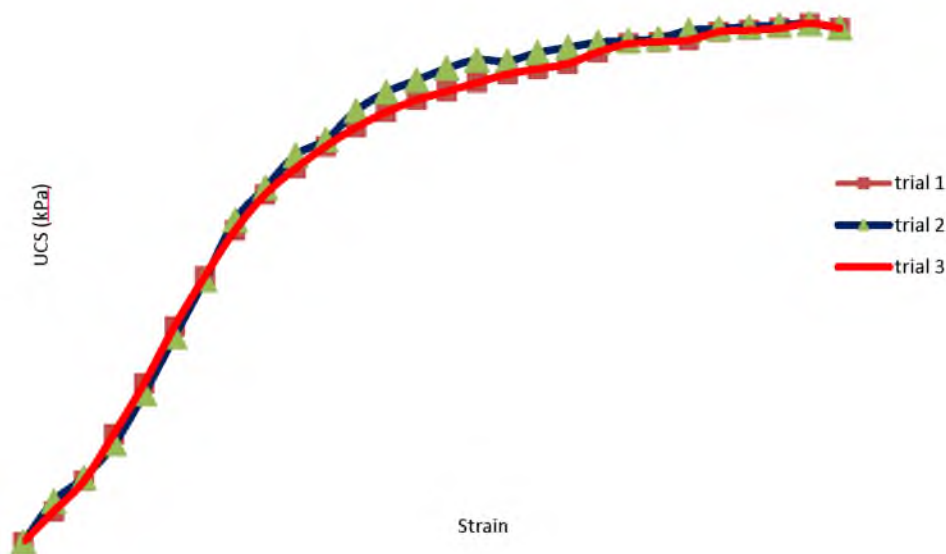


Fig.1. Unconfined Compressive Strength of natural sample.

From the figure 1it can be inferred that the peak increase in resistance is obtained after a drastic strain increase in soil sample. From the three trials nearly equal strain was observed. Medium consistency of clay and high compressibility of clay can be found out from the UCS test of natural sample.

Variation in Unconfined Compressive Strength of 0.5% Nano-Silica Amended Marine Clay

The results of unconfined compression test of marine clay stabilized with 0.5% nano-silica are shown in Figure 2. The peak value of UCS increases with increase in curing time. At the end of 14, 28 days peak resistance of stress-strain curve had shown closeness in strength. Addition of nano-silica improved strength compared to the natural marine clay sample.

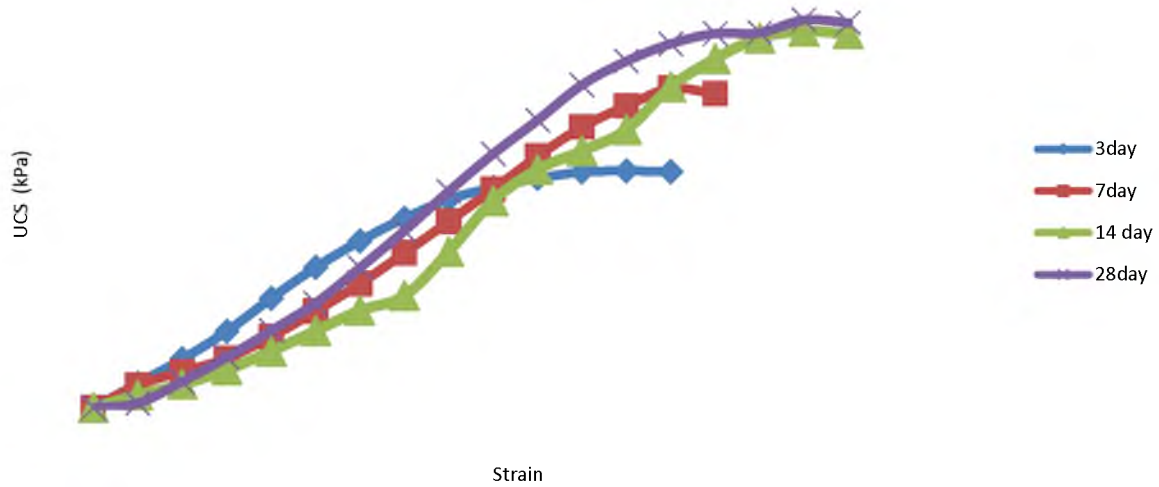


Fig.2. Unconfined Compressive Strength of 0.5% nano-silica amended clay

Variation in Unconfined Compressive Strength of 0.8% Nano-Silica Amended Marine Clay

The results of unconfined compression test of marine clay stabilized with 0.8% nano-silica are shown in Figure 3.

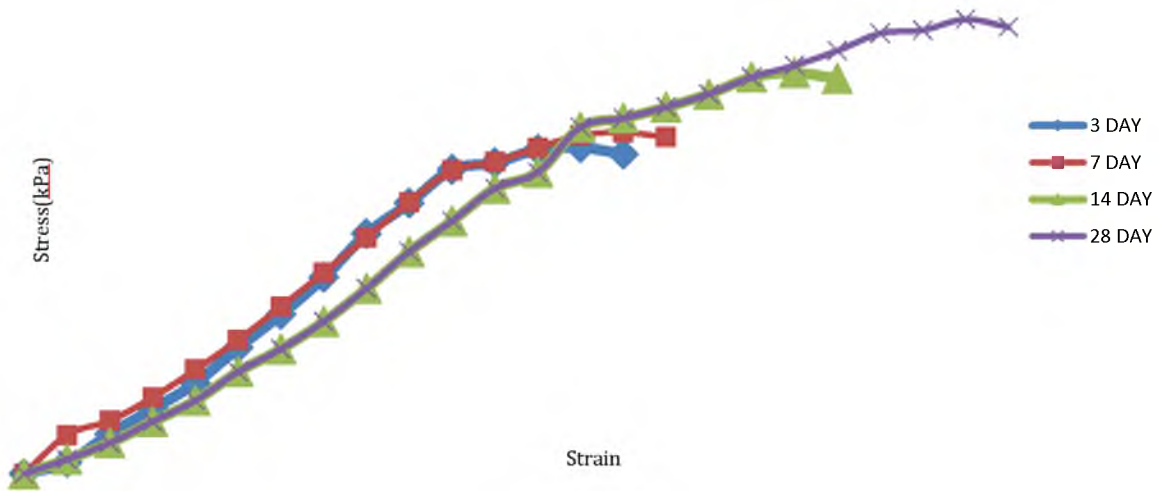


Fig.3. Unconfined Compressive Strength of 0.8% nano-silica amended clay

The figure 3 indicates that increase in nano-silica content improved the UCS characteristics of nano-silica amended clay. 0.8% nano-silica amended clay improved UCS better than 0.5% nano-silica amended clay. At the end of 28days UCS attained peak strength of 300kPa.

Variation in Unconfined Compressive Strength of 1% Nano-Silica Amended Marine Clay

The figure 4 presented the variation of UCS of 1% nano-silica amended clay with curing time. The peak value of UCS exhibited an increasing trend with curing time. But the 0.8% and 1% showed nearly equal peak value of resistance. 1% nano-silica amended clay had shown a peak resistance of 305kPa. While considering the cost of stabilization 0.8% nano-silica content can be taken as optimum content.

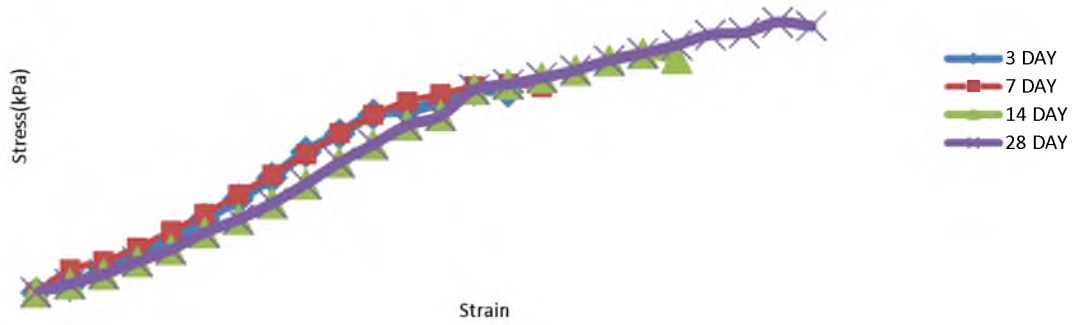


Fig.4. Unconfined Compressive Strength of 1% nano-silica amended clay

The results of unconfined compression test of marine clay stabilized with 0.5%, 0.8% & 1% nano-silica are depicted in Figure 5. The peak value of UCS increases with increase in curing time for all percentages of nano-silica content.

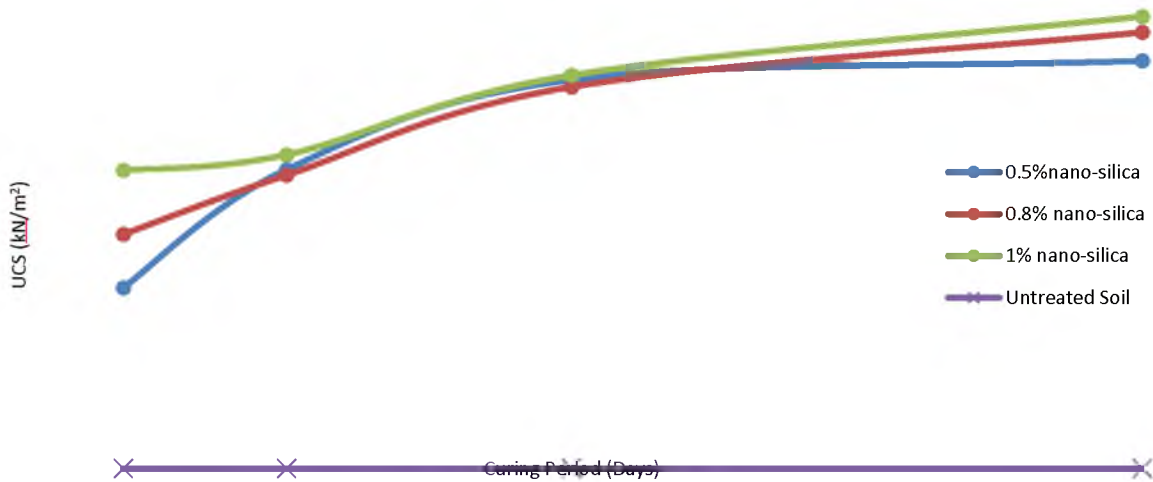


Fig.5. Variation of UCS for nano-silica amended clay

Table 3. UCS variation of nano-silica amended clay with curing time

Curing Time (Days)	Untreated Soil	0.5% nano-silica	0.8% nano-silica	1% nano-silica
3	97.07	176.80	216.03	228.51
7	97.07	228.83	226.38	235.37
14	97.07	268.45	265.32	270.45
28	97.07	276.81	300.87	305.74

The microstructural evaluation of the stabilized clay with nano-silica (Changizi et.al.2017) indicated that the nano-silica covers the clay particle surfaces, the interlock force between soil particle increases. The pores between clay particles are filled with the nano-silica viscous gel. The cohesion between clay particles due to the viscous gel is stronger than the cohesion between particles of clay due to absorbed water. Viscous gel leads to an increase in the frictional strength between the clay particles. The peak UCS resistance changed with curing time. So, the variation of unconfined compressive strength depends on the curing period. Due to large surface area for nano-silica, it is highly reactive, and this is suitable in improving the properties of soil. This leads to an increase in strength of soil.

Conclusion

The peak UCS of natural clay enhanced from 97kPa to 300kPa for 0.8% nano-silica and for 0.1% nano-silica increased to 305kPa. Strength variation shown more proximity for these contents. The variation of UCS for 0.8% & 1% are close enough. From the economic point of view 0.8% can be considered as optimum content. The improvement of strength at 28 days for 0.8% nano-silica amended clay was more than 210% than natural clay. Short term strength for the amended clay was also noticeable. Specimens treated with nano-silica shown brittle behaviour. Compared with the strain rate of natural clay, after the addition of nano-silica the strain rate was decreased. Amended clay shown increase in UCS at lower strain levels compared to natural clay.

References

- Babu T Jose, A Sreedharan, BennyMA : "A Study of Geotechnical Properties of Cochin Marine Clays", *Marine Geotechnology* Vol 7, pp 189-209 (1988)
- Marzieh Kadivar, Kazem Barkhordari, Mehdi Kadivar : "Nanotechnology in geotechnical engineering", *Advanced Materials Research* Vols. 261-263, pp 524-528 (2011)
- Pham Hand Nguyen QP : "Effect of silica nanoparticles on clay swelling and aqueous stability of nanoparticle dispersions", *Journal of Nanoparticle Research* Vols. 8, pp 224-256 (2014)
- Foad Changizi, Abdolhosein Haddad : "Strength properties of soft clay treated with mixture of nano-SiO₂ and recycled polyester fiber", *Journal of Rock Mechanics and Geotechnical Engineering*, pp 367-378 (2015)
- Foad Changizi, Abdolhosein Haddad : "Improving the geotechnical properties of soft clay with nano-silica particles", *Proceedings of the Institution of Civil Engineers Ground Improvement* Vols. 170, pp 62-71 ICE, Iran (2017)
- Silvia Garcia & Paulina Trejo, "Influence of Nanosilica on compressive strength of lacustrine soft clays", *Proceedings of the 19th International Conference on Soil Mechanics and Geotechnical Engineering*, pp 56-65 Research Gate, Seoul (2017)

Effect of Enzymatic Lime on Properties of Clay

Dani Jose¹ and Dr. S. Chandrakaran²

¹PG Student, Department of Civil Engineering, National Institute of Technology Calicut, Kerala 673601

²Professor, Department of Civil Engineering, National Institute of Technology Calicut, Kerala 673601 chandra@nitc.ac.in

Abstract. Traditional stabilizers like lime, cement, fly ash, rice husk ash, and combinations of these have been widely used to improve the properties of problematic soil. Considering the environmental impacts of these stabilizers, researchers come up with an ecofriendly method called enzymatic stabilization. Recently combination of enzyme and lime known as enzymatic lime found to be effective in improvement of strength of soft soils. In the present work, the effect of enzymatic lime on engineering behaviour of clay is analysed. The purpose of this research is to verify the efficacy of enzymatic lime in soft clays. An extensive study was carried out on a soil sample using different dosages lime, enzyme and combination of lime and enzyme. The variation in liquid limit, plastic limit, plasticity index and unconfined compressive strength were investigated after 3, 7, 14 and 28 days of curing. The optimum dosage of the stabilizers was inferred from obtained results. Addition of 120ml/m³ of enzyme and 2 %lime by weight of soil will impart significant improvement of properties. Sufficient improvement of strength obtained after 14 days of curing indicates accelerated strength improvement by enzymatic lime. Utilization of enzyme and lime in combination can reduce the percentage of lime for soil treatment making the proposed method environmental-friendly.

Key words: Lime, enzyme, enzymatic lime, strength improvement

1. Introduction

Soil stabilization aims the enhancement of the strength and durability of problematic soil by controlled compaction or by the addition of admixtures and stabilizers. Stabilization may result in increased stability, shearing resistance and bearing capacity, reduced volume changes and settlement and control of the undesirable effects associated with clay. This method is widely applied in the field of construction of roads and pavements. Several techniques have been adopted for the improvement of engineering properties of soils. These methods include incorporation of lime, cement, flyash, rice husk ash, crumb rubber, bioenzyme, geosynthetics, biopolymer and different commercial available chemicals for stabilization. Among these techniques, lime stabilization is a cost effective and commonly used method of soil improvement.

The success of lime stabilization leads to utilization of various additives along with soil-lime tried over the past few decades. The effect of climatic change, environmental concerns and increase in cost of materials necessitates an innovative ecofriendly method over these traditional methods. An economically feasible solution for overcoming this problem is the introduction of enzymatic soil stabilization.

Enzymes are biological catalyst obtained from plants and animals including microorganisms by extraction using suitable solvent. These are large protein molecules which are more efficient than inorganic catalyst. Enzyme can increase the reaction rate by a factor of 10⁶ to 10¹². They usually catalyze unique reactions therefore enzymes do not produce side reaction. Enzymes are temperature sensitive and work around temperature (35° C) and lose their effectiveness at higher temperature. Also, they are pH sensitive too and work good at pH value 7 [1].

Bio-Enzyme is a naturally obtained, nontoxic, nonflammable, noncorrosive liquid enzyme formulation fermented from vegetable extracts. They catalyze the reactions between the clay and the organic cations by accelerating the cationic exchange. Enzyme provides higher soil compaction densities and enhances strength and stability of the soil [2]. Utilization of Bio Enzyme in combination with lime will also give enhanced improvement in strength. The catalytic action of enzymes in the presence of lime brought a significant improvement of strength [3]. The enzymatic lime is more effective in soil samples with higher clay fraction [4].

A very few researches have been conducted using enzymatic lime and scope of detailed study on its influence on soil properties is there. In the present work the variation of properties of a natural soil with the addition of enzymatic lime is studied in detail.

2. Materials Used and Methodology

Soil used for the present study is collected from Vytilla, Ernakulam. The bio-enzyme using is an extract from sugar molasses, and was obtained from Avijeet Agencies in Chennai, Tamil Nadu under the chemical name TerraZyme. Lime used for the study is purchased from local agent at Kunnamanglam, Calicut. The properties of soil and enzyme are given in Table 1 and 2.

The collected soil is highly plastic and of medium consistency in nature. From UCS it's found that the soil has got medium strength and so the strength can be improved. according to IS Classification the soil is highly compressible clay.

All specimens using in this study were prepared and tested using standard procedures described by the Bureau of Indian Standards. Soil sample used for the test was air dried, pulverized manually, sieved through 425micron sieve and preserved in large containers. TerraZyme was preserved in an airtight bottle in its original liquid form. Lime was sieved using a 425micron sieve and preserved in an airtight container

Table 1. Properties of soil

Properties	Obtained Values
Specific gravity	2.62
Liquid Limit (LL)	76 %
Plastic Limit (PL)	30 %
Shrinkage Limit	13 %
Plasticity Index (PI)	46%
Free Swell	14.3 %
pH	7.74
Bulk Density (kN/m ³)	17.82
Max. Dry Density (kN/m ³)	13.86
Optimum Moisture Content (%)	27
Unconfined compressive strength (kN/m ²)	106.61
Cohesion (kN/m ²)	53.31
Clay Fraction	38.76 %
Silt	34.52 %
Sand	26.72%
Soil Classification	CH

Table 2. Properties of Enzyme[3]

Properties	Obtained Values
Boiling point	100°C
pH	2.8-3.5
Vapour pressure: mmHg	As water
Melting point	Liquid
Vapour density (air=1)	1
Solubility in water	Infinite
Evaporation rate	As water
Appearance and odour	Light gold liquid, characteristic odour
Production	Extracted from sugar molasses
Major constituents	Rhodasurf B1, Calcium Chloride

Literature reveals that the optimum lime content for soil stabilization varies from 2% to 6% by weight whereas higher percentage may require for soil having higher clay fraction. The range of dosage of lime to be used was determined from Liquid limit tests. Then, the soil is treated with 2%- 3.5% lime content and unconfined compressive strength tests were conducted to verify and confirm the actual optimum lime content. 3 samples of the same mix type were tested after 3,7,14,21,28 days and the average of the values were recorded.

A dilution ratio chart provided by manufacturer (that calculated the required dosage of TerraZyme for a soil based on particle size and plasticity index) is used to determine the range of optimum Enzyme content. Soil samples were mixed with Terra Zyme dosages between 110 ml/m³ to 130 ml/m³, cured up to four weeks in air-tight bags. The

same tests were repeated on the samples and the variation in properties were studied. From the results the actual optimum enzyme content is determined.

The dosage of enzyme is fixed at optimum enzyme dosage and the lime content is varied. The combinations involve 1.5%, 2%, 2.5% of lime with 120ml/m³ of enzyme. The variation of properties on the soil lime enzyme system is studied for 3,7,14 and 28 days. From the obtained results the optimum enzymatic lime content is fixed.

3. Results and Discussions

Based on the values of tested parameters the optimum dosage of additives was fixed. Addition of 3 % lime impart maximum improvement in strength as well as reduction in plasticity. So, the optimum dosage of lime is fixed as 3% by weight of soil. The optimum dosage of enzyme was found as 120 ml/m³ based on the analysis of results. It was observed that addition of 2% of lime with 120ml/m³of enzyme will impart maximum improvement of properties. So, the optimum enzyme and lime content for enzymatic lime treatment is found as 120 ml/m³ of enzyme and 2% of lime. The results obtained when soil is treated with enzymatic lime is given in Table 3.

Table 3. Properties of Enzymatic lime treated soil after 28 days

	LL %	PL %	PI %	UCS (kN/m ²)
Untreated	76	30	45	106.61
120ml/m ³ Enzyme + 1.5 % lime	61	40	21	293.11
120ml/m ³ Enzyme + 2 % lime	57	43	14	397.20
120ml/m ³ Enzyme + 2.5 % lime	60	41	19	330.56

From the results it was found that the addition of enzymatic lime to soil will improve the strength and plasticity of soil. The performance both chemicals in combination was more successful than the individual performance. Utilization of enzyme and lime in combination can improve the strength of virgin soil substantially. Figure 1, 2, 3 shows the variation of Atterberg limits with the addition of enzymatic lime.

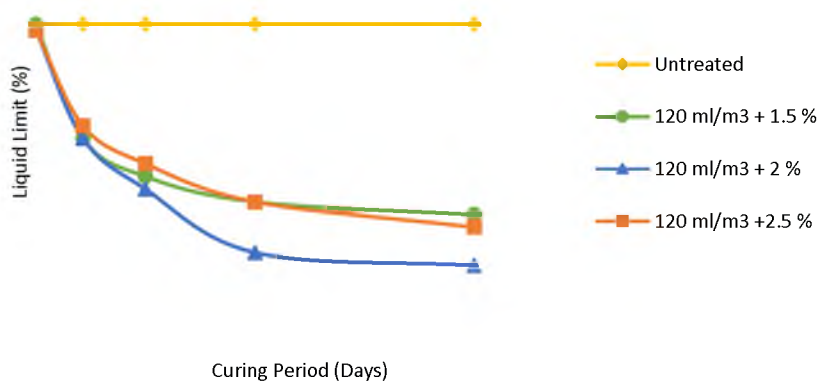


Fig.1. Variation of liquid limit of soil treated with varying percentages of enzymatic lime

By the addition of optimum dosage of enzymatic lime, the liquid limit of the soil is reduced to 57 while the plastic limit of soil has got increased to 43. The plasticity of soil is reduced to 14. The plasticity of soil is reducing with increased curing period. Enzyme acts as catalyst for the soil lime reaction and increased cation exchange will take place between clay and lime. The accelerated cation exchange imparts significant reduction of diffused double layer thickness and thus reduces the liquid limit of soil.

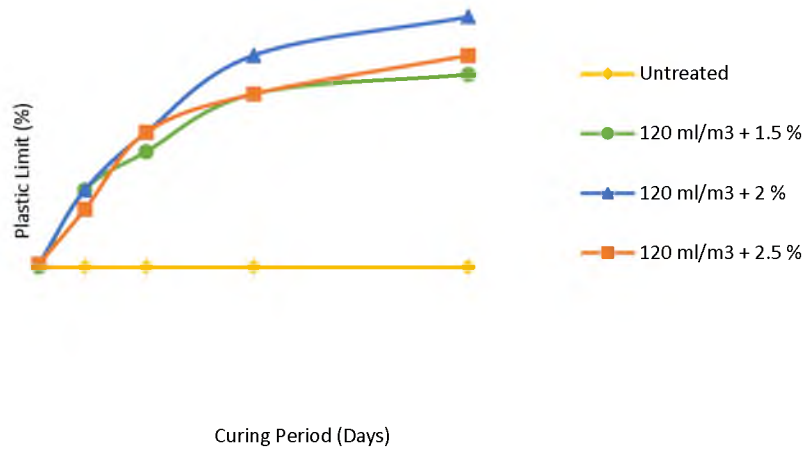


Fig.2. Variation of plastic limit of soil treated with varying percentages of enzymatic lime

The plastic limit shows an increasing trend which may be due to the reduction in thickness of diffused double layer. Decrease in the liquid limit and increase in the plastic limit leads to an overall reduction of plasticity index. Addition of enzymatic lime reduces the plasticity of the soil and sufficient curing causes significant reduction in properties too.

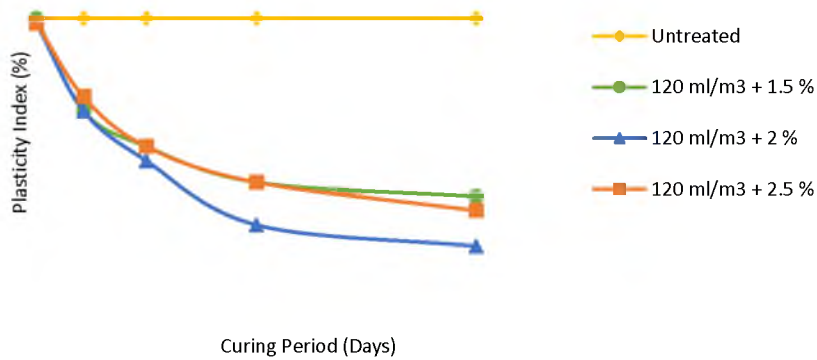


Fig.3. Variation of plasticity index of soil treated with varying percentages of enzymatic lime

From the observed data it's found that the improvement in properties of soil after 14 days of curing is significant when comparing with the untreated soil. Also, not much improvement in properties were obtained after 14 days of curing. The graph become flattened after 14 days indicates that curing after 14 days will not impart much improvement in properties. Thus, the study reveals the potential of enzymatic lime for accelerated improvement in index properties.

Figure 4 shows the variation of UCS with the addition of enzymatic lime to the untreated soil. The strength was increased to 367.9 kN/m² and 397.2 kN/m² after a curing period of 14 days and 28 days. An improvement 3.45 % was obtained after 14 days and 3.7 % increase after 28 days. The addition of 120 ml/m³ enzyme and 2% lime give maximum strength improvement after 28 days, which is considered as the optimum enzymatic lime concentration.

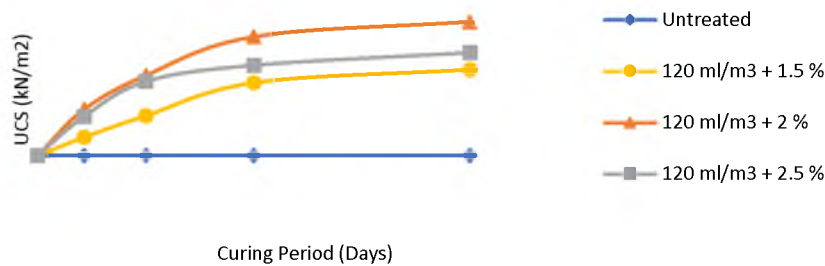


Fig.4. Variation of UCS of soil treated with varying percentages of enzymatic lime

No significant strength improvement is obtained after 14 days indicating that 2 weeks of curing is sufficient for the treatment. The enzyme catalyzes the reaction between lime and soil and this imparts an accelerated improvement in strength after 14 days. With the addition of enzyme and lime to the soil, the enzyme will modify the clay and this modified clay is reacting with the lime [5]. In addition, lime reacts with the calcium aluminate and the calcium alumina silicate by replacing the existing aluminium cations with the calcium cations in the presence of enzyme (Rhodasurf $-R(OC_2H_4)_nOH$) and form compounds which can impart high strength to soil [4].

4. Results and Discussions

Lime is commonly used for stabilization of soft soils. Utilization of enzyme and lime in combination also found to be very effective in soil treatment. By addition of enzymatic lime to soil both strength and plasticity characteristics has been improved. The liquid limit of the soil is reduced by 25% while the plastic limit of soil has got an increase of 40%. The plasticity of soil is reduced to 67% of original value. The enzyme acts as a catalyst for lime soil reaction and enhances the properties. The results show that by addition of 2% lime and 120 ml/m³ of enzyme will improve the strength within 1 week itself by a substantial amount. After 14 days the soil attained 3.4 times the initial strength and almost 90% of the strength was attained by 14 days of curing. The enzyme catalyzes the reaction between lime and soil and this imparts an accelerated improvement in strength. The lime content in optimum concentration of enzymatic lime is less than optimum lime content. This is a significant result because the reduction in lime content can reduce the impact of lime to the environment. Thus, the obtained results show that the enzyme used with lime will improve the properties as well as we can reduce the lime content and curing period making the method more economical as well as ecofriendly. The technique of addition of enzymatic lime into the soil is an innovative technique that promises to impart better and quicker stabilization according to the laboratory studies conducted in this work.

References

1. Norris R., Ryan L., Acaster D, Cambridge International AS and A Level Chemistry Coursebook. Cambridge University Press, UK, (2011).
2. Shankar A. U, Rai H. K, Mithanthaya. R., Bio-Enzyme stabilized Lateritic Soil as a Highway material, Indian Roads Congress Journal, Paper No: 553, (2009).
3. Greeshma Nizy Eujine, Dr S. Chandrakaran, Dr N. Sankar, The engineering behaviour of enzymatic lime stabilized soils, Ground Improvement, Proceedings of the Institution of Civil Engineers, Paper 1600014, 2017.
4. Greeshma Nizy Eujine, Dr S. Chandrakaran, Dr N. Sankar, Accelerated Subgrade Stabilization Using Enzymatic Lime Technique, Journal of Materials in Civil Engineering, American Society of Civil Engineers, Volume 29, Issue 9, Paper 04017085, 2017.
5. Marasteanu MO, Hozalski R, Clyne TR and Velasquez R, Preliminary Laboratory Investigation of Enzyme. Minnesota, Department of Transportation Research, Minneapolis, USA (2005).

SKIRTED STONE COLUMN WITH BAMBOO AND COIR IN KUTTANADU CLAY

S. J. Ganesh¹ and K. Balan²

¹ M. Tech. Student, Dept of Civil Engineering, Rajadhani Institute of Engineering and Technology

² Vice Principal, Rajadhani Institute of Engineering and Technology

Email : ganeshsidevika@gmail.com¹ , drkbalan@gmail.com²

Abstract. Stone column is a modern reinforcing method which is used in soft soils to support isolated footings, embankments and raft foundations. Introduction of stone column to the soft soil improves the load carrying capacity and reduces the settlement. Granular materials present in column will reduce the post consolidation settlement by improving consolidation settlement rate. During load application stone column bulges due to lateral thrust and is one of the main reasons for failure. Providing horizontal and vertical encasement to stone column is the best method to prevent lateral bulging. In this paper quarry waste is used as filling material, high stiffness bamboo strips as longitudinal reinforcement and low stiffness coir yarn as the lateral reinforcement. Strain controlled test was done to investigate the effect of spacing between longitudinal and lateral encasement in stone column. Exhumation technique was done to identify the bulging of column after load application. Test results show that longitudinal encasement with bamboo and lateral encasement with coir yarn increases the load carrying capacity of soft soil and reduces the lateral bulging.

Keywords: Stone column, Encasement, Bamboo

1. Introduction

The construction in soft clays always experiences several problems like excessive settlement and loss of global-local stability. For overcoming this the construction in soft clay was done after suitable ground improvement methods. Use of stone column as a technique of soil reinforcement is frequently implemented in soft soil. Stone columns are nothing but vertical columnar elements constructed below the ground level with compacted and uncemented stone fragments or gravels or sand. The construction of stone column increases the load bearing capacity accompanied by the significant reduction in settlement.

2. Literature review

During load application the stone column is subjected to significant vertical compression caused by the lateral bulging of aggregates. The granular materials present in the column penetrate into the soil and transfer the stress to soil [1, 2, 3]. The extra stress within the soft soil provides additional confinement to the column material. The total passive pressure developed on soft soil has a significant role in resisting the vertical loads acting over the columns [4]. Studies found that the lateral bulging of stone column will cause larger surface settlement and reduce load bearing capacity. The low confinement from the surrounding clay causes the deformation on stone column and reduces the efficiency of it [5, 9]. In such situations suitable methods want to be implemented to improve the column encasements.

Wrapping each stone column with encasements will improve the properties during load application. Geosynthetic encasement provides an additional confinement to the stone column [6, 7, 8]. The effective working of encasement depends upon the stiffness of the material used.

Placing horizontal reinforcement always reduces the lateral bulging and settlement during load application [3, 11]. There is also a significant role for the filling material in the performance of stone column. Using small sized stone filling material provides better load carrying capacity and drainage as compared to finer materials [3].

Literature reviewed shows that synthetic materials can be used as the reinforcing materials for the encasements of column. Limited work has been done in the field of horizontal reinforcement for the columns. This paper aims to

fill up this gap by studying the effect of high stiffness bamboo strips as longitudinal reinforcement and low stiffness coir yarn as the lateral reinforcement on single quarry waste column on bearing capacity improvement of soft clay.

3. Experimental programme

3.1 Material properties

Soft soil for the test was brought from the Kuttanadu region and its properties were determined and listed in Table 1. Quarry waste material passing through 4.75mm and retained on 425 μ was used as column filling material. Properties of quarry waste also determined and listed in Table 2. Air dried bamboo strips of 200mm long and 11mm width was cut from bamboo trees and used as encasement material which were placed at longitudinal spacing of 7.95, 6.62 and 5.3. Naturally available coir yarns were used for the lateral reinforcements with a spacing of 7.27, 5.88 and 4.57. Separate tests were done for different combinations.

Property	Value
Specific gravity	2.32
Liquid limit (%)	125
Plastic limit (%)	72
Plasticity Index	53
Optimum Moisture Content (%)	37
Maximum dry density (g/cc)	1.22

Property	Value
Specific gravity	2.51
Percentage of silt (%)	5
Percentage of clay (%)	4
Percentage of fine sand (%)	35
Percentage of medium sand (%)	16
Percentage of coarse sand (%)	38

3.2 Physical modeling

Model test was done in a mild steel tank of 750 x 750 x 750 mm size. After preparation of drainage bed the soft soil was filled to a depth of 500mm. Designed column of size 100mm diameter and 200 mm long are inserted into the soft soil. Footing load was applied to the stone column and surrounding soft soil by using loading plate. Schematic view of model quarry waste column is shown in Fig 1.

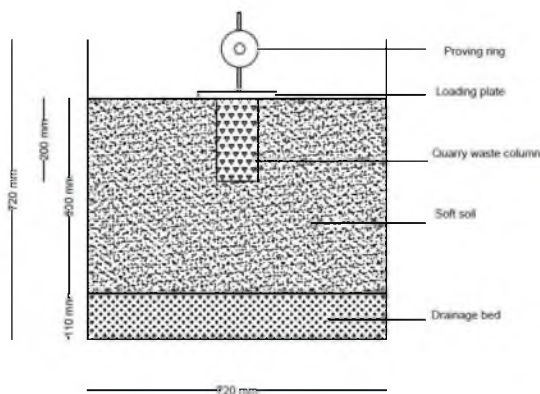


Fig 1. Test setup



Fig 2. Exhumed columns in inverted position

3.3 Preparation of soft soil

The soft soil for the testing was obtained from the river beds of Kuttanadu region. Initially the soft soil was mixed with water equal to 1.25 times liquid limit. Prepared slurry that are free from any lumps are transferred to a bucket of which was provided with sufficient drainage holes. The holes was blocked by filter papers and a load of 10kg was applied over the top of clay bed. The process of consolidation was continued for a period of 10 days. By this method the uniform moisture content and consistency were obtained throughout the test.

3.4 Column Installation

PVC pipe of 10cm external diameter was placed inside the tank. Around this pipe the clay bed was formed. Special care was done to expel the air during filling. The clay bed formed was covered with non woven coir geotextiles for 24hrs to attain thixotropic gain. The PVC pipe was removed completely without disturbing surrounding soil bed. Then the quarry waste required to fill up the column was carefully filled by funnel into three layers. Each layer was compacted using tamping rods of 12mm diameter. Encased columns are also constructed in the same manner of uncased column except the longitudinal and lateral reinforcement.

3.5 Load application

The prepared soft soil bed and quarry waste stone column together loaded with a square steel plate of 125mm size with a 12mm thickness. The test was conducted upto a maximum settlement of 50mm. Settlement was measured using dial gauge and total applied load was measured using proving ring of capacity 30kN. The applied stress at a given settlement was calculated by dividing total load by area of the plate.

3.6 Exhumation of column

After failure of column the quarry waste was removed from the column using prongs. Using plastic tubes the water from the hole was removed. A thin cement sand grout was prepared in 1:3 ratio and poured into the hole using funnel to establish the deformed shape of the column. The deformed shape was retrieved from the bed by scooping surrounding soil. From the exhumed column the depth and diameter of bulging was studied. Fig 2 shows the exhumed column.

4. Results and discussions

4.1 Effect of quarry waste column

Load penetration curve of soft soil with and without quarry waste column is shown in Fig 3. Installation of stone column highly influences the load penetration curve and shifts the curve to the right, it shows installation of stone column densifies soft soil during load application.

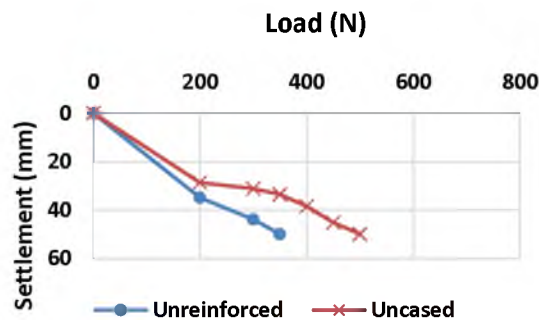


Fig 3. Load penetration curve for soft soil with uncased and without quarry waste column

Up to 20cm soil bed settlement the load carrying capacity of soft soil with quarry waste column and without column was proportional with higher value on encased quarry column. After 20cm settlement it is found that there is a sudden fall down of unreinforced soil curve to the left and shifting of soil with reinforcement to the right, it is due to the densification of soft soil with quarry waste column. The ultimate bearing capacity of the unreinforced soft soil is found as 220N and with uncased column is 325N, so the column inclusion increases the load carrying capacity by 32.3%. Studies on exhumed models of column showed there is a bulging started at 1.5d from top of the column and the diameter of bulging was about 15cm. The higher depth of bulge compared to that reported by [2] (50mm) is due to loading of soft soil and column bed together.

4.2 Effect of longitudinal bamboo encasement on stone column

High stiffness bamboo encasement was given as the longitudinal reinforcement for the column, Fig 4. It is found that the introduction of longitudinal reinforcement improves the load carrying capacity of stone column and reduces the settlement. An increasing length to spacing (L/S) ratio increases the load carrying capacity. The reason for it is

increasing length to spacing ratio reduces the space between reinforcements also the percentage of soil replaced by encasement is more. Maximum load carrying capacity stone column is with L/S ratio 7.92 with an increase of 62% with unreinforced soft bed and 52% with uncased stone column. Due to the closed spacing of L/D ratio 7.92 the diameter of bulging found to be reduced to 13.5cm and it is shifted to 1.8d depth from the top Fig 8.

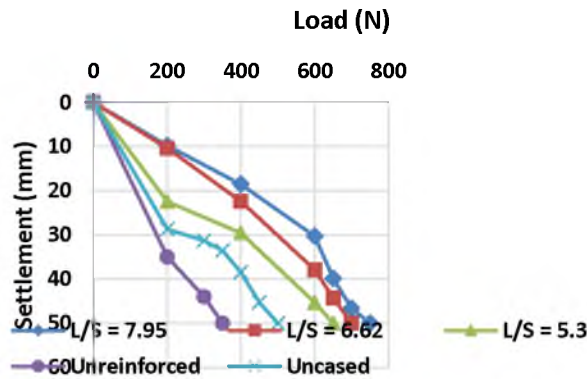


Fig 4. Load penetration curve for stone column with and without longitudinal reinforcement

4.3 Effect of longitudinal and lateral encasement in column

Coir yarn of 5mm thickness was used for the lateral reinforcement of the stone column. For the different longitudinal reinforcement spacing and the spacing between the lateral reinforcement was evaluated. Fig 5. Shows the spacing of lateral reinforcement has significant roll in load bearing. By increasing the lateral L/S ratio the mesh size of the column gets reduced also the penetration of quarry waste material. For longitudinal reinforcement L/S ratio 7.92 with lateral L/S ratio 7.27 gives 72% more load bearing capacity as compared to the unreinforced condition. By using both longitudinal and lateral encasements the diameter of bulging reduced by 16% and also depth of bulging transferred to 1.8d from the top. The percentage of elongation of coir yarn at the bottom of the column is 21% it is within the permissible limits 32% [3] so the lateral reinforcing coir yarn material is good for carrying load and reducing lateral bulging.

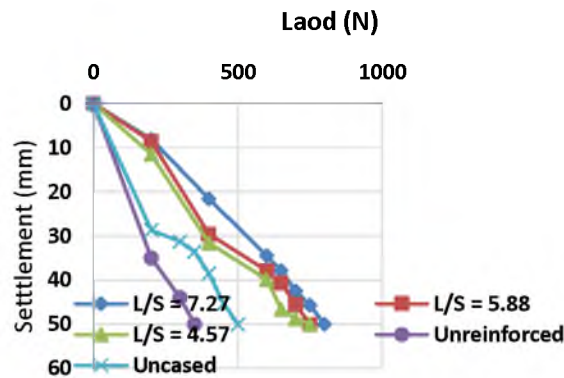


Fig 5. Load penetration curve for stone column with longitudinal L/S = 7.92

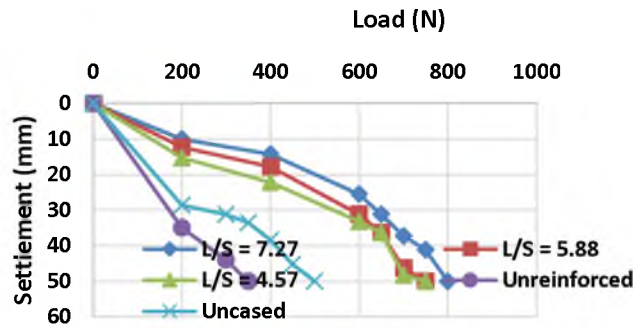


Fig 6. Load penetration curve for stone column with longitudinal L/S = 6.66

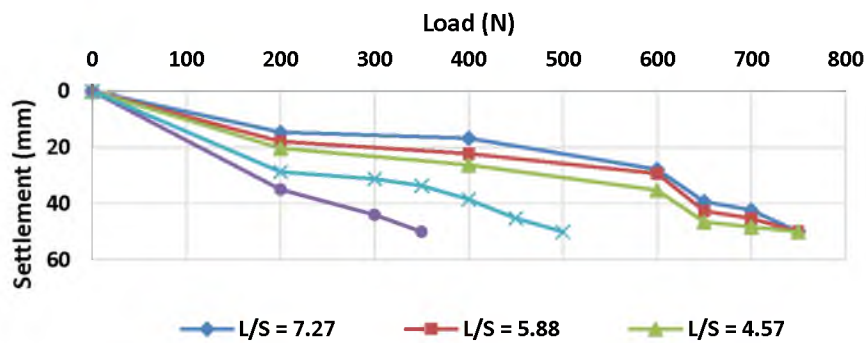


Fig 7. Load penetration curve of stone column with L/S = 5.33

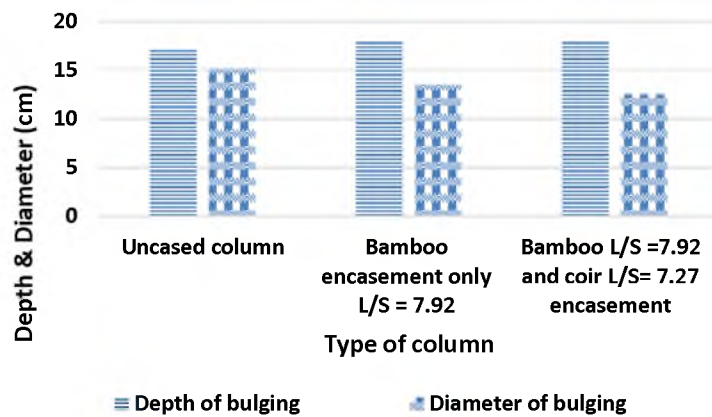


Fig 8. Depth and diameter of bulging of different combinations

4.4 Effect of stiffness of encasement on load carrying capacity

Fig 9. shows the percentage improvement of load carrying capacity stone column with and without encasements. It has been seen that if the stiffness of encasement increases the load carrying capacity of column also increases. The combination of high stiffness bamboo encasements and low stiffness coir yarn improves the load carrying capacity 72% as compared to the unreinforced soil bed conditions. This agrees the conditions suggested by [10].

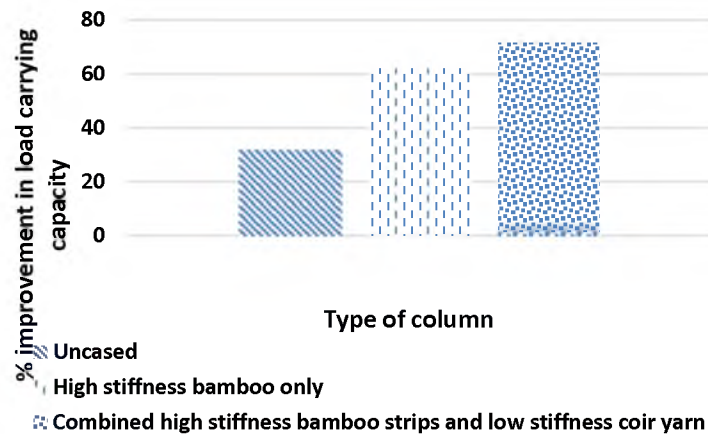


Fig 9. Variation of load carrying capacity with stiffness of reinforcement

5. Conclusion

Based on the project study it can be concluded that the quarry waste material passing through 4.75mm and retained on 425 micron can be used as a good column filling material to improve the load carrying capacity. The inclusion of stone column enhances the load carrying capacity by improving consolidation settlement. Providing both lateral and longitudinal encasements to the column will increase the stiffness of the column and enhance the load carrying capacity. Stone column with high stiffness bamboo longitudinal strips at L/S 7.92 and low stiffness coir yarn at L/S 7.27 gives better load carrying capacity and reduces the lateral bulging.

References

1. Ali, K., Shahu, J. T. and Sharma, K. G., (2012). "Model test on Geosynthetic reinforced stone columns; A comparative study", *Geosynthetic International*, Vol. 19, pp. 192-305.
2. Ambily, A. P. and Gandhi, S. R., (2007). "Behaviour of stone columns based on experimental and FEM analysis", *Journal of Geotechnical and Geoenvironmental Engineering*, Vol. 133, pp. 405-415.
3. Balan, K., Thushara, T.S. and Jayasree, P.K., (2013), "Quarry waste column laterally reinforced with coir geotextiles", *IGS journal*, Vol. 2, pp. 80-90
4. Castro, J. and Sagastro, C., (2011), "Deformation and consolidation around encased stone columns", *Geotextiles and Geomembranes*, Vol. 29, pp. 268-276.
5. Guetif, Z., Bouassida, M. and Debats, J. M., (2007). "Improved soft clay characteristics due to stone column installation", *Computers and Geotechniques*, Vol. 34, pp. 104 – 111.
6. Issac, D. S. and Girish, M. S., (2009). "Suitability of different materials for stone column construction", *Electronic journal of Geotechnical Engineering*, Vol. 14, pp. 1-12.
7. Maheshwari, P. and Khatri, K., (2011). "A non- linear model for footings on granular bed- stone column reinforced earth bed", *Applied Mathematical Modeling*, Vol. 35, pp. 2970-2804.
8. Murugesan, S. and Rajagopal, K., (2006). "Geosynthetic encased stone columns: Numerical evaluation", *Geotextiles and Geomembranes*, Vol. 24, pp. 349 – 359.
9. Rajesh, S., (2016), "Time dependent behavior of fully and partially penetrated geosynthetic encased stone columns", *IGS journal*, Vol. 26, pp. 121-132.
10. Wu, C. S. and Hong, Y. S., (2008). "The behavior of a laminated reinforced granular column", *Geotextiles and Geomembranes*, Vol. 26, pp. 302-316.
11. Zhang, L. and Zhao, M., (2016), "Effect of geogrid encasement on lateral and vertical deformations of stone columns in model tests", *IGS journal*, Vol. 23, pp. 100-112.

TREND AND CHANGE POINT ANALYSIS OF ANNUAL MAXIMUM STREAMFLOWS OF KRISHNA BASIN USING NON- PARAMETRIC TESTS AND EMPIRICAL MODE DECOMPOSITION

Athul MM¹, Nandhu AR² and Adarsh S³

¹M.Tech. National Institute of Technology Warangal, athulmmadhu@gmail.com

²B.Tech. TKM College of Engineering, Kollam, India

³TKM College of Engineering Kollam, India

Abstract: This paper presents the trend and change point analysis of the annual maximum streamflows of 42 stations of Krishna basin for 1971-2013 period. First the non-parametric Mann-Kendall (MK) test and Spearman's Rho are used for detection of trends of the different series and their statistical significance. The trend analysis revealed a significant reduction in 9 out of 42 stations of Krishna basin. The change point analysis using CUSUM method detected a change point in the third decade of study period (1991-2000) in about 52 % of the stations. The test further detected the change is statistically significant at Narsingpur, Wadakbal, Vandur, Sadalga and Shirdhon stations. The results of Sequential Mann-Kendall (SQMK) test showed that the change point was initiated much before than that obtained from CUSUM method, and the trend became significant in the due course of time. Moreover, the true inherent non-linear trends in different stations are estimated by invoking the Empirical Mode Decomposition (EMD) method. The method portrayed the true trend in different time series, which is found to be different from the linear trend in the streamflow of many of the stations. The EMD method is proven to be an improved alternative over MK method, which successfully captures the true inherent non-linear trends of annual maximum streamflow datasets of shorter length, along with their statistical significance.

Keywords : Trend, Streamflow, EMD, Change Point

1. Introduction

Trend and change point analysis of hydrologic variables has been of great concern for the hydrologists for planning and management of water resources. The trend identification is a difficult problem in practice and Sonali and Nagesh Kumar [1] performed a comprehensive review on various methods for trend analysis. The non-parametric methods such as Spearman's rho, Sen's slope method and Mann-Kendall (MK) method are still popular in analysing the trend and their statistical significance for streamflow data of different measurement scales [2-4]. Even though these non-parametric methods are still the most popular trend detection methods, it is reported that the length of the dataset can significantly influence the trend [5] and availability of long term annual maximum streamflow data (which is useful in flood forecasting studies), is rare in Indian context. Sang et al., [5] proposed the use of Empirical Mode Decomposition (EMD) for trend analysis of synthetic series and real field datasets of rainfall and runoff and it was reported to be much efficient than classical approaches for estimation of trend in datasets of shorter length, which may be often masked in the classical non-parametric methods. Moreover, it is well understood that hydroclimatic series may possess inherent non-linear trend rather than the traditional notion of linear trend [6] and capturing the true inherent non-linear trend is of great importance in hydro-meteorological studies.

The hydrologists commonly make assumption of stationarity in dealing with hydrological prediction problems. However, many of the hydrologic time series may exhibit abrupt changes owing to the land use changes, climate changes, construction of storage reservoirs etc. and the stationarity assumption may give erroneous results in prediction or forecasting exercise. There are numerous methods available for change point detection and recently Aminikhanghahi and Cook [7] provided a survey of different change point detection methods. The Cumulative Sum (CUSUM) method is a simple and practical non-parametric approach for determination of single change point in

time series datasets. The sequential version of MK test is helpful in determining the change point and also for identifying the sequential behavior of trend [8].

This study aims to perform the trend analysis of annual maximum streamflow data of 42 stations of Krishna basin using the MK method, Spearman's Rho, linear fitting and EMD; and the change points of these series are detected by the CUSUM method.

2. Materials and Methods

This study uses the traditional non-parametric methods such as Spearman's rho and MK methods for trend analysis. In general, in both of these methods, a pair-wise comparison of data points is made, and the test statistics is evaluated. The comparison of test statistics with the standard value at specified significance level along with its sign enables to comment on the nature and statistical significance of existing trend in the series. The details on computation of test statistics can be found in literature [1]. The MK test helps in determining any significant trend in the time series. However, it is of great importance to determine the starting of such a significant trend. The starting year of the trend was estimated using Sequential Mann-Kendall (SQMK) test. Sequential MK (SQMK) test is conducted upon rank values of original series, which results in sequential values of standardized variables with zero mean and unit standard deviation. The sequential values are calculated for the forward series ($u(t)$), and the backward series ($u'(t)$) in the MK framework. The SQMK test allows for the detection of approximate beginning of a change [9]. CUSUM test originally proposed by E.S. Page (stated in [10]) involves the calculation of cumulative sum of the differences. After computing the mean (\bar{x}) of a time series, the cumulative sum S_i is computed recursively as $S_i = S_{i-1} + (x_i - \bar{x})$ after assigning $S_0 = 0$. Then $\max(0, S_i)$ is considered as the test statistic. When the values of S exceed a certain threshold value, a change in values has been found. The above formula only detects changes in the positive direction. When the negative changes need to be found as well, the min operation is used and this time a change has been found when the value of S is below the negative value of the threshold value.

In this study the non-linear trend of different series is extracted using a multiscale decomposition method namely EMD proposed by Huang *et al.*, [11]. The method decomposes a time series signal into different oscillatory modes having specific periodicity in purely empirical and data adaptive manner. EMD involves (i) identification of extrema (maxima or minima) points; (ii) spline fitting through extrema to form upper and lower envelopes; (iii) computation of mean envelop curves and difference series in an iterative manner. The resulting zero mean oscillatory components are called as Intrinsic Mode Functions (IMFs) and the final component obtained by the decomposition gives the inherent non-linear trend in the series

3. Study Area and Data

In this study the trend analysis and change point analysis of annual maximum streamflow data of 42 stations in Krishna river basin (73°17' to 81°9' E and 13°10' to 19°22' N) collected from central water commission (CWC), is performed. The data of different station falls in the range 1970-2013. The basin extends over Maharashtra, Andhra Pradesh, Telangana and Karnataka. The basin extends over a total area of 258,948 Sq.km. which is nearly 8% of the total geographical area of India. join from left as shown in Figure 1.



Figure 1. Location of study area

(Source: <http://www.india-wris.nrsc.gov.in>)

The stream length of the river from its origin to where it discharges into the Bay of Bengal is about 1400 km. The principal tributaries like the Ghatprabha, the Malprabha and the Tungabhadra join the main stream from right, while the Bhima, the Musi and the Munneru. The daily maximum flow data from twenty-seven gauging stations was collected from CWC-Krishna Godavari Basin Office, Hyderabad, India.

4. Results and Discussion

In this study, first the trends of the different annual maximum datasets are determined using MK and Spearman’s Rho at 5 % statistical significance. The change point year of different series is determined using CUSUM method. The results are provided in Table 1.

Table 1 Spearman’s Rho, MK value and Change point year of annual maxima streamflow of different stations in Krishna basin. The bold figures show that the streamflow of respective show significant trend at 5 % significant level

S.no.	Station	Rho	MK	Year	S.no.	Station	Rho	MK	Year
1	Arjunwad	-1.18	-1.387	1981	22	Mantralayam	0.748	0.737	1989
2	Bastewad	-0.011	0.02	1982	23	Narsingpur	-1.981	-2.081	1998
3	Bawapuram	1.099	0.9	2005	24	Oollenur	-0.347	-0.503	1998
4	Boriomerga	-2.907	-2.865	1990	25	P.S.Gudem	-0.275	-0.21	2004
5	Cholachuguda	-0.742	-0.816	1998	26	Paleru Bridge	-0.533	-0.589	1995
6	Daddi	-2.645	-2.549	1993	27	Phulgaon	-0.569	-0.513	2002
7	Dameracherla	-0.572	-0.502	1993	28	Pondugala	-1.365	-1.534	1998
8	Dhond	-1.747	-1.949	1991	29	Sadalaga	-2.806	-2.709	1991
9	Gokakfalls	-2.141	-2.319	1983	30	Samdoli	-2.106	-2.102	1997

10	Gotur	-1.09	-1.167	2003	31	Sarati	-1.744	-1.821	2003
11	Halia	-0.349	-0.393	2009	32	Shirdhon	-1.724	-1.956	1989
12	Huvinhedgi	-0.455	-0.704	2004	33	Takli	-1.352	-1.337	1998
13	Jewangi	-0.177	-0.255	1979	34	Talikota	0.064	0.152	2010
14	Karad	-0.786	-0.889	1980	35	Terwad	-0.401	-0.237	2003
15	Keesara	-0.487	-0.44	1980	36	TR Puram	-0.524	-0.607	2004
16	Koyna	0.428	0.395	1980	37	Vandur	-2.13	-2.27	1991
17	Krishna Agra.	-0.837	-0.959	1998	38	Vijayawada	-0.45	-0.499	1998
18	Kurundwad	-1.355	-1.561	1997	39	Wadakbal	-2.841	-2.805	1991
19	Lakshmiapuram	1.027	1.184	1992	40	Wadenapally	-2.219	-2.386	1998
20	Madhira	-1.314	-1.32	1995	41	Warunji	-0.75	-1.019	1980
21	Malkhed	-0.605	-0.571	2001	42	Yadgir	-1.588	-1.758	1991

The CUSUM method is applied for different significance levels of 1%, 5 % and 10 %. The change point year obtained are categorized into four decades 1971-1980, 1980-1990, 1991-2000 and 2001-2013. Data of none of the stations except Jawangi detected a change point during 1971-1980, in which the change point year is 1979. The change points of 8 stations falls during 1980-1990. For the datasets of about 52 %of the total number of stations, the change point is observed within the decade of 1991-2000. For the data of 11 stations the change point is noticed between 2001 and 2013. On considering a significance levels of 1%,data of two stations(Wadakbal,Sadalaga) is found to be statistically significant. On considering significance level of 10%,data of four of the stations (Narsingpur,Vandur,Shirdhon and Daddi), the change is found to be statistically significant. But on considering significance levels of 5%, only data of one station (Boriomerga) the change is found to be statistically significant. All the stations except Gokakfalls that showed statistical significance trend, the change was in 1990-2000 period.

Then the linear fitting and EMD method are invoked to detect the linear and non-linear trend of different datasets. The results are presented in Figure 3. From the linear trend analysis, the data of about 71.43 % of the stations (30 out of 42 stations) shows a decreasing trend.

Table 1 shows that by MK method, the data of 9 stations showed statistically significant trend at 5 % significance level. The Spearman's rho method also displayed similar trend for all these stations. Interestingly, the data of all the stations displayed a decreasing trend. The trend analysis showed that the trend in annual maximum streamflow is increasing at 6 stations (Manthralaya, Talikota, Koyna and Bawapuram, Bestwad and Lakshmiapuram) eventhough the trend is not statistically significant. The SQMK test result for the 9 stations (Boriomerga, Daddi, Gokakfalls, Narsingpur, Sadalaga, Samdoli, Vandur, Wadakbal and Wadenapally) with significant trend at 5% significance level is shown in Figure 2. The change point at Boriormega is found to be 1975 using CUSUM method. But the trend started in the year 1975 as shown in Figure2(a). Similarly, in all these stations, except at Sadalaga and Wadakbal, the trend started atleast 9 years ago, which became significant in the due course of time. While at Sadalaga and Wadakbal, the trend started by 1990 and became significant after 1991. Perhaps, rapid changes in these adjacent catchments can be attributed for this behavior. Also, the trend started at Wadenapally by 1975 and became significant only by 1998 after 23 years. This perhaps, might be a result of gradual changes or even the climatic variations. The present study is not sufficient to attribute the reason for this characteristic.

The linear fitting and EMD of the streamflow data of 9 stations (which displayed significant change) are presented in Figure 3. From Figure 3 it is noted that all the 9 stations whose datasets show a statistically significant trend, show a decreasing trend in linear fitting method. On invoking EMD method also, data of all stations show a decreasing trend but only data of 7 stations show a monotonically decreasing trend while data of remaining 2 stations (Samdoli, Vandur) show a slight increase during the recent years as well as in the initial decades. In linear fitting method, out of 33 stations whose data are statistically insignificant, the datasets of 21 stations show decreasing trend and remaining 12 datasets show increasing trend. Data of 11 stations which showed a decreasing trend and 4 stations which showed an increasing trend in linear fitting method was not found to be monotonic in nature when EMD method was applied.

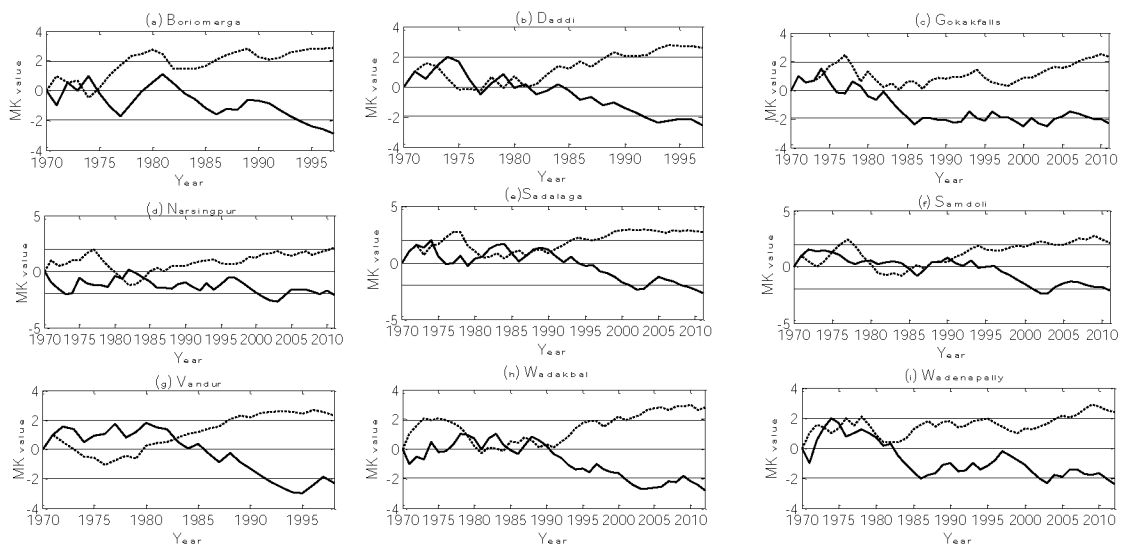


Figure 2. Sequential Mann-Kendall (SQMK) test at stations with significant linear trend.

On applying EMD method the data of 26 out of 42 stations are monotonically increasing or decreasing and out of these stations, data of 19 stations are monotonically decreasing and 7 stations are monotonically increasing. In one station (Halia), linear trend is showing increase and EMD showing monotonically decreasing trend. In the 8 stations showing change point in 1981-1990 period, data of 4 stations show decreasing trend and that of 4 stations show increasing trend. In the 11 stations showing change in 2001-2013 period, data of 6 stations show decreasing trend and that of 5 stations show increasing trend. In the 22 stations showing change in 1990-2000 period, data of 19 stations show decreasing trend and that of 3 stations show increasing trend. The station Jawangi is showing change in 1979 and it has a decreasing trend.

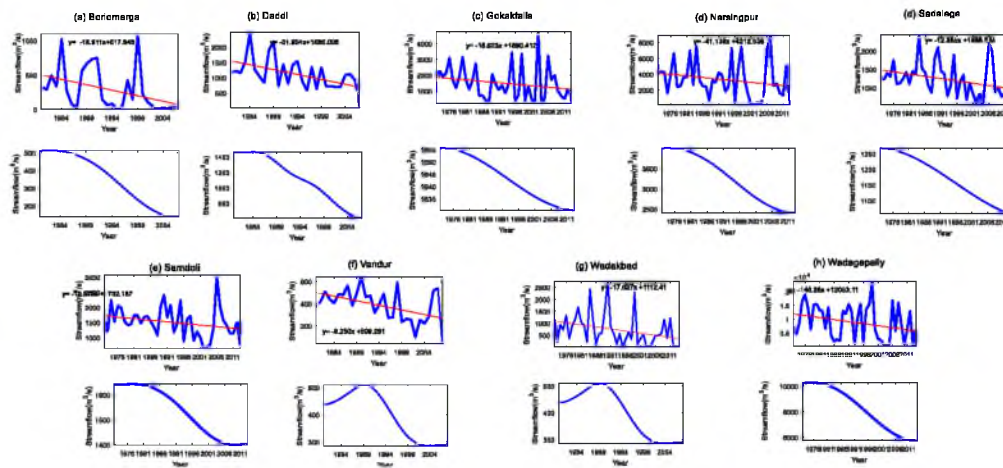


Figure3.Linear trend fitting (upper panels) and non-linear trend by EMD (lower panels) of annual maxima series of different stations of Krishna basin

5. Conclusion

The change point analysis using CUSUM method detected a change point in the third decade of study period (1991-2000) in about 52 % of the stations. The trend analysis revealed a significant reduction of annual maximum streamflow data in 9 out of 42 stations of Krishna basin. The SQMK test revealed that the trend started well before 23 years in some station like Wadenapally, and before 1 year in stations like Sadalaga and Wadakbal. This shed light to intensity of changes that might have occurred in these catchments. A logical interpretation can be made that stations like Wadenapally has undergone gradual changes while stations like Sadalaga and Wadakbal have undergone rapid changes. EMD method portrayed the true trend in different time series, which is found to be different from the linear trend in the streamflow of many of the stations. The EMD method is proven to be an improved alternative over MK method, which successfully captures the true inherent non-linear trends of annual maximum streamflow datasets of shorter length, along with their statistical significance. This is especially true in the case of data of Halia station where linear trend is showing an increase trend and EMD showing a decreasing trend. Also, the monotonic decrease in streamflow data in 19 stations implies the harmful effect of human intervention on climate and its consequences.

References

- [1] Sonali P., Nagesh Kumar D.: Review of trend detection methods and their application to detect temperature change in India. *Journal of Hydrology* 476, 212-227 (2013).
- [2] Kahya, E., Kalayci, S.: Trend Analysis of Streamflow in Turkey. *Journal of Hydrology* 289, 128-144 (2004).
- [3] Kundzewicz Z.W., Graczyk D., Maurer T., Pińskwar I., Radziejewski M., Svensson C., Szwed M.: Trend detection in river flow series: 1. Annual maximum flow. *Hydrological Sciences Journal* 50(5), 797-810 (2005)
- [4] Milan, G., Slavia, T.: Analysis of changes in meteorological variables using Mann-Kendall and Sen's slope estimator statistical tests in Serbia. *Global and Planetary Change* 100(1), 172-182 (2013).
- [5] Sang T-F., Wang Z., Liu C.: Comparison of the MK test and EMD method for trend identification in hydrological time series. *Journal of Hydrology* 510, 293-298 (2014).
- [6] Wu Z., Huang N.E., Long S.R., Peng C.K.: On the trend, detrending and variability of nonlinear and non-stationary time series. *Proceedings of National Academy of Science USA* 2007, vol 104 ,pp. 14889-14894 (2007).
- [7] [Aminikhanghahi, S.](#), [Cook, D.J.](#): A survey of methods for time series change point detection. *Knowledge Information Systems* 51(2), 339-367 (2017).

[8] Sneyers, R.: On the Statistical Analysis of Series of Observations. Technical Note No. 143, WMO No. 415, World Meteorological Organization, Geneva, pp. 192 (1990).

[9] Gerstengarbe, F.W., Werner, P.C.: Estimation of the beginning and end of recurrent events within a climate regime. *Climate Research* 11(2), 97-107 (1999).

[10] W. Taylor, "Change-Point Analysis: A Powerful Tool for Detecting Changes." Taylor Enterprises, Libertyville. 2000, <http://www.variation.com/cpa/tech/changepoint.html>

[11] Huang N.E., Shen Z., Long S.R., Wu M.C., Shih H.H., Zheng W., Yen N.C., Tung C.C., Liu H.H.: The empirical mode decomposition and the Hilbert spectrum for nonlinear and non-stationary time series analysis. *Proceedings of Royal Society London, Series A* 454, 903–995 (1998).

Modeling of Bharathapuzha River Basin Using SWAT Model and SUFI-2

Dila John¹ and Chithra N R²

¹M.Tech student, Department of Civil Engineering, National Institute of Technology Calicut

²Assistant Professor, Department of Civil Engineering, National Institute of Technology Calicut

Abstract

This paper presents the hydrologic modelling of Thuthapuzha sub-basin of Bharathapuzha river basin for efficient water management practices using the Soil and Water Assessment Tool(SWAT 2012) model. The objectives of the research were to apply Geographic Information System(GIS) and SWAT model for simulation of water discharge with input data including: Digital Elevation Model(DEM), landcover of and soil map. The SWAT 2012 model is interfaced with ArcGIS. The model was also calibrated from 2005 to 2008 and validated from 2009 to 2011 using SWAT CUP SUFI-2 Algorithm. The study shows that SWAT model is a capable tool for simulating hydrologic components of Thuthapuzha sub-basin.

Keywords: SWAT Model, Streamflow, SUFI-2

1 Introduction

Water is an extremely essential element to sustain life and increasing population is raising the demand of water. Availability of water is largely dependent on the rainfall distribution over an area, which again get distributed into various components of interflow, surface runoff, evapotranspiration etc. Due to the spatio-temporal variations in the distribution of rainfall and undulating topography with steep seaward slopes, most of the water in the Bharathapuzha river quickly drains to the Arabian Sea. Bharathapuzha lost its solemnity in the course of time due to increased sand mining, industrialization and urbanization. Many parts of Bharathapuzha has become dry. The land-water system of the area is adversely affected by the rapid growth of population and changes in the landuse or landcover. The rejuvenation of Bharathapuzha to its old pride has to be taken as a serious issue. The government and various environmental organizations have taken steps for that. This can be achieved only through a proper management of available water resources. The available land and water resources are to be effectively utilised to improve the livelihood and socio-economic conditions of the people living in the river basin. In this, the performance and feasibility of the SWAT 2012 model for prediction of flow in the river has been tested and validated.

2 Research Methodologies

2.1 Study Area

The study area is a part of Bharathapuzha river basin of Kerala extending from 10° 45' to 11° 30' N and 75° 45' to 76° 45' E. Bharathapuzha River is the second longest river of Kerala. Main tributary of study area is Thuthapuzha. This tributary starts from the Silent valley hills. It constitutes of 4 streams named as Kunthipuzha, Kanjirapuzha, Ambankadavu and Thuppanadpuzha. Area of the watershed considered in this study is 913 km² and its boundary covers a perimeter of 226 km. Thuthapuzha is one of the tributaries of Bharathapuzha. It receives an average annual rainfall of 2682.6mm. The average maximum temperature of the sub-basin is 31.43°C and a minimum temperature of 24.33°C. With a watershed of 6,186 km², the Bharathapuzha basin is the largest among all the river basins in Kerala. A little more than two-thirds of this area (4400 km²) is within Kerala and the remaining area (1786 km²) is in Tamil Nadu.



Figure 1. Index map of Thuthapuzha sub-basin

2.2 Soil and Water Assessment Tool (SWAT)

SWAT is a process-based and spatially semi-distributed hydrological and water quality model designed to calculate and route water, sediments and contaminants from individual drainage units (sub-basins) throughout a river basin towards its outlet. Within the SWAT conceptual framework, the representation of the hydrology of a basin is divided into two major parts: (a) the land phase of the hydrological cycle; and (b) the routing of runoff through the river network.

For modelling the land phase, the river basin is divided in sub-basins, each one of which is composed of one or several hydrological response units (HRUs) which are areas of relatively homogenous land use/land cover and soil types. The characteristics of the HRUs define the hydrological response of a sub-basin. For a given time step, the contributions to the discharge at each sub-basin outlet point is controlled by the HRU water balance calculations (land phase). The river network then connects the different sub-basin outlets, and the routing phase determines movement of water through this network towards internal control points, and finally toward the basin outlet. For the land phase water balance, within SWAT evapotranspiration can be calculated using one of three methods: Penman-Monteith, the Hargreaves or Priestly-Taylor. The methodology followed for the SWAT model is given as a flow chart:

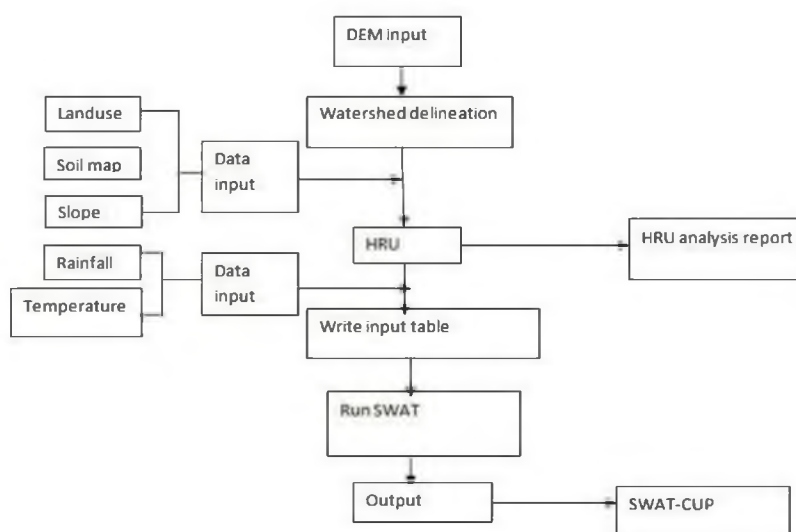


Figure 2. Flow chart showing SWAT methodology

SWAT uses water balance equation as the governing equation given by:

$$SW_t = SW + \Delta(R_{day} - Q_i - E_a - P_i - QR_i)$$

SW_t : soil water content

R_{day} : amount of precipitation

E_a : amount of evapotranspiration

QR_i : amount of return flow

t: time

Q_i : amount of surface runoff

P_i : amount of percolation

2.3 Model Data Inputs

The ArcGIS platform provides the user with a complete set of GIS tools for developing, running and editing hydrologic and management inputs and finally calibrating the model. The spatially distributed data required for ArcSWAT include the Digital Elevation Model (DEM), soil and land use data, either as shape files or grid data. The weather and measured streamflow data are also required as input for the calibration and prediction purposes.

Data collection. The data required for the study and the respective sources are mentioned below:

Table 1. Source of input data

DATA COLLECTED	SOURCE
DEM	USGS
LANDUSE MAP	USGS(2002)
SOIL MAP	FAO (2012)
METEOROLOGICAL DATA	Regional Agricultural Research Station, Pattambi(2000-2012)
OBSERVED DISCHARGE DATA	Central Water Commission(Pulamanthole)

Digital elevation model. ArcSWAT allows the user to delineate sub watersheds based on an automatic procedure using Digital Elevation Model (DEM) data. The Watershed Delineation carries out advanced GIS functions by segmenting watersheds into several hydrologically connected sub-watersheds for use in watershed modelling with SWAT. DEM is obtained from SRTM of 30 m resolution (USGS).

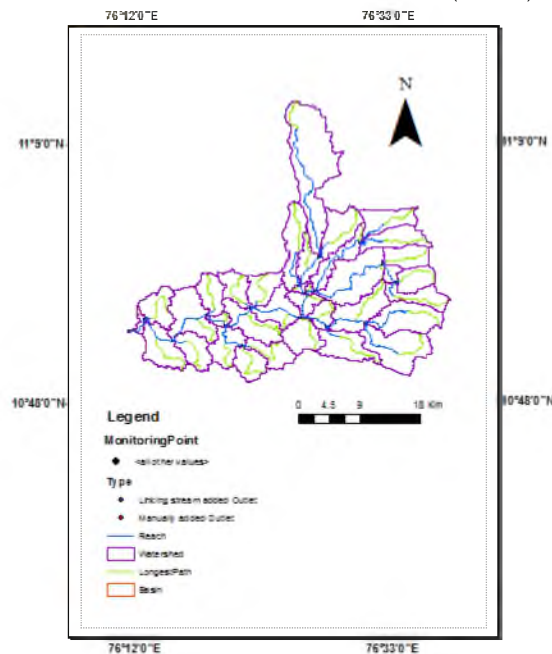


Figure 3. Delineated watershed

Climate data. The climate data required are precipitation, maximum and minimum air temperature, wind speed, relative humidity and solar radiation. Values for these parameters may be read from the records of observed data or these may be generated. The weather generator input file contains the statistical data needed to generate

2.4 Model application

In order to apply SWAT model to Thuthapuzha sub basin, the major steps involved are: 1) data preparation, 2) river basin and sub basin delineation, 3) HRU definition, 4) sensitivity analysis, and 5) model calibration and validation. The meteorological data files were created for the observed data in the format specified in SWAT. The spatial data sets required were projected to the same projection, WGS 1984 UTM ZONE 43N using ArcGIS 10.2. The DEM was used to delineate the watershed and to analyse the drainage pattern of the land surface terrain. The spatial data on LU/LC were reclassified into SWAT land cover/plant types. User defined soil types were added to the soil database and the spatial soil data were linked to the appropriate types. The multiple HRU definition of 20 percent land use, 20 percent soil and 20 percent slope threshold was applied in the study. About 39 sub basins and 990 HRU's have been created. The parameter sensitivity analysis was done for the whole river basin. The hydrologic parameters pertinent to water flow were tested for sensitivity for the simulation of streamflow in the study area. The top ranked six parameters were used for calibrating the model.

The data for the period 2005 to 2008 were used for calibrating the model for the observed flows at Pulamanthole. An independent precipitation, temperature, wind speed, relative humidity and streamflow data set (2000-2012) were prepared. Periods from 2000 to 2002 were taken as warm-up period for calibration. The warm-up period allows the model to get the hydrologic cycle fully operational.

2.5 SWAT-CUP5 software

SWAT CUP5 software was used for the calibration of the model. Sequential Uncertainty Fitting (SUFI2) algorithm was used for calibration. The model was calibrated for the top ranked parameters - Manning's "n" value for overland flow(OV_N), Threshold depth of water in the shallow aquifer required for the return flow to occur (GWQMN), Plant uptake compensation factor(EPCO), Groundwater revap coefficient(GW_REVAP), SCS Curve number (CN2) and Saturated hydraulic conductivity(SOL_K).

2.6 Evaluation of model performance

Simulated data from the SWAT model can be compared statistically to observed data to evaluate the predictive capability of the model.

2.7 Model calibration

During a calibration process, model parameters are subject to adjustment, in order to obtain model results that correspond better to discharge rates observed in the field. To calibrate a model, some aspect of watershed behaviour is selected to which the model is to be matched: typically, the streamflow hydrograph at one or more locations on the river is selected. Then the model parameters are adjusted to get the simulated streamflow hydrograph to resemble the observed hydrograph for some historical data period. The SUFI2 algorithm in SWAT CUP was used for calibration. The statistical indicators used for evaluating model performance are: The Nash-Sutcliffe modeling efficiency index (NS); The goodness of fit (R^2), and the percentage of deviation from observed streamflow (PBIAS). Comparison between the observed and calibrated streamflow values of simulation indicated that there is a good agreement between the observed and simulated flows. The closer the values of R^2 and NS to unity the better the model performance. For PBIAS the optimal value is 0; a negative value indicates an overestimation of observed discharge values, whereas a positive value indicates under estimation. The criteria suggested by Moriasi et al. (2007) for evaluating model performance are given below in Table 2:

Table 2. Performance Rating of indicators

Performance Rating	NS	PBIAS
Very Good	$0.75 < NS \leq 1$	$PBIAS < \pm 10$
Good	$0.65 < NS \leq 0.75$	$\pm 10 \leq PBIAS < \pm 15$
Satisfactory	$0.5 < NS \leq 0.65$	$\pm 15 \leq PBIAS < \pm 25$
Unsatisfactory	$NS \leq 0.5$	$PBIAS \geq \pm 25$

Source: Moriasi et al. (2007)

2.8 Sensitivity analysis

For calibrating the model, a preliminary sensitivity analysis was performed on all the flow parameters based on the available climatic and hydrologic input data for the period from 1987 to 2000. Sensitivity analysis is done to

understand which parameter is more sensitive. Two types of sensitivity analysis can be performed using SWAT-CUP. They are Global sensitivity analysis and One at a time sensitivity analysis. One at a time sensitivity shows the sensitivity of a variable to the changes in a parameter if all other parameters are kept constant at some value. Here global sensitivity analysis is used. The first six ranked parameters were selected for calibration purpose. The model was calibrated with these six parameters for the observed streamflow values.

2.8 Model validation

The streamflow for 2009 to 2011 were used for validating the predictive capability of the SWAT model with respect to Bharathapuzha river basin. The comparison statistics for observed and simulated monthly streamflow for the validation period shows that the model is very good for predicting monthly streamflow.

3 Results

The monthly average values for the simulation period is obtained for the parameters such as precipitation, surface runoff contribution, lateral flow, groundwater contribution, water yield, evapotranspiration, PET etc. – The most sensitive parameters are found out to be as in Table 3. The values of statistical indicators before calibration, after calibration and after validation are given in Table 4. The hydrograph showing the comparison between observed and simulated data for calibration and validation period is shown in Figure 6.

Table 3. Sensitive parameters

PARAMETER	SENSITIVENESS RANK
Manning’s “n” value for overland flow(OV_N)	1
Threshold depth of water in the shallow aquifer required for the return flow to occur (GWQMN)	2
Plant uptake compensation factor(EPCO)	3
Groundwater revap coefficient(GW_REVAP)	4
SCS Curve number (CN2)	5
Saturated hydraulic conductivity(SOL_K)	6

Table 4. Values of statistical indicators

Indicators	Before calibration	After calibration	After validation	Remarks
NS	0.595	0.87	0.64	Good
R ²	0.749	0.91	0.66	Good
PBIAS	41.603	13.2	4.2	Good

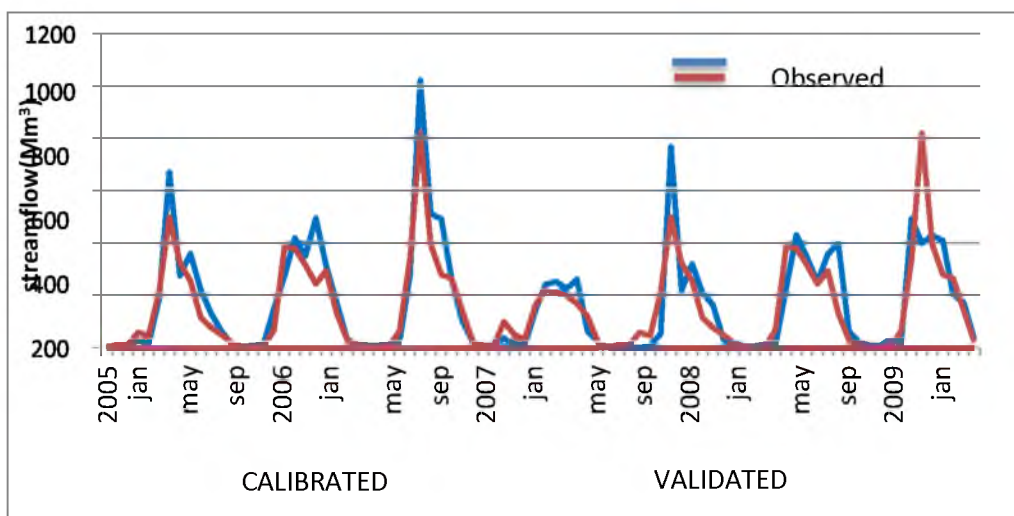


Figure 6. Hydrograph of calibration and validation

3.1 Conclusion

In this project a SWAT model was applied to simulate the discharge of Thuthapuzha river basin which is a sub-basin of the river Bharathapuzha. The model was calibrated and validated with the observed data. Based on the results of the study, SWAT model shows good performance for the Thuthapuzha sub-basin. Discharge of all the watersheds of the Thuthapuzha river basin was obtained. The results for validation of the model was slightly low compared to calibrated model. Under local conditions of data availability, the application of SWAT model for the Thuthapuzha basin confirms that SWAT is a useful tool that can be used to simulate the discharge. SWAT model can be used for future predictions also. The model can be a helpful tool to predict not only discharge but also sediment and agricultural chemical yields etc under varying soil, land use and management conditions over longer periods of time.

References

1. Alejandra S., et al., "Hydrological modelling with SWAT under conditions of limited data availability: evaluation of results from a Chilean case study", *Hydrological Sciences Journal* (2008).
2. Barthel.R., Banzhaf.S., "Groundwater and Surface Water Interaction at the Regional-scale – A Review with Focus on Regional Integrated Models" *Water Resource Management* 30, 1-32 (2016).
3. E. Kalbus., F. Reinstorf., M. Schirmer "Measuring methods for groundwater – surface water interactions: a review" *Hydrology and Earth System Sciences* 10, 873–887 (2006).
4. Kendy.E., Bredehoeft.J., "Transient effects of groundwater pumping and surface-water irrigation returns on streamflow" *Water Resources Research* 42 (2006).
5. Kundu.S., Khare.D., Mondal.A. "Past, present and future land use changes and their impact on water balance" *Journal of Environmental Management* 197, 582-596 (2017).
6. Moriasi.D., et al., "Model evaluation guidelines for systematic quantification of accuracy in watershed simulations" *American Society of Agricultural and Biological Engineers ISSN* 50(3), 885–900 (2007).
7. Nagaraj S., et al., "Runoff Modelling for Bhima River using Swat Hydrological Model" *International Journal of Engineering Research Technology* (2014).
8. P. P. Nikhil Raj, P. A. Azeez., "Land Use and Land Cover Changes in a Tropical River Basin: A Case from Bharathapuzha River Basin, Southern India" *Journal of Geographic Information System* 2, 185-193 (2010).
9. Warriar.U., Manjula.P., "River-Groundwater interaction of a tropical sub basin of Bharatapuzha, Kerala, India" *International Journal of Advanced Technology in Engineering and Science* 2 (7), 382-393 (2014).

Assessment of Meteorological Drought in Anantapur District Using Standardized Precipitation - Evapotranspiration Index (SPEI)

Athira K¹, Chithra N R², and Sathish Kumar D³

¹M.Tech student, Department of Civil Engineering, National Institute of Technology Calicut

²Assistant Professor, Department of Civil Engineering, National Institute of Technology Calicut

³Assistant Professor, Department of Civil Engineering, National Institute of Technology Calicut

Abstract: Drought is an insidious natural hazard that is generally perceived to be a prolonged period with significantly lower precipitations than normal levels. In India, over 68% of the area is drought affected. Anantapur is one such district where drought condition is prevailing for several years and its effects are severely visible in all sectors. In this study, a non-parametric test (Mann Kendall test) was used to check monotonic trend in each grid level and magnitude was calculated by Sen's slope test. The effect of meteorological parameters like precipitation and temperature assessed through a drought index called standardized precipitation-evapotranspiration index (SPEI) for a period of 1971-2003 and its spatial distribution also estimated. Studies show that the intensity and frequency of drought have increased during the same period.

Keywords: Meteorological drought, Trend test, SPEI

1. Introduction

Drought occurs virtually in all climatic regimes, and it can be defined as a prolonged period of abnormally low precipitation, unlike other hazards the footprints of drought is typically larger, which affects all sectors. In India, drought has resulted in millions of deaths over the course of the 18th, 19th, and 20th centuries. Failure of monsoon is the main reason of drought in India, it causes below average crop yield, and it adversely affects the social and economic condition. This is particularly true of major drought-prone regions such as Andhra Pradesh southern and eastern Maharashtra, northern Karnataka, Odisha, Gujarat, Telangana, and Rajasthan. Drought indices and indicators are mainly used to track drought conditions result depend upon the region and climate conditions. Drought is a recurrent phenomenon in India. About 107 million hectares of the country i.e., over 68 percent of India, spread over several administrative districts in many states, is affected by drought. Anantapur is one such district of Andhra Pradesh (AP) State where drought conditions are prevailing consistently over many years causing severe stress to the local economy, especially the agriculture (M. Srinivasa Reddy et al., 2008).

Drought indices are typically computed numerical representations of drought severity, assessed using climatic or hydro-meteorological inputs. In the last few decades lots of drought indices were developed, each index is specifically for particular climatic conditions. Recently, developed drought index called standardized precipitation- evapotranspiration index (SPEI) has incorporated the effect of precipitation and temperature so it was taken as a better approach to express the climate change in the drought scenario. In this paper, characterizing the effect of changes in precipitation and temperature on meteorological drought in Anantapur district, also analyzing the spatial distribution of drought hazard area in Anantapur.

2. Materials and Methods

2.1. Study Area

Anantapur District

Anantapur district belongs to the geographic region Rayalaseema and largest among the 13 districts of Andhra Pradesh. It is bounded on the north by Kurnool District, on the east by Kadapa District, on the southeast by Chittoor District, and on the southwest and west by Karnataka state. The district is economically backward and chronically drought affected. The district lies between North latitudes 13° 40' and 16° 15' and between East longitudes 70° 50' and 78° 38'. The geographical area of the district is 19,197 sq.km with a population of 40.83 lakhs. The population density, which was 54 persons per sq.km during 1901, has risen to 213 persons per sq.km as per 2011 census.

The average annual rainfall of the district is 535 mm, which ranges from nil rainfall in February and March to 129 mm in September. September and October are the wettest months of the year. The mean seasonal rainfall distribution is 316 mm during south-west monsoon (June-September) 146 mm during north-east monsoon

(Oct-Dec). The summer season continues from March to May, when the temperature rises to a maximum of 40°C and goes down to the minimum of 23°C (groundwater brochure Anantapur district, 2013). In this study, 9 grids of .5*.5 degree resolution are selected within the district boundary. Latitude and longitude of each grids are [14°, 77°], [14°, 77.5°], [14°, 78°], [14.5°, 77°], [14.5°, 77.5°], [14.5°, 78°], [15°, 77°], [15°, 77.5°], [15°, 78°]. The location of the grids in the map is given in the figure1.

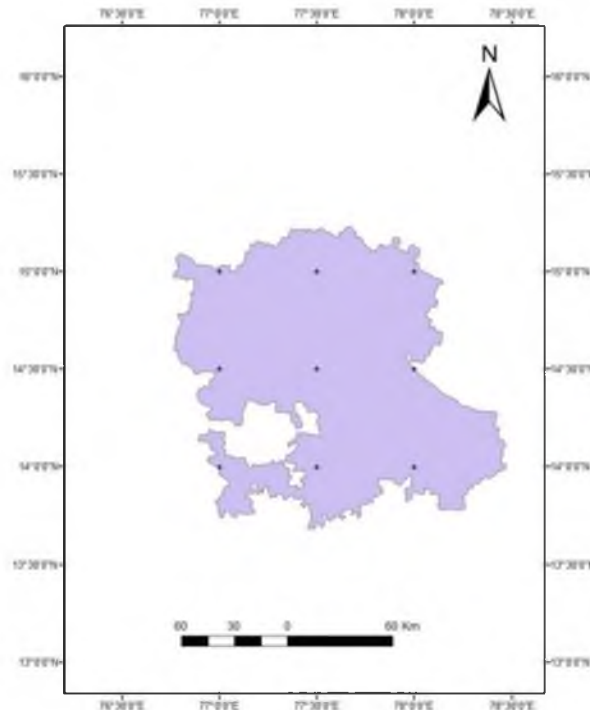


Figure 1.location of grid points

2.2. Data processing

Standardized Precipitation-Evapotranspiration Index (SPEI) is used for the drought assessment. It required monthly precipitation and temperature data as input. 0.5*0.5 degree gridded daily precipitation data and 1*1 degree gridded temperature data from Indian Meteorological Department (IMD) for the period of 1971-2003 (33 years) are used for the study. Data is given in ASCII format and c programming was used to extract the data. Linear interpolation applied for regridding the temperature data and converted to 0.5 * 0.5 resolution. Monthly, precipitation and temperature were calculated.

2.3. Trendanalysis

The statistical trend in annual meteorological data was analyzed using nonparametric Mann Kendall (MK) test (Mann, 1945; Kendall, 1975). It has been used by a number of researchers (e.g., Vijay Kumar et al., 2010; Yu et al., 1993; Douglas et al., 2000; Yue et al., 2003; Burnet al., 2004) to verify the presence of statistically significant trend in meteorological variables, such as precipitation, temperature and streamflow, with reference to climate change. MK test checks the existence of a positive or negative trend in the time series and the magnitude of the trend was determined by Sen's slope estimator. Trend analysis for precipitation and temperature was carried out at a significance limit, $\alpha = .05$ for nine grids.

2.4. Calculation of SPEI

The Standardized Precipitation Evapotranspiration Index (SPEI) is an extension of the broadly used Standardized Precipitation Index (SPI).The SPEI is designed to take into account both precipitation and potential evapotranspiration (PET) in determining drought. Thus, SPEI captures the main impact of increased temperatures on water demand. This represented simple water balance which was calculated at 1, 3, 6, 9, 12-time steps to calculate SPEI.

$$D = P - PET$$

Where P is the monthly precipitation (mm) and PET (mm) is calculated according to the method of Penman-Monteith or Hargreaves or Thornthwaite based on the availability of data. The calculated D values were aggregated at various time scales:

$$\sum_{i=0}^{k-1} (P_{n-t} - PET_{n-t}), n \geq k$$

Where k (months) was the time scale of the aggregation and n is the calculation number. The D values are undefined for $k > n$. A log-logistic probability distribution function was fitted to the data series of D , as it adapted very well to all time scales.

2.5. Mapping

Different techniques can be used to generate a continuous map of meteorological drought. One such technique generates an interpolated surface of estimated values at locations between sites based on mathematical relationships of the indicator or index between the original point data. Often this produces a map that appears “natural”, but is still based on the data from specific points and is only as accurate as the original data and the interpolation technique. No single interpolation method can be applied to all situations, and the most commonly used interpolation techniques include Kriging, Spline, and Inverse Distance Weighting (IDW).

Each interpolation technique has its advantages and disadvantages. Some techniques are more exact than others but take longer to produce the desired output. The Kriging method has geological applications and also applicable in the mining industry, assumes that there is a relationship between points that is non-random and changes over space. The Spline method is used when minimizing the overall surface curvature is important. Inverse Distance Weighting (IDW) is used when the data points are scattered but dense enough to represent local variations. The data, as the name implies, are weighted to favor data closer in proximity to the point being processed.

3. Results and Discussion

The failure of North-East monsoons and the uneven distribution of rainfall of South-West monsoons resulted in a reduction in precipitation and global warming and greenhouse effect were accelerated by the temperature rise. Gridded precipitation and temperature data were extracted and given in figure 2 and 3

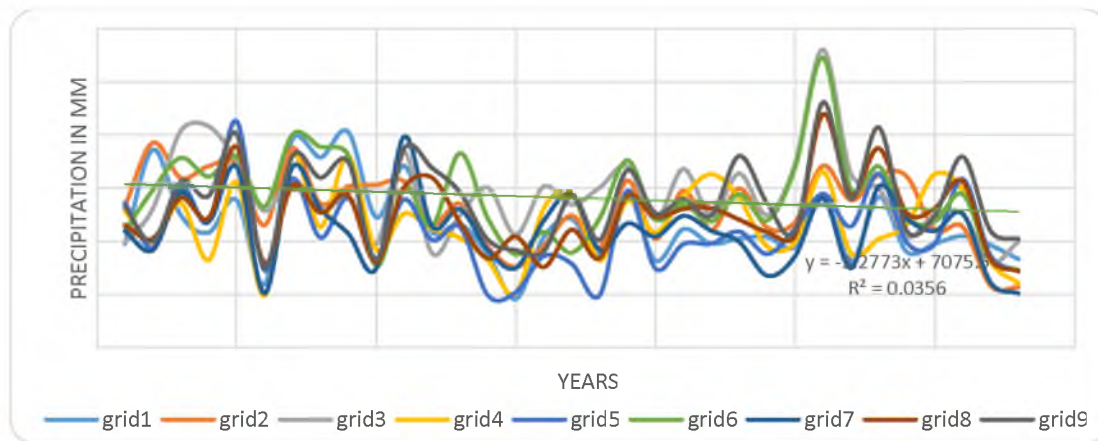


Figure 2. Gridded annual precipitation in Anantapur district (1971-2003)

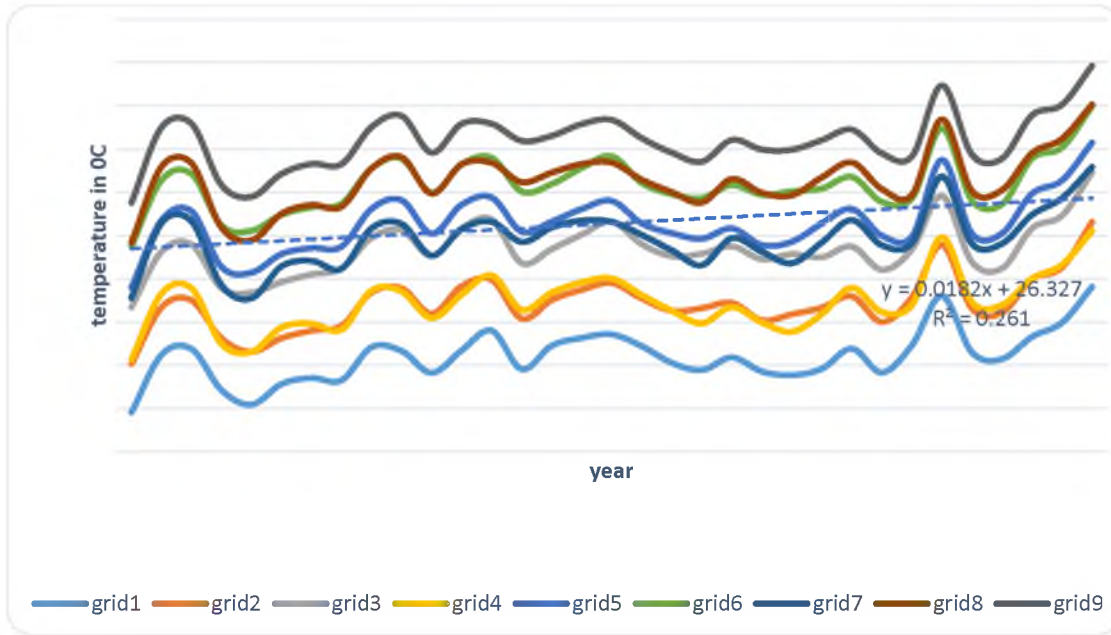


Figure 3. Gridded annual temperature in Anantapur district (1971-2003)

3.1. Trends in Precipitation and Temperature Data

MK test rejected the null hypothesis (H_0) and accepted the alternative hypothesis (H_a), i.e. monotonic trend exists in the long-term precipitation data. From Sen’s slope test, 8 grids are showing a negative trend and only one grid having a positive trend with magnitude .49mm/year in the case of temperature all grids showing a positive trend with an average magnitude .0121⁰C/year and result are given in the table1. This decrease in precipitation and increase in temperature are the main reason behind the persistent drought condition in Anantapur district.

Table1. Sen’s slope test result for annual precipitation and temperature

Grid number	Sen’s slope (mm/year)	Sen’s slope (⁰ C/year)
1	-4.87	0.014
2	-6.09	0.015
3	-2.35	0.012
4	-0.21	0.013
5	-1.83	0.013
6	-3.53	0.01
7	-3.75	0.012
8	0.49	0.011
9	-0.37	0.009

3.2. SPEI Calculation

The SPEI R library allows computing the SPEI and includes a set of additional functionalities and options. It can be obtained from the Comprehensive R Archive Network, CRAN. Using R coding SPEI was calculated for five

different time scale i.e., SPEI1, SPEI3, SPEI6, SPEI9, SPEI12 for each grid. The result of grid1 is given in figure 4.

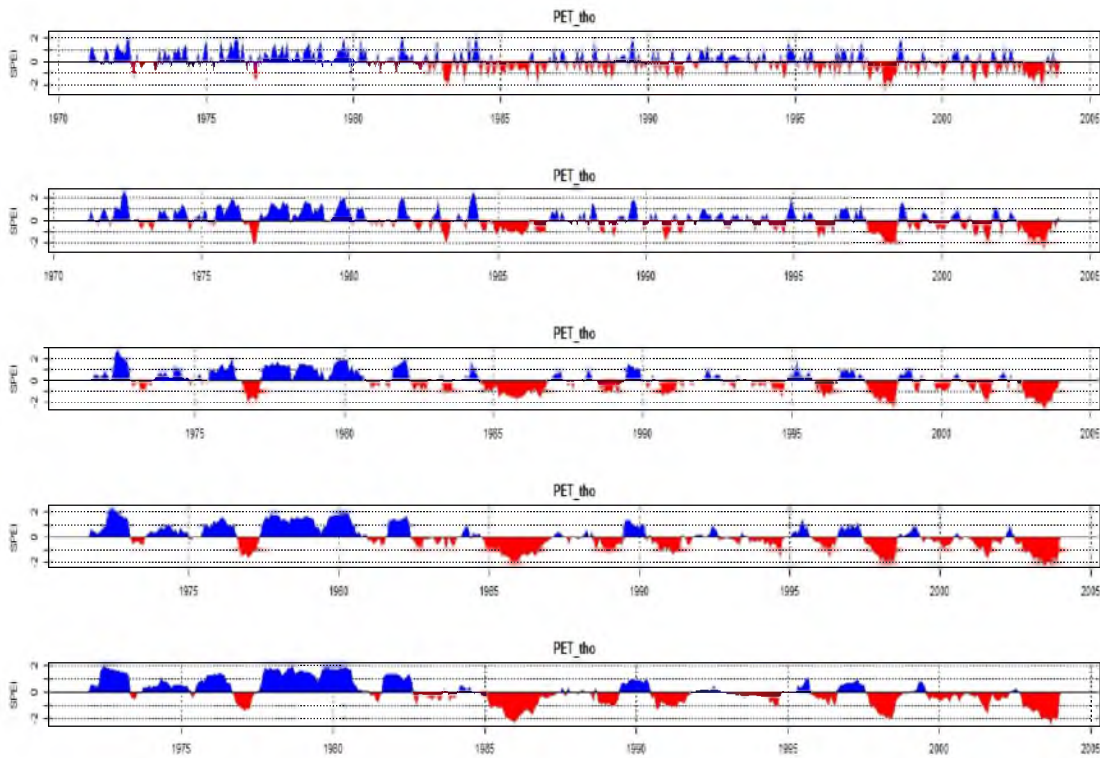


Figure.4 SPEI1, SPEI3, SPEI6, SPEI9, SPEI12 for grid1

The 1-month SPEI reproduced short-term conditions, its application can be connected closely to meteorological drought along with short-term soil moisture and crop stress, particularly during the growing season. Interpretation of the 1-month SPEI may be misleading unless climatology is understood. In regions, where precipitation was usually low during a month, large negative or positive SPEIs may result even though the withdrawal from the mean is relatively small. 3-month SPEI replicated short term and medium term moisture condition. In primary agricultural region SPEI3 represented moisture condition more effectively. The SPEI6 indicated seasonal to medium-term trends in effective precipitation it gave the effect of seasonal variation more effectively. The 9-month SPEI provided an indication of inter-seasonal precipitation patterns over a medium timescale duration. The SPEI at this timescale replicates long-term precipitation patterns. A 12-month SPEI was a comparison of the precipitation for 12 consecutive months with that recorded in the same 12 consecutive months in all previous years of available data. SPEIs of these timescales are usually tied to stream flows, reservoir levels, and groundwater levels at longer timescales.

From the figure 4, it was clear that up to 1985 the drought conditions not common, but in 1985, they experienced one the severe drought in the history. After 1985, drought was frequently observed. From 1995 – 2003 period frequency, duration, and intensity of drought increased abnormally. Consistent drought condition causes severe stress in local economy especially agriculture (M. Srinivasa Reddy et al., 2008).

3.3.SPEI Mapping

Inverse Distance Weighting (IDW) method was used to generate a continuous map and this tool is available in ArcGIS. SPEI6 was used for the mapping because 6- month time scale incorporates the seasonal variation effectively. Spatial distribution of drought condition using SPEI6 July for the years 1971, 1981, 1991, 2001 and 2003 given in the figure 5a – e.

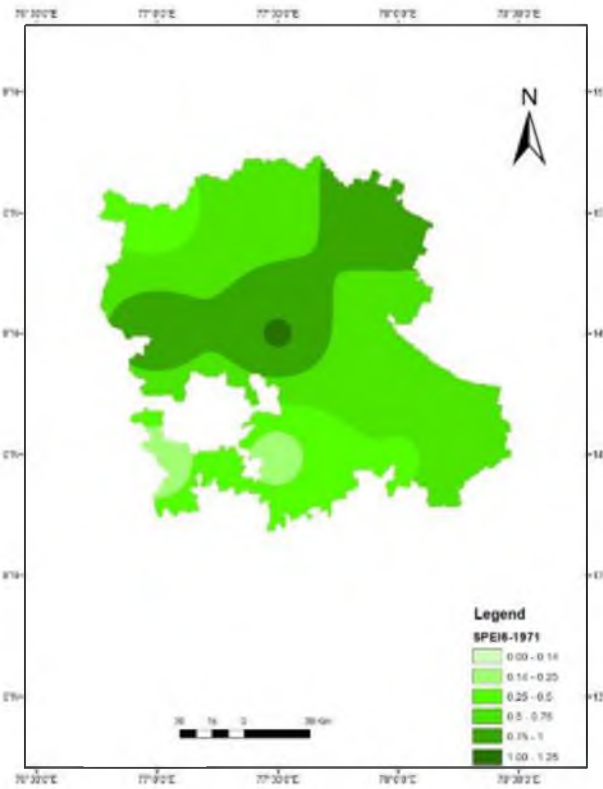


Figure 5a. SPEI6 1971 July

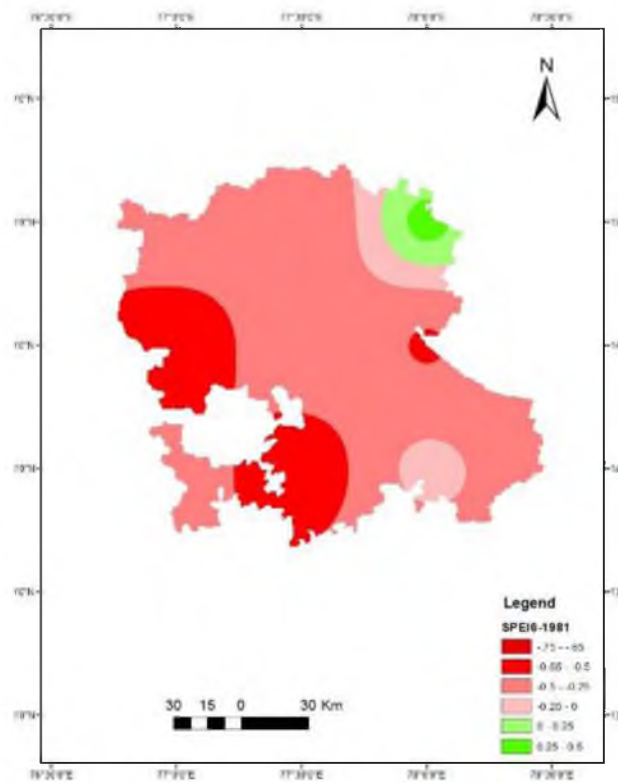


Figure 5b. SPEI6 1981 July

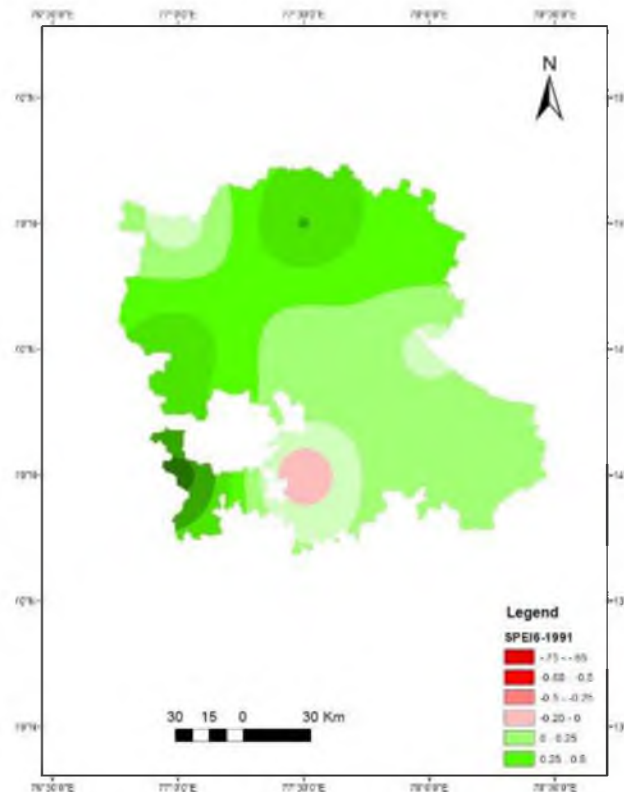


Figure 5c. SPEI6 1991 July

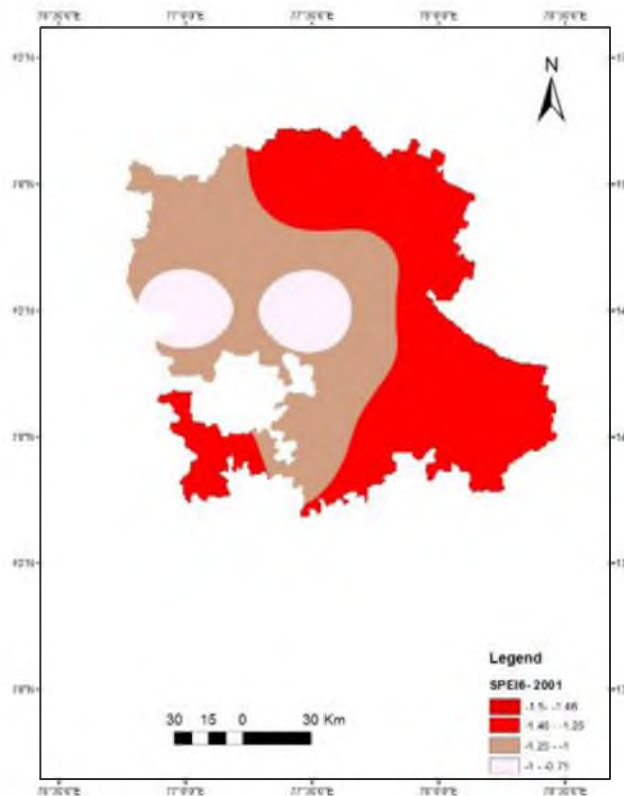


Figure 5d. SPEI6 2001 July

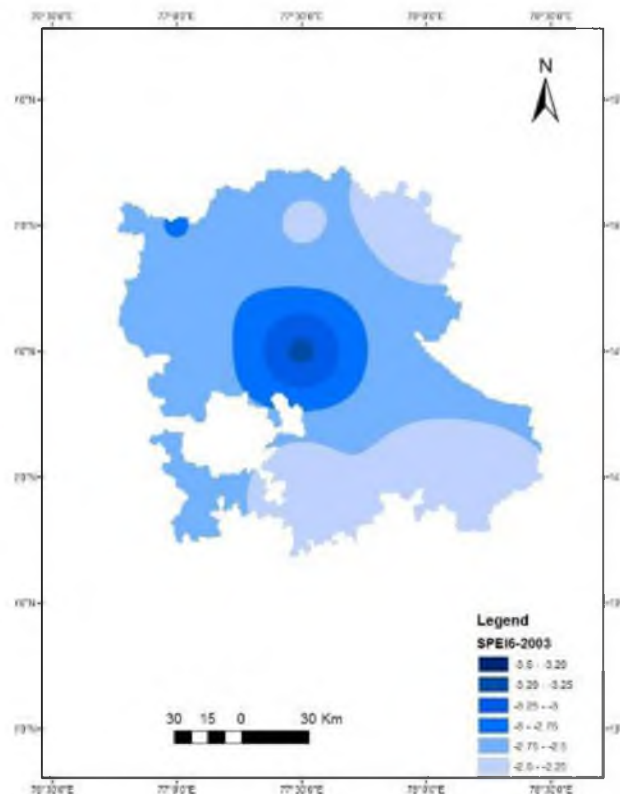


Figure 5c. SPEI6 2003 July

Southwestern side of Anantapur was the most drought-affected area. But coming to the last decades, there was a shift in the drought-prone areas i.e. Central part of the district was also experienced severe drought condition.

4. Conclusion

In Anantapur district decrease in precipitation and increase in temperature (high evapotranspiration) cause persistent drought condition. SPEI index was used to assess the drought condition in the Anantapur district. SPEI gave a better representation of climatic condition prevailing in the study area. It was incorporated the effect of precipitation as well as temperature. The results showed that, in this 33 years, from 1985 onwards Anantapur experienced more frequent and severe drought events. Duration of the drought was also increased. In the early period south-west side of the district experienced severe drought, but in the last decade, it affected the whole district. After 1985, Anantapur has experienced the severe drought in 2003, in the same year, the central part of the district experienced the most severe drought. In the last decade, seven years were drought-prone, it was seriously affected by the local economy especially agriculture.

References

1. Das P.K, Dutta D, Sharma J.R and Dadhwal V.K. (2016), "Trends and behavior of meteorological drought (1901–2008) over Indian region using standardized precipitation–evapotranspiration index", *International Journal of Climatology*, 36: 909–916
2. Gajbhiye S, Meshram C, Singh S.K, Prashant K. Srivastava and Tanvir Islam (2016), "Precipitation trend analysis of Sindh River basin, India, from the 102-year record (1901–2002)", *Atmospheric Science Letters*, 17: 71–77
3. Kim C.J, Park.M and Lee J.H (2014), "Analysis of climate change impacts on the spatial And frequency patterns of drought using a potential drought Hazard mapping approach", *International Journal of Climatology*,34: 61–80
4. Mallya G, Mishra V, Niyogi D, Tripathi S and Govindaraju R.S(2016)," Trends and variability of droughts over the Indian monsoon region", *Weather and Climate Extremes*,12: 43–68
5. NiranjanKumar K, M.Rajeevan, D.S.Pai, A.K.Srivastava and B.Preethi (2013), " On the observed variability of monsoon droughts over India", *Weather and Climate Extremes*,1:42–50

6. Zahradnicek P, Trnka M, Brazdil, Mozny M, Hlavinka P, Zalud Z and Maly A(2015), “The extreme drought episode of August 2011–May 2012 in the Czech Republic”, *International Journal of Climatology*, 35: 3335–3352
7. Rossi G, Vega T and Bonaccorso B (2006) “Methods And Tools For Drought Analysis And Management”, *Water Science and Technology Library*, Volume 62
8. Taxak A.K, Murumkar A.R and Arya D.S (2014), “Long-term spatial and temporal rainfall trends and homogeneity analysis in wainganga basin, central India ”, *Weather and Climate Extremes*, 4: 50–61



INTERNATIONAL CONFERENCE ON INFRASTRUCTURE DEVELOPMENT: ISSUES, INNOVATIONS & THE WAY FORWARD 21-23 JUNE, 2018

Website: www.icid18mbcet.in Email: icid2018@mbcet.ac.in



**KERALA INFRASTRUCTURE
INVESTMENT FUND BOARD**

Pre-Conference Workshop # 1

SUSTAINABLE PAVEMENTS AND ASSET MANAGEMENT

21 June 2018

Programme Schedule

9.00 - 10.00	Registration at Kanakakkunnu Palace	
10.00 - 10.45	Inauguration of Exhibition on “Infrastructure Development and Quality Management” by Shri G Sudhakaran , Hon’ble Minister for Public Works & Registration, Govt. of Kerala	
10.45 - 11.00	<i>Tea Break</i>	
11.00 - 11.40	Road Infrastructure Development in India – Challenges and Opportunities	Mr. Kedar Bhagwat Director, Cube Highways
11.40 - 12.20	Sustainable Road Infrastructure in Kerala - Issues and Options	Dr. Rajib Basu Mallick Professor, Worcester Polytechnic Institute (WPI), USA
12.20 - 13.00	Recycling of Pavement Materials for Sustainable Road Infrastructure – Opportunities in Kerala	Wirtgen Group
13.00 - 14.00	<i>Lunch</i>	
14.00 - 14.40	Choice and Guidelines for Selection of Binders for Long Lasting Highway Pavements	Dr. J Murali Krishnan Professor, IIT Madras
14.40 - 15.10	Sustainable Asphalt Pavement Technology & Green Initiatives in Asphalt Mixing Plants	Mr. K Saravanakumar Deputy General Manager (South) Ammann India Private Ltd.
15.10 - 15.40	Rigid Pavements – White Topping	UltraTech Cement Ltd.
15.40 - 16.00	<i>Tea Break</i>	
16.00 - 16.40	Condition Assessment and Maintenance Strategization for Highway Assets	Mr. Bhanoj Dokku Manager Maintenance (Pavements) V R Techniche
16.40 - 17.10	Moisture Resistant Durable Pavements with Nanotechnology	Mr. Vasudevan GM – International Marketing Zydex Industries
17.10 – 17.30	Interactive Session	



**INTERNATIONAL CONFERENCE ON
INFRASTRUCTURE DEVELOPMENT: ISSUES,
INNOVATIONS & THE WAY FORWARD**
21-23 JUNE, 2018

Website: www.icid18mbcet.in Email: icid2018@mbcet.ac.in



MAR BASELIOS
COLLEGE OF ENGINEERING AND TECHNOLOGY
Department of Civil Engineering



**KERALA INFRASTRUCTURE
INVESTMENT FUND BOARD**

Pre-Conference Workshop # 2

STRUCTURAL SIMULATIONS USING FEAST^{SMT} SOFTWARE

21 June 2018

Programme Schedule

9.00-10.15	Registration at MBCET
10.15-10.30	<i>Tea Break</i>
10.30-12.30	Theoretical Session on FEAST ^{SMT}
12.30-13.30	<i>Lunch</i>
13.30-15.30	Hands-on Training in FEAST ^{SMT}
15.30-15.45	<i>Tea Break</i>
15.45-17.30	FEAST ^{SMT} - Session Continues
17.30-17.45	Valedictory Function



**INTERNATIONAL CONFERENCE ON
INFRASTRUCTURE DEVELOPMENT: ISSUES,
INNOVATIONS & THE WAY FORWARD**
21-23 JUNE, 2018

Website: www.icid18mbcet.in Email: icid2018@mbcet.ac.in



MAR BASELIOS
COLLEGE OF ENGINEERING AND TECHNOLOGY
Department of Civil Engineering



**KERALA INFRASTRUCTURE
INVESTMENT FUND BOARD**

Pre-Conference Workshop # 3

**A TECHNICAL TOUR OF GREENFIELD INTERNATIONAL
STADIUM, KERALA**

21 June 2018

Programme Schedule

- 9.00 - 10.15 : Registration at MBCET
- 10.20 : Departure to Greenfield Stadium from MBCET
- 11.00 : Arrival at Greenfield Stadium
- 11.15 - 13.15 : Technical Talk
- 13.15 - 14.00 : *Lunch Break*
- 14.00 - 16.30 : Field Visit
- 16.30 - 16.50 : *Tea Break*
- 16.50 - 18.30 : Visit (Continued...)
- 18.30 : Departure from Greenfield Stadium



9.00am	Registration					
9.45-10.30	Inauguration					
10.30-10.40	Tea Break					
	Track1 : Structural Engineering		Track 2 : Transportation Engineering		Track 3 : Geotechnical Engineering	
10.40-11.20	Key Note: Mr. Immanuel Jose, Eco White		Key Note: Dr. J Murali Krishnan Professor, IITM		Key Note : Dr. T Thyagaraj Asso. Professor, IITM	
11.20-11.40	SE 108	Effect of Steel and Polypropylene Fibre on the Tension Stiffening of Ultra High Performance Concrete	TE 219	Comparative Study on Cell Filled and Whitetopped Concrete Overlay with Human Hair as Pavement Rehabilitation Methods	GT 402	Influence of Nano-Silica on Unconfined Comp. Strength of Marine Clay with Curing Time
11.40-12.00	SE 119	Strengthening of Self Compacting Concrete Using Polypropylene and Strips of Steel Scrubber	TE 220	Influence of Gauge Length on the Measurement of Resilient Modulus of Bituminous Mixtures	GT 403	Effect of Enzymatic Lime on Engineering Behaviour of Clay
12.00-12.20	SE 121	Seismic Evaluation of Different Structural Systems in Stepped Building Frame	TE 222	How to Consistently Collect Rheological Data for Bitumen in a Dynamic Shear Rheometer	GT 404	Skirted Stone Column with Bamboo and Coir in Kuttanadu Clay
12.20-12.40	SE 123	Study on Flexural Behaviour of RCC Beams Retrofitted with Biplanar Geonet	TE 225	Use of Statistical Methods for the Analysis of Axle Load Data for Pavement Design		

12.40-1.00	SE 127	Effect of Near Surface and Externally Bonded Retrofitting on Exterior Beam-Column Joint	TE203	Accurate Identification of Pavement Materials that are Susceptible to Moisture Damage with the Use of Advanced Conditioning and Test Methods and the use of Machine Learning Techniques	
1.00-2.00	Lunch Break				
	Track1 : Structural Engineering		Track 2 : Transportation Engineering		Track 3 : Hydraulics Engineering
2.00-2.40	-----		----		Key Note : Dr. Santosh G Thampi Professor, NITC
2.40-3.00	SE 102	Analysis of Concrete Silo by using ETABS 2016	TE 207	Effect of Accessibility on Potential Tourist Destinations –A Case Study of Kozhikode District in Kerala	HE 501 Trend and Change Point Analysis of Annual Maximum Stream flows of Krishna Basin Using Non- Parametric Tests and Empirical Mode Decomposition
3.00-3.20	SE 104	Seismic Analysis of RCC Buildings Considering the Flexibility of Soil	TE 208	Activity Based Transportation Modeling for Chelakottukara ward of Thrissur District	HE 502 Modeling of Bharathapuzha River Basin Using SWAT Model and SUFI-2
3.20-3.40	SE 106	Along and Across Wind Responses of Tall Buildings Considering Soil Structure Interaction	TE 209	Urban Resident’s Awareness and Readyness For Sustainable Transportation A Case Study	HE 503 Assessment of Meteorological Drought in Anantapur District Using Standardized Precipitation - Evapotranspiration Index (SPEI)
3.40-4.00	Tea Break				

				Track 1(a) : Structural Engineering	
4.00-4.20	SE 116	Thermal Response of Concrete Filled Fibre Reinforced Polymer Tube Columns	TE 211	A Study on Profit Optimisation of Kerala State Road Transport Corporation	SE 103 Finite Elemental Analysis of Idukky Dam
4.20-4.40	SE 118	Partial Replacement of Fine Aggregate with Crumb Rubber	TE 212	Estimation of PCU and Saturation Flow for Mixed Traffic Condition at Urban Signalized Intersections	SE 125 Response of Conventional and Virtual Outrigger System Subjected to Seismic Load
4.40-5.00	SE 122	Study on the Mechanical and Flexural Properties of Concrete by the Addition of Black Liquor Sludge as Admixture	TE 215	Overtaking Behaviour of Vehicles on Undivided Roads Under Heterogeneous Traffic	SE 128 Effect of Nonlinear Viscous Dampers on Irregular Shaped Buildings
5.00-5.20	SE 124	Study on Behaviour of Normal Concrete Column and Modified Reactive Powder Column	TE 224	Surrogate Safety Assessment Models for Interurban Corridors	SE 130 Numerical Study on the Flexural Behaviour of Concrete Filled Steel Tube Beam Strengthened with CFRP
6.00-8.30	Conference Dinner at Olympia, MBCET				

Programme Schedule



23 June 2018 (Saturday)

	Track 1 : Structural Engineering		Track 2 : Transportation Engineering		Track 3 : Environmental Engineering	
9.30-10.10	Key Note : Dr. Gopu R Potty Professor, University of Rhode Island		Keynote : Dr. Rajib B Mallick Professor, WPI, USA		Key Note : Mr. Shreeganesh V Nair MD, GTCS	
10.10-10.30	SE 105	Effect of Containment Reinforcement on the Seismic Performance of Un-Reinforced Masonry Buildings	TE 205	Environmental Impact Assessment of Thrissur-Vadanapally Road Project	EE 301	Environmental Issues of Buildings – Greensolutions
10.30-10.50	SE 107	Eco- Friendly Cement Blocks	TE 210	Use of Data Mining Technique for Systematic Road Safety Audit of Non-urban Highways	EE 302	Development of Noise Map Using GIS For Lucknow Metropolis
10.50-11.10	SE 109	Development of Stress Block Parameters of Concrete with Metakaolin Admixed Recycled Concrete Aggregate	TE 213	Analysis and Development of Traffic Speed-Flow-Density Relationships for Urban Roadway	EE 303	Comparative Study of Noise Descriptors and Noise Exposure Level Due to Diwali Noise in Metropolitan City: Lucknow
11.10-11.25	Tea Break					
11.25-11.45	SE 110	Study on Properties of Polythene Fibre Reinforced Concrete with Partial Replacement of Coarse Aggregate as Coconut Shell (PFRCS)	TE 214	Managing Traffic Congestion Using GIS – A Case Study In Attingal Town	EE 307	Evaluation of Groundwater Quality at Eloor, Ernakulam District, Kerala Using GIS

11.45-12.05	SE 112	Effect of Swimmer Bars on the Behaviour of Exterior Beam Column Joints Under Reverse Cyclic Loading	TE 218	Quantification and Analysis of Blindspots for Light Motor Vehicles	EE 308	Biodiesel Production from Waste Oil Using Mussel Shell as Catalyst
12.05-12.25	SE 126	Shear Behaviour of RCC Beams Retrofitted with Ultra High Performance Fibre Reinforced Concrete	TE 226	Feasibility Study of Provision for Exclusive Bus Lanes on Urban Roads	EE 309	Landfill Site Selection Using GIS and Landfill Design in Trivandrum District
12.25-12.45	SE 129	Flexural Behaviour of RCC Beams Retrofitted with Engineered Cementitious Composite (ECC)				
12.45-1.05	SE 132	Flexural Behaviour of Hybrid Fibre Reinforced High Strength Concrete				
1.05 -2.00	Lunch Break					
	Track 1 : Structural Engineering		Track 2 : Transportation Engineering		Track 3 : Environmental Engineering	
2.00-2.40	Key Note : Dr. Saravanan U Asso. Professor, IITM		Key Note : Dr. P K Sikdar President, ICT		----	
2.40-3.00	SE 101	Fire Resistance of Steel-Concrete Composite Bridge Girders	TE 201	Use of Recycled Premix Chipping Carpet (RPCC) for Rural road Construction	EE 304	Treatment of Industrial Effluent with Coir Pith and Charcoal Infused Soil Media
3.00-3.20	SE 111	Comparative Study on Hysteretic Performance of Semi Through Connections in CFT Beam - Column Joint	TE 204	Comparing The Properties of HMA With Warm Asphalt Mixes by Varying Temperatures Using Sasobit & Stearic Acid as Additives	EE 305	Optimisation of Phosphate Removal from Fertiliser Wastewater Using Polysulphone Chitosan Nanosilica Membrane

3.20-3.40	SE 115	Experimental and Analytical Study on Geopolymer Concrete Beam with Hollow Space Below Neutral Axis	TE 206	Development of a Relation Between Structural and Functional Characteristics of Pavement	EE 306	Trend and Change Point Analysis of Extreme Temperature Over India Using Non-Parametric Methods and Empirical Mode Decomposition
3.40-4.00	SE 120	Experimental Investigation on Torsional Behaviour of RCC Beams Retrofitted with High Strength Ferrocement Jacketing and GFRP	TE 221	Influence of Rest Period and Confinement Pressure on the Measurement of Dynamic Modulus of Bituminous Mixtures		
4.00-4.20	SE 133	Strength and Behaviour of RCC Beams Retrofitted by Textile Reinforced Concrete	TE 223	Moisture Conditioning Process for Large-Sized Prismatic Straight Beam Specimens of Bituminous Concrete		
4.25-5.00	Valedictory function					



NEW STANDARDS FOR THE FUTURE

AMMANN ABA UNIBATCH ASPHALT-MIXING PLANT

The Ammann ABA UniBatch sets new standards for asphalt mix production in the 100–340 t/h output classes. It delivers cutting-edge technology and includes all the features of current and future plant concepts.

- Maximum customisation combined with top performance and economic efficiency
- Designed for worldwide use, with mixing tower modules optimized for ease of transportation
- Can be fitted and extended with numerous options at any time

Ammann India Private Ltd., Near Mithakhali Circle, Navrangpura, Ahmedabad 380 009
Phone +91-79-6618-8888, Fax +91-79-2656-4705, info.ain@ammann-group.com
For additional product information and services please visit: www.ammann.com
PMP-2093-01-EN | © Ammann Group

AMMANN



BUILT FOR INDIA

AMMANN AFT 500 ASPHALT PAVER

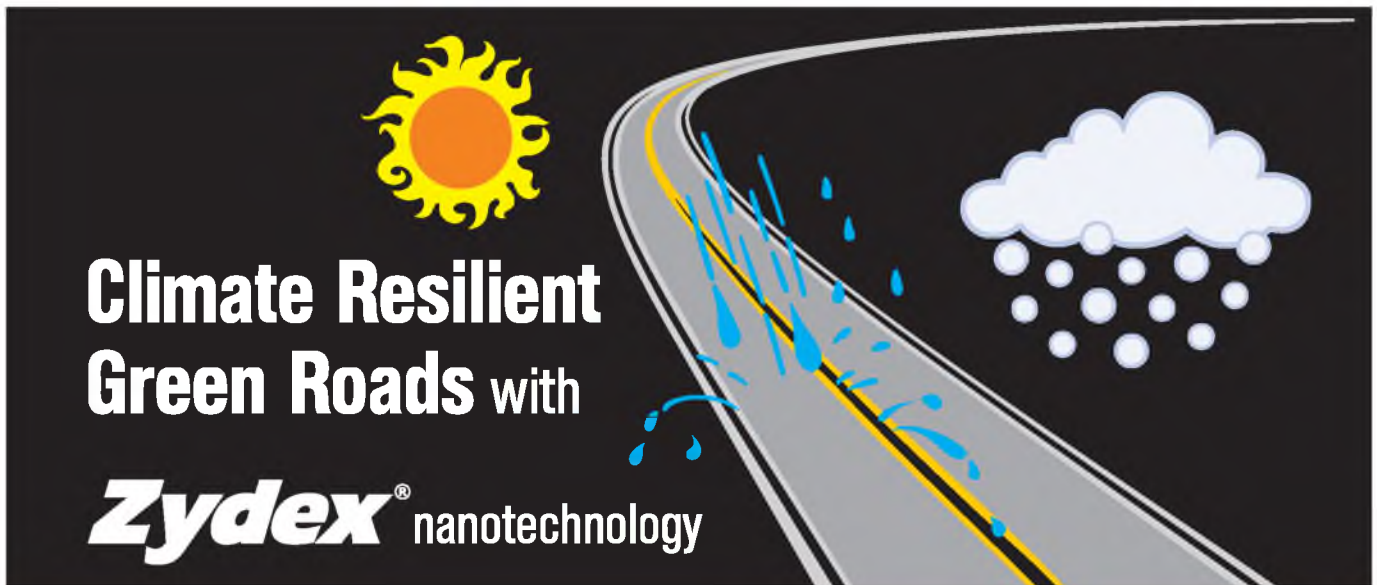
Looking for productivity on larger asphalt road projects? The Ammann AFT 500 Paver is the answer. The machine features many advantages for the operating crew, such as unmatched overview for best process control at all time. The AFT 500 offers the power, the traction and the screed options to pave roads as wide as 7 metres.

What else do you get with the AFT 500?

- A modern dashboard with 5" color display that enhances operator control
- Slidable operator stations to give the operator the best overview on the relevant side of the machine
- Open plug-and-play connections to the leveling system of your choice
- Tried-and-tested European technology that is fine-tuned for the Indian market
- Leading after-sales support through Apollo's robust service network all over India

Ammann India Private Ltd., Near Mithakhali Circle, Navrangpura, Ahmedabad 380 009
Phone +91-79-6618-8888, Fax +91-79-2656-4705, info.ain@ammann-group.com
For additional product information and services please visit: www.ammann.com
PMP-2240-00-EN | © Ammann Group

AMMANN



Water Resistant Bases

Swell control, Permeability reduction,
Improved compaction, 80+ CBR



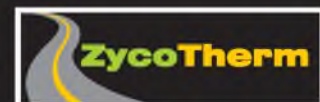
Waterproofed Prime & Tack Coats with High Performance

(also useful in Fog Seal, Slurry Seal, Chip Seal, Micro surfacing)
Strong Chemical Bonding, Waterproofing, Quick Setting,
Zero Volatile Emissions



Weather Resistant Bituminous Courses

Improved Resistance to Moisture,
Oxidation, Fatigue, Cracking & Bleed



Reduced Maintenance – Extended Life



ZYDEX INDUSTRIES 61, Gotri-Sevasi Road, Sevasi, Vadodara - 390 021. Gujarat. INDIA
Mail : roads@zydexindustries.com, info@zydexindustries.com | www.zydexindustries.com


CLOSE TO OUR CUSTOMERS

 **WIRTGEN GROUP**



For your success.

 www.wirtgen-group.com/technologies

ROAD AND MINERAL TECHNOLOGIES. The WIRTGEN GROUP owes its strength to the excellence of its product brands – WIRTGEN, VÖGELE, HAMM and KLEEMANN – with their unique wealth of experience. Put your trust in the WIRTGEN GROUP team.  www.wirtgen-group.com/india

WIRTGEN INDIA · Toll Free Number 1800-200-2600 · E-Mail: sales.india@wirtgen-group.com

WIRTGEN / VÖGELE / HAMM / KLEEMANN



UltraTech
C E M E N T
The Engineer's Choice

**Build
beautiful**



Viscometers & Rheometers



DV2T - Viscometer



DV3T - Rheometer



RST Rheometer

Texture & Powder Flow Analyzer



CT3 Texture Analyzer

- 21 CFR Part 11 Compliance
- Spreadability
- Firmness
- Gel Strength
- Tackiness

Powder Flow Analyzer

- Complies to USP 1174
- Flowability
- Angle of Friction
- Compressibility
- Cohesiveness
- Bulk Density

